NATIONAL CONFERENCE
ON
ADVANCES IN MATERIAL SCIENCES

Organized by: Department of Applied Sciences

AMS - 2014

4th & 5th April, 2014

PROCEEDINGS

Amritsar College of Engineering & Technology
NBA & NAAC Accredited

12 km stone, Amritsar - Jalandhar G.T. Road, Amritsar - 143001 (Punjab) India.

National Conference

On

Advances in Material Sciences

(AMS-2014)

April 4-5, 2014

Chief Editor

Dr. Amit Sarin

Organized By

Department of Applied Sciences

AMRITSAR COLLEGE OF ENGINEERING & TECHNOLOGY
NBA Accredited I NAAC Accredited

National Conference

On

Advances in Material Sciences

(AMS-2014)

April 4-5, 2014

Chief Patron

Advocate Amit Sharma

(Chairman & CEO, ACET Amritsar)

Patrons

Madam Ragini Sharma

(Director (Finance))

Dr. O. K. Harsh

(Group Director)

Dr. V. K. Banga

(Principal)

Organizing Secretary

Dr. Amit Sarin

(Head Department of Applied Sciences (Physics Group)),ACET

Conveners

Dr. Navdeep Singh

Varun Mehra

National Conference

On

Advances in Material Sciences

(AMS-2014)

April 4-5, 2014

International/National Advisory Board

Dr. Buta Singh	**Dean, PTU, Kapurthala**
Dr. A. P. Singh	**Dean, PTU, Kapurthala**
Dr. Satya Prakash	**Emeritus Professor, IIT Roorkee**
Dr. T. S. Sidhu	**Director, SBS Technical Campus, Ferozepur City**
Dr. Harpreet Singh	**IIT Ropar**
Dr. P. K. Sahu	**University of Petroleum, Dehradun**
Dr. Sunil Kumar	**Australia**
Dr. Nitin Sharma	**University of California, USA**
Dr. H. M. Mittal	**NIT Jalandhar**
Dr. Rohit Mehra	**NIT Jalandhar**
Dr. Sarabjit Singh	**NIT Jalandhar**
Dr. Arvinder Singh	**NIT Jalandhar**
Dr. Parveen Malik	**NIT Jalandhar**
Dr. K. Kundu	**MERADO, Ludhiana**
Sh. Vivek Talwar	**PTU, Kapurthala**
Dr. KamalDeep Paul	**Thapar University, Patiala**

National Conference

On

Advances in Material Sciences

(AMS-2014)

April 4-5, 2014

Local Advisory Board

Dr. R. C. Singh	**GNDU, Amritsar**
Dr. Adarsh Pal Vig	**GNDU, Amritsar**
Dr. Lakhwant Singh	**GNDU, Amritsar**
Dr. N. P. S. Saini	**GNDU, Amritsar**
Dr. D. P. Singh	**GNDU, Amritsar**
Dr. Atul Khanna	**GNDU, Amritsar**
Dr. Aman Mahajan	**GNDU, Amritsar**
Dr. Harminder Singh	**GNDU, Amritsar**
Dr. T. S. Bhatia	**Khalsa College, Amritsar**
Dr. Vijay Kumar	**Hindu College, Amritsar**
Sh. Sameer Kalia	**DAV College, Amritsar**
Dr. Rajesh Kumar	**DAV College, Amritsar**
Dr. Narinder Arora	**DAV College, Amritsar**
Dr. Harinder Singh Gill	**ACHMT, Amritsar**
Sh. Manoj Kumar	**ACET, Amritsar**
Dr. S. K. Aggarwal	**ACET, Amritsar**
Retd. Col. Gurmukh Singh	**ACET, Amritsar**
Prof. R. K. Mohindru	**ACET, Amritsar**
Sh. Gaurav Tejpal	**ACET, Amritsar**
Sh. Rakesh Jaitly	**ACET, Amritsar**
Sh. Harinder Singh Sarkaria	**ACET, Amritsar**
Dr. Tanupreet Singh	**ACET, Amritsar**
Er. Sandeep Kad	**ACET, Amritsar**
Er. Ajay Sharma	**ACET, Amritsar**
Er. Narinder Sharma	**ACET, Amritsar**
Prof. P. S. Sidhu	**ACET, Amritsar**
Dr. Maninder Singh Gill	**ACET, Amritsar**
Mrs. Deepti Malhotra	**ACET, Amritsar**
Er. S. B. S. Kalsi	**ACET, Amritsar**
Sh. Jayant Vats	**ACET, Amritsar**

National Conference

On

Advances in Material Sciences

(AMS-2014)

April 4-5, 2014

Organizing Committee

Mr. Baljeet Verma
Ms. Binod Kaur
Ms. Harpreet Kaur
Ms. Sharanjeet Kaur
Ms. Sapna Bhalla
Mr. Varun Mehra
Dr. Shruti Khanna
Dr. Amandeep Kaur
Dr. Navdeep Singh
Ms. Tanu Sharma

Editor

Karambir Singh

Student Coordinators

Nehal Bansal
Kunal Arora

National Conference

On

Advances in Material Sciences

(AMS-2014)

April 4-5, 2014

Publication Partners

Journal on Material Sciences (JMS) (ISSN: 2347-2235)	i-manager® Publications
Innovations in Corrosion and Material Sciences (ICMS) (ISSN: 2352-0949)	BENTHAM SCIENCE

Message

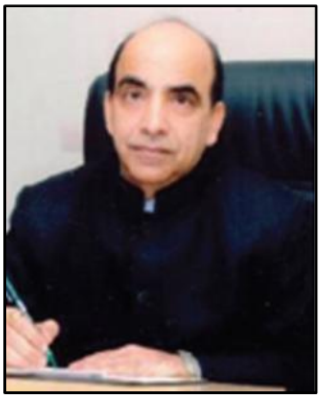

It gives me immense pleasure to witness a major milestone for us all – the publication of the proceedings of the "National Conference on Advances in Material Sciences" organized by the Department of Applied Sciences, ACET Amritsar.

Research in all the fields of Materials Science has to be undertaken earnestly, with the objective of original findings in the new realms. I am particularly happy to know that the Department of Applied Sciences of ACET, Amritsar is carrying forward the legacy of PTU by organizing such an event with a clear agenda for researchers to provide solutions to the myriad of problems in the field of Materials Science.

I am sure that the Conference will not only provide a useful forum to the participants to share their expertise in their respective fields but will also be professionally beneficial to them. The conference is being held in Amritsar, which is the place of spiritual importance in Punjab and I hope that the delegates will enjoy the traditional hospitality offered by the Institute.

I compliment the Organizers of AMS-2014 for holding this event and wish all success to the conference.

Dr. Rajnish Arora
Vice Chancellor
Punjab Technical University
Kapurthala

Message

I am glad to know that a "National Conference on Advances in Material Sciences" is being organized by Department of Applied Sciences of Amritsar College of Engineering and Technology on April 4-5, 2014.

It's a saying of wisdom that; Acquires knowledge and impart it to the people. Though the quest for knowledge has been from the beginning of time but knowledge only becomes valuable when it is disseminated and applied to benefit humankind. Academicians, Scientists and Researchers will be able to share and discuss new findings and applications of Materials Science. The primary goal of the meeting is to bring together the researchers from far and near to discuss the current understanding of the fundamental issues pertaining to the field of Materials Science. It is likely that the deeper understanding of experimental/academic observations of Materials Science will have far reaching but very positive and encouraging consequences.

Finally I would like to congratulate the organizing committee for their tremendous efforts in organizing the conference. I wish that the conference turns out to be a grand success.

Advocate Amit Sharma
Chairman & CEO
ACET Amritsar

Message

It is a matter of great pleasure that a "National Conference on Advances in Material Sciences" is being organized by Department of Applied Sciences of Amritsar College of Engineering and Technology on April 4-5, 2014.

The purpose of the conference is to unveil high quality research and experience which will set a milestone in transforming the mind set of researchers, academicians and students. Since the inception of this premier institute of Engineering and Management Studies in 2002, the main focus has always been to improve the quality of education and encourage the researchers and knowledge seekers by organizing conferences, seminars, workshops and invited guest lectures etc., and undoubtedly the current conference on Materials Science is part of our endeavor to take a step forward in this direction.

I would like to congratulate the Department of Applied Sciences for organizing this conference. I pray that the conference turns out to be a grand success.

Ragini Sharma
Director (Finance)
ACET Amritsar

Message

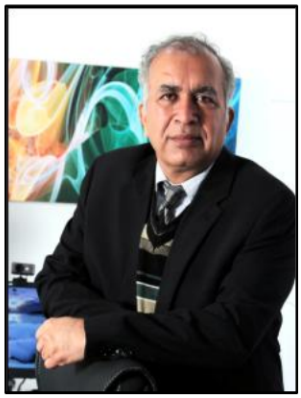

It gives me immense pleasure to note that a "National Conference on Advances in Material Sciences" is being organized by the Department of Applied Sciences of Amritsar College of Engineering and Technology, Amritsar on April 4-5, 2014.

The rich benefits of this conference are expected to have positive impact amongst the scientific and engineering communities. Special emphasis is being placed on inviting eminent scholars, researchers and engineers from various backgrounds to discuss recent advances in Materials Science and share their experiences for greater mutual benefits. The conference will surly provide comprehensive overview of the current status and potential directions for future research in search for diverse applications of Materials Science.

I on behalf of ACET, Amritsar wish all academicians and professionals for fruitful interaction in this significant field. I congratulate the Department of Applied Sciences for organizing this conference.

Dr. Om Kumar Harsh
Group Director
ACET Amritsar

Message

On behalf of Amritsar College of Engineering and Technology, I welcome all the participants to "National Conference on Advances in Material Sciences".

National level Conference on Advances in Material Sciences aims to bring together leading academic scientists, researchers and research scholars to exchange and share their experiences and research results about all aspects pertaining to Materials Sciences. It will also provide the premier interdisciplinary forum for participants to present and discuss the most recent innovations, trends, concerns and practical challenges encountered and the solutions adopted in the respective field. This conference of Materials Science aims to enhance the exchange of scientific activities in materials science and technology.

The Department of Applied Sciences at ACET, Amritsar is putting in its best efforts to make this venture not only successful but fruitful also. I want to assure the researchers and teaching community that we will continue with many more such events at ACET to reap the reward of mutual sharing for the common benefit and knowledge enrichment for all.

Dr. V. K. Banga
Principal
ACET Amritsar

Message

It is a matter of great pleasure for me that the Department of Applied Sciences of Amritsar College of Engineering and Technology is organizing a "National Conference on Advances in Material Sciences" on April 4-5, 2014.

Directions of activities of materials science and engineering are ensuring the achievements of strategic aims of the developments of societies pertaining to a humanistic mission which stands at the engineering circles. Significant contributions by researchers, academicians and scholars from all over the country are commendable and a source of great encouragement to forward many steps in the direction of many more such activities that contribute a lot in the society for the betterment of mankind.

Knowledge by sharing, undoubtedly, enhances many folds and at ACET we work with this philosophy. I hope your experience of being part of this conference will be wonderful. ACET will be a venue where exchange of applications and ideas face to face finds you a global partner for collaborations by which you can advance and explore your research and research experiences. Hopefully, the conference discussions, presentations and contributions play significant roles to update the knowledge in the concerned field.

Dr. H. S. Gill
Principal
ACHMT Amritsar

Message

I feel proud that the Department of Applied Sciences is organizing a "National Conference on Advances in Material Sciences" on April 4-5, 2014.

In today's era, new developments are occurring almost on daily basis. These developments are changing the shape of the society. Considering the fast pace of globalization and dynamic nature of trends in materials science, the need of the hour is to provide a platform where experts may share the advances in this field.

The conference paper submission opened on February 15, 2014 and in this very short period of time the conference received an overwhelming response from various researchers from esteemed institutes like IITs, UPES, Dehradun and many more across the country. We have received around 80 papers covering various areas of Materials Science. The papers received in this conference have been reviewed by reviewer committee and editorial board. After the review process around 65 papers were selected on the basis of originality, significance, clarity for the objective of the conference.

I am confident that the conference will become an occasion for academicians, professionals, researchers and students to acquire latest knowledge in the field of Materials Science.

I wish this conference a grand success.

Dr. Amit Sarin
Organizing Secretary
AMS-2014

Message

It is a matter of great pleasure for us that our department is organizing a "National Conference on Advances in Material Sciences" on April 4-5, 2014.

This conference is a platform where researchers can share their experiences and ideas. Experts will deliver keynote lectures during the conference for value addition to the professional skills of conference delegates. We believe that organizing such an event is a must for enabling professionals, scientists and educators to analyze the future needs and to keep themselves updated with the advances in the field of Materials Science.

We also take the opportunity to thank the Management, Group Director, Principal and staff of ACET for their encouragement and continuous support without which this event would not have taken shape.

Best Wishes.

Dr. Navdeep Singh
Varun Mehra
Conveners
ACET Amritsar

CONTENTS

National Conference
On
Advances in Material Sciences (AMS-2014)
April 4-5, 2014

S. No.	Title of the Paper and Authors	Page No.
1.	Nano Biomedical Applications of Carbon Nano Tubes Neetika Soni	1-3
2.	Effect of Nickel (Ni) underlayer on the field emission from carbon nanotubes Kulwinder Kaur	4-10
3.	Stability of Non Edible Oil for Biodiesel Production –A Review Gaurav Dwivedi , M.P. Sharma	11-15
4.	Corrosion Auditing in Oil & Petroleum Products Transmission Pipelines in India R.Bhaskaran, Lalit Bhalla, Vishal Sarin, Sukhpreet Kaur, Afzalur Rahman and Ashish Shukla	16-22
5.	Enhanced Antioxidant Activity Of Gold Nanoparticles Embeded Solanum Tuberosum Extract And HPTLC Quantification Roopa Rani, Kiran Singh and ManMohan Srivastava	23-26
6.	Electric properties of rare earth doped strontium M-type hexagonal ferrites Taminder Singh, Arun Katoch, Iqbal Singh	27-31
7.	Utilization of Polymer Nanocomposites for Power System Equipment's Isaac Ramalla	32-36
8.	A Review: A Secure Image Based Steganography, Cryptography and Watermarking with security key Rupesh Gupta, Dr.Tanupreet Singh	37-41
9.	Current Emerging trends in Wire EDM: A Review Sandeep Yadav, Saurabh Sharma, Shiv Ohri, Saurabh Poddar & Anmol Bhatia	42-46
10.	Comparison of the accidents at Chernobyl and Fukushima Dai-ichi Nuclear Power Stations Iqbal Preet Kaur	47-51
11.	Corrosion Mechanism Study in Waste-To-Energy Plants Harminder Singh	52-53
12.	Study of Corrosion Preventive Measures for Waste Incinerators Harminder Singh	54-55
13.	Synthesis and characterization of Dicinnamalacetone thin films for solar cell applications Sameer Kalia, J.J.Mohindroo, Rajeev Arora, Anupreet kaur, Roohi Devgan	56-58
14.	Effect of Compositional Variation of the Physical Parameters of Ge-Se-In Glass System Surbhi Sharma, Amit Sarin and Navjeet Sharma	59-64
15.	Burnishing a super finishing process – A review Aashish Sharma and S.B.S. Kalsi	65-69
16.	Synthesis Of Gold Nanoparticles From Solanum Tuberosum Extract And Evaluation Of Its Antioxidant Activity Roopa Rani, Kiran Singh, ManMohan Srivastava	70-73
17.	Essential Variables to Control the Fill Factor of Organic Photo Voltaic Cell to Improve Its Power Conversion Efficiency Karthik.B, Vedant Sumaria, P.Vijay	74-80
18.	Current Trends in ECG Compression Techniques Butta Singh	81-84
19.	Electronics with "Genes Inside" Deep Kamal Kaur Randhawa	85-89
20.	Synthesis and Characterization of Boron Subphthalocyanine Subphthalocyanine Chloride Thin Films Sameer kalia, Jasmeet Kaur, Navjot kaur	90-92
21.	Review of Load Balancing Routing Protocols in Mobile Ad Hoc Networks Er. Gaganjot Kaur, Dr. Tanu Preet Singh	93-98
22.	Photonic Integrated Circuits: Materials & Fabrication Harmandar Kaur	99-101
23.	Energy Efficient Routing Protocol for Mobile Ad hoc Networks: A Review Er. Kanwalpreet Kaur, Dr. Tanu Preet Singh	102-105
24.	Cellulosic Nanocomposites: Functional Vector for Arsenic Remediation Kiran Singh, TJM Sinha and Shalini Srivastava	106-111
25.	Photoluminescence and Dielectric Studies of Ion Induced Polyethylene Naphthalate Kusum Devgan, Navjeet Kaur, Sonika Thakur, Manpreet Kaur, Lakhwant Singh	112-113
26.	Synthesis of Copper Nanoparticles using Ascorbic acid as Reducing Agent-A Green Synthesis Jeevan Jyoti Mohindroo, Neerja Kalia, Neha and Radhika	114-117
27.	Characterisation of Polymer Gel Electrolytes Containing Imidazolium Based Ionic Liquids Dilraj Preet Kaur, S.S. Sekhon	118-120
28.	Radon Concentration in Ground Water Samples from Some Regions of Tarn Taran District of Punjab. Meetu Singh, Neerja, Asha Rani	121-123
29.	Effect of various parameters on microalgal biodiesel: A review Mukesh Kumar, M.P. Sharma	124-127

S. No.	Title of the Paper and Authors	Page No.
30.	Xanthan Gum based Gel Electrolyte containing NaOH Narinder Arora, Viney Sharma and Rajesh Kumar	128-130
31.	To study of effect of annealing on etching properties of thermal neutron irradiated CR-39 polymer Neerja, Sameer Kalia and Surinder Singh	131-134
32.	Structural Information from Nucleon Separation Energies Manpreet Kaur, Husandeep Kaur, Neeru Gupta	135-137
33.	Biodiesel Production and Performance and Emission Characteristics of Diesel Engine: A Review Puneet Verma, Gaurav Dwivedi	138-142
34.	Spin speed dependence of optical band gap of sol gel spin coated zinc oxide thin films Rajesh Kumar, Aakanksha sahu, Narinder Arora, Rabia Sareen & Gagandeep Kaur	143-145
35.	Performane Analysis on Routing Protocols in Mobile Ad Hoc Networks Er. Kavneet Kaur, Dr. Tanu Preet Singh	146-149
36.	A Study of Orthopedic Implant Materials Mohd Shahid Khan, Ghulam Anwer, Mohd Shuaib, Mohd Imran Khan	150-155
37.	Spectroscopic Investigations of Anatase Titania Nanoparticles Katlakanti Mohan Reddy, DeviL G, P K Sahoo	156-158
38.	Concrete Self-Healing Capability Using Bacterial Action – A Comparative Study Er Parampreet Kaur, Akash Bhardwaj	159-162
39.	Structural and Optical Properties of Ni Doped Zinc Oxide Nanoparticles Prepared By Coprecipitation Method Deepawali Arora, Sunil Kumar, Simranpreet Kaur, Gurinder Pal Singh, Parvinder Kaur, D.P. Singh	163-165
40.	Role of Cerium on Structural and Optical Properties of Lithium Borate and Lithium Aluminium Borate Glasses Parvinder Kaur, Simranpreet Kaur, Gurinder Pal Singh, Deepawali Arora, Sunil Kumar, D.P. Singh	166-167
41.	Investigation of Electrical Properties of Polyaniline/Silver Nanocomposite Free Standing Films Sonika Thakur, Lakhwant Singh, Navjeet Kaur, Manpreet Kaur and Kusum Devgun	168-170
42.	PMMA Based Polymer Gel Electrolyte Containing $LiCF_3SO_3$ Narinder Arora, Ajay Sharma, Amit Kumar, Rajesh Kumar	171-172
43.	Green Innovation In Technology – A Literature Review Khushal khera, Gaurav Adlakha, Shailesh Mahawal	173-176
44.	Biomimetic Materials –The Future Need Parveen Kumar, Shailesh Mahawal	177-180
45.	Characterization And Gas Sensing Properties Of Surface Modified Indium Oxide Films Amandeep Kaur Bal	181-184
46.	Time Evolution Of The Rotational States Wave Packet For The Diatomic Molecule Maninder Kaur, Mehmood Mian	185-188
47.	Effect of Gamma Irradiation on Aluminophosphate Glass doped with Titania Manpreet Kaur, Lakhwant Singh, Sonika Thakur, Navjit, Kusum Devagan	189-191
48.	Nanotechnology Role in Water Treatment Ravi Sharma	192-193
49.	Hot Corrosion Problems in Coal based Thermal Power Plants in India and Possible Solution-A Review Jaideep Singh, Amit Sarin	194-198
50.	Synthesis of Polyaniline-Zinc Oxide Composites and Its Usage as Ammonia Gas Sensor Vivek Talwar, Ravi Chand Singh	199-201
51.	Spintronics -A New Excitement in The Scientific and Electronic World Harpreet Kaur	202-204
52.	Radon Concentration in Drinking Water Samples of Some Adjoining Areas of Amritsar, Punjab Using Electronic Radon Detector Ajay Kumar	205-207
53.	Study Of Physical Parameters Of Ag-Ge-Se Glass System AmitSethi, Rajesh Kumar, AmitSarin and NavjeetSharma	208-210
54.	Effect of Gamma Irradiation on Structural and Optical Properties of Muscovite Mica Sukhnandan Kaur, Surinder Singh, Lakhwant Singh	211-213
55.	Ultrasonic Spray Pyrolysis Deposition of SDS Surfactant Assisted Copper Oxide Thin Films Iqbal Singh, Taminder Singh, Arun Katoch	214-218
56.	Transport Properties of Metallic Nanowires on Silicon Substrate Jaskiran Kaur, Surinder Singh	219-220
57.	Growth of Nanostructured Tin Oxide Thin Films for Gas Sensing Applications Kamalpreet Khun Khun	221-224
58.	Preparation and Characterisation of Rare Earth Doped Phosphate Glasses Manpreet Kaur, Mehak Mahajan, Mohini Bhatia, Sarabjit Kaur, Lakhwant Singh	225-227
59.	Comparison of Composite Proton Conducting Polymer Gel Electrolytes Containing Weak Aromatic Acids Rajiv Kumar	228-236
60.	Plastics and FRP Material Used in Railways Pawan Malik	237-239
61.	Effect of Gamma Irradiation on Structural and Optical Properties of Muscovite Mica Sukhnandan Kaur, Surinder Singh, Lakhwant Singh	240-242

Nano Biomedical Applications of Carbon Nano Tubes

Neetika Soni
Department of Electronics and Communication Engineering,
Guru Nanak Dev University Regional Campus, Jalandhar

***Abstract*-Recent progress in synthesis and characterization of carbon based nanostructured materials has demonstrated tremendous development in the field of devices used in almost every field of engineering. Carbon Nano Tube (CNT), an allotrope of carbon is one of the most probable candidate for use in nanoscale paradigm. In this paper, various applications of CNTs in the field of Biomedical engineering have been discussed.**

***Index Terms*: Carbon Nano Tubes, Functionalized CNTs, Biosensors, Targeted drug delivery.**

I.INTRODUCTION

Continuous miniaturization of electronic components and circuits has been instrumental in improvisation of systems in all fields. With the advances in technology, it has become possible to fabricate and study the nano scaled quantum systems. The silicon based transistors are no longer shrinking and the circuits based on them leaks current and gets hot. Carbon based nanostructures with high tensile strength and good thermal and electrical properties have become the prominent material in all disciplines. Various materials have been studied for use in electronics but Carbon Nano Tubes (CNTs) have raised expectations in number of different applications. CNTs, an allotrope of carbon that are hollow carbon tubes having diameter in nanometer scale and length in microns to few centimeters. These are the graphene sheets rolled up with continuous unbroken hexagonal mesh and carbon molecules at the apexes of the hexagons. These CNTs have varying structures differing in length, thickness, types of helicity and layers of graphene sheets. CNTs can be categorized as Single Wall Nano Tubes (SWNTs) with single layer of graphene sheet and diameter of 1nm to 20 nm and Multiwall Nano Tubes(MWNTs) having multi wall concentric cylinders of graphene sheets having diameter upto 50 nm.[1,2]

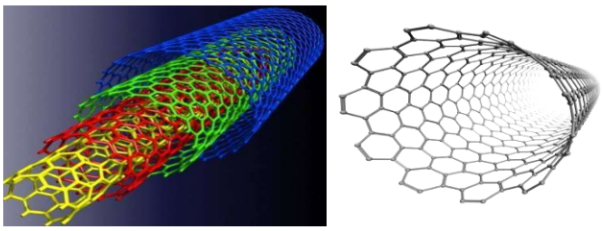

Fig1. MWNT and SWNT

Though formed with the same lattice structure the CNTs can behave as metals or semiconductors depending upon the orientations of the carbon atoms. There are three different confrontations in which these carbon atoms can be placed : arm chair, zig-zag and chiral. CNTs exhibits extra ordinary properties of high mechanical strength, low weight, excellent thermal and chemical properties, high surface area and electrical, electronics and optical properties.

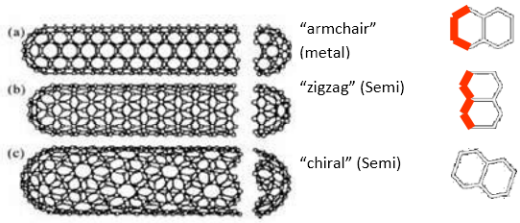

Fig 2. Different confrontations of CNTs

Owing to their unique features CNTs present exciting opportunities for scientific, research, industrial and commercial applications. Ever since its discovery ,researchers have been exploring its potential in biomedical applications. These applications include use of CNTs in energy conversion devices, nano probes, nano biosensors, actuators, bio markers(quantum dots) and bio imaging.

II.FUNCTIONALISED CNTS(*f*-CNTs)

CNTs individually are chemically inert and incompatible with almost all organic and inorganic solvents. So CNTs are being functionalized in which various functional groups are placed at the tips and around the sidewalls of CNTs[3]. Functionalized CNTs have improved surface properties for enhanced dispersion, solubility, biocompatibility ; thereby reduces cytotoxicity in biological systems for biomedical applications. Different methods that can be used for functionalization of CNTs are

1. *Covalent Functionalization*: In this method various chemical groups like COOH, OH and CO are covalently attached with CNTs that increases the oxygen content of the CNTs and decreases their cytotoxicity.
2. *Non Covalent Fuctionalization*: CNTs are non covalently interact with various molecules through weak interactions such as surface adsorption onto

the sidewalls of the CNTs , π-π stacking , electrostatic interactions, hydrogen bonding and vander walls forces . [4] π-π stacking occurs between proteins and CNTs which have been found very beneficial in biosensor fabrication, drug delivery and cancer therapy.

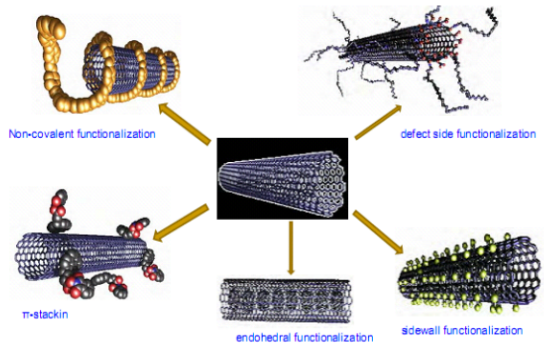

Fig3. Different types of CNT functionalization

III. APPLICATIONS OF CNTS IN BIOMEDICAL ENGINEERING

CNTs have numerous scope in the field of biomedical engineering. CNTs are playing a major role in existing and future applications in biomedical industry. In this paper few applications of CNTs in bio medical field have been discussed and their role in detection and curing the diseases have been studied. Various applications of CNTs are:

a) Diagnostic Tools And Devices: The traditional method of generating X-rays based on thermoionic emission has the limitation of slow response time , limited lifetime, and consumes high energy. Recent research has reported that field emission is better mechanism than thermoionic emission [152 153] and CNTs having high melting point and low work function can be used as cathode in field emitters. The advantage of CNT based X-ray devices are fast response time, fine focal spot, low power consumption possible miniaturization , longer life and low cost.[6]

b) Atomic Force Microscopy (AFM): AFM has been widely applied to investigate surface topographies at the nano scale. CNTs can be attached to the tip of AFM probe to make the tip sharper. This allows much higher atomic resolution of the surface under investigation. Also the flexibility of the CNTs prevents damage to the sampled surface and the probe tip if the probe tip happen to crash into the surface.[7]

c) CNT Sensors: CNT pressure or stress sensors are basically amperometric biosensor and are also based on the principle that nano tube experience a change in electric resistance when experience stress or strain. This peizo resistive effect changes the current flow through the nano tube, which can be measured to quantify the applied stress. Peizoresistive pressure sensors made by incorporating CNTs can bring drastic change to the biomedical industry. These pressure sensors can be helpful in kidney dialysis, blood pressure monitoring, eye surgery and respiratory devices. CNTs sensors can be used as to check the level of cholesterol, sodium, glucose and other ions in the blood stream in the body[7-9,16].

d) Quantum Dots: Quantum dots are basically functionalized CNTs in which the molecules with fluorescent characteristics are attached. To detect the unhealthy cells, CNT based quantum dots bound themselves to sequences of DNA that are associated with the disease. When the quantum dots are stimulated with light, they emit their unique bar codes, or labels, making the critical, diseases-associated DNA sequences visible. The diversity of quantum dots create many unique labels, which can identify numerous regions of DNA simultaneously. Another advantage of quantum dots is that they can be used in the body, eliminating the need for biopsy.

e)Targeted Drug Delivery: CNTs possess unique structure that brings opportunities for improved and fast diagnosis of the diseases and targeted drug delivery. CNTs being in the nano meter scale are small enough to enter directly into cells and hence very beneficial in targeted drug delivery and therapies. In case of cancer treatment, the chemotherapy, not only kills the infected cells but also affects the healthy cells.[] Through targeted drug delivery drugs will be punctured into the targeted cells. The CNT based drug delivery has not only been experimentally demonstrated at the cellular level ,but also applied for the treatment of cancer in animal models [10-12]. CNTs based targeted drug delivery has applications in field of cancer treatment, AIDS treatment, gene delivery and vaccine delivery.

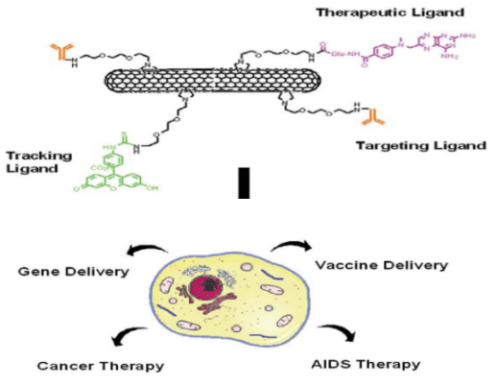

Fig4. CNTs for drug delivery to therapies

g) Tissue Engineering: CNTs have been reported as a promising material in tissue engineering. CNTs are used

for preservation of cells , delivery of growth factor and promote integration with the host tissue and are used in scaffolding the bone tissue engineering applications. The extraordinary ability of CNTs to reinforce polymeric composites is due to its high surface to volume ratio[8].

IV. CONCLUSION

This paper reviews the features of carbon nano tubes and its potential applications in the field of biomedical engineering. The cytotoxicity of the CNTs can be reduced through various methods of surface functionalazations. The exceptional physical, mechanical,and electronic properties of CNTs allow them to be used in sensors, quantum dots, actuators, nanoelectronic devices, and drug delivery systems within biomedical applications. With the increasing interest shown by the nanotechnology research community in this field, it is expected that plenty of applications of CNTs will be explored in future. At the same time, it is believed that the continued development and application of CNTs can enhance the practice of biomedical industries.

REFERENCES

1. A. Vaseashta,"Carbon Nanotubes Based Devices And Sensors", Materials And Manufacturing Processes, 2006 Vol 21, 710-716

2. Yograj Singh Duksh, Brajesh Kumar Kaushik Performance comparison of carbon nanotube, nickel silicide nanowire and copper VLSI interconnects: Perspectives and challenges ahead", Journal of Engineering, Design and Technology, Vol. 8 Iss: 3, pp.334 – 353.

3. Alberto Bianco,*a Kostas Kostarelos," Biomedical applications of functionalised carbon nanotubes", The Royal Society of Chemistry 2005, Chem. Commun., 2005, 571–577

4. Giorgia Pastorin," Crucial Functionalizations of Carbon Nanotubes for Improved Drug Delivery", Pharmaceutical Research, Vol. 26, No. 4, April 2009.

5. Xiaoming Li,Xi Liu," Biomedical investigation of CNT based coatings", Surface & Coatings Technology 206 (2011) 759–766.

6. Gianni Ciofani," Realization, characterization and functionalization of lipidic wrapped carbon Nanotubes", J Nanopart Res (2009) 11:477–484

7. Shelley A. Dougherty ,Jianyu Liang "Template-assisted fabrication of protein nanocapsules", J Nanopart Res (2009) 11:385–394.

8. Kannan Balasubramanian," Biosensors based on carbon nanotubes", Anal Bioanal Chem (2006) 385: 452–468.

9. Li G, Liao JM, Hu GQ, Ma NZ, Wu PJ (2005) Biosensors and Bioelectron 20:2140–2144.

10. Wuxu Zhang1, Zhenzhong Zhang," The application of carbon nanotubes in target drug delivery systems for cancer therapies", Nanoscale Research Letters 2011, 6:555.

11. Liu Z, Sun X, Nakayama-Ratchford N, et al. Supramolecular chemistry on water-soluble carbon nanotubes for drug loading and delivery. ACS Nano, 2007, 1: 50–56

12. Liu Z, Chen K, Davis C, et al. Drug delivery with carbon nanotubes for i*n vivo* cancer treatment. Cancer Res, 2008, 68: 6

Effect of Nickel (Ni) underlayer on the field emission from carbon nanotubes

Kulwinder Kaur

Department of Physics, Lovely Professional University, India

***Abstract*- Carbon Nanotubes were synthesized by Microwave plasma enhanced chemical vapour deposition (MPECVD) system. The CNTs were deposited on p-Si (100) wafer. The catalyst used for the growth of CNTs was Iron (Fe). A thin film (10 nm) of catalyst was coated on the Si substrate by thermal evaporation method. The introduction of Ni metal underlayer, which itself is a good catalyst for CNT growth, beneath the catalyst layer was carried out to study the structure and field emission properties of CNT films deposited on these substrates. The precursor gases used for the synthesis of CNTs were C_2H_2 and H_2. Use of Ni underlayer was observed to improve the emission from CNT films as lower turn-on fields were observed for samples with Ni underlayer.**

***Keywords*— Carbon nanotubes (CNTs), Field emission, Microwave plasma enhance chemical vapour deposition (MPECVD), Underlayer.**

I INTRODUCTION

Carbon nanotubes have a long list of outstanding properties depending on their bonding and structure. The physical properties of nanotubes make them potentially useful in Nano metric scale electronic and mechanical applications because of their unusual strength, unique electrical properties and extremely high thermal conductivity. Carbon nanotubes are one of the best known field emitters. This is understandable due to their high electrical conductivity, and the unbeatable sharpness of their tip. Because, the sharper the tip, the more concentrated will be an electric field on the tip, leading to enhanced field emission. The sharpness of the tip also means that they emit at especially low voltage, which is an important fact for building electrical devices, these include field emission displays (FEDs) [1], field emission x-ray tubes [7], plasma ignition [8] and lighting [9].An immediate application of this behaviour receiving considerable interest is in field-emission flat-panel displays. Instead of a single electron gun, as in a traditional cathode ray tube display, here there is a separate electron gun (or many) for each pixel in the display. The high current density, low turn-on and operating voltage, steady and long-lived behaviour make carbon nanotubes excellent field emitters to enable this application [1].Carbon nanotubes are generally produced by three main techniques, arc discharge, laser ablation and chemical vapour deposition. The basic requirements for the formation of CNTs are an active catalyst, a source of carbon and an adequate energy. Chemical vapour deposition (CVD) synthesis is achieved by putting a carbon source in the gas phase and using an energy source, such as plasma or aresistively heated coil, to transfer energy to a gaseous carbon molecule.

II EXPERIENTAL SETUP

Microwave plasma enhanced chemical vapour deposition technique (MPECVD) has been used to synthesize CNTs in the work reported here. MPECVD falls under the category of (Plasma enhanced chemical vapour deposition), which is a low temperature technique for synthesis of MWNTs. Plasma is formed by microwave discharge which is directly coupled to the microwave source through suitable wave guides. Microwave frequency of 2.45 GHz is applied between the source and the reaction chamber (quartz tube). The reaction chamber consists of a quartz tube of diameter 45m, inserted vertically into an aluminium cylinder and the upper end of the chamber is closed through aluminium coupler. Coupler is connected to a port for precursor's gases, through MFC (Mass flow controller; model 247 C MKS Instruments Inc.USA). Inside the reaction chamber there is a holder for keeping the substrate which lies exactly in path of the waveguide. No external heating source is used in this setup to heat the substrate. The required substrate temperature is achieved with help of plasma species which are continuously colliding with the substrate surface. The bottom of the chamber is connected to a two stage rotary pump (model 2020A, Alcatel, France). A pirani gauge is used for measuring the pressure in the reaction chamber. There is a small window provided to view the plasma. Water is circulated around the reaction chamber through copper pipes for cooling.

III EXPERIMENTAL DETAILS

Experiments with metal alloys such as FeNi, NiCo, CoMo, and FeMo have been empirically observed to produce higher growth rates and lower growth temperatures. The unique catalytic properties of bimetallic nanoparticles may be a result of the role, different metals play during critical steps in CNT growth. Therefore, dimensional and compositional tuning of catalyst nanoparticles is critical to precise control of CNT growth [2]. It is interesting to see the effect of Ni as an underlayer on the growth of CNTs, since Ni itself is a good catalyst. Ni forms alloy with Fe which increases the number of reactive sites due to clustering of bimetallic nanoparticles. So, the present work is done to study the effect of Fe and Ni combination on CNT growth and further on its field emission characteristics. Ni underlayer was deposited on a clean Si substrate of different thickness by thermal evaporation. Fe film of thickness 10 nm was deposited

over the Ni underlayer, by thermal evaporation system. Fe film of thickness 10 nm was also deposited without Ni underlayer.

After evacuating the chamber to a base pressure of 2 × 10^{-2} torr with a rotary pump, Argon was purged into the chamber and total pressure of 1 torr was maintained. Pre-treatment of Fe catalyst was done in the presence of argon plasma for 10 minutes at a pressure of (2.3 torr). After that, hydrogen was introduced into the chamber and heat treatment was done in the presence of argon and hydrogen plasma for 5 minutes.It is reported that any kind of metal can support the core according to its affinity for carbon atoms. Therefore, the Fe-Ni catalyst can support the carbon in different manners on the iron-or nickel-containing areas. This can result in different diameter distributions [6].

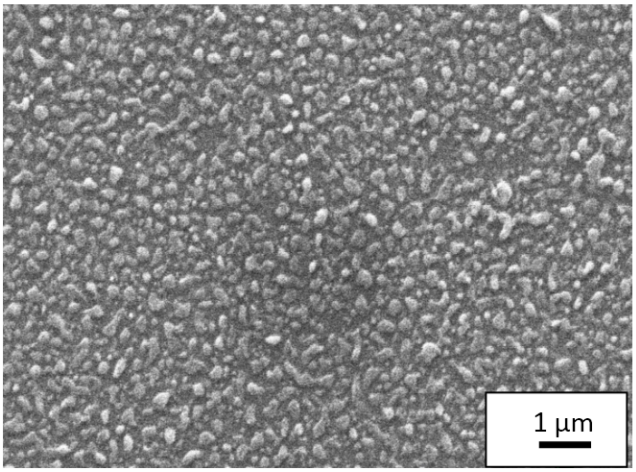

Fig. 1 SEM micrograph of sample Fe-Ni (3).

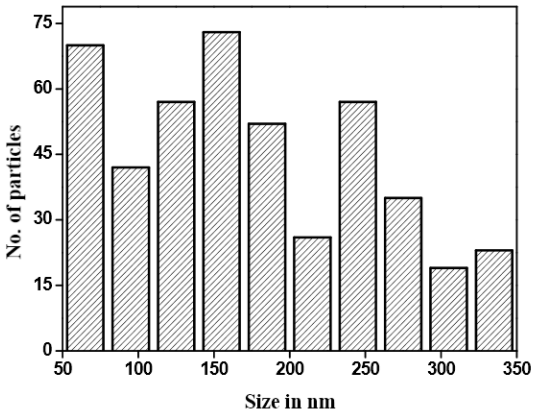

Fig. 2 Particle size distribution of Fe-Ni (3) nanoparticles

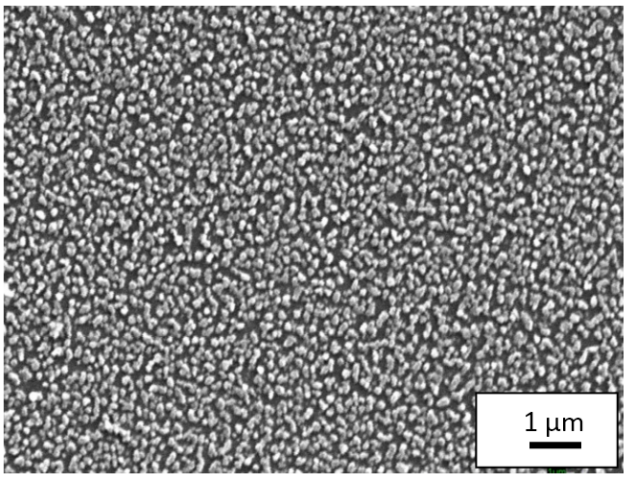

Fig. 3 SEM micrograph showing Fe film transformed into nanoparticles after heat treatment

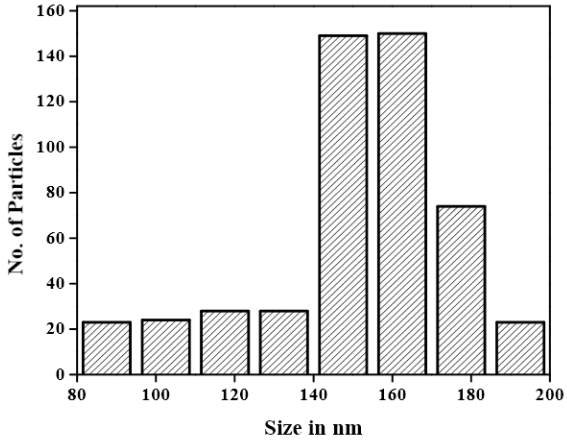

Fig. 4 Particle size distribution of Fe nanoparticles.

CNTs were grown using MPECVD on both type of samples Fe samples and Fe-Ni samples. Various samples were deposited at different deposition times. Sample preparation details are mentioned in table I and table II.

Sample	Gas flow ratios	Deposition time (sec)
Fe-2	15 : 75	90
Fe-3	15 : 75	60

Table I Details of sample prepared using Ni underlayer

Sample	Fe / Ni thickness (nm)	Gas flow ratios $C_2H_2 : H_2$ (sccm)	Deposition time (sec)
Fe-Ni (1)	10 / 10	15 : 80	90
Fe-Ni (3)	10 / 5	15 : 75	95
Fe-Ni (6)	10 / 15	15 : 75	95

Table II Details of sample prepared using Ni underlayer

It can be seen from fig. 1 and fig. 3 that the particle size varies in the range 80 – 300 nm, with maximum particles of size 150 – 200 nm for Fe-Ni sample. Large size particles are speculated to be of Fe-Ni alloy whereas particle size is small in Fe sample.

IV CHARACTERIZATION RESULTS

Glancing angle X-ray diffraction (GA XRD) pattern of one of the Fe-Ni samples indicates the presence of Fe-Ni alloys. The peaks at 43.7^0 and 52.3^0 are due to (111) and (200) planes of Fe-Ni.

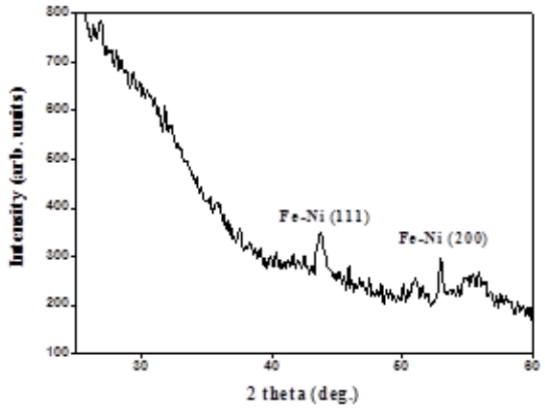

Fig. 5 GAXRD of sample Fe-Ni (1)

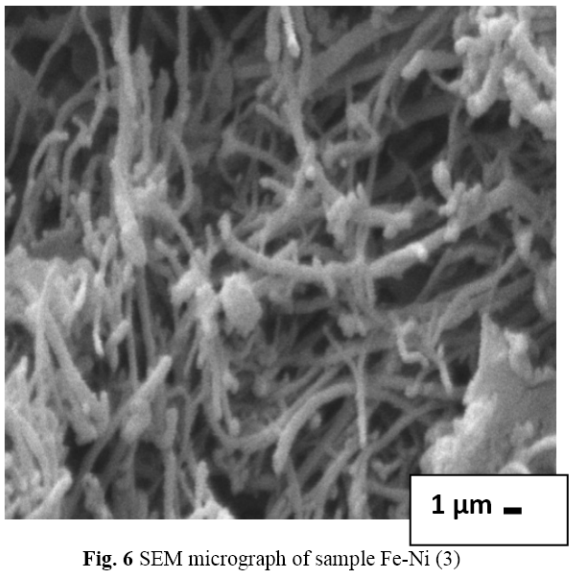

Fig. 6 SEM micrograph of sample Fe-Ni (3)

The SEM micrograph of Fe-Ni (3) and Fe-Ni (6) is shown in fig. 6and fig. 7. From the top view dense growth of CNTs is observed. The cross sectional view of the CNTs of sample Fe-Ni (1) is shown in the fig. 8. We can estimate that CNTs grown are almost vertically aligned. Length of CNTs is estimated from the SEM micrograph of Fe-Ni (1) is to be 3 µm approximately. A dense CNT growth can be seen for Fe (3) sample from fig. 9.

TEM micrograph of sample Fe-Ni (3) is shown in the fig. 10. Compartmental growth is clearly visible from the figure. Outer diameter found out to be Ranging between 50-65 nm, which is larger than in Fe samples. It is due to the larger particle size for Fe-Ni samples than Fe samples.

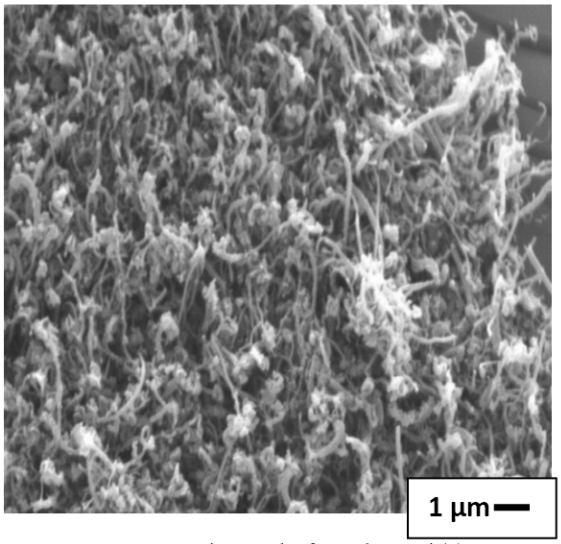

Fig. 7 SEM micrograph of sample Fe-Ni (6)

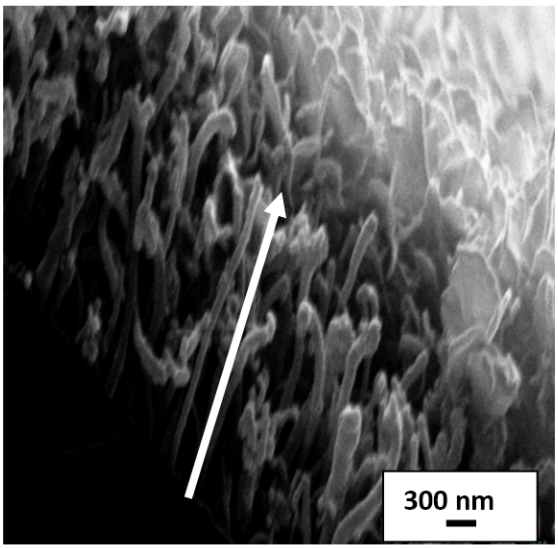

Fig. 8 SEM micrograph of sample Fe-Ni (1)

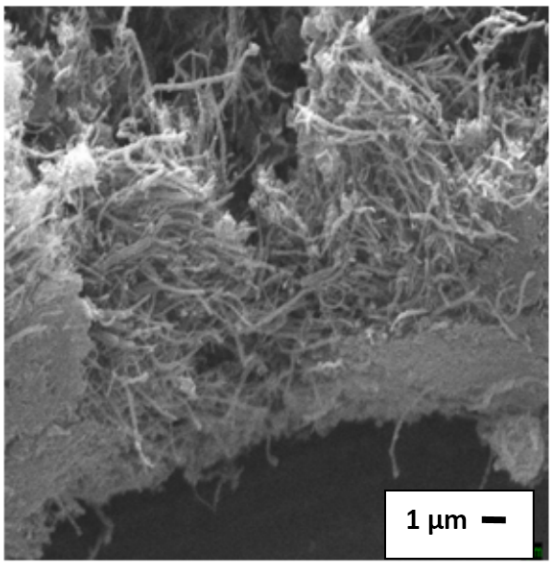

Fig. 9 SEM micrograph of sample Fe-3

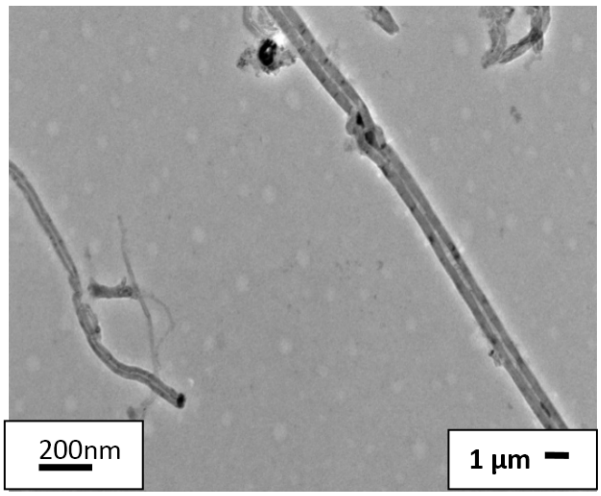

Fig. 10TEM micrograph of sample Fe-Ni (3)

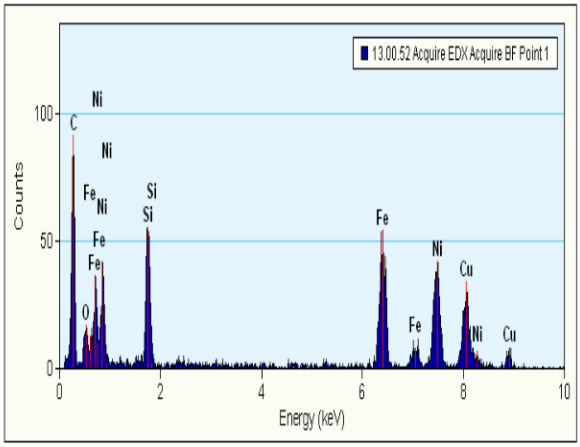

Fig. 11 EDAX of sample Fe-Ni (2)

Energy dispersive x-ray diffraction (EDAX) of sample Fe-Ni (2), which was taken from the tip of the CNT, shows peaks for both Fe and Ni. This indicates the presence of Fe and Ni both in the catalyst particle. Concentration of in at% of one of Fe-Ni sample was estimated from EDAX. It was found from the quantitative EDAX analysis that there was 54 at % of Fe and 45 at% of Ni approx in Fe-Ni samples.

V FIELD EMISSION APPARATUS

Field emission is an alternative way to extract electrons. Because the field emission current is controlled by the applied voltage rather than temperature as in the case of thermionic emission, pulsed emission with variable pulse width and repetition rate can be readily obtained by programming the applied electrical field [3].A simple model (the Fowler-Nordheim model) shows that the dependence of the emitted current on the local electric field and the work function is exponential-like. As a consequence, a small variation of the shape or surrounding of the emitter (geometric field enhancement) and/or the chemical state of the surface has a strong impact on the emitted current. The emission current from a metal surface is determined by the Fowler–Nordheim (F–N) equation:

$$\mathbf{I = aV^2 exp(-b\varphi 3/2/\beta V)} \quad \text{.....(1)}$$

where *I, V, φ, β* are the emission current, applied voltage, work function, and field enhancement factor, respectively. The constant b = 6.83×10^9 (V $eV^{-3/2}$ m^{-1}). For metal, with typical work function and a flat surface the threshold field is typically around 10^4 V/ µm which is impractically high. The work function is a basic material property that cannot be varied significantly. All the field emission sources rely on field enhancement due to sharp tips/protrusions, so they tend to have smaller virtual source sizes because of the primary role of the *β* factor. The larger the *β*, the higher the field concentration and therefore the lower the effective threshold voltage for emission [3].

The field enhancement factor β can be estimated experimentally from the slope of the F-N plot between $\ln(I/V^2)$ versus 1/V. And the value of φ can be taken as 5 eV for carbon film emitters. The slope of F-N plot is

$$(b\varphi^{3/2}\, d)/\beta \quad \text{.....(2)}$$

Field emission studies were carried out on various deposited samples. The system used to study the field emission characteristics is shown in fig. 12. It consists of a cathode and anode assembly. There is a highly polished stainless steel UHV chamber having two ports for the attachment of gauges. There is an additional port for feedthroughs for making electrical connections. A window is provided on the top of the chamber for monitoring. Inside the chamber, there are cathode and anode plates insulated from each other. The movement of the cathode plate is digitally controlled to the accuracy of 5μm, for the adjustment of distance between the cathode and anode. The sample can be mounted on the cathode plate with silver paste. The chamber is connected to the rotary pump (Varian DS 102) to create backing pressure of the order of 10^{-3} torr for turbo molecular pump (TV- 301 Navigator of Varian), which is connected to achieve high vacuum of the order of 2×10^{-6} torr. Pirani and Penning gauges are attached through feedthroughs to measure pressure.

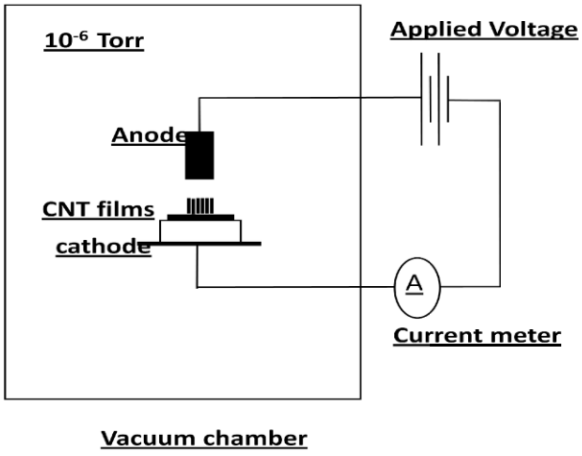

Fig. 12 Schematic diagram of field emission setup

The anode plate is connected to the positive terminal of the high voltage DC power supply unit (model no H5K02N of Aplab of 5 KV rating) through a current meter (Kethely 197 microvolt DMM). A high resistance of 7.7 MΩ is connected in series with the power supply for limiting the current and to avoid accidental damage. The cathode electrode is grounded to the power supply and also grounded to earth through chamber body. It was assembled on the window provided at the top of the chamber. For I-V characteristics, circular polished stainless steel plate having diameter 19 cm was used as an anode.

VI FIELD EMISSION RESULTS

The field emission measurements were carried out using field emission set up, discussed earlier. Samples were attached on the cathode plate by silver paste. The distance between cathode and anode was set to a value of 200μm for all samples, with the help of digital controller. The chamber was evacuated to a vacuum level of 2×10^{-6} torr. A positive voltage varying from 360V up to 3000V was applied to the anode electrode. The actual field applied was found by dividing the voltage applied (drop across 7.7 MΩ resistance was taken into account) by the distance between the cathode and anode. The current density versus electric field was plotted for the samples from which turn on field was measured for the current density of 100 μA/cm^2. The field enhancement factor was calculated from the slope of F-N plot of the samples. It is observed from the field emission results shown in fig. 13, fig. 14 and fig. 15that field emission is better in Fe-Ni samples than Fe sample. J vs. E plot for Fe-Ni samples in Fig. 12 and fig. 13 showing low turn on fields.

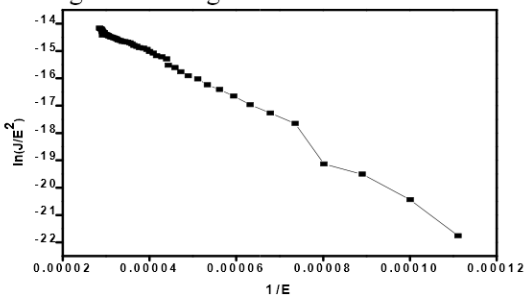

Fig. 13 (a)J vs. E plot of Fe-3

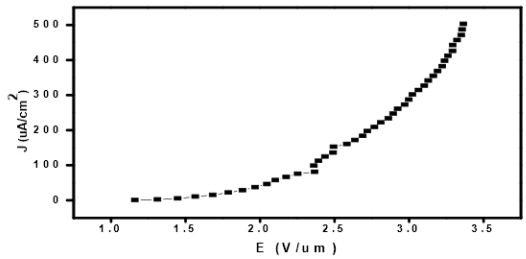

Fig. 13 (b) F-N plot of Fe-(3)

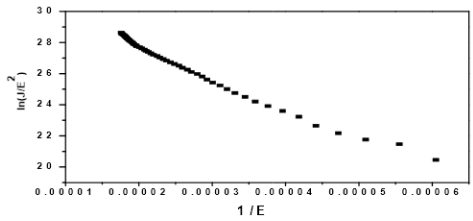

Fig. 14 (a) J vs. E plot of Fe-Ni (3)

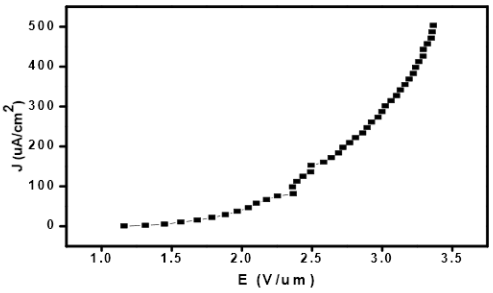

Fig. 14 (b) F-N plot of Fe-Ni (3)

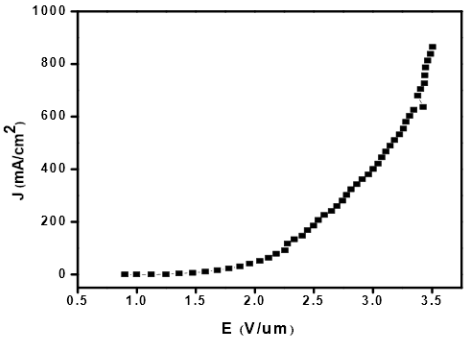

Fig. 15 (a) J vs. E plot of Fe-Ni (6)

Field enhancement factor was calculated for various samples of Fe and Fe-Ni using (2). It is found to have comparatively large values for Fe-Ni sample than Fe sample. This reflects better field emission from CNTs grown on Fe-Ni samples i.e samples where Ni underlayer has been used.

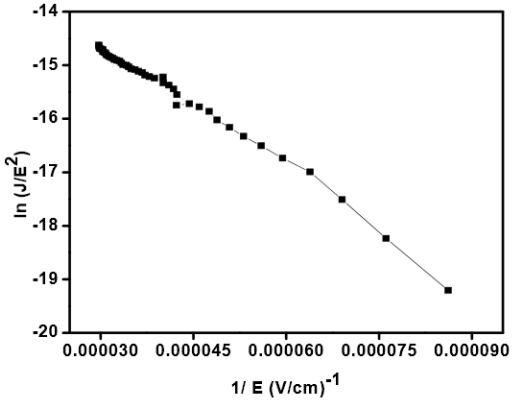

Fig. 15 (b) J vs. E plot of Fe-Ni (6)

DISCUSSION

It can be summarized from the results discussed that carbon nanotubes are excellent field emitters with low turn-on fields. Ni was used as underlayer, which was deposited beneath the Fe layer. Ni itself is a good catalyst for CNT growth. Bimetallic catalysts have stronger catalytic activity as compared to Fe and Ni substrates, reported in literature [2]. Substrates varying Ni thickness from 5 to 15 nm were prepared. X- ray diffraction confirms the formation of FeNi alloy showing peaks for FeNi (111) and (200) planes. Fe and Ni forms alloy which increases the number of reactive sites. It was seen from the nanoparticle size distribution that the nanoparticles of Fe-Ni samples were larger in size than Fe and Ni samples. It was speculated that large size particles are of FeNi alloy. It is due to large size particles, TEM studies revealed the variation in outer diameter of CNTs in Fe-Ni samples than Fe samples. Also, it was estimated that CNT growth was almost aligned in case of Fe-Ni samples.

Sample	Turn on field (V/μm)	Field enhancement factor β
Fe-3	3.31	4838
Fe-Ni (1)	1.97	9092
Fe-Ni (3)	2.25	8123
Fe-Ni (6)	2.36	7713

Table III Turn on field and Enhancement factor for various samoles.

It can be inferred from the field emission results summarized in Table III, that the sample Fe-Ni has minimum turn-on field and larger value of Field enhancement factor. The turn-on field for Fe-Ni (1) was found to be 1.97 V/ μm and field enhancement factor was found to be 9092. It was inferred from the SEM results that Fe-Ni (1) was well aligned CNTs. This is the one reason for its lower turn-on field. This is also the one reason for its better emission than other samples.

VII CONCLUSIONS

- It was found that the particle size distribution for the Fe-Ni samples was larger than others.
- It was observed from the peaks of Fe-Ni alloy in XRD that Fe and Ni has formed alloy.
- Morphology structures showed vertically aligned CNT growth for Fe-Ni samples.
- Diameter of CNTs found to be large in Fe-Ni samples and lie in the range 55-70 nm, attributed to large size nanoparticles of Fe-Ni.

- It was also observed that field emission results of Fe-Ni samples are better than Fe samples. Lower turn on fields has been observed for Fe-Ni samples.

samples. It is reported in literature that for 80-45 at% of Ni in Fe-Ni alloy, the activation energy required for the growth of the CNTs is very less [4]. So, one can study this by varying different at% of Ni and further its effect on field emission properties.

VIII ACKNOWLEDGEMENT

I wish to express my deep sense of gratitude and indebtedness to *Prof. V. D. Vankar*, for his supervision. I would like to thank him for his constant support, encouragement, motivation and guidance throughout this work. My sincere and heart-felt gratitude to my co-guide *Dr.SantanuGhosh*, for the kindness, care, help and support during my project work.I take this opportunity to express my sincere thanks to all the members of *Thin film laboratories IIT Delhi*, for their kind help and cooperation. The help provided by all the people involved in various characterizations done during the project work is also kindly acknowledged.

REFERENCES

[1] N.S. Lee et. al., Application of carbon nanotubes to field emission displays, Diamond and Related Materials 10 (2001) 265-270.

[2] Wei-Hung Chiang and R. Mohan Sankaran, Synergistic Effects in Bimetallic Nanoparticles for Low Temperature Carbon Nanotube Growth, Advanced Materials (2008) 4857-4861.

It was found from the quantitative EDAX analysis that there was 54 at % of Fe and 45 at% of Ni approx in Fe-Ni

[3] Yuan Cheng, Otto Zhou, Electron field emission from carbon nanotubes, C. R. Physique 4 (2003) 1021–1033.

[4] X.H. Chen, S.Q. Feng, Y. Ding, J.C. Ping, Z.Z. Chen, "The formation conditions of carbon nanotubes array based on FeNi alloy island films", Thin Solid Films 339 (1999) 6-9.

[5] S. B. Sinnott and R. Andreys "Carbon Nanotubes: Synthesis, Properties, and Applications". Critical Reviews in Solid State and Materials Sciences36(3): (2001) 145-249.

[6] Shuhei Inoue, Yoshihiro Kikuchi, Yukihiko Matsumura, Effect of catalyst combination on growth of single-walled carbon nanotubes, Diamond & Related Materials 17 (2008) 1888–1890.

[7] G.Z. Yue, Q. Qiu, B. Gao, Y. Cheng, J. Zhang, H. Shimoda, S. Chang, J.P. Lu, O. Zhou, Generation of continuous and pulsed diagnostic imaging x-ray radiation using a carbon-nanotube-based field-emission cathode, Appl. Phys. Lett. 81 (2) (2002) 355.

[8] R. Rosen, W. Simendinger, C. Debbault, H. Shimoda, L. Fleming, B. Stoner, O. Zhou, Application of carbon nanotubes as electrodes ingas discharge tubes, Appl. Phys. Lett. 76 (13) (2000) 1197–1199.

[9] J.M. Bonard, T. Stockli, O. Noury, A. Catelain, Field emission from cylindrical carbon nanotube cathodes: possibilities for luminescenttubes, Appl. Phys. Lett. 78 (18) (2001) 2775.

Stability of Non Edible Oil for Biodiesel Production –A Review

Gaurav Dwivedi[a], M.P. Sharma[a]
[a]*Research Scholar, Bio fuel Research Laboratory, Alternate Hydro Energy Centre, Indian Institute of Technology Roorkee, Roorkee, Uttarakhand- 247667, India, Tel.: +91 8126141004,*
[a]*Associate Professor, Alternate Hydro Energy Centre, Indian Institute of Technology Roorkee, Roorkee ,Uttarakhand-247667, India*
[*] *Corresponding Author E-mail: gdiitr2005@gmail.com*

Abstract: **The fossil fuels are depleting day by day, there is a need to find out an alternative fuel to full fill the energy demand of the world. The various oil sources are classified as edible and non edible the edible sources like groundnut, peanut etc are primarily used to meet the food requirement and the balance if any converted to biodiesel. But India is already importing 70% of the total edible oil and therefore diversion of edible oil resources for biodiesel production is not possible. The option remaining includes the growing of non edible seed crop for oil production and conversion to biodiesel. In India Jatropha and Pongamia being non edible source are being viewed as the only future hope for biodiesel production. Biodiesel is one of the best available sources to full fill the energy demand of the India. The main problem associated with biodiesel is its oxidation stability. The oxidation stability of fats and oil and their product play an important role in determining the quality. It is defined as the resistance of oil/fats/biodiesel to degradation through oxidation with air result in change of fuel quality. The rapidity of oxidation depends on the degree of un saturation, the presence of antioxidants, and prior storage conditions. This auto oxidation caused by contact with air during long term storage presents a legitimate concern for monitoring of oil fuel maturity and effect kinematic viscosity, acid value or peroxide value. The exposure of oil, fats or biodiesel to atmosphere O_2, heat, heavy metal, light, porphyrims etc generate free radicals that form peroxide radicals which subsequently led to the formation of stable secondary products. The product of oxidation stability can be measured by oil stability index or oxidation stability index. This paper focuses on oxidation stability mechanism and its effect in case of non edible oil.**

***Keywords*:** Energy, Oil, Biodiesel, Pongamia, Jatropha, Stability

I. INTRODUCTION

India ranks 6th in terms of consumption of energy, which is 3.5% of the total world's commercial energy. The current consumption of diesel in India is about 40MT (40% of the total petroleum product consumption) and is expected to reach 52MT by 2009-10 as the demand is growing at a rate 6.5% per annum. Whereas domestic production of crude oil and natural gas will remain around 33.97MT during 2009-10. Hence there will be a huge gap between demand and supply which needs to be met through increasing fuel imports or increasing production of biodiesel as substitute of diesel by growing oil seeds especially non edible plantations without sacrificing the food security of the country. Biodiesel is renewable energy resource that can be obtained by using waste and degraded lands. Biodiesel is a fuel comprising of mono-alkyl esters of long chain fatty acids of vegetable oils or animal fats, which is derived either from plant or animal. Use of bio-fuel requires very little or no modification of engine when blended with diesel up to 20% (B_{20}). Use of bio fuel results in substantial reduction of un-burnt HC by 30%, CO by 20% and particulate matters by 25%. It has no sulphur. Besides, it has nearly 10% in-built oxygen, which facilitates the combustion process and enhances Cetane number (51). [1]

II. OIL SEED CROP IN INDIA

The various oil sources are classified as edible and non edible the edible sources like groundnut, peanut etc are primarily used to meet the food requirement and the balance if any converted to biodiesel. Since the country already importing 70% of the total edible oil and therefore diversion of edible oil resources for biodiesel production is not possible. The option remaining includes the growing of non edible seed crop for oil production and conversion to biodiesel. The non edible oil resources are Jatropha, Pongamia, Mahua, Neem etc. Depending on climate and soil conditions, different nations are looking for different vegetable oils as substitute of diesel fuel for example soybean oil in USA, rapeseed and sunflower oils in Europe, palm oil in south East Asia and coconut oil in Philippines are being considered as substitutes for diesel. In India Jatropha and Pongamia being non edible source are being viewed as the only future hope for biodiesel production. Table 1 overviews the non-edible oil producing plants that can be cultivated for oil

production on suitable land and consequently the oil can be used for biodiesel production. [2]

Table: 1 Various Sources of Oil for biodiesel [3]

Vegetable Oil	Non Edible Oil	Animal Fats	Other Sources
Soya Bean	Jatropha Curcas	Lard	Bacteria
Rape seed	Jajoba oil	Tallow	Algae
Canola	Pongamia glabra	Poultry	Fungi
Sunflower	Mahua	Fish Oil	Micro algae
Barley	Tobacco seed		Tarpenes
Coconut	Rice bran		Latexes
Copra	Salmon oil		Cooking oil
Cotton seed	Sesame		Micro algae
Ground nut			
Oat			
Rice			
Sorghum			
wheat			

The non edible oil seed plant given in the above table has potential to produce oil and subsequent conversion to biodiesel apart from their uses for illumination, burning, soap making, candle making etc. It is estimated that the potential availability of such oils in India is about 2 million tons per year. The most abundant oil sources are Sal, Mahua, Neem, Pongamia and Jatropha oil. Based on extensive research, Jatropha and Pongamia have been identified as the potential feed stocks for biodiesel production in India. Table 2 gives the oil productivity of the most important non-edible oils resources in the country.

Table 2: Production of Non-Edible oils in India [4]

S. No.	Botanical Name	Local Name	Annual Productivity (Tons)
1.	Jatropha curcas	Ratanjyot	45,000
2.	Pongamia Pinnata	Karanja	135,000
3.	Schleichera oleosa	Kusum	25,000
4.	Azadirachta indica	Neem	1,00,000
5.	Shorea robusta	Sal	1,80,000
6.	Modhuca indica	Mahua	1,80,000

The above table shows the various sources of biodiesel. But according to Indian perspective Jatropha and Pongamia are the major source of biodiesel in India. Out of these non edible sources the production of pongamia is three times of jatropha oil. This has led to the expatriation of the oil for biodiesel production.

III. PROBLEM OF USING OIL AS FUEL

There are two major problem associated with oil when used in engine i.e. stability and other is cold flow properties. Both these properties are dependent on fatty acid composition of oil. i.e. saturated and unsaturated fatty acids present in oil.

A. Stability of Oil

The fuel stability is usually defined in terms of color, soluble gums and insoluble. Each is an important stability characteristic. The color is normally a predecessor of sediments. The fuel forming color does not necessarily develop gum and sediment which are predominant stability concern. The biodiesel and its blends have been found to be more prone to oxidation than the straight vegetable oils (SVO). The biodiesel & its blends can develop wide variety of alcohols, aldehydes, peroxide and other insoluble formed during its transport and long term storage and can cause acidity in the fuel and form insoluble gums and sediments that result in operational problems with plugging of fuel filter and fouling can and affect the engine operation. In view of the above problem it becomes necessary to study the oxidation, thermal and storage stability of biodiesel and its blends with diesel. The oxidation stability can be studied to establish relationship between induction period and other quality parameters. The storage stability studies require the study of the effect of storage conditions like temp., light, atmosphere, presence of natural antioxidants, metals etc on the stability of biodiesel / fuels. Thermal stability is concerned with the effect of temperature on the natural oxidation stability of fuel and the effect of adding natural synthetic antioxidants to stabilize the fuels that can be used over long period of time without any problems. In order to ensure stable biodiesel quality over long period, there is a need to enhance the oxidation, storage & thermal stability of biodiesel & its blends using various natural / synthetic antioxidants under different parameters like light, temp. metals etc. [5]

Fuel stability is the resistance of a fuel to degradation processes that can change fuel properties and form undesirable species. A fuel is considered unstable when it readily undergoes these changes. The fatty acid composition of the biodiesel fuel is an important factor in determining stability towards air. Generally, the polyunsaturated fatty acids (C18:2, linoleic acid; C18:3 linolenic acid) are most susceptible to oxidation. [6] Oil

fuel properties can degrade by one or more of the following mechanisms: (i) oxidation or autoxidation from contact with oxygen present in ambient air; (ii) thermal or thermal-oxidative decomposition from excess heat; (iii) hydrolysis from contact with water or moisture in tanks and fuel lines; or (iv) microbial contamination from migration of dust particles or water droplets containing bacteria or fungi into the fuel. [7].

Oxidation stability is more general and is distinguished from the term "storage stability" since oxidation may occur not only during storage but also during production and use.

Sarain et al. [8] states that the protection of oil quality, which remains suitable to consumers for longer time, is an important objective of quality control in the oil and fat industry. Shelf life of vegetable oils is the main characteristic that influences its suitability and market value. The consequence of lipid oxidation leads to decrease in shelf life and has been recognized as the big problem in the food industry. Oxidative stability is one of the most important indications for maintaining the quality of the vegetable oils

Tan et al. [9] state that oxidative stability is one of the most important indicators for maintaining the quality of edible oils. It has been shown that oxidation of edible oils takes place through a chain reaction that essentially consists of an induction stage. The time before a dramatic increase in the rate of lipid oxidation is a measure of oxidative stability and is referred to as the induction time. Jain and Sharma [10] states that there are various types of stabilities like oxidation, storage and thermal, playing key roles in making the fuel unstable

All fats and oils are prone to oxidation. The rapidity of oxidation depends on the degree of un saturation, the presence of antioxidants, and prior storage conditions. [11]

B. Measurement of Oxidation

During the measurement a stream of air is passed through the oil or fat sample contained in a sealed and heated reaction vessel. Oxidation of the oil or fat molecules in the sample results in the formation of peroxides as the primary oxidation products. Secondary oxidation products formed after the complete destruction of the fatty acids include low-molecular organic acids. These are transported in the stream of air to a second vessel containing distilled water whose conductivity is continuously recorded. The organic acids can be detected by the increase in conductivity. The time that elapses until these secondary reaction products appear is known as the induction time, induction period or Oil Stability Index (OSI). [8]

Shabuddin et al. [12] states that difference in oxidation stability is due to the difference are due to the various percentages of saturated fatty acid in the biodiesels. If water is present, hydrolysis can also occur. Hydroperoxides that can, in turn, produce short chain fatty acids, aldehydes, and ketones. Under the right conditions, the hydroperoxides can also polymerize. Therefore, oxidation is usually denoted by an increase in the acid value and viscosity of the fuel.

Agarwal et al. [11] State that Oxidation of the esters during the long-term storage can lead to problems in the utilization of biodiesel in the engine and can lead to rough engine operation. Contact with ambient air, exposure to sunlight, metals, and exposure to high temperature conditions accelerate the oxidation reactions leading to lower oxidation stability of biodiesel. Sarin et al. [8] state that it is not is possible to use biodiesel as a fuel having low OS.

C. Mechanism of Oxidation

The oxidation of fatty acid chain is a complex process proceeded by a variety of mechanisms. The oxidation of biodiesel is due to the unsaturation in fatty acid chain and presence of double bond in the molecule which offers high level of reactivity with O_2, especially, when it is placed in contact with air/ water. The primary oxidation products of double bonds are unstable allylic hydroperoxides which are unstable and easily form a variety of secondary oxidation products. This includes the rearrangement of product of similar molecular weights to give short chain aldehydes, acids compounds and high molecular weight materials The oxidation reactivity is related to the degree of C=C bonds in the fuel. Increased content of the C=C bonds correlates to decreased oxidative stability of the fuel. The increase in instability of a given diesel fuel molecule is generally directly proportional to the number of C=C bonds in the molecule (i.e., a molecule containing two C=C bonds has half the stability of a molecule containing one C=C bond). [13,14]

D. Primary oxidation

Peroxidation occurs by a set of reactions categorized as initiation, propagation, and termination as given in Fig 1 which shows that first set involves the removal of hydrogen from a carbon atom to produce a carbon free radical. If diatomic oxygen is present, the subsequent reaction to form a peroxy radical becomes extremely fast even not to allow significant alternatives for the carbon-based free radical. The peroxy free radical is not reactive compared to carbon free radical, but is sufficiently reactive to quickly axtract hydrogen from a carbon to form another carbon radical and a hydroperoxide (ROOH). The new carbon free radical can then react with diatomic oxygen to continue the propagation cycle. This chain reaction terminates when two free radicals react with each other to yield stable products.

Initiation:
RH + I » R· + IH
Propagation:
R· + O_2 » ROO·
ROO· + RH » ROOH + R·
Termination:
R· + R· » R-R
ROO· + ROO· » Stable Products

Fig.1 Primary Oxidation

E. Secondary oxidation.

Once the fatty oil hydroperoxides are formed, they ultimately decompose to form aldehydes such as hexenals , heptenals, and propanal. Hexanal, pentane, and 2,4-heptadienal have also been detected. Increased acidity is always a result of oxidation of fatty oils and biodiesel leading to the formation of shorter chain fatty acids [10]

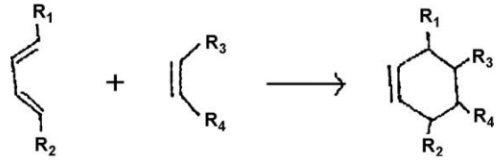

Fig. 2. Diels Alder reaction.

F. Oxidation Stability Index/Oil Stability Index

All oils and fats have a resistance to oxidation which depends on the degree of saturation, natural or added antioxidants, pro oxidants or prior abuse. Oxidation is slow until this resistance is overcome, at which point oxidation accelerates and becomes very rapid. The length of time before this rapid acceleration of oxidation is the measure of the resistance to oxidation and is commonly referred to as the 'induction period, or Oxidative Stability Index. [10] OSI is defined as the hours required for the rate of conductivity change to research a predetermined value. This method has been collaboratively studied and accepted by American Oil Chemists Society, and deter mines the relative resistance of oil/fats samples to oxidation and replaces the out dated AOM. These measurements of stability are available which do take into account double bond position and is termed Oil Stability Index. The OSI analysis, the rate of oxidation is slow until any resistance to oxidation is overcome. This time is known as the oxidation induction period. After the induction period, the rate of oxidation increases dramatically. [15] The BAPE and OSI of SVOs based on the data of table 3 has been calculated using the following equation [10]

BAPE = % C 18:2 + (2× % C 18:3)
(Equation 1)
OSI = 3.91 – (0.045 × BAPE)
(Equation 2)

Table. 3 BAPE and OSI value of various edible and non edible oil [16]

Oil	% C18:1	% C18:2	% C18:3	BAPE	OSI
Sunflower Oil	17.7	72.9	-	72.9	.62
Soybean Oil	23.2	56.2	4.3	64.8	.99
Cotton seed Oil	13	58	0	58	1.30
Rapeseed Oil	64.1	22.3	8.2	38.7	2.20
Peanut Oil	48	32	1	34	2.38
Seasame Oil	52.8	30.2	-	30.2	2.55
Jatropha Oil	35.8	28.8	0.2	29.2	2.59
Pongamia Oil	51.59	16.64	-	16.64	3.16
Palm Oil	40.5	10.2	0.2	10.6	3.43
Corn Oil	25	6	-	6	3.64
Coconut Oil	5	1	-	1	3.865

The variation of BAPE with OSI for various oil is given in table 3 which shows that oxidation stability of oil is dependent on the amount of fatty acids present in the oil. The BAPE for sunflower oil is max of all the other oil which shows that it is highly unstable while the BAPE value for coconut oil is lowest which shows that it is highly stable. The variation of BAPE with OSI is given in fig. 3.

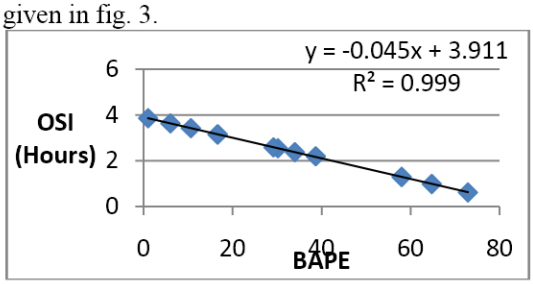

Fig. 3 OSI vs. BAPE

The above figure shows the variation of OSI with BAPE for various oil. It shows that as the BAPE increases the stability of oil going to decrease.

IV. CONCLUSION

The performance of oil as fuel is dependent on the amount of fatty acids presents in the oil. The variation of fatty acids gives the direction for oxidation stability of oil. In case of edible oil the OSI is lowest for sunflower oil which shows that it is highly unstable while the OSI value for coconut oil is maximum which shows that it is highly stable. In case of non edible oil

Pongamia oil have high OSI than Jatropha oil. So Pongamia oil can be used for biodiesel production.

REFFERENCES

[1] TERI (2011) Energy Data Directory and Yearbook

[2] Dwivedi,G. Sharma,M.P. and Siddarth Jain, (2011) Pongamia as a source of Biodiesel in India-A review, Smart grid and Renewable Energy, 2(3), pp.184-189

[3] Singh,S.P., Singh,D., (2010) Biodiesel production through the use of different sources and characterization of oils and their esters as the substitute of diesel: A review, Renewable and Sustainable Energy Reviews,14, pp.200-216

[4] Jain,S. and Sharma,M.P. (2010) Prospects of biodiesel from Jatropha in India: A review," Renewable and Sustainable Energy Reviews,14, pp. 763–771

[5] No, S.Y. (2011) Inedible vegetable oils and their derivatives for alternative diesel fuels in CI engines: A review, Renewable and Sustainable Energy Reviews, 15, pp. 131-149

[6] Mejia,J.D., Salgado,N.,and Orrego,C.E. (2013) Effect of blends of Diesel and Palm-Castor biodiesels on viscosity, cloud point and flash point, Industrial Crops and Products, 43, pp.791-797

[7] Neff, W.E. Selke, E. Mounts, T.L. Rinsch, E.N. and Zeitoun MAM. (1992) Effect of triacylglycerol composition and structures on oxidative stability of oils from selected soybean germplasm, Journal of the American Oil Chemists Society, 69(2), pp.111–118.

[8] Sarin, A. Arora, R. and Singh, N.P. (2010) Blends of biodiesels synthesized from non-edible and edible oils: Influence on the OS (oxidation stability), Energy, 35, pp.3449-3453

[9] Tan, P.C. and Man, C.B.Y. (2002) Comparative studies of oxidative stability of edible oils by differential scanning calorimetry and oxidative stability index methods, Food Chemistry, 76, pp.385–389

[10] Sharma,M.P. and Siddarth Jain, (2010), Stability of biodiesel and its blends: A review, Renewable and Sustainable Energy Reviews,14, pp. 667-678

[11] Agarwal, A.K. and Khurana, D. (2013) Long-term storage oxidation stability of Karanja biodiesel with the use of antioxidants, Fuel Processing Technology, 106, pp.447–452

[12] Shahabuddin,M. Kalam, A.M. Masjuki, H.H. and Bhuiya, K.M.M. (2012) An experimental investigation into biodiesel stability by means of oxidation and property determination, Energy, 44, pp.616-622

[13] Evangelos, G.G. (2013) A statistical investigation of biodiesel physical and chemical properties, and their correlation with the degree of unsaturation, Renewable Energy, 50, pp. 858-878

[14] Freire, L. and Santos,L. (2012) Influence of the synthesis process on the properties of flow and oxidative stability of biodiesel from Jatropha curcas biodiesel, Fuel, 94, pp.313-316

[15] Jain, S. and Sharma, M.P.(2010) Review of different test methods for the evaluation of stability of biodiesel, Renewable and Sustainable Energy Reviews, 14, pp. 1937–1947

[16] Kumar,N. Varun, G. and Chauhan,R.S. (2013) Performance and emission characteristics of biodiesel, Renewable and Sustainable Energy Reviews, 21, pp.633–658

CORROSION AUDITING IN OIL & PETROLEUM PRODUCTS TRANSMISSION PIPELINES IN INDIA

R.Bhaskaran[a], Lalit Bhalla[a], Vishal Sarin[a] Sukhpreet Kaur[a]
Afzalur Rahman[a] and Ashish Shukla[a]
[a]*School of Business, Lovely Professional University, India.*

Abstract— Pipelines are invariable used most for transporting oil and petroleum products from one end to another end. Corrosion is one of the major problems in such pipelines. It may be due to internal or external factors. In order to control corrosion and protect these pipelines, each industrial sector has to spend enormous amount. In this paper, an insitu corrosion auditing has been carried out for a 14 km long oil and petroleum products carrier pipeline in India. By using present value method, annual protection cost has been worked out as Rs.71,740. By direct extrapolation of the same to the entire pipelines in India, annual cost of corrosion is worked out Rs.106 million.

Keywords— Corrosion Auditing, Cost of Corrosion, Cathodic Protection, Pipeline Corrosion.

I. INTRODUCTION

IN 1945, Campbell Stirling [1] estimated the annual loss due to corrosion as related to underground pipelines to be US $ 50 million. He further showed through specific case studies that by application of suitable wrapping to the pipelines considerable amount could have been saved. In 1947, Anderson [2] presented a paper entitled "Our Billion – Dollar Side Show" in the annual meeting of NACE held at Chicago. According to Bureau of Standards Circular C-450, the annual cost of pipeline replacement due to corrosion was approximately US $ 200 million per year. Unruh [3] reported that for one oil company, corrosion was costing US $ 1.5 million per year on a large pipeline system prior to installation of sacrificial magnesium anodes. With installation of cathodic protection, the expenditure was drastically reduced. Talley [4] who dealt with control of pipeline corrosion has shown that cathodic protection of pipelines will lead to net annual savings of US $ 1.1 million. Peabody [5] in Chapter 16 of his book "Control of Pipelines Corrosion" published by NACE during 1967 discusses the economics of controlling corrosion of pipelines through cathodic protection by sample comparison between impressed current and sacrificial anode system. He has further shown that if the pipeline suffers leakage due to inadequate maintenance it is confronted with the following indirect losses:

(i) The average cost of making a leak repair on the pipeline understudy
(ii) An average cost for property damages associated with a simple corrosion leak repair.
(iii) The value of product lost through the average corrosion leak.
(iv) Miscellaneous costs, such as insurance, good will etc.,

During 1991-2001, Corrosion Control Technologies Laboratories (CCTL) Inc., conducted the systematic study in a cooperative agreement with the Federal Highway Administration (FHWA) and NACE International [6]. In this study, the total direct cost of corrosion for Gas and Liquid Transmission Pipelines was estimated to US $ 7 billion. In 2004, US Department of Transportation presented a detailed report [7] on cost of repairs to USA onshore pipelines. In this report, cost of repairs (non-leaking) to gas pipeline shown as US $ 20,000 – 40,000 million. Repair (leaking) to pipeline was presented as approximately US $ 200,000 – 400,000 million, According to an estimate by speakers at a symposium on the corrosion of buried metals held at London, Dec. 1952 annual cost of replacing corroded underground pipelines in Britain was of the order of £ 130 million [8]. According to an article on "the cost of corrosion" published in the Corrosion Prevention & Control [9] the annual cost of corrosion in the UK was £ 200 million during 1954. Out of these at least £ 5 million was spent towards replacement of corroded buried pipelines. In Japan, Michio Tanaka [10] during 1956 made an estimate of corrosion losses to underground cables and pipelines based on the number of failures per year caused by chemical and electrolytic corrosion, annual expenditure necessary for replacements and repairs, average repair expenditure per failure etc., The annual loss was shown as 74 billion yen.

In India, pipelines are invariably used for transporting oil and gas from one place to another place. It is a part of oil and gas industry. During 2013, the total net work of crude oil, petroleum product and LPG pipeline in India was 23,067 km. Out of this, crude oil pipeline network was 9,537 km, petroleum product pipeline network was 11,218 km and LPG pipeline network was 2,312 km [11].

Corrosion is one of the major problems in underground pipelines. It may occur either internally or externally. Internal corrosion is depending upon the nature of corrosive liquid transported through pipeline along with its transport velocity. External corrosion is due to heterogeneous nature of soils and local damage of the external coatings on the pipelines. Every year, this

industrial sector has spent huge amount of money to protect their structures. Therefore it would be of interest to carry out a systematic corrosion auditing in oil and gas transmission pipelines by collecting and analyzing data on the money spent towards control corrosion. The present value method has been adopted for estimating the cost of corrosion.

II SURVEY DETAILS

A survey was carried out on a 14 km long pipeline route of a major oil company (M/s. Indian Oil Corporation Limited), Chennai. Field data collected on carrier pipelines under road crossings has been taken for this study. There are 7 different sizes of pipelines carrying different products. These are running between Chennai Petrochemical Corporation Limited (CPCL) and Fore-Shore Terminal (FST) at Chennai Port Trust, Chennai. The details of the pipelines are as follows:

1. 0.508m dia pipeline carrying white oil
2. 0.356m dia pipeline carrying Black oil
3. 0.356m dia pipeline carrying While oil
4. 0.305m dia pipeline carrying Lube oil
5. 0.457m dia pipeline carrying Naptha
6. 0.305m dia pipeline carrying Motor Sprit and
7. 0.254m dia pipeline carrying Aviation Turbine Fuel

These pipelines cross the road at many places between CPCL and FST. The details are shown in Table 1.

Table 1: Details of Pipeline crossings between CPCL and FST

Location	Pipeline diameter (m)	Length of crossings in meter	Type of crossings
Thiruvorttiyur Road Crossings	0.305	20	Hume pipe
	0.457	20	
	0.254	20	
Manali Highway Crossings	0.305	15	Hume pipe
	0.356	15	
	0.356	15	
	0.508	15	
IOCL Inspection Road	0.254	6	Hume pipe
	0.457	6	
	0.305	6	
IOCL Inspection Road (Lube Line Diversion)	0.305	20	Underground
	0.305	8	Culvert
Concrete Pavement Road in front of Tondiarpet Installation (Western Side)	0.508	100	Underground
	0.356	100	
	0.356	100	
	0.305	100	
Tondiarpet Terminal (Southern side) Road Crossings	0.508	15	Underground
	0.356	15	Culvert
	0.356	15	
Eastern side of Tondiarpet terminal	0.457	20	Hume pipe
	0.457	360	Underground
Highway crossing (Opposite to Patel Nagar water distribution station)	0.356	15	Underground
	0.356	15	Hume pipe
Metro water road crossing	0.356	10	Culvert
	0.457	10	
	0.305	10	
Pipeline under culvert (opposite to diesel loco-shed)	0.508	15	Culvert
Diesel loco-shed crossing	0.356	8	Hume pipe
	0.356	8	
	0.457	8	
	0.305	8	
	0.305	8	
Karunanithi Road	0.508	15	Culvert
Highway crossing – near tea godown	0.508	40	Hume pipe
Pipeline under inspection road (Tea Godown)	0.356	10	Underground

	0.356	10	
	0.457	10	
	0.305	10	
	0.305	10	
	0.508	10	
Below Tondiarpet Railway bridge	0.356	120	Underground
	0.356	120	
	0.457	120	
	0.508	120	
	0.305	120	
KOKG Yard Crossings – 1	0.356	15	Culvert
	0.356	15	
KOKG Yard Crossings – 2	0.457	6	Culvert
	0.508	6	
	0.305	6	
KOKG Yard Crossings – 3	0.457	10	Underground
	0.508	10	
	0.305	10	
Total length of the pipeline in meter		**1899**	

SELECTION OF PROTECTION SYSTEM

Out of 14 km network length of pipelines, only 1.9 km length of pipelines are crossing the road at different places through underground, culvert and hume pipe. Due to environment differential, external corrosion will occur at those places. Therefore those portions are needed to be protected. Cathodic protection along with protective coatings is the best method for protecting those structures. However, application of protective coating is not possible since the pipelines are already laid in the soil. Cathodic protection is an alternative method of protection. In cathodic protection, impressed current system is likely to generate fire hazard. In order to avoid such a hazard, sacrificial system has been selected for protecting those structures. Details of suggested sacrificial system are as follows:

- Zinc strip anodes for the carrier pipelines encased in the hume pipe as well as culvert
- Magnesium alloy anodes for the underground portion of the carrier pipelines.

a. Calculation of cost of Cathodic protection system for the carrier pipelines encased in hume pipes as well as culvert.

Design parameters

Current density = $10mA/m^2$
Design life = 20 years
Coating efficiency = 50% (assumed)
Type of anode = Zinc Stripe Anode
Anode capacity = 770 AH/kg
Anode Utilization Factor = 0.8
Size of the anode = 45 mm x 45mm x 1500mm with 1 Mtr. Long of 16 sq.mm copper
Weight of anode =22 kg.

Cost Details

The supply cost per Zinc stripe anode is Rs. 12,000/- and the installation cost per anode is Rs.8,000/-. Pipe to cable connection by EUTECTIC WELD with epoxy encapsulation for cathode connection is Rs. 8,500 per location and Earth work excavation for cable laying at a depth of 1.5 Mtr. Below the ground level is Rs.275/- per running meter.

Calculation for determination of weight and size of Zinc Strip Anode

Methodology involved for determination of weight of Zinc Strip anode required for protecting the carrier pipelines encased in hume pipe as well as culvert is shown in Table 2

No. of Zinc Strip anode required = 43
Total number of locations = 14
Total length of crossings (meter) = 399

Therefore total cost of Anode required for protection = (No. of anode required x Supply cost of anode + Installation cost of anode)

43 x (Rs.12,000 + 8,000) = 8,60,000

Pipe to cable connection for all the locations
(14 x Rs.8,500) = 1,19,000

Earthwork excavation for cable laying
(399 x Rs.250) = 99,750

Total cost of Zinc strip Anode for 20 years= **10,78,750**

b. Calculation of cost of Cathodic protection system for the carrier pipelines under road crossings.

Design parameters

Current density	=	$10mA/m^2$
Design life	=	20 years
Coating efficiency	=	50% (assumed)
Type of anode	=	Magnesium alloy anode
Anode capacity	=	1100 AH/kg
Anode Utilization Factor	=	0.8
Size of the anode	=	125mm dia x 1500 mm long
Weight of anode	=	22 kg.

Cost Details

The supply cost per magnesium alloy anode is Rs. 18,000/- and the installation cost per anode is Rs.8,000/-. Pipe to cable connection by EUTECTIC WELD with epoxy encapsulation for cathode connection is Rs. 8,500 per location and Earth work excavation for cable laying at a depth of 1.5 Mtr. Below the ground level is Rs.275/- per running meter.

Calculation for determination of weight and size of Magnesium Alloy Anode

Methodology involved for determination of weight of Magnesium Alloy anode required for protecting the carrier pipelines under road crossings is shown in Table 3.

No. of Magnesium Alloy anode required	=	100
Total number of locations	=	4
Total length of crossings (meter)	=	1500

Therefore total cost of Anode required for protection = (No. of anode required x Supply cost of anode + Installation cost of anode)

100 x (Rs.18,000 + Rs,8,000) = 26,00,000

Pipe to cable connection for all the locations
(4 x Rs.8,500) = 34,000

Earthwork excavation for cable laying
(1500 x Rs.250) =
3,75,000

Total cost of
Magnesium Alloy Anode for 20 years = **30,09,000**

Determination of Annual cost of Corrosion

As can be seen from the foregoing that a Oil and Gas Pipeline industry normally spends every year quite a considerable amount towards mitigation of corrosion. Therefore in the present study, the cost of corrosion has been analyzed by considering the following

- As per the Income Tax Act, Oil and Gas Pipeline industry has to pay 35% of the net income as tax (t). This factor has been taken into account while computing the cost of corrosion.
- An interest rate (i) of 6.25% has also been considered

sData generated for cost of corrosion of cathodic protection by zinc strip anode and magnesium anode for the carrier pipelines is shown in Table 4. This table depicts annual expenditure, present worth factor, tax credit, present value, annual cost factor and equivalent annual cost in that order.

Table 2 : Determination of weight of anode required for protecting pipelines encased in hume pipe as well as culvert

Pipeline dia (meter)	Length of crossing (m)	Π	Surface area of the pipeline (m^2) [a x b x c]	Coating Efficiency	Current density (mA/m^2)	Current requirement (mA) (d x e x f)	Hours of protection (Year x day x hours)	Anode capacity x Utilization factor	Weight of anode required (g x h / I)	Weight of Commercial Available anode	No. of anode required
(a)	(b)	(c)	(d)	(e)	(f)	(g)	(h)	(i)	(j)	(k)	(m)
0.305	20	3.14	19.14	0.5	10	95.71	175200	616	27.22	22	2
0.457	20	3.14	28.71	0.5	10	143.56	175200	616	40.83	22	2
0.254	20	3.14	15.95	0.5	10	79.76	175200	616	22.68	22	2
0.305	15	3.14	14.36	0.5	10	71.78	175200	616	20.42	22	1
0.356	15	3.14	16.75	0.5	10	83.74	175200	616	23.82	22	2
0.356	15	3.14	16.75	0.5	10	83.74	175200	616	23.82	22	2
0.508	15	3.14	23.93	0.5	10	119.63	175200	616	34.03	22	2
0.254	6	3.14	4.79	0.5	10	23.93	175200	616	6.81	22	1
0.457	6	3.14	8.61	0.5	10	43.07	175200	616	12.25	22	1
0.305	6	3.14	5.74	0.5	10	28.71	175200	616	8.17	22	1
0.305	8	3.14	7.66	0.5	10	38.28	175200	616	10.89	22	1
0.356	15	3.14	16.75	0.5	10	83.74	175200	616	23.82	22	2
0.356	15	3.14	16.75	0.5	10	83.74	175200	616	23.82	22	2
0.457	20	3.14	14.36	0.5	10	71.78	175200	616	20.42	22	1
0.356	15	3.14	11.17	0.5	10	55.83	175200	616	15.88	22	1
0.356	10	3.14	11.17	0.5	10	55.83	175200	616	15.88	22	1
0.457	10	3.14	11.17	0.5	10	55.83	175200	616	15.88	22	1
0.305	10	3.14	14.36	0.5	10	71.78	175200	616	20.42	22	1
0.508	15	3.14	9.57	0.5	10	47.85	175200	616	13.61	22	1
0.356	8	3.14	9.57	0.5	10	47.85	175200	616	13.61	22	1
0.356	8	3.14	23.93	0.5	10	119.63	175200	616	34.03	22	2
0.457	8	3.14	8.93	0.5	10	44.66	175200	616	12.70	22	1
0.305	8	3.14	8.93	0.5	10	44.66	175200	616	12.70	22	1
0.305	8	3.14	11.48	0.5	10	57.42	175200	616	16.33	22	1
0.508	15	3.14	7.66	0.5	10	38.28	175200	616	10.89	22	1
0.508	40	3.14	7.66	0.5	10	38.28	175200	616	10.89	22	1
0.356	15	3.14	23.93	0.5	10	119.63	175200	616	34.03	22	2
0.356	15	3.14	31.90	0.5	10	159.51	175200	616	45.37	22	3
0.457	6	3.14	11.17	0.5	10	55.83	175200	616	15.88	22	1
0.508	6	3.14	11.17	0.5	10	55.83	175200	616	15.88	22	1
0.305	6	3.14	14.36	0.5	10	71.78	175200	616	20.42	22	1
	399										43

Table 3: Determination of weight of anode required for protecting pipelines buried underground in road crossings

Pipeline dia (meter)	Length of crossing (m)	Π	Surface area of the pipeline (m^2) [a x b x c]	Coating Efficiency	Current density (mA/m^2)	Current requirement (mA) (d x e x f)	Hours of protection (Year x day x hours)	Anode capacity x Utilization factor	Weight of anode required (g x h / I)	Weight of Commercial Available anode	No. of anode required
(a)	(b)	(c)	(d)	(e)	(f)	(g)	(h)	(i)	(j)	(k)	(m)
0.305	20	3.14	19.14	0.5	10	95.71	175200	880	19.05	22	1
0.508	100	3.14	159.51	0.5	10	797.56	175200	880	158.79	22	8
0.356	100	3.14	111.66	0.5	10	558.29	175200	880	111.15	22	6
0.356	100	3.14	111.66	0.5	10	558.29	175200	880	111.15	22	6
0.305	100	3.14	95.71	0.5	10	478.54	175200	880	95.27	22	5
0.508	15	3.14	23.93	0.5	10	119.63	175200	880	23.82	22	2
0.457	360	3.14	516.82	0.5	10	2584.09	175200	880	514.47	22	24
0.356	15	3.14	11.17	0.5	10	55.83	175200	880	11.12	22	1
0.356	10	3.14	31.90	0.5	10	159.51	175200	880	31.76	22	2
0.356	10	3.14	133.99	0.5	10	669.95	175200	880	133.38	22	7
0.457	10	3.14	133.99	0.5	10	669.95	175200	880	133.38	22	7
0.305	10	3.14	172.27	0.5	10	861.36	175200	880	171.49	22	8
0.305	10	3.14	191.41	0.5	10	957.07	175200	880	190.54	22	9
0.508	10	3.14	114.85	0.5	10	574.24	175200	880	114.33	22	6
0.356	120	3.14	14.36	0.5	10	71.78	175200	880	14.29	22	1
0.356	120	3.14	15.95	0.5	10	79.76	175200	880	15.88	22	1
0.457	120	3.14	9.57	0.5	10	47.85	175200	880	9.53	22	1
0.508	120	3.14	9.57	0.5	10	47.85	175200	880	9.53	22	1
0.305	120	3.14	9.57	0.5	10	47.85	175200	880	9.53	22	1
0.457	10	3.14	9.57	0.5	10	47.85	175200	880	9.53	22	1
0.508	10	3.14	9.57	0.5	10	47.85	175200	880	9.53	22	1
0.305	10	3.14	9.57	0.5	10	47.85	175200	880	9.53	22	1
	1500										100

Table 4 : Equivalent annual cost of corrosion for carrier pipelines encased in hume pipe / culvert and buried underground

Expenditure details	**Period of occurrence**	**Amount (Rupees)**	**Present worth factor** $\frac{1}{(1+i)^n}$	**Tax credit** $(1-t)$	**Present value (Amount in Rupees)**	**Annual cost factor** $\frac{i\,x\,(1+i)^n}{(1+i)^n-1}$	**Equivalent annual cost (Amount in Rupees)**
		(A)	**(B)**	**(C)**	**(D) [A X B X C]**	**(E)**	**(F) [D X E]**
Cathodic Protection using Zinc Strip Anode system	Once in 20 years	10,78,750	0.30	0.65	2,10,356	0.09	18,932
Cathodic Protection using Magnesium Alloy Anode system	Once in 20 years	30,09,000	0.30	0.65	5,86,755	0.09	52,808
						Total Equivalent Annual Cost	**71,740**

The annual cost of Cathodic protection for 1.9 km pipelines is estimated as Rs.71,740

Annual Cost of Sacrificial Cathodic Protection System for Carrier Pipeline in India

Assuming that the same environment is prevailing at all places, annual cost of corrosion for entire carrier pipelines in India has been estimated.

During 2012-13, the total network of carrier pipeline (crude oil and Petroleum product) in India was 20,755 km.

Length of pipeline is to be protected

Out of 14 km, only 1.9 km is needed to be protected. A direct extrapolation of the same to the entire pipelines (20,755 km) carrying crude oil and petroleum product in India is worked out

$$\frac{1.9}{14} \times 20{,}755 = 2{,}816.75\ km.$$

Therefore 2,817 km total length of pipeline is needed to be protected

Cost of protection

Annual cost of protection (corrosion cost) for 1.9 km is worked out to Rs.71,740. A direct extrapolation of the same to the pipelines carrying crude oil and petroleum product (2,817 km length) in India is worked out

$$\frac{71{,}740}{1.9} \times 2{,}817 = Rs.\,10{,}63{,}63.989.50$$

Say Rs. 106 million

III. CONCLUSION

Annual cost of corrosion for 1.9 km length of the pipeline carrying crude oil and petroleum product has been estimated as Rs.71,740. By direct extrapolation of the same to the entire pipelines in India, the annual cost of corrosion during the year 2012-13 has been worked out as Rs.106 million.

ACKNOWLEDGMENT

The authors sincerely thanks Mr.Ashok Mittal, Honorable Chancellor, Dr.Sanjay Modi, Dean of Academic Affairs, Dr.Rajesh Verma, Head, School of Business, Mr.Suresh Kashyap, Head, School of Business and other dignitary members at Lovely Professional University, Phagwara, Punjab for their support and advice. The cooperation obtained from Indian Oil Corporation Limited, Chennai is also gratefully acknowledged. The authors thank the faculties and other members in School of Business of Lovely Professional University for their kind encouragement in pursuing this study.

References :

[1] J.Campbell Stirling, "Economics of mitigation of external corrosion on underground pipelines", Corrosion, Vol.1, (No.1), Mar. 1945, p 17-30.

[2] H.H.Anderson, "Our billion-dollar side show .... for managers only", Corrosion, Vol.3, (No.6), June 1947, p 2-6.

[3] E.W.Unruh, The Petro.Eng., Vol.23, (No.8), July 1951, p D-7.

[4] R.K.Talley, "Thirty years of poof corrosion control pays off", Materials Protection, Vol.5, (No.2), Dec. 1965, p 73-75.

[5] A.W.Peabody, Control of pipeline Corrosion, National Association of Corrosion Engineers, Houston, Texas, 1967.

[6] G.HKoch, M.P.H.Brongers, N.G.Thompson, Y.P.Virmani and J.H.Payer, "Corrosion Cost & Preventive Strategies in the United States", FHWA Report No. RD-01-156, 2001.

[7] U.S. Department of Transportation. Docket RSPA-00-7666.356.

[8] "British estimate corrosion loss in U.K. to underground pipe at $ 130,000,000", Corrosion, Vol.8 (No.3), 1952, p.16-17.

[9] "The cost of corrosion", Corrosion Prevention & Control, Vol.1, (No.1), Mar. 1954, p.9.

[10]. M.Tanaka, "An estimate on corrosion losses to underground cables and pipelines in Japan", Corrosion, Vol.12, (No.10), Oct. 1956, p 513t – 514t.

[11] http://www.slideshare.net/IBEFIndia/oil-and-gas-august-2013 dated 26 Sept. 2013.

ENHANCED ANTIOXIDANT ACTIVITY OF GOLD NANOPARTICLES EMBEDED *SOLANUM TUBEROSUM* EXTRACT AND HPTLC QUANTIFICATION

Roopa Rani, Kiran Singh and ManMohan Srivastava
Department of Chemistry, Dayalbagh Educational Institute, Deemed University, Dayalbagh, Agra, India – 282110

***Abstract*– The facile synthesis of stable gold nano particles embeded solanum tuberosum (GNPST) is demonstrated using extract of Solanum Tuberosum. The best parameters for the synthesis were $NaAuCl_4$ salt (0.1M, 2 µL) at room temperature. The results were verified using UV-Vis spectrometry, XRD, AFM and SEM. GNPST were monodispersed and of the size (40 ± 20nm). DPPH and Fenton bioassay indicated that GNPST exhibit 12% enhancement in antioxidant activity. HPTLC detection identified ascorbic acid as major antioxidant compound in the potato extract.**

Keywords: Antioxidants, HPTLC, Gold nanoparticles, *Solanum Tuberosum*.

I. INTRODUCTION

Synthesis of metal nanoparticles using biological systems as an efficient sink has grabbed exceptional attention due to their anomalous optical, chemical, photo electrochemical and electronic properties [1]-[3]. Unlike chemical protocols which demands expensive instruments and results in release of inimical chemicals, biological method is more facile, eco-friendly and results in more mono dispersed nanoparticles. Gold salt when exposed to alcoholic extracts of plant have resulted in the intra cellular as well as extra cellular formation of metal nanoparticles [4]-[7]. The rate of formation fo*D.* nanoparticles and therefore the size of the nanoparticles could, to an extent, be manipulated by controlling parameters such as pH, temperature, substrate concentration and exposure time to substrate [8]-[10]. Plant extracts have been found to play an important role in biosynthesis of gold nanoparticles of pharmaceutical importance [11]-[12].

In the present work, use of methanolic extract of *Solanum tuberosum* is chosen for preparing gold nanoparticles. *Solanum tuberosum* commonly known as potato belong to the family Solanaceae. Potatoes are good sources of antioxidant compounds, including polyphenols, carotenoids and vitamins.

II. EXPERIMENTAL DETAILS

A. Reagents

Solanum tuberosum was procured from market, DPPH (0.3mM in methanol), Methanol, Deoxyribose (3mM), Ferric chloride (0.1mM), Ascorbic acid (0.1Mm), EDTA (0.1mM), H_2O_2 (1mM), Thiobarbituric acid (1% in 100 ml NaOH; 0.05 N), Trichloro acetic acid (5 % in water), Phosphate Buffer Saline (pH 7.4), α-tocopherol (0.1mM) were from Sigma Aldrich Pvt. Ltd, USA.

B. Sample extraction

Potatoes (100g) were crushed in methanol (250ml) and refluxed for 8 hours. The extract obtained was centrifuged at 10,000 rpm for 15 minutes. The supernatant was used as reducing agent for synthesis of gold nanoparticle.

C. Biosynthesis of gold nanoparticles from Solanum tuberosum extract

Doubly ionized water (10ml) was added to *Solanum tuberosum* extract (4ml) and stirred continuously at 25°C for 15 min. The stock solution of $NaAuCl_4$ solution (0.1M, 2 µL) was added to the stirring mixture. The colour of the mixture turned reddish brown from pale yellow, indicating the formation of gold nanoparticles. The gold nanoparticles thus formed were separated from potato extract immediately using filter paper (5micron).

D. Antioxidant determination DPPH assay:

The reaction mixture of dilution series (1-20 mg/ml) of potato extract were incubated with methanolic DPPH (0.03 mM, 1ml). The solution was allowed to stand for 30min at room temperature. Extracts when reacted with DPPH, a stable purple coloured free radical was converted into colourless compound (α-α diphenyl β-picryl hydrazine). The extent of decolouration indicates the amount of DPPH scavenged [13]. The absorbance was measured at 517nm using α-tocopherol as a reference antioxidant. The percent inhibition of DPPH was calculated using the formula: **[(C-T)/C]X100,** where **C** is the absorbance of control and **T** is the test sample

E. Fenton's assay:

The reaction mixture containing different dilution series of potato extract were incubated with deoxyribose, H_2O_2, $FeCl_3$, ethylene diamine tetra acetic acid (EDTA) in phosphate buffer (pH 7.4). The reaction was terminated by thiobarbituric acid (1ml, 1%w/v) and trichloro acetic acid (2% w/v) by boiling in water bath for 15 min. The pink

chromogen was formed resulting in the formation of thiobarbituric acid reactive substance (TBARS); α-tocopherol was used as a reference antioxidant. The percent inhibition of OH° generated was calculated using the same equation mentioned above.

F. Characterization of Biosynthesized Gold nanoparticles

Gold nanoparticles prepared from *Solanum tuberosum* extract was characterized by X-ray diffraction (XRD) analysis, Atomic force microscopy (AFM), Scanning Electron Microscopy, UV- Visible Spectral analysis. X-ray diffractometer (Bruker AXS D8 Advance, Germany) was used to determine the crystallinity and the lattice properties operated at 40KV, current of 30 mA with Cu Kα radiation. Scattered radiation was detected in the range 2Θ = 30°- 80°, at a speed of 2° per min. Atomic force microscope (Nanosurf easy scan Switzerland; Version 1.8) was used for the morphological observation of biosynthesised gold nanoparticles. All scans were performed in air with commercial Si nanoprobe tips. Height and phase images were obtained simultaneously in tapping mode at the fundamental resonance frequency of the cantilever with a scan rate of 0.5–0.8 Hz. The oscillating amplitude was 0.5 V. The morphological characteristics of gold nanoparticles were also evaluated using Table tops SNE-3200M Scanning Electron Microscope at working voltage 30 KV with 700X magnification. UV–Vis spectroscopy (Shimadzu 2450 UV-Vis spectrometer) is also one of the most important techniques to characterise gold nanoparticles. The absorption behaviour arises due to Surface Plasmon Resonance, which originates from coherent oscillation of the electrons in the conduction band of the nanoparticles induced by the electromagnetic field. The SPR band of gold nanoparticles at scanning range between 200-800 nm was observed.

G. HPTLC Estimation of Major antioxidant

HPTLC analysis was performed on a computerized densitometer scanner controlled by Win-CATS planner chromatography manager version 1.4.4. (Camag, Switzerland). Various steps involved in the estimation of major antioxidant of *Solanum tuberosum* (potato) extract were as follows - *Standard preparation:* Stock solution of standard ascorbic acid (1mg/ml) was prepared by dissolving ascorbic acid in methanol, *Loading of the samples:* 20cm x 10cm HPTLC plates coated with silica gel 60 F_{254} (E. Merck, Darmstadt, Germany) were used for analysis. The samples were applied at 10mm from the base of HPTLC plate by means of Camag (Switzerland) Linomat V sample applicator using a syringe (100 µl, Hamilton, Switzerland), *Developments of bands:* Plates were developed in a Camag twin-trough chamber with optimised mobile phase [Ethanol: Acetic acid: Toluene (5.5: 1: 1.5, v/v/v)], *Visualization of bands:* TLC plates were visualized in HPTLC Visualizer at 254 and 366nm, *Qualitative and quantitative assay:* Densitometric scanning of the HPTLC plates was done in HPTLC 3 Camag Scanner at 200nm controlled by WinCATS planar chromatography manager version 1.4.4. (Camag, Switzerland).

III. RESULTS AND DISCUSSION

Synthesis of gold nanoparticles

Desired Gold nanoparticles were synthesized from sodium tetra chloroaurate solution containing Au^{3+} ions by treating with *solanum tuberosum* extract. The colour of the solution changed to reddish brown within 5 min of reaction with the Au^{3+} ions. The appearance of the deep brownish colour indicated formation of gold nanoparticles with size (40 ± 20nm).

Characterization of gold nanoparticles

A. X-ray Diffraction (XRD) of gold nanoparticles

The diffraction peaks at 2θ = 38.15° (1 1 1), 44° (2 0 0), 63.9° (22 0) and 77.25° (3 1 1) obtained [Fig. 1] are identical with those reported for the standard gold metal as per recommended by Joint Committee on Powder Diffraction Standards-JCPDS, USA. The crystallite size was estimated from the full width at half-maximum intensity (FWHM) of the reflection using Scherrer's equations: $B = \sqrt{(FWHM)^2 - (0.045)^2} = x$; $B_{radian} = \frac{x\,\pi}{180} = y$; $t = \frac{K\lambda}{yCos\theta}$; where B is the breadth of the peak of a specific phase (2θ=38.15 in our case), K is a constant that varies with the method of taking breadth (K=0.94), λ is the wavelength of incident X-rays (λ=0.15418nm), θ is the centre angle of the peak, and L is the crystallite length (size). The crystalline size obtained was 32.10nm. The reference crystal size is 40 ± 20nm.

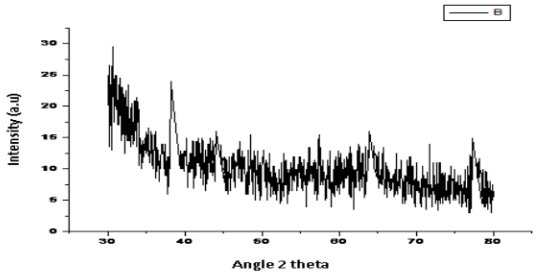

Fig.1 X-RD of gold nanoparticles

B. Atomic Force Microscopy

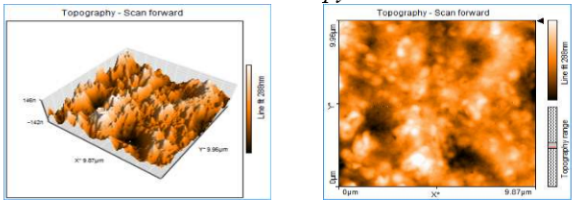

Fig.2 AFM of gold nanoparticles

From the topographical view, it is evident that the most of the nanoparticles are in spherical shape [Fig. 2]. The average roughness of the particles was found to be *13.39 nm*.

C. *SEM of gold nanoparticles*

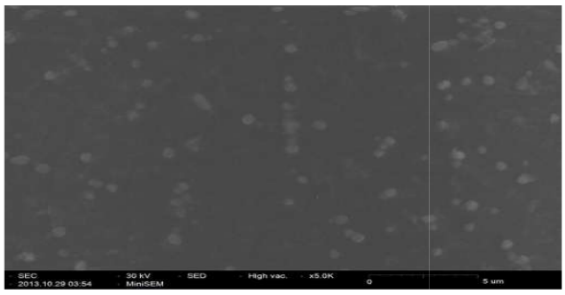

Fig. 3 SEM of gold nanoparticles

Information on the morphology of gold nanoparticles obtained from Scanning Electron Microscopy measurements**.** The image [Fig. 3] revealed that nanoparticles are mainly spherical in shape and are not in physical contact but are separated.

D. *UV-Vis Spectra of gold nanoparticles*

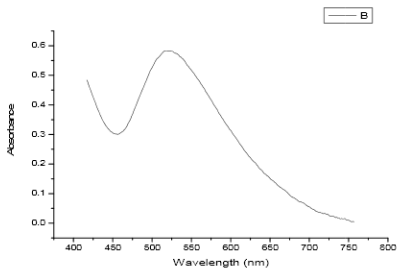

Fig. 4 UV-VIS spectra of gold nanoparticles

The UV- visible light absorption of gold nanoparticles was monitored in the range of 200-800 nm. In case of gold ions reduction, the bands corresponding to the Surface Plasmon Resonance (SPR) occurred at 530 nm [Fig. 4]. Earlier studies have established that SPR band of gold nanoparticles appears around (500-550nm).

E. *DPPH and Fenton bioassay of antioxidant activity of Solanum Tuberosum extract*

Solanum Tuberosum (potato) extract showed antioxidant behaviour in terms of percentage inhibition 83% for DPPH radicals at the concentration range 20 mg/ml. Reference antioxidant α-tocopherol inhibited 98.98% of DPPH radicals at the same concentration. The free radicals were scavenged and solution becomes yellow because of formation of α-α diphenyl-β- picryl hydrazine. The extent of decolouration indicates the amount of DPPH radical scavenged. Similarly, potato extract showed antioxidant behaviour in terms of percentage inhibition 84.1% against OH° radicals at the concentration range 20 mg/ml in Fenton's assay. Reference antioxidant α-tocopherol inhibited 99.51% of OH° radicals at the same concentration. The rate of degradation of deoxyribose sugar in test samples was compared with control in terms of appearance of pink chromogen with thiobarbituric acid. IC_{50} values of potato extract were calculated using DPPH and Fenton assay and found to be 9.34mg/ml & 8.36mg/ml, respectively.

F. *Enhanced antioxidant activity of Solanum Tuberosum embedded gold nanoparticles*

The antioxidant behaviour of synthesized gold nanoparticles of potato extract with that of the native potato extract was examined using DPPH assay. Gold nanoparticles and native potatoes showed percentage inhibition 98.34% and 83% against DPPH radicals at the concentration range 20 mg/ml respectively. It is concluded that there is 15% enhancement in antioxidant behaviour, further confirmed by lowering in IC_{50} value (9.34) to (5.87) [Fig. 5]. The observed enhancement in the antioxidant behaviour can be ascribed to the fact that, nanoparticles have advantages over bulk materials due to their surface plasmon resonance (SPR), enhanced Rayleigh scattering, surface enhanced raman scattering (SERS) in metal NPs and quantum size effect.

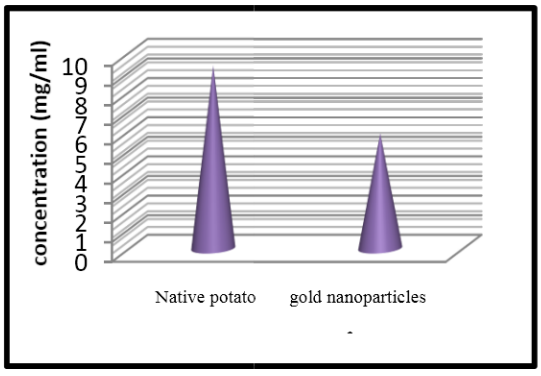

Fig. 5 IC_{50} value of raw potato and gold nanoparticles

G. *HPTLC detection of major antioxidant in Solanum Tuberosum extract*

HPTLC chromatogram was developed using optimized solvent system as ethanol: Toluene: Acetic acid [6:1:1 (v/v/v)]. A linear calibration curve was obtained on applying the increasing concentration of standard ascorbic acid in the range (2- 14 µl). The presence of Ascorbic acid in the sample was confirmed by its R_f value of 0.66 $\pm$ 0.03 matching with that of standard Ascorbic acid having R_f 0.66. Ascorbic acid in the sample was measured

quantitatively (1.30 ± 0.40 mg/g) in potato. Recording of their UV spectra further confirmed by the presence of characteristic peak of ascorbic acid in the potato extract, matching with the peak of standard ascorbic acid at λ_{max} 254nm.

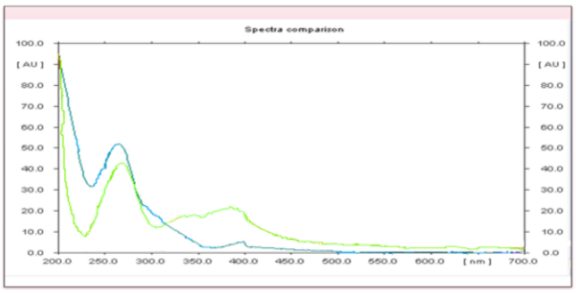

Fig 6: UV spectra of standard ascorbic acid and potato extract

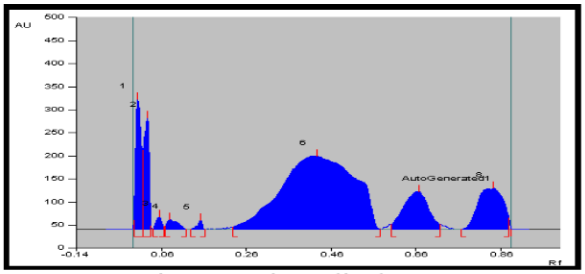

Fig. 7: Chromatographic profile of potato extract

IV. CONCLUSIONS

Biosynthesis of gold nanoparticles embeded with plant extracts having reducing agents such as citric acid, ascorbic acid, flavonoids and extracellular electron shuttlers play important role in the enhancement of various bio efficacies.

V. ACKNOWLEDGEMENT

Authors are thankful to Prof. P K Kalra, Director, DEI for providing necessary research facilities and UGC-SAP for providing financial assistant.

VI. REFERENCES

1. F. Shahidi, "Natural antioxidants: an overview, In: Natural Antioxidants, Chemistry, Health Effects and Applications" AOCS Press Champaign, Illinois, USA, pp. 1-10, 1997.
2. D. F. Mantle, Eddeb, A. T. Pickering, "Comparision of relative antioxidant activities of British medicinal plant species in vitro" *J. Appl Microbio* vol. 84 no. 4, pp. 538-544, 2000.
3. R. G. O. Rumbaoa, D. F. Cornago, I. M. Geronimo, "Phenolic content and antioxidant capacity of Philippine potato (*Solanum tuberosum*) tubers" *J Food Compos Anal vol.* 22, pp. 546-550, 2009.
4. J. Lachman, K. Hamouz, M. Orsak, V. Pivec, P. Dvorak, "The influence of flesh colour and growing locality on polyphenolic content and antioxidant activity in potatoes" *Sci Hortic* vol. 117, pp. 109-114, 2008.
5. C. R. Brown, "Breeding for phytonutrient enhancement of potato" *Am J Pot Res*. Vol. 85, pp. 163-172, 2005.
6. T. Blessington, M. N. Nzaramba, D. C. Scheuring, A. L. Hale, L. Reddivari, J. Miller, "Cooking methods and storage treatments of potato: Effects on carotenoids, antioxidant activity, and phenolics" *Am J Pot Res*. Vol. 87, pp. 479-491, 2010.
7. D. Campos, G. Noratto, R. Chirinos, C. Arbizu, W. Roca, L. Cisneros-Zevallos, "Antioxidant capacity and secondary metabolites in four species of Andean tuber crops: native potato (*Solanum* sp.), mashua (*Tropaeolum tuberosum* Ruiz & Pavón), Oca (*Oxalis tuberosa* Molina) and ulluco (*Ullucus tuberosus* Caldas)" *J Sci Food Agric*. Vol. 86, pp. 1481-1488, 2006.
8. G. Burgos, E. Salas, W. Amoros, M. Auqui, L. Munoa, M. Kimura, M. Bonbierale, "Total and individual carotenoid profiles in *Solanum phureja* of cultivated potatoes: I. Concentrations and relationships as determined by spectrophotometry and HPLC" *J Food Compos Anal* vol. 22, pp. 503-508, 2009.
9. C. M. André, M. Ghislain, P. Bertin, M. Oufir, M. R. Herrera, L. Hoffmann, J. F. Hausman, Y. Larondelle, D. Evers, "Antioxidant profiling of native Andean potato cultivars (*Solanum tuberosum*L.) as a source of antioxidant and mineral micronutrients" *J Agric Food Chem*. Vol. 55, no. 2, pp. 366-378, 2007.
10. C. M. André, M. Oufir, L. Hoffmann, J. F. Hausman, H. Rogez, Y. Larondelle, D. Evers, "Influence of environment and genotype on polyphenol compounds and in vitro antioxidant capacity of native Andean potatoes (*Solanum tuberosum* L" *J Food Compos Anal*. Vol. 22, pp. 517-524, 2009.
11. L. Leo, A. Leone, C. Longo, D. Lombardi, F. Raimo, G. Zacheo, "Antioxidant compounds and antioxidant activity in "early potatoes". *J Agric Food Chem* vol. 56, no. 11, pp. 4154-4163, 2008.
12. K. Shimada, K. Fujikawa, K. Yahara, T. Nakamura, "Antioxidative properties of Xanthan on the anti-oxidation of soybean oil in cyclodextrin emulsion" *J. Agri Food Chem*, vol. 40, pp. 945–948, 1992.
13. K. Satish, C. Nripen, S. Ravi, K. Kavita, R. Rajesh, S. T. Kulkarni, , M. Swapna, K. Raghuraman, K. V. Kattesh, "Green Nanotechnology from Tea: Phytochemicals in Tea as Building Blocks for Production of Biocompatible Gold Nanoparticles" *J Mater Chem vol.* 19 no. 19, pp. 2912–2920, 2009.

Electric properties of rare earth doped strontium M-type hexagonal ferrites

Taminder Singh[a], Arun Katoch[b], Iqbal Singh[a]
[a]*Department of Physics, Khalsa College Amritsar, India*
[b]*BKSJ College of Engineering, Amritsar, India*
dr.taminder@gmail.com

***Abstract*—TheSeebeck Coefficient for the strontium ferrites $Sr_{1-x}RE_xFe_{12}O_{19}$ (where RE = Dy, x = 0.0, 0.10, 0.20 and 0.30), which have been prepared by employing the ceramic technique, were studied in the temperature range 313-473K. The value of thermoelectric power seems to increase with increasing temperature where as the AC conductivity has been observed to be independent of frequency at high temperatures for all values of x. In the relatively low temperature region, thermoelectric power value has been found to be negative confirming that the majority of carriers are electrons thereby indicating the rare earth substituted strontium ferrites to be classified as n-type semiconductors. The X-ray diffraction patterns show that the prepared samples have a single phase. The lattice parameters 'c' and 'a' were found to decrease whereas the X-ray density increases with increasing REcontent. It has been found that the value of electrical conductivity also increases with an increase in RE content. The dispersion of dielectric constant has been discussed in the light of Koops model and hopping conduction mechanism.**

***Keywords*—**Hexagonal ferrites, X-ray diffraction, Scanning electron microscope, Thermoelectric power, AC conductivity .

I. INTRODUCTION

The hexagonal ferrites, $MFe_{12}O_{19}$ (M= Ba, Sr and Pb) are well known as permanent magnetic material which have magnetoplumbite structure and exhibit large spontaneous magnetization with strong anisotropy [1] M-type hexaferrite have widely been used in telecommunication, magnetic recording media, magneto-optics and microwave devices [2–5]. Strontium hexaferrite$SrFe_{12}O_{19}$ is a hard magnetic material due to high coercivity (6.64 kOe) which originates from its high magnetocrystalline anisotropy and is strongly dependent on the size and the shape of the particles. The Curie temperature of $SrFe_{12}O_{19}$ is around 470°C and the saturation magnetization between 74.3 and 92.6 emu/g [6–11].Hexagonal strontium ferrites have been intensively investigated during the last few decades due to their considerable importance in the electronic material industry. The hexagonal Barium (BaM) and Strontium ferrite (SrM) are considered to be excellent candidates for magnetic recording media and characterized with high magnetocrystalline anisotropy, moderate hard magnetic properties and high chemical stability, compared with other magnetic materials. The thermoelectric power of hexagonal ferrites has rarely been studied. The thermoelectric propertiesof hexagonal ferrites depend on the preparation conditions such as sintering temperature, sintering atmosphere and the soaking time as well as the type of the substituted ions.The common processing methods of hexagonal ferrites are conventional ceramic process of solid-state reaction, co-precipitation method, sol-gel process and molten salt method [12-14] etc .The conventional ceramic process includes the mixing the raw materials, calculation, milling, pressing and sintering at 1150- 1200°C. In a fine particle form, Strontium ferrite is suitable for high density recording media. Ultra fine strontium ferrite powder with narrow particle size distribution is desirable to increase the capacity of information storage as well as to reduce the medium noise [15].

In the present work the temperature and composition dependence of thermoelectric properties of rare earth doped strontium M-type hexagonal ferrites $Sr_{1-x}RE_xFe_{12}O_{19}$where RE=Dy) has been studied at different frequencies and temperatures. Structural properties and particle size of hexaferrite have also been investigated by employing XRD technique.

II. EXPERIMENTAL

Strontium hexaferrites ($SrFe_{12}O_{19}$) of nominal composition (x = 0.0, 0.10, 0.20 and 0.30) were synthesized starting from ball-milling mixtures of $SrCO_3$, $Fe_2O_3$and Dy–rare earth ion for 12h. After drying at 60°C for 6h, the powder mixture was heated at temperature of 800-1150 °C for 4 h in a lid covered alumina crucible with a heating rate of 5° C/min in air and were cooled to room temperature in furnace. In order to make the sintered magnet , the strontium ferrite powder were wet mixed in acetone medium with addition of 4% polyvinyl alcohol (PVA) binder solution by using a ball mill. The mixture were reground again for 5hrs and the final fine powder were pressed in disk-shaped pellets with thickness ranging from 2- 4mm and with diameter from 7-9mm.Subsequently the pellets were sintered in a resistance heated furnace for 3hrs at beach specified level of sintering temperature ranging from 950 to 1250°C. The samples were then slowly cooled to room temperature.

The structural characterization was carried out by employing X-ray diffraction(XRD) technique using a X-ray Diffractometer (XPERT-PRO) with CuK_α (λ = 1.5406) radiations.The electric properties of the samples were measured by HP4284A precision LCR meter having frequency range from 20 Hz-1MHz. All the measurements have been carried by using a cell having platinum electrodes.

III. RESULTS AND DISCUSSION

The XRD pattern obtained for different molar concentration in the prepared samples of $Sr_{1-x}RE_xFe_{12}O_{19}$ (where RE=Dy) ferrite sintered at 1250°C for 6hrs have been shown in Fig. 1. The analysis reveals that the prepared samples have single hexagonal M-type phase. All peaks correspond to hexaferritebut for the substitution x = 0.30, where extra peaks of hematite (α-Fe_2O_3) and tetragonal $Sr_3Fe_2O_7$have been observed, indicating that Dy for x = 0.30 did not substitute totally into the Sr M-type structure resulting in incomplete reactions between Fe^{3+} and Sr^{2+}.This is further indicated by tracing of secondary phases in these samples and is attributed to the preparation process. The respective peaks show that a magnetoplumbite structure has been formed. The variation in relative intensities of peaks may be related to the occupation of lattice sites by substituted ions . It is observed that both 'a'

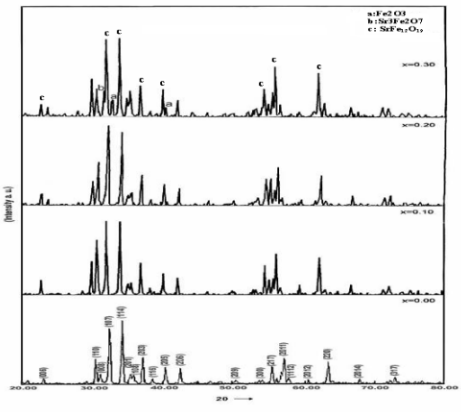

Fig.1. XRD Patterns of $Sr_{1-x}Dy_xFe_{12}O_{19}$ for compositions (a) X=0 , (b) X=0.10 , (c) X=0.20 and (d)X=0.30

and 'c' decrease continuously with increasing substituted amount of rare earth ions in the ferrites. The observed variation in the lattice constants can be explained on the basis of relative ionic radii of Sr and Dy which are 1.12 Å for Sr and 0.912Å for Dy respectively. Since Dy^{3+} ions have ionic radii less than that of the ionic radii of Sr^{2+} ions, the replacement of Sr^{2+} ions by Dy^{3+} ions results in the decrease of unit cell dimensions of hexagonal lattice. The peak for the doped strontium ferrites appears at the same position as for undoped ferrite, with different intensities[16].

The X-ray density or theoretical density (T.D.)of all the samples was determined by the relation given by equation

$$T.D. = \frac{2nM}{\sqrt{3}.N_a a^2 c}$$

where n is number of atoms, M is molecular weight, N_a is Avogadro's number per gram mole and 'a' and 'c' are lattice constants.The bulk X-ray density (B.D.) is measured using Archimedes' Principle. The porosity of all samples was calculated from the measured values of X-ray density and experimental density by using

$$P = (T.D\text{-}B.D)/T.D \times 100\%$$

The values of observed density and porosity are listed in Table 1. It has been observed that density increases continuously with increasing substituted amount of rare earth ions for the series.This can be attributed to the atomic weight and density of rare earth ions (162.5amu and 8.53 g/cm^3) for Dy^{3+} which are higher than those of Sr^{2+} (87.6amu and 2.54 g/cm^3). The replacement of Dy^{3+} by Sr^{2+} ions in the hexagonal structure leads to a variation in the bonding and consequently interatomic distance and density. The oxygen ions which diffuse through the material during sintering also accelerate the densification of the material [16]. The apparent density of the sample reflects the same general behavior as the theoretical density. The X-ray density is higher than the apparent value due to the existence of pores which depends on the sintering condition. The porosity decreases as the rare earth content increases which reflects the opposite behavior of density.

Table 1. X-ray density D_x, Observed density, D and Porosity P (%) of $Sr_{1-x}Dy_xFe_{12}O_{19}$ with (x= 0 to 0.30)

Composition (x)	D(g/cm^3)	D_x(g/cm^3)	P(%)
0	4.20	5.07	17.03
0.10	4.28	5.12	16.31
0.20	4.33	5.16	16.07
0.30	4.39	5.22	15.97

Figure 2 shows plot of log σ_{AC} against 10^3/T. It has been

observed that σ_{AC} exhibits a semi- conductive behavior with the temperature and increases with increasing temperature.The conductivity also increases with increase in x. The results of AC conductivity could be explained on the basis of Koops Model [17], which assumes that ferrite samples act as a multilayer capacitor in which the ferrite grain and grain boundaries have different properties. According to this model, the bulk material of the ferrite could be considered as consisting of two layers, one representing the grains (a conducting layer) and the other representing the grain boundaries (a poor conducting layer). The grains having high conductivity are effective at high frequencies. However the grain boundaries with low conductivity are effective at lower frequencies.

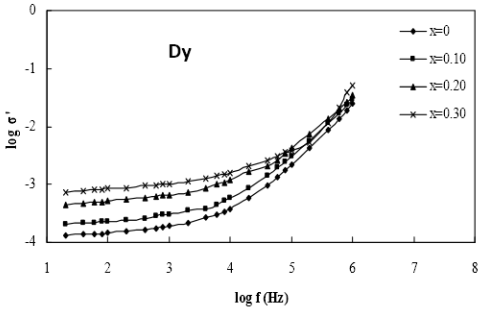

Fig. 2.Variation of AC conductivity with frequency for $Sr_{1-x}Dy_xFe_{12}O_{19}$ series at different compositions

The variation of the Seebeck coefficient with temperature for three series prepared with RE = Dy^{3+} are shown in Fig.3. It is observed that the value of thermoelectric power for Sr-Dy ferrites increases with increasing temperature. Throughout the temperature range, the thermoelectric power value has been found negative confirming that the majority of the charge carriers are electrons. On the basis of its negative sign, the rare earthsubstituted strontium ferrites have been classified as n-type semiconductors. A similar variation of the thermoelectric power with temperature has been reported for different ferrite systems [18,19]. The experimental values of Seeback coefficients have been tabulated in Table 2.

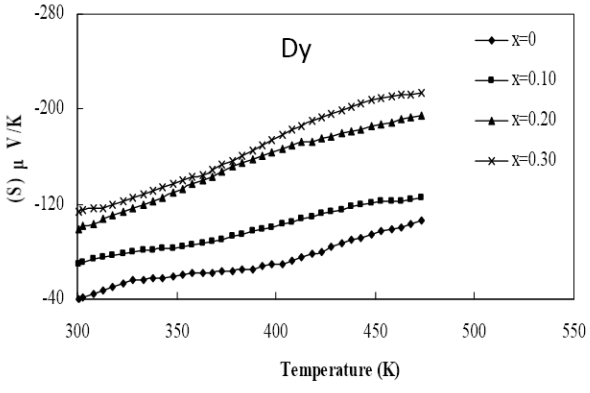

Fig.3. Variation of Seeback coefficient with temperature for $Sr_{1-x}Dy_xFe_{12}O_{19}$series for different compositions

The carrier concentration for these ferrite samples was calculated using the formula given by Morin and Gebella [20]

$$n = N\,exp\,(\frac{-Se}{k})$$

where S = Seebeck coefficient, e = charge of electron, *k*= Boltzman constant and N = density of states or concentration of electronic levels involved in the conduction process. In this case N = 2.8 x 10^{22}, the number of octahedral cation sites/cm^3 of ferrite. The variation of charge carrier concentration (n) with temperature is shown in Fig. 4. It is observed that the value of charge carrier concentration increases with increase of temperature. Similar variation of nwith temperaturehas also been observed in Ba-Zn hexaferrites [21].

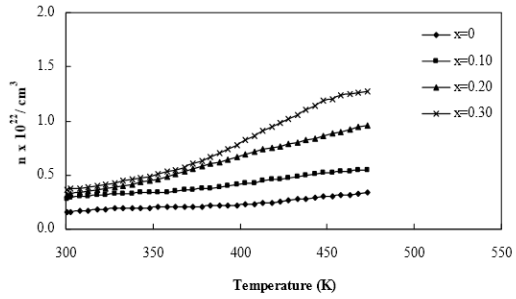

Fig.4. Variation of carrier concentration with temperature for for$Sr_{1-x}Dy_xFe_{12}O_{19}$ series for different compositions

The computed values of carrier concentration are included in Table 2. It has been observed from the table that the value of charge carrier concentration also increases with an increase in Dy content.

Table.2.Room temperature electrical conductivity and thermoelectric power data of $Sr_{1-x}Dy_xFe_{12}O_{yjyu}$for different compositions

Composition (x)	Seebeck Coefficient S(μV/K)	Carrier Concentration n(10^{22}/Cm)	Carrier Mobilityμ (cm^2/Vs)
0	-45	0.15	$8.5x10^{-12}$
0.10	-73	0.28	$6.42x10^{-11}$
0.20	-104	0.32	$2.5x10^{-10}$
0.30	-115	0.36	$8.03x10^{-10}$

Table 2 also gives the experimental values of Seebeck coefficient and electrical conductivity values at room

temperature for the series prepared with RE =Dy^{3+}. The values of Seebeck coefficient vary from -45μV/K to -115μV/K for different values of x. The values of charge carrier concentrationhave also been found to increase with an increase in RE content. Similar behavior of the electrical conductivity has been reported [21].

IV. CONCLUSIONS

The aim of the present work is to investigate the thermoelectric properties due to rare earth substitution in place of Sr^{2+} ion in hexagonal ferrites and to understand the various physical phenomena and mechanisms that lead to modifications in their properties. It has been observed that the replacement of Sr^{2+} ions by RE = Dy^{3+} ions in $Sr_{1-x}RE_xFe_{12}O_{19}$hexaferrite yields hexagonal ferrites to a certain extent of unreacted oxides with an additional phases.

The observed variation in the lattice constants can be explained on the basis of relative ionic radii of Sr and Dy , which are 1.12 Å for Sr and 0.912Å for Dy respectively. Since Dy^{3+} ions have ionic radii less than that of the ionic radii of Sr^{2+} ions, the replacement of Sr^{2+} ions by Dy^{3+} ions results in the decrease of unit cell dimensions of hexagonal lattice. The increase in bulk density with rare earth substitution may be attributed to the atomic weight and density of these ions, which are higher than those of strontium ions. The replacement of Sr^{2+} by Dy^{3+} ions in the hexagonal structure leads to a variation in the bonding and consequently interatomic distance and density. The bulk density of the sample reflects the same general behavior as of the X-ray density. The X-ray density is higher than the bulk density value due to the presence of pores which depends on the sintering conditions. The porosity decreases as rare earth content increases thereby reflecting the opposite behavior of density. The negative values of the thermoelectric power found over the entire temperature range confirm that the majority of the charge carriers are electrons. On the basis of its negative sign, the rare earth substituted strontium ferrites have been classified as n-type semiconductors.

REFERENCES

[1] S. Che, J. Wang and Q.W. Chen "Soft magnetic nanoparticles of $BaFe_{12}O_{19}$ fabricated under mild conditions"*J. Phys: Condens. Matter*Vol. 15 (22), pp L335-L339, 2003

[2] M. Sivakumar, A. Gedanken, W. Zhong, Y.W. Du, D. Bhattacharya, Y. Yeshurun, and I. Felner "Nanophase formation of strontium hexaferrite fine powder by the sono chemical lmethod using $Fe(CO)_5$",*J. Mag. &Mag. Mater.*Vol268(1-2), pp 95-104, 2004.

[3] Y.P. Fu, C. H. Lin, K..Y. Pan,"Strontium hexaferrite powders prepared by a microwave-induced combustion process and some of their properties",*J. Alloys Compd*.,Vol. 349(1-2) pp 228-231, 2003.

[4] M.J. Iqbal, M.N. Ashiq, P.H. Gomez and J.M. Munoz, "Synthesis, physical, magnetic and electrical properties of Al–Ga substituted co-precipitated nanocrystalline strontium hexaferrite", J. Mag. and Mag. Mater., Vol. 320(60) pp 881-886, 2008.

[5] S.V. Ketov, Yu.D. Yagodkin, A.L. Lebed, Yu.V. Chernopyatova and K. Khlopkov, "Structure and magnetic properties of nanocrystalline $SrFe_{12}O_{19}$ alloy produced by high-energy ball milling and annealing" *J. Mag. and Mag. Mater.*, vol. 300(1), pp e479-e481, 2006.

[6] N. Rezlescu, C. Doroftei, E. Rezlescu and P.D. Popa, "The influence of heat-treatment on microstructure and magnetic properties of rare-earth substituted $SrFe_{12}O_{19}$, *J. Alloys and Compounds*, vol. 451 (1-2), pp 492-496, 2008.

[7] J.F.Wang, C.B. Ponton and I.R. Harris, "A study of Pr-substituted strontium hexaferrite by hydrothermal synthesis" *J. Alloys and Compounds*, vol. 403(1-2), pp 104-109, 2005.

[8] J. Fang, J. Wang, L. Gan, S. Ng, J. Ding and X. Liu, "Fine Strontium Ferrite Powders from an Ethanol-Based Microemulsion", *J. Amer. Ceram. Soc*, vol. 83(5), pp 1049-1055, 2000.

[9] J. Ding, W.F. Miao, P.G. McCormick and R. Street, "High coercivity ferrite magnets prepared by mechanical alloying" *J. Alloys and Compounds,* vol. 281(1), pp 32-36, 1998

[10] L. Rezlescu, E. Rezlescu, P.D. Popa and N. Rezlescu, "Fine barium hexaferrite powder prepared by the crystallisation of glass", *J. Mag.and Mag. Mater.* vol. 193(1-3), pp 288-290, 1999.

[11] Y.P. Fu and C.H. Lin, "Fe/Sr ratio effect on magnetic properties of strontium ferrite powders synthesized by microwave-induced combustion process", *J. Alloys and Compounds*, vol 386(1-2), pp 222-227, 2005.

[12] H.Zhang , L. Li, J. Zhou, Z. Yue, and Z. Gui, "Microstructure characterization and properties of chemically synthesized Co_2Z hexaferrite", *J.Europ.Ceram.Soc*., vol 21(2) pp 149-153, 2001

[13] Y. Hayashi, T.Kanazawa and T. Yamaguchi,"Preparation of acicular NiZn-ferrite powders", *J.Mater.Sci.,* vol 21(8), pp 2876-2880, 1986.

[14] T. Kimura, T. Takahashi and T. Yamaguchi,"Preparation and characteristics of Ni-ferrite powders obtained in the presence of fused salts" *J.Mater. Sci*., vol 15(6), pp1491-1497, 1980.

[15] T. G. Carreno, M.P. Morales and C.J. Serna, "Barium ferrite nanoparticles prepared directly by aerosol pyrolysis" *Mater. Lett*., vol 43(3), pp 97-101, 2000

[16] A.Katoch and T. Singh, "Temperature and composition dependence of structural, electrical and dielectric properties of rare earth doped ferrites" in *Proc. ICETEC*, pp76-84, 2013.

[17] C.G. Koops, Phys. Rev., "On the Dispersion of Resistivity and Dielectric Constant of Some Semiconductors at Audiofrequencies", *Phy. Rev.,*vol 83(1),pp 121-124, 1951.

[18] D. Ravinder, "Thermoelectric power studies of zinc substituted copper ferrites"*J. Alloys & Compounds*, vol291(1-2),pp208-214, 1999.

[19] D. Ravinder, D and A.C.S Reddy, "Thermoelectric power studies of Co–Ge ferrites" *J. Alloys and Compounds*, vol 353(1-2), pp 86-90, 2003.

[20] F. J. Morin and T. H. Gebella, "Electrical Conductivity and Seebeck Effect in $Ni_{0.80}Fe_{2.20}O_4$"*Phys. Rev*., vol. 99(2), pp 467-468, 1955.

[21] M. Saadawy and M. M. Barakat, "Electrical conductivity of cobalt-doped BaZn hexagonal ferrites*", J. Magn. and Magn. Mater*., vol 205(2-3), pp 319-322, 1999.

Utilization of Polymer Nanocomposites for Power System Equipment's

Isaac Ramalla[a]

[a]*Research Scholar, Department of Electrical Engineering, University of petroleum and Energy Studies, Dehradun, India.*

***Abstract*—Among various types of materials for electrical insulation in power system equipment, polymers have been commonly used for more than five decades. They are usually manufactured with additives to meet design requirements. Intense researches are currently focused on nanocomposites, which are synthesized with nano-scale particles as fillers and conventional polymers as matrices. The key challenges yet to overcome are the poor dispersion and the low fillermatrix interactivity. In this paper, plasma technology, for the very first time, is utilized to engineer the surface of the nanoparticles for fabricating nanocomposites with advanced dielectric and electrical insulation properties. First, an atmospheric-pressure plasma (APP) system is developed. APPs carried by inert gas are employed to tailor the surface of silica nanoparticles with existing silane functional groups. In addition, a plasma polymerization system is developed to provide an alternative fabrication process, where the plasma is carried out under low pressure with specified monomers. In this case, plasma polymerization takes place on the pure silica nanoparticles and functional plasma polymer layers can be coated on their surfaces. For both methods, results of chemical and morphological characterization indicate that the filler-matrix bonding is enhanced and the dispersion is improved in the epoxy resinbased nanocomposites. Electrical tests showed improved partial discharge (PD) characteristics, breakdown strength, electrical ageing resistance, space charge distribution, and dielectric constant in the nanocomposites with plasma modified fillers. These improvements can be explained from the perspective of the immobilization of polymer molecules by the reinforced filler-matrix bonding, carrier trapping effects by the altered electrical double layer around the nanoparticles, and the barrier effects by good dispersion of the nanoparticles. The outcome of this research provides an effective, economic, and environment-friendly approach for synthesizing high performance nanocomposite insulation materials. It is also generic that can be utilized in the fabrication of novel nanocomposites for a wide range of applications.**

***Keywords*—** plasma polymerization technology, epoxy resin based, nanocomposite, electrical insulation technology.

I. INTRODUCTION

Polymers have been serving as electrical insulation materials in power systems for more than half a century. Polymers have been widely used in the power systems since the 1960s [1]. They can be used alone as insulators, bushings, surge arresters, cable determinations, and bus bar insulation [2].Also, polymer housing is applied to enhance the performance of porcelain insulators [3]. From the perspective of the material, polymers consist of two or more polymeric compounds with a number of structural units bound by covalent bonds [4]. Epoxy resinis the most widely used thermoset polymer due to its high mechanical properties, heat andchemical resistance, and good adhesion to metal conductors [5, 6]. Cross-linked polyethylene(XLPE) is another important thermoset polymer, which is commonly employed as the insulationof high-voltage cables [7]. Other additives, such asantioxidants, plasticizers, pigments, flame retardants, UV stabilizers, etc, are also applied toimpart desired properties to microcomposites which are extensively utilized in power systemscomponents and apparatus [2]. The improved properties of microcomposites are attributed to the high content of the fillers.

However, such a high loading rate usually results in decrease of dielectric strength [14]. Thedielectric constant may significantly increase due to the Maxwell-Wagner polarization effect[15]. These properties are considered detrimental to the electrical insulation in power systemdesign. To this end, researchers are seeking the use of nanocomposites, which consist only of asmall amount of nano-sized inorganic fillers dispersed in pristine polymer matrices, as the nextgeneration of filled resin insulation materials [16]

II. HELPFUL HINTS

A. Key problems and existing methods

Due to the enormously large specific surface area of nanoparticles, the interfacial region can take up to a few tens of percent of the total volume of the nanocomposites[34]. To achieve desired properties of the interfacial region, two major factors need to be taken into consideration. First, homogeneous dispersion is required. In the case of agglomerated or clustered nanoparticles, the average particle size is significantly increased, thus the materials may turn into microcomposites. Traditional methods to enhance the dispersion include mechanical blending and ultrasonic bathing [35]. However, the key factor dominating the dispersion is the compatibility between the surface of nanoparticles and the host polymer. Traditional methods to enhance the dispersion include mechanical blending and ultrasonic bathing [35]. However, the key factor dominating the dispersion is the compatibility between the surface of nanoparticles and the host polymer. The procedures are rather complicated and the agents are usually toxic. As an alternative, plasmas are believed as powerful tools for surface modification of nanomaterials[41]. Plasma surface modification is considered as a clean, effective, economical substitution forwet-chemical methods. It is also more versatile as the resultant surface chemistry of thesubstrate is highly

dependent on the plasma parameters, which can be customized according toparticular demands.

B. Existing modification methods for nano composites

The plasma-treated alumina was consolidated to bulk. It was found that the mechanical strength of such a material was improved due to promoted particle-particle adhesion [47]. His group used the same setup to coat polystyrene thin films on carbon nanofibres (CNFs) and found improved strength of the polystyrene/CNFs nanocomposites [48]. In 2005, *Cao* implemented a capacitively coupled plasma (CCP) reactor, and successfully performed coating hydrogenated carbon films on metallic nanowires and silica nanoparticles [49]. Plasma deposition on ceramic nanoparticles has been carried out by *Timmons*. His group employed a 360° rotating plasma reactor to break down the aggregation and introduce film deposition on the nanoparticles uniformly [50]. This techniques was then used to coat functionalize BTO nanoparticles with reactive amine groups. The epoxy/BTO nanocomposites obtained improved mechanical strength and significantly increased glasstransition temperature as compared to the epoxy resin with the non-treated BTO nanoparticles [37].

C. Nanoparticles

A series of fumed silica nanoparticles provided from EVONIK are used as the fillers forsynthesizing nanocomposites in the present thesis. The models of nanoparticles and theirparameters are given in Table 1.1. Among these nanoparticles, the AEROSIL R 812 and R 972 silica nanoparticles have been surface functionalized with silane.

Chemical Composition	Model No	Surface area	Functionalization	Wettability
SiO_2	AEROSIL 972	110*20 m^2/g	Dimethdiehlerosilane (DDS)	Hydrophobic
SiO_2	AEROSIL 812	260*30 m^2/g	Hexmethldisiloxane (HMDS)	Hydrophobic
SiO_2	AEROSIL 812	380*30 m^2/g	N/A	Hydrophobic

D. Characteristics of Epoxy/SiO_2 Nanocomposites

Epoxy resin is widely applied in electrical equipment, electronic components and integrated circuits due to its flexibility and electrical insulation properties.Its performance canbe severely degraded over long term operation under electrical, mechanical and environmentalstresses. Recent reports showed that the incorporation of nanometric particles can enhance theelectrical properties and ageing resistivity of traditional polymers [25, 74, 75]. Samples with relatively lownanoparticle content are prepared by direct mixing method. The electrical insulation propertiesare tested by carrying out a proposed surface ageing tests with self-developed needle-to-needleelectrodes. Epoxy resin is selected as the host polymer for the composite system. Specifically, bisphenol-A diglycidyl ether(BADGE), which is the reaction product of bisphenol-A and epichlorohydrin, is used as thepre-polymer resin, while triethylenetetramine (TETA) is chosen as the hardener. Thisthermosetting epoxy resin is particularly applied for electrical insulation. AEROSIL® R 972 SiO2 nanoparticles are selected as the filler. This type of nanoparticles has aspecific surface area of 110 ± 20 m2/g and an average particle size of 16 nm. The nanoparticles are after-treated with dimethyldichlorosilane (DDS).

Sample preparation and Electrical testsFirst, 0.3 g of the silica nanoparticles is dispensed into 10 g of thepre-polymer epoxy resin. Then the mixture undergoes ultrasonication for 30 min, followed by 30 minutes blending by the overhead stirrer. After that, 4 g of the curing agent is added to theslurry. Subsequently, the blending is performed for another 30 minutes. Degassing is thenperformed under low pressure (~1 Torr) until all air bubbles are extracted. Subsequently, themixture is poured into plastic moulds and undergoes another degassing process. The weightratio of resin and curing agent is 10:4, while the concentration of the nanoparticles is 2.14 wt%.A pristine epoxy resin counterpart is also fabricated according to identical procedures withoutintroducing the nanoparticles. All samples are shaped into round pellets with a thickness of 3 mm and a diameter of 20 mm. Electrodeconfiguration is suggested in ASTM Standard D495 to create highly divergent electric field on thesurface of the samples [77]. Specifically, the sample pellet is placed on an insulating stage witha pair of needle-to-needle electrodes pressing on the top surface. The electrodeneedles are made of steel and have a tip radius of 1.3 μm. The distance between the two needletips is 4 mm. They are placed at an angle of 45° to the horizontal plane and in contact with thetop surface of the pellet with equal force. Potential D activities along the surface during the ageingprocess are simultaneously monitored. For each material, the electrical test is carried out on four samples pellets withthe same composition. Results with good repeatability are obtained. Results and Discussions

With this electrode configuration, surface discharges along the surface of the sample pellet arethe predominant sources of PD activities. The PD patterns at the inception stage of each sampleare shown in figure 1.1 One can clearly observe the “hill-shape” feature, which is typical forsurface discharges, in the PD patterns of both samples. It is also noted that the inceptionvoltage of the pristine epoxy resin (1.61kV) is lower than that of the nanocomposite (1.74kV). Moreover, the integrated PD quantities, namely the average PD magnitude (*qaverage*), themaximum PD magnitude (*qmax*), and the PD repetition rate (*n*), are extracted from the PDpatterns and shown in table 1.2. The average and maximum PD magnitudes of

both samples are similar to each other. However, the PD repetition rate of the nanocomposite is dramaticallyreduced compared to the pristine sample, indicating that the surface of nanocomposite hasa suppressing effect on the occurrence.

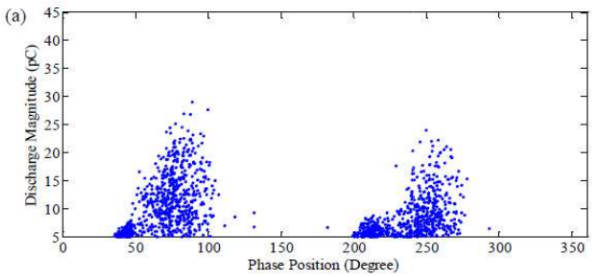

Figure 1.1: PD patterns at the inception voltage of (a) the pristine epoxy resin sample (1.61 kV)

	PD repetition rate (count per second)	Average PD magnitude (pC)	Maximum PD magnitude (pC)
Pristine	136	9.8	29.1
Nanocomposite	68	14.4	40.3

Table 1.2: Integrated PD quantities of surface discharges at the inception voltage of the pristineand the nanocomposite sample.

It is found that the PDrepetition rate of the nanocomposite sample is noticeably lower than the pristine sample atlower voltages (2kV and 2.5kV) in both half-cycles, whereas more PDs are detected in thenanocomposite sample at 3 Kv. In the surface ageing test, the applied voltage is held at 3 kV (rms). Figure 1.1demonstrates thevariation of the PD pattern of the pristine epoxy resin and epoxy resin/SiO2 nanocomposite overthe ageing time. In the beginning (0min), the PDs of the pristine epoxy resin isrelatively weak in both magnitude and repetition rate as compared to the nanocomposite. This is due to the slight difference of initial roughness of the sample pellets. However, thesurface discharge of the nanocomposite sample is weakened at later stages (20 min and 40 min). It is clear evidence that the insulationperformance is degraded.

E. Discussion

The inclusion of silica nanoparticles can increase the inception voltageand enhanced the ageing resistivity of the host epoxy resin. In particular, the "self-healing"feature of the nanocomposite exhibited through the surface ageing test is a significant advantagecompared to the pristine epoxy resin, in which the surface discharge finally develops to surfacetracking at the end of the ageing process. However, nanofillers, which are more stable than thepolymer molecules, are exposed on the surface and acting like "humps" on the paths of charges.This may effectively reduce the kinetic energy of the charges travelling along the surface,thereby preventing the formation of surface tracking. As the erosion depth is expected to increase over time, more and more nanoparticles areexposed on the surface, leading to a better hindering effect and more suppressed PDs. However, it has to be noted that the initial PD magnitude at the applied voltage of 2 kV, 2.5 kV,and 3 kV of the nanocomposite has been little suppressed from that of the pristine epoxy resin. This is probably due to the surface incompatibility between thenanofillers and the polymer matrix, which normally leads to the agglomeration of the nanofillersand weak chemical bonds forming between the two phases [37]. Therefore, appropriate surface pre-treatment is needed to accommodatethe surfaces of the nanoparticles to the host polymer properly, in order to maximize the positiveinfluence of the nanoparticles.

III. CONCLUSION

In the present study, nanocomposites have been fabricated by introducing silica particles toepoxy resin. PD test and surface ageing test have been carried out on the nanocomposite and thepristine epoxy resin sample with a pair of needle-to-needle electrodes. The nanocompositeexhibited better PD resistance in the negative half-cycle (in relation to the applied AC voltage)in terms of the reduced PD repetition rate and lowered PD magnitudes. A higher inceptionvoltage has also been found in the nanocomposite sample. From the result of the surface ageingtest, it has been found that the development of surface discharges was decelerated in thenanocomposite sample. In contrast, surface discharges in the pristine sample have eventually
developed to surface tracking with intermittent sparks after being aged for 40 minutes.In the present study, nanocomposites have been fabricated by introducing silica particles toepoxy resin. PD test and surface ageing test have been carried out on the nanocomposite and thepristine epoxy resin sample with a pair of needle-to-needle electrodes. The nanocompositeexhibited better PD resistance in the negative half-cycle (in relation to the applied AC voltage)in terms of the reduced PD repetition rate and lowered PD magnitudes. A higher inceptionvoltage has also been found in the nanocomposite sample. From the result of the surface ageingtest, it has been found that the development of surface discharges was decelerated in thenanocomposite sample. In contrast, surface discharges in the pristine sample have eventuallydeveloped to surface tracking with intermittent sparks after being aged for 40 minutes. Certainmodification methodologies are to be employed to increase the surface compatibility of thenanoparticles and the host polymer. Strong chemical bonds between these two phases are alsoexpected to be created. With these

issues solved, it is expected that the electrical insulationproperties can be further promoted.

SUGGESTIONS FOR FUTURE WORK

As the present research involves background knowledge of multiple discipline includingelectrical engineering, materials science, physics, chemistry, nanotechnology, and plasmatechnology, the future of the present research is wide open. In particular, the next stage of thisproject might take the following aspects into account; the effect of the plasma polymerization can be further investigated by comparing nanoparticlesfunctionalized by plasma polymerization and conventional wet chemical methods with the samemonomer agent. The monomer agent might be a kind of existing coupling agent. As morecomplicated and highly cross-linked polymer networks can be created in the plasmaenvironment, the plasma polymerized layers might have better adhesion with both thenanoparticles and the host polymer of the nanocomposites, leading to potentially improveddielectric and electrical insulation performance. In this way, it can be testified that plasmapolymerization is more favourable than coupling agent methods from the perspective ofnanocomposite performance.

Besides, more kinds of nanocomposites can be synthesized using the plasma functionalizednanoparticles. However, as the requirement of polymers for the nanofiller surfaces may vary,specific monomers for plasma polymerization need to be identified for different host polymersfor the nanocomposites. An index or criteria needs to be established to match monomers withhost polymers as a reference.

Material Characterization

In the present thesis, the author estimates the dispersion solely by observation. This canmarginally describe how homogeneously the nanoparticles distribute. In future investigation,quantitative methods of evaluating the dispersion might be deployed. For instance, digitalgraphic processing techniques can be applied on the SEM or TEM images of the nanocompositeso that distribution parameters can be obtained from computation, which is much more preciseto indicate the property of dispersion.Moreover, due to the limit of time and equipment, there are still a number of characterizationsof the nanocomposites that need to be carried out. For example, the thermal conductivity andthermal expansion rate of the nanocomposites are worth studying as these properties are ofequal importance as the electrical properties when the nanocomposites are engaged in powersystem equipments.

Electrical Insulation Test

With more and more academic research and industrial development carried out onnanocomposite dielectrics, it is foreseeable that nanocomposites will be applied in commercialpower system equipment. It is possible that the PD behaviour in nanocomposite is diverse fromthat in conventional insulation materials. Therefore, the PD characteristics of nanocompositeswith different defects need to be carefully investigated to precisely correlate the PD activitieswith the type of faults.On the other hand, dielectric fluids, *e.g.* mineral oils, also play an important role in powersystem equipments, especially in oil impregnated transformers. The incorporation ofnanoparticles into such insulation media has rarely been carried out. The plasma treatmentmethodologies proposed in this thesis might be able to improve the compatibility of the surface

REFERENCES

[1] D. Thornley and A. Shocket, "25 Years Experience of Outdoor Polymeric Insulation," inProceedings of *IEEE Power Engineering Society Transmission and Distribution Conference*,1994, pp. 67-72.

[2] J. Mackevich and M. Shah, "Polymer Outdoor Insulating Materials. Part I: Comparison ofPorcelain and Polymer Electrical Insulation," *IEEE Electrical Insulation Magazine,* vol. 13, pp.5-12, 1997.

[3] D. W. Lenk, J. L. Koepfinger, and J. D. Sakich, "Utilization of Polymer EnclosedIntermediate Class Arresters to Improve the Performance of Modern Power Systems," inProceedings of *IEEE Power Engineering SocietyTransmission and Distribution Conference*,
1991, pp. 424-431.

[4] R. Arora and W. Mosch, "Solid Dielectrics, Their Sources, Properties, and Behavior inElectric Fields," in *High Voltage and Electrical Insulation Engineering*, Wiley & Sons, Inc.,2011.

[5] H. Q. Pham and M. J. Marks, "Epoxy Resins," in *Ullmann'sEncyclopaedia of industrialchemistry*, Wiley-VCH, 2000.

[6] J. F. Hall, "History and Bibliography of Polymeric Insulators for Outdoor Applications," *IEEE Transactions on Power Delivery,* vol. 8, pp. 376-385, 1993.

[7] R. J. Densley, "An Investigation into the Growth of Electrical Trees in XLPE CableInsulation," *IEEE Transactions on Electrical Insulation,* vol. EI-14, pp. 148-158, 1979.

[8] C. Calebrese, H. Le, L. S. Schadler, and J. K. Nelson, "A Review on the Importance ofNanocomposite Processing to Enhance Electrical Insulation," *IEEE Transactions on Dielectricsand Electrical Insulation,* vol. 18, pp. 938-945, 2011.

[9] M. Kozako, N. Fuse, Y. Ohki, T. Okamoto, and T. Tanaka, "Surface Degradation ofPolyamide Nanocomposites Caused by Partial Discharges Using IEC(B) Electrodes," *IEEETransactions on Dielectrics and Electrical Insulation,* vol. 11, pp. 833-839, 2004.

[10] Y. Cao, P. C. Irwin, and K. Younsi, "The Future of Nanodielectrics in the Electrical PowerIndustry," *IEEE Transactions on*

Dielectrics and Electrical Insulation, vol. 11, pp. 797-807,2004.

[11] T. Enis, S. Isidor, D. R. James, R. E. Alvin, M. P. Paranthaman, A. Tolga, *et al.*, "ElectricalProperties of Epoxy Resin Based Nano-Composites," *Nanotechnology,* vol. 18, pp. 025703,2007.

[12] C.W. Reed, "The Chemistry and Physics of the Interface Region," in *Dielectric PolymerNanocomposites,* J. K. Nelson, Springer, 2010.

[13] F. Bellucci, D. Fabiani, G. C. Montanari, and L. Testa, "The Processing ofNanocomposites," in *Dielectric Polymer Nanocomposites*, J. K. Nelson, Ed., 1st ed: SpringerUS, 2010, pp. 31-64.

[14] N. Mukherjee, D. Wavhal, and R. B. Timmons, "Composites of Plasma SurfaceFunctionalized Barium Titanate Nanoparticles Covalently Attached to Epoxide Matrices:Synthesis and Evaluation," *ACS Applied Materials & Interfaces,* vol. 2, pp. 397-407, 2010.

[15] W. Yan, Z. Han, W. Liu, X. Lu, B. ToanPhung, and K. Ostrikov, "DesigningAtmospheric-Pressure Plasma Sources for Surface Engineering of Nanomaterials," *Plasma Chemistry and Plasma Processing,* vol. 33, pp. 479-490, 2013.

[16] D. L. Shi, P. He, S. X. Wang, W. J. van Ooij, L. M. Wang, J. G. Zhao, *et al.*, "InterfacialParticle Bonding Via an Ultrathin Polymer Film on Al2O3 Nanoparticles by PlasmaPolymerization," *Journal of Materials Research,* vol. 17, pp. 981-990, 2002.

[17] D. L. Shi, J. Lian, P. He, L. M. Wang, F. Xiao, L. Yang, *et al.*, "Plasma Coating of CarbonNanofibers for Enhanced Dispersion and Interfacial Bonding in Polymer Composites," *AppliedPhysics Letters,* vol. 83, pp. 5301-5303, 2003.

[18] J. Cao and T. Matsoukas, "Nanowire Coating by Plasma Processing," *IEEE Transactionson Plasma Science,* vol. 33, pp. 829-833, 2005.

[19] J. Cho, F. S. Denes, and R. B. Timmons, "Plasma Processing Approach to MolecularSurface Tailoring of Nanoparticles: Improved Photocatalytic Activity of TiO2," *Chemistry ofMaterials,* vol. 18, pp. 2989-2996, 2006.

[20] R. Sarathi, R. K. Sahu, and P. Rajeshkumar, "Understanding the Thermal, Mechanical andElectrical Properties of Epoxy Nanocomposites," *Materials Science and Engineeringa-Structural Materials Properties Microstructure and Processing,* vol. 445, pp. 567-578, 2007.

[21] H. Kirkici, M. Serkan, and K. Koppisetty, "Nano-Dielectric Materials in ElectricalInsulation Application," presented at the 31st Annual Conference of IEEE Industrial ElectronicsSociety, 2005.

[22] J. Mathias and G. Wannemacher, "Basic Characteristics and Applications of Aerosil: 30. The Chemistry and Physics of the Aerosil Surface," *Journal of Colloid and Interface Science,*vol. 125, pp. 61-68, 1988.

[23] ASTM D495, "Standard Test Method for High-Voltage, Low-Current, Dry Arc Resistanceof Solid Electrical Insulation," ASTM, 2004.

[24] N. A. Muhamad, B. T. Phung, and T. R. Blackburn, "Discrimination of Corona and SurfaceDischarge Patterns in Soy Seed-Based Transformers Insulation Oil," in Proceedings of *10th International Power and Energy Conference*, 2010, pp. 915-920.

[25] L. A. Dissado and J. C. Fothergill, "Overview of Electrical Degradation and Breakdown,"in *Electrical Degradation and Breakdown in Polymers*, 1st ed. vol. 9. London: Peter PeregrinusLtd., 1992.

[26] M. G. Danikas and T. Tanaka, "Nanocomposites - A Review of Electrical Treeing andBreakdown," *IEEE Electrical Insulation Magazine,* vol. 25, pp. 19-25, 2009.

[27] E. Tuncer, I. Sauers, D. R. James, A. R. Ellis, M. P. Paranthaman, A. Goyal, *et al.*,"Enhancement of Dielectric Strength in Nanocomposites," *Nanotechnology,* vol. 18, pp. 325704, 2007.

A Review: A Secure Image Based Steganography, Cryptography and Watermarking with security key

[a]Rupesh Gupta [b]Dr.Tanupreet Singh
[a]*M.Tech Student, Punjab Technical University*
Amritsar College of Engineering and Technology. Amritsar
[b]*Professor & Head Electronics & Communication Engineering Department*
Amritsar College of Engineering and Tech. Amritsar
[a]gupta_rupesh_mani@yahoo.co.in
[b]tanupreet.singh@gmail.com

***Abstract*-Since the rise of internet, the most important factor of information technology and communication has been the security. Many different methods have been developed to encrypt & decrypt the data in order to keep the message secret. Cryptography stegnography and watermarking and many more methods are introduced but when we combine these method with a security key which provides us a 4-tier security level which is touted as higher protection of data from external threats results in better results for different parameters. This paper will explore some of the key security issues and identify concerned solutions provided.**

Keywords- MSE, PSNR, Video frames, LSB, Encryption, Decryption, Steganography

I. INTRODUCTION

Information hiding is the technique of hiding secret data into the host medium so that the hidden data are imperceptible but known to the intended recipient [1]. The host medium can be anything like digital media, digital image, audio, video or any other type of media. Among the different kinds of media, the digital image is most popularly used as the host media to convey secret information. In the image hiding system, the image used to embed secret data is called the host image (cover image). The resultant image, which is embedded with secret data, is called the stego-image. Cryptography) [3] [11] can be defined as the conversion of data into a scrambled code that can be deciphered and sent across a public or private network. Cryptography uses two main styles or forms of encrypting data; symmetrical and asymmetrical. Symmetric encryptions, or algorithms, use the same key for encryption as they do for decryption. Other names for this type of encryption are secret-key, shared-key, and private-key. The encryption key can be loosely related to the decryption key; it does not necessarily need to be an exact copy. Symmetric cryptography is susceptible to plain text attacks and linear cryptanalysis meaning that they are hack able and at times simple to decode. With careful planning of the coding and functions of the cryptographic process these threats can be greatly reduced. Asymmetric cryptography uses different encryption keys for encryption and decryption. In this case an end user on a network, public or private, has a pair of keys; one for encryption and one for decryption. These keys are labeled or known as a public and a private key; in this instance the private key cannot be derived from the public key.

Steganography [1] is one of the data hiding scheme which is the science that involves communicating secret data in an appropriate multimedia carrier. It can embed any image, audio and video files. Steganography's [15] ultimate objectives which are undetectable, robustness resistance to various image processing methods and compression, and capacity of the hidden data, are the main factors that separate it from related techniques such as watermarking and cryptography. Steganography hides the existence of the message

Digital image watermarking: It is the process of inserting data into in image can be used to protect the rights of their owners [3] in a variety of ways:

1) Copyright identification – provide a proof of ownership.
2) User identification (fingerprinting) – encode identity of legal users to encode sources of illegal copies.
3) Authenticity determination – if the watermark will be destroyed by modification in an image, its presence quarantines authenticity.
4) Automated monitoring – monitor when and where images are used (for royalty collection or the location of illegal uses).
5) Copy protection – they can specify rules of image usage and copying (for instance, for DVD players only)

Block diagram

The basic block diagram representation for Steganography mechanism [1] is shown in the below figure.

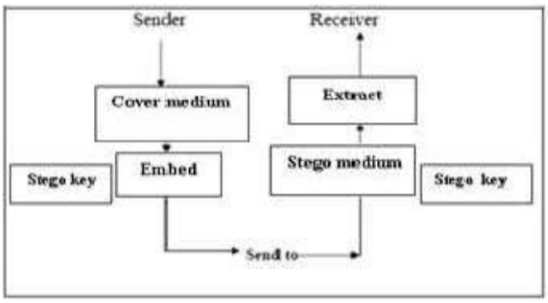

Fig 1: Steganography mechanism

Block Diagram Explanation

The above figure shows a simple representation of the generic embedding and extraction process in Steganography. In this example, a secret data is being embedded inside a cover image to produce the stego image. A key is often needed in the embedding process. The embedding procedure is done by the sender by using the proper stego key. The recipient can extract the stego cover image in order to view the secret data by using the same key used by the sender. The stego image should look almost identical to the cover image.

Steganography is the science of hiding information. Whereas the goal of cryptography is to make data unreadable by a third party, the goal of Steganography is to hide the data from a third party. In this article, I will discuss what Steganography is, what purposes it serves. The following formula provides a very generic description of the pieces of the Steganography process: cover_medium+hidden_data + stego_key = stego_medium

In this context, the cover_medium is the file in which we will hide the hidden_data, which may also be encrypted using the stego_key. The resultant file is the stego_medium (which will, of course. be the same type of file as the cover_medium). The cover_medium (and, thus, the stego_medium) are typically image or audio files. In this article, I will focus on image files and will, therefore, refer to the cover_image and stego_image. The simplest approach to hiding data within an image file is called least significant bit (LSB) insertion. In this method, we can take the binary representation of the hidden_data and overwrite the LSB of each byte within the cover_image. If we are using 24-bit color, the amount of change will be minimal and indiscernible to the human eye.

II. COMBINATION OF STEGANOGRAPHY AND CRYPTOGRAPHY AND THE WATERMARKING:

Steganography and cryptography are closely related. Cryptography [11] [6] scrambles messages so it can't be understood. Steganography on the other hand, hide the message so there is no knowledge of the existence of the message. With cryptography, comparison is made between portions of the plaintext and portions of the cipher text. In Steganography, comparisons may be made between the cover-media, the stego-media, and possible portions of the message. The end result in cryptography is the cipher text, while the end result in Steganography is the stego-media. The message in Steganography may or may not be encrypted. If it is encrypted, then a cryptanalysis technique is applied to extract the message. Those who seek the ultimate in private communication can combine encryption and Steganography. Encrypted data is more difficult to differentiate from naturally occurring phenomena than plain text is in the carrier medium. There are several tools by which we can encrypt data before hiding it in the chosen medium. In some situations, sending an encrypted message will across suspicion while an invisible message will not do so. Both methods can be combined to produce better protection of the message. In case, when the Steganography fails and the message can be detected, it is still of no use as it is encrypted using cryptography techniques.

III. LITRATURE SURVEY

A lot of research has been done in the field of image de-noising but yet the area of image de-noising, especially for the medical images remains to be a popular area of research. Stress has been laid to summarize the concept of different authors who has worked in this field

Sunil.K. Moon Rajshree.D.Raut (2013) [1] has proposed a scheme which is very important to us for studying the basic concept of Steganography. The author deals which Steganography using image file as a cover carrier. Image based Steganography can be used as one image file having separate images in frames. Since that the use of the image based Steganography can be more eligible than other multimedia files. This author is mainly concerned with how to embed data in a image file in from of bmp images and how we can make use of the internal structure of the image to hide data to be secured. The basic concept of this author which we have used in my research work and the second concept which has been implemented in our research work is how to use Steganography using image file as a cover carrier

Mr Ersin Esen, A. Aydin Alatan (2012) [19] purposed a Digital Image Watermarking Algorithm Based on DCT Domain. In order to solve the conflict with robustness and invisibility of image watermark, the algorithms proposed in this paper select certain blocks according to the texture. By using the binary image to deal with logistic chaotic map and error correction coding as watermarked data can improve the robustness and security. The low frequency

signals of the selected blocks are modified such that their Discrete Cosine Transform (DCT) fulfills a constraint imposed by the watermark code. Experiment results show that this algorithm provides a larger embedding capacity and has a certain robustness and invisibility. Digital image watermarking technology is one of the current research focuses, which has a broad prospect of application. At present, there are many scholars who put forward many image watermarking algorithms, and have their own advantages and deficiencies. In this paper, we introduce a new image watermarking scheme. Experiments show that this algorithm owns greater capacity, and has certain robustness in allowing range of image watermark's invisibility. Of course, there are still many unresolved issues, such as how to prevent lower quality after compressing, how to resist random attacks in real time request, and how to resist the frame attack. These are all the challenges to meet in the watermarking technology. We will give further research in these fields in the future.

Mr B. Subramanan (2011) [3] proposed an AES technique which presents fundamental mathematics behind the algorithm along with a brief description of some cryptographic primitives that are commonly used in the field of communication security. AES provides better security and has less implementation complexity. It has emerged as one of the strongest and the most efficient algorithm.

Mr A.K.Jain, P.Mohan Kumar and K.L.Shunmuganathan (2011) [13] proposed a techniques for the digital watermarking. According to him the retrieval can be faster if the query is made by multimodal keywords i.e. use of image as well as textual keywords. He used three MPEG-7 descriptors out of seven color descriptors in his experiment. He made the query in the form of a matrix by concatenating visual keywords and textual keywords.

Ms Punita Meelu (2011) [5] gave a different concept from above the authors using a new approach of hiding image in image. The algorithm is replaces 1 LSB of each pixel in image frame. It becomes very difficult for a intruder to guess that an image is hidden in the image as individual frame are difficult to analyze in a image running at 30 frame per second. We have seen that the author has used only 1 LSB substitution technique here. This is the basic concept of the author which is implemented in my research work.

Mr A.K. Al Frajat (2010) [6] presented a similar concept with stenography, is the art of communicating a message embedded it into multimedia data. It is desired to maximize the amount of hidden information while preserving security against detection by unauthorized parties. The image based stenography issues has been illustrated to hide secret information in images and the possibility of using the image as a cover carrier for hiding secure data

Mr Ali K Hmood (2010) [9] proposed an image encryption algorithm combining the image encryption based on S-boxes scrambling with error correcting code was developed. The error correcting code could effectively improve the security of image encryption algorithm based on S-boxes scrambling. The basic concept of this author which we have used in my work focuses on maximizing security, capacity factor of data hiding and secures the data through AES.

Mr Saurabh Singh (2010) [7] dealt with three main stenography challenges capacity imperceptibility and security. This is achieved by hybrid data hiding scheme in corporate LSB technique with a key permutation method. In my work I have implemented this basic concept of using LSB substitution and the ways to increase the system performance as well as its security.

Mr L.Rondney Long, M.Wu ,E. Tang and B.Liu (2010) [8] proposed in their paper the basics about the Steganography techniques. They suggested the features of an embedding message in the Steganography. Steganography is the art of hiding information and an effort to conceal the existence of the embedded information. It serves as a better way of securing message than cryptography which only conceals the content of the message not the existence of the message. Original message is being hidden within a carrier such that the changes so occurred in the carrier are not observable. In this paper we will discuss how digital images can be used as a carrier to hide messages. This paper also analyses the performance of some of the Steganography tools. Steganography is a useful tool that allows covert transmission of information over and over the communications channel. Combining secret image with the carrier image gives the hidden image. The hidden image is difficult to detect without retrieval. This paper will take an in-depth look at this technology by introducing the reader to various concepts of Steganography, a brief history of Steganography and a look at some of the Steganography technique.

Mr Niu Jiping (2008) [10] uses an algorithm based on AES expansion in which the encryption process is a bit wise exclusive or operation of a set of image pixels along with the 128 bit key, which changes for every set of pixel. The keys to be used are generated independently at the sender and receiver side based on AES key expansion

process. Hence the initial key is shared rather than scaring the whole set of keys. The author gives the information about AES. The AES is provides high encryption quality with minimum memory requirement and computational time.

Mr Liu bin, Li zhitang, Li Yao (2005) [12] presented Digital watermarking, the technology of embedding special information into multimedia data, is a topic that has recently gained increasing attention all over the world. The watermark of digital images, audio, image, and other media products in general has been proposed for resolving copyright ownership and verifying the integrity of content. The paper first introduced the definition and basic framework of watermark techniques, and then the basic theoretical and evaluation criteria are expatiated. Finally, the application field and possible research direction of digital watermark technology is pointed out. Nowadays due to the new technology and the communication network huge development, to enter the digital multimedia world easier and easy, it's easier to unauthorized copying and multimedia information of illegal spread, such as images, image and audio. Because the present digital watermarking technology is difficult to solve collusion against attacks of opportunity, and interpretation attack, make digital watermark in the copyright protection, access and copy control, digital fingerprints, and other aspects of the application by a limit, many researchers are working to address these issues. In addition, the watermarking algorithm design, lack the general framework of is instructive, if can put forward the feasible has guiding significance for the robustness of the watermarking model framework, will give watermarking algorithm design great convenience. Can foresee a digital watermark is used to protect the multimedia information will become a more and more popular in the world.

Mr Tao Zhang, Wenxiang Li, Yan Zhang, Xijian Ping (2005) [14] describe a method for integrating together cryptography and steganography through image processing. In particular, we present a system able to perform steganography and cryptography at the same time using images as cover objects for steganography and as keys for cryptography. We will show such system is an effective steganographic one and is also a theoretically unbreakable cryptographic one (demonstrating its equivalence to the Vernam Cipher).

Mr Fafael C.Gonzalez,Richard E.Woods Addison (1995) [17] proposed the use of Steganography. He also discussed the current status and future directions. He discussed the image features as color, texture, and shape in details. He also gives a summary of all the features with examples. For e.g. for texture there are texture co-occurrence, Fourier power spectrum, Gabor features and tamura features. He also discussed various similarity measures classifier-based, elastic deformation and graph matching.

IV. PROPOSED WORK

* To propose a new algorithm for transmitting the secret image over a network by combining the cryptography steganography & watermarking techniques.

* To implement the new algorithm on various Picture format like (JPG, PNG, TIFF, and Bmp) & video format like (mpeg, avi, flv)

* To evaluate the performance of proposed algorithm on the basis of parameters like (PSNR, MSE, EMBEDDING CAPACITY, SECURITY, RD %)

* To perform the comparison of above algorithm (Analysis of Secured Video Steganography Using Computer Forensics Technique for Enhance Data Security) with the existing algorithm (A Secure Image Based Steganography, Cryptography and Watermarking with security key) based on following parameters PSNR, MSE, Embedding capacity, SECURITY,RD%

V. CONCLUSION

In this paper, I have proposed the A Secure Image Based Steganography, Cryptography and Watermarking with security key using matlab technique which will combine all these technique results in better PSNR, MSE, Embedding capacity, security, RD% and the algorithm will work on major picture formats like Jpeg, Bmp also on major video formats like Mpeg, Avi, Flv. i.e the improved technique for database security with different picture and video formats which will qualify it to be a suitable for internet security.

REFERENCES

[1]. Sunil.K. Moon Rajshree.D.Raut "Analysis of Secured Video Steganography Using Computer Forensics Technique for Enhance Data Security" Proceedings of the 2013 IEEE Second International Conference on Image Information Processing (ICIIP-2013)

[2] Ersin Esen, A. Aydin Alatan: Comparison of Forbidden Zone Data Hiding and Quantization Index Modulation. Digital Signal Processing 22(1): 181-189 (2012)

[3]. B. Subramanan "Image encryption based on aes key expansion" in IEEE applied second international

conference on emerging application of information technology, 978-0-7695-4329-1/11, 2011.
[4]. Marghny Mohamed"Data hiding by LSB substitution using genetic optimal key permutation" in International arab journal of e-technology, vol.2, no 1,11-17, January 2011.
[5]. Punita Meelu "AES Asymmetric key cryptographic system" in international journal of information technology and knowledge management, volume 4, 113-117, 2011
[6].A.K. Al Frajat "Hiding data in image file An overview" Journal of applied sciences 10(15):1644-1649, 2010.
[7]. Saurabh singh "Hiding Image to Image" International Journal of engineering science & technology Vol. 2(12), 6999-7003, 2010.
[8]. L.Rondney Long, M.Wu ,E. Tang and B.Liu,"Data hiding in digital binary image ,"in IEEE ICME New York City, NY,USA ,July 2010.\
[9]. Ali K Hmood "An overview on hiding information technique in images" Journal of applied sciences 10(18)2094-2100, 2010
[10]. Niu Jiping "Image encryption algorithm based on rijndael S-boxes" in IEEE applied International conference on computational intelligence and security 978-0-7695-3508-1\08, 2008.
[11] Z.Zhou, G.R.Arce, and G.Di Crescenzo, "Halftone Visual Cryptography", IEEE Tans. On Image Processing,vol.15, No.8, August 2006, pp. 2441-2453.
[12. Liu bin, Li zhitang, Li Yao an Image method based on correlation analysis and image fusion "International conference on parallel and distributed computing, Application and technology 0-7695-2405-2/05 ,2005.
[13]. A.K.Jain, P.Mohan Kumar and K.L.Shunmuganathan "A New approach for hiding data in images using image domain method" in International Journal of computer and internet security ISSN 0974-2247 volume 3 ,number PP 69-80, 2005
[14] Tao Zhang, Wenxiang Li, Yan Zhang, Xijian Ping" Detection of LSB Matching Steganography Based on Distribution of Pixel Differences in Natural Images"(2005)
[15] Fridrich , J ., Goljan M., and Hogea , D ; New Methodology for Breaking Steganography Techniques for JPEGs. "Electronic Imaging 2003".
[16] Katzenbeisser and Petitcolas , "Information Hiding Techniques for Stenography and Digital watermaking" Artech House, Norwood, MA. 2000.
[17]. by Fafael C.Gonzalez,Richard E.Woods Addison, J.L. Rodgers, J. L. and W.A. Nicewander, "Thirteen Ways to Look at the Correlation Coefficient", American Statistician 42, 59-66, 1995.
[18] Robert Ulichney, "The void-and-cluster method for dither array generation", IS&T/SPIE Symposium on Electronic Imaging and Science, San Jose, CA, 1993, vol.1913, pp.332-343.
[19]. F. A. P. Petitcolas, R. J. Anderson, and M. G. Kuhn, "Information hiding – A survey,"Proceedings of IEEE, Vol. 87, 1999, pp. 1062-1078.

Current Emerging trends in Wire EDM: A Review

Sandeep Yadav[a], Saurabh Sharma[a], Shiv Ohri[a], Saurabh Poddar[a] & Anmol Bhatia[b]

[a] *B.Tech Students, Department of Mechanical Engineering, ITM University,Sector-23A Gurgaon, India*

[b] *Assistant Professor, Department of Mechanical Engineering, ITM University,Sector-23 A Gurgaon, India*

***Abstract*— This paper presents a review on the research trends in WEDM which deals with the relation between different process parameters such as pulse on time, pulse off time, peak current, flow rate of dielectric, wire tension etc on different process responses viz surface roughness (Ra), material removal rate (MRR), Kerf width, wire lag and Cutting speed. The paper also gives conclusions & recommendations about the trends for future WEDM researches.**

***Keywords*—**Wire Electric Discharge Machining (WEDM), Surface roughness, Material Removal Rate, Kerf width

I. INTRODUCTION

Wire EDM is defined as a technique of thermal Welectrical erosion in which material is worn away by the sequence of sparks between the work piece and the wire electrode which is a good conductor of electricity[1].WEDM is identical to isopleths cutting with a band saw a slow speed wire moves along a defined path. In this process there is no communication between the work piece and the electrode and the material of any hardness can be used, so it is used to cut plate of thickness around 300mm [2].In WEDM, wire does not touch the work piece, so hence no pressure is exerted on the component and a negligible pressure is used for clamping to hold the workpiece [1].The array of modern wire EDM machines are automatic control of the cutting path of the wire. Huge sparks can be seen at a time this is because real discharge can take place about 100 thousand times.[3]The temperature of heat of electrical discharge is about 8315 to 11093 Celsius[2].The application of Wire EDM is Aerospace, Nuclear and Automobile industries [3].

II. WIRE EDM PARAMETERS

A. Pulse On/Off time

During electric discharge machining process there are start and stop intervals known as ON time and OFF time. The machining is performed during the pulse ON time when in the gap between work piece and electrode the voltage is applied. Alternatively the time during which no voltage is applied is the pulse off time. A greater value of On time is selected to obtain a long duration of electric discharge to increase the material removal rate but also leads to poor surface finish. During the pulse off time re-ionization of dielectric occurs and it is also essential to avoid any short circuit leading to wire breakages.

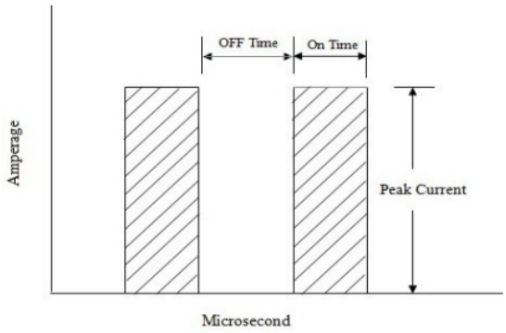

Fig. 1 Pulse on & off time

B. Peak Current & Gap Voltage

In WEDM, the most important machining parameter is the peak current. Measured in unit of amperage it is basically the amount of power used in WEDM. Peak current is the preset level reached by the increasing current during each pulse on-time.

In both processes, die sinking and wire-EDM, the surface area of cut governs the maximum amount of amperage. In roughing operations and in cavities or details with large surface areas, a higher amperage is used.

The supply voltage to be placed on the gap is expressed as the gap voltage or open circuit voltage. The electric discharge energy is directly proportional to this value i.e. greater the gap voltage value greater is the electric discharge energy. Moreover gap voltage and peak current are also dependent and peak current increases with the increase in gap voltage. In some WEDM machines machining voltage is shown by both of these factors.

C. Servo Voltage & Servo Feed

For controlling the advances and retracts of the wire a servo voltage is used. Depending on the state of machining between the work piece and electrode the mean machining voltage is varied. The reference voltage for governing the advances and retracts of the wire is established using the servo voltage.

The wire advances when the mean machining voltage is greater than the set voltage and retracts if it is lower. A superior value of servo voltage will lead to widening of gap between electrode and work piece. The number of electric sparks also decreases thus steadying the electric discharge albeit the machining rate slows down. For a smaller value of servo voltage the mean gap gets

attenuated which results in rise in number of electric sparks. It speeds up the process but may also result in wire breakage as it gets unstable.

The feed rate of table during machining is detailed by the servo feed rate. Normally this factor is selected automatically by the WEDM machines in accordance with the servo voltage but it can also be controlled manually. In such a case the machining table will have a constant speed with no remark of servo voltage.

Overall the feed rate can be altered by both servo voltage and servo feed rate.

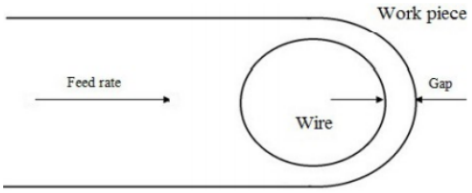

Fig. 2. Feed rate & gap size [20]

D. *Dielectric flow rate*

Electro discharge which occurs in the air can't be used for rough cut machining as it is not stable. Thus, in order to have stable electric discharge, dielectric fluid is required. Electric discharge machining can be stabilized, within the dielectric fluid, with efficient cooling and chip removal. Because of its environmental friendly characteristic, typically the de-ionized water is used as a dielectric in wire EDM. For example in Titanium alloy material, due to low thermal conductivity, high flushing pressure is completely necessary for rough machining , otherwise wire breakage will be caused by the short circuit phenomenon.

E. *Wire speed & Wire Feed*

In WEDM the speed of the wire is given by wire speed. With the increase in wire speed both the wire consumption as well as machining cost increases. On the opposite side a low wire speed can lead to wire breakage in high cutting speed.

F. *Wire tension*

In WEDM the tension of wire is disciplined by the wire tension. For the wire to remain straight the wire tension should be sufficiently high or the wire will sway behind.

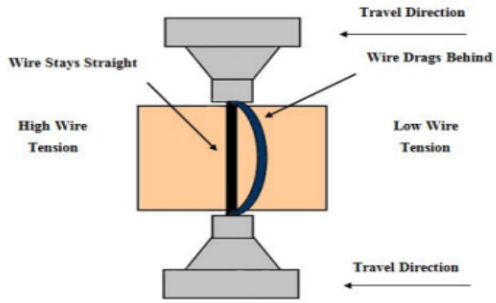

Fig. 3 Wire drag & wire tension

III. TYPES OF WIRES AS TOOL

The main problem that arose when wire EDM was first introduced was wire material as this material should possess lots of properties, the key properties include, *Conductivity.* A high conductivity rating means the wire can carry more current which in turn means to a 'hotter' spark and increased cutting speed. *Tensile Strength,* which is the ability of the wire to withstand the wire tension, imposed upon the wire in order to make a vertically straight cut during cutting. *Elongation,* which describes how much the wire plastically deforms just before the breakage. *Melting Point*,it is preferred to have the wire electrode be resistant to being melted too quickly by electric sparks. *Straightness*, is the property which helps the wire to stay straight. *Flush ability*, a better flush ability will result in the faster cutting of the wire and also helps in decreasing the chance of wire breakage. *Cleanliness,* the wire should be clean from the contamination by residual metal powder left over from drawing process, drawing lubricant, or paraffin added to wire prior to spooling by some manufacturers.

A. *Copper*

Copper: it was the inceptive material used in wire EDM. In spite of its excellent conductivity its potential is severely restrained due to its low tensile strength, low vapour pressure and high melting point. Now a days it's confined to older machines which have power supplies designed for copper wire.

B. *Brass*

Brass was the first alternative to copper. It is an alloy of copper and zinc with 63-65% Cu and 35-37% Zn. A higher tensile strength, lower melting point and higher vapor pressure rating is provided by the addition of zinc, which reduces the losses in conductivity. It is most widely used electrode material for general purposes and is available in a wide range of tensile strengths and hardness.

C. *Coated Wires*

The inefficient fabrication of brass wires with any higher concentration of zinc led to the development of coated wires or stratified wires. These wires have a core of brass or copper and are electroplated with pure or diffused zinc. The brass or copper core enhances conductivity and tensile strength and the coating of zinc enhances the spark formation and flush characteristics. Coated wire are also referred as speed wires due to their potential to cut at notably higher metal removal rates. The coated wires are best suited for all-round performance despite their high cost when compared to copper and brass.

D. *Fine wires*

These include the wires with diameters in the range of 0.006-0.012 inches. High precision work requiring small

inside radii is done by wires with diameters in range of 0.001-0.004 inches. Molybdenum and tungsten wires are used as brass and coated wires have low load carrying capacity in these sizes and hence are not practical. However they are not suitable for very thick work and tend to cut slowly due to the limited conductivity, high melting points and low vapor pressure ratings. Only a few scientific works have been dealing with cutting by wires with a diameter below 50µm.The wire materials are brass coated steel wire and tungsten having high tensile strength and melting temperatures.

IV. LITERATURE REVIEW

Dharmendra et al [4] found out the main parameters which are average cutting speed and surface roughness which affect the different machining criteria. They studied the trend of variation of these important machining criteria with four control factors which has been studied simultaneously to establish the trend of variation.

Bijendra Diwakar et al [5] analyzed that metal removal rate is most affected by pulse frequency as and predicted optimal parameter setting with the help of Taguchi's approach.

Scott F. Miller et al [6] investigated the effects of pulse on time and spark cycle on micro features with the help of wire EDM. They studied the uses of low MRR EDM cutting for complaint mechanisms and machining of thin sections. They further utilized the findings of EDM surface, subsurface, Debris from SEM micrograph.

Kamal Jangra et al [7]proposed a methodology to evaluate the machinability in terms of metal removal rate of tungsten carbide which is based on diagraph and matrix method. It was further investigated that other machining performances such as surface finish, dimensional precision, cutting forces, tool life etc. also determine the machinability.

Y.s Liao et al [8]proposed for fault diagnosis and the maintenance schedule of wire EDM a prototype ANN based expert system which is a powerful developmental tool for a complicated system such Wire EDM.

Satyaveer Singh et al [9] experimentally investigated the effects of pulse on time, pulse off time and peak current in machining of HSLA steel by utilizing WEDM process by taking into account Taguchi method. It was also demonstrated in this paper that Taguchi method is very effective in optimizing machining parameters while carrying out minimum number of experiments.

Neeraj Nirmal et al [10] concluded that both pulse duration and charge current can be utilized in order to enhance surface roughness by reducing the above parameters. It can be shown that by combining high peak value with a short pulse duration gives out a better surface roughness which is unachievable by using long pulses.

Maringostimirovic et al [11] by effectively carrying out analytical and experimental investigation suggested that metal removal rate is increased by the increasing discharge energy and the surface roughness is also directly proportional to discharge energy and hence uniform increase of surface roughness can be achieved by increasing discharge power and discharge duration by effectively carrying out analytical and experimental investigation.

J.T. Huang et al [12] with the assistance of taguchi quality design, ANOVA and F-test identified current limiting resistance, machine voltage, type of pulse generating circuit and capacitance as the significance parameters affecting the surface roughness. They also analyzed that in order to have good surface roughness traditional circuit utilizing low power for ignition is modified for machining.

Goswami Amitesh et al [13] summarized that cutting speed can be increased by increasing the peak current and is inversely proportional to pulse of time spark gap set voltage and same is the case with material removal rate.

Saeed Daneshmand et al [14] studied the capabilities of NiTi60 and investigated the effect of input parameters such as wire speed, pulse current and pulse on time on MRR and surface roughness. It was also inferred that surface roughness increases rapidly with the increase in machining speed resulting from the increase in power.

S.Sivanaga et al [15] summarized the effect of various process parameters like discharge current, job thickness etc. on machining parameters like cutting speed, spark gap and material removal rate. Optimal cutting time, machining cost and cutting accuracy for any job size were estimated using mathematical relations. An error of less than 2% was observed between the calculated and experimental values.

Gautam kocher et al [16] made an observation that for WEDM machining of D3 tool steel good surface finish was obtained using copper tungsten electrode in place of cooper and graphite electrodes. For roughing graphite electrode is used while for semi finishing process copper electrode is preferred. It was found that for final finishing process copper tungsten electrode is the best giving good surface finish.

Basil Kuriachen et al [17] showed that the pulse time, dielectric pressure, voltage pulse interactions on time are some important parameters affecting surface roughness. Further it was shown that by adopting a high value of dielectric pressure (15 kgf/cm^2) and a low value of pulse on time (20 µs) minimum surface roughness can be achieved. The marginal error in the comparison of conformation test with the predicted results was found to be 7%.

S. B. Prajapati et al [18] concluded that pulse ON and pulse OFF time are the most significant factors for determining the surface roughness and cutting rate. The spark gape set voltage was found to be significant for kerf and high confidence was indicated by all the probability distribution measurements.

Pankaj Agrawal et al [19] made the observations that with the increase of peak current the surface roughness increases. Further it was reported that with the increase of peak current the MRR of tungsten carbide increased for

short pulse duration. For high electrical energy micro cracks were exhibited on the machined surface.

V. CONCLUSION

Wire EDM is a thermal metal removal process that can produce complicated parts which cannot be machined by conventional machining processes. There is a need to optimize the process parameters of WEDM because it is costly & widely acceptable method. Many researchers have suggested various methods to optimize parameters thereby increasing the metal removal rate & lowering surface roughness. But still there is difficulty in selecting wire EDM parameters. After reviewing the literature it is found that more research needs to be done on comparision of different wire types on response characteristics. More research can further improve the contouring process. Additionally,there is no information about dry Wire EDM process.Mostly, GA is used for optimization,some other optimization method can also enhance the process capabilities.

Finally,more research on this process can further increase productivity,accuracy & efficiency of the process.

REFERENCES

[1] Kalpakjian ,*Manufacturing Engineering & Technology*, Addison wesely publication, 1995

[2] P N Rao, *Manufacturing Technology*, Tata McGraw Hills issue 2000.

[3] Roya Lindberg ,*Processes And Materials of Manufacturing*, Prentice Hall of India PVT LTD issue 2005.

[4] Dharmender, Rajeev Kumar and Anmol Bhatia, "Investigation of the effect of Process Parameters on Surface Roughness in Wire Electric Discharge of En31 Tool Steel", *Proceedings of the National Conference on Trends and Advances in Mechanical Engineering, YMCA University of Science & Technology, Faridabad, Haryana*, Oct 19-20, 2012.

[5] Bijendra Diwakar, Vedansh Chaturvedi and Jyoti Vimal , "Application of Taguchi approach for optimization of CNC wire electrical discharge machining process parameters" , *IJREAS Volume 2, Issue 7 (July 2012)* ISSN: 2249-3905.

[6] Scott F. Miller, Chen-C. Kao, Albert J. Shih, Jun Qu," Investigation of wire electrical discharge machining of thin cross-sections and compliant mechanisms", *International Journal of Machine Tools & Manufacture* 45 (2005) 1717–1725.

[7] Kamal Jangra, Sandeep Grover , Felix T. S. Chan and Aman Aggarwal," Digraph and matrix method to evaluate the machinability of tungsten carbide composite with wire EDM", *Int J Adv Manuf Technol* (2011) 56:959–974 ,DOI 10.1007/s00170-011-3234-5.

[8] J. T. HUANG and Y. S. LIAO," A wire-EDM maintenance and fault-diagnosis expert system integrated with an artificial neural network", *int. J. Prod. Res*., 2000, VOL. 38, NO. 5, 1071- 1082.

[9] Noor Zaman Khan, Mohd Atif Wahid, Satyaveer Singh, Arshad NoorSiddiquee and Zahid A. Khan," A study on micro hardness in wire electrical discharge machining based on taguchi method", *International Journal of Mechanical and Production Engineering* , Volume – 1, Issue – 1, 2013.

[10] Sorabh, Manoj Kumar and Neeraj Nirmal, "A literature review on optimizationof machining parameters in wire EDM",*International Journal of Latest Research in Science and Technology*, Volume 2,Issue 1 :Page No.492-494 , January-February (2013).

[11] Marin Gostimirovic, Pavel Kovac, MilenkoSekulic and BrankoSkoric," Influence of discharge energy on machining characteristics in EDM", *Journal of Mechanical Science and Technology* 26 (1) (2012) 173~179

[12] J.T. Huang, Y.S. Liao and Y.H. Chen," A Study to Achieve a Fine Surface Finish in Wire-EDM", *Journal of Materials Processing Technology* 149 (2004) 165–171.

[13] Goswami Amitesh, Kumar Jatinder," An investigation into the machiningcharacteristics of nimonic 80a using cnc wire EDM", *International Journal of Advanced Engineering Technology* E-ISSN 0976-3945.

[14] Saeed Daneshmand, Reza Hessami, Habib Esfandiar," Investigation of Wire Electro Discharge Machining of Nickel-Titanium Shape Memory Alloys on Surface Roughness and MRR", *Life Science Journal* 2012;9(4).

[15] S.SivanagaMalleswaraRao, Ch.V.S. ParameswaraRao," Parametric Evaluation for Machining Die-Steel with WEDM," *International Journal of Scientific and Research Publications*, Volume 3, Issue 4, April 2013,ISSN 2250-3153.

[16] Gautamkocher, Karan Chopra, Sandeep Kumar,"Investigation of Surface integrity of AISI D3 tool steel After EDM," *International Journal of Emerging Technology and Advanced Engineering* ISSN 2250-2459, Volume 2, Issue 4, April 2012.

[17] Basil Kuriachen, Dr. Josephkunju Paul, Dr.JoseMathew," Modeling of Wire Electrical Discharge Machining Parameters Using Titanium Alloy (Ti-6AL-4V)," *International Journal of Emerging Technology and Advanced Engineering,* ISSN 2250-2459, Volume 2, Issue 4, April 2012.

[18] S. B. Prajapati, N. S. Patel,"Effect of Process Parameters on Performance Measures of Wire EDM for AISI A2 Tool Steel,"*International Journal of Computational Engineering Research*||Vol, 03||Issue, 4||.

[19] Pankaj Agrawal, Ashish Manoria, Richa Thakur and Hemant Jain," *advancement in micro-manufacturing using medm and its applications*," ISSN 2278-0149, Vol.1, No.2, July 2012.

[20] Roger Kern, 2008. *EDM Today magazine*, March/April Issue.

Comparison of the accidents at Chernobyl and Fukushima Dai-ichi Nuclear Power Stations

Iqbal Preet Kaur
Department of Physics,DAV College,Chandigarh,India

***Abstract*-The Chernobyl and the Fukushima Dai-ichi Nuclear disasters have put a question mark on the process of replacing the fossil fuel based power plants with the nuclear power plants.The current paper studies the progression of the accidents at Chernobyl and Fukushima Dai-ichi Nuclear Power Stations.It also compares the two accidents in terms of the radioactive elements released, people evacuated,current status,long term health effects etc. In almost every respect, the consequences of the Chernobyl accident clearly exceeded those of the Fukushima accident. In both accidents, most of the radioactivity released was due to volatile radionuclides (noble gases, iodine, cesium, tellurium).For Chernobyl, a total release of 5300 PBq (excluding noble gases) has been established as the most cited source term. For Fukushima, we estimated a total source term of 520 (340–800) PBq. In the course of the Fukushima accident, the majority of the radionuclides (more than 80%) was transported offshore and deposited in the Pacific Ocean.**

***Keywords*-** Accident, Chernobyl, Comparison, Fukushima

I.INTRODUCTION

The Chernobyl Nuclear Power Plant Accident occurred on 26th April 1986 in Ukraine. The accident took place when a low-power engineering test of the Unit 4 reactor was being conducted.It caused widespread damage due to release of radionuclides in the environment.The Fukushima Dai-ichi Nuclear Power Station Accident occurred on 11th March 2011 when a magnitude 9 earthquake and a tsunami hit the Nuclear Plant causing extensive damage to the power station.The present paper compares the two accidents .

II.THE ACCIDENT AT CHERNOBYL NUCLEAR POWER STATION

The accident at the Chernobyl nuclear power station occurred when a low-power engineering test of the Unit 4 reactor was being conducted .The Chernobyl reactor was of the type RBMK ,which is an abbreviation of Russian terms meaning reactor of high output ,multi channel type. It is a pressurized water reactor which uses light water as a coolant and graphite as a moderator. The events leading to the accident at the Chernobyl Unit4 reactor at about1.24 a.m. on 26April1986 resulted from efforts to conduct a test on an electric control system, which allows power to be provided in the event of a station blackout[1].Actions taken during this exercise resulted in a significant variation in the temperature and flow rate of the inlet water to the reactor core(beginning at about1.03a.m.).The unstable state of the reactor before the accident is due to two factors :1. basic engineering deficiencies(such as graphite-tipped control rods, instability at low power levels and large positive coefficient of reactivity under certain conditions) 2. faulty actions of the operators (e.g., switching off the emergency safety systems of the reactor)[2].The relatively fast temperature changes resulting from the operators' actions weakened the lower transition joints that link the zirconium fuel channels in the core to the steel pipes that carry the inlet cooling water[3].Other actions resulted in a rapid increase in the power level of the reactor [4], which caused fuel fragmentation and the rapid transfer of heat from these fuel fragments to the coolant (between 1.23:43 and 1.23:49a.m.) . This caused the generation of a shockwave in the cooling water, which led to the failure of most of the lower transition joints. As a result of the failure of these transition joints, the pressurized cooling water in the primary system was released, and it immediately flashed into steam. The steam explosion occurred at1.23:49. It is believed that the reactor core might have been lifted up by the explosion [3], during which time all water left the reactor core. This resulted in an extremely rapid increase in reactivity, which led to vaporization of part of the fuel at the centre of some fuel assemblies and which was terminated by a large explosion attributable to rapid expansion of the fuel vapour disassembling the core. This explosion, which occurred at about1.24a.m.,blew the core apart and destroyed most of the building. Fuel, core components, and other structural items were blown from the reactor hall onto the roof of adjacent buildings and the ground around the reactor building. A major release of radioactive materials into the environment also occurred as a result of this explosion. The core debris dispersed by the explosion started multiple (more than 30) fires on the roofs of the reactor building and the machine hall, which were covered with highly flammable tar. Some of those fires spread to the machine hall and, through cable tubes, to the vicinity of the Unit3 reactor. A first group of 14 firemen arrived on the scene of the accident at1.28a.m.

Reinforcements were brought in until about 4a.m., when 250 firemen were available and 69 firemen participated in fire control activities. These activities were carried out at upto 70m above the ground under harsh conditions of high radiation levels and dense smoke. By 2.10a.m., the largest fires on the roof of the machine hall had been put out, while by 2.30 a.m. the largest fires on the roof of the reactor hall were under control .By about 4.50a.m. ,most of the fires had been extinguished. These actions caused the deaths of five fire fighters.It is unclear whether fires were originating from the reactor cavity during the first 20 h after the explosion. However, there was considerable steam and water because of the actions of both the fire fighters and the reactor plant personnel. Approximately 20h after the explosion, at9.41 p.m.,a large fire started as the material in the reactor became hot enough to ignite combustible gases released from the disrupted core, e.g. hydrogen from zirconium-water reactions and carbon monoxide from the reaction of hot graphite with steam. The fire made noise when it started (some witnesses called it an explosion) and burned with a large flame that initially reached at least 50m above the top of the destroyed reactor hall[3].The first measures taken to control the fire and the radionuclide releases consisted of dumping neutron-absorbing compounds and fire-control materials into the crater formed by the destruction of the reactor.The total amount of materials dumped on the reactor was approximately 5,000t , including about 40 t of boron compounds, 2,400 t of lead, 1,800 t of sand and clay, and 600 t of dolomite, as well as sodium phosphate and polymer liquids[10].About 150t of materials were dumped on 27 April, followed by 300 t on 28 April, 750 t on29 April, 1,500 t on 30 April, 1,900 t on1 May, and 400 t on 2 May.About1,800 helicopter flights were carried out to dump materials onto the reactor. During the first flights, the helicopters remained stationary over the reactor while dumping the materials .However, as the dose rates received by the helicopter pilots during this procedure were judged to be too high, it was decided that the materials should be dumped while the helicopters travelled over the reactor. This procedure , which had a poor accuracy, caused additional destruction of the standing structures and spread the contamination. The radionuclide releases from the damaged reactor occurred mainly over a10-day period, but with varying release rates. An initial high release rate on the first day was caused by mechanical discharge as a result of the explosions in the reactor. There followed a five-day period of declining releases associated with the hot air and fumes from the burning graphite core material. In the next few days, the release rate of radionuclides increased until day 10, when the releases dropped abruptly, thus ending the period of intense release. The increasing release rates on days 7 through 10 were associated with the rising temperature of the fuel in the core. Cooling of the reactor structure with liquid nitrogen using pipelines originating from Unit3 was initiated only at late stages after the accident. The abrupt ending of the releases was said to occur upon extinguishing the fire and through transformation of the fission products into more chemically stable compounds [2]. Table I gives radionuclide inventory in Unit 4 reactor core at time of the accident on 26 April 1986[2].

Table I

Radionuclide	Halflife	Activity(PBq) Estimates by [11]	Activity (PBq) Estimates by [1]
^{3}H	12.3a*	1.4	
^{14}C	5730a	0.1	
^{85}Kr	10.72a	28	
^{89}Sr	50.5d*	3960	
^{90}Sr	29.12a	230	220
^{95}Zr	64.0d	5850	
^{95}Nb	35d	5660	
^{99}Mo	2.75d	6110	
^{103}Ru	39.3d	3770	
^{106}Ru	368d	860	850
^{110}Ag	250d	1.3	
^{125}Sb	2.77a	15	
^{129}Te	33.6d	1040	
^{132}Te	3.26d	4480	4200
^{129}I	15700000a	0.000081	
^{131}I	8.04d	3080	3200
^{132}I	2.3h*	4480	4200
^{133}I	20.8h	6700	4800
^{134}I	52.6min*		2050
^{135}I	6.61h		2900
^{133}Xe	5.25d	6510	
^{134}Cs	2.06a	170	150
^{136}Cs	13.1d	110	
^{137}Cs	30.0a	260	260
^{138}Cs	32.2min	6550	
^{140}Ba	12.7d	6070	
^{140}La	40.3h	6070	
^{141}Ce	32.5d	5550	
^{144}Ce	284d	3920	3920
^{147}Nd	11.0d	2160	
^{154}Eu	8.6a	14	
^{235}U	704000000a	0.000096	
^{236}U	23400000a	0.0085	
^{238}U	4470000000a	0.0023	
^{237}Np	2140000a	0.00026	

239Np	2.36d	58,100	58100

*a-years,d-days,min-minutes,h-hours

III.GROUND CONTAMINATION IN EUROPE

Table II gives contaminated areas in European countries following the accident contaminated areas are defined as areas where the average ^{137}Cs deposition densities exceeded 37kBqm^2 (1 Cikm^2). [2].

Table II

Country	Area in deposition density ranges (km2)				
	37-185kBqm^{-2}	185-555kBqm^{-2}	555-1480kBqm^{-2}	>1480kBqm^{-2}	
Russian Federation	49800	5700	2100	300	
Belarus	29900	10200	4200	2200	
Ukraine	37200	3200	900	600	
Sweden	12000				
Finland	11500				
Austria	8600				
Norway	5200				
Bulgaria	4800				
Switzerland	1300				
Greece	1200				
Slovenia	300				
italy	300				
Republic of Moldova	60				

IV.ACCIDENT AT FUKUSHIMA-DAI-ICHI NUCLEAR PLANT

The Great East Japan Earthquake on 11 March 2011, a magnitude 9 earthquake, generated a series of large tsunami waves that struck the east coast of Japan, the highest being 38.9 m at Aneyoshi, Miyako[5]. Several nuclear power facilities were affected by the severe ground motions and large multiple tsunami waves including TEPCO`s Fukushima Dai-ichi. The operational units at this facility were successfully shutdown by the automatic systems installed as part of the design of the nuclear power plants to detect earthquakes. However, the large tsunami waves caused serious consequences at Fukushima Dai-ichi. Although all off-site power was lost when the earthquake occurred, the automatic systems at Fukushima Dai-ichi successfully inserted all the control rods into its three operational reactors upon detection of the earthquake, and all available emergency diesel generator power systems were in operation, as designed. The first of a series of large tsunami waves reached the Fukushima Dai-ichi site about 46 minutes after the earthquake. These tsunami waves overwhelmed the defences of the Fukushima Dai-ichi facility, which were only designed to withstand tsunami waves of a maximum of 5.7 m high. The larger waves that impacted this facility on that day were estimated to be over14 m high. The tsunami waves reached areas deep within the units, causing the loss of all power sources except for one emergency diesel generator (6B), with no other significant power source available on or off the site, and little hope of outside assistance. The station blackout at Fukushima Dai-ichi and the impact of the tsunami caused the loss of all instrumentation and control systems at reactors 1–4, with emergency diesel 6B providing emergency power to be shared between Units 5 and 6. The tsunami and associated large debris caused widespread destruction of many buildings, doors, roads, tanks and other site infrastructure at Fukushima Dai-ichi, including loss of heat sinks. The operators were faced with a catastrophic, unprecedented emergency scenario with no power, reactor control or instrumentation, and in addition, severely affected communications systems both within and external to the site[6]. They had to work in darkness with almost no instrumentation and control systems to secure the safety of six reactors, six nuclear fuel pools, a common fuel pool and dry cask storage facilities. With no means to confirm the parameters of the plant or cool the reactor units, the three reactor units at Fukushima Dai-ichi that were operational up to the time of the earthquake quickly heated up due to the usual reactor decay heating. Despite the brave and sometimes novel attempts of the operational staff to restore control and cool the reactors and spent fuel, there was severe damage to the fuel and a series of explosions occurred. These explosions caused further destruction at the site, making the scene faced by the operators even more demanding and dangerous. Moreover, radiological contamination spread into the environment (TableIII). These events are provisionally determined to be of the highest rating on the International Nuclear Event Scale.

Table III-Estimated amount of radionuclide released into the air due due to the accident

	Released Amount (PBq)*			
	Rare Gas	^{131}I	^{134}Cs	^{137}Cs
TEPCO	About 500	About 500	About 10	About 10
JAEA Nuclear Safety Commission 12th April 2011		150		13
NISA (Nuclear and Industrial Safety Agency) 12th April 2011		130		6.1
IRSN(Institut de Radioprotection et de Surete Nucleaire)	2000	200		
Accident at Chernobyl Nuclear Power Plant[1]	6500	1800		85

V.COMPARISON OF FUKUSHIMA AND CHERNOBYL NUCLEAR DISASTERS

Table IV-Comparison of Fukushima and Chernobyl Nuclear Disaster

Date of accident	Fukushima	11 March 2011
	Chernobyl	26 April,1986
Accident details	Fukushima	A magnitude-9.0 earthquake and resulting tsunami damaged the plant's power systems
	Chernobyl	A sudden power output surge during a systems test caused a reactor vessel to rupture
Severity rating	Fukushima	Level 7 - major accident
	Chernobyl	Level 7 - major accident
Number of reactors	Fukushima	Six; but only three of concern, plus pools storing spent fuel
	Chernobyl	Four; but only one reactor involved
Type of reactors	Fukushima	Boiling-water reactors
	Chernobyl	Graphite-moderated boiling water reactor
Containment	Fukushima	Containment remains intact
	Chernobyl	No containment to stop the trajectory of radioactive materials into the air
Area affected	Fukushima	Officials say areas extending more than 60km (36 miles) to the north-west of the plant and about 40km to the south-southwest have seen radiation levels exceed annual limits
	Chernobyl	Contamination of an area as far as 500 km (300 miles) from the plant, according to the UN. But animals and plants were also affected much further away9Table II[I]
Evacuation zone	Fukushima	20km; 20-30km voluntary zone
	Chernobyl	30km
People evacuated	Fukushima	Tens of thousands
	Chernobyl	The authorities evacuated, in 1986, about 115,000 people from areas surrounding the reactor and subsequently relocated, after 1986, about 220,000 people from Belarus, the Russian Federation and Ukraine
Related deaths	Fukushima	No deaths so far due to radiation
	Chernobyl	A UN report places the total confirmed deaths from radiation at 64 as of 2008.
Long-term health damage	Fukushima	Not yet known, but risks to human health are thought to be low
	Chernobyl	Among the residents of Belarus, the Russian Federation and Ukraine, there had been up to the year 2005 more than 6,000 cases of thyroid cancer reported in children and adolescents who were exposed at the time of the accident, and more cases can be expected during

		the next decades
Current status	Fukushima	Engineers have brought the plant to a "cold shutdown condition", a key milestone in bringing it under control. It will take decades to dismantle it completely however.
	Chernobyl	The damaged reactor is now encased in a concrete shell. A new containment structure is due to be completed by 2015

VI.CONCLUSION

Both the accidents occurred due to a shoddy accident management plans.Monitoring campaigns after both accidents reveal that the environmental impact of the Chernobyl accident was much greater than of the Fukushima accident. Both the highly contaminated areas and the evacuated areas are smaller around Fukushima and the projected health effects in Japan are significantly lower than after the Chernobyl accident. This is mainly due to the fact that food safety campaigns and evacuations worked quickly and efficiently after the Fukushima accident. In contrast to Chernobyl, no fatalities due to acute radiation effects occurred in Fukushima.

REFERENCES

[1] Kaur,Iqbal Preet.A Study Of Physical Consequences of the Chernobyl Nuclear Disaster in Ukraine. Published in Bulletin of The Indian Association of Physics Teachers, Volume-6, Number 2, February 2014, ISSN 2277-8950 and Presentation at Third International Geo-Hazards Research Symposium, Tehri Garhwal, June 2012.

[2] United Nations. Exposures and effects of the Chernobyl Accident,Annex J to Volume II of the United Nations Scientific Committee on the Effects of Atomic Radiation , 2000 Report to the General Assembly (2000).

[3] Purvis,E.E. III . The Chernobyl 4 accident sequence: update -April1995. Report of the Ukrainian Academy of Sciences , Intersectorial Scientific and Technical Center (ISTC) "UKRYTIE". Kiev (1995).

[4] International Atomic Energy Agency .The Chernobyl accident: updating of INSAG-1 .Safety Series No.75-INSAG-7.IAEA, Vienna (1992).

[5] The Accident at TEPCO's Fukushima Nuclear Power Stations .Report presented by The Japanese Government to the IAEA Ministerial Conference on Nuclear Safety, Vienna, June 20,2011 .

[6]Kaur,Iqbal Preet .The study of Events leading to Fukushima Dai-ichi Nuclear Disaster and the Measures that Would have Prevented it. Presentation at 14th International Conference of International Academy of Physical Sciences, Jabalpur, March 2014.

Corrosion Mechanism Study in Waste-To-Energy Plants

Harminder Singh
Guru Nanak Dev University, Regional Campus, Jalandhar, Punjab, India
harminder10@gmail.com +91-9914405782

***Abstract*— The waste-to-energy (WTE) plants are running at very low efficiency. The main reason is the hot corrosion failure of the heat transfer tubes in the plants. The corrosion problem in these plants is very complex due to heterogeneous nature of the fuel used in these plants. The fuel used in these plants is the waste which is usually dumped in the rivers and in land. In this study efforts are made to study the complex corrosion mechanism in these plants.**

***Keywords*— Hot Corrosion, WTE, Chlorine**

I. INTRODUCTION

Due to shortage to electricity worldwide and especially in developing countries like in India, there is need to install the waste-to-energy (WTE) plants. These plants use the waste as fuel to generate heat in controlled condition. This heat can be further recovered to generate power (electricity). But the waste which is used as fuel is heterogeneous in nature. It is not selected possible to select the fuel of these plants. These plants are primarily a project of waste management and energy recovery is secondary. The waste usually contains chlorine. This element usually reacts with alkali and other elements to make corrosive compounds which are molten in the plant conditions. Thus the environment of these plants is very harsh and corrosive in nature. This study is done to understand the corrosive nature of the WTE environment and mechanism involved which cause the degradation of the heat exchanger tubes.

II. CORROSION MECHANISM IN WTE PLANT

Several authors [1-3] suggests that the corrosion in WTE plants is more severe than the fossil fuel based plants because corrosion in these plants, is chlorine based called active oxidation and the melting temperature of the chloride salt mixture deposits on the tubes of boiler is less than sulfate salt mixture. So the deposition of chloride salt mixture accelerates the corrosion at low temperature than the sulfate salt mixture. To found the stability of protective oxide films formed on the metal in molten salt corrosion environment, similar to the waste incinerator plants. Tetsuo [4] study the solubility of several oxides in NaCl-KCl, melting point 660°C and NaCl-KCl-Na_2SO_4-K_2SO_4, melting point 518°C, salt mixtures in three different basic environments and Ishitsuka [5] study the solubility of protective oxide films Cr_2O_3, NiO, Co_3O_4, Fe_3O_4 and SiO_2 in molten chlorides NaCl-KCl at 727°Cand NaCl-KCl-Na_2SO_4-K_2SO_4at 550°C in the basic environment similar to the WTE plant. In this environment the Cr_2O_3 film changed to Cro^{2-}_4 by molten chlorides contained in the deposits, because basicity of molten chloride increases due to the presence of water in the combustion gas. So in the presence of low melting point salts in WTE plants the protective oxide film dissolves in the salts [4].

In WTE plants upon burning waste, gaseous alkali chlorides are expected to vapor-condense on the tube surfaces in a wide temperature range from flue gas at 650–950 °C, on the tube surface at 350–650 °C as reported by otsuka [6]. In this regime, vapor- condensation of gaseous NaCl and KCl from flue gas on the tube surface is favorable. The molecular quantity of vapor-condensed NaCl and KCl increased with increasing the flue gas temperature at 550–750 °C and leveled of at above 750 °C. The pure sodium and potassium chlorides cannot vapor-condense on the tube surfaces at higher than 700 °C because the pure solid NaCl and KaCl became unstable and disappeared from the deposit at higher than 650 °C. But at the tube surface temperature lower than 400 °C, exposed to flue gas at higher than 750 °C the vapor-condensed deposits $PbCl_2$, $PbSO_4$, $ZnCl_2$, and $ZnSO_4$ are considered to be responsible for the fireside corrosion of waterwall tubes, because these salts can lower the melting-point temperature of the tube deposits. Also it was found that vapor-condensation of these lead and zinc salts can only be possible on tube surfaces at lower than 400 °C. The vapor-condensation of NaCl and KCl salts, on the tube surface at 500 °C from the flue gas at 750 °C was found to be two-orders of magnitude greater than that from the flue gas at 550 °C because the high-temperature flue gases generally have high concentration of vapor NaCl and KCl and hence have greater capability to vapor-condense these species on tube surfaces. This enhanced vapor-condensation of NaCl and KCl salts on tube surfaces exposed to high-temperature flue gases increases the amount of molten salts in tube deposits, resulted in a severe fireside corrosion of boiler tubes.

Now the vapor-condensation of sodium and potassium sulfates (as solid solution) can occur for flue gases at higher than 750 °C and became heavier at higher temperatures. For flue gas at lower than 700 °C, vapor-condensation of sodium and potassium sulfates is not likely. At 650 °C, Na_2SO_4 can exist as solid phase involved in fly ash particles, instead of vapor phase in flue gases. The superheater tubes in most WTE plants are located in the region where the flue gas temperature is lower than

650 °C, hence the sodium sulfate found in superheater tube deposits is presumed to accumulate not by vapor-condensation from flue gas, but rather by impingement and/or adhesion of fly ash particles containing solid Na_2SO_4 to superheater tube surfaces. So the deposits on the boiler tubes is influenced by the flue gas temperature, rather than tube wall temperature and is also affected by the contents in the waste as reported by otsuka [6].

A corrosion mechanism based on literature available for fullscale deposit and corrosion studies in the waste-to-energy plants is based upon the chlorine-containing deposits, the sulfation of alkali chloride to sulfates and due to high partial pressures of gas-phase HCl or Cl_2. The theory is based on gaseous alkali chlorides condensing on the heat transfer surfaces and subsequently gaseous SO_2 enhanced the corrosion of metals covered with deposits containing alkali chloride, due to the in-deposit sulfation of alkali chloride to alkali sulfate by reacting with SO_2 that diffuses from the bulk gas stream to the deposit surface, forming the thermodynamically stable alkali sulfate, leading to the generation of high partial pressure chlorine. The alkali-chloride forms a melt with alkali-sulfate and iron components (Fe_xO_y, $FeCl_2$) adjacent to the oxide layer. The sulfation occurs fast in the melt and HCl or Cl_2 is formed close to the metal. Also the bulk of the salt containing chloride and sulfate did not melt it appeared that the salt grains in contact with the metal sample had formed a small amount of liquid phase (in both O_2-SO_2 and O_2-Cl_2 environments). Now the chlorine gas has the ability to diffuse through the oxide layer to the metal surface where it reacts with chromium and iron to form volatile metal chlorides. Chlorides of iron and chromium are thermodynamically stable and have high partial pressures at the conditions of low oxygen partial pressure prevailing at the metal/scale interface. The volatile iron chlorides diffuse out through the scale and oxidize as they reach areas with higher partial pressures of oxygen, forming a loose non-protective oxide layer. The iron oxides formed either in the metal oxide layer or in the dense mixed layer. The net reactions in the melt phase are that iron chloride is transformed to iron oxide and alkali chloride to alkali sulfate and release of chlorine. In this mechanism corrosion behavior shift with temperature, at low metal temperatures the solid-phase sulfation is slow and the metal suffers only from general oxidation and as the metal temperature increases from the lowest melting temperature of the deposit on the boiler tubes, the formation of sulfates from alkali-chloride increases in the melt, generating a high partial pressure of Cl_2/HCl. This causes accelerated oxidation and possibly selective corrosion on the fireside of boiler tubes in the waste to energy plants.

II. CONCLUSION

The following conclusions are derived from this study:

1. The reason for the harsh fireside corrosion in WTE plants lies in the characteristic waste chemistry. It is not only one element but the complex chemistry involving elements like sodium, potassium, calcium magnesium, lead, zinc, sulfur, and chlorine contents in the waste which cause severe corrosion problem in WTE plants.
2. The high-Cl, low-S, and moderate sodium/potassium contents, with small addition of heavy metals such as Pb and Zn has created the severe corrosion environment for boiler tubes in waste incinerators.
3. The effect of Cl in the deposits can be hindered and subsequently decrease in the corrosion, by the capture of alkali compounds in the waste.
4. The nature or composition of waste which is used as a fuel in WTE plants can not be selected, since waste incinerator is primarily a project of waste management and energy recovery is secondary.

REFERNCES

[1] Perez F. J., Nieto J., & Trilleros J. A. Hot Corrosion Monitoring of Waste Incineration Corrosion Processes Using Electrochemical Techniques. Materials Science Forum, 2006, 522-523, PP. 531-538.

[2] Lee Shang-Hsiu, & Themelis Nickolas J. High-Temperature Corrosion in Waste-to-Energy Boilers. Journal of Thermal Spray Technology, 2007, 16(1), PP. 104-110.

[3] Pedersen Anne J., Frandsen Flemming J., & Riber Christian. A Full-scale Study on the Partitioning of Trace Elements in Municipal Solid Waste Incinerations Effects of Firing Different Waste Types. Energy & Fuels, 2009, 23(7), PP. 3475-3489.

[4] Ishitsuka Tetsuo, & Nose Koichi. Stability of protective oxide films in waste incineration environment – solubility measurement of oxides in molten chlorides. Corrosion Science, 2002, 44, PP. 247-263.

[5] Ishitsuka T., & Nose K. Solubility study on protective oxide films in molten chlorides created by refuse incineration environment. Materials and Corrosion,2000, 51(3), PP. 177-181.

[6] Otsuka Nobuo. A thermodynamic approach on vapor-condensation of corrosive salts from flue gas on boiler tubes in waste incinerators. Corrosion Science, 2008, 50, PP. 1627–1636.

Study of Corrosion Preventive Measures for Waste Incinerators

Harminder Singh

Guru Nanak Dev University, Regional Campus, Jalandhar, Punjab, India

harminder10@gmail.com

+91-9914405782

Abstract— **The corrosion degradation of boilers tubes in waste incinerator environment is a serious issue. The presence of chlorine in the waste which is used as fuel in these plants is the main reason of highly corrosive environment. These plants are still running at low efficiency due to the boiler tube failures. So there is need to study the corrosion preventive measures especially for the waste incinerators and waste-to-energy (WTE) plants. In this study various corrosion preventive measures which can be adopted in these plant is reported.**

Keywords— Corrosion, Waste Incinerators, WTE

I. INTRODUCTION

The difficulty of combating corrosion in WTE plants is that there are many contributing factors and their effects may be overlapping effects and also the nature or composition of waste which is used as a fuel in WTE plant can not be selected. Now the effects of these factors vary widely among WTE facilities, due to the heterogeneous nature of the fuel used and differences in grate and boiler designs of WTE plants. In the past several years of the operation of the WTE plants the general approaches developed to reduce the corrosion can be classified as primary and secondary measures. Most of these methods have been applied to actual WTE facilities and shown different levels of effectiveness. The prevailing methods of protection from high temperature corrosion are described in this section.

II. Primary measures

The primary measures of protection to minimize the adverse effects of the corrosion factors are by influencing the process conditions in the boiler of the plant. Some of the primary methods include:

a) Changing the aggressive nature of the environment of plant by altering the fuel content used in the plants. The addition of some elements such as Mo, V or W in the fuel reduce the solubility of protective oxide film like Cr_2O_3 or addition of some elements like Si or Ni produce the protective oxide film having low solubility in a basic solution [1]. Other remedies as suggested by Khan et al. [2] is the successful removal or at least hindering the effect of Cl in the deposits and subsequently decrease in the corrosion, by the capture of alkali compounds. It is suggested that the use of different materials such as bauxite, kaolinite, limestone etc., produce high melting point alkali compounds relative to alkali chlorides and hence increase the melting point of the ash formed during combustion. But the corrosion effect will not be totally eliminated, because by the use of these additives, Cl will be released in the gas phase [2]. Also the addition of clay in the industrial waste fuel, can form high fusion point compound by reacting with the low fusion point materials and hence increase the operating temperature of plant [3].

Another measures include a new technique named ‘‘Targeted In-Furnace Injection’’ (TIFI) which makes the ash deposits more friable by means of injecting chemicals, such as MgO, directly into the combustion chamber [4].

b) Change in furnace design as suggested by Krause [5] so that there is uniform combustion, and avoid reducing conditions and also minimizing fluctuations in gas temperature[4]. Also it is suggested by Wenchao [6] that there is need for further research considering residence time, air ratio, temperature, fuel rate etc., to run the WTE plants at high efficiency.

III. Secondary Measures

Secondary methods of protection are applied to extend the lifespan of the boiler tubes. The life of tubes and hence efficiency of plant can be increased by protection from high temperature corrosion. Some of these methods require either the retrofit of existing WTE boilers or the redesign of boilers of new WTE facilities. In the case of

retrofits, the construction time for making equipment changes is a very important parameter since the required shutdown can affect the economic viability of the WTE facility [4]. Some of the protection methods applied in WTEfacilities, or are under investigation, are described in the following section:

A. Corrosion Resistant Materials

Many kinds of corrosion-resistant materials like high Cr- high Mo nickel base alloys and high Cr-high Si ferronickel alloy tubing products are used in WTE plants. From the previous study [7] it is found that the corrosion resistance of alloys can be improved by the addition of Mo or Si, but the effect of silicon is smaller than that of molybdenum, due to the discontinuity of silica layer**.**

B. PROTECTIVE COATING

It is learnt from the published literature that one possible, practical, reliable and economically viable way to control or prevent the problem of the high temperature corrosion, is an application of a thin layer of coatings having good thermal conductivity, such as nickel based alloys. Due to the continuously rising cost of the bulk materials as well as increased material requirements, the coating techniques have been given more importance in the recent times. Therefore, the use of protective overlay coatings has been emerging as a potential area and is successfully used to increase the life of superheater tubes of fossil fuel based energy recovery plants [8]. But this technique is not fully explored till now in WTE plants. Porosity, stress generation and interlayer separation between the different deposited layers are the prominent parameters to be considered for selecting a particular process for deposition of the coating. The easiness, economy and convenience of operations are the other major factors that must be considered for applying the coatings to industrial installations at site.

IV. CONCLUSION

After studying the literature critically it is found that there is very rapid surface degradation and hence failure of tubes of WTE plants in short duration due to aggressive nature of the environment in the plants.

The following conclusions are derived from this study:

1. The use of protective overlay thermal spray coatings has been emerging as a potential area and is successfully used to increase the life of superheater tubes of fossil fuel based energy recovery plants. But this technique is not fully explored till now in energy recovery plants based on waste as fuel.
2. Coatings based on nano-scale material also need to be explored because nano-scale materials have achieved much attention in recent years.
3. WTE plants are still operating at low efficiency as compared to fossil fuel based plants, so ways has to be found out to increase the efficiency of plant by decreasing the surface degradation of boiler tubes at high temperature. This area needs to be explored in the future.
4. New corrosion resistant alloys must be found, which are resistant towards chlorine corrosion.

REFERENCES

[1] Ishitsuka T., & Nose K. Solubility study on protective oxide films in molten chlorides created by refuse incineration environment. Materials and Corrosion, 2000, 51(3), pp.177-181.

[2] Khan A.A, Jong W. De, Jansens P.J., H. Spliethoff. Biomass combustion in fluidized bed boilers: Potential problems and remedies. Fuel processing technology, 2009, 90, pp. 21-50.

[3] James Cheng-Hsien Chu. Design and Operating Experience for a Fluidized Bed Incinerator to treat Industrial Hazardous Scum and Waste Oils. J. Chemical Engineering, 1999, 16(6), pp.795-797.

[4] Lee Shang-Hsiu, & Themelis Nickolas J. High-Temperature Corrosion in Waste-to-Energy Boilers. Journal of Thermal Spray Technology, 2007, 16(1), pp. 104-110.

[5] Krause H. H. Boiler tube failures in municipal waste to energy plants. Materials performance, 1996, 35 (1), 46-53.

[6] Wenchao Ma, & Susanne Rotter. Overview on the chlorine origin of MSW and Cl-originated corrosion during MSW & RDF combustion process. Bioinformatics & Biomedical Engineering, ICBBE, 2008, pp. 4255-4258.

[7] Ishitsuka Tetsuo, & Nose Koichi (2002). Stability of protective oxide films in waste incineration environment – solubility measurement of oxides in molten chlorides. Corrosion Science, 2002, 44, pp. 247-263.

[8] Sidhu T. S., & Prakash S. Hot corrosion and performance of nickel-based Coatings. Current Science, 2007, 90 (1), pp. 41-47.

Synthesis and characterization of Dicinnamalacetone thin films for solar cell applications

Sameer Kalia^, ^J.J.Mohindroo^, Rajeev Arora^, Anupreet kaur*, Roohi Devgan*

^*Assistant Professor, PG Department of Physics, DAV College, Amritsar*

**PG Students, PG Department of Physics, DAV College, Amritsar*

AbstractThe **emerging energy demands of the world have put the renewable source of energy in focus. Solar energy is one of the cheapest and greenest energy available to mankind. Inorganic material based solar cells have been in use for long time but low efficiency and high initial cost of such solar cells have inhibited their wide spread use.**

Organic solar cells (OSCs) have received much attention recently due to several potential applications, including compatibility with flexible substrates, low-manufacturing cost, and roll-to-roll fabrication process [1–3]. In organic materials, light absorption leads to the formation of excitons (bound electron-hole pairs) rather than the free electron-hole pairs. The research field of organic electronics experiences tremendous developments since organic conjugated materials are typically disordered, the charge carriers are mostly localized over a single molecule and charge transfers between molecules occur very efficiently [4]. The mobility is affected by many parameters such as molecular packing, disorder, electric field amplitude, and temperature, impurities, pressure and charge carrier density. During the past three decades conjugated organic compounds have attracted a strong interest in laboratories worldwide. The high mobility and broad light absorption band make them attractive materials for photovoltaic applications. The charge carrier mobility is the key quantity in order to get better solar cells devices made of organic conjugated material. It has been known that the dielectric constants of organic materials are largely influenced by orientations of the constituent molecules [5].

In the present work Dicinnamalacetone which is a green organic material with large conjugation, has been studied for its optical properties. The band gap has been found to be in the UV-Visible region, making it suitable candidate for solar cells.

KEYWORDS: - Dicinnamalacetone, organic solar cells (OSCs)

Introduction

The energy demands of the world have seen an exponential growth over the last century. The fossil fuels have been contributing significantly to fulfill the energy demands. But the rising cost and diminishing reserves have put the focus of the world to other sources of energy. Solar energy is the greenest and cheapest source. Photovoltaic cells to harness the energy are commercially available, most of which are inorganic material based. These solar cells have high initial cost of installation and low efficiency. The scientific fraternity has been looking for organic material which can replace the inorganic material based solar cells. Materials like Phthalocyanine and sub Phthalocyanine chloride have shown some potential but the expected efficiencies have not been achieved. In organic materials the electron hole pairs are generated but the high recombination rates before reaching the electrodes reduces the open circuit voltage $V_{OC.}$ Thus the charge transport properties of the organic material are the main parameter, after their absorption band, on which a material is rated. The conjugation of double bonds seems to enhance the charge transport properties. In the present work we are proposing Dicinnamalacetone as a potential material for solar cell applications. The thin films of the material were deposited under high vacuum conditions and were studied for their structural, optical and electrical properties [1-6].

The structure of Dicinnamalacetone is shown in fig1, having high conjugation. There is chain of five alternate double bonds on every side of the oxygen atom which can be considered as the centre of gravity of the molecule.

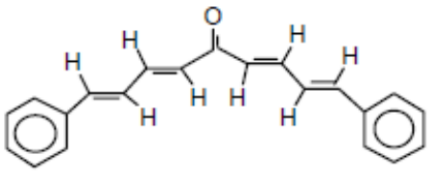

Fig.1 Structure of Dicinnamalacetone

I.EXPERIMENTAL TECHNIQUES

The high purity Dicinnamalacetone was deposited on ultrasonically cleaned glass substrates by thermal evaporation method at pressure of about 10^{-5} mbar. Aluminum electrodes were deposited under the same conditions by masking techniques. A molybdenum boat was used for depositing the Dicinnamalacetone. The structural and optical analysis of films under investigation was done by using X-ray Diffraction (XRD) technique U-V Visible spectroscopy. The C-V studies were done using Pico ammeter and function generators supplied by SES company, Roorkee.

STRUCTURAL PROPERTIES

XRD was done from SAIF, PU Chandigarh using Diffractrometer XPERT-PRO.

X-ray spectra have been recorded in the range 5°-79° (2θ).The graph is plotted between 2θ and counts.

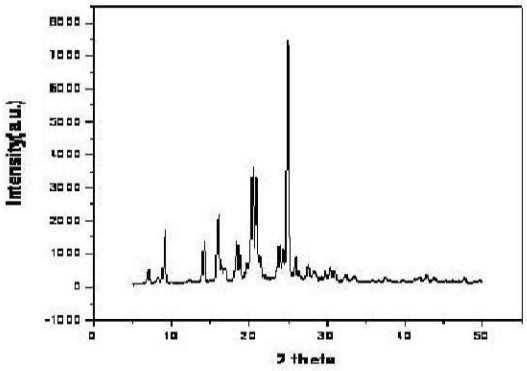

The XRD graph a strong peak at around 2θ = 25, indicating a preferential orientation for the deposited films.

II.OPTICAL PROPERTIES

UV-Visible analysis was done from SAIF, PU, Chandigarh using apparatus Perkin Elmer model no. lambda 750. The graphs were plotted between hv and (αhv)2. From graph we measure band gap for different samples. The band gap obtained for the samples was found to be about 2.2eV. The band gap found is in the UV region. This implies that the material chosen cannot alone be suitable for solar cell applications because of mismatch between the peak of solar spectrum and the peak of absorption band of the material. However the semi transparent kind of texture makes it suitable for making multilayer photo voltaic cells. The upper layer may absorb the energy from the UV part of the spectrum and for making optimum use of the solar energy underlying layer of some other material with absorption peak in the visible region can be used.

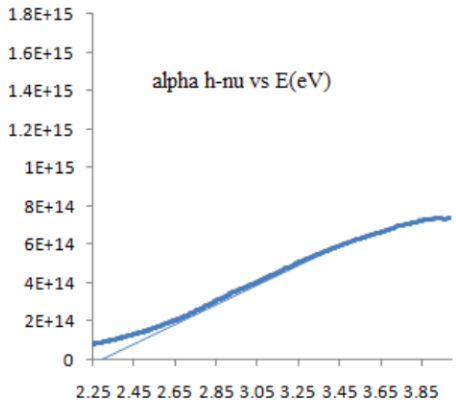

Fig.1 Optical band gap of Dicinnamalacetone

III.ELECTRICAL PROPERTIES

The dielectric properties of the samples were studied by forming aluminum electrode. The V-I characteristics showed that the electrodes were non rectifying in nature. The dielectric constant was determined using Goswami equivalent circuit model [7]. The capacitance of the film was obtained by measuring ac current at various frequencies (10-1000 Hz). The asymptotic value of this curve gives the geometric capacity of the film.

$C = \varepsilon_o KA/d.$

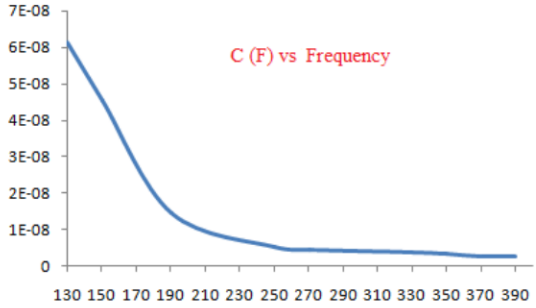

Fig.2 Variation of film capacitance with frequency

Dielectric constant was found to be 2.25.

IV.RESULTS AND CONCLUSIONS

The thermally deposited films were crystalline in nature and the junctions formed were non rectifying. The optical band gap of the films was found in the UV region. Thus the material is suitable for making multilayer solar cells. The dielectric constant was found to be 2.25.

Reference

1. J. Y. Kim, K. Lee, N. E. Coates et al., "Efficient tandem polymer solar cells fabricated by all-solution processing," .
2. F. C. Krebs, S. A. Gevorgyan, B. Gholamkhass et al., "A round robin study of flexible large-area roll-to-roll processed polymer solar cell modules," Solar Energy Materials and Solar Cells, 2009.
3. F. C. Krebs, H. Spanggard, T. Kjær, M. Biancardo, and J. Alstrup, "Large area plastic solar cell modules," Materials Science and Engineering B, vol. 138, no. 2, pp. 106–111, 2007. View at Publisher · View at Google Scholar · View at Scopus
4. C. W. Tang, "Two-layer organic photovoltaic cell," Applied Physics Letters, vol. 48, no. 2, pp. 183–185, 1986. View at Publisher · View at Google Scholar · View at Scopus
5. R. F. Bailey-Salzman, B. P. Rand, and S. R. Forrest, "Near-infrared sensitive small molecule organic photovoltaic cells based on chloroaluminum phthalocyanine," Applied Physics Letters, vol. 91, no. 1, p. 013508, 2007. View at Publisher · View at Google Scholar · View at Scopus

6. 6.J. Dai, X. Jiang, H. Wang, and D. Yan, "Organic photovoltaic cells with near infrared absorption spectrum," Applied Physics Letters, vol. 91, no. 25, Article ID 253503, 2007

7. A. Goswami and A. P. Goswami, Thin Solid Films 16, 175
8. A.Wang, L.Long, and C.J.Zhang, J. Incl. Phenom. Macrocycl.chem.71 (2011)
9. Graham E.Morse and Timonthy P.Bender "Boron Subphthalocyanines as Organic Electronic Materials", Dept. of chemical Eng. And Appl. Chemistry, Dept of chemistry,Dept. of Materials Sci. uni. Of Toronto.
10. Zur Erlangung des akademischen Grades, Doktor der Naturwissenschaften,(Doctor rerum naturalium) vorgelegt von, Wolfgang Tress" Device Physics of Organic Solar Cells Drift-Diffusion Simulation in Comparison with Experimental Data of Solar Cells Based on Small Molecules".

Effect of Compositional Variation of the Physical Parameters of Ge-Se-In Glass System

Surbhi Sharma[a], Amit Sarin[b] and Navjeet Sharma[c]
[a]*Research Scholar, Punjab Technical University, Kapurthala, India*
[a*]*Department of Applied Sciences, C.T. Institute of Engineering, Management & Technology, Jalandhar, India*
[b]*Department of Physics, Amritsar College of Engineering & Technology, Amritsar, India*
[c]*Department of Physics, DAV College, Jalandhar, India*

Abstract:-
In this paper an attempt has been made to theoretically find the variation of some important parameters of one of the arsenic free Ge-Se glass system by the addition of In content. Various parameters like co-ordination number, floppy modes, bond energy, electronegativity, heat of atomization, cohesive energy and glass transition temperature have been calculated for $Ge_{16}Se_{84-x}In_x$(x=0,1,2,3,4,5,6) glass system. Glass transition temperature (Tg) is calculated by using two approaches i.e.Tichy-Ticha and Lankhorst approaches. Tg seems to be increasing in theoretical calculations while average single bond energy is decreasing with the increase in content of In.

Keywords: Chalcogenide, Cohesive Energy, Glass transition temperature, Lone pair electrons, Heat of Atomization.

I. INTRODUCTION:

Chalcogenide Glasses (C.G) has recently attracted attention of various researchers due to their wide applications in electronics and optical devices. Among these due tothe reversible phase transformation property, high transparencies in low and middle IR region, Selenium (Se) finds numerous applications in photocells, rectifiers, switching, memory etc. [1]. But Sealso finds some disadvantages like short life time, aging, low sensitivity [2],[3],[4]. To improve its properties, it is alloyed with the elements of 3rd, 4th, 5thgroup of periodic table. The second element make bonds with Se chain and thus strengthens the average bond thereby increases the glass transition temperature. Ge-Se system is found to have wide glass forming ability. Whereas third element like In added to Ge-Se host structure in turn disturbs the long Se chains and results into the short range ordering and increase in defect concentration which helps in the network flexibility and thereby widens glass forming region.

So, in this paper an attempt has been made to theoretically study the effect of partial replacement of Se by In on the physical parameters (i.e co-ordination number, floppy modes, bond energy, electronegativity, heat of atomization, cohesive energy and glass transition temperature) of $Ge_{16}In_xSe_{84-x}$ (x=0,1,2,3,4,5,6) system.

II. THEORATICAL METHODOLOGY

Co-ordination number is an important parameter in describing the geometrical arrangement of particles in a unit cell of a crystal and is helpful in explaining some structural properties. In a multicomponent glasses, the average co-ordination number describes the cross linking in the covalently bonded solids. Higher the co-ordination number is, stronger is the bonding between the atoms.Average Co-ordination number <r> has been calculated by the standard result [5-6].Average Co-Coordination number <r> for the composition $Ge_{16}In_xSe_{84-x}$(x=0,1,2,3,4,5,6) is given by

$$\langle r\rangle = \frac{aN_{Ge}+bN_{In}+cN_{Se}}{a+b+c} \quad (1)$$

Wherea,b,c are concentration (at %) of Ge, In, Se respectively and N_{Ge}= 4, N_{In}=4, N_{Se} = 2 are their respective co-ordination number.

Mechanical constraint theory proposed by Philips and Thorpe [5-6] explains the glass formation tendencies of the material structure. These constraints are associated with the breaking of long rage ordering and resulting into short range order whichprovides the flexibility required for the formation of glass. Philips and Thorpe approach compares the degree of freedom per atom and degree of constraints acting on it. Number of constraints in an atomic species with average co-ordination <r> arises from Bond Bending N_B (angular) and Bond Stretching Ns (linear).

Bond Bending per atom is given by:

$$N_B = 2\langle r\rangle - 3 \quad (2)$$

Bond stretching per atom Ns is given by

$$N_S = \langle r\rangle/2 \quad (3)$$

Total number of constraints is given by

$$N_T = N_B + N_S \quad (4)$$

It has been further suggested that the composition at which the covalently bonded glassy system shows a sudden change from floppy (polymeric) state to rigid or stressed state is referred to as the Rigid Percolation (RPT) or Mechanical Threshold [6]. For covalently bonded network, rigid percolation occurs at <r>= 2.4 and at this point the degree of freedom per atom and total number of constraints becomes equal. At this composition glass forming ability of alloys is maximum. For <r>>2.4 the system is said to be over-stressed or rigid and for <r>< 2.4 the system issaid to be under coordinated or floppy.

The effective co-ordination number $<r_{eff}>$ is also related with the total number of constraints

$$<r_{eff}> = 2(<r> +3)/5 \quad (5)$$

Number of floppy modes signifies the degree of cross-linking and is the function of average co-ordination number. The number of floppy modes can be determined by the following relation

$$f = 2-\frac{5}{6}<r> (6)$$

Number of lone pairs can be calculated by using following formula

$$L= V- <r> (7)$$

Where L is the number of lone pairs and V is the number of valence electron [7]. Number of lone pairs signifies the degree of flexibility. More the number of lone pairs, more is the possibility of formation of amorphous network which enhances the glass formation ability. Thus lone pairelectrons in the structure of a system are a necessarycondition for obtaining the system in vitreous state [8].

Heat of atomization (Hs) is the energy required to dissociate the molecule into individual atoms. In case of the ternary compounds the relation is given as

$$Hs = \frac{(aHs_{Ge}+ bHs_{In} +cHs_{Se})}{a+b+c} (8) \quad (8)$$

whereHs_{Ge}, Hs_{In}, Hs_{Se} areheat of atomization of Ge,In,Se. Average single bond energy which is a measure of bond strength can be calculated by heat of atomization as Hs/<r>. For ternary compounds, energy can be estimated using the relation [10]

$$Eg = aEg_{Ge} + bEg_{In}+ cEg_{Se} (9)$$

In $Ge_{16}In_xSe_{84-x}$system there is relatively more probability of formation of Ge-Se, Se-In, Ge-In bonds then homopolar bonds Se-Se. According to Chemically Ordered Network model formation of hetropolar bonds dominates over homopolar bonds and the formation of bonds is in the decreasing order of their bond energy [9]. The energies of their hetropolarbondsis given by

$$E_{A-B} =(E_{A-A}\times E_{B-B})^{1/2} + 30(\chi_A-\chi_B)^2 (10)$$

where E_{A-A} , E_{B-B} are homopolar bond energies and $\chi_A,\chi_B$are corresponding electro-negativities.

Cohesive Energy of the system is the stabilization energy per atom of the large cluster. It is the amount of energy released when the crystalline structure is formed or amount of heat absorbed when crystalline structure is broken into individual atoms. Cohesive energy can be calculated by using the relation

$$C_E = \sum P_iE_i \quad (11)$$

where P_i is the number of bond expected and E_i is the energy of corresponding bond.

Various properties of C.G depends on mean bond energy E of the system which is the function of degree of crosslinking, average co-ordination number and bond energy. Mean bond energy as proposed by Tichy-Ticha [11,12], is a combination of two factors, contribution to the bond energy by hetropolar bonds Ec and contribution by the remaining matrix Erm. Thus mean bond energy can be given as

$$E = Ec+ Erm (12)$$

E_c and E_{rm} can be calculated by using following relations:

$$Ec = aE_{Ge-Se}r_{Ge}+ bE_{Se-In}r_{In} (13)$$

and

$$E_{rm} = \frac{(cN_{Se} - aN_{Ge}- bN_{In})\times Ese\text{-}se}{<r>} (14)$$

WhereN_{Ge}, N_{Se}, $N_{In}$are coordination numbers and a, b, c are concentration (at %) of Ge, Se, In respectively.

Parameter R is the ratio of covalent bonding of chalcogen atoms to non-chalcogen bonds. Parameter R indicates the deviationrepresent that eitherchalcogen or metal bonds dominates the structure.

$$R = \frac{cN_{Se}}{(a N_{Ge} + b N_{In})} (15)$$

wherea,b,c are concentration (at %) of Ge, In, Se respectively. R>1 signifies that the system is chalcogen rich and R<1 indicates chalcogen poor material i.e. metal-metal bonds dominates the structure.

Another parameter which can be determined is the glass transition temperature Tg. Glass transition temperature Tg is the transition from a pliable or "rubbery" state to more viscous, hard or rigid state. Or in other words, below Tg The material is rigid or glassy and above Tg the material is first super cooled liquid and then finally a liquid. Decrease in temperature hinders the mobility of molecular chains [13]. Tg is the function of overall mean bond energy, degree of crosslinking, types of bonds and bond energy of network formation [14].

According to Tichy-Ticha bond energy of the system also influences glass transition temperature [12]. They proposed an empirical relation between the mean bond energy and glass transition temperature is given as

$Tg_T = 311 (E-0.9)$ (16)

Glass transition temperature is also related to the heat of atomization by a relation given by Lankhorst [15]. This is expressed by the relation

$Tg_L = 3.44\ Hs - 488$ (17)

III. RESULTS AND DISCUSSION

The values of average coordination number, constraints, floppy modes and lone pairs electrons calculated for $Ge_{16}In_xSe_{84-x}$ (x = 0, 1, 2, 3, 4, 5, 6) are shown in table 1*. From the table it is inferred that average coordination number, number of constraints and hence effective coordination number increases with the increasing concentration of In. For x = 0, 1, 2, 3, 4, 5, 6 $Ge_{16}In_xSe_{84-x}$, average co-ordination number is first <r>< 2.4 then becomes equal to 2.4 and finally <r>> 2.4 and similarly total number of constraints ranges from $0 \geq N_T \geq 3$. Thus the system is showing transition from under stressed or floppy to Stressed, rigid and over coordinated glass. Number of floppy modes and lone pair electrons decreases with the increasing concentration of In, indicating that the system is getting more and more rigid. Variation of effective coordination number, number of constraints, floppy modes and lone pair electrons with In concentration is shown in figure 1.

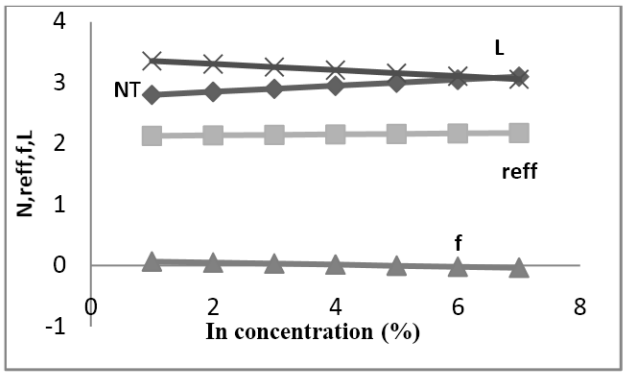

Fig: 1 shows the variation of Number of constraints (N), Effective Coordination number (r_{eff}), number of floppy modes (f) and lone pair electrons (L) with In concentration for *$Ge_{16}In_xSe_{84-x}$ (x = 0, 1, 2,3, 4,5, 6).*

Table 2* is showing the variation of heat of atomization, average single bond energy, glass transition temperature with x = 0, 1, 2, 3,4, 5 ,6. Values of glass transition temperature are calculated using Lankhorst relation for $Ge_{16}In_xSe_{84-x}$system. Variation of glass transition temperature with Se concentration is shown in figure 2.

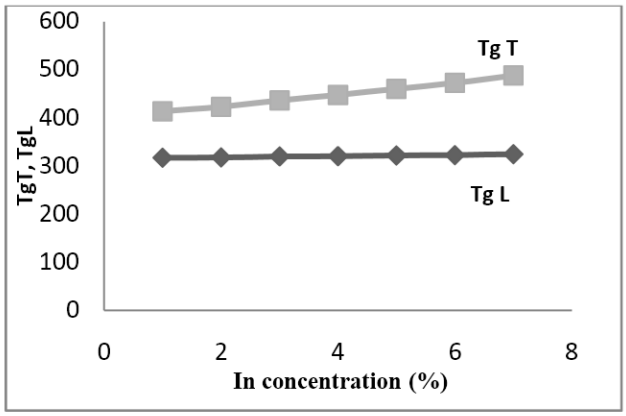

Fig. 2.Variation of glass transition temperature (Tg) with In concentration for *$Ge_{16}In_xSe_{84-x}$ (x = 0, 1, 2,3, 4,5, 6).*

Heat of Atomization of the system increases with In content while average single bond energy decreases with the increasing content of In. In chalcogenide glasses, the lone pair of Se atom forms the top of the valence band. The lone pair of Se atoms has energy higher than the electronegativity of Se atoms. When electronegative Se atom ($\chi = 2.55$) is replaced by electropositive In (χ = 1.78), the energy of lone pair gets enhanced and valence band moves towards the energy gap. Thus Energy gap decreases (Eg). Table 3* shows the variation of electronegativity, deviation of stoichiometry (R), distribution of bonds and cohesive Energy for $Ge_{16}In_xSe_{84-x}$system. From the table 3 it can be observed that electronegativity is decreasing with electropositive content of In. Decrease of parameterR factor shows that the system is becoming chalcogen poor which implies that hetro-polar bonds are increasing over homopolar bonds. Variation of number of bonds of Ge-Se, Se-In, Ge-In and Se-Sewith the increasing content of In is also shown in the table 3. Since bond energy of Se-In bonds is highest among the bonds for the present system and number of Se-In bonds is increasing at the faster rate than Se-Se, Ge-In bonds and leading to increase in glass transition temperature. Cohesive energy is also increasing due to the increase in Ge-Se, Se-In content. This reflects that stabilization energy per atom increases with increasing In concentration. Variation of heat of atomization, cohesive energy and mean bond energy with In concentration is shown in figure 3.

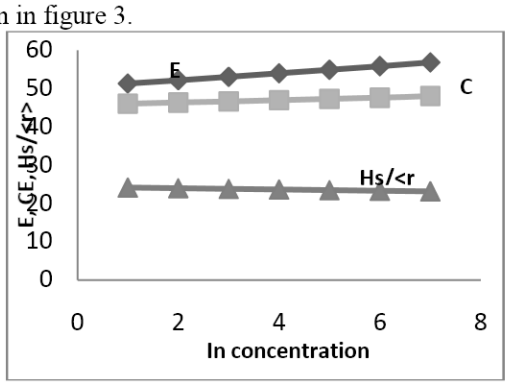

Table 4* shows the variation of mean bond energy with x = 0,1,2,3,4,5,6. As In increases it is observed from the table 4 that hetero-polar bonds are increasing thus E_c is increasing at the cost of weaker bonds resulting in the decrease of E_{rm}. Values of glass transition temperature are also calculated from Tichy-Ticha formula. Bond energies of Ge-Se, Se-In, Ge-In, Se-Se are also shown in the table 5*.

IV. CONCLUSION

Increasing concentration of In increases the number of hetero-polar bonds in the system and system becomes more and more rigid. It is seen that average coordination number, number of constraints, cohesive energy is also increasing with the increase in the concentration of In or decrease in concentration of Se whereas number of lone pairs and bond energy is decreasing with the increase in In content. Mean bond energy and heat of atomization increases with increase in In concentration leading to increase in glass transition temperature.

Fig.3. Variation of Average single bond energy (Hs/<r>), Cohesive energy (C_e) and Mean bond energy (E) with In concentration for $Ge_{16}In_xSe_{84-x}$ *(x = 0, 1, 2,3, 4,5, 6)*

*Tables are given at the end

ACKNOWLEDGMENT

Authors would like to thank Punjab Technical University, Kapurthala, India for extending its help and support.

TABLE 1

Values of Average Coordination No. (<r>), Constraints Bond bending (N_B), Bond Stretching (N_S) and Total (N), Effective Coordination Number, Floppy Modes (f) lone pairs of electrons(L) for $Ge_{16}In_xSe_{84-x}$ (x = 0, 1, 2,3, 4, 5, 6).

	<r>	N_B	N_S	N_T	r_{eff}	f	L
$Ge_{16}In_0Se_{84}$	2.32	1.64	1.16	2.8	2.128	0.066666667	3.36
$Ge_{16}In_1Se_{83}$	2.34	1.68	1.17	2.85	2.136	0.05	3.31
$Ge_{16}In_2Se_{82}$	2.36	1.72	1.18	2.9	2.144	0.033333333	3.26
$Ge_{16}In_3Se_{81}$	2.38	1.76	1.19	2.95	2.152	0.016666667	3.21
$Ge_{16}In_4Se_{80}$	2.4	1.8	1.2	3	2.16	0	3.16
$Ge_{16}In_5Se_{79}$	2.42	1.84	1.21	3.05	2.168	-0.01666667	3.11
$Ge_{16}In_6Se_{78}$	2.44	1.88	1.22	3.1	2.176	-0.03333333	3.06

TABLE 2.

Values of Heat of Atomisation (H_S), Average Single Bond Energy (H_S/<r>), Glass Transition Temperature (T_{gL}(Lankhorst)), Band Gap (E_g)*for* $Ge_{16}In_xSe_{84-x}$*(x = 0, 1, 2,3, 4, 5, 6).*

	H_s (kcal/g-atom)	H_S/<r>	T_{gL} (K)	E_g (eV)
$Ge_{16}In_0Se_{84}$	55.89	24.09051724	316.96	1.79
$Ge_{16}In_1Se_{83}$	55.98	23.92307692	317.7168	1.77
$Ge_{16}In_2Se_{82}$	56.07	23.75847458	319.55333	1.75
$Ge_{16}In_3Se_{81}$	56.15	23.59243697	320.16608	1.73
$Ge_{16}In_4Se_{80}$	56.24	23.43333333	322.00304	1.71
$Ge_{16}In_5Se_{79}$	56.32	23.27272727	322.61192	1.69
$Ge_{16}In_6Se_{78}$	56.41	23.11885246	324.44888	1.67

TABLE 3.

Values of Electronegativity (χ), Deviation from Stoichiometry (R), Distribution of Bonds, Cohesive Energy(C_E), for $Ge_{16}In_xSe_{84-x}$(x = 0, 1, 2, 3, 4.5, 6)

	χ	R	Distribution of Bonds				C_E
			Se-Ge	Se-InGe-InSe-Se			(Kcal/mol)
$Ge_{16}In_0Se_{84}$	2.46	2.63	0.38	-	-	0.62	46.0596
$Ge_{16}In_1Se_{83}$	2.456	2.44	0.385	0.0481	0.24	0.54	46.3494
$Ge_{16}In_2Se_{82}$	2.45	2.28	0.39	0.09756	0.04878	0.4637	46.6574
$Ge_{16}In_3Se_{81}$	2.44	2.13	0.395	0.1481	0.0741	0.383	46.9576
$Ge_{16}In_4Se_{80}$	2.43	2	0.4	0.2	0.1	0.3	47.2789
$Ge_{16}In_5Se_{79}$	2.425	1.88	0.40506	0.253	0.1265	0.2152	47.5979
$Ge_{16}In_6Se_{78}$	2.41	1.77	0.41	0.31	0.1538	0.1282	48.0425

TABLE 4.

Values of Mean Bond Energy (E), Glass Transition Temperature (T_{gT} (Tichy-Ticha)), for$Ge_{16}In_xSe_{84-x}$(x = 0, 1, 2, 3, 4, 5, 6,)

	E_c	E_{rm}	E (Kcal/mol)	T_{gT} (K)
$Ge_{16}In_0Se_{84}$	31.63	19.72	51.35	413.63
$Ge_{16}In_1Se_{83}$	33.79	18.427	52.217	422.96
$Ge_{16}In_2Se_{82}$	35.95	17.15	53.1	436.2086
$Ge_{16}In_3Se_{81}$	38.11	15.899	54.009	447.84
$Ge_{16}In_4Se_{80}$	40.27	14.66	54.93	460.28
$Ge_{16}In_5Se_{79}$	42.43	13.455	55.885	472.72
$Ge_{16}In_6Se_{78}$	44.59	12.26	56.85	488.27

Table 5.Values of Bond Energy for Ge-In-Se System.

Bonds	Bond Energy (Kcal/mol)
Ge-Se	49.42
In-Se	54.02
Ge-In	35.0774
Se-Se	44

REFERENCES

[1] K. Tanaka, K. Shimakawa," Structural phase- transitions in a chalcogenide glasses", Phy Rev. B. 39, 1989, pp1270-1279.

[2] Shimakawa K., "*Residual photocurrent decay in amorphous chalcogenides*", J. Non-Crystalline Solids, 77-78, Part 2, ,1985, pp.1253-1256.

[3] Shim,JaeYeob, Park, Sang Wook and Baik, Hong Koo, "*Silicide formation in cobalt/ amaorphous silicon, amorphous Co_Si and bais-induced Co_Si films*", Thin Solids, 292 (1-2), 1997, pp. 31-39.

[4] Saiter, J.M, Ledru, J.Hamou, A. and Saffarini, G., "*Crystallization of As_xSe_{1-x} from the glassy state (0.005<x<0.03)*", Physica B: Condensed Matter, 245(3), 1998, pp. 256-262.

[5] J.C Phillips, "*Topology of Covalent Non-Crystalline Solids 1: Short Range order in Chalcogenide Alloys*",Journal of non-crystalline solids, Vol. 34, 1979, pp. 153.

[6] *Phase transitions and self-organization in electronic and molecular networks,* edited by J.C.Phillips and M.F. Thorpe, Kluwer academic/Plemun Publishers, 2001, pp161-164.

[7] R. Zallen, *The Physics of Amorphous Solids* ,NewYork ,Wiley, 1983.

[8] PrashantKumar, VivekModgil, SubhashChand , V.S. Rangra,"*The Study of Physical Parameters of Pb ModifiedGermanateChalcogenide Glass*",Journal of nano- and electronic, Vol. 5 No 4, 2013, 04076(6pp).

[9]S.R Elliot, *Physics of Amorphous Solids* , New York, Longman Inc.,1984.

[10] A. Dahshan and K. A. Aly, "*Characterization of New Quaternary Chalcogenide As-Ge-Se-Sb Thin Films*," Philosophical Magazine, Vol. 88, No. 3, 2008, pp. 361-372.

[11] L.Tichy and H.Ticha, "*On the chemical Threshold in Chacogenide Glasses,*" Materials Letters, Vol. 2, No. 3-4, 1994, pp. 313-319.

[12] L.Tichy and Ticha , " *Covalent Bond Approch to the glass transition temperature of Chalcogenide Glasses"*,Journal of Non- crystalline Solids, Vol 189, No 1-2, 1995, pp 141-146.

[13] William D. Callister," *Fundamentals of Material Sciences and Engineering*" Edition 5, John Willey and Sons., 2001.

[14] C.Kittle,"*Interpretation of thermal conductivity of glasses*", Physical Review", 75(9), 1949, pp. 972-974.

[15] M.H.R Lankhorst, "*Modelling Glass Transition Temperatures of chalcogenide glasses, Applied to Phase – Change optical Recording*",Journal of Non Crystalline Solids, Vol 297 (2-3), 2002, pp. 210- 219.

Burnishing a super finishing process – A review

Aashish Sharma and S.B.S. Kalsi
Amritsar College of Engineering and Technology, Amritsar, Punjab, India

***Abstract*— Burnishing is considered as a super finishing process. In this process, the metallic surface of the work piece undergoes plastic deformation by the pressing action of a hard and highly polished rotating ball or roller. Improvements in surface finish, surface hardness, wear resistance and corrosion resistance can be achieved by the application of this process. But how to select the burnishing parameters to reduce the surface roughness and to increase the surface hardness is especially crucial. The aim of this paper is to critically discuss the affect of different parameters on burnishing.**

I. INTRODUCTION

Burnishing is a method of finishing the surfaces by applying the pressure on the surface by a hard ball or a roller. In these days, finishing processes are becoming more and more important. Surface finish not only give the good appearance to the material but it also increases the properties of the material such as increase in the surfaces hardness, decrease in surface roughness and increase the load carrying capacity of the material. Surface roughness occurs due to irregularities left by the machining tool. Owing to the inherent irregularities in the machining process, some other operations such as grinding, polishing, honing are performed to increase its surface finish. Now, in recent years, a process namely burnishing is commonly used to increase the surface finish of the material. In this process, surface characteristics are improved by plastic deformation. Such operations are sometimes referred to as plastic surface deformation. The different researchers (1-7) had tried to optimize the different parameters to achieve best possible surface finish.

A. EFFECTS OF DIFFERENT PARAMETERS

Adel Mahmood hassan and Ayman Mohammad Maqableh [1] in 2000 review the effects of initial burnishing parameters such as initial surface roughness & hardness of work piece, the ball diameter & the use of different lubricants on two non-ferrous work piece material namely Brass & Cast Al-Cu alloy. In their experiment, they comes out with the result that an increase in initial surface roughness will cause an increase in the final surface roughness of ball-burnished work piece but it has no effect on the surface hardness of these metallic work pieces. An increase in initial surface hardness will cause a decrease in the reduction of surface roughness and in total amount of the increase in surface hardness.

S.Rajesham and Jem Cheong Tak [2] in 1989 has studied the surface characteristics of aluminium alloy after its burnishing. They also done the experimental work on it and comes out with the result that as the burnishing force is increased the surface finish improves. A higher burnishing speed also has brought up an improvement in the surface finish. The micro hardness increases with the increased value of burnishing force.

S.B.S Kalsi, J. Singh, B.B. Saini [3] in 2006 carried out the experimental work on the effect of the burnishing parameters on EN-31 material. In their experiment, they comes out with the result that the surface hardness and surface roughness depends upon the burnishing parameters such as burnishing feed, burnishing speed and burnishing burnishing force. With the increase in the burnishing force, the surfaces roughness decreases to a certain limit, then it starts to increase with increase in burnishing force. The surfaces hardness decreases with an increase in feed rate and burnishing speed.

R.Rajasekariah and S.vaidyanathan [4] in 1975 carried out experimental work on steel components to increase the wear resistance of steel by ball burnishing process. They concluded that the finishing of the burnished surface depends on the burnishing load, feed rate and initial surface roughness. The burnishing load is the main factor affecting work hardening and wear- resistance of the surface. Fig.1 shows the relations between burnishing force (load) and surface hardness.

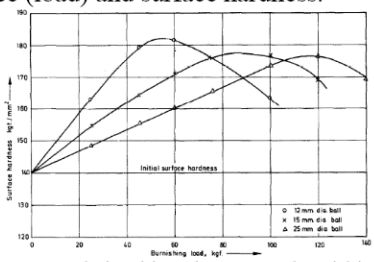

Fig. 1 Relationship between burnishing load and surface hardness.[4]

N.H. Loh, S.C. Tam and S.Miyazawa [5] in 1990 carried out the experiment on the surface hardness of material by ball burnishing process. They worked on the four ball burnishing parameters namely depth of penetration, type of lubricant, burnishing force and hardness of the material. They comes out with the result that as the feed increases, the normal and tangential forces and the hardness increase upto a maximum point. The hardeness of the material decreases with increase in the feed. Their is a variation of hardness at different depths below the surface.

R.L.Murthy and B. Kotiveerachari [6] in 1980 done the review work on the burnishing on the metallic surfaces. They concluded that the parameters such as burnishing force, feed forces in burnishing, characteristics of

components which are being burnished, smoothness of the surfaces and fatigue strength of the components. They studied some important applications of burnishing process such as finishing of inner hole, inner and outer diameter of the hydraulic cylinder, face seale, press fits, salvage operations.

N.H. Loh and S.C. Tam [7] in 1988 done the survey on the effect of ball burnishing parameters on surface finish. They studied the different ball burnishing parameters such as burnishing force, ball diameter, ball material and nature of work material. They concluded that the ball burnishing not only give the good look to the material but also increases the characteristics of the material. A required surface roughness and surface hardness can be achieved by this process.

S.S. Pande and S.M. Patel [8] in 1983 did the investigations vibratory burnishing process. They done the experimental work to study the influence of various process parameters such as burnishing speed, feed, ball force , frequency and amplitude of vibration on the surface finish micro hardness of surface layers produced by vibratory burnishing process. They also present the commercial models to correlate these parameters. They comes out with the result that very good surface finish can be obtained with the combination of large frequency and high force. Actually the effect on the surface finish is an interaction between the various process parameters rather than the total dependence of an individual parameter.

N.H. Loh and S.C. Tam [9] in 1989 did the statistical analyses of the effects of ball burnishing parameters on surfaces hardness of the material. They showed that the main effects on the surface hardness is of the lubricant used, feed and depth of penetration. The ball burnishing process can increase the surface hardness of the material to a desired amount. An interaction effect between the ball material and the linear feed was also evident. Fig.2,Fig.3 and Fig.4 shows the ball burnishing tool, set up of ball burnishing operations and schematic illustration of terminology respectively.

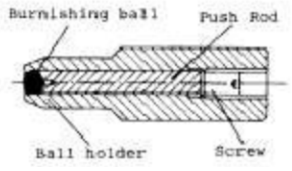

Fig. 2 The ball burnishing tool.[9]

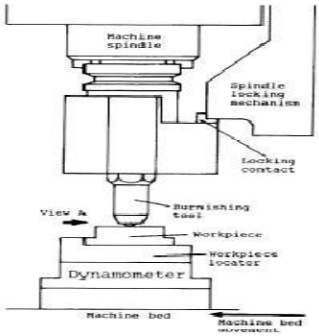

Fig.3 Schematic set up of ball burnishing operations.[9]

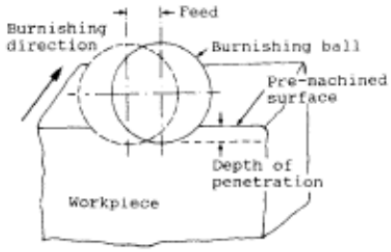

Fig.4 Schematic illustration of terminology.[9]

N.H. Loh, S.C. Tam and S.Miyazawa [10] in 1990 did the experimental work on the surface roughness produced by ball burnishing. They works on the various ball burnishing parameters such as speed, feed, burnishing force, depth of penetration, lubricant used on the surface roughness of AISI 1045 material. Results showed that the above written parameter effects the surface roughness. Increase in the depth of penetration surface roughness decreases up to an optimum point and then increases. Surface roughness increases with speed.

N.H. Loh, S.C. Tam and S. Miyazawa [11] in 1992 did the experimental work on the application of design in ball burnishing. They use ASSAB XW -5 tool steel for bunishing process. They use grease as lubricant. To establish the mathematical models to correlate these three parameters, they use response surface methodology (RSM). Finally they comes out with the result that in increase in the depth of penetration the surface roughness first decreases and then increases. Fig.5 Shows the relationship between surface roughness and depth of penetration:

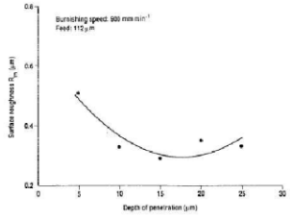

Fig.5 Effect of depth of penetration on surface roughness.[11]

Tokio Morimoto and Kentaro Tamamura [12] in 1991 carried the experimental work on the effect of tool material on the burnishing process. They use five types of

ball – tools namely silicon nitride, cemented carbide (JIS-G2), silicon carbide, alumina ceramic and high carbon chromium bearing steel(JIS-SUJ2). The turned surfaces of the steel bars were burnished using these tools. The results showed that the cemented carbide and silicon nitride ball – tools achieved the good surface finish among all types of ball – tools used.

Adel Mahmood Hassan and Aiman Sharef AI – Bsharat [13] in 1995 did the experimental work on the influence of burnishing process on surface roughness, surface hardness and microstructure of two non – ferrous metals, i.e, Brass and Aluminium. The burnishing parameters such as feed, speed, force and number of tool passes were taken into considerations. It was found that with increase in the feed rate the surface roughness decreases to a certain limit and then it starts increasing. Same results were found for the other considered parameters. With an increase in feed rate and burnishing speed the surfaces hardness decreases but surface hardness increases with the increase in burnishing force and number of tool passes. Their is an elongation in the grain near the surface of the burnished workpiece.

Adel Mahmood Hassan [14] in 1996 did the experimental work on the effects of ball and roller burnishing on the surface roughness and surface hardness of two non - ferrous metals i.e, brass and aluminium. The results showed that with increase in the burnishing force the surface roughness first decreases and then starts increasing with further increase in the burnishing force. The surface hardness increases with increase in the burnishing force. The relation between burnishing force and surface roughness shown in fig.6

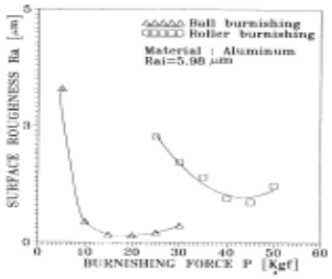

Fig.6 Relationship between surface roughness and burnishing force.[14]

M.H. EL – Axir [15] in 2000 did an investigation into the roller burnishing. The burnishing done on the steel – 37 to determine the surface hardness and surface roughness of the material. The result shown that the parameters of burnishing such as burnishing force, burnishing feed, spindle speed and number of passes of tool effect the characteristics of the material. At very high spindle speed, feed rate and number of passes, an increase in the burnishing force results in an increase in surface roughness. The workpiece over hardening and then flaking generally occurs when using a combination of high burnishing force with a high number of passes and the great deforming action of the tool and the increase of structural homogeneity of the surface layers that occurs when using low burnishing feed. The residual is maximum near the surface and decreases with an increase in the depth beneath the surface.

F. Klocke and J. Liermann [16] in 1998 carried out the experimental work on the roller burnishing of hard turned surfaces. In this hard roller burnishing operation, a hydrostatically borne ceramic ball rolls over the component surface under high pressures. The result shown that the hard roller burnishing transforms tensile residual stress present in the surface zone after hard turning into compressive residual stress. It also improve the surface roughness and surface hardness of the specimen. This process has no effect on the formation of white layers in the surface zone.

Adel Mahmood Hassan and Sulieman Z.S AL – Dhifi [17] in 1999 reviewed the improvement in the wear resistance of brass components by ball burnishing process. They investigated that with the increase in the burnishing force or the number of burnishing tool passes the wear resistance of brass component increases upto certain limits. The ball burnishing process also increases the surface finish and the surface hardness of the non- ferrous metals. It can be stated that the use of ball – burnishing process increases the wear resistance of brass component.

A.M. Hassan [18] in 1997 investigated into the surface characteristics of burnished cast Al – Cu alloys. He studied the effects of different burnishing parameters such as burnishing force, burnishing speed and burnishing feed on suface roughness and surface hardness of cast Al – Cu alloys. The result shown that with the in increase in burnishing force, speed and feed, the surface roughness seems to fall to a certain limit, and then starts to rise via an increase of each of the above – mentioned parameters. The relation between burnishing force and surface roughness is shown in fig.7(a) and the relation between burnishing speed and the surface roughness is shown in fig.7(b). Surface hardness increases with increase in the burnishing force and it decreases with burnishing speed and feed.

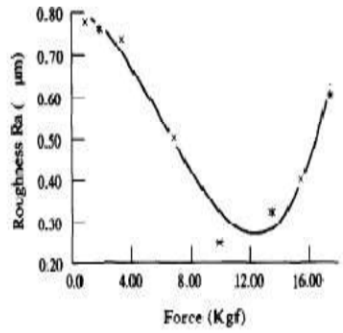

Fig.7(a). Burnishing force (*v=30 m/min,f=0`1mm/rev*).[18]

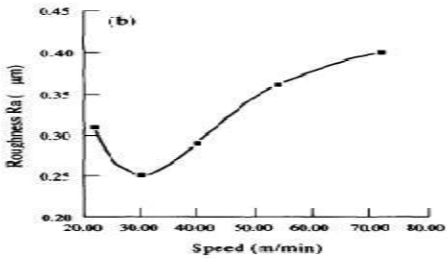

Fig.7(b). Burnishing speed (*p=10* kgf, *f=0`1 mm/rev*)[18]

B. CONCLUSION

The review show that the burnishing as a finishing process is not only technically viable but also has commercial potential. The burnishing parameters should be put under close control for the beneficial application of this process to improve the surface characteristics of the specimen. The increase in the burnishing force and speed decreases surface roughness to certain limits, and then starts to increase through the increase of each of the above – mentioned burnishing parameters. Surface hardness increases with burnishing force and it decreases with burnishing speed.

C. REFERENCES

[1] A.M. Hassan, and A.M. Maqableh, " The effects of initial burnishing parameters on non-ferrous components," Journal of materials processing technology, Vol. 102, pp. 115-121, 2000.

[2] S.Rajesham, and J.C. Tak, " A study on the surface characteristics of burnished components," Journal of mechanical working technology, Vol. 20, pp. 129-138, 1989.

[3] R. Rajasekariah, and S.Vaidyanathan, " Increasing the wear-resistance of steel components by ball burnishing," Wear, Vol. 34, pp. 183-188, 1975.

[4] N.H. Loh, S.C. Tam, and S. Miyazawa, " Surface hardening by ball burnishing," Tribology International, Vol. 23, No. 6, pp. 413-417, 1990.

[5] S.S. Pande, and S.M. Patel, " Investigations on vibratory burnishing process," International Journal of Machine Tool Design Resources, Vol. 24, No.3, pp. 195-206, 1984.

[6] N.H. Loh, and S.C. Tam, " Statistical analysis of the effects of ball burnishing parameters on surface hardness," Wear, Vol. 129, pp. 235-243, 1989.

[7] N.H. Loh, S.C. Tam, and S. Miyazawa, " Investigations on the surface roughness produced by ball burnishing," International Journal of Machine Tools & manufacture, Vol. 31, No.1, pp. 75-81, 1991.

[8] N.H. Loh, S.C. Tam, and S. Miyazawa, " Application of experimental design in ball burnishing," International Journal of Machine Tools & manufacture, Vol. 33, No. 6, pp. 841-852, 1993.

[9] T. Morimoto, and K. Tamamura, "Burnishing process using a rotating ball - tool – effect of tool material on the burnishing process," Wear, Vol. 147, pp. 185-193, 1991.

[10] A.M. Hassan, and A.S. AI- Bsharat, " Influence of burnishing process on surface roughness, hardness, and microstructure of some non – ferrous metals," Wear, Vol. 199, pp. 1-8, 1996.

[11] A.M. Hassan, " The effects of ball – and – roller burnishing on the surface roughness and hardness of some non – ferrous metals," Journal of Materials Processing Technology, Vol. 72, pp. 385-391.

[12] M.H. EL-Axir, " An investigation into roller burnishing," International Journal of Machine Tools & Manufacture, Vol. 40, pp. 1603-1617, 2000.

[13] F. Klocke, and J. Liermann, " Roller burnishing of hard turned surfaces," International Journal of Machine Tools & Manufacture," Vol. 38, No. 5-6, pp. 419-423, 1998.

[14] A.M. Hassan, and S.Z.S. AI-Dhifi, " Improvement in the wear resistance of brass components by the ball burnishing process," Journal of Materials Processing Technology, Vol. 96, pp. 73-80, 1999.

[15] A.M. Hassan, " An investigation into the surface characteristics of burnished cast Al –Cu alloys," International Journal of Machine Tools & Manufacture, Vol. 37, No. 6, pp. 813-821, 1997.

[16] R.L. Murthy, and B. Kotiveerachari, " Burnishing of mettalic surfaces – a review," Precision Engineering, Vol. 0141, pp. 172-179, 1981.

[17] N.H. Loh, and S.C. Tam, " Effects of ball burnishing parameters on surface finish – A literature survey and discussion," Precision Engineering, Vol. 10, No. 4, pp. 215-220, 1988.

[18] S.B.S. Kalsi, J. Singh, and B.B. Saini, " Effects of burnishing parameters on EN – 31," i – manager's journal of mechanical engineering, Vol. 1, No. 4, pp. 41-47, 2011.

SYNTHESIS OF GOLD NANOPARTICLES FROM SOLANUM TUBEROSUM EXTRACT AND EVALUATION OF ITS ANTIOXIDANT ACTIVITY

Roopa Rani, Kiran Singh, ManMohan Srivastava

Department of Chemistry, Dayalbagh Educational Institute, Deemed University, Dayalbagh, Agra, India - 282110

***Abstract*–Naturally occurring antioxidants are presumed to be safe since they are of plant origin and are as desirable as their synthetic counterparts. Thus, the strategy of implementing the diet with antioxidants especially deriving from natural sources is becoming more and more convincing against oxidative stress damages. This has promoted the investigation and characterization of active natural antioxidant compounds in various plant derived foods. The present piece of work is aimed to estimate antioxidant behaviour of the potato extract under different conditions (boiled, baked and raw) and synthesis of gold nanoparticles of potato extract followed by the estimation of its enhanced antioxidant behaviour.**

Keywords: Antioxidants, characterization, oxidative stress, Gold nanoparticles.

I. INTRODUCTION

Antioxidants are compounds that inhibit or delay the oxidation of other molecules by inhibiting the initiation of oxidizing chain reactions. They reduce the risk for chronic diseases including cancer and heart disease by trapping free radicals generated in our body. Synthetic antioxidants such as butylated hydroxyl anisole (BHA), butylated hydroxyl toluene (BHT), ter-butyl hydro quinine (TBHQ) and propyl gallate (PG) are effective in the protection of unsaturated fats and oils. However, the use of synthetic antioxidants in foods is discouraged because of their toxicity and carcinogenicity [1]. They may also cause liver swelling and non-selective killing of the cells. The presence of antioxidants in fruits and vegetables may reduce the risk of chronic diseases [2]. Naturally occurring antioxidants such as polyphenols, flavonoids, tocopherols and ascorbic acid are presumed to be safe since they are of plant origin and are as desirable as their synthetic counterparts. Plant sourced food antioxidants like vitamin C, vitamin E, carotenes, phenolic acids, phytate and phytoestrogens have been recognized as having the potential to reduce disease risk. Potatoes are also known as sources of antioxidant compounds, including polyphenols, carotenoids and vitamins, pointing to their relevance not only as a starchy food, but also as a vegetable. Potatoes contain phenolics compounds in the range of 0.3–4.8 mg/g dry weight [3]-[4]. Total carotenoids contents in potatoes were reported in the range of 0.6 – 233 µg/g [5]-[8]. As far as the vitamins content is concerned, potatoes contain 0.3 – 5.6 mg/g of vitamin C [9]-[13]. The present piece of work reports the estimation of *in vitro* antioxidant activity of potato extract in different conditions (raw, boiled and baked) using DPPH and Fenton assay and evaluation for enhanced antioxidant activity of gold nanoparticles synthesised from raw potato extract.

II. EXPERIMENTAL DETAILS

A. Reagents

DPPH (0.3mM in methanol), Methanol, α-tocopherol, Deoxyribose (3mM), Ferric chloride (0.1mM), Ascorbic acid (0.1Mm), EDTA (0.1mM), H_2O_2 (1mM), Thiobarbituric acid (1% in 100 ml NaOH; 0.05 N), Trichloro acetic acid (5 % in water), Phosphate Buffer Saline (pH 7.4), α-tochopherol (0.1mM).

B. Sample extraction

Potato (100g) was extracted with methanol (250ml) in a reflux extractor for 8 hours. The filtrates obtained were concentrated to a fixed volume (100 ml) using rota vapour distillation.

C. Antioxidant determination

DPPH assay:

The reaction mixture of dilution series (1-20mg/ml) of potato extracts were incubated with 1ml of 0.3 Mm DPPH solutions in MeOH. The solution was allowed to stand for 30min at room temperature. Extracts when reacted with DPPH, a stable purple coloured free radical was converted into colourless compound (α-α diphenyl β-picryl hydrazine). The extent of decolouration indicates the amount of DPPH scavenged [14]. The absorbance was measured at 517nm using α-tocopherol as a reference antioxidant. The percent inhibition of DPPH was calculated using the formula:

[(C-T)/C]X100 (1)

C is the absorbance of control and **T** is the test sample

Fenton's assay:

The reaction mixture containing different dilution series of potato extracts were incubated with deoxyribose,

H_2O_2, $FeCl_3$, ethylene diamine tetra acetic acid (EDTA) in phosphate buffer (pH 7.4). The reaction was terminated by 1ml thiobarbituric acid (1%w/v) and trichloro acetic acid (2% w/v) by boiling in water bath for about 15 min. The pink chromogen which was formed eventually results in the formation of thiobarbituric acid reactive substance (TBARS); α-tocopherol was used as a reference antioxidant. The percent inhibition of OH generated was calculated using equation 1.

Synthesis of gold nanoparticles from Solanum tuberosum extract

Doubly ionized water (10ml) was added to 4ml of *Solanum tuberosum* (potato) extract and stirred continuously at 25°C for 15 min. To the stirring mixture $NaAuCl_4$ solution (0.1M, 2 µL) was added. The colour of the mixture turned reddish brown from pale yellow within 5 minutes of the addition, indicating the formation of gold nanoparticles. The reaction mixture was stirred for an additional 15 minutes. The gold nanoparticles thus formed were separated from potato extract immediately using a 5 micron filter.

Characterization of Gold nanoparticles

Gold nanoparticles prepared from *Solanum tuberosum* (potato extract) was characterized by X-ray diffraction (XRD) analysis, Atomic force microscopy (AFM), Scanning Electron Microscopy, UV- Visible Spectral analysis.

III. RESULTS AND DISCUSSION

Estimation of antioxidant activity of potato extract by DPPH and Fenton assay

Different forms of potato (baked, boiled and raw) showed antioxidant behaviour in terms of percentage inhibition 83%, 92.46%, 97% for DPPH radicals at the concentration range 20mg/ml respectively. Reference antioxidant α-tochopherol inhibited 98.98% of DPPH radicals at the same concentration [Fig.1 (a)]. The free radicals were scavenged and solution becomes yellow because of formation of α-α diphenyl-β- picryl hydrazine.

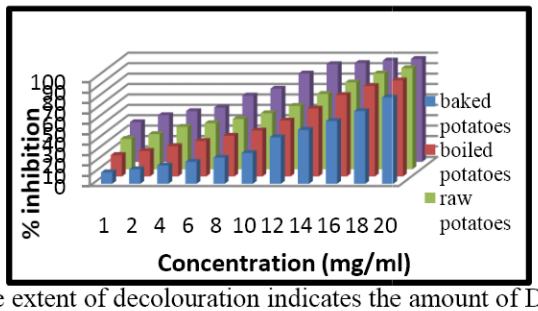

The extent of decolouration indicates the amount of DPPH radical scavenged. Similarly, baked, boiled and raw potatoes showed antioxidant behaviour in terms of percentage inhibition 84.1%, 93.04%, 97.02% against OH radicals at the concentration range 20mg/ml, respectively, in Fenton's assay. Reference antioxidant α-tochopherol inhibited 99.51% of DPPH radicals at the same concentration [Fig.1 (b)]. The rate of degradation of deoxyribose sugar in test samples was compared with control in terms of appearance of pink chromogen with thiobarbituric acid. The order of antioxidant activity was found to be - baked potatoes < boiled potatoes < raw potatoes < α-tochopherol. IC_{50} values of potato extract were calculated using DPPH and Fenton assay and found to be baked potatoes (13.95mg/ml & 13.00mg/ml), boiled potatoes (11.53mg/ml & 10.95mg/ml) and raw potatoes (9.34mg/ml & 8.36mg/ml), respectively.

(a)

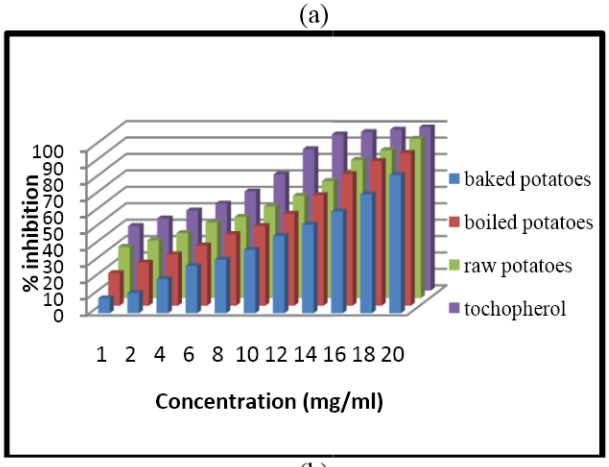

(b)

Fig.1: a) Percentage inhibition of DPPH radical, concentration dependency of baked potatoes, boiled potatoes and raw potatoes against reference α-tochopherol

b) Percentage inhibition of OH radical, concentration dependency of baked potatoes, boiled potatoes and raw potatoes against reference α-tochopherol

Synthesis of gold nanoparticles

Gold nanoparticles were synthesized from sodium tetra chloroaurate solution containing Au^{3+} ions by treating with the potato extract. The colour of the solution changed to reddish brown colour within 5 min of reaction with the Au^{3+} ions .The appearance of the deep brownish colour indicated formation of gold nanoparticles.

Characterization of gold nanoparticles

A. X-ray Diffraction (XRD) of gold nanoparticles

The diffraction peaks at 2θ = 38.15° (1 1 1), 44° (2 0 0), 63.9° (22 0) and 77.25° (3 1 1) obtained [Fig. 2] are identical with those reported for the standard gold metal (Joint Committee on Powder Diffraction Standards-JCPDS, USA).

The crystallite size was estimated from the full width at half-maximum intensity (FWHM) of the reflection using Scherrer's equation.

$$B = \sqrt{(FWHM)^2 - (0.045)^2} = x \quad (2)$$

$$B_{radian} = \frac{x\,\pi}{180} = y \quad (3)$$

$$t = \frac{K\lambda}{y Cos\theta} \quad (4)$$

Where B is the breadth of the peak of a specific phase (2θ=38.15 in our case), K is a constant that varies with the method of taking breadth (K=0.94), λ is the wavelength of incident X-rays (λ=0.15418nm), θ is the centre angle of the peak, and L is the crystallite length (size). The

crystalline size obtained was 32.10nm. The reference crystal size is 40 ± 20nm.

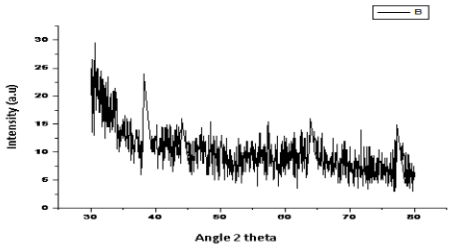

Fig.2 X-RD of gold nanoparticles

B. Atomic Force Microscopy

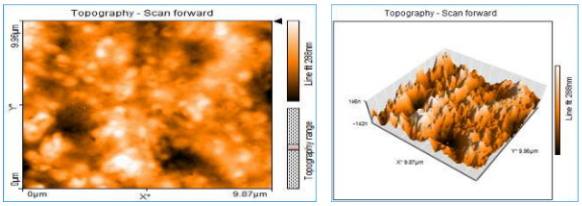

Fig.3 AFM of gold nanoparticles

From the topographical view, it is evident that the most of the nanoparticles are in spherical shape [Fig. 3]. The average roughness of the particles was found to be *13.39 nm*.

C. SEM of gold nanoparticles

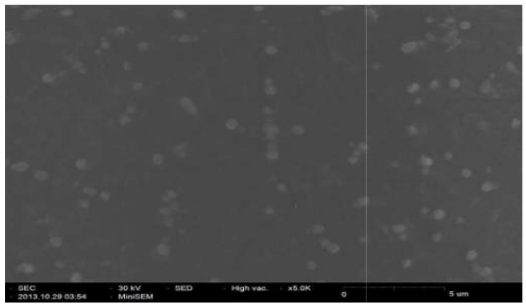

Fig. 4 SEM of gold nanoparticles

Information on the morphology of gold nanoparticles obtained from Scanning Electron Microscopy measurements**.** The image [Fig. 4] revealed that nanoparticles are mainly spherical in shape and are not in physical contact but are separated.

D. UV-Vis Spectra of gold nanoparticles

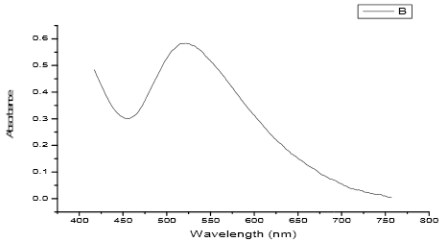

Fig. 5 UV-VIS spectra of gold nanoparticles

The UV- visible light absorption of gold nanoparticles was monitored in the range of 200nm-800nm. In case of gold ions reduction, the bands corresponding to the Surface Plasmon Resonance (SPR) occurred at 530 nm [Fig. 5]. Earlier studies have established that SPR band of gold nanoparticles appears around (500-550nm).

Antioxidant activity of potato embedded gold nanoparticles

The antioxidant behaviour of synthesized gold nanoparticles of potato extract with that of the raw potato extract was examined using DPPH assay. The comparison indicates that gold nanoparticles and raw potatoes showed percentage inhibit and 97% against DPPH radicals at the con ıge 20mg/ml respectively. Reference antioxidant ascorbic acid inhibited 98.98% of DPPH radicals for the same concentration.

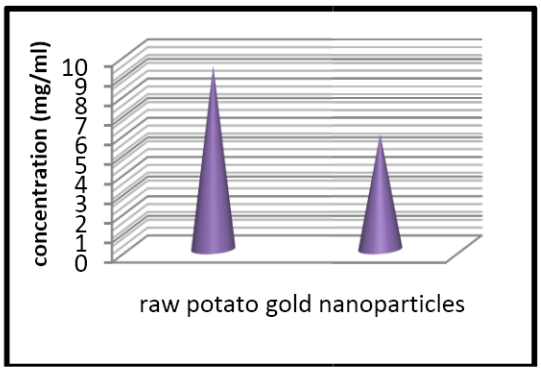

Fig. 6 IC_{50} value of raw potato and gold nanoparticles

The synthesized gold nanoparticles of potato extract showed significant increase in its antioxidant behaviour which is confirmed by the lowering in IC_{50} value (9.34) to (5.87) when compared to raw potato extract [Fig. 6]. The observed enhancement in the antioxidant behaviour can be ascribed to the fact that, nanoparticles have advantages over bulk materials due to their surface Plasmon resonance (SPR), enhanced Rayleigh scattering and surface enhanced Raman scattering (SERS) in metal NPs, quantum size effect in semiconductors.

IV. CONCLUSIONS

The present study showed that the potato extract possesses strong antioxidant activity against DPPH and OH radicals. The order of free radical scavenging activity was found to be α-tochopherol> raw potato> boiled potato> baked potato at concentration 20mg/ml. The observed trend showed that the antioxidant behaviour of different forms of the potato might be lost during boiling and baking. Synthesis of gold nanoparticles of potato extract has been carried out. The formation of gold nanoparticles were confirmed by UV-Visible spectra, X-RD, AFM, and SEM. Results indicated that nanoparticles

are spherical with 32nm in size and a broad peak at 530nm for gold nanoparticles was observed. The antioxidant behaviour of synthesized gold nanoparticles of potato extract with that of the raw potato extract was compared which indicates that the synthesized gold nanoparticles of potato extract showed significant increase in its antioxidant behaviour.

V. REFERENCES

1. F. Shahidi, "Natural antioxidants: an overview, In: Natural Antioxidants, Chemistry, Health Effects and Applications" AOCS Press Champaign, Illinois, USA, pp. 1-10, 1997.
2. D. F. Mantle, Eddeb, A. T. Pickering, "Comparision of relative antioxidant activities of British medicinal plant species in vitro" *J. Appl Microbio* vol. 84 no. 4, pp. 538-544, 2000.
3. R. G. O. Rumbaoa, D. F. Cornago, I. M. Geronimo, "Phenolic content and antioxidant capacity of Philippine potato (*Solanum tuberosum*) tubers" *J Food Compos Anal vol.* 22, pp. 546-550, 2009.
4. J. Lachman, K. Hamouz, M. Orsak, V. Pivec, P. Dvorak, "The influence of flesh colour and growing locality on polyphenolic content and antioxidant activity in potatoes" *Sci Hortic* vol. 117, pp. 109-114, 2008.
5. C. R. Brown, "Breeding for phytonutrient enhancement of potato" *Am J Pot Res*. Vol. 85, pp. 163-172, 2005.
6. T. Blessington, M. N. Nzaramba, D. C. Scheuring, A. L. Hale, L. Reddivari, J. Miller, "Cooking methods and storage treatments of potato: Effects on carotenoids, antioxidant activity, and phenolics" *Am J Pot Res*. Vol. 87, pp. 479-491, 2010.
7. D. Campos, G. Noratto, R. Chirinos, C. Arbizu, W. Roca, L. Cisneros-Zevallos, "Antioxidant capacity and secondary metabolites in four species of Andean tuber crops: native potato (*Solanum* sp.), mashua (*Tropaeolum tuberosum* Ruiz & Pavón), Oca (*Oxalis tuberosa* Molina) and ulluco (*Ullucus tuberosus* Caldas)" *J Sci Food Agric*. Vol. 86, pp. 1481-1488, 2006.
8. W. L. Morris, L. Ducreux, D. W. Griffiths, D. Stewart, H. V. Davies, M. A. Taylor, "Carotenogenesis during tuber development and storage in potato" *J Exp Bot* vol. 55, pp. 975-982, 2004
9. G. Burgos, E. Salas, W. Amoros, M. Auqui, L. Munoa, M. Kimura, M. Bonbierale, "Total and individual carotenoid profiles in *Solanum phureja* of cultivated potatoes: I. Concentrations and relationships as determined by spectrophotometry and HPLC" *J Food Compos Anal* vol. 22, pp. 503-508, 2009.
10. C. M. André, M. Ghislain, P. Bertin, M. Oufir, M. R. Herrera, L. Hoffmann, J. F. Hausman, Y. Larondelle, D. Evers, "Antioxidant profiling of native Andean potato cultivars (*Solanum tuberosum*L.) as a source of antioxidant and mineral micronutrients" *J Agric Food Chem*. Vol. 55, no. 2, pp. 366-378, 2007.
11. C. M. André, M. Oufir, L. Hoffmann, J. F. Hausman, H. Rogez, Y. Larondelle, D. Evers, "Influence of environment and genotype on polyphenol compounds and in vitro antioxidant capacity of native Andean potatoes (*Solanum tuberosum* L" *J Food Compos Anal*. Vol. 22, pp. 517-524, 2009.
12. L. Leo, A. Leone, C. Longo, D. Lombardi, F. Raimo, G. Zacheo, "Antioxidant compounds and antioxidant activity in "early potatoes". *J Agric Food Chem* vol. 56, no. 11, pp. 4154-4163, 2008.
13. K. Shimada, K. Fujikawa, K. Yahara, T. Nakamura, "Antioxidative properties of Xanthan on the anti-oxidation of soybean oil in cyclodextrin emulsion" *J. Agri Food Chem*, vol. 40, pp. 945–948, 1992.
14. K. Satish, C. Nripen, S. Ravi, K. Kavita, R. Rajesh, S. T. Kulkarni, , M. Swapna, K. Raghuraman, K. V. Kattesh, "Green Nanotechnology from Tea: Phytochemicals in Tea as Building Blocks for Production of Biocompatible Gold Nanoparticles" *J Mater Chem vol.* 19 no. 19, pp. 2912–2920, 2009.

Essential Variables to Control the Fill Factor of Organic Photo Voltaic Cell to Improve Its Power Conversion Efficiency

Karthik.B[a], Vedant Sumaria[a], P.Vijay[b]

[a]*Department of Power System Engineering,University of Petroleum and Energy Studies, India*
[b]*Assistant Professor, Department of Chemical Engineering,University of Petroleum and Enrgy Studies, India*

email: pvijay@ddn.upes.ac.in

Abstract- The ll factor is an important parameter that determines the power conversion efficiency of an organic photo-voltaic solar cell. There are several factors that significantly infuence FF and these factors interact with each other in-tricately. Due to this understanding FF is quite important. The relationship between Fill Factor(FF) and process variables have been demonstrated with series and shunt resistances and this provided a chance to understand the electrical de-vice behavior in the blend layer, series resistance(R_s) and shunt resistance(R_{sh}) were varied by controlling the morphology of the blend layer, the region regularity of conjugated polymer, and the thickness of the blend layert the interface between the cathode including PEDOT:PSS and the blend layer, cathode conductivity was controlled by varying the structure of the cathode or adding an additive.

KEYWORDS: Organic PhotoVoltaic Cell; PE-DOT:PSS; P3HT; PCBM; Fill factor.

I INTRODUCTION

Solar cell or Photovoltaic cell (or PV cell for short), is the device that converts the radiation of the sun to electricity. Every leaf of a green plant does something similar | they convert sunlight to chemical energy. Actually, a group of solar cells, the so-called "organic cells", started by borrowing the idea from leaves. Pigments (including chlorophyll [1]) were used to sensitize titanium-based materials [1,2]. The importance of developing e cient solar cells is obvious. The
sun supplies us a clean and unlimited resource of energy, helping us relieve the energy crises and world pollution. The source is out of question while the approach to e ciently utilize it remains a challenge.

Ever since 1954, when the rst modern Si p-n junction solar cell is invented at bell lab[3], many attempts have been done looking for a high-efficiency low-cost solar cells, leaving several signi cant milestones. In 1970, Zhores Alferov's team at USSR developed rst highly e ective GaAs heterostructure cell. In 1980, the rst thin- lm cell using Cu_2S/CdS was devel-oped at the University of Delaware with e - ciency of 10%. In1991, the rst dye-sensitized cell was invented. In 1994, there came the rst cell that exceeds 30% conversion e ciency using GaInP/GaAs. And in 2006, the "40% e cient barrier" was broken. Besides material research, much has been done for increasing sunlight con-centration, carrier collection, and cell stabil-ity[4]. Moreover, researches have gone beyond the inorganic world. Despite their low e ciency, the organic polymers have attracted much in-terest. The poly (3-hexylthiophene) (P3HT) and [6,6]-phenyl C61-butyric acid methylester (PCBM) blends is one of the promising organic solar cell materials. It is the most e cient fullerene derivate based donor-acceptor copoly-mer so far[5,6].

P3HT:PCBM has reported an e ciency as high as 10%, which is unusual in the organic cell material[7-10]. Their structures are as shown (Fig 1).PCBM is a fullerene derivative. Because of high hole mobility, it plays the role of elec-tron acceptor in many organic cells. P3HT is among the Polythiophene family, which is a kind of conducting polymer. It is the excitation of the - orbit electron in P3HT that gives the photo-voltaic e ect in the blend[11].All devices showed

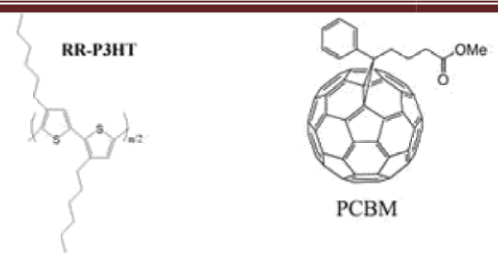

Figure 1: Structure of P3HT and PCBM[11].

that the eld-e ect transistor (FET) hole mo-bility values close to 0.1 $cm^2V^{-1}s^{-1}$ have been obtained in P3HT[13-16]. To maximize PCE of

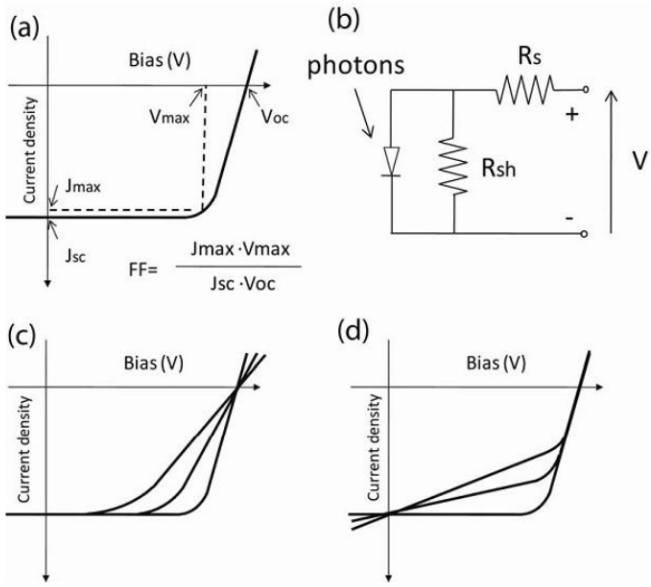

Figure 2: (a) The de nition of ll factor(FF), J_{max}:current density at the maximum of J x V in 4thquadrant, V^{max}:bias at the maximum of J x V in 4thquadrant. (b) Circuit of photovoltaic device, R^s: series resistance, R_{sh}: shunt resistance(c) Model of series resistance (R_s) impact-ing FF (d) Model of shunt resistance (R_{sh}) im-pacting FF[10].

OPVC, understanding on the parameters that a ect on J_{sc}, V_{oc}, and FF should be made. FF is de ned by (J_{max} x V_{max}) / (J_{sc} x V_{oc}) (Fig 2(a)) and its characteristic is determined by se-ries resistance (R_s) and shunt resistance (R_{sh}) of the device (Fig 3(c),(d))[17]. R_s is the measure of the series resistance of the organic semicon-ductor layer, which is related with the intrin-sic resistance, morphology, and thickness of the semiconductor layer. R_s determines the slope of J-V curve in the 1st quadrant and is calculated by V/J. On the other hand, the shunt resistance R_{sh} is correlated with how much charge are re-combined and generate the leakage current that are closely related to the amount and character of the impurities and/or defects in the active or-ganic semiconductor layer. R_{sh} determines the slope of JV curve in the 4th quadrant.

Monojit Bag Dhritiman Gupta, and K.S.Narayana investigated the concaved-up shape of S-like JV curve having drastically small FF. In their investigation, the con-caved up shape JV curve was explained by charge accumulation at the interface between an electrode and the organic semiconducting layer[18]. To verify that hypothesis, the au-thors prepared two types of OPVCs - one was ITO/PEDOT:PSS/P3HT+CB/Al and the other was ITO/PEDOT:PSS/P3HT+PCBM/Ca/Al. The former device showed the concaved up shape IV curve and the obtained FF was only 0.12. In the latter device, the thin calcium layer at the interface of Al and the organic layer facilitates the charge collection due to the ohmic contact and the resulting FF was improved up to 0.37. Instead of Christoph J.Brabec, Sean E.Shaheen, Christoph Winder, and N.Serdar Sariciftci added a lithium uoride layer between the blend layer and the aluminum cathode and observed enhanced FF from 0.5 up to 0.6[19].In this case, the authors explained that the enhanced FF originates from the dipole formation induced by LiF rather than the ohmic contact formation.

In this paper, we report the relationships be-tween FF and various parameters including the quality and thickness of the OPVC blend layer and the two interfaces between the electrodes and the blend layer. Through the study island-type electrode geometry was used to prevent the additional charge collection observed form the crossbar type device con guration[20].

II DISCUSSION

It had been tested that the e ect of the character of the organic layers, such as, the morphology, thickness, and regioregularity of the conjugated polymer to the FF. The device structure was ITO/PEFOT:PSS/P3HT+PCBM/LiF/Al.The following data and observations were made:

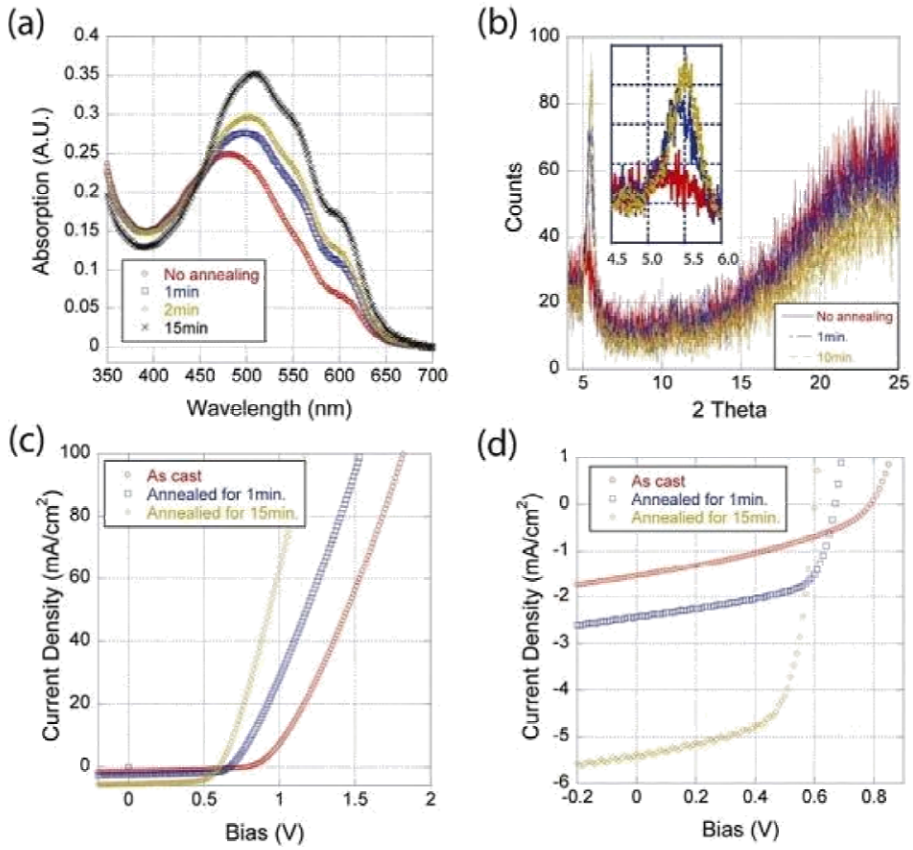

Figure 3: The annealing e ect on the FF of OPVCs (a)Absorption change a ect by thermal an-nealing. (b)Crystallinity evolution during thermal annealing(c) and(d) JV curve evolution during thermal annealing for 15min in di erent scale[10].

Annealing time(min.)	Jsc (mA/cm^2)	Voc(V)	PCE(%)	R_s(! cm^2)	FF
0	1.54	0.8	0.44	9.6	0.36
1	2.43	0.67	0.99	6.7	0.61
15	5.36	0.6	2.10	3.8	0.65

Table 1: The performances of P3HT and PCBM blend photovoltaic devices under di erent various annealing conditions[10].

Types	J_{sc} (mA/cm^2)	V_{oc}(V)	PCE(%)	FF	R_s(! cm_2)	R_{sh}(! cm^2)
Regiorandom P3HT+PCBM	0.65	0.59	0.12	0.31	0.05	1.6
Regioregular P3HT+PCBM	5.40	0.60	2.12	0.65	0.005	1.1

Table 2: Device performances of P3HT and PCBM blend photovoltaic devices having Device performances of P3HT and PCBM blend photovoltaic devices having di erent regioregularity ofthe conjugated polymer[10].

P3HT:PCBM layer thickness	J_{sc}(mA/cm^2)	V_{oc}(V)	PCE(%)	R_s(! cm^2)	R_{sh}(! cm^2)	FF
150nm	5.36	0.60	2.10	0.005	0.83	0.65
320nm	5.47	0.58	1.620	0.007	0.36	0.51
800nm	4.31	0.55	0.91	0.059	0.29	0.38

Table 3: The device performance depending on blend layer thickness e ect[10].

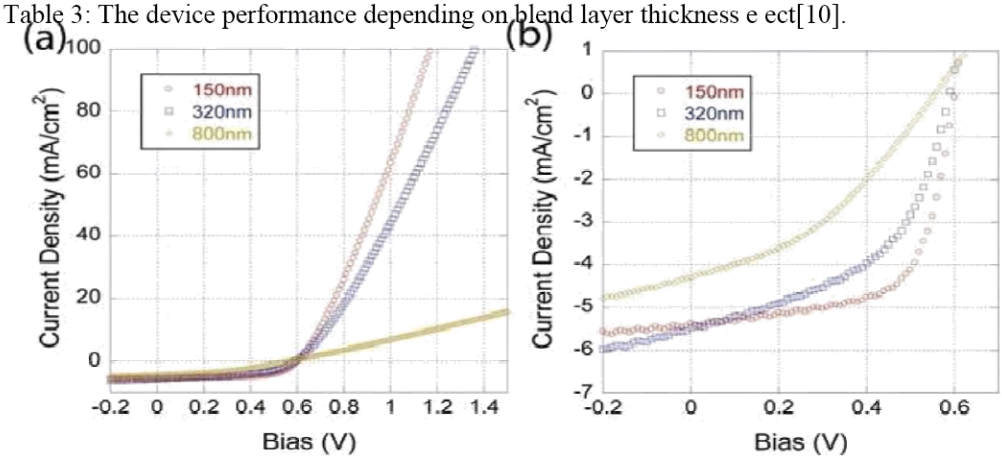

Figure 5: Thickness e ect on FF[10].

Types	J_{sc}(mA/cm^2)	V_{oc}(V)	PCE(%)	FF
Not annealed	5.06	0.42	0.92	0.43
Annealed for 10min	4.5	0.52	1.37	0.59
Annealed for 20min	5.4	0.56	1.81	0.6

Table 4: FF change depending on the interface between cathode and blend layer[10].

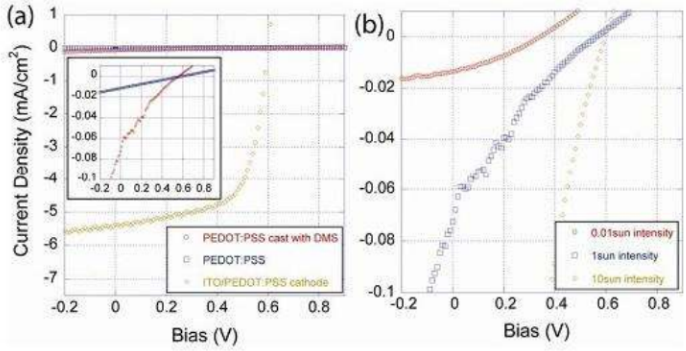

Figure 7: (a) The e ect of anode conductivityon FF and (b) Illumination intensity e ect on FF[10].

Intensity	$J_{sc}(mA/cm^2)$	$V_{oc}(V)$	FF
0.01 sun	0.01	0.35	0.3
1 sun	0.08	0.57	0.2
10 sun	0.53	0.59	0.17

Table 5: Device performances depending on anode conductivity[10].

Types	$J_{sc}(mA/cm^2)$	$V_{oc}(V)$	FF
PEDOT:PSS	0.02	0.59	0.16
PEDOT:PSS(w/10% DMS)	0.07	0.57	0.20
ITO/PEDOT:PSS	5.26	0.60	0.65

Table 6: Device performances depending on illumination intensity[10].

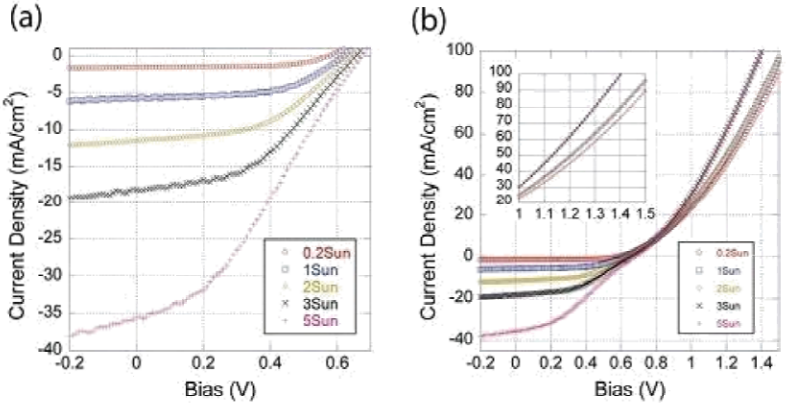

Figure 8: JV curves of a P3HT and PCBM blend photovoltaic device under various illumination intensities. (a) JV curves from -0.2V to 0.7V (b) JV curves from -0.2V to 1.5V. The larger scale JV curves are added to provide the graphical information of R_s[10].

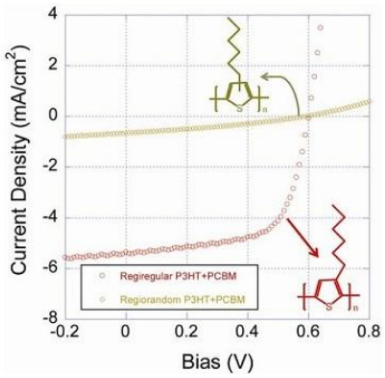

Figure 4: The regio regularity e ect of conju-gated polymers on FF[10].

Illumination intensity	^{J}sc (mA/cm^2)	^{V}oc (V)	PCE	FF
0.2 Sun	1.64	0.57	2.84	0.61
1 Sun	5.83	0.61	2.00	0.56
2 Sun	11.5	0.64	1.76	0.48
3 Sun	18.2	0.66	1.63	0.41
5 Sun	35.5	0.68	1.62	0.34

Table 7: The device performances of a P3HT and PCBM blend photovoltaic device under various illumination intensities[10].

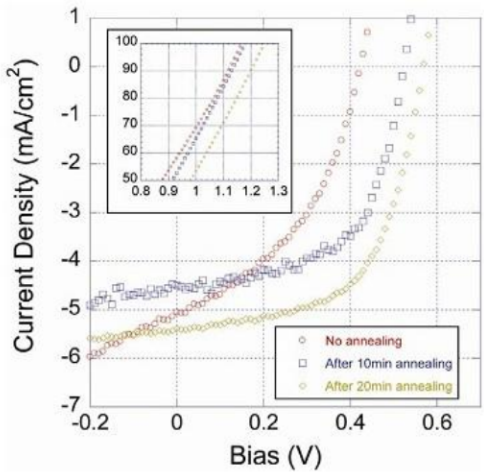

Figure 6: The interface e ect between the cath-ode and the blend layer on FF. (inset) currents from 0.8V to 1.3V which shows R_s[10].

III CONCLUSION

In this paper, the effective variables having im-pact on FF of OPVC having P3HT and PCBM were systematically identi ed. Systematic un-derstanding of the way to control FF and the correlation between the device variables and R_s and R_{sh} are important to achieve high perfor-mance OPVC. As the variable in the blend layer component, the blend morphology, the region regularity of the conjugated polymer, and the thickness of the blend layer showed large in uence on FF and through a ecting on R_s and R_{sh}. When the crystallinity of the blend layer was increased by thermal annealing, R_s decreased. When the regioregular P3HT was used one order of magnitude lower R_s was also observed. The higher crystallinity induced by thermal anneal-ing and regio-regularity should enhance the e - ciency of the intermolecular and intramolecular charge transport. On the contrary, as the thick-ness of the blend layer increased, R_s increased

and R_{sh} decreased due to the increased distance the charges should travel until they reach the electrodes and this will increase the resistivity and the charge recombination. The quality of the two interfaces between the blend layer and the electrodes was revealed to play a signi cant role in determining FF as well. When a less con-ducting cathode was used FF decreased due to more charge recombination and leakage current that was evidenced by lower R_{sh}. By controlling the amount of the photo-induced charges in the blend layer through various illumination condi-tions, it could proved that the R_{sh} and resulting FF are largely in uence by how e ciently ex-tract the generated charge through the cathode. As the chance of charge recombination increased in the experimental condition of the higher il-lumination intensity, R_{sh} and FF gradually de-creased indicating more charge recombination in the blend layer. The nature of the interface be-tween the Al anode and the blend layer turned out to be detrimental to FF as well. As the PV cells were thermally annealed after Al deposition FF R_{sh} increased indicating the interface became more favorable for charge extraction. It is likely due to the better contact between Al and the blend layer.

REFERENCE

[1]Tang, CW.Albrecht, AC. "Photovoltaic e ects of metal-chlorophyll-a-metal sandwich cells" J.Chem.Phys.62, No.6, 1975 pp. 2139-2149.

[2]O'Regan, B.Gr•atzel, "A low-cost, high-e ciency solar cell based on dye-sensitized col-loidal TiO2 lms." Nature 353,1991, pp. 737-740.

[3]Chapin,D.M.Fuller, C.S.Pearson,"A New Silicon p-n Junction Photocell for Converting Solar Radiation into Electrical Power".Appl.Phys.25, 1954, pp. 676.

[4]"Timeline of solar cells" from http://en.wikipedia.org/

[5]Perzon,E. Wang, X.Zhang,F. Mammo, W.Delgado, J.L.Cruz, P.Ingan•as, O.Langa, F.Andersson, "Design, Synthesis and Properties of Low Band Gap Poly uorenes for Photovoltaic Devices". Synthetic Metals 154,2005, pp.53-56.

[6]Al-lbrahim, M.Ambacher, "E ects of sol-ventand annealing on the improved performance of solar cells based on poly(3-hexylthiophene):Fullerene". Appl.Phys.Lett. 86201120, 2005.

[7] M. Helgesen, R. Sondergaard, F.C. Krebs, Advanced materials and processes for polymer solar cell devices, Journal of Materials Chemistry 20,2010,pp.36-60.

[8] J. Nelson, Polymer:fullerene bulk het-erojunction solar cells, Materials Today 14,2011,pp.462-470.

9] G. Li, R. Zhu, Y. Yang, Polymer solar cells, Nature Photonics 6,2012,pp.153-161.

[10] M.Su Kim. Understanding Organic Pho-tovoltaic Cells: Electrode, Nanostructure, Relia-bility, and Performance. Dissertation, The Uni-versity of Michigan.

[11] Nalwa, H.S."Handbook of Organic Con-ductive Molecules and Polymers" Vol.3: "Con-ductive Polymers: Spectroscopy and Physical Properties" ISBN: 0-471-96595-2

[12] Ge, Weihao, Solid State Physics II, Spring 2009,pp.1-2.

[13] C.Goh, R.J.Kline, M.D.McGehee, E.N.Kadnikova, L.M.J.Frechet, Appl.Phys.Lett. 122110, 2005, pp.86.

[14]A.J.Mozer,.N.Sariciftci,Chem.Phys.Lett.2004, pp. 389,438. [15] C.Tansase, E.J.Meijer, P.W.M.Blom, D.M.de Leeuw, E.J. Meijer, Phys. Status SolidiA 2004, pp. 201,1236.

[17] Jenny Nelson, The Physics of Solar Cells. Imprerial College Press, 2002.

[18] Monojit Bag Dhritiman Gupta, and K.S. Narayana, Appl. Phys. Lett. 093301,2008, pp. 92.

[19] C.J. Brabec, S.E. Shaheen, C. Winder, and N.S. Sariciftci Appl. Phy. Lett. 1288, 2002,pp.80.

[20] M.-G.Kang M.-S Kim, L. Jay Guo and J. Kim, Appl. Phy. Lett. 133301, 2008, pp. 92.

[21] Guo et al.,Thin Solid Films, 3138, 2008,pp. 516.

[22] Wu et al., Appl. Phy. Lett. 052103, 2005, pp. 87.

[23] F.C.Grozema, P.Th.van Duijnen, Y.A.Berlin,M.A.Ratner, L.D.A.Siebbeles 7791, 2002, pp. 106.

[24] Kim et al., J. Kor. Phys. Soc. 441, 2006, pp.48.

[25] Zhang et al., Adv. Mater.662, 2002, pp. 14.

Current Trends in ECG Compression Techniques

Butta Singh
Guru Nanak Dev University Regional Campus, Jalandhar

Abstract: **Compression methods have taken an important role in recent years in many areas including health monitoring. Electrocardiogram (ECG) is a physiological signal widely used in diagnosis and treatment of cardiac abnormalities. Large amount of signal data need to be stored and transmitted. Particularly, taking into account the limited band width of the transmission channels together with the imposing amount of the data to be transmitted, there is obviously a need for introducing the data compression. ECG Data Compression is intended to attain a lossless compressed data with relatively high compression ratio (CR) and low PRD (Percent Root Mean Square Difference). This proposed paper discusses various techniques proposed earlier in literature for compression of an ECG signals and provide comparative study of these techniques.**

Keywords: ECG, Compression ratio (CR), Percentage mean square, Discrete, Cosine transforms Wavelet transform.

I Introduction

The electrocardiogram (ECG) is a physiological signal containing information about the cardiac disease of the heart. The PQRST complex of ECG cycle and the various time intervals between peaks contains valuable information about the cardiac abnormalities afflicting the heart. The study of ECG pattern and heart rate variability has to be carried out over extended periods of time [1]. Therefore the storage size of the ECG data to be handled is enormous [2]. The advanced techniques must required a way to minimize the data storage without making major error in the reconstructed ECG signal and is exactly the aim of many existing ECG data compression techniques projected in literature over the last 3 decades [2, 3].The goal of ECG compression techniques is to achieve a reduced information rate, while preserving the relevant diagnostic information in the reconstructed signal.

ECG signal compression techniques can be broadly classified into three major categories: i) Direct data compression, ii) Transformation methods and iii) Parameter extraction techniques. Many algorithms have been proposed in the literature on direct data handling [4] transformation method, [5, 6, 7] and parameter extraction methods [8]. Direct methods generally preserve samples that contain important information about the signal and discarding the rest. The basic idea of all these methods is to break the ECG signal into consecutive linear segments. This is done by selecting a set of significant samples in the encoder. Whereas parameter extraction methods are mainly based on linear prediction and long-term prediction methods. It is an irreversible process, where a pre-processor is employed to extract some features that are later used to reconstruct the signal.

II Performance Measure of ECG Compression

One of the most difficult problems in ECG compression applications and reconstruction is defining the error criterion. The main purpose of the compression system is to remove redundancy and irrelevant information. The error criterion has to be defined so that it will measure the ability of the reconstructed signal to preserve the relevant information.

2.1 Percentage of root mean square difference (PRD)

PRD is one of the important parameters of any algorithms analysis and the small value of PRD shows success of algorithm. PRD is a most common used distortion measure that is given by

$$PRD = 100 \times \sqrt{\sum (ORG(i) - REC(i))^2 \Big/ \sum (ORG(i))^2}$$

Where ORG is the original signal and REC is reconstructed signal.

2.2 Compression ratio

Compression efficiency is measured by the compression ratio (CR). The CR is defined as the ratio of the number of bits representing the original signal to the number of bits required to store the compressed signal. The ECG signal calculation for compression ratio is explained as

CR=original file size /compressed file size

Higher the CR, smaller will be the size of compressed file.

III ECG Compression Methods

There are mainly three methods of ECG data compression

3.1 Direct methods

In these methods, signal samples are directly used to provide the compression. We classify the direct data compression methods into three categories: tolerance comparison Compression, differential pulse code modulation (DPCM), and entropy coding methods [4]. This section presents the direct data compression schemes developed specifically for ECG data compression. The Amplitude Zone Time Epoch Coding (AZTEC), Fan/SAPA, TP, and CORTES ECG compression schemes, which are

mainly, based on the tolerance- comparison compression methods. The (AZTEC) technique was proposed by J.R. Cox *et al*. [9] converts the original ECG data into horizontal lines (plateaus) and slopes. Plateaus use a zero-order Interpolator algorithm to compress the data, where amplitude and a length are stored. Slopes are formed when the length of a plateau is less than three. The information stored from a slope is the length of the slope and its final amplitude. Although the AZTEC algorithm provides a CR of around 10:1 (500 Hz sampled ECG with 12 b resolution) but the step-like reconstruction of the ECG signal is unacceptable for accurate analysis by the cardiologist, especially in the P and T portions of the ECG signal. W.C. Mueller proposed the Turning Point (TP) [10] data reduction algorithm was for the purpose of reducing the sampling frequency of an ECG signal from 200 to 100 Hz without reducing the elevation of large amplitude QRS's.

TP always provides CR of 2:1 and retains the important features of the ECG signal. It achieves this by replacing every three data points with the two that best represent the slope of the original three points. The second of the two saved points is used for the calculation of the next two points. A demerit of the TP method is that the saved points do not represent equally spaced time intervals. S.C. Tai proposed a real-time ECG data compressor SLOPE. This method considers some adjacent samples as a vector, and this vector is extended if the next sample falls in a fan spanned by this vector and a threshold angle; otherwise, it is delimited as a linear segment. By this way SLOPE continuously delimits linear segments of different lengths and different slopes. Fan and Scan-Along Polygonal Approximation (SAPA) algorithms [11] are ECG data compression techniques. These are based on the First-Order Interpolation with two Degrees of Freedom (FOI-2DF) technique. J.R. Cox *et al*. [9] proposed a technique in which Huffman coding was applied to the frequent codeword set, while a fixed word length coding technique was applied to the infrequent set. In this data compression ratio of 2.8:1 was reported using 250 Hz sampled ECG's with 10 b resolution. An ECG delta coding system is presented in[12] and implemented in Stewart *et al.* [2] proposed a modified technique called delta coding with threshold for compression of three-lead (X, Y, Z) ECG signals. Whenever the absolute value of the difference between successive samples in any of the three ECG leads signals exceeds above a preset threshold, data are stored. Otherwise data are considered redundant and hence, removed. DPCM system for data compression comes under the delta coding. In this system the actual signal is replaced by the first-difference signal (amplitude between successive samples).

3.2 Transformation methods

In this original samples of ECG are subjected to a (linear) transformation and the compression is performed in the entirely new domain like Fourier transform (FT), discrete cosine transform (DCT) and wavelet etc [5,15,16,17]. With FT the frequency-amplitude representation of the signal is obtained [17]. To reconstruct the signal apply inverse FFT. Limitation of FT is it fails to provide the information regarding the exact location of frequency component in time.

In DCT compression signal information can restore in a restrict number of DCT coefficients [17]. At first, the ECG signal is partitioned into its periods or beats. A beat is defined here as the signal between two R waves. As ECG signal is quasiperiodic, the lengths of the partitioned beats are not equal. These partitioned beats are then period normalised. These normalised beats are DCT transformed. For reconstruction of a signal, DCT coefficient blocks are IDCT transformed. Limitation of DCT is that the distortion is more in reconstructed signal.

ECG signal is non-stationary signal which includes different frequency components at different times and locations. Wavelet transform may localize the signal analysis in the both time and frequency domains simultaneously [22, 23]. This algorithm firstly decomposes the original signal using wavelet transform to get the coefficients. Process the wavelet coefficients by using the hard threshold. Apply inverse wavelet transform to reconstruct the signal [17].

3.3 Parameter extraction methods

In this a preprocessor is used to extract some features that are later used to reconstruct the signal. Methods belonging to this group are: peak picking linear prediction methods, syntactic methods neural nets methods and Long Term Prediction [18-21]. Parameter extraction method is an irreversible process in which a particular parameter or characteristic of the signal is extracted. The extracted parameters are used for classification based on a *priori* knowledge of the signal features. The peak picking compression techniques are usually based on the sampling of a continuous signal at peaks (maxima and minima) and other significant points of the signal. Imai *et al.* presented an ECG peak-picking compression system where the signal reconstruction was achieved by using spline functions. The system finds out the points of maxima and minima, as well as those of large curvature. The performance of compression method was compared to the AZTEC method. Nave *et al.* proposed the Long-Term Prediction (LTP) model which is based on the Sub-Auto Regression (SAR) model [18]. The "periodicity" of the ECG signal is used in order to further reduce redundancy, thus producing high compression ratios. It was detected that the PRD error (at 250 Hz sampling frequency) of LTP is lower than the conventional linear

prediction (short term prediction- STP) method at any bit rate [21].

IV Conclusion

This proposed paper provides an over view of various ECG compression techniques Table I, evaluates the performance of different algorithms that were proposed earlier for ECG compression. The future work mainly concentrates on developing an algorithm for efficient storage of ECG.

Table .1 Performance of Some ECG Signal Compression Technique

Method	**CR**	**PRD (%)**
TP[10]	2:1	28.0
AZTECH[9]	10:1	5.3
CORTES[24]	4.8:1	7.0
FAN/SAPA[11]	3:1	4.0
Entropy coding of second difference ECG[29]	2.8:1	-
Peak Picking (spline) with Entropy Coding [12]	10:1	14.0
DPCM Delta Coding with threshold [2]	4:1	-
DPCM linear Prediction [3]	2.5:1	-
DPCM-Linear Predict Interpolation and Entropy Coding[19]	7.8:1	3.5
Fourier Descriptor[5]	7.4:1	7.0
DWT using direct binary representation[7]	23:1	1.95

References

[1] S. M. Blanchard and R. C. Barr, "Comparison of methods for adaptive sampling of cardiac electrograms and electrodcardiograms" , *Med. Biol. Eng. Compur.*, vol. 23, pp. 377-386, July 1985.

[2] D. Stewart, G. E. Dower, and 0. Suranyi, "An ECG compression code", J. Electrocardiol., vol. 6, no. 2, pp. 175-176, 1973.

[3] Jalaleddine, C. Hutchens, R. Strattan, and W.Coberly,"ECG data compression techniques—A unified approach" , *IEEE Trans. Biomed.* Eng., vol. 37, pp. 329–343, 1990.

[4] J. R. Cox, F. M. Nolle, H. A. Fozzard, and G. C. Oliver, "AZTEC, a preprocessing program for real-time ECG rhythm analysis", *IEEE Trans. Biomed. Eng., vol. BME*-15, pp. 128-129, Apr. 1968.

[5] B. R. S. Reddy and I. S. N. Murthy, "ECG data compression using Fourier descriptors", *IEEE Trans. Biomed. Eng.,* vol. BME- 33, pp. 428-434, Apr.1986.

[6] M. L. Hilton, "Wavelet and wavelet packet compression of electrocardiograms", *IEEE Trans. Biomed. Eng.,* vol. 44, pp. 394–402, May 1997.

[7] B. A. Rajoub, "An efficient coding algorithm for the compression of ECG signals using Wavelet Transform", *IEEE Trans. Biomed. Eng*., vol. 49, No. 4pp. 849–856, April 2002

[8] A. Iwata, Y. Nagasaka, and N. Suzumura, " Data compression of the ECG using neural network for digital Holter monitor" , *IEEE Eng. Med. Biolo .Mag*. pp. 53-57 Sept.1990.

[9] J. R. Cox, F. M. Nolle, H. A. Fozzard, and G. C. Oliver, "AZTEC, a preprocessing program for real-time ECG rhythm analysis", *IEEE Trans. Biomed. Eng., vol. BME*-15, pp. 128-129, Apr. 1968.

[10] W. C. Mueller, Arrhythmia , " Detection program for an ambulatory ECG monitor" *Biomed. Sci. Instrument*., vol. 14, pp. 81-85, 1978.

[11] J. Sklansky and V. Gonalez, "Fast polygonal approximation of digitized curves Pattern Recog", vol. 12, pp. 327-331, 1980.

[12] P. Borjesson, G. Einarsson, and 0. Pahlm, "Comments on compression of the ECG by prediction or interpolation and entropy encoding", *IEEE Trans. Biomed. Eng*., vol. BME-27, pp. 674-675, Nov. 1980

[13] H. Imai, N. Kimura, and Y. Yoshida , "An efficient encoding method for electrocardiography using Spline functions", *Syst. Comput. Japan*, vol. 16, no. 3, pp. 85-94, 1985.

[14] M. Bertrand, R. Guardo, G. Mathieu, P. Blondeau, and R. Le-Blanc, "A microprocessor-based system for ECG encoding ana transmission" , *in Proc. 28th Annu. Con$ Eng. Med. Biol*., 1975, pp.435

[15] M. E. Womble, J. S. Halliday, S. K. Mitter, M. C. Lancaster, and J. H. Triebwasser, *,Data compression for storing and transmitting ECGs/VCGs Proc*. IEEE, vol. 65, pp. 702-706, May 1977.

[16] W. S. Kuklinski, "Fast Walsh transform data-compression algorithm", *ECG applications Med. Biol. Eng. Comput*., vol. 21, pp. 465-472, July 1983.

[17] A. A. Shinde, P. Kanjalkar, "The comparison of different transform based methods for ECG data compressionion", *ICSCCN 2011international conference on signal processing, communication, computing and networking technology*, pp332-335, 2011.

[18] G. Nave and A. Cohen, "ECG compression using long-term prediction", *IEEE Trans. Biomed. Eng.*, vol. 40, pp. 877–885, Sept. 1993.

[19]U. E. Ruthann and H. V. Pipberger, "Compression of the ECG by prediction or interpolation and entropy encoding", *IEEE Trans. Biomed. Eng.,* vol. BME-26, pp. 613-623, 1979.

[20] B. Furht and A. Perez, "An adaptive real-time ECG compression algorithm with variable threshold" *IEEE Trans. Biomed. Eng.,* vol. 35, pp. 489-494, June 1988.

[21] P. Trahanias and E. Skordalakis, "Syntactic pattern recognition of ECG", *IEEE Trans. Pattern Anal. Machine Intell.,* vol.12, pp.648-657,1990.

[22] T. Djohan, Q. Nguyen, and W. J. Tompkins, "ECG compression using discrete symmetric wavelet transform" *presented at the 17th Int. Conf. IEEE Medicine and Biology*, 1995.

[23] Z. Lu, D. Y. Kim, and W. A. Pearlman, "Wavelet compression of ECG signals by the set partitioning in hierarchical trees (SPIHT) algorithm", IEEE Trans. Biomed. Eng., vol. 47, pp. 849–856, July 2000.

[24] J . P. Abenstein and W. J. Tompkins, "New data-reduction algorithm for real-time ECG analysis", *IEEE Trans. Biomed. Eng., vol. BME-29,* pp. 43-48, Jan. 1982.

Electronics with "Genes Inside"

Deep Kamal Kaur Randhawa, ECE Department,
Guru Nanak Dev University Regional Campus, Jalandhar, India.

***Abstract*—Continuous miniaturization of electronic devices has been instrumental in development of computational and communication technology. Due to decreasing sizes lead to change in the physical mechanisms controlling the charge propagation. So there is search for new materials with new and novel properties will lead to new circuit architectures that can fundamentally change the way electronic circuit designing and the technologies evolved hence. DNA is one of the foremost contenders for use in electronic circuits.**

***Keywords*—**DNA, DNA based electronic devices, Single Electronics,

I. INTRODUCTION

The technical and economic growth of the twentieth century was marked by evolution of electronic devices and gadgets. The day-to-day lifestyle has been significantly affected by the advancement in communication systems, information systems and consumer electronics. The lifeline of progress has been the invention of transistor and it's dynamic up gradation. Discovery of fabricating Integrated Circuits (IC's) revolutionized the concept of electronic circuits. With advent of time the size of components decreased which led to increase in component density. The increase in density was as per Moore's Law. [1] The transistor has seen a consistent decrease in size over last six decades. This trend of decreasing device size and denser integrated circuits is being limited by the current lithography techniques. Non-uniformity of doping, quantum mechanical tunneling of electrons from source to drain and leakage of electrons through gate oxide limit scaling down of devices. Heat dissipation and capacitive coupling between circuit components becomes significant with decreasing size of the components. Along with the intrinsic technical limitations, downscaling of devices to nanometer sizes leads to a change in the physical mechanisms controlling the charge propagation. Some researchers predict that silicon based devices are going to face a bottleneck in near future. To deal with this constraint, search is on to look around for alternative materials, which might facilitate even more dense packing of transistors in a given space. While transistor –based electronic circuit design will continue to be the fundamental aspect of technology, the search for new materials with new and novel properties will lead to new circuit architectures that can fundamentally change the way electronic circuit designing and the technologies evolved hence.

Last decade has seen significant efforts aimed at developing new materials for electronic device application and new methods for electronic device fabrication. Contrary to the present technique of making devices out of bulk material, completely new approach of fabrication is being envisioned where one starts with a nanometer-scale material and assembles them into macro scale circuit architecture. This bottom –up approach, which has been observed to exhibit very accurate results, is cheap and ensures exact reproduction of a structure.

One of the concepts of bottom up approach is to utilize organic molecules, which can be grown in laboratory. Many molecules show interesting electronic properties, which make them probable candidates for electron device applications. The challenge is to interpret their electronic properties at nanoscale so as to exploit them for use in new generation electronic devices. Need to trim down size and have higher component density have ushered us into an era of DNA Electronics. [2] DNA, the building block of life is being predicted to be the building block of bottom-up electronics. DNA is a nanowire, which exhibits property of self-assembly and self-replication. Both these properties of DNA are most vital for electronics, as they would help in reproducing nanostructures with precision that is not possible with classical silicon based techniques. Further the techniques used for fabrication of DNA based device will be cheaper leading to economical and sophisticated gadgets. So it can be stated that miniaturization trend in semiconductor technology would lead experts into the realm of organic chemistry and biology.

II. WHAT IS DNA?

DNA or Deoxyribonucleic Acid, encodes the architecture and function of cells in all living organisms. Its size is of the order of ~ 10μm for animal cells and 100μm for plant cells. DNA comprises of a sequence of four bases namely A (Adenine), T (Thiamine), G (Guanine) and C

(Cytosine).These bases are organic compounds attached to a backbone built from repeating phosphate and sugar molecules. The bases can be attached in any sequence forming a single strand of DNA. Two strands may get coupled through hydrogen bonding of bases as per fixed pairing combination i.e. A with T and G with C. The bonding of two strands forms the double helix structure discovered by Watson and Crick .The base pairs look like rungs of a helical staircase as shown in Fig.1. Phosphate molecules in the backbone are negatively charged.

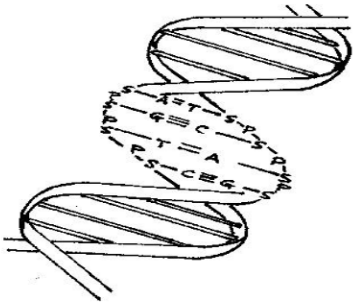

Fig. 1 Helical Structure of Double Stranded DNA

In the helical structure some of the electronic orbitals belonging to bases overlap each other along the long axis of DNA providing a path for conduction. There is difference in the energy levels of base pairs of DNA. This energy difference is larger than the thermal energy of the charge carriers. DNA's electronic and self-assembly properties make it an interesting aspirant for nanoelectronics.

During the course of research various experiments have been carried out to study the charge transport characteristics of DNA. The first direct electrical measurements on small bundles of DNA were made in 1999.[3] DNA sequences with various lengths and random base arrangements were observed. DNA was reported to act as conductor, semiconductor and insulator in different observations, which seem to be contradictory results. Porath et al observed poly (dG)- poly (dC) sequence and suggested that this type of sequence acts like a large –gap semiconductor.[4,5] On further probing it was observed that various parameters like base sequence, base length, orientation and temperature played a major role in defining conduction properties of DNA.

Experiments have demonstrated that DNA exhibits rare super conducting properties similar to those of carbon nanotubes. [6-8] By depositing long DNA molecules across a 500nm gap between special electrodes, scientists were able to apply voltages to the quantum wires and measure their conductivity at various temperatures. While most molecular wires become insulating at low temperatures, the DNA exhibited an increased conductance. [9] Superconductivity refers to a complete loss of electrical resistance, and DNA is normally not a superconductor. However, by connecting it to super conducting electrodes the scientists were able to induce super conducting effects when the temperature was lowered to 1 Kelvin and below, hence the term "proximity-induced superconductivity". [10]Charge transport measurements were also carried out at room temperature, both in and out of solution. In order to confirm that the electricity was indeed flowing through the DNA, the scientists added DNA degrading enzymes to the solution, after which the resistance increased by orders of magnitude. [11-14] At room temperature, the conductance seemed unaffected by addition of a biological buffer solution to the dried sample. This is good news for nanoengineers who might want to build solid-state nanoelectronic devices with DNA. The unique properties of DNA, self assembly and molecular recognition has rendered the "molecule of life" a promising candidate in mo0lecular nano-electronics.[15-20]

III. WHAT ARE SINGLE ELECTRON MOLECULAR DEVICES?

The incessant downscaling in the size of electronic components leads the integrated circuits into the domain of so called "mesoscopics", a dimension between microscopic and macroscopic worlds. Singular handling of electrons was conceptually possible even in the beginning of the century, but could not be realized practically as there were no means of fabricating small structures with accurate terminals. Availability of nanofabrication techniques in the past two decades have made possible a new field in electronics called Molecular Electronics. The properties of nanoscale materials are often dominated by their surface chemistry due to increased surface to volume ratio.

Silicon devices operate based on the movement of a large number of electrons n bulk matter while molecular devices take advantage of the quantum mechanical effects taking place at the nanometer scale. The building blocks of molecular electronics are single or small packets of molecules. [21, 22]

The main component of single electronics is a tunnel junction with a very small capacitance. Theses junctions can be implemented using a variety of materials: metal insulator structures, GaAs quantum dots, silicon structures, large molecules with conducting cores, etc. If the size of junction is sufficiently small, then the tunneling of only one electron may produce a noticeable change e/C of

voltage across the junction. The discreteness of this change, which is a consequence of the electrical charge discreteness, leads to a number of effects, which constitute the field of single electronics.

The single electron devices comprise of a quantum dot connected to tunnel junctions and are able to control the motion of single electrons. Injection/ ejection of electron through the quantum dot controlled by charging effect on the dot and the phenomenon is called Coulomb blockade effect. This is suppression of tunneling at voltages $|V| < e/2C$ because in this case tunneling would increase the electrostatic energy of the capacitor: $C(V\pm e/C)^2/2 > CV^2/2$. Condition for Coulomb Blockade Effect is expressed as

$$W_C = \frac{e^2}{2C} >> k_B T \qquad (1)$$

Where C is the self-capacitance of quantum dot sphere and is described as $C = 4\pi\varepsilon\varepsilon_0 r$ (ε-permittivity of medium surrounding the sphere; ε_0- vacuum permittivity, r- radius of the sphere). As the size of sphere decreases (i.e. 'r' decreases 0, the capacitance of the sphere decreases which increases the coulombic interactions of the electrons as there is lesser space separating the electrons. Capacitances as small as 10^{-19}F can be achieved in principle in the molecular electronic devices using conducting clusters of atoms embedded in a molecular matrix. The increased interactions of electrons enhance the charging energy. As the size of sphere is reduced below 10nm in diameter, this charging energy exceeds the thermal energy of the system (k_BT) and the charge states of the sphere become quantised. Term quantised implies that energy difference between sphere containing 'N' electrons 'N+1'electrons is observable and measurable. This implies that charging of sphere can be observed one electron at a time. This phenomenon of quantised charging energies of nanoparticles is exploited in single electron molecular devices [23-25].

Molecular devices offer many advantages apart from reduction of size. They operate at much lower voltage and current levels; hence saving on power consumption, which is also complemented by more densely packed ICs. As single electron molecular devices offer multiple stable current states they can allow multibit computing paradigms, opening the possibility of information processing.

IV. DNA BASED ELECTRONIC DEVICES

The electronics world is in pursuit to utilize the abundance of nature, which is full of physical and biological phenomenon. The molecular concepts, which support these phenomenons, are being interpreted for use in electronic devices and circuits. Various molecules are being analyzed for the possibility of use. DNA is one of the hot candidates for use as electronic material. It has rare quality to store information, which might prove useful in artificial storage devices.

DNA strands virtue their electrical characteristics are being considered for fabrication of electronic devices. There are certain significant facts, which support this prophecy. The energy difference between the base pairs and p and n-type of properties of the base pairs form the initial basis of this concept. Further the size of DNA molecules gives it an edge over the semiconductors especially in single electron devices. The small size can be utilized to enhance the temperature range of operation of these devices. Self-assembly property of DNA can be exploited for multiple replications. This would be a revolutionary improvement as far as uniformity of devices is concerned. DNA bases can be engineered to assemble sequences so that they are characterized by properties similar to the semiconductor devices.

Sugar molecule of backbone is connected to a base and the assembly is called a grain. Phosphate bridges forming a strand connect the grains to each other. The bases of the strand are connected to complementary bases of another strand through hydrogen bonds. In the phosphate bond the two transverse oxygen atoms connected to phosphorous give rise to two σ and one π bond as shown in fig.3. The tunneling and the capacitive effects exhibited at the bonds of DNA sequence [26,27] can be exploited to realize devices, which are characterized by these electrical parameters.

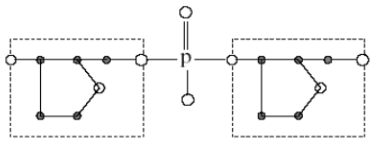

Fig.2 Schematic image of two grains of DNA connected by P bond

The energy level of A-T pair is higher than G-C pair. If an AT sequence is sandwiched between two G-C sequences the energy difference thus formed can be considered as a barrier for flow of charge carriers. [28-31] For the carrier to move from one edge of the sequence to other, the carrier has to overcome this barrier. The movement of carrier can be achieved by making the energy of carriers comparable to the barrier energy or by reducing the energy level of A-T pair. The energy levels of HOMO and LUMO molecular orbits are calculated to find the energy gap of the molecule. Analysis is also done to

visualize charge distribution on the molecule so as to predict the electrical characteristics of the DNA molecule. [32-37]

V. CONCLUSION

The unique self-assembly property of DNA along with exhibition of electrical and electronic characteristics suggests that DNA may be forecasted as one of the most effective species in molecular electronics. DNA might be used as a wire, transistor or rectifier depending on the electronic properties of the DNA sequence. DNA might become the driving force of new generation of nanodevices with gadgets labeled as "genes inside".

VI. REFERENCES

[1] Schailer, "Moore's Law: Past, Present And Future," IEEE Spectrum, pp.53-59, June (1997)

[2] M. Di. Ventra, M. Zoolak, "DNA Electronics,"Encyclopedia of Nanoscience and New Technology, Vol. 10, PP 1-19, (2004)

[3] H.W.Fink and C Schonenberger 1999, Electrical conduction through DNA molecules" Nature 398 407.

[4] Danny Porath, Noa Lipidot and Julio Gonrez-Herrero, "Charge Transport in DNA-based Devices", Lect. Notes Phys. 680, PP- 411-444, (2005.)

[5] D Porath et al., "Direct measurement of electrical transport through DNA molecules" Nature 403 635 (2000).

[6] Y. Kasumov et al., "Self assembled DNA networks and their electricalConductivity", Science 291, 280 (2001).

[7] K. H. Yoo et al., "Electrical conduction through poly (dA)-poly (dT) andpoly(dG)-poly(dC) DNA molecules", Phys. Rev. Lett. 87, 98102 (2001).

[8] E.Meggars, M.E. Michel-Beyerle, and B.Giese, J.Am. Chem.Soc. 120, 12950 (1998)

[9] Calzolari, R. Di Felice, E. Moliuari, " Electronic properties of Guanine-based Nanowires", Solid State Communication 131, PP 557-564, (2004)

[10] A.Yu. Kasumov, et.al., "Proximity-Induced Superconductivity in DNA", Science 291,280 (2001)

[11] M. Bixon, Jshua Jortner, "Incoherent change Hopping and Conduction in DNA and Long Molecular Chains", Chemical Physics 319, PP 273-282, 9(2005)

[12] Daphne Klotsa, Rudolf A. Romer, Matthew S. Turner, " Electronic Transport in DNA", Biophysical Journal, Vol. 89, PP 2187-2198, (2005)

[13] Hezy Cohan, Claude Nogues, Ron Naaman, Danny Porath, " Direct Measurement of Electrical Transport through single DNA Molecule of complex Sequence, " DNA Molecule of complex Sequence. " DNAS, Vol 102, no. 33 PP 11589-11593, (2005)

[14] Shawn D. Wettig, David O. Wood, Palok Aich, Jeremy S. Lee, "M-DNA: A novel metal ion complex of DNA studied by fluorescence techniques", Journal of Inorganic Biochemistry 99 2093–2101(2005)

[15] V.M. Apolkov, Tapash Chakraborty, "Electron Dynamics in a DNA Molecule", Physical Review B, 71. 033102(1-4), (2005)

[16] Janusz Rak, Joanna Makowska, Alexander A. Voityuk, "Effect Of Proton Transfer On The Electronic Coupling In DNA",Chemical Physics 325 567–574(2006)

[17] Tomoharu Inoue, Jun Qian , Sicheng Liao , Yang Li , Vaishnavi Narayanamurty , Milana Vasudev ,Mitra Dutta , Michael A. Stroscio, " Comparison Of Calculated And Measured *I–V* Curves For DNA" J Comput Electron DOI 10.1007/s10825-008-0172-z Springer Science+Business Media LLC (2008)

[18] Janusz Rak, Joanna Makowska, Alexander A. Voityuk, "Effect Of Proton Transfer On The Electronic Coupling In DNA",Chemical Physics 325 567–574(2006)

[19] B.P.W. de Oliveira, E.L. Albuquerque, M.S. Vasconcelos, "Electronic density of states in sequence dependent DNA molecules", Surface Science 600 3770–3774 (2006)

[20] J. Songa, D.C. Zhang, D.S. Liu, L.M. Meia, S.J. Xie , "Density of states of DNA molecules with varied itinerant electrons",Synthetic Metals 155 607–610 (2005)

[21] M. Jagadesh Kumar, "Molecular Diodes and Applications", Recent Patents on Nanotechnology, 1, 51-57 51,(2007)

[22] Douglas Natelson, Lam H. Yu, Jacob W. Ciszek, Zachary K. Keane, James M. Tour, "Single-molecule transistors: Electron transfer in the solid state", Chemical Physics 324 267–275(2006)

[23] Denis Chouvaev, Leonid Kuzmin, Dmitri Golubev, Andrei Zaikin , "Coulomb blockade in a SET transistor and a single tunnel junction: Langevin equation approach", Physica B 284-288 1786-1787 (2000)

[24] Konstantin K. Likharev "Single–Electron Devices and Their Application, "Proc IEEE, Vol 87, PP 606-632, April (1999.)

[25] Kastner M A," The Single Electron Transistor", Review of Modern Physics Vol 64,no 3, pp 849-858 July (1992)

[26] Frederick D. Lewis et. al., "Donor-bridge-acceptor energetics determine the distance dependence of electron tunneling in DNA", PNAS ,vol. 99 , no. 20 12536–12541 October 1, (2002)

[27] M. A. Kastner, "The single electron transistor and artificial atoms", Ann. Phys. (Leipzig) 9 11–12, 885 – 894(2000)
[28] Ben Jacob et al, " DNA Based Electronics", US Patent, Patent No-7, 176,482 B1, (Feb 13,2007)
[29] E. Ben-Jacob, Z. Hermon, S. Caspi, "DNA transistor and quantum bit element: Realization of nano-biomolecular logical devices". Physics Letters A 263 199–202 (1999)
[30] Mali, R.K. Lal, " The DNA Set: A novel Device for Single Molecule DNA Sequencing," IEEE Transaction on Electron Devices, vol 51, no. 12, 2004-2012, (2004).
[31] Ch. Adessi, S. Walch, and M. P. Anantram, "Environment and structure influence on DNA conduction", PHYSICAL REVIEW B 67, 081405 R (2003)
[32] Sanjasi Sitha, K Bhanuprakash, B.M. Chaudhary, "Electrical Rectification through Cumulenic Bridge: A computational Study, " Synthetic Metals, 148, PP 227-235, (2005)
[33] Sergey Kubatkin , Andrey Danilov , Mattias Hjort , J_er^ome Cornil ,Jean-Luc Br_edas , Nicolai Stuhr-Hansen , Per Hedegard , Thomas Bjørnholm, "Single electron transistor with a single conjugated molecule", Current Applied Physics 4 554–558(2004)
[34] You Lin Wu et.al.,"An Improved Single Electron Transistor Model for SPICE Application",Nanotech Vol. 3,www nsti.org, ISBN 0-9728422-2-5 (2003)
[35] Takashi Nakamura, Kazuhiko Nakatani and Isao Saito, "DNA HOMO as a new landmark for nucleic acid properties, abinitio calculations and experimental mapping", Oxford University Press Nucleic Acids Symposium Series No. 42 119-120 (1999)
[36] Palok Aich,et .al., " M-DNA: A Complex Between Divalent Metal Ions and DNA which Behaves as a Molecular Wire", J. Mol. Biol. 294, 477-485(1999)
[37] Prashant Damle, Titash Rakshit, Magnus Paulsson, and Supriyo Datta, "Current–Voltage Characteristics of Molecular Conductors: Two Versus Three Terminal", IEEE Transactions On Nanotechnology, Vol. 1, No. 3, pp 143-153,September (2002)

Synthesis and Characterization of Boron Subphthalocyanine Chloride Thin Films

Sameer kalia, Jasmeet Kaur, Navjot kaur
PG Department of Physics, DAV College, Amritsar, India

***Abstract*-There has been exponential growth in energy demands of the world in recent years. The reliability on fossil fuels has increased the pollution concerns. The world is now committed to bring to use the greener energies. Solar energy is the most abundant energy on the surface of earth and is the most nature friendly form of energy as well. The last two decades have seen the growth of inorganic solar cells put to use but their high initial cost of installation has inhibited their use. The scientific fraternity has been looking for the use of organic materials for solar cell applications. However till date no material has been able to achieve the efficiencies attained by their inorganic counterparts. The low efficiencies in organic solar cells (OSCs) has encouraged the people to look for other highly conjugated organic materials which can help in transporting the electron hole pairs generated as excitons [1–3]. This area of research found due attention with pioneer work reported by Tang [4] forming a two layer hetrojunction solar cell. Since then many new multi layer and composite materials have been put to use for OSCs [5–8].**

Boron Subphthalocyanine Chloride (BSubPc) is a highly conjugated organic material. It has specific properties different from other members of Phthalocyanine family due to its non planner structure [9]. In the present work BSubPc films were prepared by vacuum coating technique. The films prepared were studied for their structural, optical and electrical properties.

I.INTRODUCTION

Boron Subphthalocyanine Chloride is a highly conjugated organic material with 14 Π electron aromatic system. Their slight non planner bowl kind structure with octupolar character is different from other Phthalocyanines. The BSubPc based solar cells have great advantage of having high power conversion effeciencies, high open circuit V_{oc}. When used as a layer in hetrojunction cells, it has been reported to have VOC 27% more than Phthalocyanine/C60 cells [10]. But the most important of all its properties is its absorption band in the visible region with peak matching the peak of energy spectrum of sun at around 575 nm. Electronic properties organic semiconductors are strongly depending on the overlap of the neighboring molecule orbits [11, 12].

An interesting feature of all of the OPVs of BsubPc is that they in general display a particularly high open circuit voltage (Voc) [10] likely due to their HOMO and LUMO energies, a property that has been desirable in photovoltaics since their inception. The emission wavelength of BsubPc is around 575 nm, and has a narrow emission band with a full width half maximum of only 30 nm [14].

Boron Subphthalocyanine chloride is composed of three diiminoisoindole around a boron core. These isoindoles are connected through imino nitrogen, giving BsubPc an aromatic π-system of 14 π-electrons (Fig 1). SubPcs have a coned shaped structure because of constraints arising from the coupling of the three isoindoles units. These molecules indeed have a strong aromaticity [13]. The 14π-electron aromatic core system of Cl-BsubPc along with their nonplanar cone shaped structure and octupolar character make them potential candidates to design hybrid inorganic-organic materials with outstanding tunable properties for photo-induced electron energy transfer, optical data storage, nonlinear optics and sensing applications [10]. The atomic radius of boron is slightly larger than cavity causing the SubPc ligand to adopt nonplanar conformation. The symmetrical 14- π electron system of BsubPcs both absorbs and emits radiation in the visible spectrum [14]. Their most prominent and lowest energy absorption band, known as the Q band, is seen generally between 560-600 nm equating to an optical band gap of 2.1-2.0 eV.

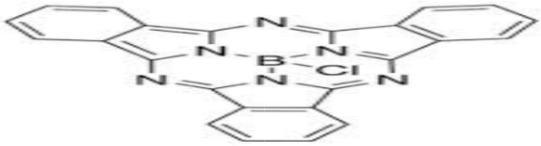

Fig.1 Structure of B SubPc

II.EXPERIMENTAL TECHNIQUES

The Boron subphthalocyanine chloride powder was purchased from eldritch company. The heterostructure was deposited on to cleaned glass substrate by vacuum coating unit. The deposition of organic material was done at the pressure of (10^-5) mb. The thickness of BsubPc-Cl

was found to be 100nm. The structural analysis of films was done by using X-ray diffraction (XRD) technique. The optical properties were studied using uv vis analysis of the sample. The electrical studies were done using Pico ammeter and function generator supplied by SES company, Roorkee. All the measurements were carried out at room temperature.

III.UV-VISIBLE ANALYSIS

UV-Visible analysis was done from SAIF, PU, Chandigarh using apparatus Perkin Elmer model no. lambda 750. The graphs were plotted between hv and (αhv)2. From graph we measure band gap for different samples. The band gap obtained for the samples was found to be about 3.57eV.

IV.X-RAY DIFFRACTION (XRD)

X-Ray Diffraction (XRD) was done from SAIF, PU, Chandigarh using Diffractrometer XPERT. PRO. X-ray spectra have been recorded in the range 5-80 (2θ).

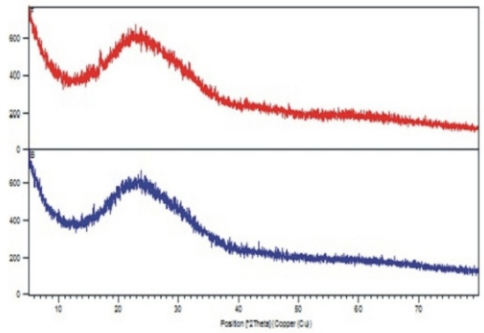

The graph shows that used material is of amorphous type and only hump at 22 degree is due to the glass substrate only. The broad peak centered at 2theta =22deree has been observed in the X-ray diffraction spectrum of Cl-BsubPc films and this peak represented (002) plane. This

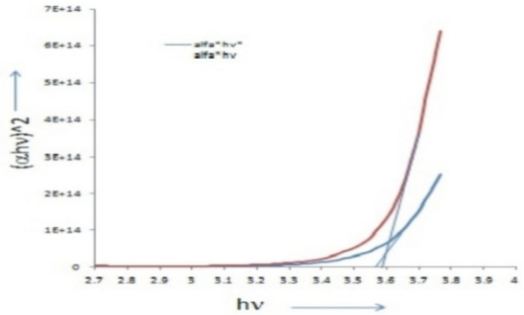

Fig.2 U-V visible analysis of the films

indicates that Cl-BsubPc molecule exhibit a preferential alignment of the molecular crystals with the (002) orientation perpendicular to the substrate [10].

V.DIELECTRIC PROPERTIES

The dielectric properties of the samples were studied by forming aluminum electrode. The V-I characteristics showed that the electrodes were non rectifying in nature. The dielectric constant was determined using Goswami equivalent circuit model[15]. The capacitance of the film was obtained by measuring ac current at various frequencies (10-1000 Hz). The asymptotic value of this curve gives the geometric capacity of the film.

$C = \varepsilon_o KA/d$

Dielectric constant was found to be 2.7.

VI.RESULTS AND CONCLUSION

The Cl-BsubPc has made significant mark as potential candidate for photo voltaic applications. The band gap of the films made were found to be corresponding to visible part of the spectrum. The XRD studies have shown that the films were amorphous in nature. The dielectric constant of the material has been found to be 2.7.

VI.REFERENCES:

[1] J. Y. Kim, K. Lee, N. E. Coates et al., "Efficient tandem polymer solar cells fabricated by all-solution processing," .

[2] F. C. Krebs, S. A. Gevorgyan, B. Gholamkhass et al., "A round robin study of flexible large-area roll-to-roll processed polymer solar cell modules," Solar Energy Materials and Solar Cells, 2009.

[3] F. C. Krebs, H. Spanggard, T. Kjær, M. Biancardo, and J. Alstrup, "Large area plastic solar cell modules," Materials Science and Engineering B, vol. 138, no. 2, pp. 106–111, 2007. View at Publisher · View at Google Scholar · View at Scopus

[4] C. W. Tang, "Two-layer organic photovoltaic cell," Applied Physics Letters, vol. 48, no. 2, pp. 183–185, 1986. View at Publisher · View at Google Scholar · View at Scopus

[5] R. F. Bailey-Salzman, B. P. Rand, and S. R. Forrest, "Near-infrared sensitive small molecule organic photovoltaic cells based on chloroaluminum phthalocyanine," Applied Physics Letters, vol. 91, no. 1, p. 013508, 2007. View at Publisher · View at Google Scholar · View at Scopus

[6] 6.J. Dai, X. Jiang, H. Wang, and D. Yan, "Organic photovoltaic cells with near infrared absorption spectrum," Applied Physics Letters, vol. 91, no. 25, Article ID 253503, 2007

[7] 7.G. Yu, J. Gao, J. C. Hummelen, F. Wudl, and A. J. Heeger, "Polymer photovoltaic cells: enhanced efficiencies via a network of internal donor-acceptor heterojunctions," Science, vol. 270,

[8] 8.J. Xue, B. P. Rand, S. Uchida, and S. R. Forrest, "A hybrid planar-mixed molecular heterojunction photovoltaic cell," Advanced Materials, vol. 17, no. 1, pp. 66–71, 2005.

[9] Kan- Lin Chen, D.W. Chou, Chien – Jung Huang , Jhong-Cioe Ke, Wen Ray Chen and Teen Hang Meen, "Effect of various Structures on the efficiency of organic solar cells".

[10] Mandeep Singh, Aman Mahajan, R.K.Bedi, and D.K.Aswal,"Dielectric Spectroscopic Studies of Boron Subphthalocyanine chloride thin films" Material sci. research lab., Dept. of phys., GNDU, Asr.

[11] Wang Jingchuan "Light absorption broadening and exciton diffusion length enchancement for solar cells" dept.of mech. Eng

[12] Andrew Simon Paton Altering the Crystal Packing of Boronsubphthalocyanine Derivatives through Molecular Engineering dept of chemical eng. And appl. Phys 2013.

[13] Kobayashi, N.; Ishizaki, T.;Ishii,K.;Konami, H. J. Am. Chem, 1999.

[14] Meller, A., and Ossko, A. Monatsh. Chem., 1972, 103, 150

[15] A. Goswami and A. P. Goswami, Thin Solid Films 16, 175

[16] A.Wang, L.Long, and C.J.Zhang, J. Incl. Phenom. Macrocycl.chem.71 (2011)

[17] Graham E.Morse and Timonthy P.Bender "Boron Subphthalocyanines as Organic Electronic Materials", Dept. of chemical Eng. And Appl. Chemistry, Dept of chemistry,Dept. of Materials Sci. uni. Of Toronto.

[18] (12)Zur Erlangung des akademischen Grades, Doktor der Naturwissenschaften,(Doctor rerum naturalium) vorgelegt von, Wolfgang Tress" Device Physics of Organic Solar Cells Drift-Diffusion Simulation in Comparison with Experimental Data of Solar Cells Based on Small Molecules".

[19] Simon Bates" Advanced Analysis of Non-Crystalline (X-ray Amorphous) Materials and Dispersions".22 (10) 3. Kristin L. Mutolo, Elizabeth I. Mayo, Barry P. Rand, Stephen R. Forrest, and Mark E. Thompson, J. Am. Chem. Soc. 128, 108 (2006). 22 (15)

REVIEW OF LOAD BALANCING ROUTING PROTOCOLS IN MOBILE AD HOC NETWORKS

Er. Gaganjot Kaur[a], Dr. Tanu Preet Singh[b]
[a]*M.Tech Research Scholar*
Department of Computer Science & Engineering
Amritsar College of Engineering & Technology, Amritsar
Er.gagan.acet@gmail.com
[b]*Professor & HOD,Department of Electronics & Communication Engineering*
Amritsar College of Engineering & Technology, Amritsar
tanupreet.singh@gmail.com

***Abstract*- Load balancing is the crucial part of the MANET routing protocols. It has been seen that many experts proposed many new techniques for balancing the load in MANETs. Here this paper includes many load balancing techniques in MANETs and also measures their performances by taking several parameters like PDR, DELAY, Control Packets. This paper contains the basic knowledge about the MANETs with their applications and limitations. It also contains MANET's routing protocols like FARP, AODV, LBPRP, and NCLBR.**

***Index terms*- load balancing, MANETs, routing protocols, FARP, AODV, LBPRP, and NCLBR.**

1. INTRODUCTION

Load balancing plays an important role in routing protocol for efficient data transmission in MANETS (mobile ad hoc network).Today, the most challenging Task in designing an adhoc network is the development of efficient routing protocol that provides high quality communication. In MANETS, the role of the routing protocol is to distribute the routing tasks among the mobile host. If the node with heavy routing duties i.e. has large queuing delay and high packet loss ratio which results in the serious problem like congestion, power depletion and queuing delay. To remove these problems, a load balancing tool is emerged for better use of MANET's resource and also to enhance MANET's performance. With the use of the load balancing techniques, MANETS can be able to minimize the traffic congestion, end to end delay and to maximize the lifetime of mobile nodes.

2. MOBILE ADHOC NETWORK

MANETS are the wireless communication network in which nodes are not in the direct range of each other. They separately establish their communication by using the different nodes to forward the data between them. They will occur without any fixed infrastructure and also comes under the multi-hop wireless networking

2.1 APPLICATIONS OF MANETS

MANETS are often used in the situations where fixed networks are either very much expensive or they are impractical in nature. They are used in large no of applications for example [1]

A. **PERSONAL AREA NETWORK (PANs):** PANs are particularly designed for individual users. They are derived from different types of mobile devices. The main role of PANs is to build an embedded network by combining some nodes that are inside or near the human body to exchange the digital data between them. The communication between nodes of different PANs can take advantage of using the facilities provided by adhoc network for example a doctor can distribute different set of devices (sensors) on the patient's body so that he can able to get the medical information also named as Wireless Body Area Network which has many applications in medical field[1].

B. **MILITARY APPLICATIONS**: In the area of battle field military applications can be considered as the most popular application of adhoc network because of providing an infrastructure less network which gives reliable communication and fast failure recovery. In the battle field, it is not so complicated to set up a fixed network for military communications.

2.2 LIMITATION OF ADHOC NETWORK [1]

There are many restrictions that need to be accounted for when designing routing protocols for MANETs which is indeed a challenging task. These physical constraints include the following.[1]

A. Limited CPU Capacity: Nodes have limited processing operations.
B. Limited Storage Capacity: Memory resources are normally restricted in the mobile nodes.
C. Limited Battery Power: where each node has a limited life time battery.
D. Limited Bandwidth: Bandwidth is shared by a number of mobile nodes.
E. Nodes have limited transmission range since they are depends on the radio waves.
F. Rapidly changing topology, where the nodes are continuously moving and changing their places.

3. ROUTING FOR ADHOC NETWORK

Routing is the essential component of any adhoc network which is responsible for balancing the load between the source and the destination. It is a mechanism of finding an appropriate route between the source and the destination in order to send the packets between them. They are divided into two basic types which are [1]:

a. Static Routing: Static Routing is the type of routing which is done manually by the administrator. Administrator assigns the route manually to send the packet in the network. From this it has been concluded that the source and the destination are fixed during the whole transaction. Here the router is not responsible for building a routing table.
b. Dynamic Routing: Dynamic routing is the routing technique which is responsible for building and exchanging the routing table information. It is much more flexible than the static routing since it detects congested paths. It comes under the following three categories:[1]

1. Reactive Protocols
2. Proactive Protocols
3. Hybrid Protocols

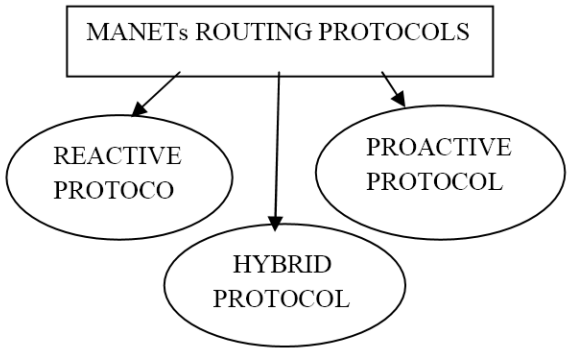

Fig1. Types of MANETs Routing Protocols

I. Reactive Protocols: They are also called On Demand routing protocols because it does have any prior knowledge about the routes between the nodes until the source node sends a Route Request to the destination node. They are used to reduce the no of control overhead by determining routes to a destination whenever required. This can be achieved by a process called two-phase route discovery which is initiated by source node. This include Route Request Packet (RREQ) and Route Reply Packet (RREP).When large no of flows, reactive protocols shows significant drop in data throughput due to global flooding. To reduce this global flooding two protocols are introduced Location aided routing (LAR) and RDMAR. Reactive protocols have the following four characteristics [1]

1. The route should be found only when needed.
2. Flooding technique is used in order to broadcast the route request.
3. Saving bandwidth by decreasing control packets.
4. Bandwidth is used when source node decides to transmit data to a destination node. Adhoc On-Demand Distance Vector Routing Protocol (AODV) is an example of on-demand protocol.

II. Proactive Protocols: It is the first step in designing the routing protocol. They include two protocols DSDV and GSR which are used to maintain the routes to all nodes within the network. They contain full information regarding the routes between each pair of nodes whether the nodes need to send data or not. This lead to disadvantage of having lack of scalability and large no of overhead. This can be removed by introducing two protocols i.e. OLSR and TBRPF by reducing the no of re-broadcasting nodes in the network. The advantages and disadvantages of proactive protocols are given below.

Advantages: [1]

a. Nodes can easily obtain routing information.
b. Nodes can easily initiate a session.

Disadvantages: [1]

a. Consuming bandwidth because of the large overhead caused by the control messages exchange

b. A huge amount of data needs to be saved in the memory of each node in the network.

III. Hybrid Protocols: It is a combination of both reactive and proactive protocols to utilize the advantages of each of them. The most popular example of the hybrid routing is Zone Routing Protocol (ZRP). In these routing protocols all the network nodes are groups into zones. The nodes having the same zone come under the proactive protocol where as the nodes having different zones comes under the reactive protocols. Fig1 shows an example of the ZRP protocol with two hops.

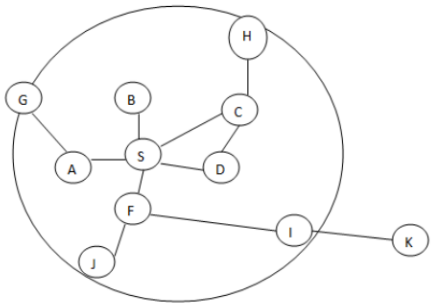

Fig2. Example of routing zone with two hops

In the fig1 we notice that the nodes in ZRP protocol are differentiating into three categories [1]

A. Peripheral Nodes: Peripheral nodes are the nodes which are at the same distance from the central node with equal zone radius. The nodes J, I, G and H are the peripheral nodes.

B. Interior Nodes: The interior nodes are the nodes which are placed at a distance from the central node smaller than the zone radius. The nodes A, B, C and d are the interior nodes.

C. Nodes outside the routing zone: Those nodes which are separated from the central nodes by a distance more than the zone radius. The node k is the only node which resides outside the routing zone.

4. FLOW AWARE ROUTING PROTOCOL

Flow Aware Routing Protocol is the protocol whose purpose is to reduce the amount of control overhead so that a better distribution of the traffic between the nodes takes place. To reduce congestion or the creation of the bottleneck nodes, they introduce a utility metric for restricting the propagation of route request (RREQ) over the nodes having minimum no of the active data flows from different source nodes.

4.1 PERFORMANCE METRICS IN FARP [4]

There are three different types of performance metrics to compare the FARP routing strategies. They are:

A. Packet Delivery Ratio(PDR)
B. Control Packets
C. Delays

A. Packet Delivery Ratio (PDR): Packet Delivery Ratio measures the percentage of data packets generated by nodes that are successfully delivered. [2]
In case of 20 nodes – both AODV and FARP achieves over 98% of PDR. [4]
In case of 100 nodes- The PDR performance of FARP is much more than AODV in case of having high node mobility. This is due to FARP reduces the establishing routes over bottleneck. Also FARP introduces a more selective approach to flooding than AODV.[4]

B. Control Packet: In case of 20 or 100 nodes, FARP produces fewer control packets than AODV because of having restriction of flooding over nodes which are further break down the no of rebroadcasting nodes as compared to AODV.

C. Delays: In case of 20 nodes- both AODV and FARP obtaining equal levels of end-to-end delay because of introducing lower level of traffic in the network than that of the available bandwidth and capacity of each node.[4]
In case of 100 nodes- when the mobility is high 50 flows of FARP obtains significantly lower end-to-end delay than AODV. This is due to the AODV protocol produces more control overhead than FARP. [4]

5. MANET NETWORK MODEL

The MANET network model consists of a collection of nodes that have the capacity to connect on a wireless medium and form either an arbitrary and dynamic network with the wireless links that will change with respect to time. They have no permanent infrastructure.

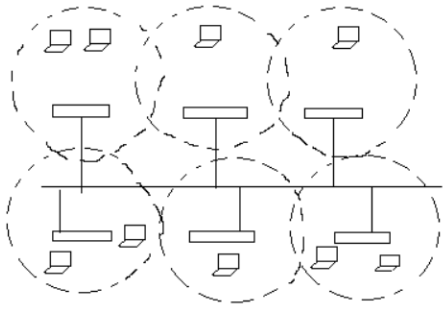

Fig3. Wireless Network Structure (Infrastructure Networks)

6. Ad hoc On Demand Distance Vector Routing Protocol (AODV)

In case of the MANETs, AODV protocol is a reactive unicast routing protocol in which it maintains a routing table for storing each entry of the routing data for all the nodes. If the routing table entry is not used for such a long period it will get expires or reactivated for a pre-specified expiration time. The AODV routing table contains the following main fields. [1]

a. Destination IP Address: It contains the IP address of the destination nodes.
b. Destination Sequence Number: It increment the sequence number for every new route to the destination node.
c. Hop Count: It gives a total number of hops needed to reach a specific destination.
d. Next Hop: It indicates the next node in the route.
e. The states routing flags(e.g. valid, invalid, repairable, being repaired): These flags indicates the states of the route in the routing table.

7. NODE CENTRIC LOAD BALANCING ROUTING PROTOCOL (NCLBR)

The working of this protocol is same as like the AODV protocol. In this protocol it performs three distinct roles for the nodes named as Terminal, Trunk and Normal Nodes. The nodes which are connected through a single link are called Terminal nodes. They contains only one neighboring nodes. The nodes which are connected to two distinct networks are called Trunk nodes. Normal nodes are those nodes which are neither the Terminal nodes nor the Trunk nodes.

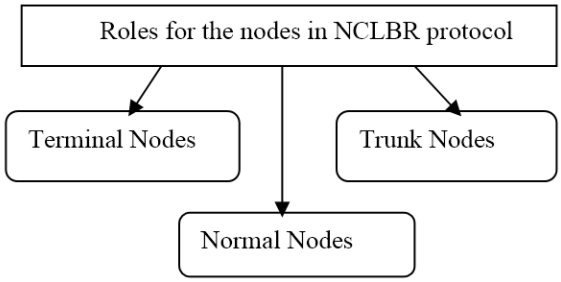

Fig4. Roles for the nodes in NCLBR protocol

PARAMETERS	NCLBR	AODV
Routing path	Single Path	Single Path
Category	Traffic Size	Packet in interface Queue
Metric Used	Current congestion status	interface queue length
Complexity of capturing load	Low	High
Routing structure	Reactive	Reactive

Table1. Compares the delay-oriented load balancing routing protocols [8]

8. OVERVIEW OF CORMAN

CORMAN stands for the Cooperative Opportunistic Routing in mobile ad hoc network. It is an extension of EXOR. Unlike EXOR, CORMAN also forwards the information in batch oriented fashion i.e. information packets are divided into batches. To support CORMAN, we have proactive source routing which provides complete routing information to each node in the network.

9. LOAD BALANCING PARALLEL ROUTING PROTOCOL (LBPRP)

The main aim of this system is to develop a product which results in increase in the MANETs lifetime by using Load Balancing multipath technique representing parallelism in sending data using disjoints multipath. Here disjoints multipath means

all the selected nodes will send data at the same time. Hence, it results in solving the overloading problem and prevention of the node starvation.

10. COMPARISON CHART

ROUTING PROTOCOLS	PDR(PACKET DELIVERY RATIO)	DELAYS
FARP(FLOW AWARE ROUTING PROTOCOL)	A	A
AODV(Ad hoc on demand Distance Vector Routing Protocol)	B	B
LBPRP(LOAD BALANCING PARALLEL ROUTING PROTOCOL (LBPRP)	D	C
CORMAN	C	D

A- EXCELLENT B- GOOD C- AVERAGE D- POOR

Table2. Comparison of routing protocols based on parameters like PDR and Delay.

PARAMETER	LBPRP	CORMAN	AODV
PDR	650*10^3	700*10^3	750*10^3

Table3. The Packet Delivery Ratio Vs Network Dimension [2]

PARAMETER	LBPRP	CORMAN	AODV
Packet Delay	7*10^3	48*10^3	15*10^3

11. CONCLUSION

In this study many load balancing techniques for MANETs are discussed. It includes routing protocols like FARP (Flow Aware Routing Protocol), AODV (Adhoc on demand Distance Vector Routing Protocol), LBPRP (LOAD BALANCING PARALLEL ROUTING PROTOCOL (LBPRP), CORMAN, NCLBR (NODE CENTRIC LOAD BALANCING ROUTING PROTOCOL). On comparing all these protocols on the basis of the following parameters like PDR (Packet Delivery Ratio), Control Packets, Delay. It has been observed that FARP has higher level of packet delivery than AODV which further have a higher packet delivery than CORMAN AND LBPRP. So from this it has been concluded than FARP has overall higher PDR among all the routing protocols. Also FARP achieves lower end-to-end delay than AODV. AODV achieves more packet delay than LBPRP and corresponding less packet delay than CORMAN. So overall it is seen that FARP has lower packet delay among all routing protocols. So from here it is concluded that FARP has high packet delivery ratio with less delay.

REFERENCES

[1] Yahya Tashtoush a,*, Omar Darwish a, Mohammad Hayajneh b, “Fibonacci Sequence Based Multipath Load Balancing Approach for mobile ad hoc network”, journal, 2014

[2] M.Selladevi, P. KrishnaKumari, “Load Balancing Parallel Routing Protocol in Mobile AD Hoc Network”, International journal of engineering and computer science, Volume 2, 2013, pp. 2728-2732.

[3]Shashank Bharadwaj #1, Vipin Kumar #2, Ankit Verma #3,” A Review of Load Balanced Routing Proocols in Mobile Adhoc Networks”, International Journal of engineering and technology, 2011, pp. 2231-5381.

[4] Mehran Abolhasan, Justin Lipman, Tadeusz Wysocki,” Load-Balanced Route Discovery for Mobile Ad hoc Networks”, Conference, 2004.

[5]Amjad Ali, Wang Huiqiang, “Node Centric Load Balancing Routing Protocol for Mobile Adhoc Networks”, Conference, Volume1, 2012

[6] Zhijing Xu1, Kang Wang2, Liu Qi 1,” Adaptive Threshold Routing Algorithm with Load-balancing for Ad Hoc Networks”,2009, pp. 351-354

[7] Bahram Najafpour1, Behzad Mahdavi2, Vahab Ashrafian3, Narges Latifi Avid4, Mehdi Sadeghzadeh5," Comparative Study of Delay-Oriented and Hybrid Load Balancing Routing Protocols in Mobile Ad Hoc Networks", Journal of Basic and Applied Scientific Research, 2013, pp.498-502

[8] Behzad Mahdavi1, Bahram Najafpour2, Hadi Mojez3, Hamed Masoomi4, Feridon Babazadeh5, " An Overview of Traffic-Oriented load Balancing Routing Protocols Based on the Multiple Metrics in Mobile Ad Hoc Networks", Journal of Basic and Applied Scientific Research, 2013, pp.751-755

[9] Yashar Ganjali, Abtin Keshavarzian ," Load Balancing in Ad Hoc Networks: Single-path Routing vs. Multi-path Routing", Conference, 2004

[10] Vinh Dien HOANG, Zhenhai SHAO and Masayuki FUJISE, "Efficient Load balancing in MANETs to Improve Network Performance", International Conference on ITS, 2006, pp.753-756

[11]Jie Gao, Li Zhang," Load Balanced Short Path Routing in Wireless Networks", Conference, 2004,

Photonic Integrated Circuits: Materials & Fabrication

Harmandar Kaur
Department of Electronics & Communication Engg., GNDU, India

***Abstract*— An ever increasing demand for data has led to the invent of smaller, faster and efficient devices. But the thermal and signal delay problems impose a limitation on the speed of the device.[1-3]Large-scale photonic integrated circuits (PICs) in Indium Phosphide represent a significant technology innovation that simplifies optical system design, reduces space and power consumption, and improves reliability. In addition, by lowering the cost of optical-to-electrical-to-optical (OEO) conversion in optical networks, they provide a transformational opportunity to embrace the use of electronic ICs and system software in a "digital" optical network to maximize system functionality, improve service flexibility, and simplify network operations.**

***Keywords*—**microelectronics, photonics, optical materials

I. INTRODUCTION

The most commercially utilized material platform for photonic integrated circuits is indium phosphide, which allows for the integration of various optically active and passive functions on the same chip. Initial examples of photonic integrated circuits were simple 2 section distributed bragg reflector lasers, consisting of two independently controlled device sections - a gain section and a DBR mirror section. Consequently, all modern monolithic tunable lasers, widely tunable lasers, externally modulated lasers and transmitters, integrated receivers, etc. are examples of photonic integrated circuits. Current state-of-the-art devices integrate hundreds of functions onto single chip.[4]

it has been shown that silicon can, even though it is an indirect bandgap material, still be used to generate laser light via the raman nonlinearity. Such lasers are not electrically driven but optically driven and therefore still necessitate a further optical pump laser source. [5]

II. MATERIALS AND FABRICATION

A. *Materials*

Unlike electronic integration where silicon is the dominant material, system photonic integrated circuits have been fabricated from a variety of material systems, including electro-optic crystals such as lithium niobate, silica on silicon, Silicon on insulator, various polymers and semiconductor materials which are used to make semiconductor lasers such as GaAs and InP. The different material systems are used because they each provide different advantages and limitations depending on the function to be integrated. For instance, silica (silicon dioxide) based PICs have very desirable properties for passive photonic circuits such as AWGs due to their comparatively low losses and low thermal sensitivity, GaAs or InP based PICs allow the direct integration of light sources and Silicon PICs enable co-integration of the photonics with transistor based electronics.[3]

The fabrication techniques are similar to those used in electronic integrated circuits in which photolithography is used to pattern wafers for etching and material deposition. Unlike electronics where the primary device is the transistor, there is no single dominant device. The range of devices required on a chip includes low loss interconnect waveguides, power splitters, optical amplifiers, optical modulators, filters, lasers and detectors. These devices require a variety of different materials and fabrication techniques making it difficult to realize all of them on a single chip.

Newer techniques using resonant photonic interferometry is making way for UV LEDs to be used for optical computing requirements with much cheaper costs leading the way to PHz consumer electronics.

Photonic integrated circuits are usually fabricated with a wafer-scale technology (involving lithography) on substrates (often called chips) of silicon, silica, or a nonlinear crystal material such as lithium niobate ($LiNbO_3$). The substrate material already determines a number of features and limitations of the technology:

Silica-on-silicon integrated optics builds on silicon wafers, for which many aspects of the powerful microelectronics technology can be used. Silica waveguides allow the realization of couplers, filters (e.g. for multiplexers and demultiplexers in wavelength division multiplexing technology), power splitters and combiners, and even active elements with optical gain. They can also be connected to optical fibers.

An area of strong current interest is silicon photonics, where photonic functions are implemented directly on silicon chips.

An already commercialized photonic integrated circuits technology is based on indium phosphide (InP); it is used mainly in optical fiber communications.

Waveguides can be fabricated on silica glass (fused silica) e.g. with lithographic techniques involving chemical processing or indiffusion of dopants, or with laser micromachining. The latter techniques can be used for fabricating waveguides far below the surface (embedded waveguides), so that three-dimensional circuit designs become possible. Amplifiers and lasers can be made by using rare-earth-doped glasses.

Lithium niobate ($LiNbO_3$) as a nonlinear crystal material is suitable for devices performing nonlinear functions, for example electro-optic modulators or acousto-optic transducers. Waveguides can be fabricated on lithium niobate substrates e.g. via proton exchange or by indiffusion of titanium, in any case controlled by a lithographic method. Doping with rare earth ions makes possible amplifiers and lasers. The birefringence of this material creates opportunities for polarization control, which may then be used e.g. for filtering purposes. On the other hand, the birefringence makes it more difficult to obtain polarization-independent devices, as are often required for optical fiber communications.[6]

An important distinction is that between devices with smaller or larger mode areas:

Some waveguides (e.g. made in silicon-on-insulator technology) exhibit strong confinement, leading to small effective mode areasand allowing for tight bends without excessive bend losses. They are therefore potentially suitable for chips with a very high level of integration. However, such devices are essentially always polarization dependent, having a strong built-it birefringence. Polarization-insensitive designs would be possible in principle, but would introduce unrealistic fabrication tolerances.

Other waveguides exhibit much weaker guidance and can be made in polarization-insensitive form. However, such waveguides do not allow tight bends and thus prevent a high level of integration.[7]

B. Fabrication

There are two techniques to design these ultra-compact waveguides. One can use a scaled down version of conventional index-guided waveguides. These *photonic wires* are typically 300−500*nm* wide. Alternatively, light can be guided in a photonic crystal, a periodic structure with a high refractive index contrast and a period of the order of the wavelength of the light[8].This strong contrast and periodicity can create a photonic band gap (PBG), i.e. a wavelength range where light cannot propagate through the crystal. A waveguide can be made by confining the light to a line defect in a photonic crystal.

In a photonic crystal slab, a 2-D periodic structure is used, and in the third, vertical, direction, the light is confined in a simple slab waveguide. These structures can be fabricated using high resolution lithography and dry etching in a semiconductor layer stack.

At 1.3μ*m* and 1.55μ*m*, both photonic wires and photonic crystals have dimensions of a few hundred nanometers. However, the accuracy required of the fabrication is of the order of 10*nm*. Therefore, we can rightfully speak of nanophotonics. For research purposes, nanophotonic components are traditionally fabricated using e-beam lithography. While this is a very accurate technique, it is slow and unsuitable for mass-fabrication. Conventional photolithography, as used for the fabrication of current photonic ICs, lacks the resolution to define nanophotonic structures. Deep UV lithography at 248*nm* or 193*nm*, the technology used for advanced CMOS fabrication, offers both the resolution and throughput needed for commercial applications.

Deep UV Lithography

Photonic nanostructures typically consist of a variety of structures and for accurate alignment all nanostructures should be printed in the same lithography step. This is not trivial, as not all structures print on target for the same lithography conditions. Especially the exposure dose, i.e. the amount of light in the photoresist, has a large influence on the feature size [3, 4]. For higher doses, the illuminated areas, like the holes of a photonic crystal or the trenches adjacent to photonic wires, will expand. The dose-to-target for photonic crystals and photonic wires can therefore differ significantly. To fabricate both simultaneously, a bias needs to be applied to one or the other, preferably the isolated wires. As this bias between lines and holes needs to be applied directly on the photomask, it should be known in advance. Therefore, we have included on our first photomask a large number of test structures, representative of many nanophotonic circuit elements. From this, we could extract the necessary bias on the etched features.

Etching

After lithography, the patterns in the photoresist are transferred to the underlying SOI by dry etching. We can choose between etching only the top Silicon, or the underlying oxide as well. For a nano-photonic waveguide, etching the oxide is better, as it increases the lateral and the vertical index contrast. For our first experiments [9], we etched the top Silicon layer with a low pressure/high density ICP etch based on *Cl*2/*HBr*/*He*/*O*2. This is a highly selective etch process. Subsequently, the oxide was etched using medium density *CF*4/*O*2-plasma chemistry at medium pressure. In between the etch processes, the wafer is not exposed to the outside atmosphere. However, as we can see in Fig. 3(a), this deep etching causes considerable sidewall roughness[10], because of the limited thickness of the photoresist which is used as an etch mask.

The sidewall roughness can be reduced by thermal oxidation of the top Silicon layer [11]. However, this technique only reduces roughness in the top layer, not in the underlying oxide. A better solution is not to etch the buried oxide altogether, as shown in Fig. 2(b). In our optimized fabrication process, a plasma treatment of the photoresist is carried out, which smoothens irregularities present in the photoresist patterns. Then the top Silicon is etched

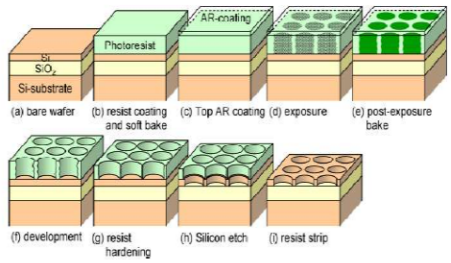

Fig.1. Fabrication process for photonic nanostructures in SOI using deep UV lithography and dry etching[13]

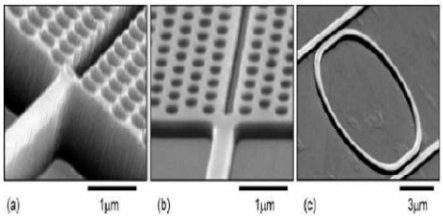

Fig.2. Photonic crystal waveguides fabricated with deep UV lithography and dry etching. a). trench defect in deeply etched photonic crystal, b). silicon only etch, c). racetrack resonator with silicon only etch[13]

Conclusion

Photonic integrated circuits can allow optical systems to be made more compact and higher performance than with discrete optical components. They also offer the possibility of integration with electronic circuits to provide increased functionality. [12]

One challenge to achieving this level of integration is the size discrepancy between electronic and photonic components.[13] The emerging field of nanoplasmonics is focused on creating ultracompact components for realizing truly nanoscale photonic devices to match their electronic counterparts.

An example of the new breed of components is a recently proposed novel type of bandpass plasmonic filter that uses a response similar to electromagnetically induced transparency to achieve multichannel filtering.[14] This allows easy control over the filtering wavelengths and bandwidths for applications in wavelength multiplexing systems for optical computing and communications in highly integrated all-optical circuits.

Photonic integrated circuits should also be immune to the hazards of functionality losses associated with electromagnetic pulse (EMP), though may not be immune to high neutron flux.

References

1. Bohr, M. T., Tech. Dig. IEDM (1995).
2. Chiang, T.-Y., et al., Impact of joule heating on scaling of deep sub-micron Cu/low-k interconnects. IEEE Symp. VLSI Circuits, Dig. Tech. Papers (2002)
3. Banerjee, K., et al., Tech. Dig. IEDM (1996).
4. Larry Coldren; Scott Corzine, Milan Mashanovitch (2012). "Diode Lasers and Photonic Integrated Circuits" (Second edition.). John Wiley and Sons.
5. Rong, Haisheng; Jones, Richard; Liu, Ansheng; Cohen, Oded; Hak, Dani; Fang, Alexander; and Paniccia, Mario (February 2005). "A continuous-wave Raman silicon laser"
6. F. A. Kish et al., "Current status of large-scale InP photonic integrated circuits", IEEE Sel. Top. Quantum Electron. 17 (6), 1470 (2011)
7 W. S. Zaoui et al., "Bridging the gap between optical fibers and silicon photonic integrated circuits", Opt. Express 22 (2), 1277 (2014)
8. J. D. Joannopolous, R. Meade, and J.Winn, Photonic Crystals - Molding the Flow of Light (Princeton University
Press, Princeton, N.J., 1995).
9. W. Bogaerts, V.Wiaux, D. Taillaert, S. Beckx, B. Luyssaert, P. Bienstman, and R. Baets, "Fabrication of photonic
crystals in silicon-on-insulator using 248-nm deep UV lithography," IEEE J. Sel. Top. Quantum Electron. 8, 928–934 (2002).
10. W. Bogaerts, V. Wiaux, P. Dumon, D. Taillaert, J. Wouters, S. Beckx, J. Van Campenhout, B. Luyssaert,
D. Van Thourhout, and R. Baets, "Large-scale production techniques for photonic nanostructures," Proc. SPIE
5225, 101–112 (2003).
11. J. Arentoft, T. Sondergaard, M. Kristensen, A. Boltasseva, M. Thorhauge, and L. Frandsen, "Low-loss siliconon-
insulator photonic crystal waveguides," Electron. Lett. 38, 274–275 (2002).
12. "Silicon Photonics" Intel Technology Journal, Volume 08, Issue 02. 10 May 2004.
13. Zia, Rashid; Schuller, Jon A.; Chandran, Anu; Brongersma, Mark L. (2006). "Plasmonics: The next chip-scale technology". Materials Today
14. Lu, Hua; Liu, Xueming; Wang, Guoxi; Mao, Dong (2012). "Tunable high-channel-count bandpass plasmonic filters based on an analogue of electromagnetically induced transparency".Nanotechnology

Energy Efficient Routing Protocol for Mobile Ad hoc Networks: A Review

Er. Kanwalpreet Kaur, Dr. Tanu Preet Singh
M.Tech Research Scholar
Department of Computer Science & Engineering
Amritsar College of Engineering & Technology, Amritsar
Kanwal.preet0511@gmail.com
Professor & HOD
Department of Electronics & Communication Engineering
Amritsar College of Engineering & Technology, Amritsar
tanupreet.singh@gmail.com

***Abstract*-An mobile Ad-hoc network forms the temporary network with the wireless mobile hosts. It is a local area network and doesn't use the base station for the communication [1].Ad-hoc network is used for short range .mobility; energy efficiency and the looping free path are the main part in ad-hoc network.Enrgy efficient routing protocols are used for the efficient energy to the mobile ad-hoc network. We consider DSR , MMBCR and AODV protocols and also the performances of routing protocols in terms of life time[2][7][1].**

***Keywords*-** *Ad-hoc network, AODV, DSR*, MMBCR, mobile AD-hoc network.

INTRODUCTION

An ad-hoc network is used for short range and it is temporary network. Ad-hoc network is used for the local area and the messages can transfer from one end to another. Wireless devices also can communicate with each other with the help of ad-hoc network in local area network. Mobility is the major feature of mobile ad-hoc network. MANET is the end-to-end network and can transfer messages from one end to another and so communication can takes place but in case of large network not all the nodes can directly communicate with each other so the multi-hop is used in ad-hoc network. In this intermediate nodes are used and through these intermediate nodes the communication can takes place from source to destination.ad-hoc network forms the temporary network with the help of wireless hosts. Mobile ad-hoc is a multi hop wireless network because of the mobility of the nodes. The nodes in the ad-hoc network forward packets of data to and from each other this node is also behave like a router that routes the data and can communicate with each other. Mobile ad-hoc network is dynamic in nature.

The main drawback of ad-hoc network is that devices are communicating by passing messages but if the devices or nodes are not there then whole network fails nodes in ad-hoc network uses the limited battery power. So the energy management is the important aspect in ad-hoc network. The energy can be saved with the designing of good protocols so as to decrease the energy consumption. In case of network layer, where the load is distributed to the different paths and then increases the life time. So the routing protocols which selects the path that save the power and increases the life time of the ad-hoc network [1][2][7].

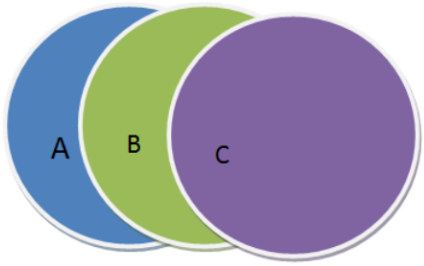

Figure1: Simple Ad hoc Network[2]

CLASSIFICATION OF ROUTING PROTOCOLS

1. Proactive Routing Protocol (table-driven)

2. Reactive Routing Protocol (on-demand)

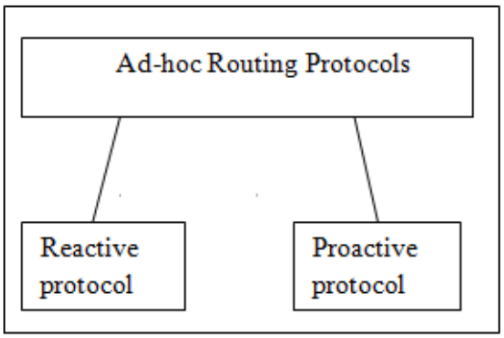

Figure2: Classification of Routing Protocol

Proactive routing protocol or table driven

In Proactive Protocol, the nodes transfer the data packets from one node to the other node and so they update the position of entire node. So the nodes create the Routing table for the other nodes in the network and update the information in the routing table:

The benefit of these Protocols is that for find the route to a destination node , the source node does not require the travels from the source and the limitation of these protocols is that is creates the routing table which is contains the information but increase overhead of messages, uses the more energy and using output . various table driven protocol are Destination Sequenced Distance Vector Routing (DSDV) ,Wireless Routing Protocol (WRP), Fish Eye State Routing Protocol (FSR), Optimized Link State Routing Protocol (OLSR) Cluster Gate Way Switch Routing Protocol[2].

REACTIVE ROUTING PROTOCOL -(On Demand)

Reactive protocol is also called on demand routing protocol. Reactive protocol is used mostly as compared to proactive protocol the reactive protocol is better. Because, it is on demand protocol AODV, PAAMODV are the reactive protocol[2].

2. DESCRIPTION OF SELECTED ROUTING PROTOCOLS

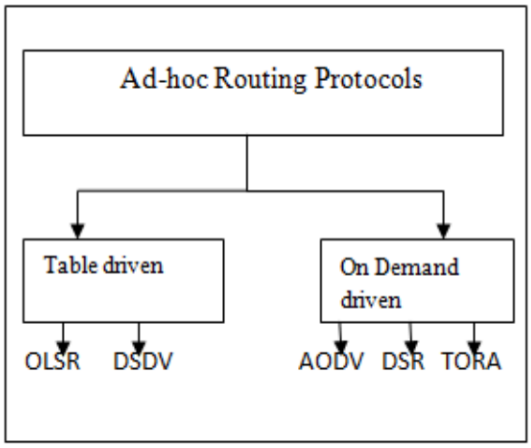

Figure3: Different Routing Protocols

(a)Ad-hoc on demand distance vector (AODV)-

AODV routing protocol is used for ad-hoc network. AODV is also called on –demand algorithm because it maintains the route AODV makes trees and this tree structure create by the group members and all the nodes of the tree connect with each other so the group members connects with each other . In AODV, the messages flows and creates the path and this process is done by first sends the route request (RREQ). The nodes which receives the request is called intermediate node replies to the requesting the nodes by using the nodes reply message. the intermediate nodes replies to the requesting node . if it has a destination path . The intermediate node replies with the route reply message. The intermediate node which replies to the source node have the sequence number which is greater or equal to the sequence number contained in RREQ and also the node which have to reply the RREQ is either the destination or the path to the destination the nodes which contains the RREQ [2][7]if this node is have processed before than the RREQ will be discard the data packets forwards by the source node , if it receives the RREP from the destination if the data packets the source to destination than the route will be active and if the source node doesn't sends the packets then this link will be deleted from the network but if the link is deleted from the network but the path is active then the route error messages(RERR)[7] will receives by the source node[7].In case of ERS, the RREQ goes to the neighbors in the route. if this request receives by the node for the first time , then it will relay the request otherwise the packets will be drop. So the information about the source and destination wastes so this design propose and makes the efficient design in which some nodes will be silent and these and these nodes doesn't

sends the packets so in this way the energy used by the nodes will be efficient and its name after improves is E2AODV i.e. energy efficient AODV[7][2].

Advantages of AODV

AODV protocol is the on demand and finds the route from source to destination &this route will be latest.
The delay is less in AODV protocol. It is on demand so the message overhead is not in case of AODV[2].

Disadvantages

The disadvantages of this protocol is that if the intermediate node does not have latest sequence number then it leads inconsistent routes and also the multiple route reply packets to the one route request packets and this leads to greater overhead[2].

(b)Minimum maximum battery cost routing (MMBCR)

In MMBCR, the selection of route is done on the basis of battery capacity of the nodes which have minimum battery capacity and selects the having the maximum life time or maximum value. If Ci is the cost of battery at any instant t FCIT is the function and the route contains the N nodes then the total cost for the route Ri is the sum of the cost function of all nodes .If f(cit)=1/Git for example the function having higher value ,the more unwilling nodes participating in the route selection algorithm is used for uniform distribution of batteries[7].

(c)DYNAMIC SOURCE ROUTING (DSR)
DSR is the routing protocol. The sender knows the route and the route cache is used to store the route. Data header is used in DSR. The data packets carry the source route in the packet header. When the data packet travel from source to destination and it do not already knows or than it uses the route discovery process to find the route. The route discovery process first it sends the ROUTE REQUEST (RREQ)[7]. The node which receives the RREQ rebroadcast it, whether it is a destination or the route to the destination then RREQ makes the path than Route REPLY (RREP) traverse the path backwards. If the link on the route is break than the source node notified by route error (RERR) packet. The source detect the route with the link of error from it cache and new route discovery process starts to find the route[2][7].

ADVANTAGES

DSR is a reactive or table driven protocol. In this, the intermediate nodes use the route cache to reduces the control overhead.

(d)Destination-Sequenced Distance-Vector Routing (DSDV)
DSDV is a proactive protocol i.e. it is a table- driven routing scheme. It eliminates route looping, increase speed and reduces control message overhead. Each node maintains a next –hop table, which exchanges with its neighbours[2].

3. Comparison between DSR, AODV, DSDV

Sr No.	AODV	DSR	DSDV
1	It is Reactive protocol	It is Reactive protocol	It is Proactive protocol
2	It delivers virtually all packets at low mobility	It is very good at all mobility rates.	It performs almost as DSR, but requires transmission overheads of many packets.
3		It has low end to end delay	It has high for pause time 0 but it starts decreasing as time increases.
4	It performs better for larger number of nodes	It performs better for larger number of nodes	It performs better for few number of nodes
5	For real time traffic AODV is preferred		

Table1: Comparison b/w Different Protocols[2]

4. Simulation Tool

The simulation tool for analysis is NS-2 which is highly preferred by research communities[2].NS-2 is suitable for designing new protocols. Comparing different protocols and traffic evaluation.NS-2 is an object oriented simulator

written in C++, with TcL interpreter as a fronted. This means that most of the simulation scripts are created in TCL(Tool Command Language).If the component have to be developed for NS-2 then both TcL and C++ have to be used[2].

5. Simulation Analysis

We creates the network of seven nodes, node 0,1,2,3,4,5&6 with an energy with energy level of 1.5W[7].Initially node 5 has to send the data to node 1,2&3. MMBCR first finds the node having the minimum battery capacity and having the maximum value of the selected route i.e. the route with maximum lifetime is selected. Node 0 has to transmit the data from 0 to 4. These are 0-5-4,0-1-6-4&0-2-3-4[7].MMBCR initiates route discovery process and selects the route with maximum lifetime i.e. MMBCR selects 0-2-3-4 from the route discovery process. Source node is 0 and the Destination node is 4 via route 0-2-3-4.Before the link failure takes place source node 0 initiates the route discovery process and transmit the packet through route 0-1-6-4 for increasing the network lifetime. Thus the DSR does not take into consideration the energy levels of nodes or the lifetime of the network resulting in link failure whereas MMBCR increases the network lifetime by selecting route with maximum battery capacity[7][2].

Simulation Parameter	Value
Simulator NS-2	NS-2
No. of nodes used	7
Selected Route	0-2-3-4
After link failure route will	0-1-6-4

Table2: Parameters Used

6. CONCLUSION

In this paper, we have considered four routing protocols i.e. AODV, DSR, DSDV & MMBCR and compared the performances of two protocols i.e MMBCR and DSR in terms of network using NS-2.From the simulations we observed that MMBCR selects the route with nodes containing maximum battery value i.e the route with maximum lifetime is selected.DSR does not consider the lifetime of the network and chooses the route based on route discovery process. It is also clear from the result that minimum energy routing protocol should employ a unified link cache graph data structure to store the routing and power information so that it can converge to the minimum energy route faster with reduced overhead[7].

7. REFERENCES

[1] Anu Kumari,Arvind Kumar,Akhil Sharma, "Survey Paper On Energy Efficient Routing protocol in MANET" Proceedings of International journal of Advanced Research in computer science and software engineering ,Vol.3,Issue3,pp-396-403,March-2013.

[2] Tanupreet Singh,Shivani Dua,Vikrant Das,"Energy Efficient Routing Protocol In Mobile Ad-Hoc Networks" Proceeding Of International journal of Advanced Research in computer science and software engineering,Vol.2,Issue 1,January 2012.

[3] Ajay Singh, Hitesh Gupta,Mukesh Baghel,"Energy Efficient Routing Protocol For Mobile AD-Hoc Networks" Proceeding Of International journal of Engineering Research & Technology(IJERT),Vol.1,Issue 5,July 2012.

[4]Kadiveti .Koteswar Rao, Ragendra.C, Ramesh.Ragala"An Enhanced Energy Efficient Routing Protocol For MANETs" Proceeding Of International journal of Computational Engineering Research (IJCER), Volume. 2, July 2011.

[5] Shiva Prakash,J.P.Saini,"A Review Of Energy Efficient Routing Protocols For Mobile AD HOC Wireless Networks" Proceeding Of International journal of Computer Information Systems,Vol.1,Issue 4, January 2010.

[6] Rupali Mahajan, Rupali Jagtap "Energy Efficient Routing Protocols For Mobile Ad-Hoc Networks" Proceeding Of International journal of Science and Modern Engineering (IJISME),Vol-1,Issue-3,February 2013.[7]Ajay Shah, Hitesh Gupta, Mukesh Baghel, "Energy Efficient Routing Protocols for Mobile Ad Hoc Networks " , International Journal of Engineering Research & Technology, Volume1,2012,1-5

[8] Ravneet Kaur," Energy Efficient Routing Protocols in Mobile Ad hoc Network based on AODV Protocol ", International Journal of Application or Innovation in Engineering & Management, Volume 2, 2013,322-327

[9] Bartosz Wietrzyk, Milena Radenkovic ," Energy Efficiency in the Mobile Ad Hoc Networking Approach to Monitoring Farm Animals ",Conference, 2007

[10] Thomas Kunz," Energy-Efficient MANET Routing: Ideal vs. Realistic Performance", Conference, 2008

Cellulosic Nanocomposites: Functional Vector for Arsenic Remediation

Kiran Singh[a*], TJM Sinha[b] and Shalini Srivastava[a]
[a]*Department of Chemistry, Faculty of Science, Dayalbagh Educational Institute, Agra, 282105, India*
[b]*ACS Chemical Innovations, Navi Mumbai, Maharashtra*
e-mail: kiransdei@email.com

***Abstract*— Surface functionalization of nanocrystalline cellulose using diethyl amine was carried out to form an anion adsorbent (3-N-N' dimethylamino-2-hydroxypropyl nanocrystalline cellulose ether) for arsenic remediation. The product was thoroughly characterized using modern tools. Nano-biosorbent had high efficiency of removal of trivalent (85.20 %) and pentavalent (97.60 %) arsenic from aqueous solutions, even at low concentrations. Adsorption capacity was found to be 8.28 and 9.56 mg/g for As (III) and As (V) respectively. Functionalized nano-biosorbent is ideally suited for economic biosorbent for pretreatment step before large scale chemical treatments for arsenic remediation.**

Keywords— Arsenic, Functionalization, Isotherms, Kinetics Nano-biosorbent.

I. INTRODUCTION

Among various toxic pollutants, arsenic released into the environment tends to persist, circulate and eventually accumulating throughout the food chain, thus becoming a serious threat to the environment [1]. The presence of various environmental oxidation states of arsenic, toxicity and health hazards have been comprehensively reviewed [2-6]. World Health Organization has revised the guidelines for arsenic in drinking water from 50 to 10 µg/L [7]. However, arsenic concentrations, about 100 times more than permissible limit, were found in many parts of world [8,9]. Of these regions, India and Bangladesh are most seriously affected in terms of the size of the population at risk and the magnitude of the health problems [10].

Several methods of arsenic removal are available including precipitation, electrochemical reduction, adsorption, ion exchange, solvent extraction, nano filtration and reverse osmosis [11-14]. However, their use is limited due to high operation cost, sludge formation with high wastage of water, and other technical difficulties. Lime precipitation is in frequent use, but suffers from the problem of gypsum formation and is not capable of reducing arsenate to the optimum level, thus requiring an additional ferric treatment [15]. Calcium arsenate formed in the process has to be disposed off in a landfill site where it may interact with carbon dioxide in air to form calcium carbonate thus releasing arsenic back into the environment [16]. Alum precipitation is in practice but its performance has not been considered to be satisfactory [17]. Arsenic precipitation using sodium sulfide has also been considered in reducing arsenic levels; however, being colloidal in nature cause a filtration problem and is also readily oxidized when exposed to the atmosphere there by making it difficult to dispose off in a land fill site [18-20]. Lanthanum compounds and iron (III)-loaded chelating ion exchange resins having either an acidic or basic moiety as the functional group [21-23]. Treatment with such chelating ion exchange resins is expensive because of the materials cost associated with the removal process[24-27]. This sludge contains a mixture of gypsum, heavy-metalloid hydroxides and carbonates in addition to a large amount of water, this may leak arsenic back to the environment after exposure to water and air. In addition, to remove arsenite directly by these adsorbents, it should be oxidized into the pentavalent state prior to treatment by using oxidizing agents like hydrogen peroxide [28,29].

Biosorption has gained important credibility in recent years for remediating even heavily metal-loaded waste water because of its eco-friendly nature, excellent performance and low cost [30,31]. Over the past years, intensive research on metal biosorption has established solid base of knowledge, principles and highlighted enormous potential of this effective metal removal phenomenon for commercialization. The highest priority of commercially available bioremediation technology is the assessment of the commercial potential, practicability of the developed technology, competition with other technologies, market size, and cost of raw biosorbents [32-33]. Association with the industries to carry out biomass formulation, processing, into a product for its tuning to meet out the technical requirements is yet another important aspect. Green Nanotechnology integrates Nanomaterial science and environmental chemistry and creates significant step forward in biosorption processes whose efficiency depend on the size of particles of sorbent [34-35].

Currently, research is being conducted in toxic metals removal from water using inorganic nanomaterials [36-42]. However, inorganic nanostructured materials are coupled with toxicity issues [43-45]. One approach to tackle such issues associated to sustainability is to incorporate organic nanomaterials of plant origin. The increasing interest in the organic bio nanomaterials of plant origin and their unique properties has led to intensive research in the area of nanocellulose materials [46-49].

Cellulose is considered as one of the most economic biomass for the preparation of nano-biosorbent. Chemical reactivity of cellulose is largely a function of the high donor reactivity of the OH groups which becomes the sorption site of cationic form of metals; however, it does not have sorption capacity for anionic metal species. Using smart processing it could be used as nano reinforcing biopolymer triggering various functionalizations. A critical challenge in the fabrication of nano-biosorbent is to make nanoscale building blocks with a particular surface structure, charge, and functionality. Nanocrystalline cellulose is ideal building block due to their lightweight, high aspect ratio, large specific surface area, reactive surface of –OH groups, high mechanical strength and stiffness, and ability to form superstructures. In order to improve the performance of NCC-based composite materials, there has been a strong desire to develop an environmentally friendly procedure for tailoring the surface functionality of nanocrystalline cellulose.

This communication reports the unexplored removal efficiency of dimethyl amine functionalized nano crystalline cellulose for negatively charged arsenic species ($H_2AsO_3^{-1}$, $HAsO_3^{-2}$, $H_3AsO_4^{-1}$, $H_2AsO_4^{2-}$) from aqueous solutions. This nanotech and synthetically functionalized nano-biosorbent has significant potential as economic, biodegradable, non-toxic nature with enhanced sorption and environmental stability.

A. Reagents and chemicals

All chemicals were of analytical grade. Stock solutions of arsenic containing 1,000 mg/L As(III) and As(V) were prepared by dissolving $NaAsO_2$ and $Na_2HAsO_4 \cdot 7H_2O$ in double distilled water and stored in darkness at 4 ºC. Working solutions of the desired concentrations were prepared by diluting the stock solution.

B. Preparation of Nanocrystalline cellulose

NCC was prepared by sulphuric acid hydrolysis of microcrystalline cellulose (MCC) [50]. MCC (50.0 g oven dried weight) was mixed with H_2SO_4 solution (62 %, w/w) with continuous stirring at 45º C for 45 min. The hydrolysis reaction was stopped by adding excess (10 fold) of distilled water followed by the removal of acidic solution by successive centrifugation at 12,000 rpm for 10 min. until the supernatant became turbid. After washing, the content was sonicated for 30 min. The cloudy supernatant, containing NCC, was collected and the remaining sediment was again mixed with water, sonicated and centrifuged to obtain additional NCC, this procedure was repeated till the supernatant was clear.

C. Preparation of Tertiary Aminated Nanocrystalline cellulose (TA-NCC)

Epichlorohydrin (50 ml in 0.1 moles DMF; 60 ml) was reacted with dimethyl amine (1.5 moles; 25 ml). A viscous chlorohydrin was resulted and treated with 50% solution of sodium hydroxide (4.0 g; 0.1 moles). Amine epoxide was extracted with dioxane and filtered. It was separated from sodium chloride formed during the reaction. NCC (10 g) was taken as slurry in dioxane and made alkaline with 50% aqueous sodium hydroxide (0.1 moles). Amine epoxide in dioxane was added to NCC and allowed to react for 4 hours at 50-60º C. The product was filtered, washed and neutralized with 75% methanol and air-dried. 3-N-N' dimethylamino-2-h hydroxypropyl cellulose ether.

D. Characterization of NCC and TA-NCC

Native NCC and TA-NCC were dried at 105 ºC for 6 h and cooled to room temperature for analysis. The average crystallite size and crystallinity pattern of both the samples were recorded using glancing angle X-ray diffractometer (Bruker AXS D8 Advance, Germany) with Cu Kα radiation at 40 kV and 30 mA. Scattered radiation was detected in the range 2θ = 5-40º, at a speed of 2 º/min. Nanosurf Easyscan, Switzerland (V 1.8 atomic force microscope) was used for surface roughness and topography observation of native and modified biosorbents before and after arsenic ion sorption. All the scans were performed in air with commercial Si nanoprobe tips. Images were obtained simultaneously in tapping mode at the fundamental resonance frequency of the cantilever with a scan rate of 0.5-0.8 Hz and oscillating amplitude of 0.5 V. The morphological characteristics of the oven dried NCC and freeze dried TA-NCC before and after arsenic ion sorption were evaluated using Scanning Electron Micrograph Zeiss EVO40 at bar length equivalent to 10 µm, working voltage 15 kV with 500X magnification. FTIR analysis in solid phase in KBr was performed using a Shimadzu 8400 Fourier Transform Infrared spectroscope. Absorption mode FT-IR spectra were recorded in 600-4,000 cm^{-1} range and scanned for 64 times.

E. Biosorption studies

Batch experiments using standard practices were performed as functions of biomass dosage (0.1 - 1.0 g), contact time (10-50 min), volume of test solution (100-300 ml), pH (1-10) and arsenic ion concentration (0.005-50 mg/L) at shaking rate 250 rpm at room temperature in clean air-conditioned environmental laboratory. The solutions of trivalent and pentavalent arsenic were taken into separate erlenmeyer flasks. After proper pH adjustments, a known quantity of biosorbent was added and arsenic bearing suspension was kept under stirring until the equilibrium conditions were reached. After shaking, suspension was allowed to settle down. Arsenic treated biosorbent was filtered using whatman 42 filter paper (Whatman International Ltd., Maidstone, England). Filtrate was collected and subjected for arsenic ions estimation using ICP OES Perkin Elmer Optima™ 8x00.

Percent arsenic sorption was computed using the equation: $\%\ \text{Sorption} = [\frac{(C_0 - C_e)}{C_0} \times 100]$, where, C_0 and C_e are the initial and final concentrations of arsenic ions in solution. All the investigations were carried out in triplicate to confirm reproducibility of the experimental results. The reproducibility and relative deviation are considered at ±0.5% and ±2.5%, respectively. The adsorption capacity Q_e (mg/g) was calculated from the following equation: $Q_e = [\frac{(C_0 - C_e)}{m} V]$, where C_0 and C_e represent the initial and final concentrations of the arsenic solutions, respectively. V and m are the solution volumes and biosorbent dose.

II. Results and Discussion

A. Confirmation of preparation of NCC and TA-NCC

The prime objective of this paper was to prepare smart tertiary aminated NCC having different extents of tertiary amine group for arsenic remediation. Prepared NCC was obtained in 60–70 % yield and was aminated to obtain TA-NCC in 75-88% yield.

FTIR spectrum of NCC shows all the characteristic absorption bands of cellulose. A broad band at around 3324 cm^{-1} which is attributed to the presence of free and hydrogen bonded –OH stretching vibrations. The peaks at 2891 cm^{-1} and 1429 cm^{-1} corresponds to the –CH stretching and $–CH_2$ bending vibrations. The peak at 1152 cm^{-1} relates to C–O–C anti symmetric stretching vibration. The adsorption band at 1001 cm^{-1} is attributed to –CO stretching vibration. An absorption band at 896 cm^{-1} arises from the –glycosidic linkages. In addition to the characteristic cellulose peaks, additional peaks at 14318.1 and 1246.4 cm^{-1} in its functionalized form (TA-NCC) indicate the presence of aliphatic –CN and $–CH_2–{}^{+}NH(R)_2$–type nitrogen vibrations. These observations clearly indicate the formation of chain and the presence of $–CH2–{}^{+}NH(CH_3)^2$ groups in TA-NCC. After the amination, the characteristic absorption bands of cellulose have not shifted, indicating that amination reaction has not destroyed the basic molecular structure of cellulose.

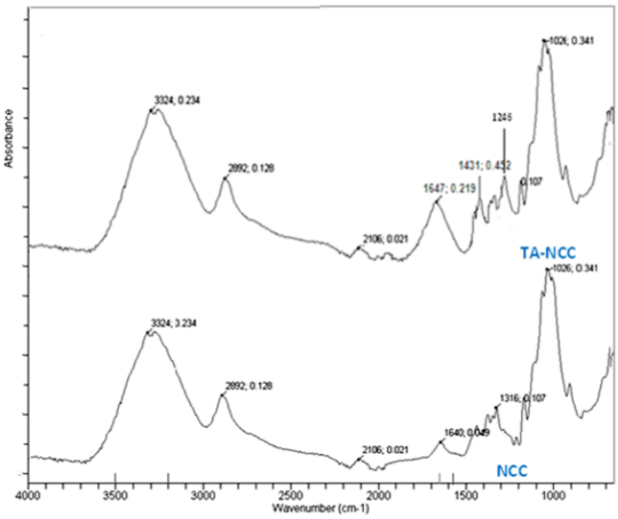

Fig. 1 – FT-IR spectrum of NCC and TA-NCC

XRD analysis shows that the acid treatment results into narrowing and higher crystallinity level of hydrolyzed cellulose. Presence of three strong peaks at 2θ= 14.84, 22.76 and 34.98 are the characteristics of cellulose I. [52]. The observed slight decrease in crystallinity index reduction may be ascribed to the incorporation of amine groups onto the TA-NCC surface. X-ray crystallinity index of native (NCC) and functionalized (TA-NCC) were calculated using equation: $CI = \frac{I_{002} - I_{101}}{I_{002}} \times 100$, and found to be 92.56 and 54.82, respectively. The average crystallite size was estimated from the full width at half-maximum intensity (FWHM) of the reflection using Debye-Scherrer equation and was found 6 and 116 nm for NCC and TA -NCC respectively.

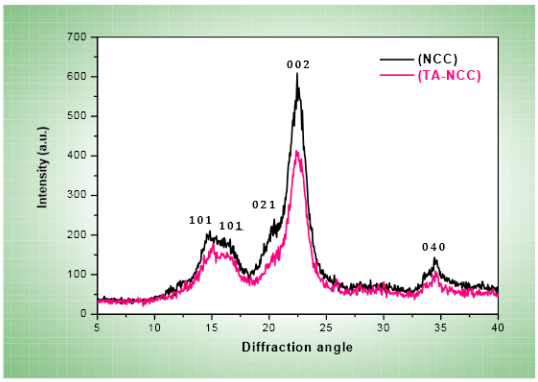

Fig. 2 – XRD spectrum of NCC and TA-NCC

Investigation of surface roughness and morphology of NCC and TA-NCC were carried out using AFM. AFM micrograph of NCC indicates that the NCC are triangular rather than spherical and with a diameter of nano meter range, uniform growth and mono disperse particle distribution without any pinhole. AFM amplitude images indicate that the TA-NCC has less well-defined structures with little evidence of triangular shape. The TA-NCC is of

same length the NCC, but wider. AFM image shows that the NCC maintained their characteristic RMS roughness even after amination process and found to be 19.491 and 18.456 for NCC and TA-NCC, respectively.

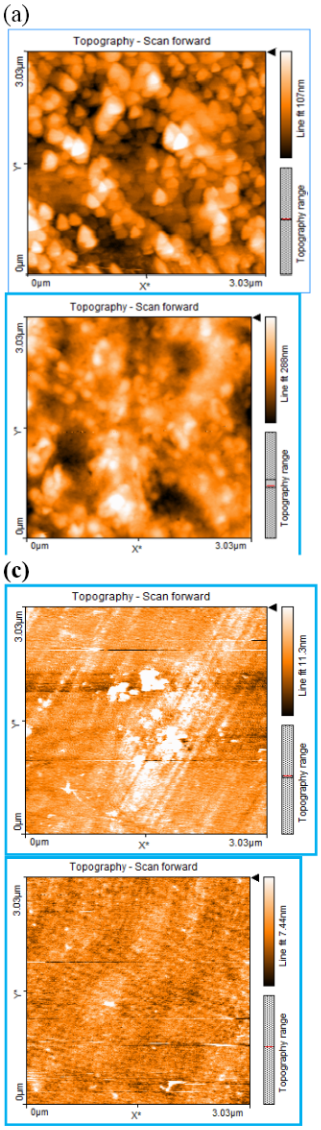

Fig. 3 - AFM images of a) NCC; b) TA-NCC; c) As (III) laden TA-NCC; and d) As (V) laden TA-NCC

SEM images of NCC and TA-NCC indicate that the surface morphology of NCC looks smooth and triangular, supporting the results of AFM. However, after amination, the shape of the NCC is slightly deformed, losing their original triangular shapes. After the amination reaction, obvious coating layers are observed. Thus, the amination reaction achieved the immobilization of the amine groups on the surface of NCC. NCC appeared to be agglomerated before functionalization and was separated from each other after amination, reason being the incorporation of relatively hydrophobic amine groups on the surface.

(a) (b)

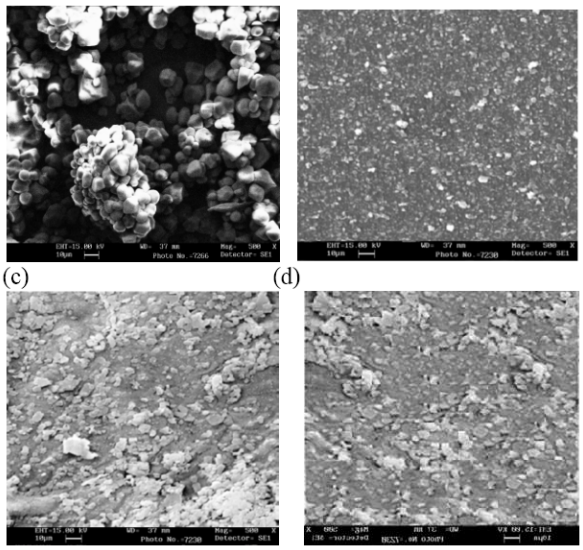

Fig. 4 - SEM images of a) NCC; b) TA-NCC; c) As (III) laden TA-NCC and d) As (V) laden TA--NCC

B. Evidences in support of the sorption of As (III and V) onto TA-NCC

Loading of both the arsenic species on TA-NCC is evident from lowering in peak intensity and shifting of –OH peak appearing at 3324 cm^{-1} in native to 3303 cm^{-1} and 3309 cm^{-1} in As (III) and As(V) laden TA-NCC, respectively. Similarly, lowering in the characteristic -N peak intensity (1245 cm^{-1}) observed in each case (As III and As V laden biosorbent) also confirms TA-NCC-Arsenic interaction.

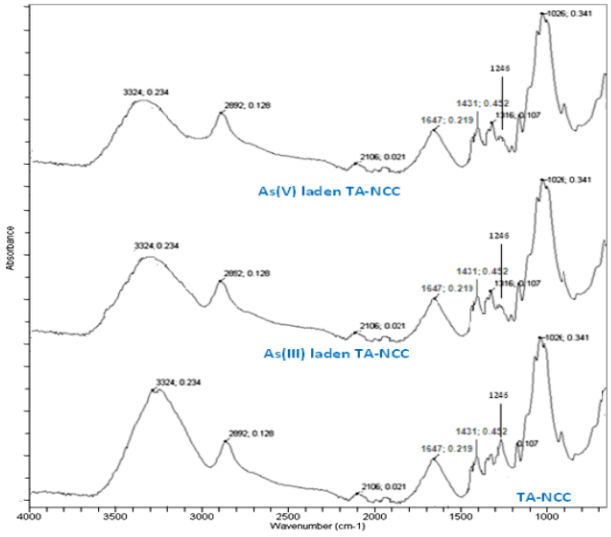

Fig. 5 –FT-IR spectrum of TA-NCC and As(III) and As(V) laden TA-NCC

AFM images points out the fact that shape and surface topography of arsenic laden TA-NCC (Fig. 3c and d) was found to be destroyed confirming sorption of arsenic on target biomass. Significant decrease in relative mean surface roughness in arsenic laden TA-NCC also provides support to the above observation.

SEM Micrographs (Fig. 4c and d) of native and As (III and V) laden TA-NCC clearly shows the change in morphological features from triangular cluster to dense agglomerated clusters. Reduction in pore area of native (10.02 μm^2 to 4.48 and 3.21 μm^2) for As (III) and As (V) laden TA-NCC respectively was also recorded confirming the accumulation of liquid phase arsenic species in the target biosorbent.

C. *Sorption Experiments*

A series of batch experiments on sorption led to the standardization of the optimum conditions for As (III) and As(V) removal at arsenic concentration (25 mg/L), contact time (40 min), volume (200 mL) and pH 7.5 for As (III) and 2.5 for As (V). A mechanistic aspect of sorption has been discussed as follows.

Fig. 7 shows the dependence of sorption behavior of arsenic species on pH at adsorbent dose (0.5g). The observed increasing and decreasing trend of sorption with lowering and rise in pH may be explained on the basis of highly pH dependent aqueous arsenic chemistry. In the pH range 7.5-9.0, As (III) exists in anionic ($H_2AsO_3^{-1}$ and $HAsO_3^{-2}$) species, exhibiting optimum sorption on cationic biosorbent because of electrostatic attraction. At pH< 7.5, As(III) exists as uncharged species $H_3AsO_3^0$ and does not show affinity towards cationic TA-NCC sorbent. However, the observed sorption (60-70 %) of As (III) in this pH range is ascribed to the structural behavior of modified nano sorbent. The increased surface area-to-volume ratio of cellulosic nanoparticles and quantum size effects not only increase the surface area providing more adsorption sites but also induce the ability to tune surface properties through molecular modification. Therefore, in the present paper, nanotech strategy has been used to enhance the sorption of arsenic species.

Appreciable sorption of As (V) is observed in the pH range 2.5 -7.5. Maximum sorption of As (V) on cationic biosorbent observed at pH 2.5 can be easily ascribed to its interaction with the anionic ($H_2AsO_4^{-1}$ and $HAsO_4^{-2}$) species, occurring predominantly in this pH range [53]. To add, designed biosorbent (TA-NCC) at lower pH has tertiary amine group in protonated form ($NR_1R_2H^+$), the electrostatic repulsion among these positive groups increases the availability of sorption sites by overcoming the tendency of the chains to aggregate. At pH below 2.5, neutral species of arsenic starts forming and becomes the reason of relative decrease of As (V) sorption on cationic biosorbent.

III. CONCLUSION

The incorporation of positively charged amino groups in NCC significantly enhanced binding capacity of negatively charged arsenic species and reusability cycles of functionalized nano-biosorbent. The work highlighted the application of nanotech and chemical functionalization approach on largely abundant, economic, biopolymer (cellulose) resulting into smart nano-biosorbent with enhanced sorption efficiency and environmental stability for a simple and cost effective pretreatment step before large scale chemical treatments for the removal of arsenic from water bodies.

ACKNOWLEDGMENT

Authors are thankful to Director, Prof. P.K. Kalra, Dayalbagh Educational Institute, Dayalbagh, Agra, for providing necessary research facilities. Kiran Singh is grateful to UGC-BSR, fellowship (New Delhi), for rendering financial assistance.

REFERENCES

[1] B.K. Mandal, K.T. Suzuki, Arsenic round the world: a review. Talanta. 58 (2002) 201–235.
[2] D. Mohan, C. U. Pittman, Arsenic removal from water/ wastewater using adsorbents-a critical review. J. Hazard. Mater. 142 (2007) 1–53.
[3] S. Kundu, A.K. Gupta, Investigations on the adsorption efficiency of iron oxide coated cement (IOCC) towards As (V) - kinetics, equilibrium and thermodynamic studies. Colloid. Surf. A. Physicochem. Eng. Asp. 273 (2006) 121-128.
[4] T.S.Y. Choonga, T.G. Chuaha, Y. Robiaha, F.L.G. Koaya, I. Azni, Arsenic toxicity, health hazards and removal techniques from water: an overview. Desalination. 217 (2007) 139–166.
[5] B.L. Rivas, M.C. Aguirre, Removal of As (III) and As (V) by Tin (II) compounds. Water. Res. 44 (2010) 5730-5739.
[6] U. Bose, M. Rahman, M. Alamgir, Arsenic toxicity and speciation analysis in ground water samples: a review of some techniques. Int. J. Chem. Tech. 3(1): (2011) 14–25.
[7] WHO (1993) Guidelines for drinking water quality, World Health Organization, Geneva, Switzerland.
[8] M.S.S. Pereira, E.Winter, J.R. Guimaraes, S. Rath, A.H. Fostier, A simple voltammetric procedure for speciation and evaluation of As removal from water. Environ. Chem. Lett. 5 (2007) 137–141.
[9] J.S. Wang, C.M. Wai, Arsenic in drinking water-a global environmental problem. J. Chem. Educ. 81 (2004) 207–213.
[10] N. Sohel, P.L. Ake, M. Rahman, S.P. Kim, Y. Muhammad, E.E. Charlotte, V. Marie, Arsenic in drinking water and adult mortality: a population based cohort study in rural Bangladesh. Epidemiol. 20 (2009) 824–830.
[11] M. Shih, An overview of arsenic removal by pressure-driven membrane processes. Desalination. 172(1): (2005) 85-97.
[12] M.I.S. Gonzaga, J.A.G Santos, L.Q. Ma, Arsenic phytoextraction and hyper accumulation by fern species. Scientia. Agricola. 63 (2006) 90–101.
[13] J.T. Mayo, C. Yavuz, The effect of Nanocrystalline magnetite size on arsenic removal. Sci. Tech. of Advanc. Mat. 8(1–2): (2007) 71–75.
[14] J. Hu, I.M.C. Lo, G. Chen, Removal of Cr(VI) by magnetite nanoparticle. Water Sci. Technol. 50 (12): (2004) 139-146.
[15] G.H. Khoe, J.C.Y. Huang, R.G. Robins. Precipitation Chemistry of the Aqueous Ferrous Arsenate System. In: EPD Congress '91. TMS, Warrendale PA, (1991) 103-105.
[16] T. Nishimura, K. Tozawa. On the Solubility Products of Ferric, Calcium and Magnesium Arsenates. Bull. Res. Inst. Min. Dress. Metall. 34 (1), (1978) 19-26.
[17] Z.K. Chowdhury, G.L. Amy, R.C. Bales. Coagulation of submicron colloids in water treatment by incorporation into aluminium hydroxide floc. Environ. Sci. Technol. 25(10), (1991) 1766-1773.
[18] G. Prasad, Arsenic in the Environment. Part 1, New York. 33 (1994).
[19] H.J. Shipley, S. Yean, A.T. Kan, M.B. Tomson, Adsorption of arsenic to magnetite nanoparticles: effect of particle concentration, pH, ionic strength, and temperature. Environ. Toxicol. Chem. 28 (3): (2009) 509-515.

[20] T. Tuutijärvi, M. Sillanpää, J. Lu, G. Chenb, As(V) adsorption on maghemite nanoparticles. J. Hazard. Mater. 166 (2009) 1415-1420.
[21] S. Tokunaga, S.A. Wasay, S.W. Park, Removal of arsenic(V) ion from aqueous solutions by lanthanum compounds. Wat. Sci. Technol. 35(7): (1999) 7-18.
[22] M. Chanda, K.F. O'driscoll, G.L. Rempel, Ligand exchange sorption of arsenate and arsenite anions bychelating resins in ferric ion form: II. iminodiacetic chelating resin Chelex 100. React. Polym. 8 (1988) 85–95.
[23] H. Egawa, T. Nonaka, H. Maeda. Studies of selective adsorption resins. XXII. Removal and recovery of arsenic ion in geothermal power waste solution with chelating resin containing mercapto groups. Sep. Sci. Technol. 20 (1985) 653–64.
[24] H. Matsunaga, T. Yokoyama, R.J. Eldridge, B.A. Bolto. Adsorption characteristics of arsenic(III) and arsenic(V) on iron(III)-loaded chelating resin having lysine-Na, Na-diacetic acid. React. Funct. Polym. 29 (1996) 167–74.
[25] I. Yoshida, K. Ueno, H. Kobayashi. Selective separation of arsenic(III) and (V) ions with ferric complex of chelating ion-exchange resin. Sep. Sci. Technol.13 (1978) 173–84.
[26] B. Petrusevski, J. Boere, S.M. Shahidullah, S.K. Sharma, J.C. Schippers, Adsorbent-based point-of-use system for arsenic removal in rural areas. J. Water SRT-Aqua. 51 (2002) 135-144.
[27] W. Driehaus, M. Jekel, Granular ferric hydroxide d a new adsorbent for the removal of arsenic from natural water. J. Water SRT-Aqua. 47 (1998) 1-6.
[28] R.W. Lawrence, T.W. Higgs, Removing and stabilizing As in acid mine water. J. Met. 51(9): (1999) 27–39.
[29] A.H. Mirza, V. Ramachandran, Removal of arsenic and selenium from wastewaters-a review. In Second International Symposium on Extraction and Processing for the Treatment and Minimization of Wastes, The Minerals, Metals & Materials Society, Salt Lake City, Utah, (1996).
[30] J.N. Egila, B.E.N. Dauda, Y.A. Iyaka, T. Jimoh, Agricultural waste as a low cost adsorbent for heavy metal removal from wastewater. Int. J. Phys. Sci. 6(8): (2011) 2152–2157.
[31] P. Goyal, S. Srivastava, Characterization of novel *Zea mays* based biosorbent designed for toxic metals biosorption. J. Haz. Mat. 172 (2009) 1206–1211.
[32] K.R. Raj, A. Kardam, J.K.. Arora, M.M. Srivastava, S. Srivastava, Neural network modeling for Ni(II) removal from aqueous system using shelled *Moringa oleifera* seed powder as an agricultural waste. JWARP. 2 (2010) 331-338.
[33] S. Guhab, M. Chaudhuri, Removal of As(III) from groundwater by low cost materials. Asian Environ. 12 (1990) 42.
[34] J. Theron, J.A. Walker, T.E. Cloete, Nanotechnology and water treatment: applications and emerging opportunities. Cri. Rev. Microbiol. 34(1): (2008) 43–69.
[35] K.T. Dhermendra, J. Behari, S. Prasenjit, Application of nanoparticles in waste water treatment. World App. Sci. J. 3(3): (2008) 417–433.
[36] W.X. Zhang, Nanoscale iron particles for environmental remediation: an overview. J. Nano. Res. 5 (2003) 323–332.
[37] M. Botes, T.E. Cloete, The potential of nanofibers and nanobiocides in water purification. Cri Rev. Microbiol. 36(1): (2010) 68–81.
[38] S. Dixit, J.G. Hering, Comparison of arsenic(V) and arsenic (III) sorption onto iron oxide minerals: implications for arsenic mobility. Environ. Sci. Technol. 37 (2003) 41-82.
[39] A.P. Grosvenor, B.A. Kobe, N.S. McIntyr, Examination of the oxidation of iron by oxygen using X-ray photoelectron spectroscopy and QUASES. Surf. Sci. 565 (2004) 151-162.
[40] S. Yean, L. Cong, C.T. Yavuz, J.T. Mayo, W.W. Yu, Effect of magnetite particle size on adsorption and desorption of arsenite and arsenate. J. Mater. Res. 20(12): (2005).
[41] C.T. Yavuz, J.T. Mayo, WW. Yu, A. Prakash, J.C. Falkner, S. Yean, L. Cong, H.J. Shipley, A. Kan, M. Tomson, D. Natelson, V.L. Colvin, Low-field magnetic separation of monodisperse Fe_3O_4 nanocrystals. Sci. 314 (5801): (2006) 964-967.
[42] T. Tuutijärvi, M. Sillanpää, J. Lu, G. Chenb, As(V) adsorption on maghemite nanoparticles. J. Hazard. Mater. 166 (2009) 1415-1420.
[43] G.T. Paul, L.J. Richard, Nanotechnologies for environmental cleanup. Nanotoday. 1(2): (2006) 44–48.
[44] B. Karn, T. Kuiken, M. Otto, Nanotechnology and in situ remediation: a review of the benefits and potential risks. Env. Health Perspec. 117(12): (2009) 1823–1831.
[45] S.K. Brar, M. Verma, R.D. Tyagi, R.Y. Surampalli, Engineered nanoparticles in wastewater and wastewater sludge-evidence and impacts. Waste. Manag. 30 (2010) 504–520.
[46] M.A. Samir, F. Alloin, A. Dufresne, Review of recent research into cellulosic whiskers, their properties and their application in nanocomposites field. Biomacromol. 6 (2005) 612–626.
[47] P.M. Visakh, S. Thomas, Preparation of bionanomaterials and their polymer nanocomposites from waste and biomass. Waste Bio. Valor. 1 (2010) 121–134.
[48] H. Ma, C. Burger, B.S. Hsiao, B. Chu, Ultra-fine cellulose nanofibers: new nano-scale materials for water purification. J. Mat. Chem. 21 (2011) 7507–7510.
[49] H. Ma, B.S. Hsiao, B. Chu, Ultrafine cellulose nanofibers as efficient adsorbents for removal of UO_2 in water. ACS Macro Lett. 1 (2012) 213–216.
[50] M. Ioelovich, Optimal Conditions for Isolation of Nanocrystalline Cellulose Particles. J. Nanosci. Nanotechnol. 2 (2): (2012) 9-13.
[51] A.I. Vogel, Elementary Practical Organic Chemistry" Part 3, "Quantitative Organic analysis" Longman Group Ltd. (London), 2nd Ed. (1975) 652.
[52] S. Park, J.O. Baker, M.E. Himmel, P.A. Parilla, D.K. Johnson. Cellulose Crystallinity Index: Measurement Techniques and their Impact on Interpreting Cellulase Performance, Biotechnol. for Biofuels. 3 (2010) 1-10.
[53] S. Cornu, D. Breeze, A. Saada, P. Baranger. The influence of pH, electrolyte type, and surface coating on arsenic (V) adsorption onto kaolinite. Soil Sci. Soc. Am. J. 67 (2003) 1127– 1132.

Photoluminescence and Dielectric Studies of Ion Induced Polyethylene Naphthalate

Kusum Devgan[a], Navjeet Kaur[b,*], Sonika Thakur[c], Manpreet Kaur[d], , Lakhwant Singh[e]
[a]*Department of Physics, S.R. Government College for Women, Amritsar, Pumjab, India*
[b]*Department of Physics, Khalsa College for Women, Amritsar, Pumjab, India*
[c]*Department of Physics, Guru Nanak Dev University College, Verka, Amritsar, Pumjab, India*
[d]*Department of Physics, DAV College, Amritsar, Pumjab, India*
[e]*Department of Physics, Guru Nanak Dev University, Amritsar, Pumjab, India*
**Corresponding Author email address: navjeetphy@gmail.com*

***Abstract*—Dielectric properties along with photoluminescence phenomenon of ion induced Polyethylene naphthalate (PEN) were analyzed. Li^{3+}, C^{6+}, Ni^{10+} ion beams were used to analyze the modifications induced by swift heavy ions as a function of ion fluence, ranging from $1x10^{11}$ to $3x10^{12}$ ions/cm^2. Blue shift is observed in PL behavior. Dielectric constant (ε′) for pristine and irradiated samples has also been calculated, which increases with the increase in ion fluence.**

***Keywords*—**Dielectric constant, Irradiation, Photoluminescence, Swift heavy ions.

I. INTRODUCTION

Swift heavy ion loses its energy by interacting with target nuclei (nuclear stopping) and by interaction with target electrons (electronic stopping). In case of polymers, electronic stopping process due to ion irradiation is more eminent, which contributes to the scissoring of original bonds, production of radicals and excited atoms. At higher ion fluences cross linking and rearrangement of bonds occur. All these processes are accountable for the modifications in structural, optical, thermal and chemical properties of the polymer due to creation of defects in the polymer [1]. Effect of swift heavy ion irradiation on Polyethylene naphthalate (PEN) has rarely been studied, therefore the aim of the present investigation is to study the alterations in structural properties of PEN films caused by lithium (50 MeV), carbon (85 MeV) and nickel (120 MeV) ion irradiation with the help of Photoluminescence (PL) and Dielectric techniques.

II. EXPERIMENTAL DETAILS

The specimens of Polyethylene naphthalate (PEN) in the form of flat polished thin films (25μm) were procured from Good Fellow Ltd. (England). These films were used as-received form without any further treatment in the size of 1 cm x 1 cm. The samples were mounted on the sliding ladder and irradiated with lithium (50 MeV), carbon (85 MeV) and nickel (120 MeV) ion beams using 15 UD pelletron facility for the general purpose scattering chamber (GPSC) under vacuum of ~10^{-6} Torr at Inter-University Accelerator Center, New Delhi.

The electronic energy loss of characterize lithium (50 MeV), carbon (85 MeV) and nickel (120 MeV) ions in PEN polymer is ~6.96, 27.85 and 563.3 eV/Å respectively. The range of all ions is more than the thickness of polymer films. The ion beam fluence was varied from 1 x 10^{11} to 3 x 10^{12} ions cm^{-2}. In order to expose the whole target area, the beam was scanned in the x-y plane. The beam current was kept low to suppress thermal decomposition and was monitored intermittently with a Faraday cup. Flouromax-3 (Jobin-Yvon, Edison, NJ, USA) equipped with a photomultiplier tube and a xenon lamp was used for (PL) analysis of samples at 300K. The Precision impedance analyzer 6500B is used to measure dielectric constant (ε′) of pristine and irradiated samples of polyethylene naphthalate at room temperature in the frequency range 20Hz-1MHz.

III. RESULTS AND DISCUSSION

A. PL Analysis

Fig. 1(a), (b) and (c) shows PL spectra of pristine and irradiated samples of Polyethylene Naphthalate (PEN) with different fluences of lithium, carbon and nickel ions respectively. The samples were excited at wavelength λ =350 nm. A prominent peak was observed at 448 nm for pristine sample. The spectra shown by samples irradiated with heavier ions (nickel ions) have intensity quite smaller than the pristine ones, which show that after irradiation the luminescent centers such as impurities, defects have disappeared [2]. The PL spectra of irradiated Polyethylene naphthalate (PEN) samples show shifting of peaks towards the lower end of wavelength (448nm-425nm) i.e. towards higher energies which is known as blue shift, might be due to compressive stress. This may be due to the reason that with irradiation, there is increase in defects concentrations in polymers [3].The PL intensity of PEN samples irradiated with lighter ions (lithium and carbon ions) decreases, when irradiated at lower fluence ($1x10^{11}$ions/cm^2), but at intermediate fluences there is increase in intensity, which may be due to increase in concentration of defects after irradiation. At higher fluences the intensity again decreases, which is due to degradation of sample with irradiation.

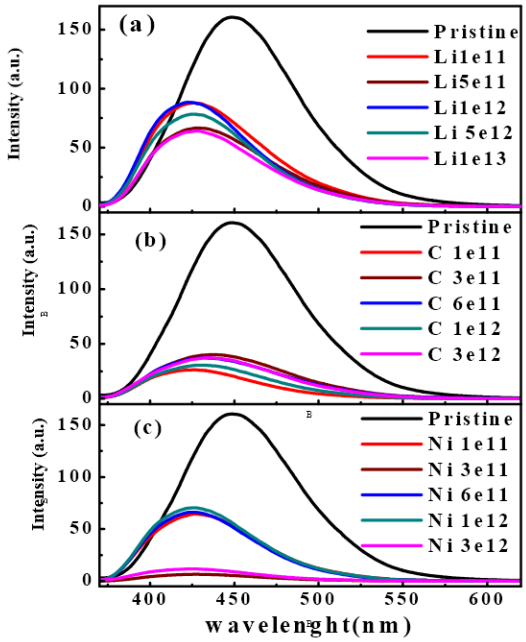

Fig. 1 PL spectra of Polyethylene Naphthalate samples irradiated with different fluences of (a) lithium (b) carbon and (c) nickel ions.

B. Dielectric studies

The dielectric constant of pristine and irradiated samples of polyethylene naphthalate (PEN) was calculated using the relation $\varepsilon' = C_p/C_0$, where C_p is capacitance measured using impedance analyzer; $C_o = \varepsilon_o A/t$, where ε_o is the permittivity in vacuum. The plots for variation of dielectric constants with frequency for pristine and irradiated samples of polyethylene naphthalate (PEN), irradiated with lithium ions, carbon ions and nickel ions are shown in Fig. 2(a), (b) and (c) respectively. It is observed that dielectric constant (ε′) decreases with increase in frequency. This is due to the fact that the charge carriers migrate through the dielectric and get trapped against a defect site, where they induce an opposite charge; hence motion of charge carriers slow down, which in turn decreases the value of dielectric constant (ε′). It is also observed from Fig. 2 that the value of dielectric constant (ε′) of irradiated samples of polyethylene naphthalate (PEN) is more as compared to dielectric constant (ε′) of pristine sample. This may be due to chain scission process due to which there is an increase in number of free radicals [4]. The increase in dielectric constant (ε′) with increase in ion fluence leads to the increase in rigidity of polymer due to irradiation [5].

IV. CONCLUSION

The irradiated samples of Polyethylene naphthalate (PEN) shows a shifting of peaks towards the lower end of wavelength (448nm-425nm) i.e. towards higher energies due to compressive stress. The increase in dielectric constant (ε′) with increase in ion fluence leads to the increase in rigidity of polymer due to irradiation.

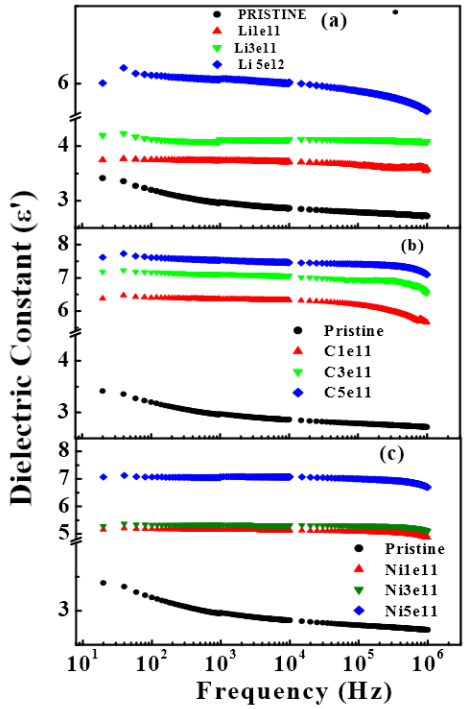

Fig. 2 Dielectric spectra of Polyethylene Naphthalate samples irradiated with different fluences of (a) lithium (b) carbon and (c) nickel ions.

ACKNOWLEDGMENT

The authors wish to thanks Instrumentation lab of Department of Physics, Guru Nanak Dev University, Amritsar for Photoluminescence studies and Department of Electronics Technology, Guru Nanak Dev University, Amritsar for Dielectric studies.

REFERENCES

[1] M.M. Nasef, K. Zaman and M. Dahlan, "Electron irradiation effects on partially fluorinated polymer films: Structure–property relationships" *Nucl. Instr. Meth. Phys. Res. B,* vol. 201, April. 2003, pp. 604-614.

[2] G. Teyssedre, P. Tiemblo, F. Massines and C. Laurent, "On the UV contribution to plasma-induced luminescence of polypropylene" *J. Phys. D: Appl. Phy.* Vol. 29, Dec. 1996, pp. 3137-3146.

[3] R.A.M. Rizk, A.M. Abdul-Kader, Z.I. Ali and M. Ali, "Effect of ion bombardment on the optical properties of LDPE/EPDM polymer blends," *Vacuum,* vol. 83, Jan. 2009, pp. 805-808.

[4] T. Phunkan, D. Kanjilal, T.D. Goswami and H.L. Das, "Dielectric response of irradiated PADC polymer track detector," *Nucl. Instr. Meth. Phys. Res. B,* vol. 234, July. 2005, pp. 520-524.

[5] T. Phunkan, D. Kanjilal, T.D. Goswami and H.L. Das, "Dielectric response of heavy ion irradiated PADC track detector," *Nucl. Instr. Meth. Phys. Res. B,* vol. 155, July. 1999, pp. 116-119.

Synthesis of Copper Nanoparticles using Ascorbic acid as Reducing Agent-A Green Synthesis

Jeevan Jyoti Mohindroo[a] Neerja Kalia[b] · Neha[c] and Radhika[c]

[a]*Dept. of Chemistry DAV College Amritsar*

[b] *Dept. of Physics DAV College Amritsar*

[c]*PG students Dept. of Physics DAV College Amritsar*

E Mail: jjmdav@gmail.com

***Abstract*—In the present work a green method of synthesising Copper Nanoparticles using Ascorbic Acid as reducing agents is proposed. The method involves adding Polyethylene glycol(PEG) as capping agent for stabilising the copper nanoparticles. The synthesised Nanoparticles were characterised by UV, IR Spectroscopy. The UV Spectrum gave a Characteristic Band at 570nm indicating the synthesis of copper nanoparticles. The TEM Analysis was carried out to confirm the size distribution of nanoparticles. The size distribution of synthesised particles was in the range80-100nm.The same particles were synthesised by using traditional reducing agent such as NaBH4 via chemical reduction method and a comparison of size distribution was made. It was concluded that the particles synthesised by Green Synthetic method showed a better size distribution pattern which was confirmed by TEM and XRD studies,**

***Keywords*—**Copper Nanoparticles, Ascorbic Acid, Reductants, Green Synthesis.

I. INTRODUCTION

The emerging field of green Nanoscience faces considerable research challenges to achieve the maximum performance and benefit from nanotechnology while minimizing the impact on human health and the environment. The principles of green chemistry, applied to Nanoscience, provide a framework for designing greener nanomaterials and developing greener Nanosynthesis methods. As Nanoscience emerges from the "discovery phase" to the production level, the need for larger quantities of highly purified, structurally well defined and precisely functionalized materials will require significant improvements in Nanoparticles synthesis. The literature in this area illustrates a few of the many approaches that are being explored in the pursuit of Greener Nanosynthesis and provides some examples of how these steps can yield high-performance materials with higher efficiency and enhanced safety.

The nature of engineered nanomaterials and their proposed uses provides compelling reasons for the implementation of green chemistry in the development of the new materials and applications. Nanomaterials are expected to (i) exhibit new size-based properties (both beneficial and detrimental) that are intermediate between molecular and particulate, (ii) incorporate a wide range of elemental and material compositions, including organic, inorganic, and hybrid structures, and (iii) possess a high degree of surface functionality. Assessment of the potential toxicological and environmental effects of nanoscale materials before they are accepted as mature technologies presents an opportunity to minimize putative negative consequences[2] from the outset and ultimately lead to the design of higher performance materials.

It is a well known fact that green chemistry has been employed successfully in the preparation of highly functionalized products (e.g., pharmaceuticals) that have a strong analogy to functionalized nanomaterials that have been proposed for a range of future applications, one would expect successful application of this approach for these nascent materials. Application of green chemistry to Nanoscience should also prove beneficial in developing production-level commercial scale materials. The development of high-precision, low-waste methods of Nano manufacturing will be crucial to commercialization. In addition to providing enhanced research and development strategies, green chemistry offers an opportunity to improve public perception of Nanoscience, as this approach is relatively easy to explain and can be used to convey a responsible attitude toward the development of this new technology. For these reasons, green chemistry can play a prominent role in guiding the development of nanotechnology to provide the maximum benefit of these products for society and the environment.

II. METHODOLOGY

Metal Nanoparticles via Greener Routes have been synthesized by using an Environmentally Benign Method .In this approach we intend to use different available Environmentally Benign Biodegradable Reductants such as **Sugars** like Glucose and Sucrose;

Vitamins Like Ascorbic Acid. This approach has certain advantages

(i) sugars (glucose, fructose, and sucrose) and other biodegradable reductants are easily available to be used as reducing agents,

(ii) upon their exploitation no other stabilizing agent or capping agent is required to stabilize the Nanoparticles,

(iii) sugars are very cheap and biofriendly and instead of keeping the Nanoparticles in aqueous solution one can safely preserve the particles in a desiccators for months and can be redispersed in aqueous phase whenever required.

The Method would involve mixing the standard solutions of Cu^{+2} ions with the Poly ethylene Glycol (PEG) solution and the mixture is stirred for 30min at about 70°C. Aqueous solution of NaOH was added slowly to the above solution to adjust the pH to alkaline. The resulting mixture was stirred for half an hour. Ascorbic Acid was added in small portion to complete reduction. Colour of the solution changes indicating the formation of copper nanoparticles. The nanoparticles were separated by ultracentrifugation, washed with distilled water and dried in oven at 80°c for half an hour.

III. RESULTS AND DISCUSSION

Characterization of Synthesized Copper (Cu) Nanoparticles

The characterization of Synthesized Nanoparticles will be done by using following techniques

A. UV-Visible and FTIR characterisation:

The formation of Copper Nanoparticles was indicated by the change in colour of solution from blue to copper yellow and Dark black, which is also supported by the λmax value at 572nm.The value clearly indicates that copper nanoparticles have been formed in the colloidal form. The Nanoparticles were separated by ultracentrifugation and the dried powder was analyzed by FTIR. The FTIR spectra showed a Characteristic pattern as reported for copper nanoparticles.(figure1 and 2)

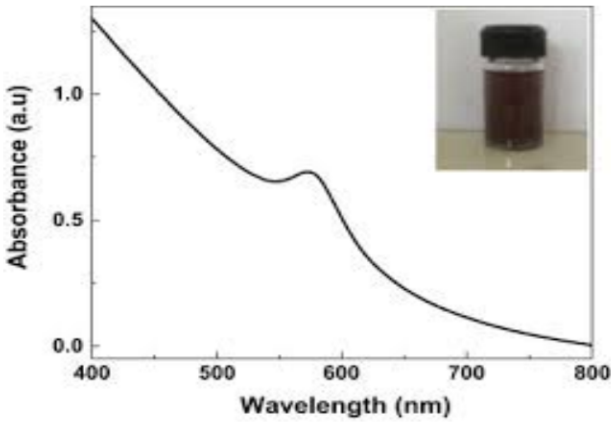

Figure 1: UV spectra of Copper Colloidal solution showing Absorption Maxima-572nm

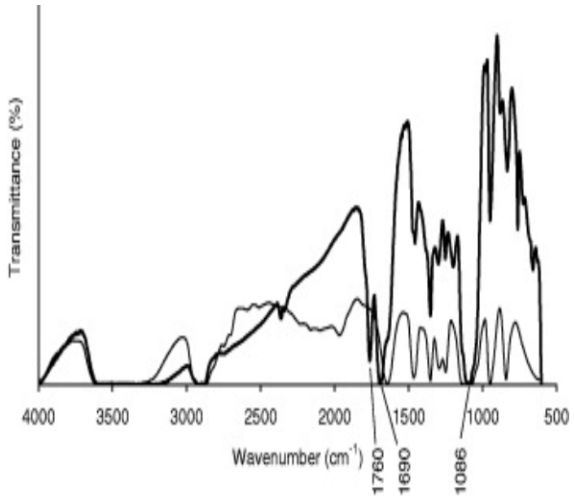

Figure 2: FT IR Spectrum of Copper Nanoparticles

B. X-Ray Diffraction (XRD)

The intensity of the diffracted X-rays is measured as a function of the diffraction angle. The intensities of the spots provide information about the atomic basis. The sharpness and shape of the spots are related to the perfection of the crystal or a powder. These studies determine the lattice constants, porosity and approximate size of the metal nanoparticles. Il also tell us about the purity of the synthesized materials.

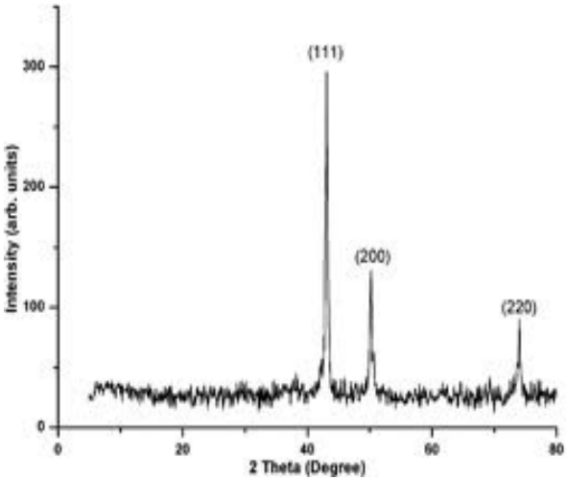

Figure 3: XRD of Synthesized Copper Nanoparticles

C. SEM Studies:

In these studies Electron beams are used to produce images. SEM **(Scanning-Tunneling Microscope)** studies will be applied to confirm the particle size of metal nanoparticle obtained by varying the reductants. Analysis pertaining to the determination of size of nanoparticles is the TEM Analysis for which the samples are being send to IIT Mumbai for Analysis. Further studies in this regard were carried out to check the size distribution of copper nanoparticles the TEM Image showed that the size of particles was in the range of 80-100nm.

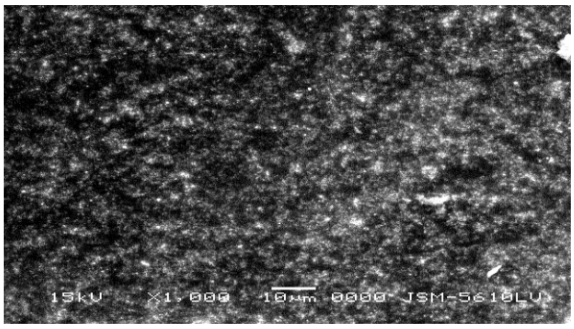

Figure 4(a): SEM Image and size distribution of synthesized copper

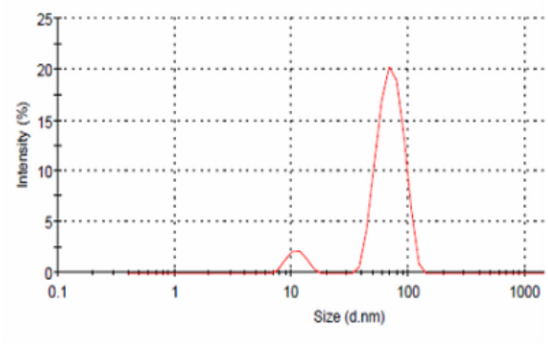

Figure 4(b): SEM Image and size distribution of synthesized copper

The particle size distributions of the freshly prepared Cu nanoparticles is shown in the figure3. It is seen that thesize of the majority of the nanoparticles when prepared fresh was about 90 nm but after storage for 2 days the same was increased to about 300 nm. This is due to the aggregation of nanoparticles. Cu nanoparticles because of their high reactivity tend to form aggregates. The tendency of getting aggregated was controlled by the starch and PEG (poly ethylene glycol which act as the stabilising agent.

IV. CONCLUSION

- Copper nanoparticles were successfully prepared, by reducing Cu^{+2} ions, using environmentally benign reducing agents ie Ascorbic Acid. The absorbance spectrum of the solution was taken showing characteristic absorption at 572nm.
- The particle size and theirdistribution, of freshly prepared system and after storing for two days in atmospheric condition, were examined by particle size analyzer shows that the maximum size of the particle was increased from 90nm to 300 nm .
- The stability of the particles was improved by the introduction ofstarch solution along with PEG in the colloidal system.the antimicrobial activity of these particles were studued and it showed that they resist the growth of gram positive bacteria.

V. REFERENCES

1. *Nanostructured Materials, Processing, Properties and Applications*; Koch, C. C., Ed.; Noyes Publications: Norwich, New York, 2002
2. Albrecht, M. A.; Evans, C. W.; Raston, C. L. *Green Chem.* 2006, *8*, 417.
3. Jennifer A. Dahl, Bettye L. S. Maddux, and James E. Hutchison* *Chem. Rev.* 2007, 107, 2228-2269
4. YANG Jian-guang, et al/Trans. Nonferrous Met. Soc. China 17(2007) 1181-1185
5. Sudipa Panigrahi, Subrata Kundu, Sujit Kumar Ghosh, Sudip Nath and Tarasankar Pal* Journal of Nanoparticle Research 2004, 6:411– 414,.
6. Zhen Yin, Ding Ma* and Xinhe Bao* Chem. Commun., 2010, 46, 1344–1346

7. XUEGENG YANGa, SHENHAO CHENa,b*, SHIYONG ZHAOa, DEGANG LIa and HOUYIMA
J. Serb. Chem. Soc. 2003*68*(11)843–847
8. Pillai, Z. S.; Kamat, P. V. *J. Phys. Chem. B, American Chemical Society* ,2004,*108,* 945
9. David D. Evanoff, Jr. and George Chumanov* *J. Phys. Chem. B*, 2004, *108* (37), pp 13948–13956
10. Eric C. Njagi, Hui Huang, Lisa Stafford, Homer Genuino, Hugo M. Galindo, John B. Collins,
George E. Hoag, and Steven L. Squib*, s Langmuir 2011, 27(1), 264–271
11. Lin, Y.; Wen, C.; Chen, F. Sep. Purif. Technol. 2008, 64, 26–30.
12. Valle-Orta,M.; Diaz, D.; Santiago-Jacinto, P.; V_ azquez-Olmos, A.; Reguera, E. J. Phys. Chem. B 2008, 112, 14427–14434.
13. Ahmad, A.; Mukherjee, P.; Mandal, D.; Senapati, S.; Khan, M. I.; Kumar,R.; Sastry, M. J. Am.
Chem. Soc. 2002, 124, 12108–1210
14. Bharde, A. A.; Parikh, R. Y.; Baidakova, M.; Jouen, S.; Hannoyer, B.; Enoki, T.; Prasad, B. L. V.;
Shouche, Y. S.; Ogale, S.; Sastry, M. Langmuir 2008, 24, 5787–5794.
15. Nadagouda, M. N.; Castle, A. B.; Murdock, R. C.; Hussain, S. M.; Varma, R. S. Green Chem. 2010,
12, 114–122.
16. Sathishkumar, M.; Sneha, K.; Kwak, I. S.; Mao, J.; Tripathy, S. J.; Yun, Y.-S. J. Hazard. Mater.2009, 171, 400– 404.
17. Philip, D. Physica E: Low Dimens. Syst. Nanostruct. 2010, 42, 1417–1424.
18. Chandran, S. P.; Chaudhary, M.; Pasricha, R.; Ahmad, A.; Sastry, M. Biotechnol. Prog. 2006, 22, 577–583.
19. Hoag, G. E.; Collins, J. B.; Holcomb, J. L.; Hoag, J. R.; Nadagouda, M. N.; Varma, R. S. J. Mater. Chem. 2009, 19, 8671–8677.
20. Herrera-Becerra, R.; Zorrilla, C.; Ascencio, J. A. J. Phys. Chem.C 2007, 111, 16147-53.
21. Huang, J.; Li, Q.; Sun, D.; Lu, Y.; Su, Y.; Yang, X.; Wang, H.; Wang, Y.; Shao, W.; He, N.; Hong, J.; Chen, C. Nanotechnology 2007, 18, 105104–105115
22. Weare, W. W.; Reed, S. M.; Warner, M. G.; Hutchison, J. E. *J. Am.Chem. Soc.* 2000, *122*, 12890.
23. Gardea-Torresdey, J. L.; Parsons, J. G.; Gomez, E.; Peralta-Videa, J.; Troiani, H. E.; Santiago, P.; Yacaman, M. J. *Nano Lett.* 2002, *2*,397
24. Shiraishi, Y., and Toshima, N., *Journal of Molecular Catalysis A: Chemical*, 1999, 141, 187–192.

Characterisation of Polymer Gel Electrolytes Containing Imidazolium Based Ionic Liquids

Dilraj Preet Kaur[a], S.S. Sekhon[b]

[a]*Department of Physics, Dolphin (PG) College of Science and Agriculture, Chandigarh, Punjab, India*

[b]*Department of Physics, The University of West Indies, St. Augustine, West Indies*

***Abstract*— Poly(vinylidene fluoride-co-hexafluoropropylene) (PVdF-HFP)-ionic liquid gel electrolytes have been synthesized using ionic liquid 2,3-dimethyl-1-hexylimidazolium bis(trifluoromethanesulfonyl)imide (DMHxImTFSI) and propylene carbonate. Ionic conductivity of the ionic liquid is 2.47 x 10^{-3} Scm^{-1} at 30°C and polymer gel electrolytes also possess conductivity of the same order. The dependence of ionic conductivity on the concentration of ionic liquid, polymer and temperature has been studied. TGA/DSC studies shows that the polymer gel electrolytes containing ionic liquid are thermally stable upto 100°C.**

***Keywords*—**Ionic Liquids, Ionic Conductivity, Polymer Gel Electrolytes, Thermal Stability

I. INTRODUCTION

Room temperature molten salts or ionic liquids (IL), as they are generally known, are salts with melting point below 100°C and are composed of large organic cations and weakly coordinating anions. Due to the unique physicochemical properties of IL such as high ionic conductivity, negligible vapor pressure, non-flammability and high thermal and chemical stability [1]-[3], polymer electrolytes containing ionic liquids in gel or solid form are being widely studied for their potential applications in solid state ionic devices [4]-[9].

In the present work, polymer gel electrolytes containing imidazolium based ionic liquid have been prepared and characterized for their ionic conductivity and thermal stability.

II. EXPERIMENTAL

Ionic liquid 2,3-dimethyl-1-hexylimidazolium bis(trifluoromethane sulfonyl)imide (DMHxImTFSI) was synthesized by the metathesis reaction of 1,2-dimethylimidazole with 1-bromohexane to obtain 2,3-dimethyl-1-hexylimidazolium bromide (DMHxImBr) followed by an anion exchange reaction of DMHxImBr with lithium trifluoromethanesulfonimide. The formation of ionic liquid was checked by ^{1}H and ^{13}C NMR with JEOL AL-300 MHz NMR spectrometer. The details of the preparation procedure for the ionic liquid is available in earlier publications.[10,11] Polymer gel electrolytes having different concentrations of IL and polymer poly(vinylidenefluoridecohexafluoropropylene) (PVdF-HFP) were prepared by first solvating the IL in the high dielectric constant solvent propylene carbonate (PC, ε = 64.4) to prepare liquid electrolyte and then immobilizing this liquid electrolyte by the gradual addition of polymer along with continuous stirring. Ionic liquid and polymer gel electrolyte were characterized by impedance spectroscopy (computer interfaced Hioki 3532-50 LCR Hi-Tester), FTIR spectroscopy (Shimadzu 8400S FTIR spectrometer) and simultaneous DSC/TGA/DTG measurements (Perkin Elmer Pyris Diamond)

III. RESULTS AND DISCUSSION

A. *Ionic Conductivity and Viscosity*

As a function of temperature, the viscosity of IL decreases from 109 mPas at 30°C to 19.8 mPas at 80°C, and a corresponding increase in conductivity from 2.47x10^{-3} Scm^{-1} at 30°C to 1.21x10^{-2} Scm^{-1} at 80°C has been observed. The decrease in the viscosity results in an increase in mobility and hence increases ionic conductivity of ionic liquid.

Liquid electrolytes with the composition PC+0.5M IL has been subsequently utilized to prepare polymer gel electrolytes. The ionic conductivity of polymer gel electrolytes containing different concentrations of PVdF-HFP in PC+0.5M IL is given in Fig.1(a).

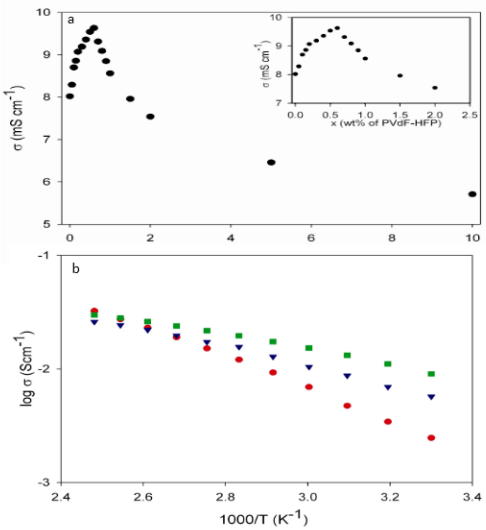

Fig. 1(a) Variation of ionic conductivity of gel electrolyte PC+0.5M IL+ x (wt%) PVdF-HFP with concentration of polymer. Inset shows the conductivity at lower concentrations of polymer. (b) ionic conductivity of IL(●), PC+0.5M IL(■), and PC+0.5M IL+10 wt% PVdF-HFP(▼) as a function of temperature.

At very low concentrations of PVdF-HFP (0-0.6wt %), conductivity of electrolytes increases, reaches a maximum and then starts decreasing at higher concentrations of PVdF-HFP. This small increase in ionic conductivity with the addition of polymer is due to the dissociation of some ion aggregates, which are generally present in these electrolytes due to the higher concentration of ions. This results in an increase in free ion concentration, thereby increasing the ionic conductivity. The decrease in ionic conductivity at higher concentrations of PVdF-HFP is due to an increase in viscosity, which reduces mobility and hence conductivity decreases.

The variation of ionic conductivity of IL, PC+0.5M IL and PC+ 0.5M IL+ 10wt% PVdF-HFP as a function of temperature has been shown in Fig. 1(b). At room temperature the addition of PC to the IL results in an increase in conductivity and liquid electrolyte PC + 0.5 M IL show higher conductivity than IL at all temperatures which is due to lower viscosity of PC as compared to the IL and higher dielectric constant and both these factors contribute to higher conductivity.

However polymer gel electrolytes containing 10 wt% PVdF-HFP show lower conductivity as compared to the liquid electrolytes at all temperatures which is due to an increase in viscosity with the addition of polymer.

B. FTIR

The formation and dissociation of ion aggregates has been checked by FTIR spectroscopy. In the FTIR spectrum of (PC+0.1M IL), peaks due to free ions contributed by the ionic liquid are observed at 739 (δ_s CF_3) and 761(ν_s SNS) cm^{-1} and 1056cm^{-1} (ν_a SNS) (Fig. 2(a)). On further increasing the concentration of IL in PC to 0.5M, an additional shoulder is observed at 757cm^{-1} and also a shoulder appears adjacent to 1056cm^{-1} peak suggesting the presence of ion aggregates.

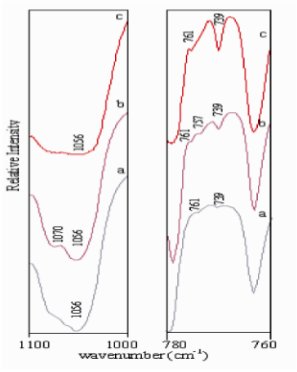

Fig. 2 FTIR spectrum of electrolytes PC+0.1M IL (a), PC+0.5M IL (b) and PC+0.5M IL+ 10 wt% PVdF-HFP (c).

However, the addition of PVdF-HFP in small concentrations (0.1wt %), results in the disappearance of the shoulders at 757cm^{-1} and 1070cm^{-1}, indicating the dissociation of ion aggregates. These observations are consistent with the results obtained from ionic conductivity measurements.

C. DSC/TGA

TGA thermogram, of PC+0.5M IL+ 10wt% PVdF-HFP (Fig. 3) shows that the polymer gel electrolyte is stable upto 100°C.

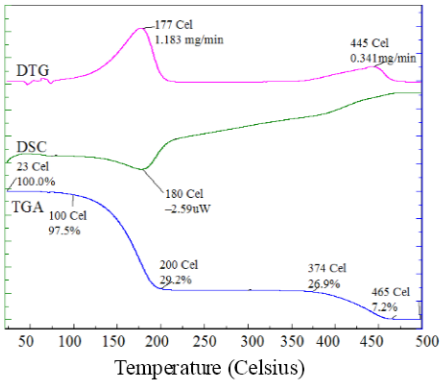

Fig. 3 DSC/TGA/DTG plots for PC+0.5M IL+ 10 wt% PVdF-HFP

Above 100°C, weight loss by a large amount takes place due to the loss of PC which also corresponds to the endothermic peak at 180°C in DSC curve. The second weight loss by a small amount at 374°C in the TGA thermogram is due to the degradation of IL and PVdF-HFP.

IV. CONCLUSION

PVdF-HFP based polymer gel electrolytes containing ionic liquid DMHxImTFSI have been found to show ionic conductivity higher than 0.01 Scm^{-1} at all temperatures above 50°C. The polymer has been observed to play an active role and helps in the dissociation of ion aggregates present in these electrolytes. The polymer gel electrolytes are thermally stable upto 100°C which is suitable for their use in many devices.

REFERENCES

[1] J. S. Wilkes and M. J. Zaworotko, "Air and water stable 1-ethyl-3-methylimidazolium based ionic liquids," J. Chem Soc Chem Commun vol.13, pp 965, 1992.

[2] P. Bonhote, A. P. Dias, N. Papageorgiou, K. Kalyanasundaram and M. Gratzel, "Hydrophobic, highly conductive ambient temperature molten salts," Inorg Chem. vol 35, pp 1168, 1996.

[3] D. R. MacFarlane, P. Meakin, J. Sun, N. Amini and M. Forsyth, "Pyrrolidinium Imides: A new family of molten salts and conductive plastic crystal phases J. Phys. Chem. B , vol. 103, pp 4164, 1999.

[4] M. Watanabe, S. I. Yamada and N. Ogata, "Ionic conductivity of polymer electrolytes containing room temperature molten salts based on pyridinium halide and aluminium chloride," Electrochim. Acta, vol. 40, 2285, 1995.

[5] J. Fuller, A. C. Breda and R. T. Carlin, "Ionic liquid-polymer gel electrolytes," J. Electrochem. Soc. 144, L67, 1997

[6] M. Morita, T. Shirai, N. Yoshimoto and M. Ishikawa, "Ionic conductance behaviour of polymeric gel electrolyte containing ionic liquid mixed with magnesium salt," J. Power Sources vol. 139, pp 351, 2005.

[7] S. S. Sekhon, B. S. Lalia, J. S. Park, C. S. Kim and K. Yamada, "Physicochemical properties of proton conducting membranes based on ionic liquid impregnated polymer for fuel cells," J. Mater. Chem. , vol. 16, pp 2256, 2006.

[8] D. P. Kaur, K. Yamada, J. S. Park and S. S. Sekhon, "Correlation Between Ion Diffusional Motion and Ionic Conductivity for Different Electrolytes Based on Ionic Liquid," J. Phys. Chem. B , vol. 113, pp 5381, 2009.

[9] S. Zhang, K. H. Lee, C. D. Frisbie and T. P. Lodge, " Ionic conductivity, capacitance, and viscoelastic properties of block copolymer based ion gels," Macromolecules vol. 44, pp 940, 2011.

[10] B. Singh and S. S. Sekhon, "Ion conducting behaviour of polymer electrolytes containing ionic liquids," Chem. Phys. Lett. , vol. 414, pp 34, 2005.

[11] B. Singh and S. S. Sekhon, "Polymer Electrolytes Based on Room Temperature Ionic Liquid: 2,3-Dimethyl-1-octylimidazolium Triflate," J. Phys. Chem. B, vol. 109, pp 16539, 2005.

RADON CONCENTRATION IN GROUND WATER SAMPLES FROM SOME REGIONS OF TARN TARAN DISTRICT OF PUNJAB.

[a]Meetu Singh, [b]Neerja, [c]Asha Rani

[a]*Department of Applied Sciences, Punjab Technical University, Jalandhar (Punjab), India.*

[b]*PG Department of Physics, DAV College, Amritsar (Punjab), India.*

[c]*Department of Applied Sciences, Ferozepur College of Engineering and Technology, Ferozshah (Punjab), India.*

Email: [a] meet.rajput40@yahoo.com

Abstract: **The estimation of radon level has been increasingly supervised in world due to its unsafe effects to mankind. In the present study, groundwater samples were taken from different villages of Tarn Taran district. The analysis of radon concentration in these samples was carried out by using RAD7, an electronic radon detector equipped with an appropriate unit (Aqua kit). The radon concentration in the samples has been found to be in range of 27.18 pCi/L to 189.18 pCi/L, which is well within safe limit as recommended by USEPA in all the regions from where the samples were collected.**

Keywords: Estimation, Radon Concentration, RAD7.

INTRODUCTION

Great interest has been expressed worldwide for the study of naturally occurring radiation and environmental radioactivity. This interest has led to the performance of extensive surveys in many countries (UNSCEAR, 2000). The primary reason for these studies is the simple fact that natural radiation background is the primary source of human radiological exposure. Radioactivity present in human environment is the major source of radiation dose being received by population. Naturally occurring radionuclides like Uranium have existed in the Earth's crust since its formation. Radon (Rn-222) is a radioactive gas derived from the Uranium decay series and it is the main source of internal radiation exposure to human life [1]. As radon undergoes radioactive decay, it gives off radiation and becomes another radioactive element. This is repeated several times until it becomes stable lead Radon gas is chemically inert without odor, color or taste and is responsible for about half of the radiation dose received by the general population [2]. According to the US Environmental Protection Agency (EPA) and the World Health Organization (WHO) Handbook on Indoor Radon (WHO, 2009) radon is the second leading cause of lung cancer after smoking [3,4]. The increased interest in measuring radon in recent years has stimulated instrument research radon measurement professionals, mitigators, and researchers. Overall, as a global average, at least 80 % of the radon emitted into the atmosphere comes from the uppermost ground layer.The second most important contributor to environmental radon is emanation from groundwater sources [5,6]. Since water is most important source of life and major part of total body weight. So dissolved radon in drinking water can lead to significant health problems for humans [7]. It is estimated that for every 10000 pCi/L of radon in water, about 1 pCi/L is released into air [8]. The nuclides of the uranium series which can be dangerous to health because of their presence in drinking water are 226Ra and 222Rn [9]. The maximum limit of concentration of radon in water as proposed by US Environmental Protection Agency (USEPA) is 300 pCi/L which can cause a life time cancer risk of about 1 in 104 [10]. Many extensive studies have been performed on radioactivity in drinking waters worldwide in recent years [11, 12, 13]. The present work tries to explore the concentration of radon in water samples taken from some regions of Tarn Taran district of Punjab.

EXPERIMENTAL DETAILS

Water samples were taken from the study area used for drinking and radon concentrations in these samples were measured with solid state alpha detector based RAD7 [14]. The RAD7 is a continuous monitor based on the alpha spectrometry technique. It uses a solid state semiconductor detector that directly converts an alpha radiation to electrical signal. Its accessory RAD H_2O is used to measure the radon in water over a wide range of concentration [15]. The unit features the fastest response and recovery time of any system on the market, and is able to measure radon concentrations at the 200Bq/m^3 action level in less than one hour.

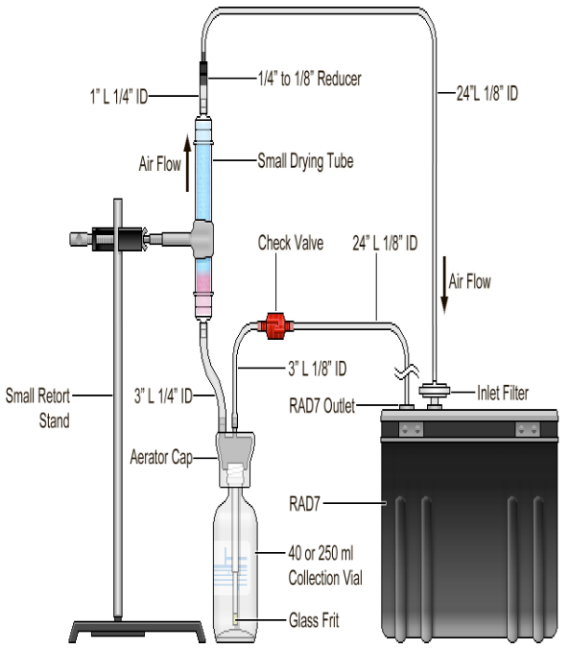

Figure 1:The RAD7 connected with RAD7H2O accessories

The RAD7-H_2O method employs a closed loop aeration scheme in which the air is recirculated through the water sample collected in vial and the radon is continuously extracted until a state of equilibrium develops. The RAD-H_2O system reaches this state of equilibrium within about 5 minutes, after which no more radon can be extracted from the water sample. The extracted radon is pumped in the test chamber the detector measures the radon concentration. The RAD H_2O gives results after 30 minutes analysis with a sensitivity that matches or exceeds that of liquid scintillation methods.

STUDY AREA

The study area covers some regions of Tarn Taran district which is one of the districts in the state of Punjab in North-West Republic of India as shown in the map in Figure 2.

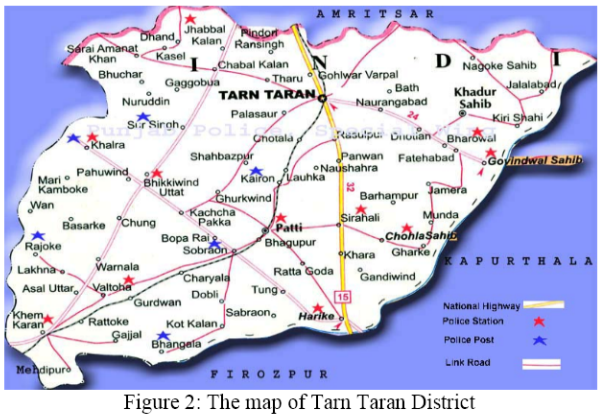

Figure 2: The map of Tarn Taran District

RESULTS AND DISCUSSIONS

The results of measurements are summarized in tables 1. A total of 20 samples were analysed. It can be seen that radon activity in water varies from 27.18 pCi/L to 189.18 pCi/L and the safe value recommended by EPA is 300pCi/L.

Sample no.	Location	Radon conc. In pCi/L
1.	Sheron	84.40
2.	Dhotian	102.76
3.	**Usmaan**	**27.18**
4.	Nasshehra pannua	37.34
5.	Jamarai	109.65
6.	Rasulpur	69.5
7.	Aladinpur	103.16
8.	Sarhali	149.58
9.	Sarhali kalan	121.43
10.	**Chaudary wala**	**189.18**
11.	Bhathal bhaike	118.04
12.	Warian	98.48
13.	New warian	108.41
14.	Thathiana mahanta	132.92
15.	Banwalipur	46.16

Table 1: Results of measurements of radon concentration

CONCLUSIONS

Present study reveals that the value of radon concentration in the water samples is well below the prescribed safe limit values in all the regions from where the samples were collected.

REFERENCES

[1] UNSCEAR 2000, Sources, Effects and Risks of ionizing radiation, New York, United Nations.
[2].United Nations Scientific Committee on the Effects of Atomic Radiation (UNSCEAR) (1994) Ionizing Radiation: Sources and Biological Effects, New York: United Nations.
[3] EPA (Environmental Protection Agency)"Radon Reference Manual", Office of Radiation Programs Washington DC 20460, EPA 520/1-87-20, September 1987.
[4] WHO handbook on indoor radon - a public health perspective, Geneva, World Health Organization, 2009.
[5]Lee KY, Yoon YY, Ko KS (2010) J Radioanal Nucl Chem 286:381–385
[6] Lee KY, Yoon YY, Cho SY, Ko KS, Yum B (2012) J Radioanal Nucl Chem 294:27–30
[7] K. N. Yu, Z. J. Guan, M. J. Stokes and ECM Young, *Appl. Radiat. Isot.,*1994, 45, 809.
[8] H. M. Prichard, J. American Water Works Association, 1987, 79(4), 159.
[9] Duenas, C., Fernandez, M.C., Carretero, J., Liger, E., Canete, S., 226Ra and 222Rn concentrations and doses in bottled waters in Spain. J. Environ. Radioactivity, 45, 283–290, 1999.
[10] USEPA:. National Primary Drinking Water Regulations for Radionuclides, Washington DC, US, 1991.
[11] L. Salonen and P. Huikuri, High Levels of Natural Radiation and Radon Areas: Radiation Dose and Health Effects. General Exposure Assessment, 2000, 24, 87.
[12] V. M. Choubey and R. C. Ramola, J. Environmental Geology 1997, 32(4), 258.
[13] Ganesh Prasad, Yogesh Prasad, G. S. Gusain and R. C. Ramola, Radiation Measurements, 2008, 43(1), 375.
[14]Durridge Company Inc., (2010), Reference Manual version 6.0.1, RAD7™ Electronic Radon Detector.
[15] N.Todorovic J.,Nikolov, S.Forkapic, I.Bikit, D.Mrdja world Academy of Science, Engineering & Technology 76 2011.

Effect of various parameters on microalgal biodiesel: A review

Mukesh Kumar[a], M.P. Sharma[b]
[a]*Research Scholar, Alternate Hydro Energy Centre, Indian Institute of Technology Roorkee, Roorkee, Uttarakhand- 247667, India, Tel.: 08126504460*
[b]*Associate Professor, Alternate Hydro Energy Centre, Indian Institute of Technology Roorkee, Roorkee ,Uttarakhand-247667, India*
Corresponding Author: E-mail: mukeshdec07@gmail.com

***Abstract*-Presently the world has facing energy crisis associated with continuous depletion of fossil fuels, emission of greenhouse gases which are responsible for global warming. The urgent need to replace fossil fuels and introduced a new source of energy which can fulfill the global energy demand. Biodiesel and biohydrogen are interesting alternatives, both of which can be obtained by non-edible and microalgae. Microalgae have several advantages over the edible and non-edible feedstocks such as it have potential to produce 25-220 times higher triglycerides than terrestrial plants, gives about 30 times or more oil yields than terrestrial oil seed crops, have greater photosynthetic efficiency, require less land area and it can provide several different types of renewable biofuels such as methane, ethanol, triglyceride and hydrogen. Microalgae can be cultivated in saline and wastewaters, in sunlight and in atmospheric CO_2. However, large-scale biodiesel and biohydrogen production from microalgae are commercialized due to their poor volumetric efficiencies. This paper provides an overview of the biodiesel production from microalgae via acid catalyst and the effect of various parameters on the biodiesel yield.**

1. Introduction

Renewable energy plays a key role to replace fossil fuel. Presently biodiesel importance is increasingly to meet the global energy demands. Biodiesel is an alkyl esters of long-chain fatty acids obtained from various sources such as edible and non edible oil or animal fats. Edible as well as non-edible feedstocks have several limitations which restricts it use for biodiesel production. Presently attention is focused on microalgae for biodiesel production. Microalgae have several advantages over the edible and non-edible feedstocks such as it have potential to produce 25-220 times higher triglycerides than terrestrial plants, gives about 30 times or more oil yields than terrestrial oil seed crops, have greater photosynthetic efficiency, require less land area and it can provide several different types of renewable biofuels such as methane, ethanol, triglyceride and hydrogen [1-3]. The tubular photobioreactors was preferred, in comparison to raceway pond for microalgae culture, because the former resulted in greater productivity with a higher microalgal oil yield with minimum contamination. The flocculation is reported as the most promising harvesting method because flocculants used having higher molecular weights and it can adsorb several particles at once. Microalgae produce 25-220 times higher triglycerides than terrestrial plants and can doubling their biomass within 24 h. Oil content in microalgae is 30 times or more than the terrestrial oil seed crops. From the available extraction method, solvent extraction method is most commonly used because of low cost of solvent and the solvent can be reused. Biodiesel production from the Chlorella protothecoides was performed by acidic transesterification. The optimum condition occurred at 100% catalyst quantity (based on oil weight) with a molar ratio of methanol to oil of 56:1 at a temperature of 30 °C, which give biodiesel yield 63 % within~4h of reaction time [4].

2. Algae Cultivation

Two types of system are used of algae cultivation named is open system and closed system. In earlier time open system is most successful method of microalgae cultivation because of easily availability of natural water (lakes, lagoons) and artificial ponds. But low productivity and contamination limited its use to industrial scale. Open system can be classified into circular ponds, inclined ponds and unmixed ponds. In order to overcome the limitation of open ponds such as contamination and low productivity, closed system is used for microalgae cultivation. Closed system permits single strain culture, high productivity and increases the light availability to each cell [5]. Closed system can be classified into vertical tubular reactor, flat plate bioreactors.

3. Harvesting of Algae

Harvesting consist of removing of water from microalgae and recover the biomass for further processing. Due to the small size of microalgae cells (1-20 μm), it may account 20 to 30 % of the total biodiesel production cost [6-7]. Various methods available for harvesting including ultra filtration sedimentation,

filtration, centrifugation, combination of flocculation-flotation, etc [8].

4. Oil Extraction Technique

After harvesting, several extraction methods like solvent, mechanical and chemical extraction methods can be applied to extract oil from microalgae. Solvent extraction is usually applied to get high oil yields from microalgae [2].

Table 1: Comparison of various extraction methods [9]

Extraction methods	Advantages	Disadvantages
Mechanical extraction	Easy to use, no solvent required for extraction	Slow technique, higher amount of sample required for extraction
Solvent extraction	Solvent used are of low cost, solvent can be recycled	Solvent used are highly flammable and toxic, large amount of solvent required
Ultrasound	Fast process, low volume of solvent needed	Very difficult for scale up, required high power
Supercritical fluid extraction	Easy to use, no need of organic solvent	Interaction between CO2 and sample is insufficient

The above table shows the advantages and disadvantages of various extraction systems. It is concluded that solvent extraction method is most promising method for oil extraction and can be widely used.

5. Conversion of microalgal oil into biodiesel

The direct use of oils in an engines is not possible, because it can creates several problems such as, their characteristics (high viscosity, high density, difficulty to vaporize in cold weather) cause deposits in the combustion chamber, with a risk of fouling and an increase in emissions [10]. To overcome all these problems, the conversion of microalgal oil into biodiesel is necessary. The main advantage of acid catalyst transesterification is that it allows to use of high free fatty acid content feedstocks and overall theoretical yield is more than the alkaline catalyst. The main drawback of this method is that high molar ratios of alcohol to oil are required to drive the reaction forward, reactions time is more than alkali-based catalysis. It was reported that biodiesel production from microalgae via acid catalysis are much more abundant than those of the alkali base catalyst method. Other acid catalyst (HCl) is used for biodiesel production with similar reaction conditions of sulphuric acid [11].

6. Effect of various parameters on the transesterification

The biodiesel from microalgal oil is depends on the following parameters [4]:-

(1) Catalyst and its quantity

(2) Molar ration of methanol to oil

(3) Reaction Temperature

(4) Reaction time

6.1 Catalyst and its quantity

Homogenous as well as heterogeneous both catalysts can be used for transesterification of microalgal oil into biodiesel. Homogeneous alkaline catalysts include sodium or potassium hydroxide (NaOH or KOH) while homogeneous acid catalysts include sulfuric acid or hydrochloric acid (H_2SO_4 or HCL). Homogeneous acid catalyst is mostly used because of higher biodiesel yield while these catalysts are slower and more expansive than the homogeneous alkaline catalysts. Different acid-alkaline catalysts used for biodiesel production such as sulfuric acid-Potassium methoxide (H_2SO_4-CH_3OK) or potassium hydroxide-hydrochloride (KOH-HCl). Alkaline catalysts can be used to increase the biodiesel yield. [4, 12, 13] take the (2-100%) catalyst concentration, the specific gravity is less while biodiesel yield is also lower because at this concentration some of oil is burned. [14-18] used NaOH as catalyst and obtained biodiesel yield by 91.4% while [19-20] used KOH as a catalust and they obtained biodiesel yield by approximately 100%. Some author used Mg-Zr, CH_3ONa and CaO/Al_2O_3 as a catalyst for biodiesel production from microalgal oil [21-22]

6.2 Molar ration of methanol to oil

Alcohol is necessary in the transesterification process for breaking the glycerine–fatty acid linkages. The alcohols used for biodiesel production are methanol, ethanol or butanol. Methanol is most commonly used because of low cost. The optimum molar ration of methanol to oil is from 30:1 to 56:1 and H_2SO_4 as a catalyst while molar ratio is from 6:1 to 12:1 in case of KOH as catalyst while 11:50 to 220:100 (based on Volume of methanol to volume of oil) [4, 14-20, 23]. The presence of excess methanol is essential while higher amount slow down the separation of biodiesel.

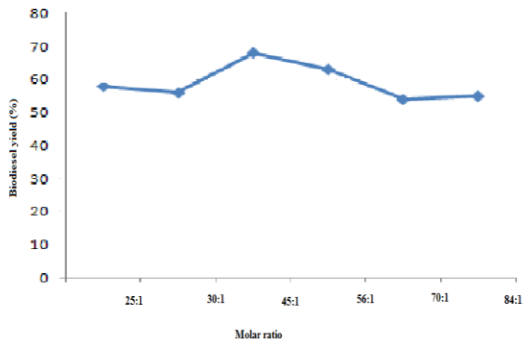

Fig.1. Influence of molar ratio on biodiesel yield

The above shows the variation of biodiesel yield with molar ration. High volume of methanol is required to break the glycerine–fatty acid linkage and to move the reaction in forward direction. The above figure can be helpful to choose the optimum molar ration for biodiesel production.

6.3 Reaction Temperature

The temperature seems to have less effect on the microalgae biodiesel production. Miao found that same biodiesel yield at temperatures of 30 and 50˚C, respectively while at higher temperature the biodiesel yield dropped [4]. The optimum biodiesel achieved in transesterification is from 30-110 [4, 14-20, 23].

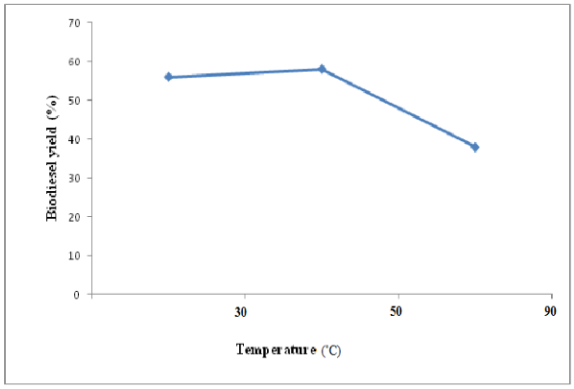

Fig.2. Influence of temperature on biodiesel yield

The above sows the variation of biodiesel yield with temperature. It is concluded that at a specific temperature, the biodiesel yield is maximum, so we can select this optimum temperature.

6.4 Reaction time

Reaction time gives a positive effect on the transesterification. Ehimen *et al.* (2010) found that the SG decreased from 0.914 to 0.884 when the reaction time was increased from 0.25 to 12h. Maio et al found that SG of the biodiesel varied with time, the SG decreased with reaction time in a roughly exponential fashion. The optimum reaction time achieved in transesterification is from 20 min to 11 hrs [4, 14-20, 23].

7. Conclusion

Microalgae can be considered as the most efficient and most promising feedstocks for biodiesel production due to their wide spread availability, potential to produce 25-220 times higher triglycerides than terrestrial plants, gives about 30 times or more oil yields than terrestrial oil seed crops, have greater photosynthetic efficiency, require less land area and it can provide several different types of renewable biofuels such as methane, ethanol, triglyceride and hydrogen. The main difficulty associated with large scale biodiesel production from microalgae is their poor volumetric efficiencies. This paper provides an overview of the biodiesel production from microalgae via acid catalystand the effect of various parameters on the biodiesel yield.

References

[1] Kumar M, Sharma MP, Dwivedi G. Algae Oil as Future Energy Source in Indian Perspective. International journal of renewable energy research 2013; 3:913-21.

[2] Kumar M, Sharma MP. Potential assessment of microalgal oils for biodiesel production: A review. J. Mater. Environ. Sci. 2014; 5.

[3] Kumar M, Sharma MP. Production Methodology of Biodiesel from Microalgae. International Journal of Applied Engineering Research 2013; 8:1825-32.

[4] Miao X, Wu Q. Biodiesel production from heterotrophic microalgal oil. Bioresource Technology 2006; 97:841–46.

[5] Sahoo D, Elangbam G, Devi SS. Using algae for carbon dioxide capture and bio-fuel production to combat climate change. Phykos 2012; 42:32 – 38.

[6] Lam MK, Lee KT. Microalgae biofuels: A critical review of issues, problems and the way forward. Biotechnology Advances 2012; 30:673–90.

[7] Suali E, Sarbatly R. Conversion of microalgae to Biofuel. Renewable and Sustainable Energy Reviews 2012; 16:4316– 42.
[8] www.intechopen.com/download/pdf/33981
[9] Singh J, Sai Gu S. Commercialization potential of microalgae for biofuels production. Renewable and Sustainable Energy Reviews 2010; 14: 2596–10.
[10] Basha SA, Gopal KR, Jebaraj S. A review on biodiesel production, combustion, emissions and performance. Renewable and Sustainable Energy Reviews 2009; 13:1628-34.
[11] Daroch M, Geng S, Wanga G. Recent advances in liquid biofuel production from algal feedstocks. Applied Energy 2013; 102:1371–81.
[12] Kaur S, Sarkar M, Srivastava RB, Gogoi1HK, Kalita MC. Fatty acid profiling and molecular characterization of some fresh water microalgae from INDIA with potential for biodiesel production. New biotechnology; 29:332-44.
[13]Nailwal S, NailwaL TK, Sharma M, Garg S. Physico-chemical characterization of algal oil (oilgae) of kumaun himalayan origin for potential biofuel application. Journal of Applied Phytotechnology in Environmental Sanitation 2013; 2:91-98.
[14] Afify EMR, Shalaby EA, Shanab SMM. Enhancement of biodiesel production from different species of algae. Octubre-diciembre 2010; 61:416-22.
[15] Al-lwayzy SH, Yusaf T. *Chlorella protothecoides* Microalgae as an Alternative Fuel for Tractor Diesel Engines. Energies 2013; 6:766-83.
[16] www.eprints.usq.edu.au/18178
[17] Hossain ABMS, Salleh A. Biodiesel Fuel Production from Algae as Renewable Energy. American Journal of Biochemistry and Biotechnology 2008; 4:250-54.
[18] Maceiras R, Rodrı´guez M, Cancela A, Urrejola S, Sanchez A. Macroalgae: Raw material for biodiesel production. Applied Energy 2011; 88:3318–23.
[19] Chen L, Liu T, Zhang W, Chen X, Wang J. Biodiesel production from algae oil high in free fatty acids by two-step catalytic conversion. Bioresource Technology 2012; 111:208–14.
[20] Chen YH, Huang BY, Chiang TH, Tang TC. Fuel properties of microalgae (Chlorella protothecoides) oil biodiesel and its blends with petroleum diesel. Fuel 2012; 94:270–73.
[21] Tang H, Abunasser N, Garcia MED, Meng Chen, Ng KYS, Salley SO. Potential of microalgae oil from Dunaliella tertiolecta as a feedstock for biodiesel. Applied Energy 2011; 88:3324–30.
[22] Umdu ES, Tuncer M, Seker E. Transesterification of Nannochloropsis oculata microalga's lipid to biodiesel on Al_2O_3 supported CaO and MgO catalysts. Bioresource Technology 2009; 100: 2828–31.
[23] D'Oca MGM, Vieˆgas CV, Lemo˜es JS, Miyasaki EK, Moro´n-Villarreyes JA, Primel EG, Abreu PC. Production of FAMEs from several microalgal lipidic extracts and direct transesterification of the Chlorella pyrenoidosa. biomass and bioenergy 2011; 35:153-38.

Xanthan Gum based Gel Electrolyte containing NaOH

Narinder Arora, Viney Sharma and Rajesh Kumar
P.G. Dept. of Physics, D.A.V. College, Amritsar-143001 (Pb) India
**email: n_arora2k@yahoo.com*

Abstract **- Ionic conductivity of xanthan gum based gel electrolytes containing NaOH has been studied and the maximum ionic conductivity (σ = 88.8 mS/cm) at room temperature has been recorded. The behavior of ionic conductivity with the rise in temperature has been observed and shows contradiction to the theoretical explanation. Small change in ionic conductivity of xanthan gum based gel electrolytes containing sodium hydroxide (NaOH) has been observed with the passage of time. pH value of gel electrolyte containing NaOH shows their basic in nature.**

Keywords: **Natural gum, Gel electrolyte, Ionic conductivity, pH**

I. INTRODUCTION

A Gel is defined as substantially dilute cross linked system and is categorized principally as weak or strong (in terms of less or more viscous) depending upon their flow behavior in steady state [Ferry, 1980] [1]. Gel electrolyte is the hybrid mixture of salt, solvent and polymer; in which salt provide ions upon it's dissociation in solvent and create conducting medium**.** Along with solvent property is to dissolve the salt; whereas polymer increases the mechanical stability of the electrolyte [2-4].

Number of proton conducting polymer gel electrolytes has been studied since last two decades and categorized as: strong acid based gel electrolytes, weak acid based gel electrolytes and natural gum based gel electrolytes [4]. Strong acid (like HCl, H_3PO_4 and H_2SO_4 etc.) based gel electrolytes are mostly not suitable for a device application due to their corrosion in nature that results the degradation of the gel electrolytes. Whereas, weak acid based gel electrolytes are materials of current interest due to their high ionic conductivity at room temperature and also non-degradable nature.

Also natural gums consist of polysaccharides which are extracted from trees and plants, they are materials of high molecular weight, which are mostly soluble in water and provide high ionic conductivity and also capable of large increase in a liquid viscosity even at small concentrations. They are also used as adhesives, binding agents, encapsulating agents, flocculating agents, swelling agents, foam stabilizers, etc. [5-7].

In the present research work, the ionic conductivity and pH of xanthan gum based gel electrolytes containing NaOH have been reported.

II. EXPERIMENTAL TECHNIQUE

Xanthan gum is a polysaccharide secreted by the bacterium xanthomonas campestris, mainly composed of pentasaccharide repeat units containing glucose, sucrose and lactose and is produced by fermentation of glucose, sucrose and lactose.

Xanthan gum based gel electrolyte was prepared by dissolving salt (NaOH) in distilled water and then an appropriate amount of xanthan gum (Aldrich) in NaOH solution. With continuous stirring and kept for 24 hours resulting in the formation of homogeneous gel electrolyte in viscous form.

The extent of ion transport in gel electrolyte represents it's ionic conductivity i.e. $\sigma = nq\mu$, where n represents the number of charge carriers, μ be the mobility of ions and q be the charge on the ion [8, 9]. The ionic conductivity of gel electrolyte was measured with conductivity meter (WTW 3210), which is based upon four probe method. To check the acidic/basic behavior of gel electrolyte; pH measurement was done with the help of pH meter.

III. RESULTS AND DISCUSSION

Xanthan gum is highly soluble in both cold and hot water and this bahaviour is related with polyelectrolyte nature of the xanthan molecule. Due to their special properties, xanthan gum is useful in many industrial applications, especially in the food industry as well as xanthan gum is used as a thickener and to stabilize suspensions and emulsions [10].

Ionic conductivity of liquid electrolyte (solvent: distilled water) has been studied as a function of salt (NaOH) concentration at room temperature and is as shown in Fig.1.

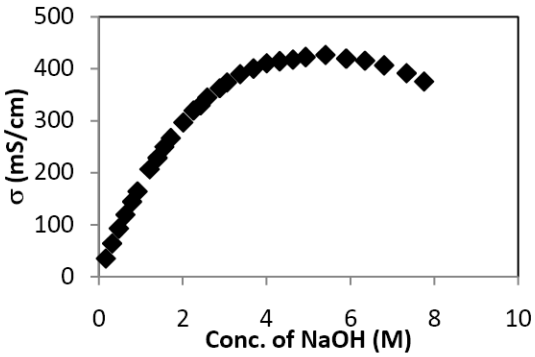

Fig. 1. Variation of room temperature conductivity of liquid electrolyte with salt concentration.

The conductivity of solvent (distilled water - DW) ($\sigma \sim 10^{-6}$ S/cm) increases by four order of magnitude with the addition of small concentration of NaOH salt, which may be explained to be due to the dissociation of salt into ions in distilled water resulting an increase in number of charge carriers and hence conductivity value. As the ionic conductivity is given by $\sigma=nq\mu$, where n represents the number of charge carriers, μ be the mobility of ions and q be the charge on ion. The mobility of ions is given by $\mu=q/6\pi r\eta$. Here η is the viscosity of electrolyte, q is the charge on the ion and r is radius of carrier ion.

From figure 1, also it has been observed that conductivity increases linearly (upto 270 mS/cm) with the increase of salt (NaOH) concentration in distilled water, which has already been explained and is due to the dissociation of salt (NaOH) into ions (Na^+ & OH^-) and at higher salt concentration, a small decrease in conductivity value has been recorded, which may be due to the formation of ion aggregates alongwith the increase in viscosity of liquid electrolyte.

The conductivity of liquid and gel electrolyte has been studied with increase in temperature and the results are shown in figure 2. It has been observed that the conductivity of liquid and gel electrolyte decreases with increase in temperature, which is in contradiction to the theoretical explanation {i.e. $\sigma = \sigma_o \exp(-E_a/K_BT)$}. This may be due to the evaporation of water on raising the temperature of gel electrolyte leads to decrease in mobility of ions and hence conductivity [11]. Also the decrease in conductivity with increase in temperature is small which may make suitability of these gel electrolytes for device application particularly for fuel cell application.

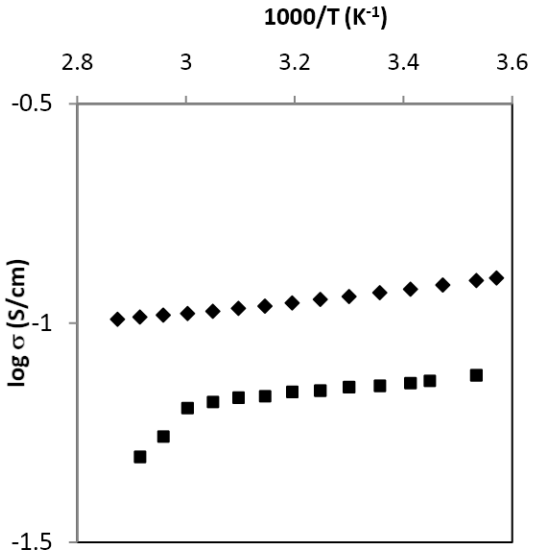

Fig. 2. Conductivity variation of liquid (♦) and gel (■) electrolyte with temperature

It has been further observed that the conductivity of xanthan gum based gel electrolyte is lower than that of liquid electrolyte at all temperature region. This may be explained to be the due to the higher viscosity of gel electrolyte as compared to that of liquid electrolyte with the addition of xanthan gum.

The conductivity of gel electrolyte has also been studied at different time span and results are shown in figure 3. The conductivity of xanthan gum based gel electrolyte containing NaOH increases upto 20 days and then decreases with the passage of time. This may be explained due to continuous movement and interactions of OH^-, H^+, H_3O^+, Na^+ ions in gel electrolyte with the passage of time [12]. As there is not much change in conductivity and gel electrolyte has been observed fungus free even after 50 days, this indicates about their suitable candidature for fuel cell application.

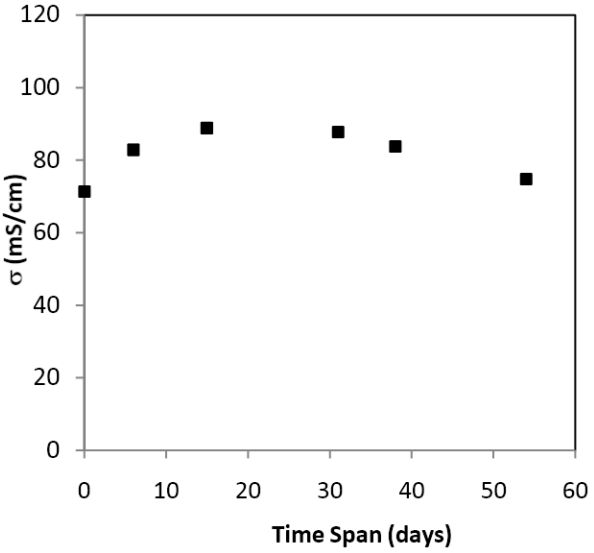

Fig.3. Variation of ionic conductivity of gel electrolyte with the passage of time at room temperature.

pH value of xanthan gum based gel electrolyte containing sodium salt was studied with the passage of time and it's observed values for different gel electrolytes lies between 12 - 14. This shows that these gel electrolytes are basic in nature.

CONCLUSION

The ionic conductivity of xanthan gum based gel electrolyte containing sodium hydroxide is lower than the liquid electrolyte. Also the conductivity of the gel electrolyte decreases with increase in temperature. Conductivity of gel electrolyte varied with passage of time is small and is factor-wise only, which may make it suitable for fuel cell application. pH value of gel electrolyte shows their basic behaviour.

ACKNOWLEDGMENT

The author would like to pay thanks to Dr. K.N. Kaul, Principal, DAV College, Amritsar for providing the necessary infrastructure at my work place.

REFERENCES

[1] J. D. Ferry Viscoelstic properties of polymers, John Wilet & sons, NewYork (1980) pp. 486-544.
[2] Min Hyuk Lee and Yeon–Taik Kim, Electrochemical & Solid State Letters, 2, 72 (1999).
[3] J. Fricke and T. Tillotson, Thin Solid Films, 297, 212 (1997).
[4] J.P Sharma, S.S Sekhon/ Material Science and Engineering B 129(2006) 104-108.
[5] Ariura et al, U.S. patent, patent no.: 4,474,570; Oct. 1984.
[6] Starz et al, U.S. patent, US 2012/0077671A1, Mar. 2012.
[7] J.R. Daniel, R.L. Whistler, A.C.J. Voragen, W. Pilnik, in: B. Elvers, S. Hawkins, W. Russey (Eds.), Ullmann's Encyclopedia of Industrial Chemistry, VCH, Weinheim, 1994, p. 1.
[8] O. Bohnke, G. Frand, M. Rezrazi, C. Rousselot and C. Truche, Solid State Ionics, Vol.66 (1993) 97-104; 105-112.
[9] S.S. Sekhon, Pardeep, S.A. Agnihotry, in: B.V.R. Chowdari, K Lal, S.A. Agnihotry, N.khare , S.S. Sekhon, P.C. Srivastva, S. Chandra (Eds), Solid state ionics: Science & Technology, World Scientific, Singapore, 1998, P. 217.
[10] F. GarcÂõa-Ochoa et al., Biotechnology Advances, 18 (2000) 549-579
[11] Karmann, U.S. Patent (4,299,231) Nov. 10, 1981
[12] S. Chandra, S.S.Sekhon and Narinder Arora, *Ionics,* Vol.6 (2000) pp.112

To study of effect of annealing on etching properties of thermal neutron irradiated CR-39 polymer

Neerja[a], Sameer Kalia[a] and Surinder Singh[c]

[a]*P G Department of Physics, D.A.V. College, Amritsar-143001, Punjab, India*

[b]*Department of Physics, Guru Nanak Dev University, Amritsar-143001, Punjab, India*

Email : neerjakalia@yahoo.co.in

***Abstract*-Here in this work, the polycarbonate CR-39 with average thickness 260μm was irradiated with different neutron fluences from Cirus reactor BARC, Mumbai. For all the samples the isochronal annealing was done in temperature zone 130^0 to 150^0C, each for 45 minutes [1, 2]. The effect of annealing on irradiated samples was studied using etching studies via bulk etch rate V_B, track etch rate V_T, sensitivity S, activation energy for bulk etch rate E_B and activation energy for track etch rate E_T [3,7].**

Keywords: CR-39 polymer, Thermal neutron-irradiation, bulk etch rate, track etch rate, sensitivity, activation energy for bulk etch rate, activation energy for track etch rate, Annealing.

I.INTRODUCTION

Solid State nuclear track detectors (SSNTD) are used in a very broad field of technical applications for the detection of charged particles from protons to heavy ions [8].Besides the simple use of it in the environmental dosimeter, the extraordinary properties of SSNTDs are manifested in reasonable resolution of particle charge and energy makes them very useful for many complicated experiments in particle physics like space research, neutron and plasma physics and biology [9-11]. Out of a large number of solid state nuclear track detectors, polymers have been found to be most sensitive, efficient, easily processable and low weight. The use of different irradiation to modify polymer properties, opened a wide area of research and utilization in various fields like industry agriculture, ecology [12], sensors [13, 14], micro-electronics[15] and nano-technology[16-18]. When a nuclear particle passes through a SSTD, it leaves behind its impression in the form of a damage trail called latent track which gives us very important information about particle and its interactions with the medium for analysis. The tracks are developed at a track etch rate V_T and with increasing etching time, the removal of blank sample layers proceeds with a different bulk etch rates V_B. Along with it, some useful information can also be made if we can remove the impressions of these recorded particles and this process is known as annealing. The annealing mechanism has been mainly studied in minerals and glasses due to its extensive application in fission track dating [19] .The effects of radiations such as gamma-rays, X-rays and heavy ions etc. On track etch rates, optical and structural properties of SSNTD,s have been extensively used [20] whereas a little work has been carried out on neutron induced effects [21-23].A large number of plastic detectors have been extensively used in neutron dosimeters and attempts have been made to improve neutron detection efficiency and their retention properties [24-26].

II.EXPERIMENTAL SETUP

Here, in the present work the main focus is to study the influence of the thermal neutrons on the fission fragment etching properties, optical and structural properties of CR-39 polymeric track recorder with average thickness of 260μm (monomer as shown below and is procured from Pershore Moulding Ltd. U.K.) after isochronal annealing.

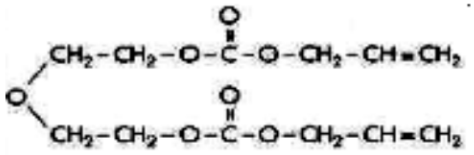

Fig.1Structure of CR-39

The small sample pieces of size 1x1cm^2 were sent to CIRUS Reactor as a Neutron Source at Bhabha Atomic Research Centre, Trombay, Mumbai. Thermal neutron flux up to $6.7x10^{13}$ ncm^{-2} s^{-1} is available in the thermal column of the reactor with very low fast neutron flux [27]. In the present work, the samples of CR-39 detector was irradiated with thermal neutrons in the fluence range upto 10^{17} ncm^{-2} with gamma background in the range of $1.11x10^{-3}$kGy to1.1kGy in the IC-1 self serve position of the reactor. The gamma dose in the thermal column is less than that in the Co^{60} source which is purely for gamma irradiation and gives sufficiently high gamma dose (of the order of Mrad). Then these neutron irradiated samples were annealing at 130° and 150°C each for 45 minutes.

To study the variation of fission track registration in irradiated and pristine samples after annealing, these were exposed to Cf^{252} source in the 2π geometry. After then, these exposed samples of the detectors were etched in 6.25N NaoH at different

etching temperature viz 328, 333, 338 and 343K.The track lengths were measured with an optical microscope at 400x magnification at different etching time. The bulk etching rates were estimated by measuring the thickness for defined time [28] while the track etch rates were calculated from the slope of linear part of curve between the track length and etching time [29]. These calculated values of bulk and track etch rates of the different detectors are reported in tables (I-IV). The sensitivity S ($=V_T/V_B$) was also calculated and the values are mentioned in table (5).

The dependence of V_B on the temperature and concentration of the etchant is given by the relation.

$V_B = \alpha C^n \text{Exp}(-E_B/kT)$;

where α is constant of proportionality, n is slope of plot of $\ln V_B$ Vs lnC, C is the etchant concentration in normals. E_B is the activation energy for bulk etching. Here we take C as a constant, so the above relation becomes

$$V_B = A \text{ Exp}(-E_B/kT)$$

$$\text{or } E_B = -k T \ln V_B \quad (1)$$

This relation is also valid for activation energy of track etching

$$E_T = -kT \ln V_T \quad (2)$$

In the ongoing investigations an attempt has also been made to estimate the effects of dose as well as the effect of annealing temperature both have been studied. The irreparability of the damages caused at high-doses at optimum annealing temperatures has been revealed.

III.RESULTS AND DISCUSSION

Here, to study the etching studies, the thermal neutron irradiated and the pristine samples were exposed to Cf^{252} source in 2π geometry and then annealed at 130 and 150^0 C for 45mintues.After then, these exposed samples of the detectors were etched in 6.25N NaoH at different etching temperature viz 328, 333, 338 and 343K and bulk and track etch rates of the these samples are calculated and reported here in tables I-IV respectively. The sensitivity S ($=V_T/V_B$) was also calculated and the values are mentioned in table V. For annealed samples, bulk etch rate sightly decreases with increase of annealing temperatures. By annealing studies, it is found that the track etch rate, V_T, and the track registration sensitivity ,S, decreases with the healing of latent tracks (tables III- V). Here the activation energy associated with bulk and track etch rates for all the samples (neutron irradiated and pristine) is calculated using the equation (1 and 2). The calculated values (from the graphs fig.1-4) of E_B and E_T are mentioned in table 6. A decreasing trend has been found for irradiated samples. Here this decrease is much more prominent in case of CR-39 polymer. This decrease in E_B and E_T may be due to scission which breaks down the size of the polymer chain and facilitates the movement of the functional groups. The values of bulk and track etch activation energies almost remain constant with annealing temperatures.

Table I The variation of the bulk etch rate V_B with neutron fluence in the gamma background at different temperatures after annealing at 130°C.

Temp. (K) → Neutron fluence (n/cm^2)↓	328	333	338	343
Pristine	0.43± 1.02	.54± 0.03	1.01±0.01	1.45± 0.05
10^{15}	2.09± 0.04	3.89± 0.11	5.0± 0.16	5.89± 0.08
10^{17}	24.05±1.07	29.03±1.02	30.8±0.74	45.79±1.76

Table II The variation of the bulk etch rate V_B with neutron fluence in the gamma background at different temperatures after annealing at 150°C.

Temp. (K) → Neutron fluence (n/cm^2)↓	328	333	338	343
Pristine	0.44± 0.05	0.5± 0.08	0.95± 0.06	1.39± 0.09
10^{15}	1.91± 0.03	3.56± 0.18	4.75± 0.07	5.63± 1.01
10^{17}	21.76±1.58	26.89±0.09	29.06±1.59	43.89±1.74

Table III

The variation of the track etch rate V_T with neutron fluence in the gamma background at different temperatures in case of CR-39 after annealing at 130°C.

Temp. (K) → Neutron fluence (n/cm^2)↓	328	333	338	343
Pristine	5.01± 0.11	7.5± 0.20	12.48±0.31	14.21±0.58
10^{15}	7.39± 0.19	8.67± 0.28	13.48±0.50	18.69±0.63
10^{17}	85.3± 1.69	88.92±2.45	99.57±3.20	102.03±4.45

Table IV

The variation of the track etch rate V_T with neutron fluence in the gamma background at different temperatures in case of CR-39 after annealing at 150°C.

Temp. (K) → Neutron fluence (n/cm^2)↓	328	333	338	343
Pristine	4.89±0.04	7.32± 0.32	12.32±0.67	14± 0.71
10^{15}	7.2± 0.39	8.56± 0.28	13.01±0.52	18.45±0.65
10^{17}	84.7±2.22	88.29±3.29	99.49±4.28	101.89±4.45

Table V

The variation of the sensitivity, S(= V_T /V_B) with neutron fluence in the gamma background at different temperatures after annealing at 130°C and at 150°C.

Temp. (K) → Neutron fluence (n/cm^2)↓	Annealed at 130°C			Annealed at 150°C				
	328	333	338	343	328	333	338	343
Pristine	11.65	13.88	12.35	9.80	11.11	14.64	12.96	10.07
10^{15}	3.53	2.22	2.69	3.17	3.76	2.40	2.73	3.27
10^{17}	3.54	3.06	3.23	2.22	3.89	3.28	3.42	2.32

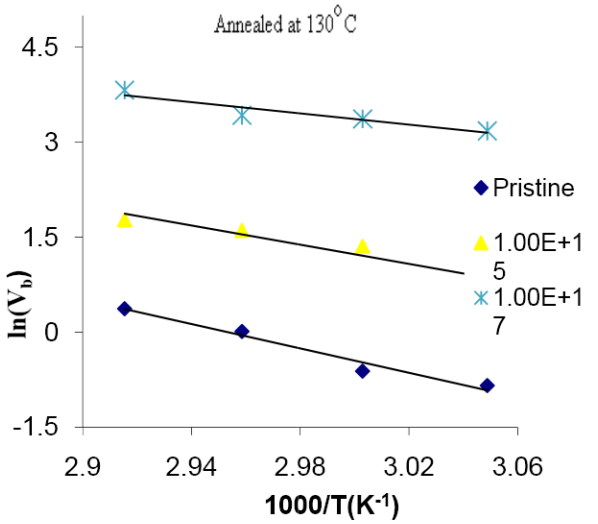

Fig 1 shows the variation of bulk etch rate with etching temperatures at different fluence of neutrons after annealing at 130°C.

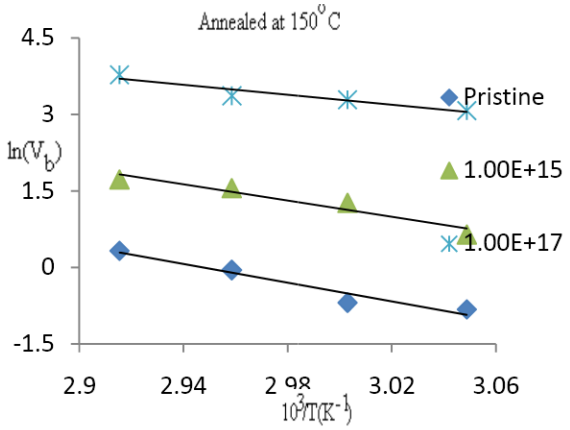

Fig 2 shows the variation of bulk etch rate with etching temperatures at different fluence of neutrons after annealing at 150°C

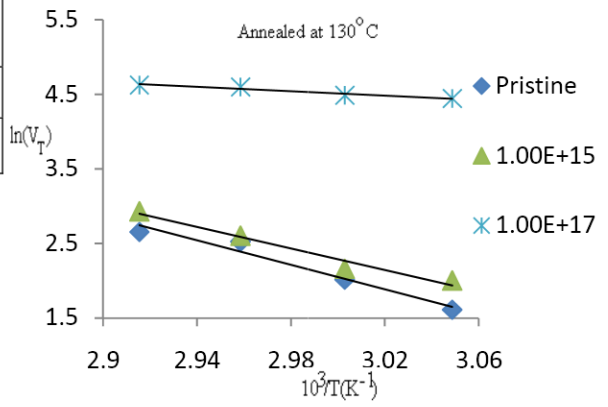

Fig 3 shows the variation of track etch rate with etching temperatures at different fluence of neutrons after annealing at 130°C

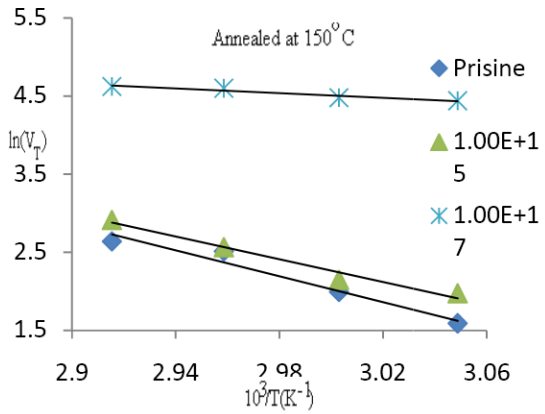

Fig 4 shows the variation of track etch rate with etching temperatures at different fluence of neutrons after annealing at 150°C

Table VI The variation of the bulk etch and track etch

Neutron fluence (n/cm^2)	E_B(eV)		E_T(eV)	
	130°C	150°C	130°C	150°C
Pristine	0.82	0.79	0.70	0.70
10^{15}	0.65	0.68	0.62	0.62
10^{17}	0.38	0.42	0.12	0.12

activation energies with neutron fluence in the gamma background after annealing at 130°C and150°C temperatures .

IV.REFERENCES

[1] A. Rana Mukhtan, I.E. Qureshi, E.U. Khan, S. Manzoor, M.I.Shahzad, H.A.Khan, *Nucl. Instrum. Methods*, **2000**, B170,149-155.

[2] A. Rana Mukhtan, I.E. Qureshi,S. Manzoor ,E.U. Khan, M.I.Shahzad, H.A. Khan, *Nucl Instrum. Methods*, **2001,** B179, 249-254.

[3] S. Singh and S. Prasher ,. *Nucl. Instrum. Methods* **2004**, B215 (1-2), 169-173.

[4] P.C. Kalsi , and C. Agarwal, *Radiat. Effects. Defects S.* **2007**, 162(1), 25-30.

[5] S.A. Nouh , *Radiat. Meas*., **2004,** 38,167.

[6] S.A. Nouh , M.H. Abdel-Salam, A. Morsy Ahmed, *Radiat. Meas*. **2003,** 37, 25- 29.

[7] S.A. Nouh, M.H. Salam, A. Morsy Ahmed, *Radiat. Meas.* **2003**, 30**,** 25-29.

[8] Rad.Meas. 42(2007)1-7.D. Hermsdorf, M. Hunger, S. Starke, F. Weickert.

[9] Dorschel et al..,2003; Nucl. Instrum. Meth.B 207,154-164.

[10] Gaillard et al.,2005 Radiat.Research 163,343-350.

[11] Gaillard et al.,2005 Radiat. Meas. 40,279-282.

[12] S. Karegeorgive et al., Ecol. Sci. 52 1997,15

[13] M. Mateev et al., Radiat.Phys.Chem.48(4),1996,437.

[14] M. Mateev, Radiat.Def. Sol. 129,1994,223.

[15] M. Mateev, Radiat. Phy.Chem. 44(3),1994,329.

[16] C. Daubresse et al., Nucl. Instr. And Meth. B122, 1997,89.

[17] H.S.Viork et al., J.Phys.D:Appl.Phys. 31,1998,3139.

[18] L.P.Biro et al., Vaccum 50(1998)263.

[19] R.K. Bhatia and H. S. Virk. Radiat. Eff. 1989, 107,167-173.

[20] P.C. Kalsi and C. Agarwal. J. Mater. Sci. 2008, 43, 2865-2868.

[21] S. Singh, A, K Sandhu S Prasher, O P Pandey, Radiat. Meas. (in Press)

[22] S A Nouh, T M Hegazy 2006, Radiat. Meas. 41:17.

[23] Morsy Ahmed 2003, Radiat. Meas. 37:25.

[24] Cartwright, B.G., Shirk E.K. and Price, P.B. 1978. *Nucl. Instrum. Methods.* **153**: 457.

[25] Cassou R.M. and Benton, E.V. 1978. *Nucl. Track Detection* **2**:173.

[26] Khan H.A, 1975. *Nucl. Instrum. Meth.* **125**:419.

[27] Srivastva, A. and Ramesh, N., 2006. *Proceeding of DAE-BARNS.* DiscussionMeet on Current Trends and Future Perspectives of Neutron Activation Analysis (16-17Nov.) Pg 121-123.

[28] Enge,W., . Grabisch,K., Dallmeyer,L., Bartholoma K.P. and Beaujean,R. 1975. *Nucl. Instr. Meth.* **127**: 125.

[29] Fleischer, R.L. and Price P. B., Walker, R. M. and Hubbard, E. L.1967. *Phys. Rev.* **156:** 353.

Structural Information from Nucleon Separation Energies

[a]Manpreet Kaur, [a]Husandeep Kaur, [c]Neeru Gupta
[a]M.Sc. Student, [c]Astt Prof , D A V College, Amritsar
e-mail: gneeru2007@yahoo.co.in

Abstract:

In this work nuclei from Z=70 onward are of interest. A strong sudden shape transition between deformation is predicted to occur in the region N>Z nuclei. New shell gaps are predicted using nucleon and two-nucleon separation energies. Nucleon separation energy plays a major role in the prediction of new magicity .Shell closures play very important role in predicting the mgic nuclei. In this work separation energies of one and two neutrons are studied, with and without shell corrections and results are compared.

Keywords: Separation Energy; Stability; Shell Closures; Shape Transition

1. INTRODUCTION

The landscape of nuclear binding energy spanned in the co-ordinate system of proton and neutron is well structured as evident by the measured binding energies. At the magic proton or neutron numbers 2, 8, 20, 28, 50 and 82 the nuclei have an increased binding energy relative to average trend. For neutron, N=126 is also identified as a 'magic number'. Among other special properties, the doubly magic nuclei are spherical and resist deformation.

The stability of the heaviest and super heavy elements has been a long-standing fundamental question in nuclear science. Theoretically, the mere existence of the heavy elements with Z>104 is entirely due to the quantal shell effects.

If the heaviest nuclei were governed by the classical liquid drop model, they would fission immediately from their ground states due to the large electric charge. However in themid 1960s, with the invention of the shell-correction method, it wasrealized that atomic numbers could exist due to the strong shell stabilization [1], [2], [3]. Most of the heaviest elements found recently are believed to be well deformed. Many nucleus structure models have been proposed, including, Liquid drop model, Collective model, Shell model. None of these could completely explain experimental data of nuclear structure. The nuclear radius (R) is considered to be one of basic things that any model must explain for stable nuclei.

2. LIQUID DROP MODEL AND SHELL CORRECTION

Semi empirical mass formula given by Von Weizsacker [4] can be used to predictaccurately the masses of nuclei which ranges from light nuclei to heavy nuclei .In reality this situation is complicated. The inability of the liquid drop model proposed by Bohr and Wheeler [5] to account for the observed asymmetry in the mass yield curve of binary fission was demonstrated by Cohen and Swiatecki [6]. It does not explain the peaks in Binding energy curve at certain key values of N and Z.

There might be local variation of masses due to effects known as shell effects. Introduction of shell correction explains magicity in the binding energy curve.A.E.L.Deperink[7] has shown that if in addition to an improved version of liquid drop mass formula with modified symmetry and coulomb terms, shell effects are modelled, a very simple formula is obtained with a rms deviation from the 2003 database of atomic masses of about 800keV.

3 .METHODOLOGY

Two nucleon separation energies are difference of binding energies. They provide information on the relative stability of the nuclei.G.G.Bunatyan[8] has studied the behaviour of change of slope of two-nucleon separation energies and has shown that the maximum slope, at closed shells is due to Wigner energy.

It is shown by V.Yu. Denisov[9] that position of deep local minima of shell correction associated with magic numbers in the region of super heavy nuclei depend on the parameters of central spin-orbital mean-field potentials.

The separation energies of two protons for Odd Z and Even N nuclei have been calculated using theformula

$$S_{2n} = B(Z,N) - B(Z,N-2) \quad \text{.....1}$$

The Binding energies have been calculated by using semi empirical formula.

$$E_B = a_v A - a_s A^{\frac{2}{3}} - \frac{a_c Z(Z-1)}{A^{\frac{1}{3}}} - \frac{a_A (A-2Z)^2}{A} + \delta(A,Z)$$

.....2

The values of these coefficients are are calculated by "Wapstra"[10] as

$a_v = 14.1MeV \quad a_s = 13MeV a_c = .595MeV \quad a_A = 19MeV$.....3

Due to pairing, a nucleus with an even number of protons is tightly bound than odd number of proton nucleus [11]. As we are taking Odd nucleons, therefore pairing term is taken as zero.

The Binding energies of elements having atomic numbers from 1 to 112 with all their possible isotopes have been calculated. Then we calculate the separation energy of two protons as well as one proton for Odd Z and Even N nuclei. Fig. 1 is a plot of separation energies of two neutrons as a function of Z (S_{2n}).It is observed that this curve is not in agreement with the experimental plot.

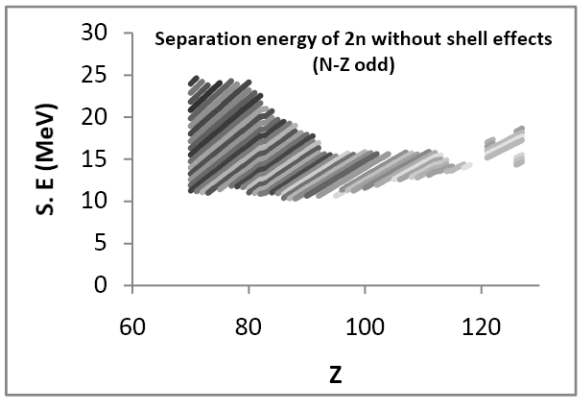

Fig. 1: Plot of theoretical values of separation energies of two neutrons with Z without shell corrections

This problem is resolved by taking in account the shell effects. Seeger gave a formula for calculating binding energies [12]

$\Delta M_0(Z,A) = 7.2887\mathrm{Z} + 8.0713(\mathrm{A}-\mathrm{Z}) - \alpha\mathrm{A} + 0.8076\mathrm{Z}^2\mathrm{A}^{-1/3}\left(1 - 0.7636\mathrm{Z}^{-2/3} - 2.29\mathrm{A}^{-2/3}\right) + \gamma A^{2/3} + \left(\beta - \eta A^{-1/3}\right)A^{-1}[(A-2Z)^2 + 2|A-2Z|] - S_{jk}(N'Z')$.....4

The last term in the above equation is a shell correction term, which is the function of parameter N and Z defined as

$$N' = \frac{N - N_j}{N_{j+1} - N_j}$$

$Z' = \frac{Z - Z_k}{Z_{k+1} - Z_k}$.....5

Here N_j and Z_k are magic numbers

N_j, Z_k=8, 20, 50, 82, 126, 184 and$N_j \leq N < N_{j+1} Z_k \leq Z < Z_{k+1}$

Thus the function $S_{jk}$is different for different intervals between magic numbers. The formula for S_{jk} is

$$S_{jk}(N',Z') = \xi_j sinN'\pi + \xi_k sinZ'\pi + \nu_j sin2N'\pi + \nu_k sin2Z'\pi + \left(\phi_{j+}\phi_k\right)(sinN'\pi)(sinZ'\pi) + \chi$$

.....6

The adjustable constants have been determined by method of least squares. The constants are the same for the full range of masses listed from A =19 to A =260.

α= 17.06 MeV β = 33.61MeVγ= 25.00 MeVη =59.54 MeV

In our calculation we use Von Weisacker'sformula [4] to calculate the binding energy as

$\Delta M(Z,A) = a_v A - a_s A^{2/3} - \frac{a_c Z(Z-1)}{A^{\frac{1}{3}}} - \frac{a_A (A-2Z)^2}{A} - S_{jk}(N',Z')$.....7

Using this formula, separation energies for two neutrons are calculated for all the possible isotopes from Z= 70 to Z=112. Now these separation energies include shell corrections. The experimental values of separation energies of two neutrons are taken from the table compiled by Audi and Wapstra[10] and separation energies of two neutrons are calculated and plotted against Z. From comparison of Fig 2 and Fig 3, we see the change of slope at Z=81 proving the magic character of Z=82.

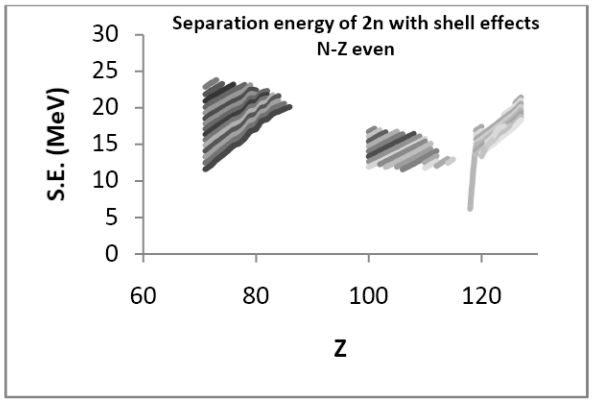

Fig. 2: Plot of theoretical values of separation energies of neutrons with Z with shell corrections

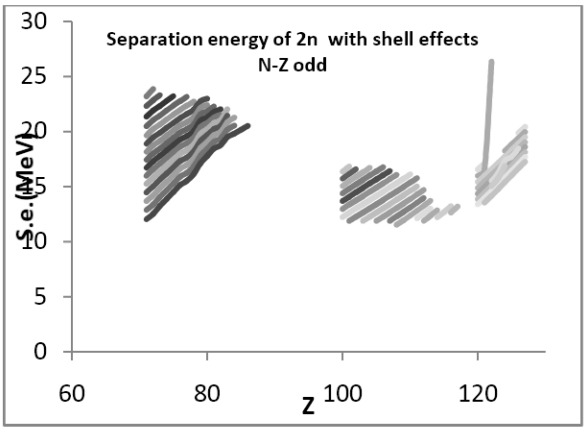

Fig. 3: Plot of theoretical values of separation energies of neutrons with Z with shellcorrections

4. CONCLUSION

Liquid drop model of the nucleus structure explains all the binding energies but cannot explain the existence of magic nuclei. Shell corrections play very important role in nuclear structure. By following this methodology we can guess the next magic nucleus in super heavy elements.

5.ACKNOWLEDGEMEMT

The authors thank the D A V College, Amritsar for the support rendered in doing this theoretical work.

REFERENCES

[1] A.Sobiczewski et al., phys. Let. 22, (1966) 500
[2] U.Mosel and W. Greiner, Z. Phys. 222, (1969) 261
[3] W.D.Myers and W.J.Swiatecki, Nucl. Phys.,81, (1966)
[4] Von Weizscker, "C. F., Z. Physik," 96, 431 (1935)
[5] Bohr, N., Wheeler, J: Phys. Rev. 56, 426, (1939)
[6] Cohen, S., Swiatecki, W.J., Ann. Phys. 19, 67 (1962), 22,406 (1963)
[7] A.E.L.Dieperink, P.VanIsackerEur.Phys.J. A 42, 269 (2009)
[8] G.G.BunatyanYad.Fiz. 29, 38 (1979); Sov.J.Nucl.Phys. 29, 18 (1979)
[9] V.Yu.DenisovPhys.Atomic Nuclei 70, 244 (2007); Yad.Fiz. 70, 267 (2007)
[10] G. Audi, A.H.Wapstra, C.Thibault,J. Blachot and O. Bersillon in Nuclear Physics A729 (2003).
[11] A. Abbas, et al, Mod. Phys. Lett. A16 (2001) 755.
[12] P. A. Seeger, Nucl. Phys. 25, 1 (1961)

Biodiesel Production and Performance and Emission Characteristics of Diesel Engine: A Review

Puneet Verma[a], Gaurav Dwivedi[b]
[a]*B.Tech (ME), KC College of Engineering & IT, Nawanshahr, India*
[b]*Biofuel Research Laboratory, Alternate Hydro Energy Centre, IIT Roorkee, Roorkee, India*

***Abstract*- The increased demand for energy, climate change, and energy security concerns has driven the research interest for the development of alternative fuel from plant origin. Biodiesel derived from plant oils, which include edible and non-edible oil have gained interest for the last two decades as alternative for diesel around the world. Performance and emissions are two distinct factors that decide the use of fuels in engines; a brief discussion is made on the performance and emission characteristics of various bio-diesel sources like Jatropha Oil, Pongamia Oil, Cottonseed oil etc. Biodiesel produced from saturated feedstock reduce NOx emission and resistive to oxidation but exhibit poor atomization. However,many further research needs to be carried out to understand the relationship between the type of biodiesel feedstock and performance and emissions.**

***Keywords*—**Biodiesel, BTE, BSFC, Non-edible oil

I. INTRODUCTION

Biofuels are globally considered sustainable and eco-friendly source of energy to enhance national energy security and decrease dependence on imported fossil fuels. Main user of diesel fuel in India is the agriculture sector next to transport sector. The demand for diesel fuel exceeds its availability resulting in its scarcity and is projected to increase at an annual rate of 5.8% [1]. Biodiesel demand and over-capacity in Europe, US and Asia are driving investment in the global trade of alternative feedstocks. As the demand of these fuels increases, the price of the fuel also keeps on increasing which has become a great setback for the nation's economy. It is becoming increasingly important to develop sustainable solutions to our energy needs. As fossil fuels are depleting at a faster rate and global warming more heavily affects our lives, the urgency of finding a solution to these problems is more obvious. Energy is considered a critical reason for economic growth, social development, and human welfare. Since their exploration, the fossil fuels continued as the major conventional energy source. With the trend of modernization and industrialization, the world energy demand is also growing at a faster rate. To cope up the increasing energy demand, the majority of the developing countries import crude oil. This puts extra burden on their home economy [2]. Biodiesel is an alternative fuel similar to conventional or fossil diesel which can be produced from raw vegetable oil, animal oils/fats, tallow oil and waste cooking oil [3]. Biodiesel has many environmental beneficial properties as it has the potential to be a ''carbon neutral'' fuel. Biodiesel fuels are attracting increasing attention worldwide as a blending component or a direct replacement for diesel fuel in vehicle engines [4]. Biodiesel is often used as a blend rather than pure. Biodiesel blends up to B20 can be used in nearly all diesel engines and are compatible with most storage distribution equipment [5,6]. FAME (Fatty Acid Methyl Ester) biodiesel is the most common biofuel employed in Europe and is mainly produced from types of raw vegetable oils from energy crops, but waste oils can also be used in small percentages as feedstock. FAME from vegetable oils is considered a first generation biofuel as it is exclusively produced from energy crops using the conventional transesterification technology. The basic feedstock for FAME production is vegetable oil from seeds of various crops such as sunflower, rape, soy, jatropha etc, raising economic and social implications due to the associated ''food versus fuel'' debate and problematic glycer- ine disposal. Nevertheless, the growing need for biodiesel and the above considerations directed research focus into alternative technologies that can exploit residual biomass [7].

II. BIODIESEL AS A SOURCE OF FUEL

The name Biodiesel was introduced in the United States during 1992 by the National Soy diesel Development Board (presently national bio diesel board) which has pioneered the commercialization of Biodiesel in the United States. Biodiesel can be used inany mixture with petroleum diesel as it has very similar characteristics but it has lower exhaust emissions. Biodiesel has better properties than that of petroleum diesel such as renewable, biodegradable, non-toxic, and essentially free of sulfur and aromatics. Biodiesel fuel has the

potential to reduce the level of pollutants and the level of potential or probable carcinogens [8]. Various researchers [9] in literature have reported that the following advantages are noted with bio-diesel:

- Bio-diesel is non-toxic and degrades four times faster than diesel.
- Its oxygen content improves the bio-degradation process.
- Pure bio-diesel degrades 85–88% in water.
- Blending of bio-diesel with diesel fuel increases engine efficiency.
- Bio-diesel has a lower vapor pressure and higher flash point than its petroleum counterpart, making it safer to handle and store.
- Oxygen content of bio-diesel improves the combustion process and decreases its oxidation potential.

In contrary, various other authors reported the following disadvantages [9]:

- Higher viscosity.
- Higher copper strip corrosion.
- Slight decrease in fuel economy on energy basics (about 10% for pure bio-diesel).
- Bio-diesel offers unfavorable cold flow properties since it begins to form gel at low temperature which can clog filters or even become so thick that it cannot be pumped from the fuel tank to the engine.
- Density is more than diesel fuel, but may need to use the blends in sub-freezing conditions.
- More prone to oxidation than petroleum diesel and in its advanced stages, this can cause acidity in the fuel and form insoluble gums and sediments that can plug filters.

III. BIODIESEL PREPARATION

The main problems associated with the use of vegetable oils are due to their high viscosity and poor volatility. Some methods to overcome these difficulties are:

- Blending
- Micro-emulsion
- Pyrolysis (Thermal cracking)
- Transesterification

A. Blending

A mixture of 10% vegetable oil is used to run the engine without any modifications. At present, it is not practical to substitute 100% vegetable oil in diesel engines, but a blend of 20% vegetable oil and 80% of diesel fuel can be used. Some short-term experiments are conducted with a 50% blend of Jatropha oil in diesel engine without any major operational difficulties, but further study is required for the long-term durable operation of the engine. Direct use of vegetable oils and the use of higher percentages of blends of oil have generally been considered not satisfactory for either direct or indirect injection diesel engines. High viscosity, acid composition, free fatty acid content, as well as gum formation due to oxidation polymerization during storage and combustion, carbon deposits and lubricating oil thick ening aresome of the problems [10].

B. Micro-emulsions

A micro-emulsion is defined as a colloidal equilibrium dispersion of optically isotropic fluid microstructure with dimensions in the 1–150 nm range, formed spontaneously from two normally immiscible liquids. They can improve spray characteristics by explosive vaporization of the low boiling constituents in the micelles. A brief study shows that the performance of micro- emulsions of aqueous ethanol in soya bean oil was nearly as good as that of diesel, in spite of lower cetane number and energy content [11].

C. Pyrolysis (thermal cracking)

Pyrolysis is the conversion of one substance into another by means of heat in the presence of a catalyst. The pyrolised material can be vegetable oil, animal fats, natural fatty acids or methyl esters of fatty acids. The pyrolysis of fats has been investigated for more than 100 years, especially in those areas of the world where there is lack of deposit of petroleum. Many investigators have studied pyrolysis of triglycerides to obtain products suitable for diesel engines. Thermal decompositions of triglycerides produce alkanes, alkenes, alkadines, aromatics, and carboxylic acids [12].

D. Transestrification

Transesterification (also called alcoholysis) is the reaction of a fat or oil with an alcohol to form esters and glycerol. A catalyst is usually used to improve the reaction rate and yield. Excess alcohol is used to shift the equilibrium toward the product because of reversible nature of reaction. For this purpose primary and secondary monohybrid aliphatic alcohols having 1-8 carbon atoms are used [13].

Singh et al. [14] evaluated the use of magnesium oxide (MgO) impregnated with potassium hydroxide (KOH) as a heterogeneous catalyst for the transesterification of mutton fat with methanol. This process yielded more than 98% of bio-diesel in 20 min. Fig. 1 shows the reaction of transesterification used for preparation of biodiesel.

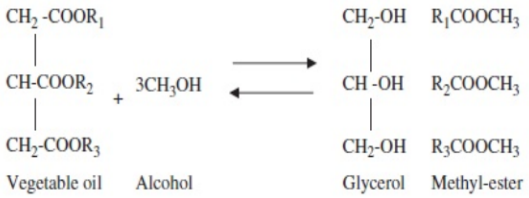

Fig. 1: Transesterification reaction of triglycerides.

IV. ENGINE PERFORMANCE

To use biodiesel as a fuel, the first consideration is its economic aspect. If the crude oil is not widely available, it cannot be used as engine fuel. Engine performance is the next parameter which indicates whether a fuel is economical or not. Brake power, brake specific fuel consumption (BSFC) and brake thermal efficiency are the performance indicators for engines. Not only fuel properties but also fuel injection pressure and timing, air-fuel mixture, amount of injected fuel, fuel spray pattern etc. affect engine performances. Usually engine brake power, brake torque and BSFC are tested against load or speed. Engine performance parameters for different biodiesel and their blends are discussed here. Articles reviewed here reveal that biodiesel generally gives lower power, torque and thermal efficiency at higher fuel consumption than that of pure diesel. Usually calorific value of biodiesel is lower than pure diesel thus use of pure biodiesel or its blends as fuel reduces heat release during combustion and decreases engine performance. However, in some cases, irregular change of power [15,16] and efficiency [16] were observed. It may be because, the engines were not modified for biodiesel used and the amounts of fuel injected at different load conditions were not properly tuned.

A. Jatropha Biodiesel

Bhupendra Singh et al. [17] conducted an experiment on the performance and emission of a diesel engine fueled with Jatropha biodiesel oil and its blends. The results show that biodiesel from Jatropha oil has higher density but lower calorific value than that of diesel, however, the difference is not significantly higher. The kinematic viscosity of biodiesel derived from Jatropha oil is higher than that of diesel. The engine performance with biodiesel of Jatropha and its blends were comparable to the performance with diesel fuel. The oxides of nitrogen from Jatropha biodiesel during the whole range of experiment were higher than diesel fuel. While running the engine with biodiesel and its blends, emissions such as CO, smoke density and HC were reduced as compared to diesel. These reductions of emissions could be due to complete combustion of fuel.
P.K. Sahoo et al. [22] evaluated that the maximum increase in power is observed for 50% jatropha biodiesel and diesel blend at rated speed. Brake specific fuel consumptions for all the biodiesel blends with diesel increases with blends and decreases with speed. There is a reduction in smoke for all the biodiesel blends. Smoke emission reduces with blends and speeds during full throttle performance test.The average fuel economy at rated speed measured with JB20, JB50, JB100 was found to be 181.63, 184.56, 191.28 g/BHP-hr. It is observed that there is an improvement in fuel economy with JB20 when compared with reference fuel. The brake specific energy consumption improvement is observed with JB20. Biodiesel proportion of more than 20% in the blend tends to decrease BSEC. The energy content of the fuel tends to decrease by increasing biodiesel proportion from B20 to B100. This consequently affects the fuel economy.

B. Karanja (Pongamia) Biodiesel

Gaurav Dwivedi [18] did Performance Evaluation of Diesel Engine Using Biodiesel from Pongamia Oil and found that BSFC for B_{10} (580 g/kWh) which is almost equal to the diesel, (601 g/kWh) for B_{20}, (642 g/kWh) for B_{30}, (661 g/kWh) for B_{40}, (669 g/kWh) for B_{50} is respectively 3.2, 10.3, 13.5and 14.9% respectively higher than diesel. The BSFC of B_{10} is same as that of diesel. The reason may be due to high viscosity higher volumetric fuel delivery of fuel per stroke of the engine. The BTE for B_{10} (22.08), B_{20} (22) and B_{30} (21.03) was found about nearly equal to diesel (23.39) respectively. The low efficiency may be due to low volatility, slightly higher viscosity and higher density of the biodiesel of Pongamia oil.

C. Cotton Seed Oil

Nurun Nabi et al. [19] reported that biodiesel mixtures showed less CO, PM, smoke emissions than those of neat diesel fuel. NOx emission with biodiesel mixtures showed higher values when compared with neat diesel fuel. Compared to the neat diesel fuel, 10% biodiesel mixtures reduced PM, smoke emissions by 24% and 14%, respectively. Biodiesel mixtures (30%) reduced CO emissions by 24%, while 10% increase in the NOx emission was experienced with the same blend. Thermal efficiency with biodiesel mixtures was slightly lower than that of neat diesel fuel due to lower heating value of the mixtures.A. Siva Kumar et al. [20] reported thatcompared to the neat diesel fuel, 10% biodiesel mixtures reduced smoke emission by 24% and 14% respectively. Biodiesel mixtures (30%) reduced CO emission by 24%, while10% increase in the NOx emission was experienced with the same blend. The reason for reducing CO emissions and increasing NOx emission with biodiesel mixtures was mainly due to the presence of oxygen in molecularstructure.

D. Rubeer Seed Oil

A.S. Ramadhas et al. [21] prepared biodiesel from rubber seed oil and performance of diesel engine showed that. The maximum brake thermal efficiency obtained is about 28% for B10, which is quite higher than that of diesel (25%). The maximum brake thermal efficiency obtained while using B50, B75 and B100 are, respectively, 25, 25 and 24%. Initially the thermal efficiency of the engine is improved with increasing concentration of the biodiesel in the blend. The possible reason for this is the additional lubricity provided by the biodiesel.Using lower percentage of biodiesel in biodiesel–diesel blends, the brake specific fuel consumption of the engine is lower than that of diesel for all loads. In case of B50 to B100, BSFC is found to be higher than that of diesel. At maximum load condition, BSFC consumption of 100% biodiesel is more than 12% than that of diesel. Table 1 shows results found by various researchers for different biodiesel feedstocks.

Table 1: Effect of biodiesel on Performance and Emission of Diesel Engine

S. No.	Fuel	Results	References
1	Jatropha Biodiesel, Diesel	• BTE of Jatropha biodiesel oil and its blends were found to be lower than diesel fuel. • Brake specific consumption of Jatropha methyl ester and its blends, when used in an unmodified diesel engine was higher than the diesel fuel. • With increase in biodiesel percentage in biodiesel-diesel blends, CO emission decreases. • NO_xemissions increased with the increasing engine load.	[17]
2	Karanja Biodiesel, Diesel	• BSFC is more for biodiesel than diesel • Decrease in BTE for biodiesel. • CO, NO_x and HC emission increase for biodiesel	[23]
3	Rubber seed methyl esters, Diesel	• BSFC increases for biodiesel • CO, NO_x and HC decrease for biodiesel.	[24]
4	Poon Oil Biodiesel, Diesel	• Increase in BSFC • Decrease in BTE • Exhaust Gas Temperature increases. • CO_2 and NO_x emissionsdecrease.	[25]
5	Pongamia Biodiesel, Diesel	• BTE of diesel is higher as compared to biodiesel by (3–5%). • $CO_2$and NOx emission are lower in case of diesel • CO and unburnt hydrocarbon emission are lower in case of Pongamia biodiesel	[26]
6	Neem Oil	• BSFC was slightly higher at all loads for B20 compared with pure diesel. • Higher brake thermal efficiency (BTE) of biodiesel blends than the standard diesel	[27,28]

V. CONCLUSION

The choice of feedstock for biodiesel often depends upon domestic source. Being renewable and sustainable source of fuel, biodiesel will play dominating role in transport sector in the near future. The properties of biodiesel depend on the fatty acid compositions of the parent oil or fat, which are highly influenced by the nature of the feedstock. Most of the researchers have reported that the BTE of bio- diesel operated engine decreased with increase in bio-diesel– diesel blends. One possible explanation for this trendcould be as a result of higher BSFC of bio-diesel due to the presence of fuel-borne oxygen.

REFERENCES

[1] Annoy, 2008. Biodeisel-2020. Global market survey, feedstock trends and forecasts. Multiclient study, 2nd eds. Multi-Client Study, 2nd Edition (2008 release), 685 pages Published by Emerging Markets Online.

[2] Agarwal AK. Bio fuels (alcohols and bio diesel) applications as fuels for internal combustion engines. Progress in Energy and Combustion Science 2007;33:233–71.

[3] Dennis Leung YC, Xuan Wu, Leung MKH. A review on biodiesel production using catalyzed transesterification. Applied Energy 2010;87:1083–95.

[4] Dermibas A. Progress and recent trends in biodiesel fuels. Energy Conversion and Management 2009;50:14–34.
[5] MustafaB.Potentialalternativestoedibleoilsforbiodie selproduction—a review ofcurrentwork.EnergyConversionandManagement 2011;52:1479–92.
[6] Mofijur M, Masjuki HH, Kalam MA, Hazrat MA, Liaquat AM, Shahabuddin M, et al. Prospects of biodiesel from jatropha in Malaysia. Renewable and Sustainable Energy Reviews 2012;16:5007–20.
[7] Stella Bezergianni, Athanasios Dimitriadis, Comparison between different types of renewable diesel, Renewable and Sustainable Energy Reviews 21 (2013) 110–116.
[8] Martini N, Shell JS. Plant oils as fuels—present state of science and future development. Berlin: Spinger; 1998. p. 276.
[9] Subramaniam D, Murugesan A, Avinash A, Kumaravel A, Bio-diesel production and its engine characteristics—An expatiate view, Renewable and Sustainable Energy Reviews 22 (2013) 361–370.
[10] Pramanik K, Propertiesanduseof Jatropha curcas oilanddieselfuelblendsin a compressionignitionengine.RenewableEnergy (2003) 28:239–48.
[11] Srivastava A, Prasad R. Triglycerides-based diesel fuels. Renewable & Sustain- able Energy Reviews 2000;4:111–33.
[12] Ma F, Hanna MA. Biodiesel production: a review. Bioresource Technology 1999;70:1–15.
[13] Sprules FJ, Price D. Production of fatty esters. US Patent 2; 1950, p. 366–494.
[14] Vishal Mutreja Satnam Singh, Amjad Ali. Biodiesel from mutton fat using KOH impregnated MgO as heterogeneous catalysts. Renewable Energy 2011;36:2253–8.
[15] Sahoo PK, Das LM, Babu MKG, Arora P, Singh VP, Kumar NR, et al. Comparative evaluation of performance and emission characteristics of jatropha, karanja and polanga based biodiesel as fuel in a tractor engine. Fuel 2009;88:1698–707.
[16] Karabektas M, Ergen G, Hosoz M. The effects of preheated cottonseed oil methyl ester on the performance and exhaust emissions of a diesel engine. Applied Thermal Engineering 2008;28:2136–43.
[17] Chauhan BS, Kumar N, Cho HM, A study on the performance and emission of a diesel engine fueled with Jatropha biodiesel oil and its blends, Energy 37 (2012) 616e622.
[18] Dwivedi G, Sharma MP, (2013), Performance Evaluation of Diesel Engine Using Biodiesel from Pongamia Oil, International Journal of Renewable Energy Research, Vol.3, No.2
[19] Nabi N,Rahman M, Akhter S, Biodiesel from cotton seed oil and its effect on engine performance and exhaust emissions, Applied Thermal Engineering 29 (2009) 2265–2270
[20] Kumar AS, Maheswar D, Reddy KVK, Comparision of Diesel Engine Performance and Emissions from Neat and Transesterified Cotton Seed Oil, JJMIE, Volume 3, Number 3 (ISSN 1995-6665).
[21] Ramadhas AS, Muraleedharan C, Jayaraj S, Performance and emission evaluation of a diesel engine fueled with methyl esters of rubber seed oil, Renewable Energy 30 (2005) 1789–1800.
[22] Sahoo PK,Das LM, Babu MKG, Arora P, Singh VP, Kumar NR, Varyani TR, Comparative evaluation of performance and emission characteristics of jatropha, karanja and polanga based biodiesel as fuel in a tractor engine, Fuel 88 (2009) 1698–1707.
[23] Srivastava PK, Verma M. Methyl ester of karanja oil as an alternative renewable source energy. Fuel 2008;87:1673–7.
[24] Lin L, Ying D, Chaitep S, Vittayapadung S. Biodiesel production from crude rice bran oil and properties as fuel. Applied Energy 2009;86:681–8.
[25] Devan PK, Mahalakshmi NV. Performance, emission and combustion char- acteristics of poon oil and its diesel blends in a DI diesel engine. Fuel 2009;88(5):861–7.
[26] Chauhan BS,KumarN,ChoHM, Astudyonthe performance and emission of a diesel engine fueled with Pongamia biodiesel and its blends, Energy 2013;56:1–7.
[27] Sharma D,SoniSL,MathurJ, Emissionre ductionina direct injection diesel engine fueled by neem-diesel blend, EnergySourcePartA2009;31:500–8.
[28] Dhar A, Kevin R, Agarwal AK. Production of biodiesel from high-FFA neem oil and its performance, emission and combustion characterization in a single cylinder DI CI engine.Fuel Processing Technology 2012, 97:118–29.

Spin speed dependence of optical band gap of sol gel spin coated zinc oxide thin films

Rajesh Kumar, Aakanksha sahu, Narinder Arora, Rabia Sareen & Gagandeep Kaur
P.G. Department of Physics, D. A. V College, Amritsar, India
e-mail: dk_rk@rediffmail.com

Abstract: **The zinc oxide (ZnO) thin films have been obtained by sol gel spin coating technique on to the glass substrates kept at 400^{O}C. The conditions have been optimized to obtain quality films. Optical absorption studies to find optical band gap of the films have been made through UV-Visible spectroscopy in the spectral range 200 -1100 nm. Effect of spin speed on the optical band gap of these films has been studied. Results show that optical band gap of the films gets modify on increasing the spin speed of films.**

Keywords: Spray pyrolysis, Zinc oxide, optical band gap.

I INTRODUCTION

ZnO is a wide band gap semiconductor with interesting electro optical properties because of large exciton binding energy and its high thermal as well as chemical stability at room temperature. ZnO thin film has been extensively used as transparent conductive film and the solar cell window material because of the its high optical transmittance in the visible region. With such a technological important properties ZnO has wide range of applications as sensors [1, 2], heat mirrors [3], transparent electrodes [4], solar cells [5-7] and piezoelectric devices [8].These films can be deposited by several techniques including, sputtering [9], metal organic chemical vapour deposition [10], sol gel [11] and spray pyrolysis [12]. A sol-gel method has advantages over other techniques due to low cost instrumentation involved for obtaining films, the easy control over chemical components and thickness of the film along with the simple route for film deposition. Optical absorption coefficient, optical band gap and refractive index of semiconductors are important parameters for the design, fabrication and analysis of various optical and optoelectronic devices. The optical transmittance through the samples can be used to obtain direct and indirect optical band gap along with other optical constants. In the present work, low cost sol-gel spin coating technique has been exploited to obtain ZnO thin films onto the glass substrate. The effect of spin speed on optical band gap of the films so obtained has been discussed.

II EXPERIMENTAL DETAILS

Chemically and thermally stable films of zinc oxide were prepared using the spin coating method. Microscope glass slides were used as the substrates for thin films. Prior to deposition, the glass slides were sequentially cleaned in an ultrasonic bath with acetone and ethanol. Finally they were rinsed with distilled water and dried. 0.1M solution of zinc acetate dehydrate ($Zn(CH_3COO)_2.2H_2O$) in ethanol was taken as precursor solution for all the films. The solution was continuously stirred for an hour with the help of magnetic stirrer in an air tight container. The resulting solution was allowed to get settled for 24 hours. The solution so obtained was stirring at room temperature for half hour in an air tight container. 40μl of this spreading solution was dispensed on to the substrate from a distance of 5mm above the substrate and spinner (Apex system model NXG M1) was employed to spin the substrate at different speeds ranging from 2000 to 5000 rpm with spin time 15 sec. for each film. The amorphous gel films were left to dry in air at 100^{0}C for ten minutes. The films were then cooled down to room temperature in open air. This process was repeated four times/cycles for each film. The films were further kept at 400^{O}C for half an hour in open air. The UV-visible-IR optical transmission spectra of ZnO thin films were recorded by using Shimadzu UV-VIS-2450 scanning spectrophotometer in the range of 300-1100 nm. The measurements were taken at a normal incidence using a reference blank glass substrate. From the transmittance and absorbance spectra were used to calculate the absorption coefficient and optical band gap of the films. The thickness of the thin films were estimated using max-min method, using the formula: $t = \lambda_1 \lambda_2/4n (\lambda_2 - \lambda_1)$, where 't' is the thickness of the film, λ_1 and λ_2 are the wavelengths which corresponds to the maxima and minima of the transmittance spectra and 'n' is the refractive index to ZnO. Thickness of the films was also confirmed using microbalance method and has been shown in table 1.

III RESULTS AND DISCUSSION

The most direct and perhaps the simplest method for probing the band structure of semiconductors is to measure the absorption spectrum. The absorption and percentage transmission spectra of ZnO thin films deposited at different temperature is shown in Figs. 1 and 2 respectively.

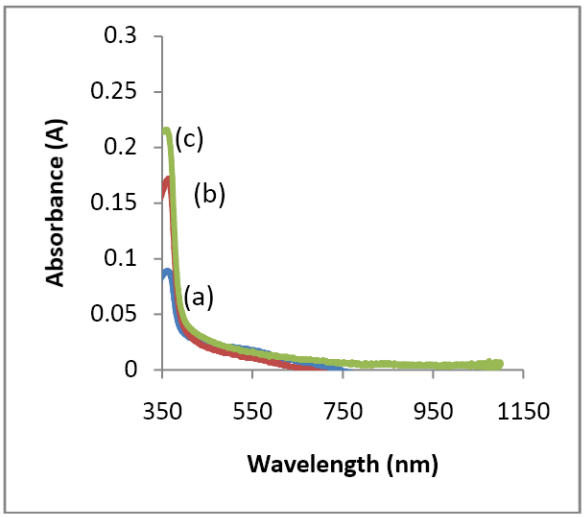

Fig. 1: Optical absorbance spectra of ZnO films deposited at spin speed (a) 2000 rpm (b) 3000 rpm (c) 4000 rpm

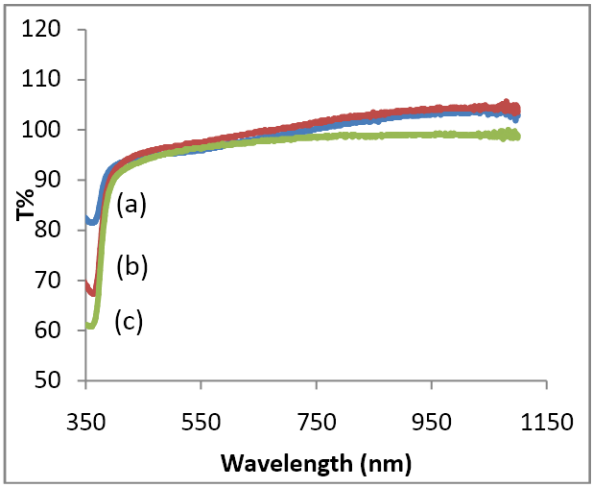

Fig. 2: Optical transmittance spectra of ZnO films deposited at spin speed (a) 2000 rpm (b)3000 rpm (c) 4000 rpm.

In order to determine the optical band gap of the films, the absorbance spectra of the films were recorded at room temperature. The absorption coefficient (α) was calculated from the absorbance spectrums using the formula: $\alpha = 2.3026\ (A/d)$, where d is the film thickness and A is the optical absorbance. The absorption edge of the ZnO has been examined in terms of a direct transition using the equation of Bardeen et al [13], stating that: $\alpha h\nu = B(h\nu - E_g)^n$, where α is the absorption coefficient, hν is the photon energy, E_g is the optical band gap, B is a constant which does not depend on photon energy and n is respectively 1/2 and 2 for direct and indirect transitions. The direct and indirect band gap was determined by plotting $(\alpha h\nu)^2$ vs. hν and $(\alpha h\nu)^{1/2}$ vs. hν curves and have been shown in figs. 3 and 4 respectively.

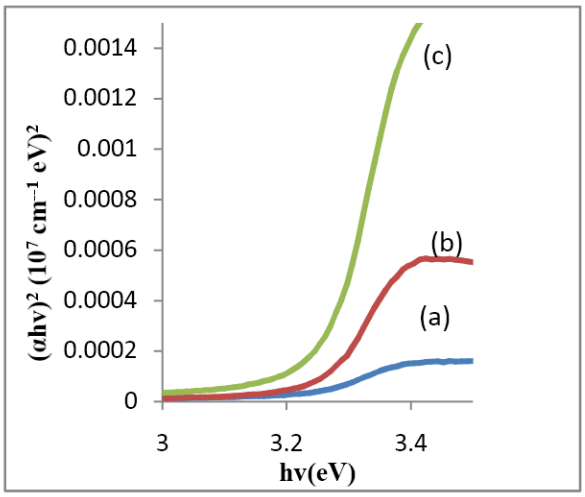

Fig. 3: Variation of $(\alpha h\nu)^2$ as a function of photon energy hν of ZnO films deposited at spin speed (a) 2000 rpm (b) 3000 rpm (c) 4000 rpm.

The intercepts (extrapolations) of these plots (straight lines) on the energy axis give the optical energy band gaps. It has been observed that both direct and indirect optical band gap increases from 3.22 eV to 3.27 eV and from 2.98 eV to 3.08 eV respectively with the increase in spin speed. This increase in band gap energy may be attributed to the improvement of crystallinity of the films with the increase in spin speed and due to the fact that homogeneity of the films increases with increase in the spin speed of films hence more ordered films causing comparatively less contribution to the absorption is obtained at higher spin speeds. Results are in good agreement with the findings of Halin et al [14] and Capan et al [15]. The direct and indirect band gap energy of zinc oxide films obtained on glass substrate at different spinning rates have been listed in table 1.

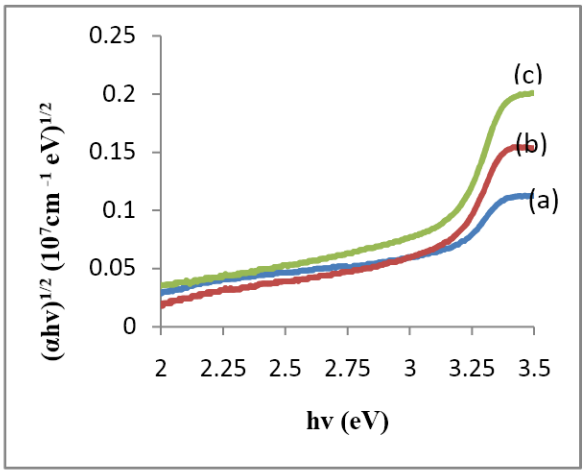

Fig. 4: Variation of $(\alpha h\nu)^{1/2}$ as a function of photon energy hν of ZnO films deposited at spin speed (a) 2000 rpm (b)3000 rpm (c) 4000 rpm.

TABLE 1

Band gap energy of spray deposited zinc oxide films on glass substrate kept at different spin speeds.

Spin Speed (rpm)	Thickness (nm)	Direct Band Gap (eV)	Indirect Band Gap (eV)
2000	60	3.22	2.98
3000	57	3.26	3.05
4000	43	3.27	3.08

IV CONCLUSION

The spin coated zinc oxide films at different spin rates have been obtained on glass substrates. The optical absorbance and transmittance spectra of the films so obtained has been recorded in the wavelength range of 200-1100 nm. It has been observed that both the allowed direct and indirect optical band gap of the films increases with the increase in spinning rate.

ACKNOWLEDGMENT

The author would like to pay thanks to Dr. K.N.Kaul, Principal, DAV College, Amritsar for providing the necessary infrastructure at my work place.

REFERENCES

[1] P. Mitra, A. P. Chatterjee, H.S. Maiti, Mater. Lett. 35,33 (1998).
[2] C. H. Kwon, H. K. Hong, D. H. Yun, K. Lee, S. T. Kim, Y. H. Roh, B. H. Lee, Sens. Actuators B 25,610 (1995).
[3] K. L. Chopra, S. Major, D. K. Pandya, Thin Solid Films 102, 1 (1983).
[4] S. Major, A. Banerjee, K. L. Chopra, Thin Solid Films 143, 19 (1986).
[5] J. B. Yoo, A. L. Fahrenbruch, R. H. Bube, J. Appl.Phys. 68, 4694 (1990).
[6] D. Dimova-Malinovska, J. Lumin. 80, 207 (1999).
[7] Z.-C. Jin, I. Hamberg, C. G. Granqvist, B. E.Sernelius,K.-F. Berggren, Thin Solid Films 164, 381(1988).
[8] J. G. E. Gardeniers, Z. M. Rittersma, G. J. Burger, J.Appl. Phys. 83, 7844 (1998).
[9] Soon-Jin So, Choon-Bae Park Journal of Crystal Growth 285, 606 (2005).
[10] S. T. Tan, B. J. Chen, X. W. Sun, X. Hu, X. H.Zhang, S. J. Chua, Journal of Crystal Growth 281,571 (2005).
[11] Young-Sung Kim, Weon-Pil Tai, Su-Jeong Shu, Thin Solid Films 491, 153 (2005).
[12] R. Martins, R. Igreja, I. Ferreira, A. Marques, A.Pimentel, A. Gonçalves, E. Fortunato, Materials Science and Engineering B 118, 135 (2005).
[13] J.Bardeen, F.J.Blatt and L.H.Hall, Photoconductivity Conf., Ed. R.Breckenridge, B.Russel and T.Hahn, John-Weiley, New York (1956).
[14] D.S.C Halin, I.A.Talib, A.R.Daud and M.A.A.Hamid, Solid state science and technology,Vol. 17, No. 1 (2009),119-125
[15] R Capan, N.B.Chaure, A K Hassan and A K Ray, Semicod. Sci. Tech.19 (2004), 198-202.

PERFORMANE ANALYSIS ON ROUTING PROTOCOLS IN MOBILE AD HOC NETWORKS

Er. Kavneet Kaur, Dr. Tanu Preet Singh
M.Tech Research Scholar
Department of Computer Science & Engineering
Amritsar College of Engineering & Technology, Amritsar
Kavneet_003@yahoo.com

Professor & HOD
Department of Electronics & Communication Engineering
Amritsar College of Engineering & Technology, Amritsar
tanupreet.singh@gmail.com

***Abstract*-Mobile ad-hoc network (MANETs) is a network without fixed infrastructure. In MANETs path routing and protocol selection are the strategies to design a wireless network. MANET should selected the protocol which has the high capability of data delivery and used in large network, So performance analysis on routing protocols is carried out i.e. AODV,DSR,TORA,OLSR and DSDV using OPNET simulator. The delay, throughput and load are the three parameters used for the comparison of the performance of above protocols.**

***Index terms*- performance analysis, MANETs, routing protocols, AODV, TORA, DSR, OLSR and DSDV.**

1. INTRODUCTION

The mobile ad-hoc networks (MANETs) contain the ad-hoc network which consists of wireless network without any fixed infrastructure. It provides the facility to get access to the network for the communication or exchanging information from anywhere. It has the facility of changing the network structure dynamically due to the move ability of nodes. In this nodes behave or act as a host or routes for the transmission of data from one node to another node in the network. In MANETs the security of information during transmission has guaranteed. In MANETs to transfer information from source to destination i.e. to get the efficient routing. The routing protocols take some parameters.

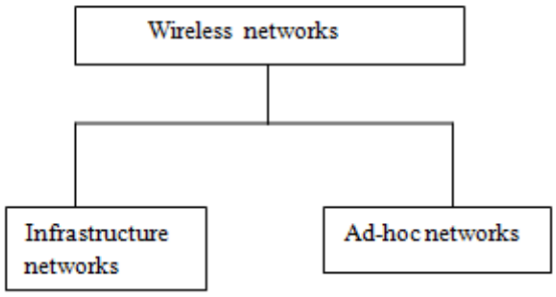

Figure1: Wireless Networks Categories

The routing protocols that used are AODV, DSR, OLSR, TORA and DSDV for finding the routing paths and efficient data delivery and data integrity. Through these protocols, it can find the best performance metrics, so the output of these performance metrics decide which routing protocols is the best to transfer large information from one source to another source. There are some operations i.e. performance analysis of protocol to judge their delay, throughput, and packet delivery ratio. To calculate their performance using simulation software.

2. MANET ROUTING PROTOCOLS

There are some important features of these protocols that can be studied in simulations and we have some parameters to implement these protocols. There are some differences in routing protocols i.e. lies on protocols. The routing strategy based on two classifications i.e. reactive and proactive. So through this the protocols find the way to launch the terms like scalability, mobility support and energy consumption.

A. Reactive Routing Protocols

It represents the determination of routes, only and only when there is availability of packets to send. So this reactive routing protocol describes about the AODV, DSR, TORA protocol in detail .The routing protocol is used for large networks.

B. Proactive Routing protocols

Proactive routing protocols are basically used to maintain routes to all the destinations of all the time. It cannot be used for large networks. There is slow reaction where any link breakage or failures. the facility of this routing is quickly obtain routing information and establish routes. It describes about the OLSR and DSDV.

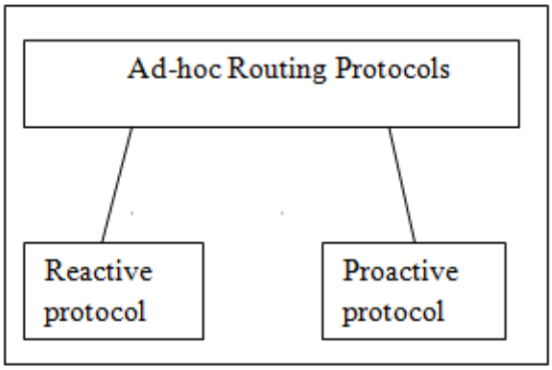

Figure2: Classification of Routing Protocols

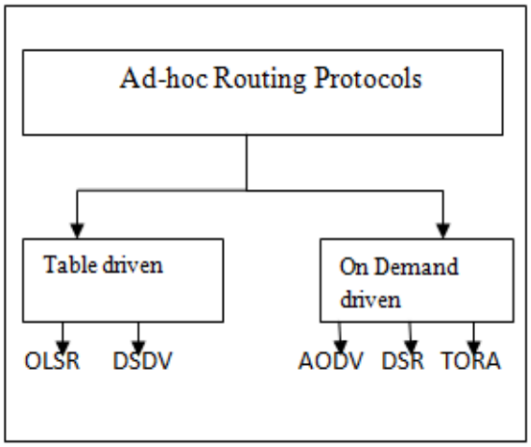

Figure3: Represents Family Tree

3. Ad-hoc On-Demand Distance Vector Routing Protocol (AODV)

AODV is a combination of on-demand and distance vector i.e. hop-to-hop methodology. This protocol performs routing discovery when a node needs to know the route from source to destination, it creates a ROUTE REQUEST and ROUTE REPLY, it creates when the request reaches a node with route to destination. And there is a ROUTE ERROR which is sent to the effected source nodes. When a source node receives, it again creates a route discovery, if route is needed.

4. Dynamic Source Routing (DSR)

It is a reactive routing protocol.DSR is also known as on demand routing protocol, It is very simple and efficient protocol designed for the use in multichip wireless ad-hoc networks. It has two mechanisms i.e. [3]

1. Route Discovery
2. Route Maintenance

In route discovery we use ROUTE REQUEST and ROUTE REPLY for sending data packets. The data packet that we sent it carries in its header to know that from which source the packet is sent or at which destination.

5. Temporally Ordered Routing Algorithm (TORA)

TORA is reactive routing protocol. It is a distributed algorithm, adaptive and efficient protocol. It is basically known for their three main functions that are creating routes, mentioning routes and erasing routes. It creates the route when we required not at all time the route establishment is achieved through the directed acyclic graph. Characteristics of TORA:-

1. Distributed execution
2. Loop-free routing
3. Multipath routing

6. Destination Sequenced Distance Vector (DSDV)

DSDV is a proactive routing protocol(table driven routing protocol).It is based on hop-by-hop distance vector .In this routing protocol, each node in the routing table, in which all destinations and number of hops that used them in network. It also generates the sequence number for the route generated by nodes.

7. Optimized link State Routing (OLSR)

OLSR also comes under the proactive routing protocol. It provides the link state routing for mobile ad-hoc networks. It also maintains the routing table by the link state called MPR (multipoint relays) for forwarding control traffic. It helps in exchanging of messages. It creates two types of packet: [1]

1. Hello packets
2. TC packets (topology control) through its MPR.

8. SIMULATION and ANALYSIS [1]

In this study, the simulation software is Optimized Network Evaluation Tool (OPNET), which is to simulate and analyze for network communication and distributed system. It provides three-tier model, where the top layer is the network layer that reflects the topology of the network, the middle layer is the node layer that is composed of the corresponding protocol modules and the bottom layer is the process model that is described by finite state machines.

Aim is to analyze the performance of the routing protocols of AODV, DSR, TORA, DSDV and OLSR which takes the parameters of throughput (bits per second), delay (sec).The analyzing of routing protocols is done by the simulation tool OPNET. The communication over the wireless nodes with the transmission range of 1500 with transmission power of 0.05w. The traffic generator starting time has set to 10(sec), pause time (0) size and the duration period constant 10(sec). The random mobility model was used. The simulation was 300 seconds in length.

These routing protocols can be configured on:

1. MANET routing protocols
2. Routers

Performance indexes:

1. Throughput
2. Delay
3. Load

In the OPNET simulator first create a design of the network and by applying individuals statistics to each node the performance is viewed by view result.Figure3 shows the workflow of OPNET simulator.

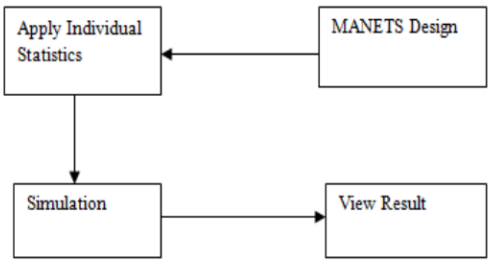

Figure 3: Simulation Flow

Routing protocols	AODV,DSR,TORA,OLSR,DSDV
Number of wireless nodes	5,10,15,20
Simulator	OPNET
Transmit power	0.05(watt)
Data rate	11Mbps
Simulation seconds	300(sec)

· **Table1**: Simulation Parameters.

8.1 PARAMETER ANALYSIS [2]

There are some performance evaluations with respect to the parameters of the routing protocol. The parameters are delayed, load, throughput.

DELAY: It is time taken for an entire message to completely arrive at the destination from the source. It includes the components i.e. propagation time (PT), transmission time (TT),

Queuing time (QT) and processing delay (PD).

It is evaluated as:

Delay=PT+TT+QT+PD

THROUGH PUT: It is a measure of how fast a node can actually sent the data through a network. Through put is the average rate of the control information sent to the data actual received at each node.

$$\text{Throughput (bits/sec)} = \frac{\text{no of delivered packets*packet size*8}}{\text{Total simulation period}}$$

LOAD: It represents with respect to bits/sec, which is put forward to wireless LAN layers.

Routing protocols	Delayed	Network load	Throughput
AODV	Excellent	Very good	Average
DSR	Worst	Good	Very good
TORA	Very good	Excellent	Average
OLSR	Average	Average	Good
DSDV	Good	Average	Excellent

Table2: Comparison of routing protocols depending upon number of nodes.

9. CONCLUSION

In this study, an effort has been made to concentrate on the comparative performance analysis of routing protocols are reactive (AODV, TORA, DSR) and proactive (OLSR, DSDV) routing protocols on the basis of above mentioned performance metrics using OPNET simulator. While comparing five routing protocols, in OLSR load and delay is low while the number of nodes is less, so OLSR can use in small network areas. While DSDV because of its proactive nature it provides delay is low. The average load and delay is high for DSR and throughput is also high in DSR when the number of nodes increases and hence it can be used for large networks but not suitable for wireless transmission. TORA and AODV both have less, load while increasing number of nodes. So TORA and AODV have the capability of higher packet delivery than DSR.

REFERENCES

[1] Uma Mani, Ramasamy Chandrasekhar and v.R.Sarma Dhulipala,"Study and analysis of routing protocols in mobile ad-hoc network", science publications,9(11),2013,1519-1525.

[2]S.Mohapatra,P.Kanungo,a*,"Performance analysis of AODV,DSR,OLSR AND DSDV routing protocols using NS2 simulator", International Conference on communication Technology and System Design 2011/Proscenia Engineering,30,2012,69-76.

[3]GinniTonk, InduKashyap,S.S.Tyagi,"Performance comparison of ad-hoc network routing protocols using NS-2",International Journal Of Innovative Technology Engineering,1,june2012,53-57.

[4] Parma Nanda, S.C. Sharmab,a*."Probability Based Improved Broadcasting for AODV Routing Protocol", International Conference on Advances Science and Contemporary Engineering, 2012,pp. 222 – 23

[5] Peter P. Pham and Sylvie Perreau," Performance Analysis of Reactive Shortest Path and Multi-path Routing Mechanism With Load Balance", Conference, 2003

[6] Samyak Shah1, Amit Khandre2, Mahesh Shirole3 and Girish Bhole4 ," Performance Evaluation of Ad Hoc Routing Protocols Using NS2 Simulation",2008,pp.168-171

[7] Dr. Aditya Goel & Ajaii Sharma," Performance Analysis of Mobile Ad-hoc Network Using AODV Protocol" , International Journal of Computer Science and Security, Volume (3), pp.334-343

[8] Manu Srivastava,Parul Yadav, "A Performance Analysis Of Routing Protocols In Mobile Ad-Hoc Networks ",International Journal of Engineering Research & Technology, Vol. 1,2012,1-10

[9] Kaliyaperumal Karthikeyan1 Sreedhar Appalabatla2 Mungamuru Nirmala3 Teklay Tesfazghi4 ," Comparative Analysis of Non-Uniform Unicast Routing Protocols for Mobile Adhoc Networks", International Journal of Advanced Research in Computer Science and Software Engineering , Volume 2, 2012,pp.227-232

[10] Dr.S.S.Dhenakaran1, 1 Assistant Professor, Department of Computer Science and Engineering, Alagappa University, A.Parvathavarthini2, "An Overview of Routing Protocols in Mobile Ad-Hoc Network", International Journal of Advanced Research in Computer Science and Software Engineering, Volume 3, 2013, pp.251-259

A Study of Orthopedic Implant Materials

Mohd Shahid Khan[a], Ghulam Anwer[a], Mohd Shuaib[a], Mohd Imran Khan[a]
[a]*Department of mechanical Engineering, JamiaMilliaIslamia*

***ABSTRACT*—As there are many research going on in the field of surgical implanting materials. One of the major factors that affect the materials is chemical reaction and environmental conditions inside the body during the internal fixation in surgical implantation. This paper is based on comparing materials(like stainless steel, cast cobalt, and titanium) under the internal conditionsof body in order to describe the susceptibility and corrosion of these materials. The work is done by considering different paper published in this field. Based on these results it can be analyses which material is best suitable under the given circumstances.**

***KEYWORDS*:** Bio-material, Corrosion, Implantation Surgical materials.

INTRODUCTION

Human body is a very complex system consisting of many organs. These organs are enclosed by an structure of bones, which protects organs along with it stores blood cells and other essential nutrients. The study of entire structure of bones is well-known as skeletal system. During a birth of a child there are 306 bones which get fuse into one another and become single one as growth occur. In an adult 206 bones is identified. All the bones consists of a living cells, if somehow, any bones get fractured or broken then it is capable of repairing itself by multiplication of its cells through the process of mitosis and meiosis.Ligaments and tendons are like rubber bands that hold the musculoskeletal system together. Ligaments are used to join one bone to another and having 50-60% of water along with 70-80% of collagen and 10-15% of elastin while Tendons are used to join the muscles with the bones and having 75-85% of collagen and 5% of elastin [1].

At the time of joint fracture when bones are incapable of repairing itself, certain materials known as biomaterials are used to replace that segment of bone. As early as the first material implants, surgeon identified some of the problem regarding material and designthat resulted in premature loss of implant function, as evidenced by mechanical failure, corrosion, and poor biocompatibility. Design, material selection, and biocompatibility remain the three critical issues in today's biomedical implants and devices.

The main problems with these materials are as

- Either the body accepts these types of materials or not
- Corrosion and stability of the metals
- Infections on other parts of tissues and bones
- Chemical reaction that take place inside a body

Orthopedic biomaterials are generally limited to those materials that withstand cyclic loadbearing applications. While metals, polymers, and ceramics are used in orthopedics, it remains metals, which have over the years uniquely provided appropriate material properties such as high strength, ductility, fracture toughness, hardness, corrosion resistance, formability, and biocompatibility necessary for most loadbearing roles required in fracture fixation and total joint arthroplasty (TJA). The environment to which biomaterials are exposed during prolonged use (i.e., the internal milieu of the body) can bedescribed as an aqueous medium containing various anions, cations, organic substances, and dissolved oxygen. The anions are mainly chloride, phosphate, and bicarbonate ions. The principal cations are Na+, K+, Ca2+, and Mg2+, withsmaller amounts of many others, also protein content of the environment is known to have a significant influence on the corrosive nature of body fluids [2],[3]. The pH in this well-buffered system is around7.4, although because of inflammation it may change for shortperiods following surgery to as low as 4 or 5 [4],while temperature remains constant around 37◦C.

Material selection should be strong and stable under these type of variable body environment also one of the major factor effect the material is corrosion.Since corrosion is a surface phenomenon, however, itmay be possible to optimize corrosion resistance byattention to or treatment of the surface rather than bymanipulation of the bulk chemistry[5].This offers the possibility of developing sufficientcorrosion resistance in materials of excellent bulkmechanical and physical properties. Thus, noble metalssuch as gold and platinum are rarely used for structuralapplications (apart from dental restoration) because oftheir inferior mechanical properties, even though theyhave excellent corrosion resistance; instead, base metalalloys with passivated or protected surfaces offer betterall-around properties.

The metal can be corroded either by

In body environment which contain a number of cations and anions, electrons will flow from that metal withthe greater potential in an attempt to make the two electrodes equipotential. This upsets the equilibrium and causes continuedand accelerated corrosion of the more active metal (anodicdissolution) and protects the less active (cathodic protection).Galvanic corrosion may be seen whenever two different metals are placed in contact in an electrolyte. It has beenfrequently observed with complex, multi component surgicall implants such as modular total joint designs consisting

of titanium alloy femoral stems and cobalt alloy femoral heads[6].

It is not necessary for the components to be macroscopic, monolithic electrodes for this to happen ,and the same effect can be seen when there are different microstructural features within one alloy, such as the multiphase microstructure evident in implants of sensitized stainless steel where the grain boundaries become depleted in chromium and corrode preferentially to the remaining surface [7].

In practice, it is the regional variations in electrode potential over an alloy surface that are responsible for much of the generalized surface corrosion that takes place in metallic components. Many of the commonly used surgical alloys contain highly reactive metals (i.e., with high negative electrode potentials),such as titanium, aluminum, and chromium. Because of this high reactivity, they will react with oxygen upon initial exposure to the atmosphere. This initial oxidation leaves an impervious oxide layer firmly adherent to the metal surface; thus all other forms of corrosion may be significantly reduced because the oxide layer acts as a protective barrier, passivating the metal. The manufacturing process for implant alloys may include a passivating step to enhance the oxide layer prior to implantation, for example nitric acid treatment of 316L stainless steel [8].

2. The stability of the oxide layer depends on the electrode potential and the pH of the solution. Proteins and cells can be electrically active and interact with the charges formed at the interface and thus affect the electrode potential [4]. Bacteria and inflammatory cells can alter the pH of the local environment through the generation of acidic metabolic products that can shift the equilibrium.

3. The stability of the oxide layer is also dependent on the availability of oxygen. The adsorption of proteins and cells onto the surface of materials could limit the diffusion of oxygen to certain regions of the surface.This could cause preferential corrosion of the oxygen-deficient regions and lead to the breakdown of the passive layer. Alternatively the biomolecule adsorption layer could act as a capacitor preventing the diffusion of molecules from the surface [9].

The need to ensure minimal corrosion has been the major determining factor in the selection of metals and alloys for use in the body. Two broad approaches have been adopted. The first has involved the use of noble metals, that is, those metals and their alloys for which the electrochemical series indicates excellent corrosion resistance. Examples are gold, silver, and the platinum group of metals. Because of cost and relatively poor mechanical properties, these are not used for major structural applications, although it should be noted that gold and its alloys are extensively used in dentistry; silver is sometimes used for its antibacterial activity; and platinum-group metals(Pt, Pd, Ir, Rh) are used in electrodes.

The second approach involves the use of the passivated metals. Of the three elements that are strongly passivated (i.e.,aluminum, chromium, and titanium), aluminum cannot beused on its own for biomedical purposes because of toxicity problems; however, it has an important role in several Ti alloys.

Chromium is very effectively protected but cannot be used inbulk. It is, however, widely used in alloys, especially in stainless steels and in the cobalt–chromium-based alloys, where it is normally considered that a level of above 12% gives good corrosion resistance and about 18% provides excellent resistance. Titanium is the best in this respect and is used as a pure meta lor as the major constituent of alloys [10]. In alloys the passivating layer promoting the corrosion resistance is predominantly composed of one of these metal oxides. For example, chromium oxide passivates 316L stainless steel andCo–Cr-based alloys and Ti oxide in Ti alloys. The other alloying elements may be present in the surface oxide and this can influence the passivity of the layer [11].

Carefu lpretreatment of the alloys can be used to control the passivityof these alloys [5],[12]. In particular, production procedures need to be controlled because of their influence on the surface oxides, for example, the cleaning[13] and sterilization [14]procedures. Although these metals and alloys have been selected for their corrosion resistance, corrosion will still take place when they are implanted in the body. Two important points have to be remembered. First, whether noble or passivated, all metals will suffer a slow removal of ions from the surface, largely because of local and temporal variations in microstructure and environment. This need not necessarily be continuous and the rate may either increase or decrease with time, but metal ions will be released into that environment. This is particularly important with biomaterials, since it is the effect of these potentially toxic or irritant ions that is the most important consequence of their use. Even with a strongly passivated metal, there will be a finite rate of diffusion of ions through the oxide layer, and possibly a dissolution of the layer itself. It is well known that titanium is steadily released into the tissue from titanium implants [15],[16]. Fig 2 such type of implanting material.

Fig.2

According to the Rang, 2000 [17],the first metallic implant for a hip replacement, introduced in 1940, was constructed of Vitallium, form of cobalt-chromium alloy. Along with stainless steel, this became a standard metal for large-joint replacement and internal fracture fixation. In 1926 18% chromium, 8% nickel stainless steel was introduced into surgical applications [18]. This material was noted to be much more corrosion resistant in body fluids. This was stronger and more resistant to corrosion than the vanadium steel initially introduced by Sherman for his fracture fixation plates. Later in 1926, 18-8SMo stainless steel, which contained a small percentage of molybdenum, to improve the corrosion resistance in salt water, was introduced. This alloy became known as 316 stainless steel. . In the 1950's the carbon content of 316 stainless steel was reduced from 0.08% to 0.03% for better corrosion resistance and became known as 316L stainless steel [18].

The next alloy to be introduced into orthopedic practice was titanium and its alloys. In 1947 possible applications for titanium surgical implants were considered. The pure metal had shown excellent inertness in an environment of seawater, so that corrosion resistance seemed likely to be good in the human environment. A few surgical implants were made and inserted into human subjects. Upon their removal, excellent corrosion resistance was confirmed. Subsequently, Maurice Down introduced a variety of titanium orthopedic fracture devices such as plates and screws.

In order to determine whether a newly developed implant material conforms to the requirements of biocompatibility, mechanical stability and safety, it must undergo rigorous testing both in vitro and in vivo. Results from in vitro studies can be difficult to extrapolate to the in vivo situation. For this reason the use of animal models is often an essential step in the testing of orthopedic and dental implants prior to clinical use in humans. This review discusses some of the more commonly available and frequently used animal models such as the dog, sheep, goat, pig and rabbit models for the evaluation of bone-implant interactions.

There were only minor differences in bone composition between the various species and humans. The pig demonstrates a good likeness with human bone, however difficulties may be encountered in relation to their size and ease of handling. In this respect the dog and sheep/goat show more promise as animal models for the testing of bone implant materials. While no species fulfils all of the requirements of an ideal model, an understanding of the differences in bone architecture will assist in the selection of a suitable model for a defined research question.

This paper is focused on materials like tungsten, stainless steel and cast cobalt alloys. Titanium and stainless steel are known for its good corrosion resistance property because of its inertness and presence of chromium, nickel respectively. Since the materials which is implanted inside the body is always the selection of material in animals depends on many factors out of which some properties like density and elastic modulus of the material are compared with the cortical bonein tabular form in table 1 while summary of orthopedic biomaterials and their primary use are listed in Table II.

Table I: Density and elastic modulus of selected biomaterials [19]

Material	Density	Elastic Modulus
Cortical Bone	~ 2.0 $g.cm^{-3}$	7-30 GPa
Cobalt-Chrome alloy	~ 8.5 $g.cm^{-3}$	230 GPa
316L Stainless Steel	~ 8.0 $g.cm^{-3}$	200 GPa
CP Titanium	~ 4.51 $g.cm^{-3}$	110 GPa
Ti-6Al-4v	~ 4.40 $g.cm^{-3}$	106 GPa

Table II: common metals used in implantation

METAL	PRIMARY USE
Co-Cr-Mo alloy	TJA components
Stainless Steel	TJA components, screws, plates, cabling
Ti alloy (Ti-6Al-4V)	Plates, screws, TJA components (non-bearing surface)

METALS AS BIOMATERIALS

Stainless Steels

The primary stainless steel alloy presently recommended for device manufacture used in implantation is the American Iron and Steel Institute (AISI) type 316L (Table III).This steel has less than 0.03% carbon in order to reduce the possibility in vivo corrosion. The "L" in designation316L denotes low carbon content. The exact composition may vary slightly relative to the casting or forging variant; however, both forms are derived from the very common 18-8 stainless steel alloy (18% chromium, 8% nickel) used in tableware and other commercial applications. The composition differences between the 18-8 and 316L alloy are necessitated by the superior corrosion resistance required of implant devices. Very briefly, the addition of molybdenum (3%) to the 18-8 alloy and the reduction of carbon content (0.03% max) confers improved corrosion resistance particularly to pitting and intergranular attack, respectively. Such compositional changes, however, necessitate the addition of nickel (12%) to maintain the stability of the desired microstructure, austenite.

The mechanical properties of surgical-grade stainless steel are considered to be good relative to other implant alloy systems but certainly not outstanding in the general engineering field. To maintain the specified austenitic microstructure, the normal hardening and tempering heat treatments of carbon-and low-alloy steels cannot be performed. Indeed, within the composition and phase specifications of SS316, hardening can be achieved only by a process known as cold-working. The cold-worked alloys relative to a fully annealed alloy can produce a twofold to threefold increase in yield strength, a 40% increase in ultimate strength, but a corresponding 80% decrease in ductility, thus making the material far more brittle. This is an important consideration when cold-working stainless steel fracture-fixation devices, as in the plate-contouring process. Although such a contoured device may have improved ultimate properties, it is somewhat more prone to catastrophic brittle failure.

TableIII: composition of surgical implant alloy [20]

COMPOSITION (% WEIGHT)	STAINLESS STEEL ASTM F55 OR F56 WROUGHT TYPE 8	CO-CR ASTM F75 CAST	CO-CR ASTM F90 (VITALLIUM) WROUGHT
Tungsten	—	—	14–16
Cobalt	—	Bal (57.4–65)	Bal (46–53)
Chromium	17–20	27–30	19–21
Nickel	10–14	2.5 max	9–11
Molybdenum	2–4	5–7	—
Iron	Bal (59–70)	0.75 max	3.0 max
Carbon	0.03 max	0.35 max	0.05–0.15
Manganese	2.00 max	1.0 max	2.0 max
Phosphorus	0.03 max	—	—
Sulfur	0.03 max	—	—
Silicon	0.75 max	1.00 max	1.00 max
COMPOSITION (% WEIGHT)	STAINLESS STEEL ASTM A296 CAST	TITANIUM (PURE) ASTM F67 GRADE 4, FLAT PRODUCT CAST/WROUGHT	TITANIUM 6A1-4V ALLOY ASTM F136 CAST/WROUGHT
Cobalt	—	—	—
Chromium	16–18	—	—
Nickel	10–14	—	—
Molybdenum	2–3	—	—
Iron	Bal (62–72)	0.5 max	0.25 max
Aluminum	—	—	5.5–6.5
Vanadium	—	—	3.5–4.5
Titanium	—	Bal (99+)	Bal (88.5–92)
Carbon	0.06 max	0.10 max	0.08 max
Manganese	2.00 max	—	—
Phosphorus	0.045 max	—	—
Sulfur	0.030 max	—	—
Silicon	1.0 max	—	—
Oxygen	—	0.40 max	0.13 max
Nitrogen	—	0.07 max	0.05 max
Hydrogen	—	0.015 max	0.015 max
TRADE NAME	TYPE	MANUFACTURER	
Alivium	Co-Cr	Zimmer Orthopaedic Ltd., London, England	
CoCroMo	Co-Cr	Orthopaedic Equipment Co., Bourbon, Indiana	
Francobal	Co-Cr	s.a. Benoist Girard & Cie, Heronville, France	
Orthochrome	Co-Cr	DePuy, Warsaw, Indiana	
Protosul-2	Co-Cr	Protek & Sulzer, Zurich, Switzerland	
Tivanium	Ti-6A1-4V	Zimmer USA, Warsaw, Indiana	
Vinertia	Co-Cr	Deloro Surgical Ltd., Stratton St., Margaret, England	
Vitallium	Co-Cr	Howmedica, Rutherford, New Jersey	
Zimaloy	Co-Cr	Zimmer USA, Warsaw, Indiana	

(Black J.: Biomaterials for internal fixation. In Heppenstall B (ed): Fracture Treatment and Healing. Philadelphia, WB Saunders, 1980)

The forged stainless steel alloy is used most commonly for fracture-fixation devices because of the desirable effects the forging process has on the grain structure of the fixahon device. For example, the selective directional deformation in forging a plate from bar stock or in making wire results in an optimum "fiber texture" or grain structure in which grains are elongated into fibrous or spindle shapes parallel to the long axis of the device and the expected deforming forces. This microstructure provides greater resistance to crack propagation and breakage than fully-annealed or as-cast devices having equi-axed grain structure. Of the alloys currently specified for device manufacture, stainless steel is the cheapest and most easily fabricated. To obtain high quality devices, however, careful attention must be given to the melting process, the carbon and impurity content, and the various thermal treatments necessary for shaping and developing desirable mechanical properties. Surface preparation is typically accomplished by mechanical polishing or electro-polishing to remove draw marks, pits, burrs, and surface contamination. The final step in processing stainless steel implants is that of surface passivation in nitric acid to remove surface iron particles and to artificially thicken the surface oxide layer

COBALT-BASED ALLOYS

Two main types of cobalt-based alloys are used for surgical implant purposes; a cast alloy and a wrought alloy, which vary significantly in composition (Table III). Despite these differences, however, the trade designation of Vitallium (or in Britain, "Stellite") is often applied erroneously to both alloys. The cobalt-based alloys display a useful balance between mechanical properties and biocompatibility, both forms being somewhat superior to stainless steel in strength and corrosion resistance but more expensive to manufacture

The casting variant is a cobalt-chromium-molybdenum alloy referred to as cast cobalt chromium alloy, which because of its high rate of work hardening cannot be contoured at the time of surgery. Accordingly, this alloy is typically reserved for implantable devices having a fixed configuration (e.g. total hip prosthesis), and because of its high abrasion resistance is sometimes used for bearing applications including metal-on-metal devices.

The wrought cobalt-chromium alloy is composed primarily of cobalt, chromium, nickel, and tungsten and mechanically exhibits a lower rate of work hardening than the cast alloy. In the fully annealed state the wrought alloy displays a yield stress similar to the more brittle cast variant yet has a much improved ductility (60% strain at fracture) and an ultimate tensile strength approaching that of a heavily cold-worked stainless steel. Moreover, with appropriate working and annealing treatments, the wrought alloy can be made to yield a useful range of strengths and ductilities, giving it much versatility as an implant alloy. The wrought alloy, however, is somewhat less resistant to crevice corrosion than the cast cobalt-chromium-molybdenum alloy. Its use for fracture-fixation purposes is not as yet commonplace, probably as a result of its increased cost compared with that of stainless steel.

TITANIUM- BASED ALLOYS

This third alloy system used in manufacturing structural implants includes two titanium-based alloys: commercially pure titanium and the Ti-6AI-4V, containing a nominal 6% aluminum and 4% vanadium (Table III). Commerically pure titanium must adhere to specified impurity maxima, particularly with respect to oxygen, since mechanical properties vary markedly with impurity content; the higher the impurity content, the stronger but less ductile the metal. Mechanically, the disadvantages of pure titanium include its relatively low elastic modules (approximately one half that of stainless steel and cobalt-chromium), low shear stength, and its poor abrasion resistance causing it to gall or seize when it is in sliding contact with another metal surface. In addition, it is more difficult to fabricate than stainless steel and is more expensive. Beyond its light weight, its major advantage lies in its inherent corrosion resistance. This is attributable to the spontaneous formation of a strong passivating oxide layer particularly resistant to saline solutions.

The addition of 6% aluminum and 4% vanadium to commercially pure titanium results in an alloy having mechanical properties similar to cold-worked stainless steel (including superior fatigue resistance) yet retaining excellent corrosion resistance. In addition, the Ti-6AI-4V alloy is more easily weldable and machinable than the pure form. Its principal drawback remains its poor resistance to erosion, making it unacceptable for bearing surfaces.

The titanium-based alloys, because they have been more recently introduced and are more costly, have not found widespread application, particularly in veterinary surgery; however, they are the material of choice for patients having known hypersensitivity reactions to any of the constituents of stainless steel or cobalt-chromium alloy.

CONCLUSION:

Along with the advances in biomedical technology and tissue engineering, biomaterials are desired to exhibit low elastic modulus, shape memory effect or super elasticity, wear resistance and workability. In addition, they are required to eliminate all possibility of toxic effects from leaching, wear and corrosion. Nowadays, some metal implants have been replaced by ceramics and polymers due to their excellent biocompatibility and bio-functionality. However, for implants which require high strength, toughness and durability, they are still made of metals. This demand leads to the development of new generation of metallic biomaterials and their novel processing

REFRENCES

[1] Mcdowell, Julie. Encyclopedia of Human Body System.
[2] Khan, M. A., Williams, R. L., and Williams, D. F. (1999a). The corrosion behaviour of Ti-6Al-4V, Ti-6Al-7Nb and Ti-13Nb-13Zr in protein solutions. Biomaterials 20(7): 631–637).
[3] Williams, D. F. (1985). Physiological and microbiological corrosion. Crit. Rev. Biocompat. 1(1): 1–24
[4] Bundy K. J. (1994). Corrosion and other electrochemical aspects of biomaterials. Crit. Rev. Biomed. Eng. 22(3/4): 139–251 [5] Trepanier, C., Leung, T. K., Tabrizian, M., Yahia, L. H., Bienvenu, J.-G., Tanguay, J.-F., Piron, D. L., and Bildeau, L. (1999). Preliminary investigation of the effects of surface treatments on biological response to shape memory NiTi stents. J. Biomed. Mater. Res.(Appl. Biomater.) 48: 165–171.)
[6] Jacobs, J. J., Gilbert, J. L., and Urban, R. M. (1998). Current concepts review corrosion of metal orthopaedic implants. J. Bone Joint Surg.
80-A: 268–282).
[7] Disegi, J. A., and Eschbach, L. (2000). Stainless steel in bone surgery. Injury 31(suppl 4): 2–6.)
[8] 1985Fraker, A. C., and Griffith, C. D., eds. (1985). Corrosion and Degradationof Implant Materials. ASTM S.T.P. No. 859, American Society for Testing and Materials, Philadelphia).
[9] Hiromoto, S., Noda, K., and Hanawa, T. (2002). Development of electrolytic cell with cell-culture for metallic biomaterials. Corr. Sci. 44: 955–965.).
[10] Long, M., and Rack, H. J. (1998). Titanium alloys in total joint replacement—a materials science perspective. Biomaterials19: 1621–1639).
[11] Sittig, C., Textor, M., Spencer, N. D., Wieland, M., and Vallotton, P.-H. (1999). Surface characterization of implant materials c.p.Ti,Ti-6Al-7Nb and Ti-6Al-4V with different pretreatments. J. Mater. Sci.: Mater. Med. 10: 35–46.).
[12] Shih, C.-C., Lin, S.-J., Chung, K.-H., Chen, Y.-L., and Su, Y.-Y. (2000). Increased corrosion resistance of stent materials by converting current surface film of polycrystalline oxide into amorphous oxide. J. Biomed. Mater. Res. 52: 323–332.
[13] Aronsson, B.-O., Lausmaa, J., and Kasemo, B. (1997). Glow discharge plasma treatment for surface cleaning and modification of metallic biomaterials. J. Biomed. Mater. Res. 35: 49–73.
[14] Thierry, B., Tabrizian, M., Savadogo, O., and Yahia, L'H. (2000). Effects of sterilization processes on NiTi alloy: Surface characterization.J. Biomed. Mater. Res. 49: 88–98.
[15] Jacobs, J. J., Gilbert, J. L., and Urban, R. M. (1998). Current concepts review corrosion of metal orthopedic implants. J. Bone Joint Surg.
80-A: 268–282.
[16] Hanawa, T., Asami, K., and Asaoka, K. (1998). Repassvation of titanium and surface oxide film regeneration in simulated bio liquid. J. Biomed. Mater. Res. 40: 530–538.
[17] Rang, M. (2000), The Story of Orthopedics, Saunders, Philadelphia.
[18] Nag, Soumya and Banerjee, Rajarshi. Fundamentals of Medical Implants Materials. [ed.] R. Narayan. Vol. 23.
[19] www.azom.com /Titanium and Titanium Alloys as Biomaterials.
[20] Black J: Biomaterials for Internal Fixation. In Hep- penstall B (ed): Fracture Treatment and Healing, p 113. Philadelphia, WB Saunders,

Spectroscopic Investigations of Anatase Titania Nanoparticles

Katlakanti Mohan Reddy[*, a], DeviL G[b], P K Sahoo[c]

[*, a]*Department of Chemistry, College of Engineering Studies, University of Petroleum & Energy Studies, India.*

[a, b]*Central College, Department of Chemistry, Bangalore University, India*[c]*Department of Mechanical Engineering, University of petroleum and Energy Studies, India.*

***Abstract*—To investigate the relationship between the particle size and the Raman bands of TiO2 nanoparticles, two different size-selected samples of TiO2 nanoparticles wereinvestigatedusing transmission electron microscopy (TEM), High resolution TEM (HRTEM), Xray photoelectron absorption spectroscopy (XPS), and Fourier Transform Raman spectroscopy (FT-Raman). In the Raman spectra, both broadening and shifts of the Raman bands with decreasing particle diameter were observed. In this paper, these Raman shifts are attributed to the effects of decreasing particle size on the on theforce constants and vibrational amplitudes of the nearest neighbor bonds.**

***Keywords*—** nanoparticles, titania, Raman spectroscopy, resonance Raman scattering

I INTRODUCTION

Various metal oxides (i.e. TiO_2, ZnO, MoO_3, CeO_2, ZrO_2, WO_3, Fe_2O_3, and SnO_2) and metal chalcogenides (i.e. ZnS, CdS, CdSe, WS_2 and MoS_2) are used as catalysts in semiconductor photocatalyst reactions[1-4]. In this regard, Titanium Dioxide (TiO_2) mediated photocatalysis has been of particular interest [5]. TiO_2 is most widely used for heterogeneous photocatalysis due to its special characteristics such as: 1. It is environmental friendly and TiO_2 is plenty full (it is widely used as pigment in paint industry and it is inexpensive), 2. It is chemically stable and non-toxic, 3. It has excellent electronic and optical properties, 4. It is chemically and biologically inert, 5. It is stable with respect to photocorrosion or chemical corrosion, 6. It is available at relatively modest cost and can be recycled in a technical scale, 7. Most of the studies are only on $TiO_2$and No other semiconductor has proven to be as best as TiO_2. Because of these reasons TiO_2 is the special photocatalyst with a wide band gap whose absorption onset occurs in the lower end of the UV-spectrum [6-10]. Sensitization and modification of this catalyst leads to the visible light response. Because of high photocatalytic activity and stability, TiO_2 has become bench mark photocatalyst.In recent years, the preparation and characterization of TiO_2 nanostructures have attracted much interest due to their unique properties and potential applications in catalysis [10-15]. It has been demonstrated that the physical and chemical properties of TiO_2 nanostructures, and their potential applications depend strongly on their crystalline structure, morphology and particle size. TiO_2 occurs mainly in three crystalline phases namely Anatase, Rutile and Brookite. Rutile is the thermodynamically most stable phase. They differ in their physical properties, such as refractive index, dielectric constant, chemical and photochemical reactivity. Though various forms of TiO_2 have been reported [16-20], rutile, anatase and brookite are the naturally occurring forms of TiO_2. The rutile structure is based on a slightly distorted hexagonal close packing of oxygen atoms with the half of the octagonal interstices being occupied by the titanium atoms. The octahedral coordination of titanium atoms and the trigonal planar coordination of oxygen atoms. This is the structure commonly adopted by ionic dioxides and difluorides. The relative sizes of ions are such that they favour 6 : 3 coordination. Anatase and brookite are based on cubic rather than hexagonal close packing (ccp/hcp) of oxygen atoms where Ti^{4+} ions occupy half-the octahedral interstices [20].

II RESULTS AND DISCUSSIONS

FT-RamanSpectral Analysis

Figure 1a1b & 1cshows the Raman spectra of three types of TiO_2nanoparticles and the reference spectrum of anatase TiO_2.Bulk anatase has a tetragonal structure containing twelve atoms per unit cell with latticeparameters a = 3.784 A°and c = 9.514 A°[21]. According tofactor group analysis, anatase has six Raman active modes(A_{1g} + $2B_{1g}$ + 3_{Eg}). Ohsaka reported the Raman spectrum of an anatase single crystal that the six allowed modes appear at 144 cm^{-1} (E_g), 197 cm^{-1} (E_g), 399 cm^{-1} (B_{1g}), 513 cm^{-1}(A1g), 519 cm^{-1} (B1g), and 639 cm^{-1} (Eg) [22]. The main spectralfeatures of samples N (~27 nm) and M (~10 nm) are closelysimilar to those of the reference TiO_2, which mean that the prepared samples N and M possess a certain degree of longrangeorder of the anatase phase. However, the spectrum of sample P (~5 nm) is quite different from the others, showingthe band broadening with decrease in intensity. This

difference in Raman spectra of TiO_2 nanoparticles can be attributed to the effect of smaller particle size and it affectsthe force constant and vibrational amplitudes of the nearestneighbor bond.

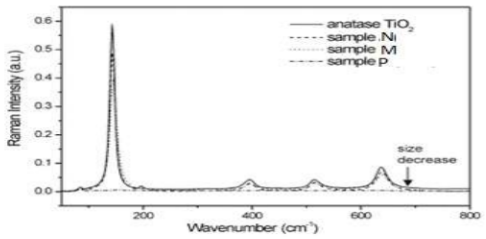

a

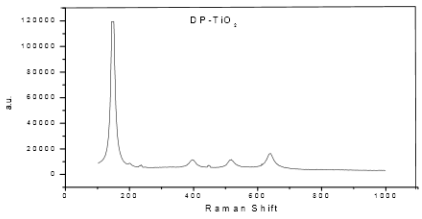

b

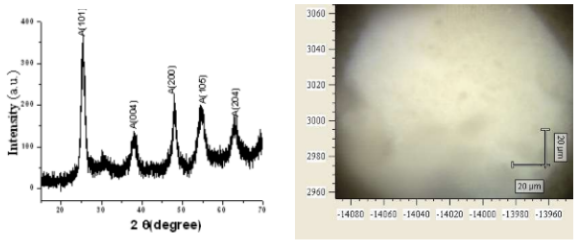

c

Fig. 1a, 1b & 1c Raman spectra of all the samples of anatase TiO_2(XRD of anatase TiO_2)

B. TEM and HRTEM analysis

TEM image of the TiO_2 sample of particles have sizes in the range 6-10 nm and homogeneously distributed TiO_2 grains. TEM image shows the particles of the TiO_2 sample possess sphericalshapes and of same sizes: some small spherical particles approximately 10 nm in diameter and agglomerates approximately 20-30 nm in length and 2 nm width. The high resolution transmission electron microscopy of the TiO_2 catalysts were shown in the Figure. 2 (a, b&c).The HRTEM shows that titania particles were present in nano spherical shapes: smaller round particles of diameter ~10 nm and long prismatic particles with an end to end distance of ~ 30 nm. The distance between the lattice planes in the latter case is 2.8 A^o. HRTEM images of anatase TiO_2 particles were obtained, hexagonal crystal was 5 nm across its edges. As can be seen from the TEM image, the TiO_2 powder shows a wide particle size distribution ranging from 10 to 30 nm. Moreover, some small particles with diameters of less than 10 nm were also observed. In this case, it seems that the crystallite size of the TiO_2 is the most important factor affecting the phase transformation.

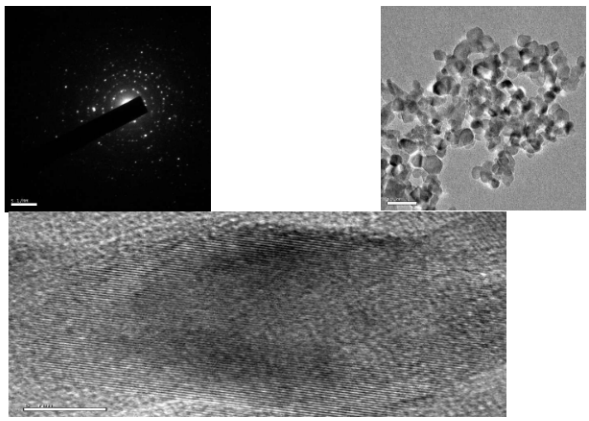

Fig. 2 (a, b & c) the TEM and HRTEM images of anatase TiO_2 nanoparticles

C. XPS analysis

The chemical state and the composition of anatase TiO_2 surface was studied by XPS as shown in Figure. 3(a & b). The Ti binding energies were observed at 458.43 eV and 464.196 eV which can be assigned to Ti $2p_{3/2}$ and Ti $2p_{1/2}$ with a peak separation of 5.739 eV which can be assigned to Ti^{4+} in TiO_2. The O_{1S} peaks were observed at 529.668 eV. The surface atomic concentration of O 1s is 72.7 and 70.5%, Ti 2p is 27.3 and 24.2%, TiO_2.

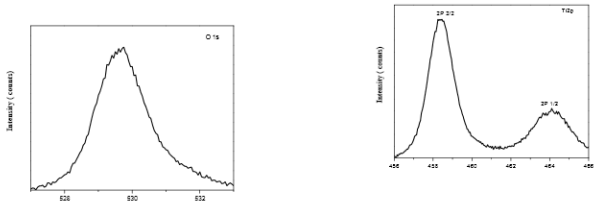

Fig. 3 (a&b) the XPS spectra of anatase TiO_2 nanoparticles

III CONCLUSION

The broadening and shifts of Raman bands of anataseTiO_2 nanoparticles with decreasing particle size were investigatedusing X-ray absorption spectroscopy and Ramanspectroscopy. The TEM results show that the prepared 25 and 10 nm TiO_2 nanoparticles have an anatase structure,and that there is no difference between the oxidation state ofthe titanium ions in the nanoparticles and that of titaniumions in bulk TiO_2. Both broadening and shifts of theRaman bands were observed with decreasing particle diameter.The observed Raman shifts are thus due

to the effectsof decreasing particle size on the force constants andvibrational amplitudes of the nearest neighbor bonds.

IV ACKNOWLEDGMENT

Authors are grateful to thank the Management of UPES, Dehradun and Bangalore University, Bangalore for the continuous support this work to present and publish.

REFERENCES

[1] A. Fujishima, K. Honda, "Electrochemical Photolysis of Water at a Semiconductor Electrode" *Nature*, Vol. 238, pp. 37 – 38, Jul. 1972.

[2] H. Sun, Y. Bai, Y. Cheng, W. Jin, N. Xu, "Preparation and characterization of visible-light-driven carbon-sulfur-codoped TiO2 photocatalysts" Ind. Eng. Chem.Res., Vol. 45, No. 14, pp. 4971- 4976.Jul. 2006.

[3] S. Tojo, T. Tachikawa, M. Fujitsuka, T. Majima, "Iodine-Doped TiO_2 Photocatalysts: Correlation between band structure and mechanism "J. Phys.Chem, Vol. 112, No. 38pp.14948 – 14954, Aug. 2008.

[4] M. S. Wong, S. W. Hsu, K. K. Rao, C. P. Kumar, "Influence of crystallinity and carbon content on visible light photocatalysis of carbon doped titntania thin films", J. Mol.Catal. A: Chem., Vol. 2 79, pp.2–26, Jun. 2008.

[5] H. Kato, A. Kudo, "Visible-Light-Response and Photocatalytic Activities of tio_2 and $srtio_3$ Photocatalysts Codoped with Antimony and Chromium", J. Phys. Chem. B, Vol.106, No. 16, pp. 5029-5034, Apr. 2002.

[6] T. Matsunaga, R. Tomoda, T. Nakajima, H.Wake, "Ph otoelectrochemical sterilization of microbial cells by semiconductor powders", FEMS Microbiol. Lett., Vol. 29, pp. 211-214, 1985.

[7] V. Nadtochenko, N. Denisov, O. Sarjusiv, D. Gumy, C.Pulgarin, J. Kiwi, "Laser kinetic spectroscopy of the interfacial charge transfer",J. Photochem. Photobiol. A Chem, Vol. 181, pp. 401-407, 2006.

[8] A.G. Rincón and C. Pulgarin, "Effect of pH, inorganic ions, organic matter and H_2O_2 on E. coli K12 photocatalytic inactivation by TiO_2: implications in solar water disinfection," Appl.Catal. B, vol. 51, no. 4, pp. 283–302, 2004.

[9] J. C. Yu, W. Ho, J. Lin, H. Yip, P.K. Wong, "Photocatalytic activity, antibacterial effect, and photoinduced hydrophilicity of TiO_2 films coated on a stainless steel substrate", Environ. Sci.Technol.,Vol.37 pp. 2296 – 2301, May 2003.

[10] J. S. Hur, Y. Koh, "Bactericidal activity and water purification of im- mobilized TiO2 photocatalyst in bean sprout cultivation", Biotechnol. Lett.,Vol.24, pp. 23-25, 2002.

[11] E. Szabo-Bardos, H. Czili, A. Horvath,"Photocatalytic oxidation of oxalic ... a TiO_2 surface", J. Photochem. Photobiol. A: Chem.,Pp.154,pp. 195–201, 2003.

[12] Erzsébet Szabó-Bárdos, Erika Pétervári, Viktória El-Zein, Attila Horváth:„Photocatalytic decomposition of aspartic acid over bare and silver deposited TiO_2"*J. Photochem. & Photobiol. A:Chem.,* Vol.184, No 1-2, pp. 221-227, 2006.

[13] M.R. Hoffmann, S.C. Martin, W. Choi, D.W. Behne mann, "Environ-
mental applications of semiconductor photocatalysis"Che m. Rev. Vol. 95, No. 1, pp. 69 – 96, Jan. 1995.

[14] B. O'Regan and M. Grätzel, A Low-cost, "High-efficiency Solar Cell Based on Dye-sensitized Colloidal TiO_2 Films", Nature, Vol. 353, pp. 737 – 740,1991.

[15] M. R. Hoffmann, S. T. Martin, W. Choi, and D. W. Bahnemann, "Environmental applications of semiconductor photocatalysis," Chemical Reviews, vol. 95, no. 1, pp. 69–96, 1995.

[16] M. Anpo, H. Yamashita, in: M. Anpo (Ed.), Surface Photochemistry, Wiley, Chichester, 1996, pp. 117-164.[17] P. V. Kamat, Chem. Rev. 93(1993)267-300.

[18] D.M. Blake, P.C. Maness, Z. Huang, E.J. Wolfrum, J. Huang, W.A.Jacoby, "application of the photocatalytic chemistry of Titanium dioxide to disinfection and the killing Of cancer cells"Sep.Purif. Methods Vol. 28, No. 1, pp 1-50, 1999.

[19] L. Gomathi Devi, K. Mohan Reddy, "Enhanced photocatalytic activity of silver metallized TiO2 particles in the degradation of an azo dye methyl orange: Characterization and activity at different pH values"Appl. Surf. Sci. Vol. 256, No. 10, pp. 3116 – 3121, March 2010.

[20]. L. Gomathi Devi, K. Mohan Reddy," Photocatalytic performance of silver TiO_2: Role of electronic energy levels"Appl. Surf. Sci., Vol. 257, No. 15, pp. 6821–6828, May 2011.

[21] O.A. Ileperuma et al, "Photocatalytic behavior of metal doped titanium dioxide.", Appl. Catal. vol. 62, No. 1, Jun.1990, pages L1-L5.

[22] K. Kalyanasundaram, and M. Graetzel,"Photosensitization and Photocatalysis Using Inorganic and…"Coordin. Chem. Rev., Vol. 196, pp. 219, 2000.

Concrete Self-Healing Capability Using Bacterial Action – A Comparative Study

Er Parampreet Kaur*, Akash Bhardwaj*
*Department of Civil Engineering
Shaheed Bhagat Singh State Technical Campus, NH-95 , Moga Road , Ferozepur-152004

Abstract- Cracking is a frequent cause of complaints in the concrete industry. Cracking can be the result of one or a combination of factors such as drying shrinkage, thermal contraction, restraint (external or internal) to shortening, sub grade settlement, and applied loads or can also be caused by freezing and thawing of saturated concrete, alkali- aggregate reactivity, sulphate attack, or corrosion of reinforcing steel. So there is a need for the development of such an inherent biomaterial which is an self-repairing material and can remediate the cracks and fissures in concrete.

Bacterial concrete is one among such a material, which can successfully remediate cracks in concrete. This Technique is an eco-friendly desirable as well as a natural method that can be taken into consideration in recent concrete industry era. The Paper discusses the comparative study of concrete self healing capability using different types of bacteria viz Bacillus Sphacricus, B. Cohnii. Hence this is a Biological Remediation of cracks repairment.

Keywords:- Cracking , Bacterial Concrete , Biological Remediation.

Introduction

Usually Concrete plays a major role in the construction era due to its strength acquiring capability and various other factors like ease to use, less cost and good workability, But the concrete with passage of time start undergoing losing its strength due to various environmental parameters . This strength can be acquired by polymer based resins and chemicals but there use is restricted to a limited extent.

So, Bacteria action in concrete is an advance method that can be implemented in recent construction technology as bacteria is a biological substance that is capable of healing concrete using biomechanics reactions. Bio methodology to be used in concrete can lead to a new concrete type called as bacteria concrete.

The Use of bacteria in concrete is a new rational approach for biologically precipitation of calcite in cracks. It is of a vital importance for the identification of concrete microbial behaviour towards crack. This method is basically a microbiologically induced calcite precipitation technique based on bio mineralization Concept. Concrete, however, is due to its high internal pH, relative dryness and lack of nutrients needed for growth, a rather hostile environment for common bacteria, but there are some extremophilic spore forming bacteria may be able to survive in this artificial environment and increase the strength and durability of cement concrete. The following reaction summarizes the bacterial role in formation of nucleation site on cracked concrete specimen:-

$$Ca^{2+} + Cell \rightarrow Cell - Ca^{2+}$$

$$Cl^- + HCO_3^- + NH_3 \rightarrow NH_4Cl + CO_3^{2-}$$

$$Cell\text{-}\ Ca^{2+} + CO_3^- \rightarrow Cell\text{-}\ CaCO_3$$

Basically this paper is based on the behaviour of B. Pasteruii, B. sphaericus , B. Cohnii & Bacillus subtiles, bacteria due to its higher stability in environmental conditions and also helps in reduction of permeability to avoid bacterial nutrients losses during the phenomenon.

This phenomenon is based on the concept of metabolic process of $CaCO_3$ Precipitation, the Calcium Carbonate Microbial Precipitation leads to various applications like Crack remediation of concrete, Sand Consolidation, repairment of cracks in historical Monuments and various other applications.

The Use of Bio mineralogy leads to the invention of Bacterial concrete- A Bio potential Material which is considered as a green technology and is a crossbreed between biology and engineering study of concrete which involves bacterial utilization. The microbial precipitation of calcite is visualized using X-ray Diffraction analysis along with scanning electron microscopic analysis of the specimens.

Requirement of the Study

This study is carried out for visualization & analysis of the following aspects:-

- Effect of Different Bacterial concentrations on strength & crack repairing ability of the specimen.
- Bacterial Efficiency in different medium concentrations and their reaction tendency.
- Comparison of various categories of bacteria in crack repairing ability and their survival duration in the specimen.
- Bacteria inherent ability to precipitate calcite continuously.
- Evaluation of Crack Repair.

The main purpose of this paper is to observe the bacterial tendency to act as a self-repairing agent in concrete as usually bacteria are considered to be alkali-resistant and produces spores which act as a protecting agent for the cell-wall against extreme environmental and chemical stresses. Bacterial spores are specialized cells which can remain viable for up to 200 years. Spores are dormant but viable bacterial spores immobilized in the concrete matrix will become metabolically active when revived by water entering freshly into the concrete.

As usually many terminologies are there for crack remediation using different biological species but mostly there output is not up to the desired level of the requirement so there is a need to compare the different biological species and there outputs in order to get that particular bio mineral method and species which provide better results.

Looking at the challenges of our infrastructure - self repairing concrete would be a advancement, as Cracks permit water to penetrate concrete, water in contact with reinforcing steel causes rust, rust takes up 7 times the volume of steel and causes concrete to crack more and spall, exposing more steel to water.

Literature Review

In this study four calcite forming precipitation bacteria were compared on the parameters like compressive, strength, their reactivity, These bacteria are B. Pasteruii, B. sphaericus , B. Cohnii & Bacillus subtiles. The microstructure examinations are analyzed out using Scanning electron Microscopy micrograph of these four bacteria. From the SEM Micrograph of these four bacteria it was found that there is no crystal growth in concrete without bacteria but when bacteria is added the rod shape Fabulous deposition is observed due to bacterial interaction with concrete. During this study the enhancement of compressive strength , Reduction in permeability and concrete optimum performance has been observed as due to calcifying micro-organisms growth in concrete.

These Four Bacteria are prepared by following Biomechanism:-

Bacteria	**Formation Mechanism**	**Nutrients Required**
B. Pasturii	Oxidative Determination of amino acids	trypticase, yeast extract, tricine ammonium sulphate, glutamic acid , agar solution.
B. Subtiles	Hydrolysis of Urea	Urea ,ammonium chloride, sodium biocarbonate , Calcium salts.
B. Sphaericus	Bio oxidative urea analysis	Extract Yeast , urea, Calcium Salts.
B. Cohnii	Urea Hydolysis	Peptone , yeast extract , Actical , Natamycine.

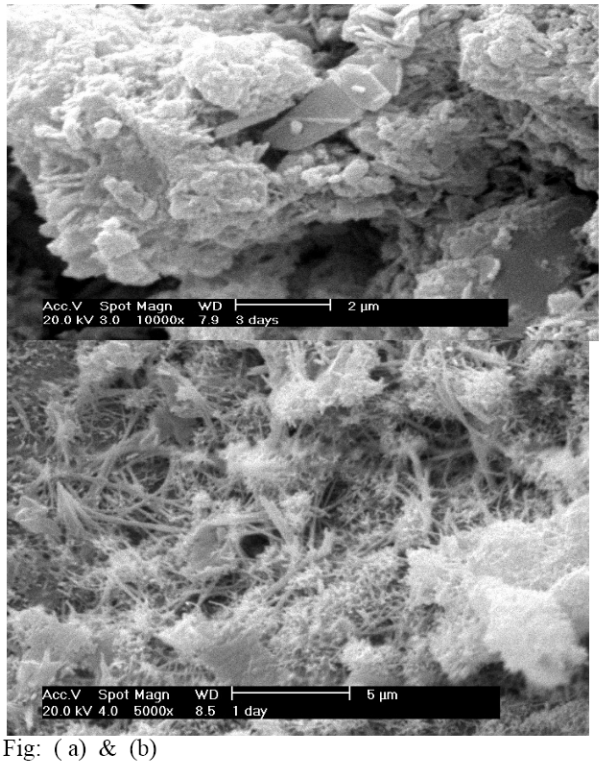

Fig: (a) & (b)
Fig:(a). shows the Concrete SEM without Bacteria,
Fig: (b) shows the Concrete SEM with B.Subtiles Bacteria.

Compressive Strength Comparison of Concrete Specimen:-

Bacteria	Specimen Compressive Strength (7 days)
B. Pasturii	**30 N/mm^2**
B. Subtiles	**33 N/mm^2**
B. Sphaericus	**28 N/mm^2**
B. Cohnii	**29 N/mm^2**

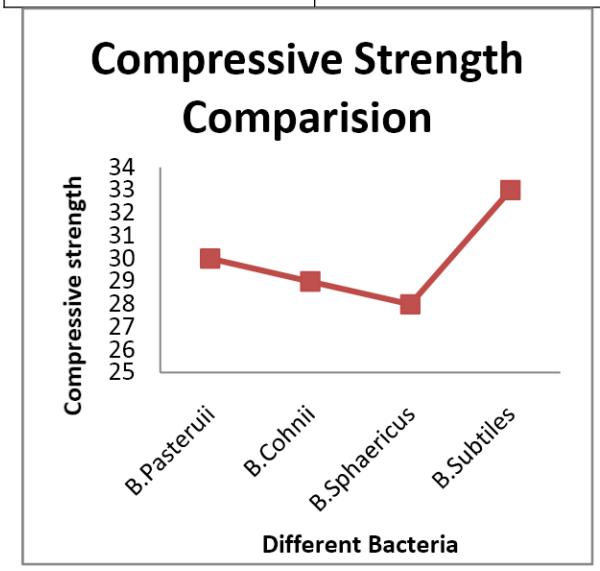

Graph No. 1: Compressive Strength of concrete for Different Bacteria.
The units of Compressive Strength of concrete is kN/m^2

Result of Comparative study the Graph is

B.Subtiles is found as the most effective microbiome after studing this graph.

Conclusion

In this comparative study of the literature ,it is conclude that the B.Subtiles is the most effective microbiome for the crack remediation of the concrete as it remediates the cracked specimen easily . Out of the four bacteria , study reveals that Bacillus subtilis

contribute marked increase in strength during early age. It appears that the increase in strength due to the inclusion of microbe in concrete is comparable from the Literature Review . However, the strength enhancement made from a microbe in concrete was not able to surpass the strength enhancement made by silica fume replacement (Average Strength of 34 N/mm^2) . Microbial concrete has proved to be better than many conventional technologies as of its eco friendly nature, self-healing abilities and increase in strength of various building materials.

References

[1]Benini S, Rypniewski W, Wilson KS, Miletti S, Ciurli S, Mangani S., "A new proposal for urease mechanism based on the crystal structures of the native and inhibited enzyme from Bacillus pasteurii: why urea hydrolysis costs two nickels." *Structure7,* 1999.

[2]H. M. Jonkers and E. Schlangen, "A two component bacteria-based self-healing concrete," *Concrete Repair, Rehabilitation and Retrofitting II*, 2009, pp. 215–220.

[3] Ramakrishnan, V., Bang, S.S., Srinivasan Neelamegam., and Ramesh, K.P., "Durability of Cement Mortar Made With Different Concentrations of Bacteria", Proceedings of 25th International Conference of Cement Microscopy, Richmond, Virginia, April 2003.

[4] Ramachandran, S.K., Ramakrishnan, V., and Bang, S.S., "Remediation of Concrete using Microorganisms", ACI Materials Journal, v.98, No.1, pp. 3-9, Jan-Feb 2001.

[5] Kantzas, A., Ferris, F.G., Jha, K.N., and Mourits, F.M., "A Novel Method of Sand Consolidation through Bacteriogenic Mineral Plugging", paper presented at the CIM Annual Technical Conference, Calgary, June 7-10, 1992.

[6] Gollapudi, U.K., Knutson, C.L., Bang, S.S., and Islam, M.R., "A New method for Controlling Leaching through Permeable Channels", Chemosphere, v. 30, No. 4, pp. 695-705, 1995.

[7]De Muynck W., Cox K., De Belie N. and Verstraete W."Bacterial carbonate precipitation as an alternative surface treatment for concrete", *Constr Build Mater,* **22,** 875 -885 **(2008)**

[8]F. Hammes, N. Boon, J. De Villiers, W. Verstraete, S. D. Siciliano, and J. De Villiers, "Strain-Specific Ureolytic Microbial CalciumCarbonate Precipitation," *Applied And Environmental Microbiology*, vol.69, no.8, 2003, pp. 4901–4909.

[9] Ghosh P, Mandal S, Chattopadhyay BD, Pal S., "Use of microorganism to improve the strength of cement mortar." *Cement and Concrete Research 35*, 2005, pp.1980-1983.

[10] González-Muñoz M.T., Ben-Chekroun K., Ben-Aboud A., Arias J.M. and Rodriguez-

Structural and Optical Properties of Ni Doped Zinc Oxide Nanoparticles Prepared By Coprecipitation Method

Deepawali Arora[a], Sunil Kumar[a], Simranpreet Kaur[a], Gurinder Pal Singh[a], Parvinder Kaur[a], D.P. Singh[a]

[a]*Department of Physics, Guru Nanak Dev University, Amritsar 143005, India*

***Abstract*— The samples of $Zn_{1-x}Ni_xO$ (x= 0.00 and 0.05) were prepared with coprecipitation method at different annealing temperatures. The effect of Ni ion substitution on the structural and optical properties has been studied using X-ray Diffraction (XRD), Ultraviolet-Visible and Photoluminescence Spectroscopy. XRD measurements demonstrate that all the prepared samples are polycrystalline single phase in nature and belong to the wurtzite structure ruling out the presence of any secondary phase formation. Ultraviolet visible measurements showed a decrease in band gap with the increase in annealing temperature and doping concentration. The PL data shows the red shift in all the samples with the increase in the annealing temperature.**

***Keywords*—** Coprecipitation, Nanopowders, Photoluminescence, XRD

I. INTRODUCTION

Currently, ZnO is attracting attention for its application to transparent high power electronics, surface acoustic wave devices, UV light-emitters, gas-sensing and as a window material for display and solar cells [1],[2]. Zinc oxide (ZnO) has a direct wide bandgap (3.4 eV at Room temperature), which is n-type semiconductor. In ambient condition, ZnO has a stable hexagonal wurtzite structure with lattice spacing a = 0.325 nm and c = 0.521 nm [3]and composed of a number of alternating planes with tetrahedrally-coordinated $O^{2-}$and Zn^{2+} ions, stacked alternately along the c-axis. All these predominant properties make ZnO a great potential in the field of nanotechnology. Usually ZnO is doped with different types of metallic ions, like Ga, In, Sn, Al, Sc, Ti, V, Ni, Co and Mn in order to improve its transparent conducting oxide properties [4],[5]. ZnO nanoparticles can be prepared at low cost by simple solution based method, such as, sol-gel synthesis, chemical precipitation and hydrothermal reaction [6] ,[7]. Coprecipitation method is a promising alternative synthetic method because it can be achieved at low working temperature as well as particle size could be easily controlled.

In the present work undoped and Ni doped ZnO nanoparticles were synthesized by using chemical coprecipitation method and thus we attempt to study structural and optical properties of undoped and Ni doped ZnO nanopwders

II. EXPERIMENTAL DETAILS

$Zn_{1-x}Ni_xO$ (x= 0.00 and 0.05) powders were prepared by coprecipitation method. Sol was synthesized using sol-gel solution route technique in order to obtain the Ni doped ZnO powders. For the preparation of sol, stoichiometric amounts of metal nitrate, $Zn(NO_3)_{3\cdot6}H2O$, $Ni(NO_3)_{3\cdot6}H_2O$ was dissolved in deionized water to get 0.6 M solution. No stabilizer was added. This solution was kept for 1 hour for stirring at room temperature. In this solution, 5 M NH_4OH was added drop wise, till the pH value reached to 7,the solution was stirred for 3 hours and then filtered and washed with deionized water and ethanol 3 times. The mixture was then dried at 800° C for 15 hours. The dried mixture was then grounded .The obtained powders were annealed at 400°C and 600^{0}C temperature. Structural characterization of undoped and Ni doped ZnO nanopwders were done using Shimadzu XRD-7000 x-ray diffractometer (Cu Kα, λ= 1.5418 Å) and optical studies were done using ultra-violet visible spectrometer (Perkin Elmar, Lambda 35). Photoluminescence studies were done with fluoremeter LS 45 to excite the luminescence with fixed wavelength light and to measure the intensity of the PL emission at a single wavelength or over a range of wavelengths.

III. RESULT AND DISCUSSION

Fig.1 and Fig.2 shows XRD spectra of undoped and Ni doped ZnO annealed at 400 and 600°C temperatures respectively. The data analyzed exhibits single phase behavior with wurtzite lattice and excludes the formation of any secondary phase. No significant change were observed in the peak position as the annealing temperature of undoped ZnO was increased from 400 to 600°C, but the intensity of all the peaks were found to decrease indicating a little degradation in the crystallinity of ZnO. No peaks corresponding to Ni ions (clusters or precipitates) were observed in all the samples, this clearly indicates that Ni-incorporation does not change the wurtzite crystal structure of the ZnO matrix, hence it can be said that Ni

ions intrinsically substituted Zn ion without disturbing the parent structure of the host matrix.

The lattice parameter values were calculated using XRDA analysis and tabulated (Table 1), compared with standard ZnO (a = 3.25 and c = 5.21 nm), c parameter decreased with annealing temperature and doping of Ni ions. This decrease can be justified since the ionic radius of Ni^{2+} (0.069 nm) is less than that of Zn^{2+} (0.074nm) [8].The particle size d, of ZnO:Ni nanoparticles were estimated by Debye- Scherer's equation (1)

$$D=\frac{k\lambda}{\beta cos\theta} \quad (1)$$

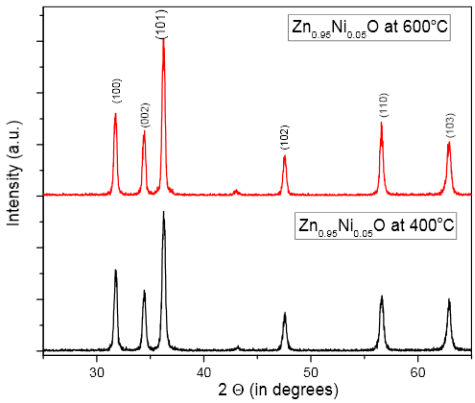

Fig.1 XRD pattern of $Zn_{0.95}Ni_{0.05}O$ powders annealed 400 and 600°C temperatures.

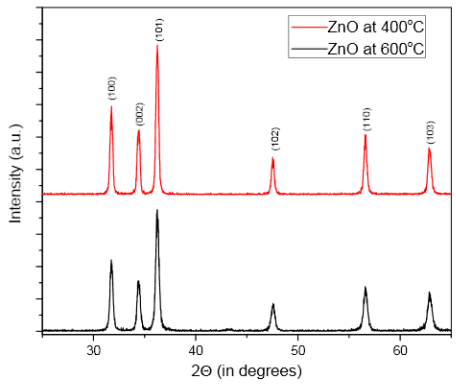

Fig.2. XRD pattern of ZnO annealed 400 and 600°C temperatures.

Uv-Vis spectra of both undoped and Ni doped ZnO nanoparticles are shown in Fig. 3 and Fig. 4.The calculated band gaps are tabulated in Table 1.The band gap was found to decrease with doping, since doping of ZnO with Ni adds defects sites in the vicinity of valence band and reduces the effective band gap [9].The decrease in the band gap with annealing temperature may be attributed to the better substitution of Ni ions annealing out of some defects.

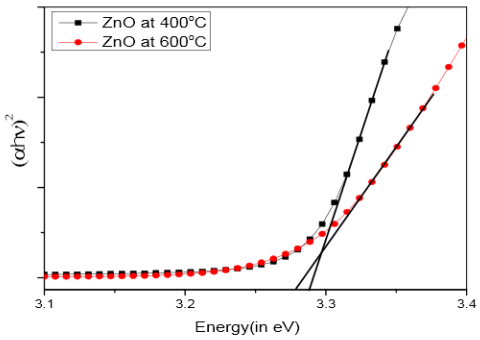

Fig.3 Optical Band gap of ZnO of annealed 400 and 600°C temperatures.

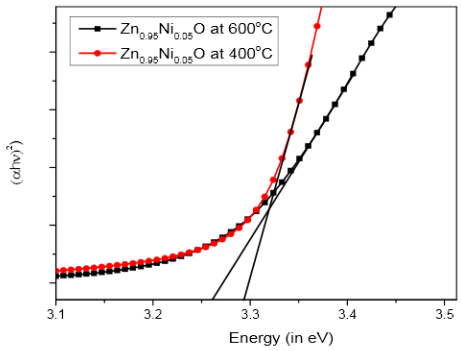

Fig.4. Optical Band Gap of $Zn_{0.95}Ni_{0.05}O$ powders annealed 400 and 600°C temperatures.

Fig.5 and Fig.6 illustrate the photoluminescence spectra of undoped and Ni doped ZnO respectively with 290 nm excitation under room temperature. The PL emission consists of broad visible region, which can be attributed to the electronic transitions from the level of interstitial zinc as associated with ionized oxygen vacancies to the valence band. [10].A peak at 423 nm refers to the violet luminescence which is probably due to radiative defects related to the interface traps existing at the grain boundaries and emitted from the radiative transition between this level and the valence band [11].Another peak at 485 nm refers to the blue emission and can be attributed to the transitions between the oxygen vacancy and lattice defects related to oxygen and zinc vacancies[12].The PL intensity becomes stronger as the annealing temperature increases from 400 to 600° C which might be attributed to the recovery of microstructural

defects [13].However as, Ni doping concentration is increased the peak at 485 nm quenched with the significant value .This quenching might be due incorporation of Ni ions into the ZnO host matrix and hence leads to decrease in the crystalline quality of the samples, which is consistent with the XRD results.

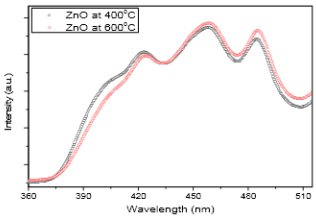

Fig. 5 PL spectra of ZnO annealed at 400 and 600°C temperature

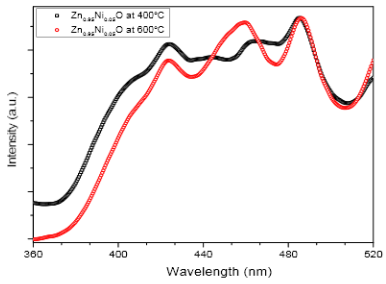

Fig. 6 PL spectra of $Zn_{0.95}Ni_{0.05}O$ powders annealed at 400 and 600°C temperatures.

TABLE 1. Variation of Lattice parameters and Band Gap with of undoped and Ni doped ZnO annealing temperature and doping concentration.

Parameters	**Pure ZnO**	**ZnO**		**$Zn_{0.95}Ni_{0.05}O$**	
Temperature		**400**	**600**	**400**	**600**
a(nm)	3.250 3.27	3.279		3.279	3.279
c(nm)	5.204 5.212	5.208		5.205	5.202
Band Gap (eV)	3.3 3.288	3.278		3.293	3.260
Crystallite Size(nm)	20.80	20.96		22.10	24.6

IV. REFERENCES

1. D.C. Look, *Mater. Sci. Eng*. **B80,** 383 (2001)
2. P. Zu, Z.K. Tang, G.K.L.Wong, M. Kawasaki, A. Ohtomo, K. Koinuma, Y. Sagawa, *Solid State Commun.***103,** 459. (1997)
3. Nakahara, K.; Takasu, H. *Appl. Phys. Lett.,* **25 (79),** 4139-4141 (2001)
4 V.N. Zhitomirsky, E. Cetinorgu, R.L. Boxman, S. Goldsmith, *Thin Solid Films* **516,** 5079 (2008)
5. B.D. Ahn, S.H. Oh, C.H. Lee, G.H. Kim, H.J. Kim, S.Y. Lee *J. Cryst. Growth* **309,** 128 (2007)
6. Z. Hui, Y.Deren, M. Xiangyang, J.Yujie, X. Jin, *Nanotechnology* **15,** 622 (2004)
7. J.Zhang, L. D. Sun, J.L. *Yin, Chem. Mater*. **14,** 4172 (2002)
8. M. El-Hilo, A.A. Dakhe, A.Y. Ali-Mohamed, *J. Magn. Magn. Mater*. **321,** 2279–2283(2009)
9. S. Kant and A. Kumar *Adv. Mat. Lett.* **3(4),** 350-354 (2012)
10. R. Elilarassi, and G. Chandrasekaran *Optoelec. Lett*. **6,** 1 (2010)
11. B.J. Jina ,S.Imb, S.Y. Leec, *Thin Solid Films* **366**, 107-110 (2000)
12. S. Kumar, N. Kumari , S. Kumar, S. Jain, N. K. Verma *Appl Nanosci* **2**, 437–443 (2012)
13. D.J. Qiua,*, H.Z. Wua,b , A.M. Fengc , Y.F. Laob , N.B. Chena, T.N. Xua. *Appl. Surf. Sci.* **222,** 263–268 (2004)

Role of Cerium on Structural and Optical Properties of Lithium Borate and Lithium Aluminium Borate Glasses

Parvinder Kaur[a], Simranpreet Kaur[a], Gurinder Pal Singh[a], Deepawali Arora[a], Sunil Kumar[a], D.P. Singh[a]

[a]*Department of Physics, Guru Nanak Dev University, Amritsar 143005, India*

Corresponding Author e mail: dpsinghdryahoo.com

Abstract- **Melt quench technique has been used to prepare lithium aluminium borate glasses doped with CeO_2 at the expense of Al_2O_3 and lithium borate glasses doped with cerium but without aluminium. An intense fluorescence has been observed when excited at 380 nm which has been attributed to 5d→4f transition of Ce^{3+}. A comparatively more increase in fluorescence intensity and a decrease in band gap have been observed in the samples in which cerium is added at the expense of Al_2O_3 as compared to the samples in which aluminium is absent. The densification of glass network has been studied using density and molar volume calculations.**

Keywords: Optical absorption; Fluorescence; Borate glasses.

INTRODUCTION

Rare earth doped glasses have attracted a great attention of researchers world over for a number of years due to the specific electronic structure of rareearth elements [1]. Cerium doped glasses are used in many practical purposes such as protection of fibre optic materials against radiation, laser active media and scintillating materials [2-5]. It has been accepted that solids, including glasses having Ce^{3+} possess strong optical absorption and fluorescence in near UV and/or visible and infrared range [6]. Trivalent cerium ($4f^1$) holds parity allowed transitions between 4f and 5d electronic configurations. The energy gap between 4f levels and lowest of 5d levels is very large which is helpful for the nonradiative decay to be less probable and hence 5d fluorescence can be observed. In this report, we have tried to put some light on the cerium doped lithium aluminium borate and lithium borate glasses and compared their roles to show that which can give us better spectroscopic and physical properties.

EXPERIMENTAL

Glass samples of composition (i) x CeO_2- (10-x) Al_2O_3- 10Li_2CO_3- 80 B_2O_3 and (ii) x CeO_2- (10-x) Li_2CO_3- 90B_2O_3 with x= 0.5 and1% mole fraction are prepared by melt quench technique. The raw materials of lithium carbonate (Li_2CO_3), aluminium oxide (α-Al_2O_3), borate (B_2O_3) and cerium oxide (CeO_2) in appropriate amounts are mixed and grinded finely to make a batch of 15g. The grinded mixture was melted in silica crucible in an electric furnace for 1 hour at a temperature of 1150^0 C in normal atmosphere until a bubble free liquid was formed. The melt is then dispensed into preheated steel mould and annealed at a temperature of 350^0 C for a time of one and a half hour to remove the internal strains. The samples so prepared are ground with different grades of SiC and polished with
cerium oxide to have maximum flatness. The nominal composition of the prepared glasses is given in Table 1.
Archimedes principle is used to find the density and molar volume (V_m) is calculated by using the formula:
$V_m=\Sigma\, x_iM_i/D$
where x_i is the molar fraction of the component and M_i is its molecular weight.
The fluorescence spectra of the samples are recorded with the help of Perkin-Elmer Fluorescence LS-Spectrophotometer.

Results and Discussion

Density

The density of glass samples is given in Table1. It is clear that an increase in CeO_2 concentration causes a gradual increase in the glass density. The density of glass samples given in series (i) is found to be more than that of series (ii) glass samples. The increase in density indicates that CeO_2 has a contracting effect. An accordingly decreasing pattern of molar volume has also been observed.

UV-Vis Spectroscopy

The Urbach plots between $(\alpha h\nu)^{1/2}$and energy ($h\nu$) have been plotted to determine the optical band gap (as shown in fig. 1). It is clear from Table 1 that the optical band gap decreases (from 3.49 to 2.95 eV) with an increase of cerium oxide content. This is due to the presence of Ce^{3+} or Ce^{4+} ions in the glasses. This can be explained by the reaction Ce^{3+} + HC→Ce^{4+} and Ce^{4+} + EC→Ce^{3+}, where HC is the hole center captured by the cations and EC is the electron centre captured by the anions [7]. The slight shift of band edge of cerium doped glass shows that Ce^{4+} +EC→Ce^{3+} reaction has taken place predominantly. This decrease is more in series (i) glass samples than that of series (ii) glass samples. So it is clear from the above result that the series (i) glasses are showing more

prominent results than the glasses of series (ii) which are in agreement with the density and molar volume calculations.

Fluorescence

The emission spectra of the prepared glass samples are shown in fig.2. The excitation wavelength used is 380 nm. The fluorescence emission of Ce^{3+} is due to transition from one or more of 5d levels to the ^2F ground state. Each emission band is composed of two peaks due to doublet ground state of Ce^{3+} ($^2F_{5/2}$ and $^2F_{7/2}$) with a separation of about 2000 cm^{-1} [8]. In our present study, the emission peaks are present around 455 nm 498 nm which is due to 5d→ $^2F_{5/2}$ and 5d→ $^2F_{7/2}$ transitions of Ce^{3+} respectively. The emission spectra of series (i) and (ii) reveal both the quantitative and the qualitative difference in luminescence intensity. In series (i) luminescence intensity increases with increase in cerium concentration at the expense of aluminium with a slight red shift in first peak i.e. 455 nm. On comparing emission spectra of series (ii) with series (i) we can observe that addition of aluminium results in enhancement of luminescence intensity. From this we may conclude that aluminium helps in maintaining reduced valence state of cerium ions (Ce^{3+}).

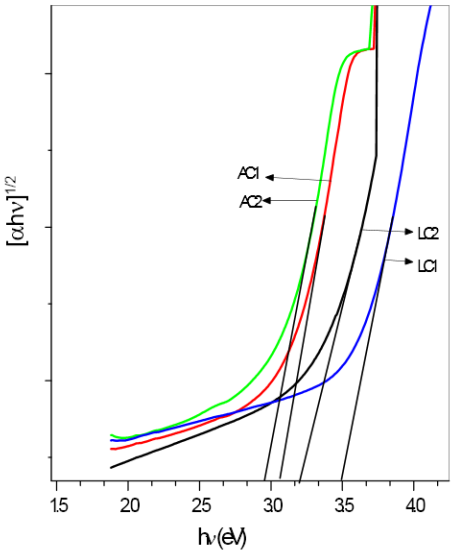

FIGURE 1. Optical Band Gap of the Glass Samples

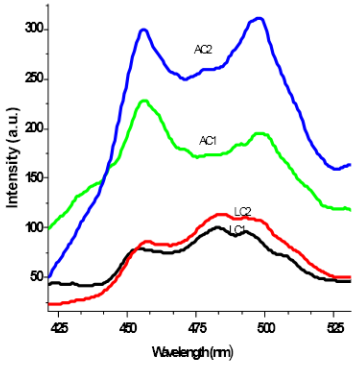

FIGURE 2. Fluorescence Spectra of the Glass Samples

•

Nominal composition (mole fraction), density, molar volume and band gap of the glass samples.

Sample	Density(g/ cm^3)	Molar Volume(cm^3/gm)	Optical band Gap(eV)
(i) LC1(Ce =0.5, Li=9.5)	2.23	31.57	3.49
	2.34	30.32	3.20
(ii) LC2(Ce=1. 0, Li=9.0)			
(iii) AC1(Ce=0 .5, Al=9.5)	3.17	23.21	3.06
(iv) AC2(Ce1.0 , Al=9.0)	3.35	22.11	2.95

REFERENCES

[1] M. L Maczka, L. Stoch, J. Less- Common Met. 166 (1990) 163.
[2] Y. Ishii, K. Arai, H. Namikawa, M. Tanaka, A. Negishi, T. Handa, J. Am. Ceram. Society 70 (1987) 72.
[3] N. Chiodni, M. Fasoli, M. Martini, E. Rosetta, G. Spinolo, A. Vedda, M. Nikl, N. Solovieva,a. Baradli, R. Capelletti, Appl. Phys. Lett. 81 (2002) 4374.
[4] E.J.J. Friebele, Appl. Phys. Lett. 27(1975) 210.
[5] M.V. Korzhik, W.P.J. Trower, Appl. Phys. Lett. 66 (1995) 2327.
[6] M.J. Weber, J. Solid State Commun. 12 (1973) 741.
[7] G. Pal Singh, D.P. Singh, Physica B 406 (2011) 3402.T.P.J. Botden, Philips Res. Rept. 7 (1952) 197

Investigation of Electrical Properties of Polyaniline/Silver Nanocomposite Free Standing Films

Sonika Thakur[a*], Lakhwant Singh[b], Navjeet Kaur[c], Manpreet Kaur[d], and Kusum Devgun[e]
[a]*Department of Physics, Guru Nanak Dev University College Verka, Amritsar, Punjab, India*
[b]*Department of Physics, Guru Nanak Dev University, Amritsar, Punjab, India*
[c]*Department of Physics, Khalsa College for Women, Amritsar, Punjab, India*
[d]*Department of Physics, DAV College, Amritsar, Punjab, India*
[e]*Department of Physics, S.R. Govt. College for Women, Amritsar, Punjab, India*
**Corresponding address-thakur.sonika7@gmail.com*

***Abstract*—This work reports the synthesis and electrical characterization of polyaniline/silver (PA/Ag) nanocomposite free standing films. The dc conductivity measurements in the temperature range of 80-300K, Hall effect studies at room temperature and dielectric measurements of the synthesized films, inferred semiconducting behavior of the samples. Significant improvement in the electrical properties of nanocomposites has been observed and discussed in this manuscript.**

***Keywords*—**Electrical properties, nanocomposites, polyaniline, silver nanoparticles.

I. INTRODUCTION

The study of conducting polymer-metal nanocomposite materials has received much attention in the past few years. It is interesting to observe the improvements in the optical, mechanical and electrical properties of conducting polymers by the incorporation of the metal nanoparticles [1]. These organic-inorganic hybrid materials are found to have numerous applications in several fields such as sensors, catalysis, memory devices etc. Among the various metal nanostructures, silver nanoparticle based composite have been chosen because of their unique optical, electronic, thermal, catalytic, and biocompatible properties. So the aim of proposed investigation is not only to characterize the new materials but also provide complete experimental study of the chosen materials to pave way for their applications in the required fields.

II. EXPERIMENTAL

In the present paper, chemical method has been used to prepare good quality free standing films of pure polyaniline (PA) as well as nanocomposite [2]. Pure polyaniline as well as its nano composite with silver nanoparticles of different concentrations such as 0.30 %, and 1.0 % by weight has been synthesized in the form of free standing films. The dc conductivity measurements of the films were performed by standard four probe method in the temperature range 80-300K using Keithley 2612A System source meter and Lake Shore 340 temperature controller, after making the samples conducting by dipping them in 1M HCL solution. Hall measurements were taken using Ecopia Hall effect measurement system (HMS-3000 VER 3.51.5) at room temperature. Agilent 4285A Precession LCR meter was used for dielectric measurements of the synthesized films at room temperature. Silver paste was used on both sides of samples for making contacts.

III. RESULTS AND DISCUSSION

A. DC conductivity measurements

It is observed from fig. 1 that with increase in the concentration of silver nanoparticles within polymer matrix, the room temperature dc conductivity (σ_{dc}) significantly increases. It is found from conductivity behaviour that Mott's three dimensional (3-D) variable range hopping (VRH) model gives a better fit to the experimental results. The total observed conductivity of PA/Ag films may be correlated with the hopping of electrons along and between the molecular chains. The Mott's parameters, T_0 (energy difference between localized states), R (hopping distance), W (average hopping energy), $N(E_F)$ (density of states at Fermi energy level) are evaluated

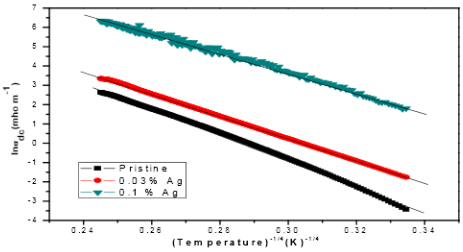

Fig.1 d.c. conductivity (ln σ_{dc}) plotted as a function of $T^{-1/4}$.

using α^{-1}=1.1nm (the coefficient of exponential decay of the electronic wave function of the localized states) and are in good agreement with the values reported earlier [3].

The variation of concentration of silver nanoparticles within polyaniline is justifying the enhancement of conductivity of PA/Ag films. The results are consistent with the Mott's requirement ($\alpha R \gg 1$ and $W \gg kT$) for conductivity by hopping to distant sites. The improvement in electrical conductivity observed in composite material relative to pure PA is due to effective dispersion of Ag nanoparticles in the given polymer matrix [4]. Properly dispersed metal nanoparticles leads to enhancement in the mobility of electrons owing to increased tunnelling probability [5].

B. Hall Effect Studies

As a further test of the electrical conductivity of modified samples, the Hall resistivity as a function of concentration was studied. The results are shown in table I. Parameters $N(E_F)$ (number density of charge carriers), μ (mobility), ρ (resistivity) & R_H (Hall coefficient) obtained from Hall measurements are of the same order as is calculated by dc measurements, indicating a very good corroboration of results.

C. AC conducting measurements

The ac conductivity (σ_{ac}) as a function of frequency at different concentration of silver nanoparticles in polyaniline at room temperature has been studied (not shown here). It is found that σ_{ac} of PA/Ag films increases with frequency as well as with concentration of nanoparticles in accordance with the correlated barrier hopping (CBH) model.

Table I. Evaluation of various parameters from DC conductivity and Hall effect measurements for different PA/Ag films.

Parameters	Pure PA Film	0.30 Ag Film	1.0% Ag Film
T_0(K)	$1.84\text{x}10^{7}$	$1.3\text{x}10^{7}$	$5.9\text{x}10^{6}$
R_{hop} (300K)	6.45nm	5.97nm	4.88nm
W (meV)	102	94	77
$N(E_F)$ $cm^{-3}eV^{-1}$	$8.76\text{x}10^{18}$	$1.2\text{x}10^{19}$	$2.67\text{x}10^{19}$
αR_{hop}	5.86	5.43	4.4
$N(E_F)$	$9.17\text{x}10^{17}$	$7.3\text{x}10^{18}$	$2.07\text{x}10^{19}$
μ	2.55	7.9	5.1
ρ	2.66	0.11	0.08
R_H	6.8	0.85	0.30

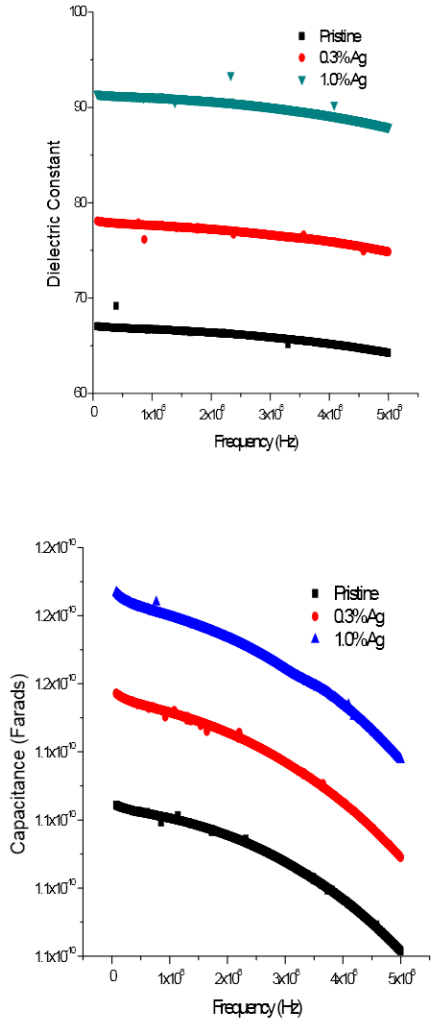

Fig. 2 Plot of (a) dielectric constant & (b) capacitance versus frequency of PA/Ag films.

Fig. 2 shows the dependence of dielectric constant and capacitance respectively on the frequency of the applied field, at different concentration of silver nanoparticles. The dielectric constant remains almost constant for wide frequency range and increases with increase of metal concentration in PA. This behaviour may be due to volume fraction of the charges (electric dipoles) in the interfaces between polymer and metal particles. Charge carriers under electric field can hop readily out of sites with low free energy barriers but tend to 'pileup' at sites with high free energy barriers. This leads to a net polarization of the dipoles and large value of dielectric permittivity [6]. Thus, the dielectric constant of the composites is higher than the pure polymer. As capacitance is directly proportional to dielectric constant therefore similar increasing trend of capacitance is observed with the increase of metal concentration.

IV. CONCLUSION

Polyaniline doped with different concentration of Ag nanoparticles has been prepared by chemical polymerization process. The dc conductivity measurement obeys the 3-D variable range hopping among localized states for non-interacting carriers. The ac conductivity of PA/Ag films increases with frequency as well as with concentration. The parameters obtained directly from hall measurement are in good agreement with that of dc measurements. Thus, the hybrid material has improved electrical conductivity, higher dielectric constant and capacitance, which may make it quite important from technology point of view.

ACKNOWLEDGMENT

Dr. K. Asokan, Scientist F, Inter University Accelerator Centre, New Delhi, has been acknowledged for extending some of the experimental facilities for this research.

REFERENCES

[1] E. Granot, E. Katz, B. Basnar, I. Willner, "Enhanced bioelectrocatalysis using Au-Nanoparticle/Polyaniline hybrid systems in thin films and microstructured rods assembled on electrodes," *Chem. Mater*. , vol. 17, pp. 4600 -4609, Jun. 2005.

[2] K. Gupta, P. C. Jana, A. K. Meikap, "Optical and electrical properties of polyaniline-silver nanocomposite," *Synth. Met.,* vol. 160, pp. 1566-1573, Jun. 2010.

[3] A. B. Afzal, M. J. Akhtar, M. Nadeem, M. Ahmed, M. M. Hassan, T. Yasin, M. Mehmood, "Structural and electrical properties of polyaniline/silver nanocomposites," *J. Phys. D: Appl. Phys.*, vol. 42, pp. 015411-418, Dec. 2008.

[4] R. Singh, A. K. Narula, R. P. Tandon, A. Mansingh, S. Chandra, "Mechanism of charge transport in polypyrrole, poly(N-methylpyrrole) and their copolymers," *J. Appl. Phys.,* vol. 79, pp. 1476-80, Feb. 1996.

[5] A. Choudhury, "Polyaniline/silver nanocomposites: Dielectric properties and ethanol vapour sensitivity," *Sens. and Act. B*, vol. 138, pp. 318-325, Apr. 2009.

[6] S. Shah, N. L. Singh, A. Qureshi, D. Singh, K. P. Singh, V. Shrinet, A. Tripathi, "Dielectric and structural modification of proton beam irradiated polymer composite," *NIM B,* vol. 266, pp. 1768-74, Apr. 2008.

PMMA based polymer gel electrolyte containing $LiCF_3SO_3$

Narinder Arora, Ajay Sharma, Amit Kumar, Rajesh Kumar
P.G. Dept. of Physics, D.A.V. College, Amritsar-143001 (Pb) India
email: n_arora2k@yahoo.com

Abstract **— Effect of polymer (PMMA) and salt ($LiCF_3SO_3$) on the conducting behaviour of polymer gel electrolytes in non-volatile solvent (PC) has been studied. The maximum ionic conductivity (σ = 2.92 mS/cm) of polymer gel electrolyte has been observed at room temperature. An anomalous conducting behaviour observed at small content of PMMA addition in gel electrolyte. Small increase in conductivity observed with increasing temperature (range 10°-70°C); is in factor-wise only, which make these gel electrolytes suitable for many device applications.**

Keywords — Ionic conductivity, polymer gel electrolytes, lithium salt.

I. INTRODUCTION

olymer gel electrolytes are materials of current research Pinterest due to their high ionic conductivity (> 10^{-4} S/cm) comparable with polymer electrolyte. Generally, polymer gel electrolytes belong to the salt-solvent-polymer hybrid system and prepared by immobilizing the salt solution with a suitable polymer matrix. Salt provide ions in solvent, whereas solvent helps to solvate the salt; retained in the electrolyte matrix and polymer provides mechanical stability to gel electrolyte [1-4]. Initial work on the gel electrolytes mainly with lithium salts since 1973 due to their small radii of lithium ion, high ionic conductivity and their use in different solid state ionic devices viz. high density batteries, electrochromic windows, supercapacitors, sensors etc. [5,6]. The conductivity (σ) of electrolyte is generally expressed in terms of the charge concentration (n) and the mobility (μ) of the ions as σ = nqμ, where q is the charge on the mobile species. Polyvinylidenefluoride (PVdF), polymethylmethacrylate (PMMA), polyethylene oxide (PEO), polyvinylidenefluoride-hexafluoropropylene (PVdF-HFP) etc. are some of the polymers commonly used in electrolyte for their jellification [7,8].

In the present research work, PMMA has been used in the synthesis of polymer gel electrolytes containing $LiCF_3SO_3$ as a salt and propylene carbonate (PC) as a solvent. The effect of smaller and higher content of polymer addition on conductivity behaviour of gel electrolyte has also been studied. Variation of conductivity has also been observed with an increase in temperature of polymer gel electrolyte containing $LiCF_3SO_3$ in PC.

II. METHODOLOGY

Polymethylmethacrylate (PMMA) (Aldrich, M_w = 1,20,000), lithium trifluoromethane sufonate ($LiCF_3SO_3$) (Aldrich), propylene carbonate (PC) (Aldrich) were used as the starting materials for the preparation of liquid and gel electrolytes. At room temperature; $LiCF_3SO_3$ in different concentrations (in molarities values) was dissolved in the solvent (PC) to obtain liquid electrolyte and with the gradual addition of PMMA along with continuous stirring at 40°C results in the formation of gel electrolyte. Ionic conductivity of liquid and gel electrolyte was measured with the help of conductivity meter (WTW 3210), which is based upon four probe method and inbuilt temperature sensor.

III. RESULTS & DISCUSSION

Variation of ionic conductivity of liquid electrolyte by dissolving $LiCF_3SO_3$ salt (in different molar ratios) in PC has been observed and as shown in figure 1. The conductivity increases linearly with the smaller addition of $LiCF_3SO_3$, reaches a maximum value and shows a decrease with further addition of salt. At low salt concentrations, salt upon dissociation in liquid electrolyte and provide free ions, results an increase in conductivity and maximum ionic conductivity obtained is 2.81 mS/cm for liquid electrolyte at 0.8 molar concentration of salt.

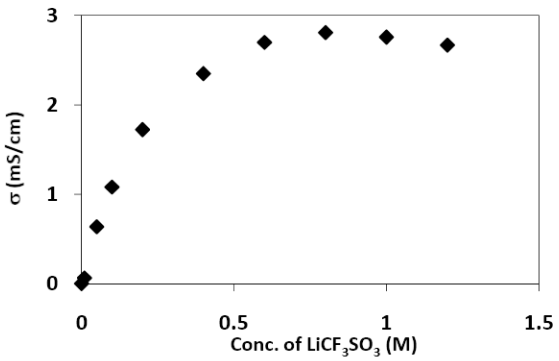

Fig. 1. Variation of conductivity (σ) of liquid electrolytes (PC– xM $LiCF_3SO_3$) with the concentration of $LiCF_3SO_3$ in PC.

But at the higher salt concentration, there is small decrease in conductivity, which may be explained to be due to the formation of ion aggregates.

Gel electrolyte was prepared by adding polymer (PMMA) to liquid electrolyte and results obtained are shown in figure 2.

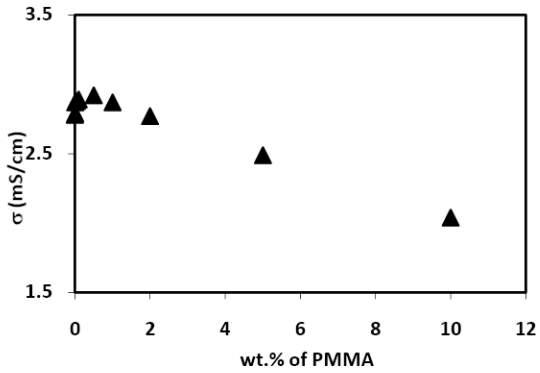

Fig. 2. Change of conductivity of polymer gel electrolyte at different content of polymer.

It has been observed that the conductivity of gel electrolyte containing 1M $LiCF_3SO_3$ increases with the addition of PMMA, reaches a maximum value of 2.92 mS/cm at 0.5 wt. % of PMMA and then decreases to a value of 2.04 mS/cm at 10 wt. % of PMMA. An increase in conductivity of gel electrolyte at small content of polymer may be explained with that the polymer chain is assumed to breathe in and out while it opens or folds occupying different volume in the process, which leads to localized pressure fluctuations assisting either in separating the neutral ion-associated pairs or ''loosen up'' of the viscosity controlled mobility or both resulting in the conductivity increment [10] and this fact has also been observed in our results and as shown in Fig.2. In 1999, Grillone et al have observed an increase in ionic conductivity on jellification of gel electrolyte containing salicylic acid and in 2000, Chandra et al. have suggested a "breathing polymeric chain model" to explain the interaction of polymer with the liquid and gel electrolyte [10,11]. But however the decrease in conductivity is small and by a factor only. A small decrease in conductivity at higher polymer content suggests that the polymer act as a stiffener resulting in an increase in viscosity tend to mobility decreases and hence conductivity.

The conductivity of gel electrolytes was also measured as a function of temperature and the results are shown in figure 3.

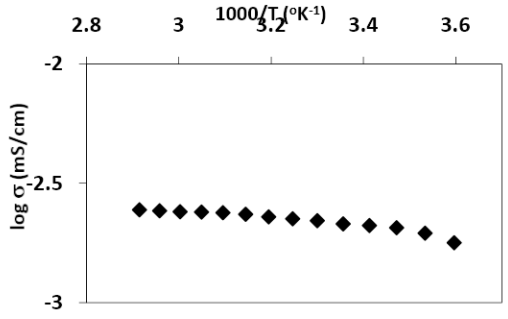

Fig. 3. Variation of conductivity of polymer gel electrolyte as a function of temperature.

Conductivity of PMMA based gel electrolyte increases with increase in temperature and this behavior follow good agreement with theoretical relation $\sigma = \sigma_0 \exp(-\beta/T)$ where β-adjustable parameter, σ_o–constant, T-temperature. Also the increase in conductivity of gel electrolyte with increase in temperature is small and factor-wise only, which make suitable for many device applications [12].

IV. Conclusion

Lithium ion conducting PMMA based polymer gel electrolyte having maximum ionic conductivity at room temperature is 2.92 mS/cm. A small increase in conductivity of gel electrolyte with lower content of polymer has already been explained with "Breathing Polymeric Chain Model" and small decrease in conductivity observed indicates that polymer act as a stiffener only at higher content of polymer. Small increase in conductivity of gel electrolyte with increase in temperature makes them suitable for many device applications.

Acknowledgment

Authors are highly thankful to Dr. K.N. Kaul, Principal, D.A.V. College, Amritsar for help to carry out the experimental work, generous support and valuable suggestions.

References

[1] P.V. Wright, *Br. polym. j.*, 7 (1975) 319.
[2] K.M. Abraham and M. Alamgir, *J. Electrochem. Soc.,* 137 (1990) 1657.
[3] F.M. Gray, "Polymer Electrolytes", *The Royal Society of Chemistry*, Cambridge, 1997.
[4] G. Feuillade, P.H. Perche, *J. Appl. Electrochem.*, 5 (1975) 63–69.
[5] B.B. Owens, *J. Power Sources,* 90 (2000) 2–8.
[6] K.D. Kreuer, *Solid State Ionics,* 97 (1997) 1–15
[7] O. Bohnke, G. Frand, M. Rezrazi, C. Rousselot, C. Truche, *Solid State Ionics,* 66 (1993) 97–104; 105–112.
[8] S.S. Sekhon, Pradeep, S.A. Agnihotry, in: B.V.R. Chowdari, K. Lal, S.A. Agnihotry, N. Khare, S.S. Sekhon, P.C. Srivastava, S. Chandra (Eds.), "Solid State Ionics: Science & Technology", *World Scientific*, Singapore, 1998, p.217.
[9] S.S. Sekhon, N. Arora, S. Chandra, *Eur. Polym. J.*, 39 (2003) 915–920.
[10]S. Chandra, S.S. Sekhon, N. Arora, *Ionics,* 6 (2000) 112–118.
[11] A.M. Grillone, S. Pancro, B.A. Retamal, B. Scrosati, *J. Electrochem. Soc.* Vol. 146 (1) (1999) pp. 27.
[12] I. Basumallick, Pankaj Roy, Abhik Chatterjee, Arup Bhattacharya, Someswar Chatterjee, Susanta Ghosh, *Journal of Power Sources*, 162 (2006) 797–799

Green innovation in technology – A LITERATURE REVIEW

Khushal khera, Gaurav Adlakha, Shailesh Mahawal
Mechanical Engg. Dept(Students)
Echelon Institute of Technology
Faridabad, Haryana
kushkhera92@gmail.com, gaurav16adlakha@gmail.com, shaileshmahawal@gmail.com

Abstract: **The importance of green innovation management is growing in practice. Environmentally benign manufacturing has become one of industry's greatest challenges from engineering, business and marketing perspective. Green manufacturing is a method for manufacturing that minimizes waste and pollution. The goals of green innovation technology are often achieved through process and product design.In this study we will also discuss over the three life cycle approaches to green product design:Design for reuse: this refers to designing of products so that they can be used in later generations.Design for disassembly: it is a method for developing products so that they can be taken apart easily. Design for re-manufacture: it is a method for developing products so that the parts can be used in other products.The paper stimulates discussion about the adequacy of research in this subject area (managing green innovation) and the dearth of comprehensive literature reviews. 'Green manufacturing' also involves product recovery activities. The former reflects on various operations, that can be directly converted into usable ones.. The various types of such activities like remanufacturing, recycling, etc. In our country, the 'Green manufacturing' concept is still young. However, the inherent scarcity of natural resources is creating motivation to make it a field of active research. The government has extensive plans to market Indian manufacturing as Green to make it stand apart from Chinese and US products that are energy-intensive. Thus, adoption of Green Manufacturing techniques reduce energy consumption, and promote development but not at the cost of environment.**

Keywords: Green innovation, Eco innovation, Environmental innovation, Sustainable innovation.

I. INTRODUCTION:

The term "Green Technology" is also used to describe sustainable energy generation technologies such as photovoltaic, wind turbines, bioreactors, etc. The Green technology is also used to describe a class of electronic devices that can promote sustainable management of resources. Green, renewable energy is already a major component of energy production in India. From the ancient period, the importance of management of green innovations is growing in practice. The research based on green innovations is divided into six sections i.e. in the first section we present different definitions for the following notions around the concept of green innovations including ecological innovations, environmental innovations, green innovation and sustainable innovations. These definitions are further discussed and compared to create an understanding of similarities and differences in this conceptualisation. In the second section, the results from a quantitative analysis of the available literature under the above given notions are provided, the third section describes our research approach to analyse the data for our literature review, in the fourth section we present our finding of our quantitative analysis, in the fifth section a brief overview and discussions of our findings of our quantitative analysis is done, the conclusion of the paper including the future research are concluded it the sixth section. To attain the goal of sustainable development, green innovation can raise resource productivity efficiently and decrease pollution effectively. Green innovation has become one of the most important strategic tools in manufacturing industry under the new environmental era.

II. THE CONCEPT OF GREEN INNOVATION:

The basic notions of the green innovation in technology are ecological innovation, environmental innovation, green innovation and sustainable innovation are used in this research. A clarification of the concept of green innovation was required to understand which literature

must be included in our analysis so this process is carried out before reviewing the literature part .the following definitions of the above mentioned notions are described as follows

i. SUSTINABLE DEVELOPMENT:

Meeting the needs of the present without compromising with the ability of future generations is termed as sustainable development. In 1980 the term "sustainable development" was first used by the International Union for Conservation of Nature (environment) and Natural Resources in their World Conservation Strategy report. This report defines sustainable development as "the integration of conservation and development of natural resources to ensure the modifications in securing the survival and well-being of all people." Open Sustainability innovation uses open innovation in the development of sustainable products, services and initiatives.

Sustainable innovation is an approach to marketing for companies which may prove to be advantageous. As a result of the conversational relationship between companies and consumers ideas about the importance of sustainability and how people relate to this through consumption can arise.

ii. ECO–INNOVATIONS:

A large variety of definitions exists for "eco – innovation". Fussler and James (1996) define eco-innovations as "new products and processes which provide Customer and business value but significantly decrease environmental impacts" (cited From Bartlett and Trifilova (2010: 2)) .eco-innovation is "the production exploitation of the product with production process followed by service or management or business method Which results in throughout its life cycle, in a Reduction of environmental danger, pollution and other bad impacts of resources use (including energy use) compared to other relevant substitutes. Eco-innovation is about the fluctuation, consumption and production styles and market uptake in technologies of products and services to eliminate our impact on the environment.

But it is not just the environment that stands to gain from eco-innovation. Every year, there is an increase in the world market for environmental products & services with the exploitation of new markets. The Europe INNOVA panel

concludes that "eco-innovation means the creation of novel and competitively priced goods, processes, systems, services, and procedures that can satisfy human needs and bring quality of life to all people with a life-cycle-wide minimal use of natural resources (material including energy carriers, and surface area) per unit output, and a minimal release of toxic substances" (cited from Reid and Miedzinski (2008: 7)). In comparison to the eco-innovation definitions, Oltra and Saint Jean (2009: 567) define environmental innovation "as innovations that consist of new or modified processes, practices, systems and products which benefit the environment and so contribute to environmental sustainability.

iii. GREEN INNOVATION:

'The creation or implementation of new, or significantly improved, products (goods and services), processes, marketing methods, organisational structures and institutional arrangements which the creation of novel and competitively priced goods, processes, systems, services, and procedures that can satisfy human needs and bring quality of life to all people with a life-cycle-wide minimal use of natural resources (material including energy carriers, and surface area) per unit output, and a minimal release of toxic substances' (Reid and Miedzinski, 2008) – with or without intent – lead to environmental improvements compared to relevant alternatives' (OECD, 2009).

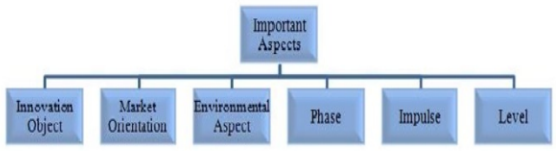

We found out the six important factors/aspects in the different definitions and they are firstly, innovation object which deals on product, services and methods. secondly we like to mention about the market orientation which deals in satisfying needs to be competitive to withstand the market, thirdly its about environmental aspects, says it reduces the negative impact which means zero impact .fourth point says about the phase which depicts about the full life cycle (for material flow reduction).in fifth point it depicts about the intention for reduction in impulse may b considered economical or ecological. Last part tell

about the level, setting up a new innovation standard to the company

III. Literature view:

The term "sustainable development" was first used in 1980 by the International Union for Conservation of Nature and Natural Resources in their World Conservation Strategy report. The report defines sustainable development as "the integration of conservation and development to ensure that modifications to the planet do indeed secure the survival and well-being of all people. In 1987 the concept of sustainable development does imply limits - not absolute limits but limitations imposed by the present state of technology and social organization on environmental resources and by the ability of the biosphere to absorb the effects of human activities (Brundtland, 1987: 24).

As stated in several publications (e.g. Mebratu (1998), Dixon and Fallon (1989)), the notion of "sustainable development" was essentially coined by the Brundtland report, commissioned by the UN where it is defined as meeting the needs of the present without compromising the ability of future generations to meet their own needs. One of the first, Fussler and James (1996) define eco-innovations as "new products and processes which provide customer and business value but significantly decrease environmental impacts"

In 2002, to define the notion 'green innovation' Driessen and Hillebrand (2002: 344) apply "a rather pragmatic definition" stating that it "does not have to be developed with the goal of reducing the environmental burden" .In 2006,Chen, Lai et al. (2006: 534) define green innovation "as hardware or software innovation that is related to green products or processes, including the innovation in technologies that are involved in energy-saving, pollution-prevention, waste recycling, green product designs, or corporate environmental management". In 2007 in a similar manner Kemp and Pearson (2007: 3) define eco-innovation as "the production, assimilation or exploitation of a product, production process, service or management or business method that is novel to the organization (developing or adopting it) and which results, throughout its life cycle, in a reduction of environmental risk, pollution and other negative impacts of resources use (including energy use) compared to relevant alternatives".
In 2008, based on the industrial dynamics perspective Andersen (2008: 5) defines eco-innovation "as innovations which are able to attract green rents on the market. In 2009, building on these two definitions Arundel and Kemp (2009: 34) conclude that eco-innovation is "a new concept of great importance to business and policy makers. It is about innovations with lower environmental impact than relevant alternatives."

IV. DISCUSSION

This paper shows that the concept of green innovation is closely related to three other notions that is sustainable innovation, innovation and ecological innovation. A minor conceptual difference was found while comparing the various definitions for these four notions. We identified six aspects (i.e. innovation object , market orientation , environmental aspects, phase, impulse and level).that are incorporated in different definitions and found one key aspect that differentiates the conceptualization of sustainable innovations from the other three notions. In its original meaning, sustainable innovation includes a social dimensions as well as ecological dimensions. Across the three other notions, ecological innovations seem to be the most precise and well developed concept, where as green innovations remain rather shallow .but if we compare all the four notions, sustainable innovation is desired.

Environmental innovation	Sustainable innovation
The most common usage of the term "eco-innovation" is to refer to innovative products and processes that reduce environmental impacts	Sustainable development is an organizing principle for human life on a finite planet. It posits a desirable future state for human societies in which living conditions and resource-use meet human needs without undermining the sustainability of natural systems and the environment, so that future generations may also have their needs met.
This is often used in conjunction with eco-efficiency and eco-design. Leaders in many industries have been developing innovative technologies in order to work towards sustainability. However, these are not always practical, or enforced by policy and legislation.	"Sustainable development is development that meets the needs of the present without compromising the ability of future generations to meet their own needs."

V. CONCLUSION:

Through this paper we have found that different notions provide reduced environmental impact in the innovations. The main focus of current research has shifted from green and environmental innovations to sustainable innovations. Most of the available definitions in the field of green innovations are focused on economical and ecological intended innovations. The further research is required for the classification of green innovations. The future research can place emphasis on two levels: at first level defining and analyzing the related problems thoroughly on a smaller scale and at the second level comparing the ecological innovations from different firms and sectors to build a theory on meso or macro level.

VI. REFERENCES:

[1] Andersen, M. M. (2008). *Eco-innovation–towards a taxonomy and a theory*. 25th Celebration DRUID Conference 2008 on Entrepreneurship and Innovation - Organizations, Institutions, Systems and Regions, Copenhagen, Denmark.

[2] Arundel, A. and R. Kemp (2009). Measuring eco-innovation. United Nations University - Maastricht Economic and Social Research and Training Centre on Innovation and Technology. Maastricht, UNU-MERIT #2009-017.

[3] Bartlett, D. and A. Trifilova (2010). "Green technology and eco-innovation: Seven casestudies from a Russian manufacturing context." *Journal of Manufacturing Technology Management* 21(8): 910-929.

[4] Brundtland, G. H. (1987). Report of the World Commission on Environment and Development: Our Common Future. World Commission on Environment and Development. New York, United Nations.

[5] Chen, Y. S., S. B. Lai and C. T. Wen (2006). "The influence of green innovation performance on corporate advantage in Taiwan." *Journal of Business Ethics* 67(4): 331- 339.

[6] Dixon, J. A. and L. A. Fallon (1989). "The concept of sustainability: origins, extensions, and usefulness for policy." Society & Natural Resources 2(1): 73-84.

[7] Driessen, P. and B. Hillebrand (2002). Adoption and diffusion of green innovations.

[8] Fussler, C. and P. James (1996). *Driving eco-innovation: A breakthrough discipline for innovation and sustainability*, Pitman London.

[9] Kemp, R. and P. Pearson (2007). Final report of the MEI project measuring eco innovation. Brussels, DG Research of the European Commission, Eurostat, the European Environment Agency (EEA) and the Joint Research Center (JRC) of the European Commission.

[10] Mebratu, D. (1998). "Sustainability and sustainable development: Historical and conceptual review." Environmental Impact Assessment Review 18(6): 493-520.

[11] OECD (2009). "Sustainable Manufacturing and Eco-innovation: Towards a Green Economy." OECD Observer(June).

[12] Oltra, V. and M. Saint Jean (2009). "Sectoral systems of environmental innovation: an application to the French automotive industry." Technological Forecasting and Social Change 76(4): 567-583.

[13] Reid, A. and M. Miedzinski (2008). Eco-innovation Final Report for sectoral innovation watch. Brussels, Technopolis Group.

Biomimetic Materials –the Future Need

Parveen Kumar[a], Shailesh Mahawal[b]
[a]faculty, [b]Student
Echelon Institute of Technology, Faridabad, India
E-mail: ssharma.parveen@gmail.com[a] , shaileshmahawal@gmail.com[b]

***Abstract*-The review of the multi-millennia long history of human civilisation indicates that the significant increase of the level of living and production is connected more often with the launching of new material groups with the properties better and better adjusted to real requirements of customers getting more sophisticated nearly each day. The given reasons enable to forecast that the future of the market and products with the required properties, which appear on the market, are inseparably connected with the development of materials science and engineering. The fundamental aim of materials science and engineering is materials selection ensuring required functions and application properties of products, which are manufactured out of them. Better understanding of the development of minerals and composites by the live organisms, biomimetic materials become the fast developing area of materials engineering, enabling to copy the biological processes and materials, both organic and inorganic ones (e.g., synthetic spider's thread, DNA chips, crystal growth within the virus crates) and are manufactured more and more accurately and efficiently, due to which their usefulness improves and new possibilities of their use become apparent (e.g., self-repair feature, ultra-hard and ultra-light composites for airplanes)**

Keyword:-Biomemetics, hydrophobicity, Anti reflective Nano materials

1. INTRODUCTION

The field of science and engineering that seeks to understand nature as a model for copying, adapting and inspiring concepts and designs is now mostly called Biomimetic. As a model for inspiration, it is important to remember that Nature's solutions are the result of the survival of the fittest and these solutions are not necessarily optimal for the required function. Many of Nature's materials and processes are far superior to man-made ones where the sea shells and the spider web are examples of such materials and structures .Natural materials like wood and bone have been used in structural applications throughout the history of the human race. Biomimetics first appeared in ancient times when natural materials and structures were replicated using artificial materials like metals and ceramics. In more recent times biomimetic materials have found applications in medicine where artificial materials have been developed that to some degree replicate the tissues they replace. Currently, the advent of nanotechnology and advances in our understanding of biological systems has enabled the methods of biological synthesis and assembly to be applied in material fabrication. This has greatly expanded the range of materials and the range of applications to which biomimetics is applicable.

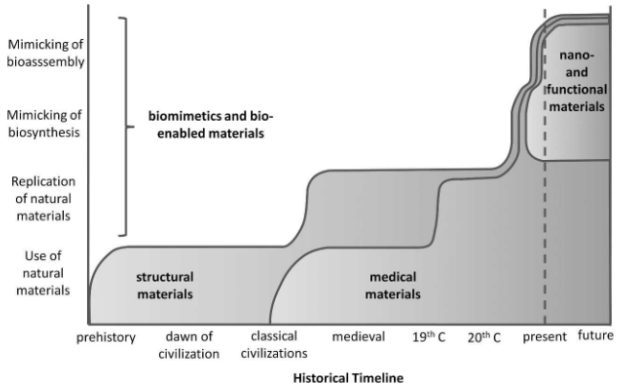

Fig.1:-Historic Development

The use of natural materials for human applications can be traced back many thousands of years and it includes the silk, bones, leather, fur, ivory and many others [12]. As a result of the recognition of these materials advantages there has been an ever-increasing need for supply and it led to the development of artificial versions. Besides their immediate use for thermal protection, food, cleaning, beauty, construction, etc., natural materials have other important capabilities many of which we don't know how to mimic. It is interesting to note that natural materials are normally produced in ambient conditions and their fabrication generates minimum waste, where the result is biodegradable and is recycled by nature. Learning how to systematically mimic nature's materials and fabrication processes will dramatically expand our capabilities and choices as well as improve our ability to recycle materials and protect the environment. Also, it can benefit humans in many other ways including the development of more life-like prosthetics as well as artificial hips, teeth, structural support of bones and others. Biological structures are made either as an integral part of the body, including the bones, shells, and nails; or made by them to support the life essentials including bird nests, cocoon shells, spider web, and underground tunnels. These structures have numerous advantages such as resilience, multi-functionality, and great fracture toughness. The spider, bees and beaver are examples of creatures that produce

amazing structures and demonstrate great engineering skill. The spider creates large flat webs; the beavers construct large habitats on water streams and the bees produce the honeycomb that is a highly efficient packing configuration for laying their eggs with nurturing material (the honey) for their off-springs [13]. The honeycomb structure is also made by humans and it is widely used to create aircraft structures benefiting from the low weight and high strength.

2. HISTORY OF BIOMIMETICS RESEARCH

The term "biomimetics" (in Japan, the term is translated literally as "Imitation of Living Things") was proposed by German-American neurophysiologist Otto Schmitt in the latter half of the 1950s. In the 1970s, biomimetics research came along in the fields of chemistry, as "Biomimetic Chemistry," aiming at molecular-level emulation of enzymes and biomembranes. The artificial photosynthesis research that became active in the 1980s laid the foundation for dye-sensitive solar cells, and the actuator research, using gel, brought about such inventions as synthetic muscles. Entering the 1990s, in spite of the prevalence of the idea "Learn from Living Things," the opportunities for linkage with biology, in effect, almost disappeared. Even the term "Biomimetic Chemistry," which represented an academic field, became almost extinct in the wake of the shift of focus toward molecular nano-technology and nano-biology.

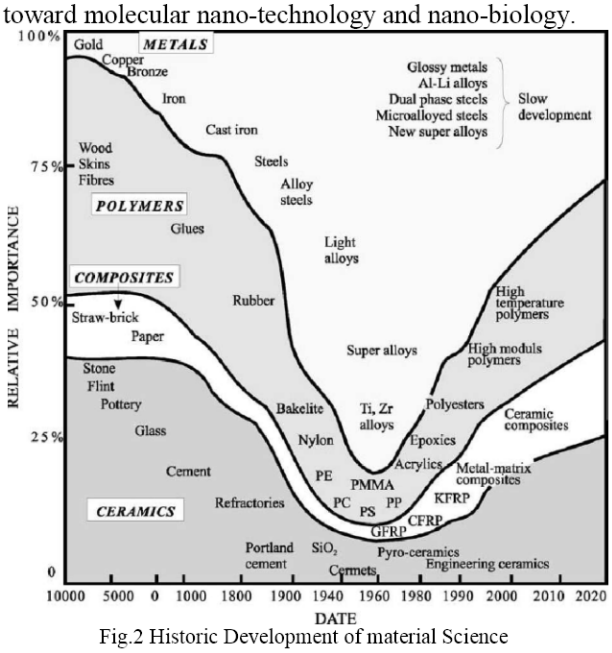

Fig.2 Historic Development of material Science

In contrast, the material research, or
new generation biomimetics, are considered to have been created through collaborations among natural history, biology, and material nano-technology, where electron microscopy and microfabrication technology provided the common platform. The characteristics of nano-technology in Europe are symbolized by the term "Nano meets Bio."

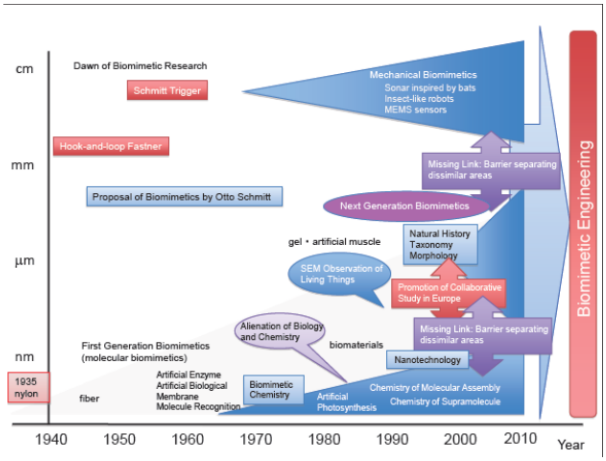

Figure 3: History of Biomimetics Research

3.APPLICATION OF BIOMIMETICS MATERIAL

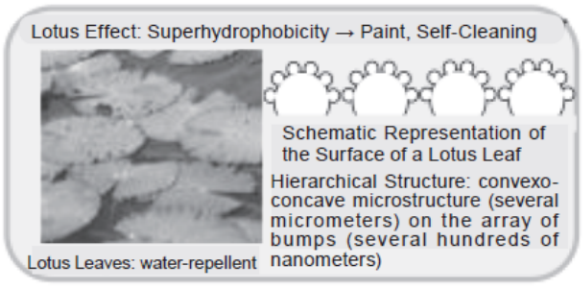

Fig. 4 Lotus Effect: Self cleaning

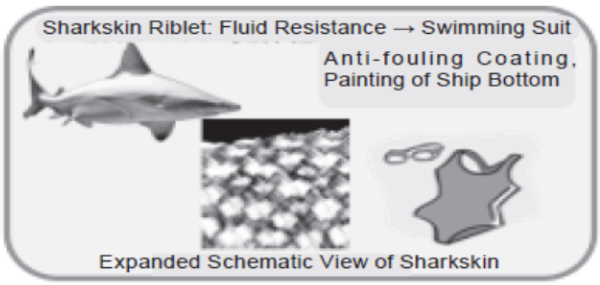

Fig. 5 Sharkskin Riblet :Fluid resistance

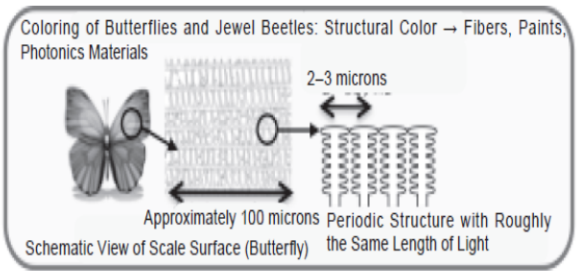

Fig. 6 Colouring of Buterflies: Structural Colour

Fig. 7 Gecko's Finger: Adhesive Hair

Sr. No.	Concept name	Concept Detail	Application
1	Lotus Effect	Super hydrophobicity	Paint, Self-Cleaning
2	Sharkskin Riblet	Fluid Resistance	Swimming Suit, Ant i - foul ing Coat ing, Painting of Ship Bottom
3	Coloring of Butterflies and Jewel Beetles	Structural Color	Fibers, Paints, Photonics Materials
4	Gecko's Finger	Adhesive Hair	Adhesive Materials
5	Moss Eye	Anti-reflective Structure	Anti-reflective Films, Photonics Materials

Table 1: Application of Biomimitics Material

4. CONCLUSION:-

Biomimetics is not a new way of adapting ideas from biology, but it is currently empirical in its approach. If it is to build on current successes, and to be able to serve our technological society, then it needs some sort of regularizing, best introduced as a set of common principles. The benefits to be gained
from biomimetics are not yet totally obvious, other than to deepen the human race's box of technical tricks. However if, biological functions and processes are less reliant on energy, then the implications could be very significant. That this change in our approach to technology and engineering could be achieved by developing nanotechnology. At the beginning of the 21st century, it is fair to say that biomimetics is ancient in its origin, but modern in terms of its potential applications and use. This area of materials research is set for rapid expansion in coming years, and this will result in substantial technological advances.

5. REFERENCES:-

[1] http://www.otto-schmitt.org/
[2] D. Ishii, H. Yabu, M. Shimomura,"Novel Biomimetic Surface Based on a Self-Organized Metal-Polymer Hybrid Structure," Chem. Mater., 21(9), 1799–1801. 2009.
[3] F. Xia, L. Jiang, "Bio-Inspired, Smart, Multiscale Interfacial Materials," Adv. Mater., 20(15), 2842–2858. 2008.
[4] T. Hariyama,"Structural Colors in Fish," Structural Colors in Biological Systems – Principles and Applications– (edited by S. Kinoshita and S. Yoshioka), Chapt. 5. Osaka University Press, 2005.
[5] L. Feng, Y. Zhang, J. Xi, Y. Zhu, N. Wang, F. Xia, L. Jiang, "Petal Effect: A Superhydrophobic State with High Adhesive Force," Langmuir, 24(8), 4114–4119. 2008.
[6] D. Ishii, H. Yabu, M. Shimomura,"Novel Biomimetic Surface Based on a Self-Organized Metal-Polymer Hybrid Structure," Chem. Mater., 21(9), 1799–1801. 2009
[7] M. Sitti, R.S. Fearing,"Synthetic gecko foot-hair micro/nano-structures as dry adhesives," J. Adhesion Sci. Technol., 17(8), 1055–1073. 2003.
[8] Boncheva, M.; Gracias, D.H.; Jacobs, H.O.; Whitesides, G.M. Biomimetic self-assembly of a functional asymmetrical electronic device. Proc. Natl. Acad. Sci. U. S. A. 2002, 99, 4937–4940.
[9] J.M. Benyus, Biomimicry Innovation Inspired by Nature, HarperCollins Publishers, New York, 1997, p. V.

[10] Compiled from http://database.biomimicry.org/
[11] http://people.bath.ac.uk/en2ral/biomimeticprocess.html, accessed April 5, 2007.
[12] Bioinspired materials for self-cleaning and self-healing. MRS Bull., 33(8) (2008).
[13] Biomolecular mimetics. *MRS Bull.* 33(5) (2008).
[14] *Biological Materials to Biomimetic Material Synthesis*, edited by N. Kröger, R. Qiu, R. Naik, and D. Kaplan (Mater. Res. Soc. Symp. Proc. 1094E, Warrendale, PA, 2008).
[15] Benyus J. M., *Biomimicry: Innovation Inspired byNature*, Perennial (HarperCollins) Press, New York, NY, 1998,pp. 1-302.
[16] Bar-Cohen, Y., *Biomimetics - Biologically Inspired Technologies*, CRC Press, Boca Raton, FL, 2005, p. 1-527.

Characterization and gas sensing properties of surface modified Indium Oxide films.

Amandeep Kaur Bal
Department of Applied Sciences, Amritsar College of Engineering and Technology, Amritsar, India

***Abstract*-Indium Oxide (In_2O_3) films have been prepared by thermal oxidation of pre deposited Indium films onto glass substrate kept at room temperature (35 °C). These films were dipped into an aqueous solution (0.1 M) of Sulphonated Copper Phthalocyanine (TsCuPc) followed by being fired at 500 °C. Based on X-ray diffraction and Field emission scanning electron microscopy results it has been observed that modification of pure film in results in deterioration of crystalline character. The gas sensing studies show increase in gas sensing response towards acetone**

Keywords: Dipping; Microstructure; UV-visible spectroscopy; Gas sensing.

1. INTRODUCTION

While synthesizing TCO materials, it is a common practice to introduce impurities using various techniques to modify structural, electrical and optical properties. For example Li, Sn, Fe, As and F have been doped in In_2O_3 using chemical synthesis, VLS, reaction route, laser ablation process and magnetron sputtering, respectively [1-5]. Among various techniques used, the coating of nanoparticles using dipping technique has been used by some research groups to enhance the surface, chemical and physical properties of nanomaterials. Depending on both the concentrations of additives and crystallization parameters, a simultaneous structural modification of the base oxide can take place which involves change in grain size, appearance of second phase and change of electrophysical and surface properties. There are examples in which dipping technique has been followed to modify the surface and to enhance the gas sensing performance of semiconducting films. The effect of various surface doping elements on the electrical and gas sensing properties of indium oxide thick film sensors was investigated by D. Sanders and U. Simon[6]. Surface modification of ZnO nanoparticles is also done to improve the compatibility between inorganic nanoparticles and organic matrix[7] and to enhance gas sensing responses [8-10]. Gas sensing properties of SnO_2 and BSST based thick films has been enhanced by modifying their surface using $PtCl_2$ and Al_2O_3 [11, 12]. However, there is lack of studies about the effect of impurities introduced by dipping technique in indium oxide. In this manuscript we focus on the structural, optical and acetone sensing properties of pure and modified indium oxide films. The modification of pure films is done by dipping them into aqueous solution of Sulfonated copper phtalocyanine (TsCuPc), followed by firing at 500 °C.

2. EXPERIMENTAL

Indium (In) films were deposited on the corning glass substrate kept at room temperature at pressure of 10^{-5} torr using thermal evaporation technique. The thickness of the film was determined by depth profiler (Dektak 3030 XT) which was found to be 0.3 μm. The films were then thermally oxidized in air at 500 °C to form pure In_2O_3. The dipping technique was adopted to incorporate TsCuPc into thermally oxidized In_2O_3 films. The In_2O_3 films were dipped into a 0.1 M aqueous solution of TsCuPc for 2, 5 and 10 minutes. These films were then fired at 500 °C.

The X-ray diffractograms (XRD) pattern of pure and modified films were taken using Cu Kα (wavelength-1.5405 A°) radiation in range 0-60° by XPERT-PRO diffractometer. Surface topography of films was analyzed using field emission scanning electron microscopy (JEOL JSM 6700 FESEM) with beam voltage 25 kV. The optical gap (Eg) were deduced from absorption spectra using the relation $(\alpha h\nu)^2 = A(h\nu - E_g)$.

The acetone sensing properties of pure and modified Indium oxide films were measured at room temperature (35 °C) using laboratory built apparatus consisting of a sealed chamber having inlet and outlet ports. During gas-sensing measurements, the outlet port was closed and acetone was injected into the chamber through inlet port. Sensing characteristics of the sensor were then studied by measuring the variation in electrical resistance using Keithley electrometer (6517) as a function of time.

3. RESULTS AND DISCUSSION

3.1 Structural Characterization

The growth, orientation and crystallite size in pure and modified In_2O_3 films have been evaluated by XRD as shown in Fig.1. XRD of pure film has five peaks corresponding to 2θ ranging from 20° to 60°. Results indicate that maximum intensity is exhibited by 222 plane corresponding to 30.58°. The 211, 400, 332, and 440

planes at 21.52°, 35.47°, 41.8° and 50.99°, respectively, of comparatively low intensity are also obtained. These peaks are characteristic of In_2O_3 crystallites with bcc structure according to the ASTM card no. 6-0416.

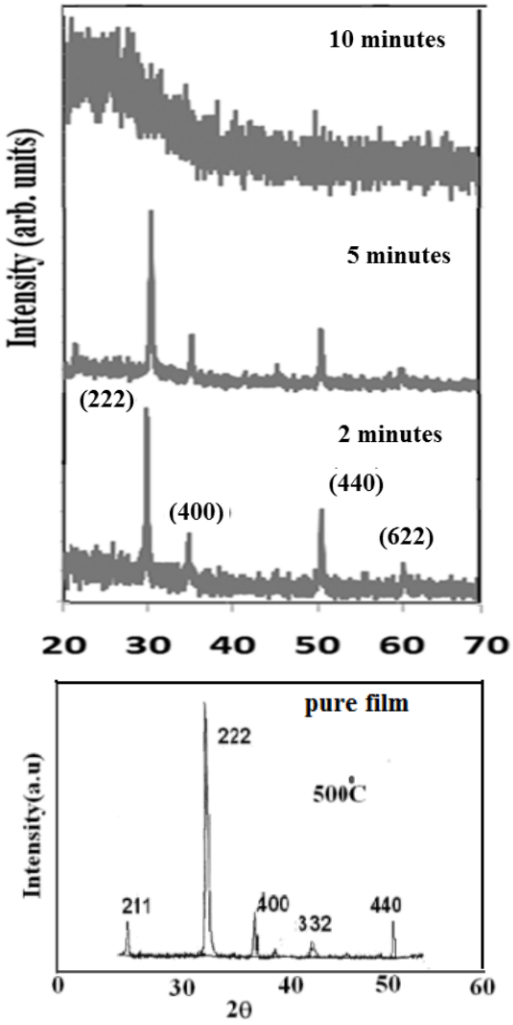

Fig.1. X-ray diffraction curve for puuPc modified In_2O_3 film.

The crystallite size is calculated from the (FWHM) of (222) peak using the Scherrer's formul [13]

$$D = \frac{0.9\lambda}{\beta \cos\theta} \quad (2)$$

where β is FWHM of most intense peak and λ is the wavelength of CuKα radiation (1.542 A °). The film dipped for 2 minutes is polycrystalline, and exhibit (222), (400), (440) and (622) peaks. The relative intensities of these peaks decrease after dipping the In_2O_3 film for 5 minutes in aqueous solution of TsCuPc. After dipping for 10 minutes, the films appear to be amorphous. Thus sulfonated copper phthalocyanine tends to destroy the crystalline phase of indium oxide.

Fig. 2 FESEM reveals the spherical morphology of particles, which are highly agglomerated. Inspection of other two images revealed the deteriorated crystallanity of films. Therefore, FESEM results confirm the same trend seen in XRD analysis.

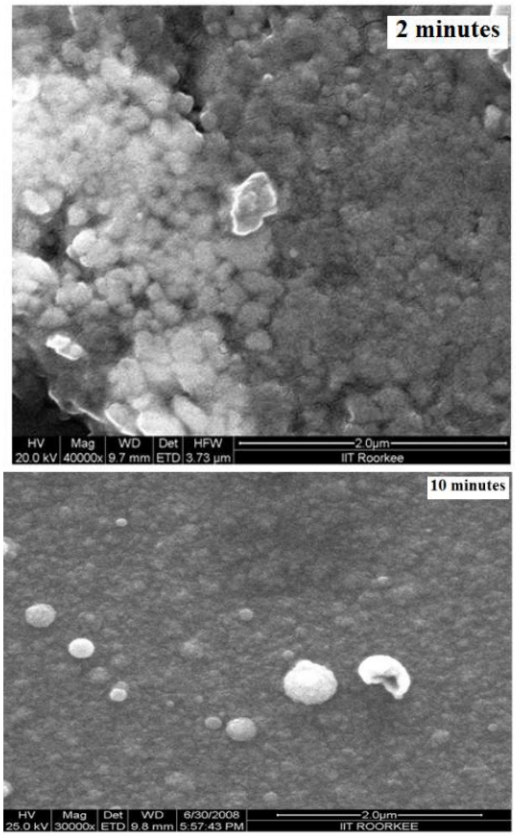

3.2 Optical properties

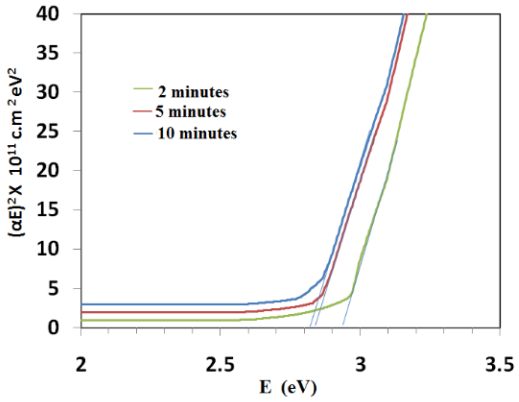

Figure 3 Plot of $(\alpha E)^2$ versus E for modified films

The absorption coefficient of the films has been determined over the energy range 1.2-4.5 eV. The absorption edge of modified In_2O_3 films is examined in terms of a direct transition using the equation of Bardeen et al. [14] stating that

$$(\alpha h\nu)^2 = A(h\nu - E_g)$$

Extrapolation of the linear portion to αhν =0 gives the value of optical band gap under direct allowed transition for pure and modified films **Figure 3** shows the plot of $(\alpha E)^2$ versus E for TsCuPc modified In_2O_3 films. There is a decrease in optical band gap of pure In_2O_3 films after modification with TsCuPc.

3.3 Response to Acetone gas

The acetone response of pure and modified In_2O_3 films has been determined using the relation

$$\frac{R_a - R_g}{R_a} X100$$

Here R_a and R_g are the resistances of sensor in air and in presence of ammonia, respectively.

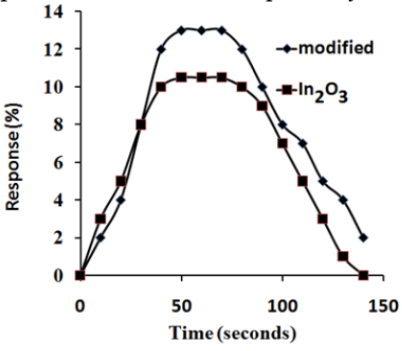

Figure 4. Response of pure and TsCuPc modified In_2O_3 film to 50 ppm of acetone.

The gas sensing studies show that modification of the surface of indium oxide films by TsCuPc also increased the response for acetone vapors. For pure and In_2O_3 film surface modified by dipping for 2 minutes in aqueous solution of TsCuPc, the response values are 8.5 and 13% respectively, shown in **figure 4**. The response does not show any significant improvement in values in case of films modified by dipping for 5 and 10 minutes. This is attributed to dense microstructure and deteriorated crystalline quality of films due to which there could not be effective diffusion of analytic gas through the film. These films also do not show any improvement in response values for other gases like ammonia and ethanol gases.

Two facts could be responsible for such an attitude of these films. When a a p type organic semiconductor like Sulfonated copper phthalocyanine is added in n-type In_2O_3, it may form some pn junctions in the sensing material giving rise to a positively charged depletion layer on surface. This will cause lowering of activation energy and enthalpy of physisorption for vapors with good electron donating characteristics. When the sensor is exposed to a volatile organic base like acetone, its molecules may diffuse into the interface of the p-n junction, and lead to variations in the sensor performance[15]. Since acetone is electron donor, it is also possible that a schottky barrier is also formed and p-n hetrojunction is destroyed, leading to obvious resistance changes in resistance of sample. Similar explanation is given by Y. H. et. al.[16] for CuO-ZnO hetrojunctions for H_2S gas. We can also explain the highest sensitivity of acetone in light of dipole interactions. The organic layer of TsCuPc is polar in nature. A. Kumar et. al.[17] also explained this fact while discussing the chlorine gas sensing property of sulfonated copper phthalocyanine films. Ethanol and ammonia has lesser dipole moment than acetone. As a consequence, the interaction between the organic layer and acetone molecules could be much stronger than any other gas, leading to the observed senstivity to acetone. L. Wang et. al. also gave a similar type of reason while explaining the selectivity of acetone towards WO_3 nanoparticles[18]

4. CONCLUSION

XRD analysis revealed that pure and modified In_2O_3 films are polycrystalline in nature with 222 plane having maximum intensity. FESEM micrographs shows small and large crystallites dispersed on pure modified In_2O_3 film surface which changes into agglomeration as time of dipping increases. There is a decrease in optical band gap of pure In_2O_3 films after modification with TsCuPc. The gas sensing studies show that modification of the surface

of indium oxide films by TsCuPc also increased the response for acetone vapors.

REFERENCES

[1] M. Sasaki, R. Kiyoshimaa, S. Kohikia, S. Matsushimab, M. Okuc, T. Shishido, *J. Alloys Compd*. **322** 220 (2001).
[2] S. Y. Li, C. Y. Lee, P. Lin, T. Y. Tseng, *Nanotechnol.* **16** 451 (2005).
[3] D. Berardan, E. Guilmeau, *J. Phys.: Condens. Mater*, **19** 236224 (2007).
[4]. P. C. Chen, G. Shen, H. Chen, Y. Ha, C. Wu, S. Sukcharoenchoke, Y. Fu , J. Liu, A. Facchetti, T. J. Marks, M. E. Thompson, C. Zhou, *ACS Nano*. **3** 3383 (2009).
[5] Y. Shigesato, N. Shin, M. Kamei, P. K. Song, I. Yasui, Jpn. *J. Appl. Phys*. **39** 6422 (2000).
[6] Sanders D. and Simon U., *J. Comb. Chem*. **9** 53 (2007).
[7] Hong R., Pan T., Qian J., Li H., J. Chem. Eng. **119** 71 (2006).
[8] D. R. Patil, L. A. Patil, G. H. Jain, M. S. Wagh, S. A. Patil, *Sens. Transd*. **74** 874 (2006).
[9] D. R. Patil and L. A. Patil, *Sens. Actuators B*. **123** 546 (2007).
[10] D. R. Patil and L. A. Patil, *IEEE sens*. **7** 434 (2007).
[11] A. D. Garje, R. C. Aiyer, *J. Mater. Sci.* **19** 547 (2008).
[12] L. A. Patil and H. M. Baviskar, *Sensors Transd*. **109** 126 (2009).
[13] R. S. Niranjan, Y. K. Hwang, D. K. Kim, S. H. Jhung, J. S. Cang, I. S. Mullah, *Mater. Chem. Phys*. **92** 384 (2005).
[14] J. Bardeen, F.J. Blatt, L.H. Hall, R. Breekeuridge, B. Russel, T. Hahn (Eds.),
Photoconductivity Conference, Wiley, New York, 1956.
[15] Wisitsoraat, A. Tuantranont, A. Comini, E. Sberveglieri, G. Wlodarski, W. (2009) Thin Solid Films, 517 (8), 2775.
[16] Y. Hu, X. Zhou, Q. Han, Cao, Q. Huang, Y. (2003) Mat. Sci. Eng. B, 99, 41.
[17] Kumar A., Singh, A. Debnath, A. K. Samanta, S. Aswal, D.K. Gupta, S.K. Yakhmi, J.V. (2010) Talanta, 82, 1485.
[18] Wang, D. Chu X. and Gong, M. (2007) Nanotechn. 18 (18), 185601.

Time evolution of the rotational states wave packet for the diatomic molecule

Maninder Kaur[a], Mehmood Mian[b]
[a]Dept. of physics, D.A.V.Colledge,Hathi Gate, Amritsar, India.
[b]*Department of Physics, G.N.D.U., Amritsar, India.*
mannu_711@yahoo.co.in

***Abstract*— In this paper we present the time evolution of the quantum wave packet, constructed by superimposing the rotational states of H_2 molecule. We use the probability density function, auto-correlation function, and the various time scales to explore the time evolution and the revival pattern of this wave packet. We show that the wave packet collapses and revives during the time evolution.**

***Keywords*—**Bound wave packets, revivals and collapses, quantum mechanics.

I. INTRODUCTION

A quantum wave packet can be defined as a superposition of a set of eigenstates in a system. The eigenstates can be, for instance, electronic states in atoms, vibrational or rotational states in molecules and photon-number states in quantum optics. The evolution and dynamics of such wave packets is the subject of interest in many areas of physics and chemistry. In physics a short laser pulse produce a Rydberg wave packet i.e. a superposition of highly excited states. These Rydberg wave packets provides a bridge between classical and quantum mechanics. In molecular physics, ultra short pulses are used to prepare and probe molecular wave packets. The technique can be used to control chemical reactions using optimized light pulses.

The phenomenon of collapses and revivals of the wave packets was first discussed in [1]. After that many authors have discussed this phenomenon focusing on the infinite square well potential [2-4], harmonic oscillator potential [5--6] and the Rydberg Atoms [7—8]. Certain variants of the infinite square well have also been discussed as the infinte square well with δ potential at the centre [1], asymmetric infinite square well [9] and the finite square well [10]. The united approach of all these authors relevant to the demonstration of the phenomenon of the collapses and revivals of the wave packets is to localize the initial Gaussian wave packet inside the well and then visualize the dynamics of the wave packet with the passage of time. The autocorrelation function has also been plotted by some authors to give the evidence of the collapses and revivals of the wave packet [11].

The study of the time evolution of the bound state wave packet illuminates many features of the wave mechanics . This includes both semi-classical features as well as purely quantum mechanical effects. Initially the wave packet moves along the classical trajectory showing the classical behavior, but afterwards spreads out due to dephasing of the subsidiary waves. Under some conditions the spreading process is reversed due to rephasing and, after long enough time, the wave packet comes back to its initial state nearly completely. This behavior demonstrates the quantum behavior of wave packets. The dynamics of the unbound and bound wave packet have been visualized by many authors .This approach of visualization of the dynamics of the wave packet has facilitated the understanding of many quantum phenomenon like tunneling, scattering, interference and reflection. As a consequence such visualizations have become increasingly relevant as pedagogical tool.

In this work we have constructed a wave packet by superimposing the rotational states of H_2 diatomic molecule. Rotational motion of molecules can be treated using the rigid rotator model. The key thing that we learn from a rotational spectrum is the bond length of the molecule. Moreover each energy level of the quantum mechanical rigid rotator is (2l+1) fold degenerate. Thus E_1 will be threefold degenerate. This is important in interpreting the intensities of the infrared spectra of gas phase molecules.

II. QUANTUM WAVE PACKETS CONSTRUCTION

Here we construct a quantum wave packet by superimposing the rotational states of a diatomic molecule. A rotating diatomic molecule could be modeled as consisting of two point masses m_1 and m_2 at fixed distance r_1 and r_2 from their center of mass (Fig.1). Because the distance between the two masses is fixed, this model is referred to as the rigid rotator model.

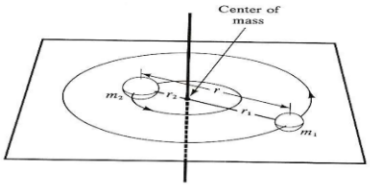

Fig. (1). Two masses m_1 and m_2 shown rotating about their centre of mass.

Next we consider a two dimensional rigid rotator where two masses are attached by a rigid rod, at a fixed distance, r, and are free to rotate about the Center of Mass in their x-y plane as in Fig. (2),

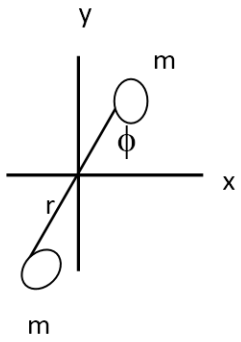

Fig. (2). Two dimensional rigid rotator

The angle φ represents the angle of rotation relative to the x-axis.

The 2D Schrödinger equation for the relative motion of two masses is given as,

$$-\frac{h^2}{2\mu}\nabla^2\psi + V\psi = E\psi,$$

where

$\mu = \frac{m_1 m_2}{m_1 m_2}$, is the reduced mass,

and

$\nabla^2 = \frac{\partial^2}{\partial x^2} + \frac{\partial^2}{\partial y^2}$, is 2D Laplacian operator.

In terms of the plane polar coordinates, the Schrödinger equation becomes,

$$-\frac{h^2}{2\mu r^2}\frac{\partial^2}{\partial \phi^2}\psi = E\psi.$$

The energy Eigen values and the normalized wave function are given as,

$$E = \frac{\hbar^2 m^2}{2\mu r^2},$$

And

$$\psi = \frac{1}{\sqrt{2\pi}} e^{im\phi},$$

Where

$m = 0, \pm 1, \pm 2, \pm 3, ...$

III. TIME EVOLUTION OF THE QUANTUM WAVE PACKET

The time-dependent wave function for the quantum wave packet formed as a superposition of rotational states is given as [1],

$$\psi(\phi,t) = \sum_v c_m \psi_m(\phi) \exp(-iE_m t).$$

(4) Here the coefficients are the weighting factors in the superposition, which are given in terms of the initial wave function as

$$c_m = \langle \psi_m(\phi,t) | \psi_m(\phi,0) \rangle$$

We model the weighting probabilities as a Gaussian distribution,

$$c_m = \sqrt{\frac{1}{2\pi\sigma^2}} e^{-(m-\bar{m})^2\pi^2 / 4\sigma^2}.$$

This model is preferred as it provides a symmetrical distribution in m with mean $\bar{m}$.

The assumption that the weighting probabilities are peaked around a mean value, it is reasonable to suppose that the states with energy near the mean value, contribute for the formation of wave packet. This allows expanding the energy in a Taylor series in v around the central value $\bar{m}$:

$$E_m \cong E_{\bar{m}} + E_{\bar{m}}'(m-\bar{m}) + \frac{1}{2}E_{\bar{m}}''(m-\bar{m})^2 + \frac{1}{6}E_{\bar{m}}'''(m-\bar{m})^3 + .., \quad (5)$$

where each prime denotes a derivative. The derivative terms in Eq.(5), define the time scales as given below [5]:

$$T_{cl} = \frac{2\pi\hbar}{E'_{\bar{m}}}, T_{rev} = \frac{2\pi\hbar}{\frac{1}{2}|E''_{\bar{m}}|}, T_{sr} = \frac{2\pi\hbar}{\frac{1}{6}|E'''_{\bar{m}}|}.$$

The first time scale is the classical time period for the shortest closed orbit. It controls the initial behavior of the wave packet. The second time scale is called the revival time. It governs the appearance of the fractional revivals and the full revivals. The third time scale is the superrevival time. It is a larger time scale. In terms of these time scales the Eq. (4) can be expressed as,

$$\psi(\phi,t) = \sum_m c_m \psi_m(\phi) \exp\left[-2\pi i\left(\frac{(m-\bar{m})t}{T_{cl}} + \frac{(m-\bar{m})^2 t}{T_{rev}} + ..\right)\right] \quad (6)$$

The expansion (6) shows that the time evolution of wave function is governed by these three time scales, which in turn are controlled by quantum number v. For small values of t, the first term in Eq. (6) dominates. Thus during this interval motion of wave packet is approximately periodic

in time with period T_{cl} . As t increases more the second term in phase modulates this behaviour, causing the wave packet to spread and collapse. However at time equal to revival time, the second term in phase equals 2πi and once again the motion is governed by the first term. As a result the wave packet regains its initial shape. This is called a full revival. Similarly at the superrevival time again the contribution of the third term is 2πi , the wave form reforms into a single wave packet that resembles the initial one better than does the full revival at time revival time. This new structure is called a superrevival.

IV. THE PROBABILITY DENSITY FUNCTION AND THE AUTO-CORRELATION FUNCTION

The probability density function is used to plot the shapes of the wave packet at various times. This function is defined as follows,

$$|\psi(\phi,t)|^2 = \psi(\phi,t)^* \psi(\phi,t)$$

Similarly the autocorrelation function is defined as [11],

$$A(t) = \psi(\phi,0)^* \psi(\phi,t)$$

Its absolute square gives a measure of the overlap between the wave packet at time t=0 and at later time t.

IV. RESULTS AND DISCUSSIONS

Here we choose a weighting factor with central value of 15 and H_2 as an example of diatomic molecule. Now for the molecule H_2 the reduced mass, bond length, moment of inertia, the classical time period and the revival time period are,

$$\mu = 8.30 \times 10^{-28}\, Kg,$$
$$r = 0.74 \times 10^{-10}\, m,$$
$$I = 4.55 \times 10^{-48}\, Kg.m^2,$$
$$T_{cl} = 1.9037 \times 10^{-14}\, s.$$
$$T_{rev} = 57.111 \times 10^{-14}\, s$$

The following figures are the plots of the probability density function at various instants of time. Fig. (3) is the plot of the probability density function at time t=0. Fig. (4) is plot of the probability density function at time $t=T_{cl}$. Fig. (5) is plot of the probability density function at time $t=T_{rev}$.

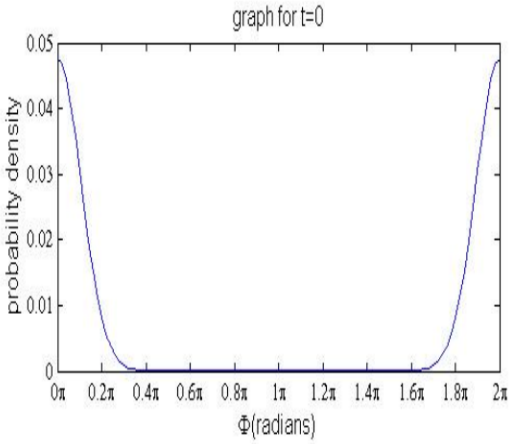

Fig. (3): Probability Density plot at time t=0

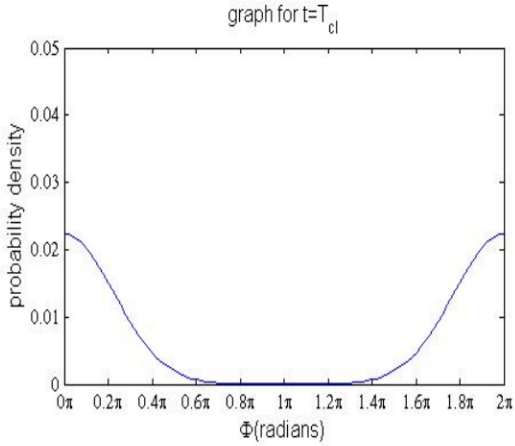

Fig. (4): Probability Density plot at time $t=T_{cl}$

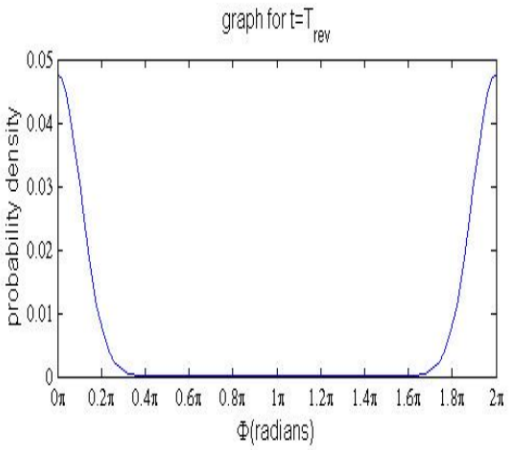

Fig. (5): Probability Density plot at time $t=T_{rev}$

From these plots it is clear that the wave packet spreads more and more after every classical time period. Ultimately the wave packet will collapse. But at the revival time period the wave packet revives to its original state. This fact is made more lucid from the following plot absolute square of the autocorrelation function verses reduced revival time (the ratio of the

revival time period and the revival time for the primitive path), Fig. (6),

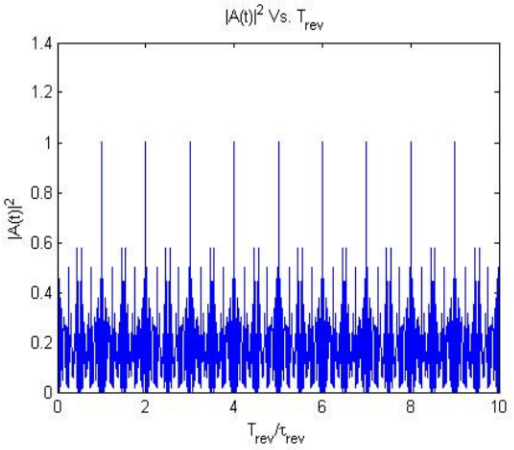

Fig. (6): Autocorrelation function vs. reduced revival time

The absolute square of autocorrelation function numerically varies between 0 and 1. When wave packet exactly matches initial wave packet the value is 1. For a completely mismatched wave packet the value is 0. From the Fig (6), it is readily seen that the wave packet shows exact revival pattern after each revival time (longer peaks). The smaller peaks show the existence of fractional revivals.

V. CONCLUSION

Quantum wave packet constructed by superimposing the rotational states of the H_2 molecule shows the exact revival pattern along with the fractional revivals.

VI. ACKNOWLEDGEMENT

The work is accomplished with the help of resources of department of physics G.N.D.U. Amritsar.

REFRENCES

[1] C. U. Segre, and J. D. Sullivan, *" Bound-state wave packets*, " Am. J. Phys, vol. 44, pp.729--732,1976.

[2] D. L. Aronstein, and C. R. Stroud, *'Fractional wave-function revivals in the infinite square well*, " Phys. Rev. A, vol. 55, pp. 4526—4537, 1997.

[3] R. W. Robinett, "*Visualizing the collapse and revival of wave packets in the infnite square well using expectation values*, " Am. J. Phys, vol. 68, pp.410-420, 2000.

[4] D. F. Styer, "*Quantum revivals verses classical periodicity in the infinite square well*, " Am, J. Phy., vol. 69, pp. 56-62, 2001.

[5] R. W. Robinett, *"Quantum wave packet revivals*, " Physics Reports, vol. 392, pp.1—119, 2004.

[6] Robert Bluhm, V. Alan Kostelecky, and James A. Porter, *"The evolution and revival structure of localized quantum wave packet,* " Am. J. Phys, vol. 64, pp.944—953, 1996.

[7] L. S. Brown, "*Classical limit of hydrogen atom*, " Am. J. Phy. vol. 41, pp. 525—530, 1973.

[8] Z. D. Gaeta, and C. R. Stroud, *"Classical and quantum mechanical dynamics of a quasiclassical state of the hydrogen atom* , " Physical review A, vol. 42, pp. 6308—6313, 1990.

[9] Todd K. Timberlake, and Seth Camp, "*Decay of wave packet revivals in the asymmetric infinite square well,* " Am. J. Phys, vol. 79, pp.607--614, 2011.

[10] Anu Venugopalan, and G. S. Agarwal, *"Superrevivals in the Quantum dynamics of a particle trapped in a finite square well potential,* " Phys. Rev. A vol.73, pp.1413—1422, 1999.

[11] Michael Nauenberg, *"Autocorrelation function and quantum recurrence of wave packets,* " Journal of Physics B, vol. 23, pp. L385--L390, 1990.

Effect of Gamma Irradiation on Aluminophosphate Glass doped with Titania

Manpreet Kaur[a], Lakhwant Singh[b], Sonika Thakur[c], Navjit[d], Kusum Devagan[e]
[a]*Department of Physics, DAV College, Amritsar, Punjab, India*
[b]*Department of Physics, Guru Nanak Dev University, Amritsar, Punjab, India*
[c]*Department of Physics, Guru Nanak Dev University College, Verka, Amritsar, Punjab, India*
[d]*Department of Physics, Khalsa College for Women, Amritsar, Punjab, India*
[e]*Department of Physics, S.R. Government College for Women, Amritsar, Punjab, India*
Corresponding author: manpreetaurora@gmail.com

***Abstract*—Titania doped aluminophosphate glass was prepared using melt-quench technique. The glass was found to be of purple color. The glass was then characterized for optical and structural variation with irradiation using gamma ray dose from 25 kGy to 200 kGy. The UV Visible spectra of the glass revealed that these glasses can act as radiation shielding materials but for low dose i.e. upto 100 kGy. Raman spectra showed the variation in intensity of different bands with irradiation. However no new bands were formed but only slight shifting of bands was observed.**

***Keywords*—**Phosphate glass, UV Visible spectra, Raman spectra, Irradiation

I. INTRODUCTION

Phosphate glasses doped with transition metals have gained interest in recent years due to their interesting optical, magnetic and electrical properties. These glasses find a wide range of technological applications like solid state laser hosts, optical fibres, TL materials and many more [1-2]. The addition of alumina and titania to phosphate glass enhances its chemical durability [3]. Generally, titanium exhibits two valence states in oxide glasses. They either exist as trivalent Ti^{3+} ions or as tetravalent Ti^{4+} ions. However in phosphate glasses the stabilisation of Ti^{3+} ions is easier to achieve as compared to Ti^{4+} ions.TiO_2 acts as glass modifier when doped in phosphate glasses. It enhances the chemical durability of glasses by forming more stable Ti-O-P bonds as compared to P-O-P bonds. It has been reported by many researchers that exposure of materials to high energy radiations produce drastic changes in the electrical, chemical, magnetic, structural and optical properties. These radiations cause ionisation and thus lead to the displacement of constituent ions in the sample. Ionisation radiations generate defect centers also called as color centers in glasses due to electron or hole capture mechanism [4]. The main objective of present work is to study the effect of different gamma ray doses on optical and structural properties of 50 P_2O_5-5Al_2O_3- 30 CaO -10 Na_2O-10 TiO_2 glass.

II. EXPERIMENTAL DETAILS

A. *Preparation of Glass sample*

The glass with composition 50 P_2O_5-5Al_2O_3- 30 CaO - 10 Na_2O-10 TiO_2 was prepared using the conventional melt quench technique. All the chemicals were weighed and thoroughly mixed in a ball mill for 24 hours to form a homogeneous mixture. This batch was then melted in an electric furnace at 1300^{0}C for 2 hours. The melt was then poured onto preheated steel plates maintained at temperature 200^{0}C to obtain the bubble free transparent glasses. The glass was then annealed at 400^{0}C to remove internal stress if any. The glass sample was then exposed to 4 different gamma doses from 25 kGy -200 kGy using ^{60}Co gamma cell at room temperature.

B. *UV Visible Spectroscopy*

Ultraviolet and visible optical absorption spectra was measured for polished glass sample without irradiation and after irradiation in 200-1100 nm range using double beam spectrophotometer Shimadzu 1601. The absorption spectrum was then used to calculate the direct and indirect bandgap energy for prepared glass before and after irradiation.

C. *Raman Spectra*

Raman spectra of polished glass samples were recorded using Renishaw inVia Raman Microscope with 488 Argon Laser in 400-1500 cm^{-1} range. The laser power used was 10% and the acquisition time was 30s. All the measurements were recorded at room temperature.

III. RESULT AND DISCUSSION

A. *UV Visible Spectroscopy*

Fig. 1 shows the absorption spectra of Ti doped phosphate glass before and after irradiation. The absorbance of the glass was found to increase with the dose but the shape of the spectrum remains the same. On subjecting these glasses upto dose of 100 kGy they

showed resistance towards irradiation and the intensities of bands remain very close to that before irradiation. However for higher dose of the range of 200 kGy the absorption increases abruptly and two new bands are observed at 383 nm and 510 nm resp.

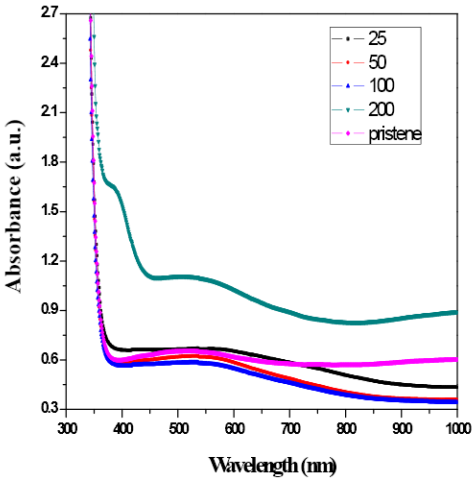

Fig1 Absorption spectra of Titania doped aluminophosphate glass before and after irradiation

The general photochemical reaction that takes place when phosphate glasses doped with Titania are irradiated is as shown:

Defect + hν ⟶ trapped electron +free hole

Ti^{3+} +free hole ⟶ Ti^{4+}

The optical band gap energy of the glass system is calculated from the ultraviolet absorption edge. This study is useful for investigating the induced optical transitions and also it provides information about the band structure. The absorption coefficient α is related to the band gap energy by the famous Davis and Mott relation given as

$$\alpha(\nu) = B\frac{(h\nu - E_g)^n}{h\nu}$$

Where n is an index and can have value 2 or 1/2 corresponding to the indirect and direct transitions, B is a constant, E_g is the optical band gap energy and hν is the incident photon energy. Fig 3 shows the plot of $(\alpha h\nu)^{1/2}$ and hν and we can calculate the optical band gap energy by extrapolating the linear region of curve to the hν axis where $(\alpha h\nu)^{1/2}$ =0. The bandgap energy was found to decrease from 3.36 eV to 2.91 eV with irradiation. This can be explained on the fact that with irradiation the spin density and hence the density of free electrons increases [5]. Also there is the probability of formation of defect centers which have their electronic states between the valence band and the conduction band. So photons may induce transitions between the valence band and the bands of defect centers.

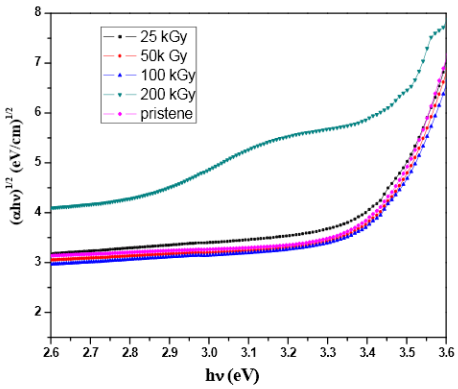

Fig2 Indirect Bandgap energy of Titania doped aluminophosphate glass before and after irradiation

B. Raman Spectra

Fig. 3 shows the Raman spectra of Ti doped phosphate glass before and after irradiation. There are mainly six bands observed in the Raman spectra. The sharp band at 1278 cm^{-1} is attributed to the asymmetrical stretching vibrations of PO_2 groups. The sharp peak at 1160 cm^{-1} is assigned to the presence of symmetrical stretching vibrations of PO_2 groups. A broad weak band at 1000 cm^{-1} is due to symmetric stretching vibrations of PO_3 groups. The band at 910 cm^{-1} is assigned to the presence of asymmetric P-O-P bonds. Sharp band at 706 cm^{-1} is attributed to symmetric P-O-P bonds [6]. The band at 620 cm^{-1} is assigned to the presence of TiO_6 tetrahedral structure. With irradiation no new bands were observed but there was a slight variation in the intensity of bands and the bands were red shifted.

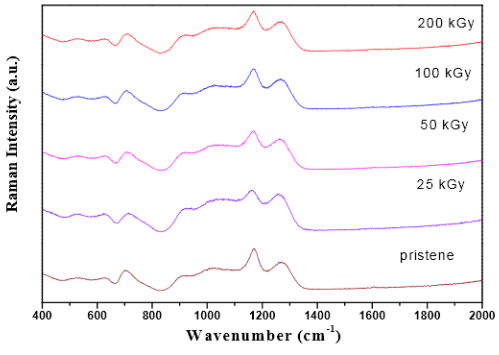

Fig3.Raman Spectra of Titania doped aluminophosphate glass before and after irradiation

IV. CONCLUSIONS

The purple colour of the glass was found to decrease with the irradiation. This was due to the absorption of holes which converts the Ti^{3+} ions to Ti^{4+} ions. The optical bandgap energy was found to decrease which was due to the formation of more free charge carriers with irradiation. The Raman spectra confirmed that no new bonds are made due to irradiation but only the intensity of bands was found to increase with irradiation.

ACKNOWLEDGMENT

The authors wish to thank Dr. Atul Khanna, Department of Physics, Guru Nanak Dev University, Amritsar for providing facilities like XRD, Raman and UV-Visible spectrophotometer. We are also thankful to Principal DAV College Amritsar for their support.

REFERENCES

[1] Hatem A. ElBatal, Zeinab E. ElMandouh, Hamida A. Zayed, Samir Y. Marzouk, Gihan M. Elkomy, Ahmed Hosney, "Gamma rays interaction with copper doped lithium phosphate glasses,"j. Molecular Structure 1054-1055, 57-64 (2013).

[2] Fatma H ElBatal, "UV Visible, Infrared, Raman and ESR spectra of gamma irradiated TiO_2 doped soda lime phosphate glasses,"Indian Journal of Pure & Applied Physics, 47, 631-642 (2009).

[3] Babita Tiwari, V. Sudarsan, Anupam Dixit, and Govind P. Kothiyal, "Effect of TiO_2 Addition on the Optical, Thermo-Physical and Structural Aspects of Sodium Alumino-Phosphate Glasses," J. Am. Ceram. Soc.1-7 (2011).

[4] AM Abdelghany, F H ElBatal, MA AZooz, MA Ouis, HA ElBatal, "Optical and Infrared absorption spectra of 3d transition metal ions doped sodium borophospahte glasses and effect of gamma irradiation," Spectrochimica Acta Part A: Molecular and Biomolecular Spectroscopy, 98, 148-155 (2012).

[5] VN Rai, BN Raja Sekhar, S. Kher, SK Deb, "Effect of gamma ray irradiation on optical properties of Nd doped phosphate glass," Journal of Luminescence, 130, 582-586 (2010).

[6] F H ElBatal, AM Abdelghany, RL Elwan, "Structural Characterisation of gamma irradiated lithium phosphate glasses containg variable amounts of molybdenum," Journal of Molecular Structure 1000, 103-108 (2011)

NANOTECHNOLOGY ROLE IN WATER TREATMENT

Ravi Sharma
Dept. of Chemistry , DAV College, Amritsar

***Abstract*— Advances in nanoscale science and engineering suggest that many of the current problems involving water quality could be resolved or greatly ameliorated using nanosorbents, nanocatalysts, bioactive nanoparticles, nanostructured catalytic membranes and nanoparticle enhanced filtration among other products and processes resulting from the development of nanotechnology. Nanoparticles have a great potential to be used in waste water treatment. Its unique characteristic of having high surface area can be used efficiently for removing toxic metal ions, disease causing microbes, organic and inorganic solutes from water. Various classes of nanomaterials are also proved to be efficient for water treatment like metal-containing nanoparticles, The paper reviews recent advances on different nanomaterials catalytic membranes, nanosorbents, membrane water treatment. Additionally, nanotechnology-derived products that reduce the concentrations of toxic compounds to sub-ppb levels can assist in the attainment of water quality standards and health advisories.**

***Keywords*—** Nanomaterials, bioactive , organic solutes, nanoabsorbents

I. INTRODUCTION

Metal oxides such as iron oxide, titaniumdioxide and alumina are effective, low cost adsorbents for heavy metals and radio nuclides. The sorption is mainly controlled by complexation between dissolved metals and the oxygen in metal oxides It is a two-step process fast adsorption ofmetal ions on the external surface, followed by the rate-limiting intraparticle diffusion along the micropore walls[1-2].

A. Method using Metals

Their nanoscale counter-parts have higher adsorption capacity and faster kinetics because of the higher specific surface area, shorter intraparticle diffusion distance and larger number of surface reaction sites (i.e., corners, edges, vacancies). Metal oxide nanocrystals can be compressed into porous pellets without significantly compromising their surface area when moderate pressure is applied. Thus, they can be applied in forms of both fine powders and porous pellets, which are the likely forms to be used in industry.

B Use of Nanofibres

Although nanofiber membranes have been commercially employed for air filtration applications, their potential in water treatment is still largely unexploited. Nanofiber membranes can remove micron-sized particles from aqueousphase at a high rejection rate without significant fouling [6]. Thus they have been proposed to be used as pretreatment prior to ultrafiltration or reverse osmosis (RO). Functional nanomaterials can be easily doped into the spinning solutions to fabricate nanoparticle impregnated nanofibers .

C Role of thin film Membranes

Development of TFN membranes mainly focuses on incorporating nanomaterials into the active layer of thin film composite (TFC)membranes via doping in the casting solutions or surface modification. Nanomaterials that have been researched for such applications include nano-zeolites, CNTs. The impact of nanoparticles on membrane permeability and selectivity depends on the type, size and amount of nanoparticles added. Nano-zeolites are themost frequently used dopants in TFN and have shown potential in enhancing membrane permeability. The addition of nano-zeolites leads to more perme able, negatively charged, and thicker polyamide active layer . Bioactive nanoparticles Water pollution has caused lots of infectious diseases due to various contaminating pathogens. Many of the microorganisms acting as pathogens are antibiotic resistance and so it's very difficult to remove them from water. Recently the concept of bioactive nanoparticles has emerged which has given the alternative of newchlorine – free biocides and also silver based nano materials do play a very promising role [7]

D Biological membranes

Many biological membranes are highly selective and permeable. Aquaporins are protein channels that regulate water flux across cell membranes. Their high selectivity and water permeability makes their use in polymeric membranes an attractive approach to improve membrane performance.

E Semiconducting photocatalyst

TiO_2 is the most widely used semiconductor photocatalyst in water/wastewater treatment owing to its low toxicity, chemical stability, low cost, and abundance as raw material. It generates an electron/hole pair upon absorbing a UV photon, which later either migrate to the surface and form reactive oxygen species (ROS) or undergo undesired recombination. The photoactivity of nano-TiO_2 can be improved by optimizing particle size and shape, reducing e/h recombination by noblemetal doping, maximizing reactive facets, and surface treatment to enhance contaminant adsorption. The overall efficiency of a photocatalytic water treatment process strongly depends on the configuration and operation parameters of the photo-reactor.

F Contaminated particles detection

In trace organic or inorganic contaminant detection, nano materials can be used in both concentration and detection. CNTs have great potential for environmental analysis of trace metal or organic pollutants as they offer high adsorption ca pacity and recovery rate as well as fast kinetics The pre-concentration factors for metal ionswere found to be between 20 and 300 with fast adsorption kinetics CNTs have also been extensively

studied for pre concentrating a variety of organic compounds, many of which were done in real water samples. Adsorption of charged species to CNTs results in changes of conductance, providing the basis for the correlation between analyte concentration and current fluctuation

II. CONCLUSION

Nanocatalysts, bioactive nanoparticles, nanostructured catalytic membranes and nanoparticle enhanced filtration among other products and processes resulting from the development of nanotechnology. Nanoparticles have a great potential to be used in waste water treatment. Its unique characteristic of having high surface area can be used efficiently for removing toxic metal ions, disease causing microbes, organic and inorganic solutes from water. Various classes of nanomaterials are also proved to be efficient for water treatment like metal-containing nanoparticles,

REFERENCES

[1] G. O. Young, "Synthetic structure of industrial plastics (Book style with paper title and editor)," in *Plastics*, 2nd ed. vol. 3, J. Peters, Ed. New York: McGraw-Hill, 1964, pp. 15–64.

[2] W.-K. Chen, *Linear Networks and Systems* (Book style). Belmont, CA: Wadsworth, 1993, pp. 123–135.

[3] H. Poor, *An Introduction to Signal Detection and Estimation*. New York: Springer-Verlag, 1985, ch. 4.

[4] B. Smith, "An approach to graphs of linear forms (Unpublished work style)," unpublished.

[5] E. H. Miller, "A note on reflector arrays (Periodical style—Accepted for publication)," *IEEE Trans. Antennas Propagat.*, to be published.

[6] J. Wang, "Fundamentals of erbium-doped fiber amplifiers arrays (Periodical style—Submitted for publication)," *IEEE J. Quantum Electron.*, submitted for publication.

[7] C. J. Kaufman, Rocky Mountain Research Lab., Boulder, CO, private communication, May 1995.

[8] Y. Yorozu, M. Hirano, K. Oka, and Y. Tagawa, "Electron spectroscopy studies on magneto-optical media and plastic substrate interfaces(Translation Journals style)," *IEEE Transl. J. Magn.Jpn.*, vol. 2, Aug. 1987, pp. 740–741 [*Dig. 9th Annu. Conf. Magnetics* Japan, 1982, p. 301].

[9] M. Young, *The Techincal Writers Handbook.* Mill Valley, CA: University Science, 1989.

[10] J. U. Duncombe, "Infrared navigation—Part I: An assessment of feasibility (Periodical style)," *IEEE Trans. Electron Devices*, vol. ED-11, pp. 34–39, Jan. 1959.

[11] S. Chen, B. Mulgrew, and P. M. Grant, "A clustering technique for digital communications channel equalization using radial basis function networks," *IEEE Trans. Neural Networks*, vol. 4, pp. 570–578, July 1993.

[12] R. W. Lucky, "Automatic equalization for digital communication," *Bell Syst. Tech. J.*, vol. 44, no. 4, pp. 547–588, Apr. 1965.

[13] S. P. Bingulac, "On the compatibility of adaptive controllers (Published Conference Proceedings style)," in *Proc. 4th Annu. Allerton Conf. Circuits and Systems Theory*, New York, 1994, pp. 8–16.

[14] G. R. Faulhaber, "Design of service systems with priority reservation," in *Conf. Rec. 1995 IEEE Int. Conf. Communications,* pp. 3–8.

Hot Corrosion Problems in Coal based Thermal Power Plants in India and Possible Solution-A Review

Jaideep Singh[a], Amit Sarin[b]
[a] *Research Scholar, PTU, Jalandhar, Punjab, India,*
[b] *Associate Professor, ACET, Amritsar, Punjab, India.*
Email: jaideep_13@hotmail.co.uk,amit.sarin@yahoo.com

***ABSTRACT*- The different chemical environments to which boiler tubes are subjected causes different types of corrosions. Hot corrosions are recognized as serious problems in coal based power generation plants in India. The coal used in Indian power stations has large amounts of ash (about 50%) which contain abrasive mineral species such as hard quartz (up to 15%) which increase the erosion propensity of coal. Many studies have correlated Hot corrosions in boiler tubes with the Chlorine content present in coal. Maximum permissible limit of Chlorine content is set at 0.3%. Hot corrosion in boilers are responsible for huge losses, in power generation. An understanding of these problems and thus to develop suitable protective system is essential for maximizing the utilization of such components. These problems can be prevented by either changing the material or altering the environment or by using a suitable coating on the surface.**

***Keywords* – Abrasive, Ash, Boiler, Corrosion**

I INTRODUCTION:

Attainment of high temperature is major requirement in the coal powered power plants. Under such extreme conditions of environment and temperature, hot corrosions are likely to occur. Gas turbines in aircraft, fossil fueled power plants, refineries, and petrochemical industries, and heating elements for high temperature furnaces are some examples where corrosion limits their use or reduces their life, considerably affecting the efficiency [1]. Coal constitutes the major source of fuel used for electricity generation worldwide. About 41% of electricity generated worldwide is generated from coal. As far as India is concerned about 59% of electricity is generated using coal. In coal based power plants, large amount of heat is produced by burning of coal. The amount of heat generated depends on thermal content of coal. Different varieties of coal have different heat content. The heat so generated is transferred to water reservoir to produce steam. This steam rotates the turbine and generator connected to turbine produces electricity.

Coal is a complex and relatively dirty fuel that contains varying amount of sulfur and a substantial fraction of non combustible mineral constituents, commonly called ash . The coal used in Indian power stations has large amounts of ash (about 50%), which contain abrasive mineral species such as hard quartz (up to 15%), which increase the erosion propensity of coal. The vast technical literature available is evidence that corrosion and deposits on the fireside of boiler surfaces or in gas turbines represent important problems. Metals and alloys may experience accelerated oxidation when their surfaces are coated by a thin film of fused salt in an oxidizing gas. This mode of attack is called hot corrosion, and the most dominant salt involved is Na2SO4 . High temperature degradation is one of the main failure modes of hot-section components in the gas turbines, so an understanding of this high temperature oxidation is very necessary [2].

(a) *COAL FIRED POWER PLANTS* - The availability of electrical power and the development of millions of devices that use it have made electricity the energy of choice in contemporary industrial societies. It is estimated that in the United States approximately 70% of the electricity is produced in fossil power plants, 15% in nuclear power plants, 12% in hydraulic power plants and the remainder from other types of sources [3]. In any event, the fossil fuel power plant is and will continue to be the mainstay of electric power production. The fossil fuel employed in a steam turbine plant can be pulverized coal (PC), oil, or natural gas. Of these, coal is the most abundant and hence the most commonly used fuel for steam turbine plants, while gas turbine plants generally employ oil and natural gas. Figure 1 shows the arrangement of the various elements of a PC fossil plant. Here, water is first preheated to a relatively low temperature in feed water heaters and pumped into tubes contained in a boiler. The water is heated to steam by the heat of combustion of pulverized coal in the boiler and then superheated. Superheated and pressurized steam is then allowed to expand in a high-pressure (HP) steam turbine and causes rotation of the turbine shaft. The outlet steam from the HP turbine may once again be reheated and made to expand through an intermediate pressure (IP) turbine and then through a low-pressure (LP) turbine. The turbine shafts are all connected to one or more generator shafts which in turn rotate and convert the mechanical energy of rotation into electrical energy in the generator. The exit steam from the LP turbine is condensed in the condenser and is once again fed back to the boiler through the feed water heater and pumps. A closed loop of the water and steam is thus maintained. Figure 1: Schematic diagram of a coal-fired steam power plant [3].

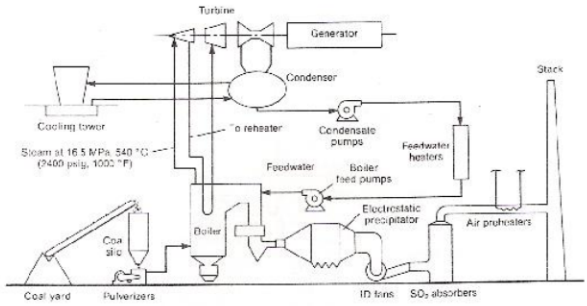

Indian Coal Contents and its Combustion- Coal gasification systems operate at temperature of up to 2000 F (1093^{0}C) and at a pressure of up to 100 atm depending on the specific process and the product, coal gas generates the greatest problems. In addition to hydrogen and carbon-containing gaseous species, there are many undesirable species including sulphides, sulphites, sulphates, ammonia, cyanides, volatilised oils, phenols and aggressive trace elements such as potassium, sodium, vanadium and lead [4].

The coal used in Indian power stations has large amounts of ash (about 50%), which contain abrasive mineral species such as hard quartz (up to 15%), which increase the erosion propensity of coal [3]. The Indian coal proved to be exceptional in that they had significant amounts of alkali feldspars, (K, Na)AlSi3O8 , and a garnet, minerals usually thought of as trace components of a coal. The garnets found in the Indian coals were found to follow the general formula (Mg, Fe2+)3Al2Si3O12. J.J. Wells et al [4] have studied the Ash content, major minerals and trace materials in 10 coals and found the maximum ash content in Indian coal. Table: 1 indicate the Indian coal with dry ash content and mineral matter [5]. Further the coal analysis data collected from Guru Gobind Singh Thermal Plant, Ropar (Punjab), is presented in Table-2. The ash and flue gases analysis of Guru Nanak Dev Thermal Plant, Bathinda (Punjab), is presented in Table 3, which also indicates the presence of these constituents.

Table 1: The ash content and mineral matter in the suite of coals [4]

Coal	Ash Content	Major minerals	Trace minerals
	(Wt%) dab		
Indian coal A	46.7	Quartz, muscovite, illitic,clay	Barites, feldspar, ilmenite,
Indian coal B	30.3	Quartz, feldspar, clay,kaolinit	Apatite, garnet, ilmenite,
Indian coal C	45.6	Quartz, feldspar, garnet,	Apatite, ilmenite, monazite,

Table 2: Coal Analysis data

Constituent	Wt. percentage
Total Moisture (Inherent + Surface)	10.43
Inherent moisture	7.55
Ash	34.74
Ash on fire basis (actual)	33.64
Volatile metal	21.59
Gross Calorific value(kcal/kg)	4187
Gross Calorific value (fire basis)	4055
Unburnt carbon in fly ash	1.35

The corrosive nature of the gaseous environments, which contain oxygen, sulfur, and carbon, may cause rapid material degradation and result in the premature failure of components [5]. Combustion of coal generates very corrosive media particularly near the superheater tubes of the boilers. In the boiler tubes suffering severe fireside corrosion, sulphate salts concentrate at the deposit/scale interface and become partially fused since these salts contain alkali metals of sodium and potassium [7]. In the combustion systems, much of the sodium and potassium is volatized from the mineral matters in the flame to form Na2O and K_2O vapours. The sulphur released from the coal, forms SO2 with a minor amount of SO3 and reacts with the volatilized alkalis to form Na2SO4 vapours, which then condense together with fly ash on the pendant superheater and reheater tubes in the boiler.

The vast technical literature available is evidence that corrosion and deposits on the fireside of boiler surfaces or in gas turbines represent important problems [4]. When a comparison is made between the amount of ash collected in a boiler or a gas turbine, in the form of deposits, and the total amount of ash released during combustion, the conclusion is clear that most of the ash passes through the unit. For particles to collect on boiler surfaces or blade surfaces, they must first be brought close to the surface itself and be of the proper size. This can be ascribed to physical phenomenon involving the reaction of particles to the forces to which they are subjected within the stream of gases passing near the surfaces [6]. A particle may hit and then rebound from the surface. If it hits or rubs the surface with sufficient force, erosion will result. On the other hand, if the particle is captured physically or chemically by the surface, a deposit is initiated whose growth appears aerodynamically inevitable. Because of high temperatures, reactions can then take place between the various particles deposited, and also with the gases passing nearby, particularly SO3 and SO2. The resulting compounds may then react, by diffusion, with the metal structure on which they are attached and cause accelerated corrosion [6].

(b) *HOT CORROSION* - Oxidation is a type of corrosion involving the reaction between a metal and air or oxygen at high temperature in the absence of water or an aqueous phase. It is also called dry-corrosion. The rate of oxidation of a metal at high temperature depends on the nature of the oxide layer that forms on the surface of metal [7]. Metals and alloys may experience accelerated oxidation when their surfaces are coated by a thin film of fused salt in an oxidizing gas. This mode of attack is called hot corrosion.

Hot corrosion was first recognized as a serious problem in the 1940s in connection with the degradation of fireside boiler tubes in coal-fired steam generating plant. Since then the problem has been observed in boilers, internal combustion engines, gas turbines, fluidized bed combustion and industrial waste incinerators [8].

(c) *General Classification of Hot Corrosion* - Hot corrosion is often divided into two forms of attack: Type I or High temperature hot corrosion (HTHC) above about 900°C where pure sodium sulfate is above its melting temperature, and Type II or Low temperature hot corrosion (LTHC), between about 700°C-750°C where a liquid salt phase is only formed because of significant dissolution of some corrosion products [9].

Mechanism of Hot Corrosion

Several mechanisms have been suggested to explain the process of hot corrosion [21]. The hot corrosion degradation process of the superalloys usually consists of two stages [10]:

1.An initiation stage during which the alloys behave much as they would have behaved in the absence of the deposits and

2.A propagation stage where the deposits cause the protective properties of the oxide scales to become significantly different then those that they would have been had no deposit been present. Khana et al. [1] , in their review of degradation of materials under hot corrosion conditions , stated that corrosion-resistant alloys depend on selective oxidation to form the dense, compact protective scales of Cr_2O_3 and Al_2O_3 for their resistance. During hot corrosion a degradation sequence consisting of the eventual displacement of a more protective reaction product barrier by a less protective product is usually followed.

PREVENTIVE MEASURES AGAINST HOT CORROSION

A case study reported by Prakash et. al. [12] pertaining to a coal fired boiler of a power plant where out of 89 failure occurring in one year duration, 50 failures were found to be due to hot corrosion by ash. Material losses due to corrosion are the major problems in many industries. Corrosion and its associated losses cannot be eliminated completely. However, 25 to 30% of annual corrosion related costs could be saved with the use of optimum corrosion preventive and control strategies. The option to use low grade fuel limits the improvement in hot corrosion environment. In that case hot corrosion preventive methods to the existing environment are (a) change of metal i.e. use of superalloy (b) use of inhibitors and (c) use of coatings. Regarding change of metal or use of super alloy, alloying elements which can improve the hot corrosion resistance of materials such as Cr, Al, etc., often have a negative effect on the mechanical properties in high temperature environments and are expensive. Regarding use of inhibitor, addition of an organic inhibitor (e.g. pyridines, pyrimidines, quinolines) is sufficient to mitigate corrosion of metals in many corrosive media [15].However, these inhibitors have shown only limited success due to solubility and/or thermal stability problems in high – temperature, concentrated salt solutions [15]. Increasingly greater demand imposed on materials makes it more difficult to combine the different properties required in one single material. Therefore, a composite system of a base material providing the necessary mechanical strength with a protective surface layer different in structure and/or chemical composition and supplied by a surface treatment can be an optimum choice in combining material properties. Single materials are at their upper performance limits in all fields and coatings offer a way to extend these limits [16]. One possible way to cope with these problems is by using thin wear and oxidation resistant coatings with good thermal conductivities [10].Following methods may be followed in order to develop thin films:

(i) *Hot Corrosion Resistant Coatings*

The coating can be defined as a layer of material, formed naturally or synthetically or deposited artificially on the surface of an object made of another material, with the aim of obtaining required technical or decorative properties [11].

Recent studies show that 80% of the total cost for the protection of metals, are related to coating applications [13]. Organic coatings cover a large part of this percentage, but also metallic ones have a relatively big market. In fact, metallic coatings possesses together with good corrosion resistance, good aesthetics, brightness, and interesting mechanical properties such as hardness and wear resistance. In general, coating systems can be classified as either diffusion or overlay type, which are distinguished principally by the method of deposition and the structure of the resulting coating-substrate bond [4].

From a production point of view [7], three methods are in current use to deposit coatings, these being chemical vapour deposition (CVD), physical vapour deposition (PVD) and Plasma spraying. The CVD process comes under the category of Diffusion coatings, in which the coating material forms a chemical bond with the substrate. Whereas the PVD and Thermal spraying processes comes under the category of Overlay coatings, in which the desired material is placed over the substrate material [1].

(ii) *Thermal Spraying*

Thermal spraying is one of the most versatile hard facing techniques available for the application of coating

materials used to protect components from abrasive wear, adhesive wear, erosive wear or surface fatigue and corrosion (such as that caused by oxidation or seawater) . Generally, any material which does not decompose, vaporize, sublimate, or dissociate on heating, can be thermally sprayed. Consequently a large class of metallic and nonmetallic materials (metals, alloys, ceramics, cermets, and polymers) can be deposited by thermal spraying. Plasma-sprayed ceramic coatings are used to protect metallic structural components from corrosion, wear and erosion, and to provide lubrication and thermal insulation [18]. In particular, coatings made of Al2O3 containing 13 wt% TiO2 (Al2O3-13 wt% TiO2) are commonly used to improve the wear-corrosion and erosion resistance of steel. In conventional plasma-spray processing of Al2O3-13 wt% TiO2 coatings, powder particles are injected into a plasma jet, causing them to melt into droplets that are propelled towards the substrate [18].

(Iii) *Physical Vapor Deposition (PVD) Process*

In physical vapor deposition (PVD) process, the coating is deposited in vacuum by condensation from a flux of neutral or ionized atoms of metals [19]. Several PVD techniques are available for deposition of hard coatings. Among them, cathodic arc vapor (plasma or arc ion plating) deposition, magnetron sputtering (or sputter ion plating), and combined magnetron and arc processes are most widely used techniques used to deposit titanium-aluminum based coatings.

PVD process is carried out in *high vacuum* at temperature between 150 and 500°C. The high purity solid coating material (metals such as titanium, chromium & aluminum) is either evaporated by heat or by bombardment with ions (sputtering). At the same time, a reactive gas (e.g. nitrogen or a gas containing carbon) is introduced; it forms a compound with the metal vapors and is deposited on the tools or components as a thin, highly adherent coating.

(iv)*Chemical Vapor Deposition (CVD)*

Chemical Vapor Deposition (CVD) process is a versatile process that can be used to deposit nearly any metal as well as non metal such as carbon or silicon [1]. The first step is the production of metal vapours. Several chemical reactions can be used: thermal decomposition, pyrolysis, reduction, oxidation, nitridation etc. The main reaction is carried out in a separate reactor. The vapors thus formed are transferred to the coating chamber where the sample is mounted and maintained at high temperature. One of the limitations of the CVD is the high substrate temperature, which in many cases changes the microstructure of the substrate, and another is the size of specimens, often smaller parts are used due to limitation of chamber size.

(v) *Nanostructured Coatings*

Nanostructured coatings [17] composed of crystalline/amorphous nanophase mixture have recently attracted increasing interests in fundamental research and industrial applications, because of the possibilities of synthesizing a surface protection layer with unique physical- chemical properties that are often not attained in the bulk materials. Nanostructured materials as a new class of engineering materials with enhanced properties and structural length scale between 1 and 100 nm. Nanostructured ceramic coatings produced by Plasma sprayed processes are being developed for a wide variety of applications that required resistance to wear corrosion, cracking and spallation, with improved properties.

environment for applying nanostructured oxide ceramic materials, as compared to APS. The superior properties of coatings applied from nanostructured powders seem to be associated with coatings that have retained a nanostructure, i.e. a bimodal structure composed of partially or unmolten particles, combined with fully molten regions. Jin-hong Kim et al [20] have successfully developed thermal sprayed nanostructured WC-Co wear resistant coatings and the resultant coatings showed significant improvement of wear resistance in comparison with the conventional counterparts. Micro structural in homogeneity of the conventional Cr2O3 based solid-lubricant coatings was successfully solved by utilizing nanostructured feedstock powder developed. Nanostructured and conventional zirconia coatings were deposited by atmospheric plasma spraying and the thermal shock resistance of as-sprayed coatings was investigated by the water quenching method [21]. The results showed that the nanostructured as-sprayed coatings possessed better thermal shock resistance then the conventional coating. This phenomenon is explained in terms of the difference in microstructure and micro-structural changes occurring during thermal shock cycling.

CONCLUSIONS

1. Hot corrosion is a serious problem in power generation equipment, in gas turbines for ships and aircrafts and in other energy conversion and chemical process systems and should be either totally prevented or detected at an early stage to avoid catastrophic failure.
2. The coal used in Indian power stations has large amounts of ash (about 50%), which contain abrasive mineral species such as hard quartz (up to 15%), which increase the erosion propensity of coal.
3. Application of a proper combination of preventive approaches should lead, in practice, to a significant decrease in the number of failures due to hot corrosion.
4. Hot corrosion preventive methods to the existing environment are (a) change of metal i.e. use of super alloy (b) use of inhibitors and (c) use of coatings.
5. The development of modern coal fired power generation systems with higher thermal efficiency requires the use of construction materials of higher strength and with improved resistance to the aggressive service atmospheres. These requirements can be fulfilled by protective coatings.

REFERENCES

1. A.S. Khanna, "Introduction to high temperature oxidation and corrosion", ASM International, ISBN 0-87170-762-4, SAN: 204-7586, 2002, pp 1-322.
2. M.H. Li, X.F.Sun, J.G.Li, Z.Y. Zhang, T. Jin, H.R. Guan, Z.Q. Hu, Oxid. Metals, Vol.59 (5/6) (2003
3. R. Viswanathan, " Damage mechanism and life assessment of high-temperature components", ASM International, 1989, ISBN: 0-87170-358-0, pp 1-483
4. B.A. Landry, J.D. Hummel, H.W. Nelson et al, "A review of available information on corrosion and deposition in coal and oil fired boilers and gas turbines", ASME research committee, Pergamon press, The American society of mechanical engineers, New York, pp1-197.
5. Buta Singh Sidhu and S. Prakash, "Evaluation of the behavior of shrouded plasma spray coatings in the platen superheater of coal-fired boilers", Metallurgical & Materials Transactions, Vol. 37A, 2006,pp 1927.
7. 7. T.S. Sidhu, R.D. Agarwal, S. Prakash, "Hot corrosion of some super alloys and role ofhigh-velocity oxy-fuel spray coatings", Surface Coatings & Technology, Vol. 198, 2005,pp441-446
8. Kevin J. Stein, Brian S. Schorr, Arnold R. Marder, "Erosion of thermal spray MCr-Cr C cermet coatings", Wear, Vol. 224, 1999, pp 153-159.
9. Robert A. Rapp, "Hot corrosion of materials: a fluxing mechanisms", Corrosion Science ,44, 2002, 209-221.
10. Y.T. Pei, D. Galvan, J. Th. M. De Hosson, A. Cavaleiro, "Nanostructured TiC/a-C coatings for low friction and wear resistant application", Surface & Coatings Technology, Vol. 198, 2005, pp 44-50.
11. Kevin J. Stein, Brien S. Schorr, Arnold R. Marder, "Erosion of thermal spray MCr- Cr3C2", Wear, Vol. 224, 1999, pp 153-159.
12. S. Prakash, S. Singh, B. S. Sidhu and A. Madeshia, (2001), "Tube Failures in Coal Fired Boilers," Proc. National Seminar on Advances in Material and Processing, Nov., 9-10, IITR, Roorkee, India, pp. 245-253.
13. L. Fedrizzi, S. Rossi, R. Cristel, P.L. Bonora, "Corrosion and wear behavior of HVOF cermet coatings used to eplace hard chromium", Electrochemica Acta, Vol 49, 2004, pp
2803-2814.
14. Chen, H. C., Liu, Z. Y. and Chuang, Y. C., (1993), "Degradation of Plasma-Sprayed Alumina and Zirconia Coatings on Stainless Steel During Thermal Cycling and Hot Corrosion," Thin Solid Films, Vol. 223, No. 1, pp. 56-64.
15. N. Priyantha, P. Jayaweera, A. Sanjurjo, K. Lau, K. Krish, "Corrosion-resistant metallic coatings for applications in highly aggressive environment", Surface & Coating Technology, Vol.163-164, 2003, 31-36.
16. M.G. Hocking, "Coating resistant to erosive/corrosive and severe environment", Surface Coatings & Technology, Vol. 62, 1993, p 460-466.
17. A.S Khanna, S.K Jha," Degradation of Materials under hot corrosion conditions". Trans Indian Inst. Met., 51(5).1998,279-90.
18. P.Bansal, N. P. Padture, A. Vasiliev, " Improved interfacial properties of Al2O3- 13wt%TiO2plasma sprayed coatings derived from nanocrytalline powders", Acta Materialia, 2003, Vol.51,pp.2959-2970.
19. S. Paldey, S. C. Deevi, "Single layer and multilayer wear resistant coatings of (Ti,Al): a review", Materials Science & Engineering, Vol: A 342, 2003, pp 58-79.
20. Jin-hong Kim, Hyun-seok Yang, Kyeong-ho Baik, Byeung Geun Seong, Chang-hee Lee, Soon Young Hwang, "Development and properties of nanostructured thermal spray coatings", Current Applied Physics, Vol. [6], issue 6, (2006), 1002-1006.
21. Bo Liang, Chuanxian Ding, "Thermal shock resistances of nanostructured and conventional zirconia coatings deposited by atmospheric plasma spraying", Surface Coatings & Technology, Vol. [197], (2005), 185-192.

Synthesis of polyaniline-zinc oxide composites and its usage as ammonia gas sensor

Vivek Talwar[a,b], Ravi Chand Singh[a]

[a]*Department of Physics, Guru Nanak Dev University, Amritsar, India*
[b]*Department of RIC, Punjab Technical University, Kapurthala, India*

***Abstract*— The synthesis of polyaniline-Zinc oxide composites and their usage as ammonia gas sensor was reported in this paper. We adopted a novel chemical route for the synthesis of polyaniline composites via chemical method. These samples were prepared by oxidation of aniline via rapid mixing method in acidic medium with the addition of fixed weight percentage of Zinc oxide. The synthesized samples were characterized using X-ray diffraction (XRD) and field emission scanning electron microscope (FESEM) techniques. The thick films of prepared salt were deposited on alumina substrate for gas sensing application. These sensors exhibited excellent response and recovery time, when exposed to different concentration of ammonia gas at room temperature.**

***Keywords*—** Polyaniline, Zinc oxide, Gas sensors, Conducting polymers, Composites.

I. INTRODUCTION

Conducting polymers has attracted a lot of attention due to its unique electrical properties [1]. The conducting polymers have relative ease of synthesis, environmental stability and very rich doping/de-doping chemistry [2]. Polyaniline (PANI) has proved to be a promising material among the conducting polymers with numerous applications like gas sensors, modified electrodes, solar cells, electrochromic materials, microelectronics and in rechargeable batteries. PANI can easily be synthesized by oxidation of aniline monomer at room temperature [3]. However its synthesis at low temperatures yields PANI with molecular weight five to ten times higher than that synthesized at room temperature [4]. Lately, the research interest of scientific fraternity is growing to study the properties and applications of organic-inorganic composites due to their low cost, ease of synthesis and their novel properties. In this regard polyaniline-metal oxide composites [5] have been investigated by several researchers.

In the present study, polyaniline-zinc oxide composites have been synthesized by oxidation of aniline using rapid mixing technique with the addition of zinc oxide powder. The synthesized samples were characterized by using X-ray diffraction (XRD) and field emission scanning electron microscope (FESEM) techniques. Further these samples were used for ammonia gas sensing at room temperature.

II. EXPERIMENTAL DETAILS

A. Synthesis of polyaniline-ZnO composites

Aniline, zinc oxide (ZnO), ammonium persulphate (APS), Hydrochloric acid (HCl), Salphuric acid (H_2SO_4), N-methyl-2-pyrrolidone (NMP) and m-cresol were procured from Spectrochem, India. All chemicals used were of analytical grade and were used without further purification. To synthesize these samples, aniline was oxidized with ammonium persulphate (APS) in aqueous acid solution with the addition of ZnO powder. The solutions of aniline and APS with monomer to oxidant molar ratio 1:1.25 were dissolved separately in 1 M H_2SO_4 solution. ZnO powder (20 wt% of aniline) was added to aniline solution with ultrasonication of few minutes. Both the solutions were placed in an ice bath (0-4° C) and then oxidant was added rapidly to aniline solution and kept in same ice bath for 4 hours. The obtained solution was kept at room temperature for polymerization for 24 hours. The polymerized salt was filtered and washed repeatedly with double distilled water to remove oligomers and excess acid. The resultant product was dried in air and then in vacuum at 60°C.

B. Material characterization

The structural and morphological analysis was done using X-ray diffraction and FESEM techniques. For crystal structure analysis, the prepared samples were characterized by powder X-ray diffraction (XRD) using Cu Kα radiation with Shimadzu 7000 Diffractometer and field emission scanning electron microscope (FESEM) with Ziess, model Supra 55.

C. Sensor fabrication and testing method

To fabricate gas sensors, a small amount of prepared powder was dissolved in m-cresol and thick films were deposited on alumina substrate by simple coating with paint brush and dried at 60°C for 30 minutes in air. The fabricated sensor was placed in the test chamber at room temperature and a known quantity of ammonia gas was injected into the test chamber. Variation of real time voltage signal across the resistance was recorded with an experimental setup consisting of Keithley Data Acquisition Module KUSB–3100 and a computer [6]. The sensor

response magnitude was determined as ratio of resistances of sensor in air-gas mixture and air ambience.

III. RESULT AND DISCUSSION

A. *X-ray diffraction spectra*

Figure 1 represents the x-ray diffraction pattern of pure polyaniline, polyaniline-zinc oxide composites and pure zinc oxide. The small characteristic peaks of ZnO were observed in the spectrum of composite, which are marked by red dots. Also large peaks of polyaniline were found in the XRD spectrum and marked by black dots. This indicates that polyaniline material is more crystalline in the composite due to some kind of formation of polyaniline fibres with the addition of ZnO.

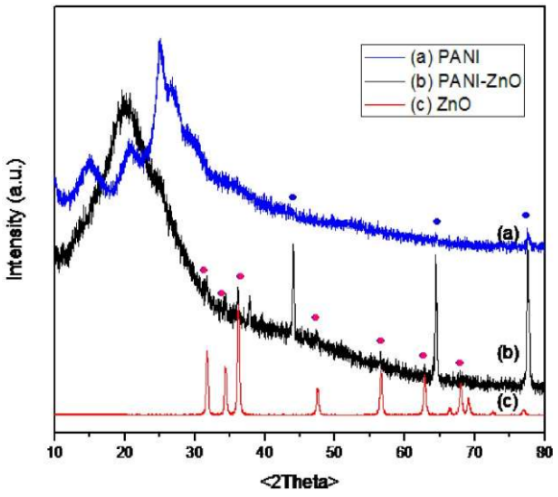

Fig 1 X-ray diffraction spectra of (a) pure PANI, (b) PANI-ZnO composites and (c) pure ZnO powder.

B. *Field emission scanning electron microscopy*

Figure 2 represents SEM image of PANI-ZnO composites prepared in acidic medium. It is observed from the morphological analysis that fibrous structures of PANI were formed with the addition of ZnO powder.

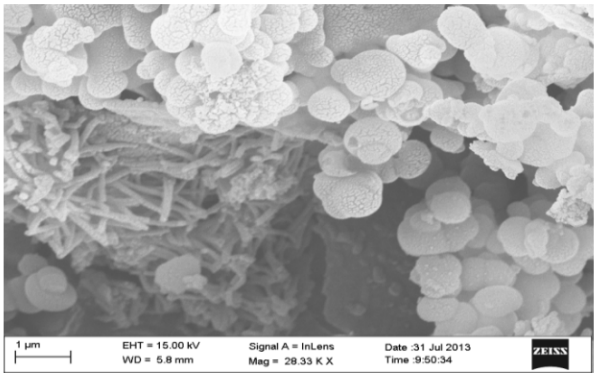

Fig 2 SEM image of PANI-ZnO composites.

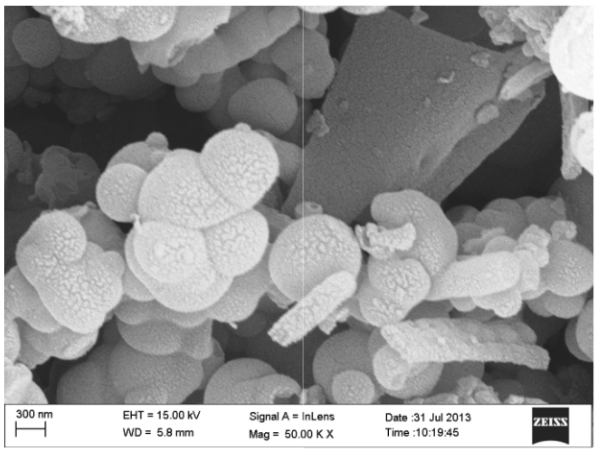

Fig 3 SEM image of PANI-ZnO composites at higher resolution.

Figure 3 represents the SEM image of PANI-ZnO composites at higher resolution. The length and width of these fibers is about 1 micrometer and 100 nanometers respectively. These fibers are made up of polyaniline material as observed by large peaks of polyaniline in the XRD spectra of composites. The presence of ZnO during the polymerization of aniline supports the formation of PANI fibers.

C. *Ammonia gas sensing*

Figure 4 represents the sensing response of the PANI-ZnO composites to different concentration of ammonia gas (50-500 ppm) at 27°C. It was found that the sensing response increases linearly with increase in gas concentration. The response time of this sensor if about 2-3 minutes while the recovery time is about 25-30 minutes.

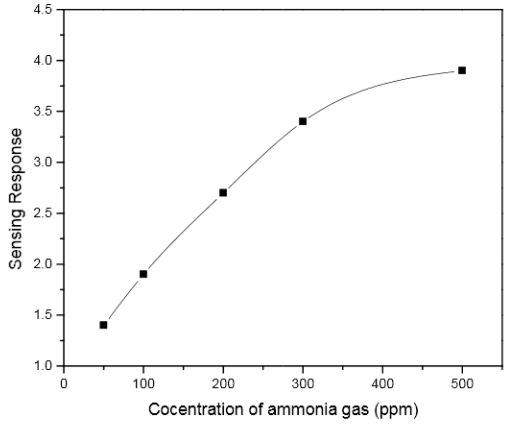

Fig 4 Sensing response for different concentration of ammonia gas.

IV. CONCLUSION

The PANI-ZnO composites were prepared chemically by rapid mixing method. The X-ray diffraction spectrum confirmed the formation of highly crystalline PANI-ZnO composites. These results were confirmed with SEM

images, which had shown the formation of polyaniline fibers in the samples. The prepared salt was used for ammonia gas sensing at room temperature and found good sensing response.

REFERENCES

[1] A.G. Mac Diarmid, *Semiconducting and metallic polymers: the fourth generation of polymeric materials*. Synth. Met., 2002, pp. 11-22.

[2] A.J. Heeger, *A novel role for organic polymers*. Synth. Met., 2002, pp. 23-42.

[3] J. Stejskal, R.G. Gilberd, *Polyaniline. Prepration of Conducting Polymer*. Pure Appl. Chem., 2002, pp. 857-867.

[4] P.N. Adams, P.J. Laughlin, A.P. Monkme, *Synthesis of high molecular weight polyaniline at low temperatures*. Synth. Met., 1996, pp. 157-160.

[5] J. Huang, T. Yang, Y. Kang, Y. Wang, S. Wang, *Gas sensing performance of polyaniline/ZnO organic-inorganic hybrids for detecting VOCs at low temperature*. J. Nat. Gas Chem., 2011, pp. 515–519.

[6] V. Talwar, O. Singh, R. C. Singh, *ZnO assisted polyaniline nanofibers and its application in ammonia gas sensing.* Sens. Actuators B, 2014, pp. 276-282.

Spintronics -A new excitement in the scientific and Electronic world

Harpreet Kaur
Department of Applied Sciences,
Amritsar College of Engineering and Technology, Amritsar

Abstract: **An emerging technology exploiting both the intrinsic spin of the electron and its associated magnetic moment, in addition to its fundamental electronic charge, in solid-state devices. Using the spin of an electron to represent binary data (0 or 1). Spintronics techniques are capable of much higher speed while requiring less power than the conventional method of using electron charges to represent data. This paper reviews about the "spintronics" which is new branch of physics and concerned with the manipulation, storage, and transfer of information by means of electron spins and not by the electron charge as in conventional electronics.**

KEYWORDS: **Spinelectronics , Fuxtronics, Electronics, Spin etc.**

INTRODUCTION

Semiconductor based devices and Magnetic materials have been known to mankind since many years. Semiconductor devices are electronic components that exploit the electronic properties of semiconductor materials, principally silicon, germanium, and gallium arsenide. Meanwhile, semiconductor based devices that use the charge of the individual electrons as the information carrier, have extensively been used in the last century in integrated devices like microprocessors, diodes used in computers, amplifiers, cell phones etc.

When we switch to magnetic materials, the most famous example is the compass needle but today magnets are used everywhere, as permanent magnets in electrical motors in our cars, in hard drives on our computers, in loudspeakers
etc. The performance of these devices is generally dependent on development in manufacturing and fabrication, due to which the dimension of the components of devices (e.g. transistors in ICs) is to be shrinked and packed more densely in order to make a faster device[1]. The dimensions are becoming so tiny that classical physics no longer is applicable and quantum effects start to become important. So the industry has found new clever ways to overcome the problem by creating such a possibility so as to combine both functionalities charge and spin of electron together. So, the ability to manipulate e^-'s spin together with controlling their charge flow has created a new branch of electronics called *SPINTRONICS*. So hopefully, the mass, charge and spin of the electron will form the foundation of information technology in the coming future [1,2].

Spintronics (a portmanteau) meaning "spin transport electronics also known as spinelectronics or fluxtronic, is an emerging technology exploiting both the intrinsic spin of the electron and its associated magnetic moment, in addition to its fundamental electronic charge, in solid-state devices. Using the spin of an electron to represent binary data (0 or 1). Spintronics techniques are capable of much higher speed while requiring less power than the conventional method of using electron charges to represent data.

REVIEW OF LITERATURE

The first use of spintronics was in the late 1980s with the development of giant magnetoresistance (GMR) read heads for disk drives. The first major breakthrough in spintronics was the discovery of the giant magnetoresistance (GMR) effect in 1988. Working independently, Albert Fert in France and Peter Grünberg in Germany found that in a material consisting of alternating layers of magnetic and nonmagnetic atoms a very small change in a magnetic field can produce a large

change in electrical resistance. Employing advances in nanotechnology, they used chemical techniques that allowed them to make layers of different materials that were only a few atoms thick. The GMR effect was used in the development of data-storage devices that were physically smaller but allowed increasingly denser packing of the information content. The first commercial devices using the GMR effect, produced in 1997, had a 40-fold increase in data density when compared with conventional electronics. The technology is now used in computer storage, personal music players, cell phones, and other devices that benefit from the increased size of readable memory. In a more sensitive effect, called tunneling magnetoresistance (TMR), an insulating material acts as a sandwich. Electrons can move through the sandwich by quantum tunneling

Another spintronic breakthrough product is magnetoresistive memory (MRAM), which uses electron spin to store information; while requiring less power than coventional magnetic storage technologies, it combines the density of DRAM (dynamic random access memory) with the speed of SRAM (static random access memory) and the nonvolatility of flash memory. In recognition of their contributions, Fert and Grünberg shared the 2007 Nobel Prize in physics. Manipulating an e-'s magnetic state in a semiconducting device is the key to successful realization of spintronics. There is currently a lot of interest in the science and potential technological applications of spin-transport electronics or spintronics, in which the spin of charge carriers; electrons or holes is exploited to provide new functionality for microelectronic devices. A number of researchers are trying to find out the materials for successful realization of spintronics. .This has paved a way to new class of materials called DILUTE MAGNETIC SEMICONDUCTORS"

The term "spintronics" usually refers to the branch of physics concerned with the manipulation, storage, and transfer of information by means of electron spins in addition to or in place of the electron charge as in conventional electronics. Introduced in 1996, spintronics (the word coined by S. Wolf) was originally the name for a Defense Advanced Re-search Projects Agency (DARPA) program managed by Wolf. Spin is a fundamental quantum-mechanical property. It is the intrinsic angular momentum of an elementary particle, such as the electron. Of course, any charged object possessing spin also possesses an intrinsic magnetic moment. Electrons are spin-1/2 fermions and therefore constitute a two-state system with spin "up" and spin "down". Conventional electronic devices rely on the transport of electrical charge carriers electrons in a semiconductor such as silicon. Now, however, physicists are trying to exploit the 'spin' of the electron rather than its charge to create a remarkable new generation of 'spintronic' devices which will be smaller, more versatile and more robust than those currently making up silicon chips and circuit elements.

Spintronics promises the possibility of integrating memory and logic into a single device. Schematic overview of spintronics is schematically shown in Figure 1

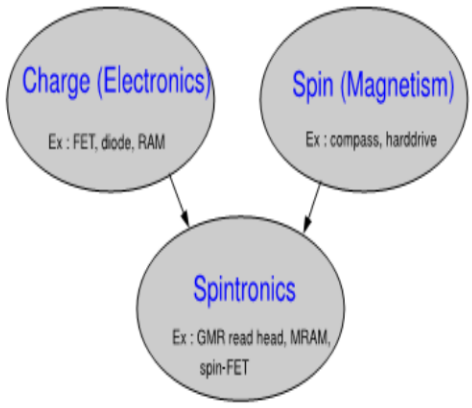

Figure1. Schematic overview of spintronics which combines both charge (electronics) and spin (magnetism) into a novel field of research and applications.

The research field of Spintronics emerged from experiments on spin-dependent electron transport phenomena in solid-state devices done in the 1980s, including the observation of spin-polarized electron injection from a ferromagnetic metal to a normal metal by Johnson and Silsbee[1] (1985) and then independently work is carried out by Albert Fert et al and Peter Grünberg et al.[2] (1988).The use of semiconductors for spintronics can be traced back at least as far

as the theoretical proposal of a spin field-effect-transistor by Datta and Das in 1990.

To make a spintronic device, the primary requirements are to have a system that can generate a current of spin polarized electrons comprising more of one spin species – up or down – than the other (called a spin injector), and a separate system that is sensitive to the spin polarization of the electrons (spin detector). Spintronic devices act according to the simple scheme: (1) information is stored (written) into spins as a particular spin orientation (up or down), (2) the spins, being attached to mobile electrons, carry the information along a wire, and (3) the information is read at a terminal.

APPLICATIONS

The use of carrier spin, in addition to charge, appears promising for a new class of devices such as polarized light emitters, chips that integrate memory and microprocessor functions, magnetic devices exhibiting gain and ultra-low power transistors[3]. The most successful application of spintronics to date is without any doubt the giant magneto resistance (GMR) read head in harddrives, an effect that was discovered by P. Grunberg and A. Fert who received the 2007 Nobel Prize in Physics. Spintronics phenomenon is expected to become widely used in sensors and non-volatile memories.

CONCLUSION

Today everyone already has a spintronics device on their desktop, as all modern computers use the spin valve in order to read and write data on their hard drive. It was followed immediately by the discovery of Giant Magnetoresistance (GMR) leading to the magnetic tunnel junction that has been utilized for the next generation computer memory known as Magnetic Random Access Memory (MRAM), another spintronics device for computers. Also, Spintronic devices are attractive for memory storage magnetic sensors applications.[9] .

Enormous application of spintronic devices such as spin-valve transistor, spin-light emitting diodes, non-volatile memory, ultra fast optical switches, inspires extensive research work to synthesize Diluted Magnetic Semiconductor (DMS)with III-V and II-VI semiconductors. Quite substantial amount of work has been done with transition metal doped III-V semiconductor particularly Mn doped GaAs[1,2].With III-V semiconductors, however, the magnetic elements are much less soluble than in II-VI semiconductors making them much more difficult to inject into a material like GaAs.

REFERENCES

[1] J. K. Furdyna, "Diluted magnetic semiconductors," J.Appl.Phys. 64 (4), 29-64 (1988).

[2] S. A. Wolf et al., "Spintronics: a spin-based electronics vision for the future," Science 294, 1488-95 (2001).

[3] S. Das Sarma, American Scientist, Vol 89(2001) 516H.

[4] H.ohno,Science,vol281(1998),951.

[5] Mauger A and Godart C 1986 Phys. Rep. 141 51.

[6] R. Janisch, P. Gopal and N. A. Spaldin. J. Phys: Condens Matter Vol 17 (2005) R657-R689.

[7] H. Ohno, Science, Vol 281 (1998), 951.

Radon Concentration in drinking water samples of some adjoining areas of Amritsar, Punjab using electronic radon detector

Ajay Kumar[a]
[a]*Post Graduate Department of Physics, DAV College, Amritsar, India*
Corresponding author: ajay782@rediffmail.com

***Abstract*-Radon and its daughter products are the major sources of radiation exposure and recognized as one of the health hazards for mankind. In the Present work, the groundwater samples taken from 10 locations of Amritsar area, Punjab were analysed for radon concentration. Radon concentrations were measured using RAD 7, an electronic radon detector. Radon concentration varies from 32.4 pci/l to 60.3 pci/l. The values are found to be within the safe limits as recommended by the International Commission of USEPA and UNSCEAR. The results reveal that these areas are safe from the health hazard point of view as for as the radon is concerned.**

***Keywords*- RAD 7, Radon, water**

1. INTRODUCTION

Radon is a radioactive inert gas, which is produced during the decay of radium in the naturally occurring uranium series. In the recent past environmental scientists all over the world have been expressing great concern about the radiation hazards from ^{222}Rn and its short lived daughter products inside buildings [1,2]. Inhalation of ^{222}Rn and its daughter products, especially ^{218}Po and ^{214}Po attached to aerosols present in ambient air, constitute a significant radiological hazard to human lungs. Radon appears mainly by diffusion processes from the point of origin [3] following α-decay of ^{226}Ra in underground soil and building materials used in the construction of floors, walls, ceilings, etc.

The earth is radioactive since its creation. The inhalation and ingestion of these radio nuclides above the permissible level becomes a health hazard. Therefore, concern of the monitoring of these radio nuclides in the environs is increasing at all levels, due to their harmful effects. If inhaled or ingested, uranium activity poses an increased risk of lung and bone cancer [4].

The magnitude of indoor radon concentration indoors depends primarily on a building construction and the amount of radon in underlying soil. The concentration of radon and its decay products show large temporal and local fluctuations in the indoor atmosphere due to meteorological variables [5, 6]. People who consume underground water for various purposes including drinking may be exposed to high levels of radon, but there is some risk from drinking water with elevated radon. The aim of the present study is to investigate the radon concentration in groundwater of some areas of Amritsar, Punjab for public health risk measurements

II. EXPERIMENTAL TECHNIQUE

A. Estimation of Radon Concentration in Water samples

For radon in water measurement, the RAD-H_2O closed loop aeration method has been employed [7-9] as shown in fig. 1. The RAD7 continually measures radon and thoron concentration, showing both on a spectrum printout, and also functions as a sniffer with audible count signal to locate radon entry points. Radon in water was measured by unit RAD-7.0 detector supplied by DURRIGDE Company INC, USA. It has a sample cell of 0.7 litre hemisphere, coated inside with an electrical conductor. A solid state Ion implanted planer silicon alpha detector is at the centre of hemisphere. A voltage of 2000V to 2500V creates an electric field. Radon 222 nucleus that decays within the cell creates polonium 218 which enters the hemisphere and the signal is amplified and counted electronically. The unit features the fastest response and recovery time of any system on the market, and is able to measure radon concentrations at the 200 Bq/m^3 action level in less than 1 hour with 10% standard deviation. The virtual absence of intrinsic background (0.2 Bq/m^3) gives the RAD7 an extremely low detection threshold, easily measuring below 4 Bq/m^3. The instrument is microcomputer controlled, featuring step-by-step instructions for ease of use. The instrument is a complete, portable stand-alone system with a built-in air pump, supplied in a rugged carrying case, total weight 5 kg. Additional accessories allow measurement of radon in soil and water (continuous and sample measurement); the RAD AQUA continuous water measurement accessory allows measurement of water radon to extremely low concentrations, whereby the air volume and water volume are constant and independent of the flow rate. The air circulates through the water and continuously extracts the radon until a state of equilibrium develops. The RAD-H_2O system reaches this state of equilibrium within about 5 minutes, after which no more radon can be extracted from the water. The extraction efficiency, or percentage of radon

removed from the water to the air loop, is very high. The RAD H_2O gives results after 30 minutes analysis with a sensitivity that matches or exceeds that of liquid scintillation methods.

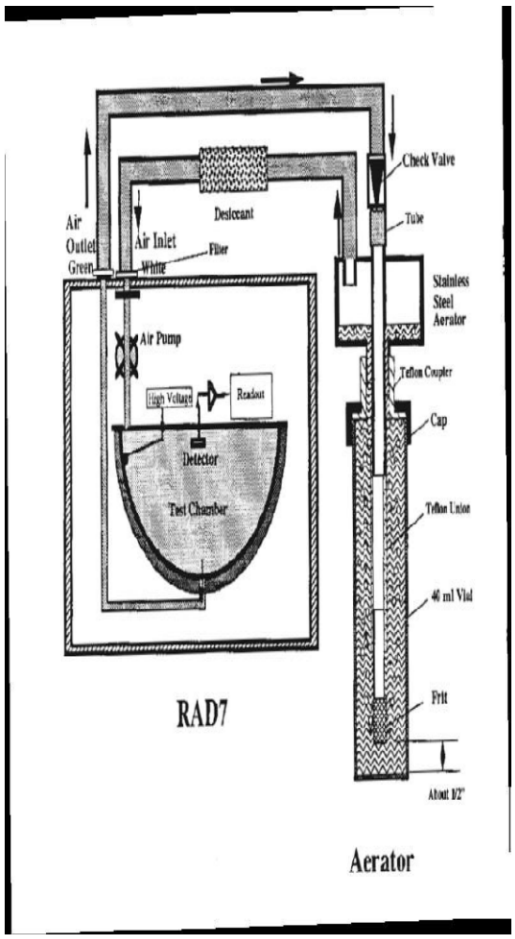

Fig.1 Schematic diagram of the RAD 7 H_2O

III. RESULTS AND DISCUSSION

The values of radon concentration in water samples of the study area are given in Table 1. The values in samples from Amritsar area lies in the range32.4±14.2 pci/l(Lauka) to 60.3±18.2pci/l (Patti). The US Environmental protection agency has proposed that the allowed maximum contamination level (MCL) for radon concentration in water is 300 pci/l (USEPA, 1991). The value of radon concentration in groundwater was compared with those reported by other investigators. Duggal et al.[7] have reported a radon concentration range 0.9 Bql^{-1} to 5.1 Bql^{-1} of Bathinda district, Punjab [7] and Rani et al. [10] have reported a radon concentration range 0.5 to 85.7 Bql^{-1} in groundwater samples of Rajasthan area, India. Radon concentration values obtained in the groundwater samples lies well within the range. The results reveal that the area is safe as for as the health hazard effects due to radon are concerned in these drinking water samples.

Table 1 The average radon concentration of 10 locations in Amritsar district

S.No.	Location	Radon Concentration (pci/l)±SD*
1	Patti	60.3±18.2
2	Kairon	39.1±4.89
3	Lauka	32.4±14.2
4	Sarhali	43.5±12.3
5	Chohla Sahib	55.3±18.4
6	Bhaggupur	45.7±14.7
7	Sangwan	49.2±11.3
8	Amarkot	57.4±9.0
9	Bhikhiwind	34.5±6.1
10	Ghariala	41.7±8.3

SD- standard deviation

IV. CONCLUSIONS

The values of Radon concentration in the groundwater samples are within the safe limit recommended by the US Environmental Protection agency [11] and United Nations Scientific Committee on the Effects of Atomic Radiation [12]. The results show no significant radiological risk for the inhabitant of the study area.

. REFERENCES

[1] J. Kumar, R. Malhotra, J. Singh and S. Singh, "Radon measurements in dwellings in radioactive areas in Himachal Pradesh, India, using LR-115, plastic track detectors" in *Nuclear Geophys.*, 1994, 8, 573-576.

[2] J. M. Lee and G. Kim, "A simple and rapid method for analyzing radon in coastal and ground waters using a radon in air monitor" in *J. Environmental radioactivity.,* 2006, 89, 219-228.

[3] A.B.Tanner, Radon migration in the ground : A supplementary review. In *The Natural Radiation Environment III.* (eds. T.F. Gesell and W.M. Lowder), National Technical Information service, Springfield, VA. CONF-780422, 1980 5-56.

[4] *Agency for Toxic Substances and Disease Registry(ATDSR),* Report TP-90-29. Atlanta, USA, 1999.

[5] T.V. Ramachandran, T.S. Murleedharan, A.N. Shaikh and M.C. Subba Ramu, "Seasonal

variation of indoor radon and its progeny concentration in a dwelling" in *Atmos. Environ.,*1990, 24A(3), 639-645.

[6] S. Singh, R. Malhotra, J. Kumar and L. Singh., Seasonal variation of indoor radon and its progeny concentration in a dwelling. *Radiation measurements.,* 2001, 34, 505-508.

[7] V. Duggal, R. Mehra and A. Rani, "Determination of ^{222}Rn level in groundwater using RAD 7 Detector in the Bathinda District of Punjab, India" in *Radiat. Prot. Dosim*., 2013 1-7 (Doi: 10,1093/rpd/net054.

[8] K.Badhan, R. Mehra and R.G. Sonkawade "Measurement of radon concentration in ground water using RAD 7 and assessment of average annual dose in the environs of NITJ, Punjab, India" in *Indian Journal of Pure and Applied Physics.,*2010, 48, 508.

[9] N. Sharma, R. Sharma and H.S. Virk "Environmental Radioactivity: A case study of Punjab, India" *Advances in Applied Science Research* 2011, 2(3),186.

[10] A. Rani, R. Mehra and V. Duggal "Radon monitoring in groundwater samples from some areas of Northern Rajasthan, India, using a RAD 7 Detector *Radiat.Prot. Dosim*, 2013, 153, 496.

[11] USEPA, National Primary drinking water regulations, US Governmental Printing Office, EPA/570/9-91/700, 1991.

[12] United Nations Scientific Committee on the Effects of Atomic Radiation. Sources and Effects of Ionizing Radiation. UNSCEAR, 2008 report to the general assembly with scientific annexes. United Nations, 2008.

Study of physical parameters of Ag-Ge-Se glass system

AmitSethi[a], Rajesh Kumar[b], AmitSarin[c] and NavjeetSharma[d]
[a]*Research Scholar, Punjab Technical University, Kapurthala, India*
[b]*Department of Physics, DAV College, Amritsar, India*
[c]*Department of Physics, Amritsar College of Engineering & Technology, Amritsar, India*
[d]*Department of Physics, DAV College, Jalandhar, India*

***Abstract*—Glasses in selenium rich region of Ag-Ge-Se are fast ionic conductors. Effect of variation of Ag content on the properties of $[Ge_{20}Se_{80}]_{100-x}Ag_x$ (x = 2, 4, 6, 8, 10) glass system has been analyzed. The variation in the properties of the system such as glass transition temperature and optical gap has been explained in terms of physical parameters such as average coordination number, number of constraints, floppy modes and lone pair electrons. Heat of atomization of the system has been calculated. Heat of atomization has been found to be increasing with increasing Ag content. Glass transition temperature has been evaluated on the basis of Lankhorst approach and variation has been discussed on the basis of chemical bond approach.**

***Keywords*—**Coordination Number, Glasses, Glass Transition Temperature, Heat of Atomisation.

I. INTRODUCTION

Chalcogenide glasses are compounds of one or more chalcogen elements with some metallic element. These glasses have numerous applications in diverse fields such opto electronic devices, as memory elements, xerography etc (Ovshinsky, 1968; Khan et al., 2002; Zhang et al., 2003). The glasses are known for high transparency in IR region. Addition of an impurity element to host glass introduces structural disorder leading to variation in peoperties of glass. So the properties of these glasses are composition dependent and can be changed by continuously varying the concentration of impurity element (Davis, 1985; Moharram et al., 2006). Many of the physical properties of these materials can be related to the Chemical bonds structure present in the system (Fouad et al., 1998). One of the most studied chalcogenide system is the Ge-Se glass system because of its wide glass forming ability. Various studies has been performed on the effect of different impurities such as Pb, Sb, Tl, Bi etc in Ge-Se system. The Ag-Ge-Se system can be classified into two categories i.e. selenium rich or germanium rich. Seleium rich glasses are fast ionic conductors and germanium rich glasses are semiconducting. In the present paper we have attempted to study the effect of variation of Ag concentration on the properties of Ag-Ge-Se glass system.

II. THEORETICAL METHODOLOGY & DISCUSSION

Constraints theory for covalent bonded glasses, proposes that mechanical constraints play an important role structure formation of a network (Philip, 1979; Thorpe, 1983). If long range order is neglected, then two types of constraints i.e. bond bending N_B and bond stretching N_S, need to be counted. For an atom with coordination number r, bond bending constraints per atom are given by

$N_B = 2r-3$

while the bond stretching constraints per atom are given by

$N_S = r/2.$

For multicomponent glasses, average coordination number $\langle r \rangle$ is taken which can be calculated as

$\langle r \rangle = (ar_A+br_B+cr_C)/a+b+c$

wherea,b,c are atomic percentages and r_A, r_B, r_C are coordination numbers, of constituents elements. Total number of constraints are given by

$N = N_S+N_B$. The effective coordination $\langle r_{eff} \rangle$ is related to total number of constraints by the relation

$\langle r_{eff} \rangle = 2(N+3)/5.$

Constraints theory further proposes rigidity percolation or mechanical threshold when total number of constraints equal the number of degrees of freedom of system, which is obtained for $\langle r \rangle = 2.4$.

For $\langle r \rangle < 2.4$ the system is said to be under coordinated or floppy and for $\langle r \rangle > 2.4$, system is over coordinated or rigid.

Number of floppy modes in the system is related to degree of cross linking, which is a function of average coordination number.

The number of floppy modes in the system is calculated by the relation

$f = 2-5/6\langle r \rangle.$

Number of lone pair electrons in the system influences the glass formation ability of the system. Presence of lone pair electrons in the bonding atoms provide a character of flexibility to the bond, which allows it to form amorphous network easily. The number of lone pair electrons in any system can be calculated by the relation (Heera et al., 2012).

$L = V - \langle r \rangle$, where V is average number of valance electrons and $\langle r \rangle$ is average coordination number.

The values of average coordination number, constraints, floppy modes and lone pair electrons calculated for $[Ge_{20}Se_{80}]_{100-x}Ag_x$ (x = 2, 4, 6, 8, 10) are shown in table 1. Average coordination number, number of constraints and hence effective coordination number increases with the increasing concentration of Ag.Number of floppy modes

and lone pair electrons decreases with increasing concentration of Ag, indicating that the system is getting more and more rigid with the addition of Ag. The Variation of Number of constraints (N) Effective coordination number (r_{eff}), Number of floppy modes (f) and Lone pair electrons (L) with Ag concentration is shown in fig. 1.

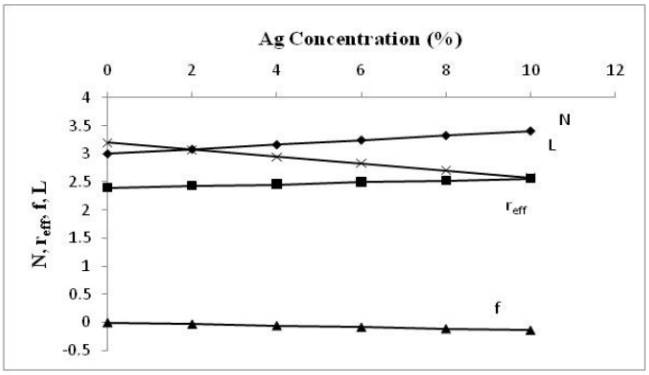

Fig.1. Variation of Number of constraints (N) Effective coordination number (r_{eff}), Number of floppy modes (f) and Lone pair electrons (L) with Ag concentration for $[Ge_{20}Se_{80}]_{100-x}Ag_x$ (x = 2, 4, 6, 8, 10).

Heat of atomization is the enthalpy change required to break all bonds dissociate the material to individual atoms. It is a measure of cohesive energy and average bond strength of the system, and for ternary and higher order compounds can be calculated using the formula (Thorpe, 1995).

$H_s = (aH_S^A+bH_S^B+cH_S^C)/a+b+c$

where H_S^A, H_S^B, H_S^C are heats of atomization for elements A, B, C.

using the value of average heat of atomization, a parameter, $H_S/\langle r\rangle$, called average single bond energy can be calculated, which can be related with the energy gap by a relation given as

$E_g = x(H_S-y)$, where x and y are characteristic constants of system.

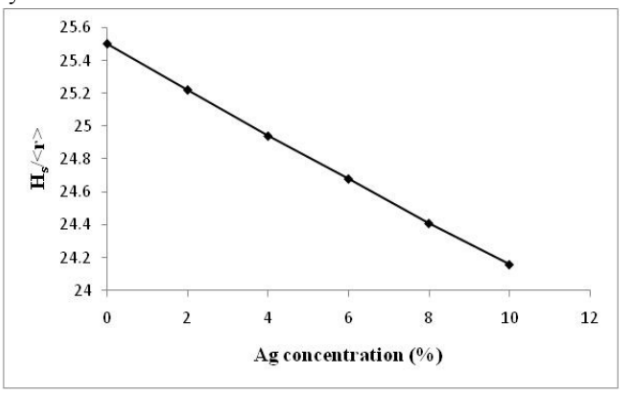

Fig.2. Variation of Average single bond energy ($H_s/\langle r\rangle$), Cohesive energy (C_E) and Band Gap (E_g) with Ag concentration for $[Ge_{20}Se_{80}]_{100-x}Ag_x$ (x = 2, 4, 6, 8, 10).

Glass transition temperature can be related to heat of atomization by a relation given as (Lankhorst, 2002) $T_g = 3.44\ H_S - 488$.

Values of heat of atomization, average single bond energy, glass transition temperature, calculated using Lankhorst formula based on heat of atomisation and band gap calculated for the $[Ge_{20}Se_{80}]_{100-x}Ag_x$ (x = 2, 4, 6, 8, 10) are shown in table 2. Heat of atomization of the system increases with Sn content while average single bond energy decreases with increasing Ag content. Glass transition temperature increases with increasing Ag concentration while the band gap decreases.

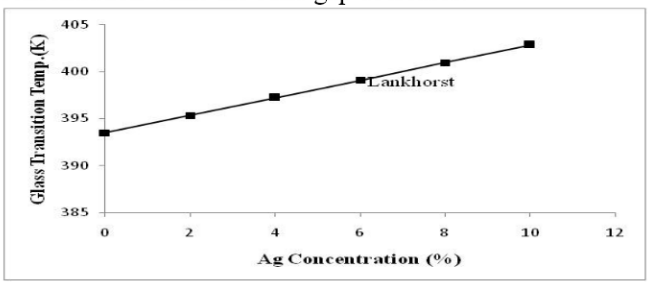

Fig. 3. Variation of Glass transition temperature (T_g) with Ag concentration for $[Ge_{20}Se_{80}]_{100-x}Ag_x$ (x = 2, 4, 6, 8, 10).

III. CONCLUSIONS

Average coordination number, number of constraints and effective coordination number increases with the increasing concentration of Ag. Number of floppy modes and lone pair electrons decreases with increasing concentration of Ag, indicating that bond deformation decreases and the system is getting more and more rigid with the addition of Ag.Heat of atomization of the system increases with Ag content while average single bond energy decreases with increasing Ag content. Glass transition temperature increases with increasing Ag content.

REFERENCES

[1] Ovshinsky S. R., Physical Review Letters, 21,1450-1453, 1968.

[2] Khan S. A., Zulfequar M. and Husain M., Solid State Communications, Vol. 123, No. 10,463- 468, 2002.

[3] Zhang.X., Ma H. and Lucas J., Journal of Optoelectronics and Advanced Materials, Vol. 5, No. 5, pp. 1327-1333, 2003.

[4] Davis E. A., J. Non-Cryst.Solids71, 113, 1985.

[5] Moharram A. H., Othman A. A., Amer H. H. and Dahshan A., J. Non-Cryst. Solids, 352, 2187, 2006.

[6] Fouad S. S., Fayek S. A., Ali M.H., Physical evolution and glass forming tendency of $Ge_{1-x}Sn_xSe_{2.5}$ amorphous system.Vacuum, 49, 25, 1998.

[7] Phillips J. C., J. Non-Crystalline Solids, 34(2), 153, 1979.

[8] Thorpe M. F., J.Non-Crystalline Solids, 57(3), 35, 1983.

[9] Heera P., Kumar A. and Sharma R., J. Ovonic Research, 8(2), 29, 2012.
[10] Thorpe M. F., J. Non-Cryst.Solids 182, 135, 1995.
[11] Lankhorst M. H. R., J. Non-Crystalline Solids, 297(2-3), 210, 2002.

Table 1.Values of Average Coordination No. (<r>), Constraints Bond bending (N_B), Bond Stretching (N_S) and Total (N), Effective Coordination Number, Floppy Modes (f) and Lone Pair Electrons (L) for $[Ge_{20}Se_{80}]_{100-x}Ag_x$ (x = 2, 4, 6, 8, 10).

Composition	<r>	N_B	N_S	N	r_{eff}	f	L
$[Ge_{20}Se_{80}]_{100}$	2.400	1.800	1.200	3.000	2.40	0.0	3.200
$[Ge_{20}Se_{80}]_{98}Ag_2$	2.432	1.864	1.216	3.080	2.43	-0.0266	3.076
$[Ge_{20}Se_{80}]_{96}Ag_4$	2.464	1.928	1.232	3.160	2.46	-0.0533	2.952
$[Ge_{20}Se_{80}]_{94}Ag_6$	2.496	1.992	1.248	3.240	2.50	-0.08	2.828
$[Ge_{20}Se_{80}]_{92}Ag_8$	2.528	2.056	1.264	3.320	2.53	-0.1066	2.704
$[Ge_{20}Se_{80}]_{90}Ag_{10}$	2.56	2.120	1.28	3.400	2.56	-0.1333	2.580

Table 2. Values of Heat of Atomisation (H_S), Average Single Bond Energy (H_S/<r>), Glass Transition Temperature (T_{gL} (Lankhorst)) for $[Ge_{20}Se_{80}]_{100-x}Ag_x$ (x= 2, 4, 6, 8, 10).

	H_s (kcal/g-atom)	H_S/<r>	T_{gL} (K)	Eg (eV)
$[Ge_{20}Se_{80}]_{100}$	61.20	25.50	393.48	2.76
$[Ge_{20}Se_{80}]_{98}Ag_2$	61.33	25.22	395.35	2.74
$[Ge_{20}Se_{80}]_{96}Ag_4$	61.46	24.94	397.23	2.72
$[Ge_{20}Se_{80}]_{94}Ag_6$	61.59	24.68	399.09	2.71
$[Ge_{20}Se_{80}]_{92}Ag_8$	61.72	24.41	400.97	2.69
$[Ge20Se80]_{90}Ag_{10}$	61.85	24.16	402.84	2.67

Effect of Gamma irradiation on structural and optical properties of Muscovite Mica

Sukhnandan Kaur, Surinder Singh, Lakhwant Singh

Department of Physics, Guru Nanak Dev University, Amritsar-143005, Punjab

**Corresponding Author's Email:sukhnandanphy@gmail.com*

***Abstract*— Present work reports the structural and optical properties of pristine and gamma irradiated muscovite mica. The XRD spectra are used to estimate structural parameters such as crystallite size and micro strain of pristine and irradiated samples. Williamson Hall analysis is employed to calculate crystallite size and micro strain of pristine and irradiated sheets. UV-VIS analysis provides the value of optical indirect, direct band gap and Urbach energy. It was found that the value of optical indirect and direct band gap increases with the increase of gamma dose upto 100 kGy and then decreases with further increase in gamma dose upto 2000 kGy. Thus, the increase of optical band gap makes natural muscovite fits for efficient optoelectronic devices.**

***Keywords*—** Gamma Radiation, Natural muscovite, XRD, UV-VIS.

I. INTRODUCTION

Muscovite mica [KAl_2 ($AlSi_3O_{10}$) (F, $OH)_2$] is abundant mineral on the earth and has a layered structure of aluminium silicate sheets weekly bonded together by layers of potassium ions. These potassium ion layers produce the perfect cleavage [1]. Muscovite is used chiefly as an insulating material and for fireproofing and are presently being used as dosimeter for monitoring absorbed doses in radiation rich environments. It is well established that the exposure of any material to ionizing radiations produces changes in the microstructural properties of the material, which in turn affects the structural and optical properties [2]. Thus, it is important to understand the effect of ionizing radiation on the structural and optical properties of these materials.

A lot of information is available on the optical [3-7] properties of natural muscovite mica without irradiation. Moreover, the effect of gamma irradiation on these properties has not been investigated so far. Therefore, in the present work, the effect of gamma dose on structural and optical properties of natural muscovite mica have been investigated to utilize this material for innovative applications in radiation technology and opto-electronic devices.

II. EXPERIMENTAL TECHNIQUES

Thin sheets of Natural muscovite mica (procured from Bhilwara mines in Rajasthan) samples were irradiated with ^{60}Co source to different doses ranging from 1 kGy to 2000 kGy at IUAC, New Delhi. The structural changes were studied using XRD-7000 SHIMADZU X-ray diffractometer. The optical changes were analysed with UV-1800 Shimadzu UV-Vis spectroscopy in the wavelength range 200-600 nm.

III. RESULTS AND DISCUSSION

A. Structural Analysis

Figure 1 shows the XRD pattern for pristine and gamma irradiated natural muscovite mica. Five peaks are observed in pristine muscovite mica at 2θ = 8.99°, 17.90°, 26.94°, 36.12° and 45.59° corresponding to crystallographic planes (003), (006), (009), (0012) and (0015), respectively. No shift in peak positions is observed after gamma irradiation.

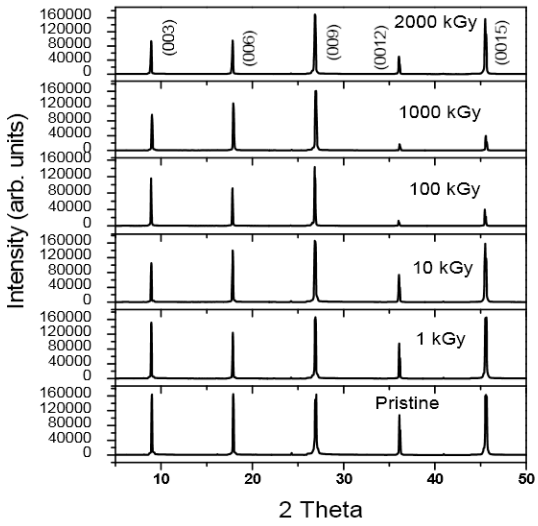

Fig. 1 X- ray diffraction pattern for pristine and gamma irradiated muscovite mica.

The average particle size and the microstrain for the pristine and gamma irradiated samples were determined using the Williamson Hall (W-H) analysis [8]. Fig. 2 shows the W-H plots for the pristine and the gamma irradiated muscovite at different absorbed doses. The values of crystallite size (D) and microstrain (ε) obtained from the intercept and slope of WH plots are listed in table

1. The crystallite size increases with the gamma dose upto 100 kGy; microstrain decreases in the dose range 1- 100 kGy. For gamma doses upto 2000 kGy, the crystallite size decreases however, unlike the microstrain which increase. This means that in the lower gamma dose range, 1 -100 kGy, the irradiation binds the crystallites in clusters, increasing their size and decreasing the microstrain. At higher gamma doses, i.e. 1000, 2000 kGy, the crystallite size decreases and the microstrain increase which indicates that the muscovite moves to a disordered structure.

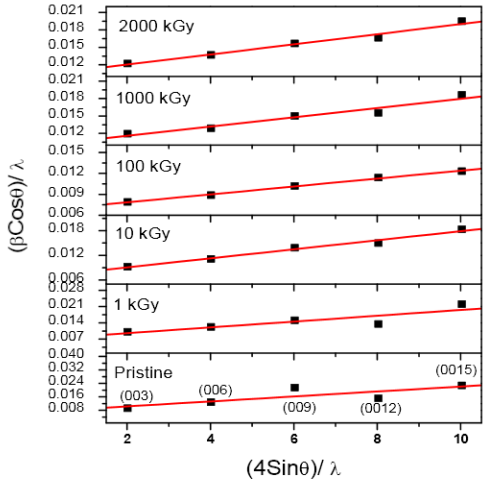

Fig. 2 W-H plots for the pristine and gamma irradiated muscovite mica.

Table 1 Variation of structural and optical parameters with gamma dose

Gamma Dose (kGy)	D nm	ε (10^{-3})	E_g (eV)		E_u (eV)
			Indirect	Direct	
Pristine	135.50	1.47	3.25	3.81	0.45
1	140.65	1.24	3.28	3.83	0.44
10	145.35	1.10	3.33	3.87	0.39
100	148.81	0.57	3.46	3.91	0.32
1000	100.10	0.79	3.30	3.85	0.43
2000	97.09	0.87	3.21	3.76	0.44

B. Optical Analysis

Fig. 3 presents the UV–visible absorption spectra of the pristine and gamma-irradiated (1-2000 kGy dose) natural muscovite mica samples. The absorption edge is shifted towards lower wavelength values by increasing the dose up to 100 kGy. However by further increasing the dose upto 2000 kGy, the absorption edge shifts towards higher wavelength values.

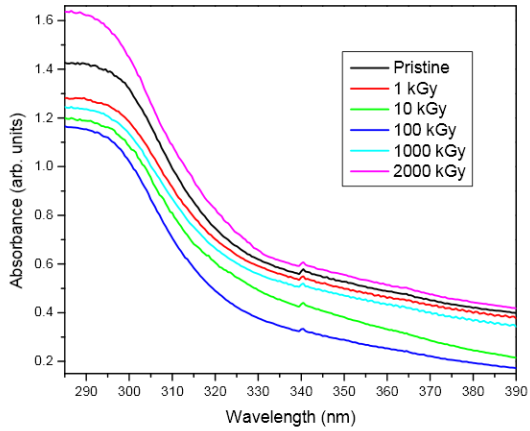

Fig. 3 UV-Vis spectra of pristine and gamma irradiated muscovite mica.

The optical band gap was determined using the following equation [9]:

$$\alpha(h\nu) = B(h\nu - E_g)^n / h\nu \quad (1)$$

where $h\nu$ is the energy of the incident photons, E_g is the value of the optical energy gap between the valance band and the conduction band, B is a constant. The value of n as 1/2 and 2 stands for direct allowed and indirect allowed transitions, respectively. The calculated values of direct and indirect optical band gap for pristine and irradiated samples are given in table 1. The values of optical indirect and direct band gap increase from 1 to 100 kGy and decrease by further increasing the gamma dose upto 2000 kGy.

The irregularities in the band gap level can be defined in terms of Urbach energy (E_u) and were estimated using relation [8]:

$$\alpha(\nu) = \alpha_o \exp(h\nu/E_u) \quad (2)$$

where α_o is a constant, E_u is an Urbach energy and ν is the frequency of radiation. The calculated values of Urbach energy for pristine and gamma irradiated muscovite at different doses are listed in table 1. The decrease of the Urbach energy at increasing γ-doses, from 1 kGy to 100 kGy, indicates the decrease in the structural disorder. By further increasing the dose upto 2000 kGy, the Urbach energy increase may be attributed to increasing of the structural disorder.

IV. CONCLUSION

Gamma irradiation upto 100 kGy leads to the increase in crystallite size and reduction in the defects, structural disorder and microstrain. Thus, irradiation of natural muscovite mica with gamma rays improves its crystallinity. The results of UV-VIS spectra show that the direct and indirect optical band gap can be monitored with the help of gamma irradiations. The increase of optical band gap with gamma irradiation makes natural muscovite fits for efficient optoelectronic devices.

ACKNOWLEDGMENT

Authors are highly thankful to Health physics and material science group at IUAC, New Delhi for providing the Gamma Irradiation, XRD and UV-Vis facilities. Financial support given by UGC, New Delhi, in the form Senior Research Fellowship is also gratefully acknowledged.

REFERENCES

[1] J. Sinkankas, Mineralogy: A First Course; East-west press Pvt. Ltd: New Delhi, 1969.
[2] B.N. Singh, J. Comput-aided Mater. Des. 6 (1999) 195-214.
[3] Popper, P. Nature. **1951**, 168, 1119-1120.
[4] Grum-Grzhimails, S.V., Anikina, L.I., Belova, E.N., Tolstikhins, K.I. Chem. Abst. **1958**, 52,13551.
[5] Dhar, R. N., Das, S.R. Nature. **1966**, 209, 185-186.
[6] Davidson, A.T., Vickers, A.F. J. Phys. C: Solid State Phys. **1972,** 5, 879-887.
[7] Le Calvez, Y., Stephen, G., Robin, S. Opt. Acta. **1968**, 15, 583-594
[8] S. Kaur, S. Singh, L. Singh and S.P. Lochab, *Nucl. Instr. Meth. B* **301,** 17-22 (2013).function networks," *IEEE Trans. Neural Networks*, vol. 4, pp. 570–578, July 1993.
[9] N. F. Mott and E.A. Davies, "Electronic processes in non crystalline materials. Claredon press, Oxford.

Ultrasonic Spray Pyrolysis Deposition of SDS Surfactant Assisted Copper Oxide Thin Films

Iqbal Singh[a], Taminder Singh[a], Arun Katoch[b]
[a]*PG Department of Physics, Khalsa College, Amritsar-143005, India*
[b]*BKSJ College of Engineering, Amritsar, India*
iqbalsgh@yahoo.com

***Abstract*— An aqueous solution of cupric nitrate trihydrate ($Cu(NO_3)_2.3H_2O$) modified with sodium dodecyl sulphate (SDS) surfactant is used to deposit CuO films on glass substrate by Ultrasonic spray pyrolysis technique. X-ray diffraction (XRD) studies of the films deposited at various substrate temperatures indicate the formation of monoclinic CuO with preferential orientation along (002) plane for all samples. Surfactant modified films showed an increase in crystallite size of 35 nm at substrate temperature of 300 ˚C. The scanning electron micrograph (FESEM) confirms the uniform distribution of facets like grains on the entire area of substrate. SDS modified films show a significant reduction in the particle agglomeration.**

***Keywords*—**Surfactant, spray pyrolysis

I. INTRODUCTION

Considerable efforts have been devoted to characterize and describe the physical and chemical properties of metal oxide due to their important applications in many technological fields [1–4]. CuO has a monoclinic crystal structure and is an important p-type semiconducting material has been utilized in different technological areas [5-10] and deposited films by various techniques [11-17]. Surfactants can play an important role in synthesizing the material in different interesting morphologies [18-20]. They may be used to control the size, shape and agglomeration among the particles. Surfactants have the tendency to absorb on the specific crystal planes hence causes an anisotropic growth of the crystal structure. The addition of surfactant reduces the surface tension of the precursor solution, which facilitates nucleation and allows its easier spreading. Surfactant with molecules composed from a hydrophilic head and a hydrophobic tail into precursor results in the formation of reverse micelles in the gel. Hydrocarbonic tail length and the formation of reverse micelles control the growth and the distance between the particles hence agglomeration [21]. SDS has been extensively used in synthesizing CuO by different routes [22-24]. Most of these studies involve the synthesis of CuO powder. However, limited data is available concerning the effect of surfactant on the aerosol spray deposited CuO thin films. In this study CuO films have been deposited by ultrasonic spray pyrolysis technique with an aim to observe the effect of SDS addition on the structural and morphological properties of the CuO films.

II. EXPERIMENTAL

The films of CuO were deposited onto glass substrates by using 0.2M aqueous solution of trihydrated cupric nitrate ($Cu(NO_3)_2.3H_2O$). To prepare 0.5 M aqueous solution of SDS, required quantity of salt has been dissolved and 10 mL of it was added to aqueous cupric nitrate solution. The resulting solution has been stirred vigorously for 4 hours to form a homogeneous sol. The solution so prepared was used to generate an aerosol using an ultrasonic nebulizer (Omron Make NE-U17) which was subsequently transferred on the ultrasonically cleaned, preheated amorphous glass substrate using an air as carrier gas. The preparative parameters of the ultrasonic spray setup such as nozzle to substrate distance, solution concentration, solution spray rate etc. were optimized to obtain pin hole free and adherent films of CuO. The substrate temperature was varied from 300 to 400˚C ± 5 ˚C in a step of 50 ˚C which is controlled by thermocontroller (DTC Selec 303). The substrates were heated to required temperature for film deposition by an electrical heater. The distance between the nozzle and the substrate was maintained at 25 cm.

The phase identification of the film was performed by X-ray diffraction (XRD) on a X'Pert Panlytical diffractometer using Cu Kα radiation (λ = 1.5405 Å, 30mA, 40 kV) in 2θ range from 30-80˚. To study the surface topography and composition analysis of copper oxide films, field emission scanning electron micrographs (FESEM), EDAX spectrum were taken on a JEOL JSM-6700F with a beam voltage of 30 kV. The thickness of the film was monitored using depth profiler (Dektek 3030 XT) and was found to be 400 ± 20 nm.

III. RESULTS AND DISCUSSION

XRD patterns of as deposited CuO films with SDS at different substrate temperature are shown in the Fig. 1. The presence of intense peaks in the XRD patterns of the films shows that the CuO films are polycrystalline in nature. Two most prominent peaks can be clearly seen at 2θ value 35.5˚ and 38.7˚ corresponding to atomic planes (002) and (111) respectively of CuO phase. No peak corresponding to Cu_2O phase of copper oxide has appeared in the XRD pattern which the formation of pure CuO films. The surfactant addition in the precursor improves the crystallinity along enhanced the growth of crystallites

along certain preferred directions as evident in Fig 1(b, c). Jiaxiang et al (2010) has deposited the ITO film by sol gel method in the presence of surfactants and shown that surfactants acts as important factor in controlling the preferred growth orientation of ITO films. Thus surfactant might help to self assemble the grains in the minimum energy growth direction. The micelle which directed the growth thermally decompose on the substrate leads to an oriented growth.

To determine the preferential orientation in CuO films with and without the addition of surfactant from the XRD data, the texture coefficient was calculated using the equation below

$$P(hkl) = \frac{I(hkl)}{I_o(hkl)}\left[\frac{1}{n}\sum_{i=1}^{n}\frac{I(hkl)}{I_o(hkl)}\right]^{-1} \qquad (1)$$

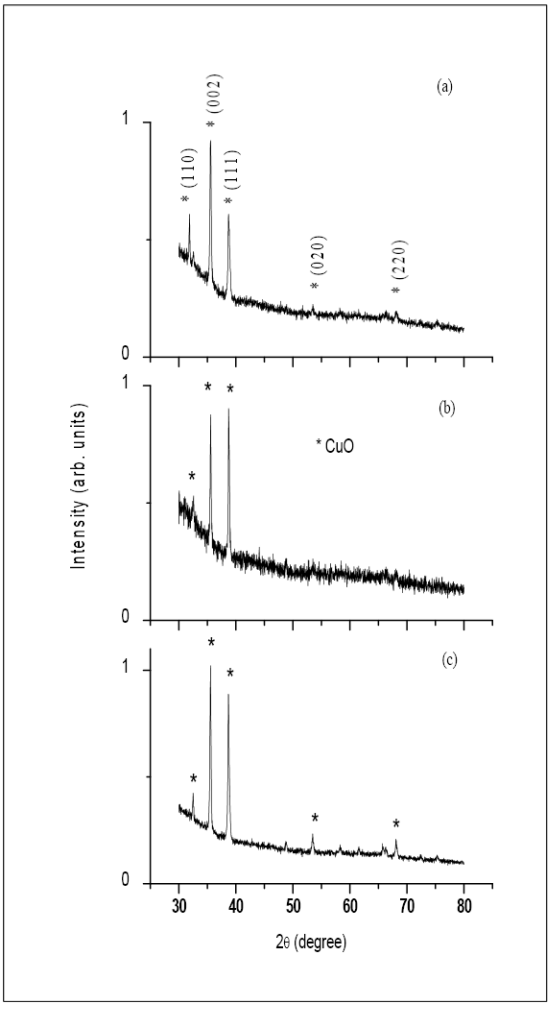

Fig.1. XRD diffractograms of SDS assisted CuO films deposited at substrate temperature of (a) 300˚C:SF1 (b) 350˚C:SF2 and (c) 400˚C:SF3

where I_0 represents the standard intensity, I is the observed intensity of the (hkl) plane and n is the reflection number. Calculated $P(hkl)$ values reveals some important structural information. For the preferential orientation $P(hkl)$ has to be greater than one [18]. $P(hkl)$ value equals to one for all the reflecting planes shows that films are randomly oriented. $P(hkl)$ values greater than one indicates the abundance of the grains in a given (hkl) direction. For the $P(hkl)$ values liying between zero and one indicates the lack of grain orientation in that direction [19]. The diffraction parameters for the as deposited CuO films have been listed in the Table 1. As can be seen from the Table 1, structural parameters are depending on the synthesis parameters. Texture coefficient values greater than one for the peak located at 2θ value corresponding to the reflection from atomic plane (002) of the films reveals the preferential orientation of the film.

The average grain size and the internal lattice strain of the film samples have been evaluated by the Hall-Williamson equation expressed as:

$$\frac{\beta\cos\theta}{\lambda} = \frac{1}{D} + \frac{\varepsilon\sin\theta}{\lambda} \qquad (2)$$

where β is the FWHM of the powder, θ the Bragg angle, λ the wavelength of X-ray used, D the grain size and ε the internal strain. The D and ε values were calculated from the least square fit to $\beta\cos\theta/\lambda$ vs $\sin\theta/\lambda$ plots for the prominent peaks of the samples as shown in Fig. 2. The intercept of the Hall equation plot on the y-axis give rise to the average grain size and corresponding values are recorded in the Table 1. It has been observed that the addition of SDS in the precursor sol results in an increase in the average grain size. The crystallite size of around 35 nm has been observed

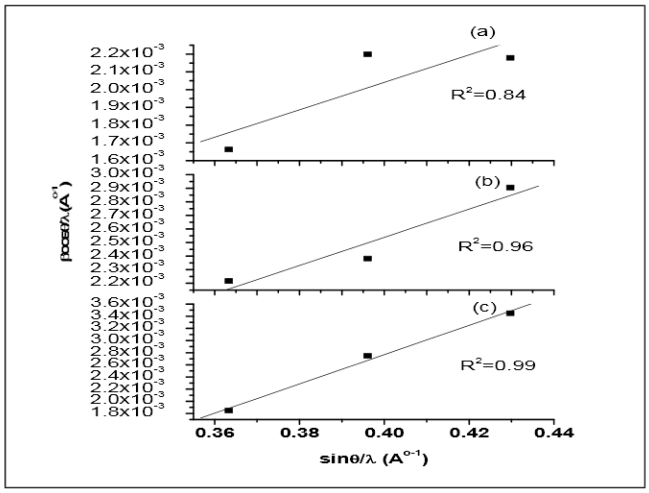

Fig. 2. Hall-Williamson equation plot of SDS assisted CuO films (a) SF1 (b) SF2 and (c) SF3

in case of the CuO film with 0.5M SDS deposited at substrate temperature of 300˚C, thus indicating the formation of nanocrystalline phase.

A positive slope has been observed in the Hall equation plot for CuO films deposited with SDS which confirms the presence of tensile strain in the crystal lattice [19]. The magnitude of the slope in SDS assisted CuO film show a

decrease which suggests the decrement of the strain. Since strain is the indication of defects in the film and a drastic decrease in strain from 0.024 to 0.007 with substrate temperature in the SDS assisted grown films suggests the formation of high quality films with improvement in crystallinity and crystallite size.

To find the effect of surfactant and substrate temperature on the CuO films, the lattice parameters ($a \neq b \neq c$, $\alpha = \gamma = 90^\circ \neq \beta$ for monoclinic structure) and the volume of unit cell were calculated using the relations

$$\frac{1}{d^2} = \frac{1}{\sin^2\beta}\left(\frac{h^2}{a^2} + \frac{k^2\sin^2\beta}{b^2} + \frac{l^2}{c^2} - \frac{2hl\cos\beta}{ac}\right) \quad (3)$$

$$V = abc\sin\beta \quad (4)$$

where d is the interplanar spacing, h,k,l are Miller indices of the crystal planes, a, b, c, β are the lattice parameters and V is the volume of the unit cell. The values of the lattice parameters are in good agreement with those of the ICDD card 41-254. The change in the lattice parameters and the unit cell volume with the surfactant assisted grown films gives the evidences of the strain. Variation in the lattice constant can also be observed with the addition of surfactant and substrate temperature Table 1. The origin of strain in the films is also related to the misfit of the lattice which in turn strongly depends upon the deposition conditions. Dislocations are the imperfections in the crystal lattice associated with the misfit of the lattice in the crystal in one part from the other part. It is an important parameter that governs the growth mechanism. Dislocations are mostly non uniform in nature and depend upon the crystallite size.

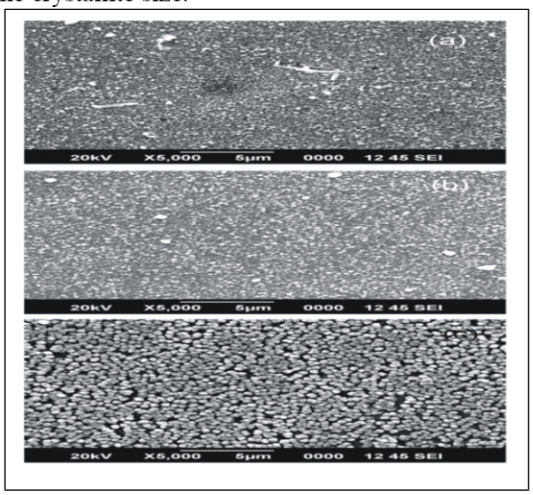

Fig. 3. EDAX spectrum of SDS assisted CuO films (a) SF1 (b) SF2 and (c) SF3

SEM micrographs were taken to investigate to study the effect of SDS on the surface morphology of the CuO films and obtained micrographs are shown in Fig. 3. The SEM micrographs show that the films deposited with surfactant are smooth, void or crack free and showing self assembling of the with nano-sized particle agglomerates into pyramid like grains. The size of the particles which form these agglomerates, however, is much smaller than the grain size and is difficult to resolve. The film texture is smoother for the films with smaller grain size. It was observed that SDS assisted CuO thin films deposited at 300˚C substrate temperature were smooth, dense and showing a uniform distribution of grains. The contrast of the images shows that when SDS was added, the particle size significantly reduces to about 45 nm, while the particle sphericity was improved. Thus SDS assisted CuO films showed low agglomeration. This might be due to the adsorption of surfactant molecules absorbed on the particle surface which acts as a spacer among the neighbouring particles and prevent the coalescence and the formation of hard agglomerates of the individual particles.

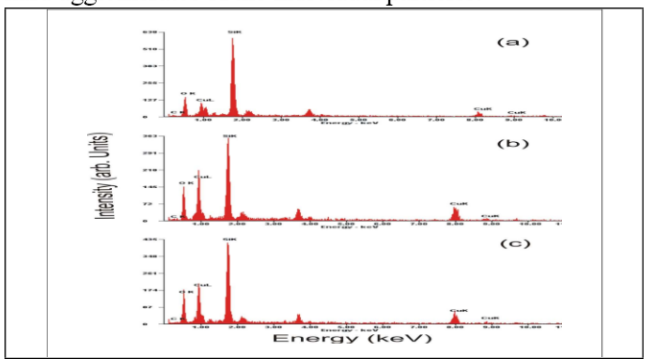

Fig. 4. EDAX spectrum of SDS assisted CuO films (a) **SF1** (b) **SF2** and (c) **SF3**

Table 1 Lattice parameters, strain and crystallite size, elemental composition

Property/sample	**SF1**	**SF1**	**SF1**
P(hkl)			
a (Å)	4.671	4.681	4.695
b (Å)	3.428	3.427	3.427
c (Å)	5.104	5.110	5.118
β (degree)	98.772	99.012	99.370
cell volume (Å^3)	80.882	80.987	81.145
Non uniform Strain (ε)	+0.024	+0.010	+0.007
Average Crystallite size, *D* (nm) XRD	35.8	38.1	45.5
Thickness (µm) ± 0.03	0.48	0.45	0.38
Cu:O at%	27.10:72.90	28.42:71.58	30.22:72.90

The EDAX spectrums of the film samples are shown in Fig. 4 and elemental composition of the samples has been tabulated in Table 1. The analysis shows that the SDS

assisted grown films are metal deficient. The elemental composition taken at different location of the film sample shows that content of oxygen increases with an increase in substrate temperature.

IV. Conclusions

A nanocrystalline CuO thin films were deposited on glass substrate by a surfactant assisted ultrasonic spray pyrolysis method. The crystallite size in CuO has been found to be around 61 nm with the addition of 0.5M CTAB. The results indicate that CuO nanocrystallites are subjected to considerable strain and decreases with the addition of CTAB in the sol. The faceted distorted spherically shaped CuO nanoparticles with minimum agglomeration are obtained. The activation energy of CuO appears to enhance with addition of surfactant. Interestingly, an enhancement of response of CuO film toward ammonia at room temperature has been recorded with the addition of SDS. The study reveals that the properties of synthesized CuO nanoparticles can be controlled by optimizing the surfactant with substrate temperature.

Acknowledgment

Authors wish to thank Director IIT Roorkee, STIC, Kochi and RSIC, Panjab University, Chandigarh for providing FESEM, EDAX and XRD facilities..

References

[1] N. Ueda, H. Maeda, H. Hosono, H. Kawazoe, Band-gap widening of CdO thin films, J. Appl. Phys. 84 (1998) 6174-6177.

[2] H. Liu, X. Zhang, L. Li, Y. X. Wang, K. H. Gao, Z. Q. Li, R. K. Zheng, S. P. Ringer, B. Zhang, X. X. Zhang, Role of point defects in room-temperature ferromagnetism of Cr-doped ZnO, Appl. Phys. Lett. 91 (2007) 0725111-3.

[3] H. Zhu, F. Zhao, L. Pan, Y. Zhang, C. Fan, Y. Zhang, J. Q. Xiao, Structural and magnetic properties of Mn-doped CuO thin films, J. Appl. Phys. 101 (2007) 09H1111-3.

[4] F. F. Ferreira, M. H. Tabacniks, M. C. A. Fantinia, I. C. Fariab, A. Gorensteinb, Electrochromic nickel oxide thin films deposited under different sputtering conditions, Solid State Ionics 86-88 (1996) 971-976.

[5] L. S. Huanga, S. G. Yanga, T. Lia, B. X. Gua, Y. W. Dua, Y. N. Lub, S. Z. Shi, Preparation of large-scale cupric oxide nanowires by thermal evaporation, J. Cryst. Growth 260 (2004) 130-135.

[6] Kari E. R. Brown, K. S. Choi, Electrochemical synthesis and characterization of transparent nanocrystalline Cu_2O films and their conversion to CuO films, Chem. Commun. (2006) 3311-3313.

[7] N. Serin, T. Serin, S. Horzum, Y. Celik Annealing effects on the properties of copper oxide thin films prepared by chemical deposition, Semcond. Sci Technol. 20(5) (2005) 398-

[8] T. Maruyama, Copper oxide thin films prepared from copper dipivaloylmethanate and oxygen by chemical vapor deposition, Jpn. J. Appl. Phys. 37 (1998) 4099-4102.

[9] K. Santra, C. K. Sarkar. M. K. Mukherjee, B. Ghosh, Copper oxide thin films grown by plasma evaporation method, Thin Solid Films, 213 (1992) 226-229.

[10] V. F. Drobny, D. L. Pulfrey, Properties of reactively-sputtered copper oxide thin films, Thin Soild Films, 61 (1979) 89-98.

[11] K. P. Muthe, J. C. Vyas, S. N. Narang, D. K. Aswal, S. K. Gupta, R. Pinto, G. P. Kothiyal, S. B. Sabharwal, A study of the CuO phase formation during thin film deposition by molecular beam epitaxy, Thin Solid Films, 324 (1998) 37-43.

[12] M. Salarian, M. S. Hashjin, S. S. Shafiei, R. Salaria, Z. A. Nemati, template directed hydrothermal synthesis of dandelion like hydroxyapatite in the presence of cetyltrimethylammonium bromide and polyethylene glycol, Ceram. Int. 35 (2009) 2563-2569.

[13] M. Pradhan, S. Sarkar, A. K. Sinha, M. Basu and T. Pal, High yield synthesis of 1D Rh nanostructures from surfactant mediated reductive pathway and their shape transformation, J. Phys. Chem. C. 114 (2010) 16129-16142.

[14] S. Alamolhoda, S. A. Seyyed Ebrahimi, A. Badiei, A study on the formation of strontium hexaferrite nanopowder by a sol–gel auto-combustion method in the presence of surfactant, J. of Mag. Mater. 303 (2006), 69-72.

[15] Y. Zhang, S. Wang, X. Li, L. Chen, Y. Qian and Z. Zhang, CuO shuttle like nanocrystals synthesized by oriented attachment, J. Cryst. Growth 291 (2006) 196-201.

[16] Y. Liu, Y. Chu, M. Li, L. Li and L. Dong, In situ synthesis and assembly of copper oxide nanocrystals on copper foil via a mild hydrothermal process, J. Mater. Chem. 16 (2006) 192-198.

[17] R. K. Bedi and I. Singh, Room temperature ammonia sensor based on cationic surfactant assisted nanocrystalline CuO, Appl. Mater. Interf., 2(5) (2010) 1361-1368.

[18] S. Kose, F. Atay, V. Bilgin, I. Akyuz, Some physical properties of copper oxide films: the effect of substrate temperature, Mater. Chem. Phys. 111 (2009) 351-358.

[19] D. Perednis, L. J. Gauckler, Thin film deposition using spray pyrolysis, J. Electroceram. 14 (2005) 103-111.

[20] S. Lv, C. Wang, T. Zhou, S. Jing, Y. Wu, C. Zhao In situ synthesis of ZnO nanostructures on a zinc substrate assisted with mixed cationic/anionic surfactants J. Alloys Compds. 477 (2009) 364-369

[21] R. Elansezhian, B. Ramamoorthy, P. Kesavan Nair The influence of SDS and CTAB surfactants on the surface morphology and surface topography of electrodless Ni-P deposits J. Mater. Process. Technol. 209 (2009) 233-240

[22] C. K. Xu, G. D. Xu, Y. K. Liu, G. H. Wang. A simple and novel route for the preparation of ZnO nanorods. Solid State Communications 122 (2002) 175-179.

[23] H. Xu, D. H. Qin, Z. Yang, H. L. Li, Fabrication and characterization of highly ordered zirconia nanowire arrays by sol–gel template method Material Chemistry and Physics 80 (2003)524-528.

[24] J. H. Liang, C. Peng, X. Wang Chromate nanorods/nanobelts: general synthesis, characterization, and properties Inorgnic Chemistry 44 (2005) 9405-9415.

[25] L. Jiaxiang, W. U. Da, Z. Nan, W. Yue Effects of surfactants on the structure and photoelectric properties of ITO films by sol-gel method Rare Materials 29 (2): (2010)143-148.

Transport Properties of Metallic Nanowires on Silicon Substrate

Jaskiran Kaur, Surinder Singh

Department of Physics, Guru Nanak Dev University, Amritsar, India.

***Abstract*— This paper presents the Electrical properties of the randomly distributed metallic (Co, Ni and Fe) nano/micro wires on Silicon. Deposition was carried out potentiostatically into the pores of the track-etch polycarbonate membrane spin coated onto the Silicon substrate. Spin coated films were irradiated with 150MeV Ni (+11) ions at a fluence of 8E7 ions/cm^2, followed by UV irradiation and chemically etching in aqueous NaOH (6N, at room temperature). Later morphological, and electrical properties of the so deposited nano-/micro structures were studied.**

***Keywords*—**Nanowires,SEM, Electrical Characterization

I. INTRODUCTION

The research on nano-/micro structures has led to the exploration of novel physics and material properties at reduced physical dimensions. There is considerable technological interest in the fabrication of arrays of high aspect ratio structures synthesized by electrodeposition for use as sensors and ultra-high-density information storage. Along with the synthesis of bare nano/micro structures, fabrication of one-dimensional nanostructures, or nanowires on the substrate (metallic or semiconducting), has been under intense investigation due to their lucrative device applications [1-3].

In the present work, the track-etched membrane is used to synthesis nano-/micro structures on the substrate itself. Structures are grown directly over the semiconducting substrate for their further characterization and obviating the need for post- synthesis manipulations. These Semiconductor based nano-/micro structures are expected to have practical applications in electronic circuit integration [4-5]. A thin polymeric layer was spin coated on the gold-coated semiconducting substrate. This gold layer acts as electrode at the time of electrodeposition and polymeric layer acts as template having the etched tracks.

II. EXPERIMENTAL DETAILS

Preparation of substrate was carried out at Inter University Accelerator Center (IUAC), New Delhi, India, and the CSIO, Chandigarh, India. We have used Si (P-doped) (111) as a semiconducting substrate. To remove the dirt and oxide layer from the surface of the substrate Si, wafer was kept in Trichloroethylene solvent at 70°C for 10 min then immersed in 1% HF acid for 1 min. Finally wafer was rinsed using deionised water for 5 min.

A thin gold layer of thickness about 95.5nm was deposited using vacuum evaporation method, onto the Au layer, polycarbonate (Makrofol) was deposited by spin coating (at room temperature with spinning speed of 4000rmp) and the thickness of coated polymer was around 10µm. The adhesion of the polycarbonate film on the substrate was improved by the use of a primer (hexamethyledisilisazan), a chemical reagent $(CH_3)_3Si\text{-}NH\text{-}Si(CH_3)_3$, consisting of ammonia substituted with two trimethylsilyl functional groups.

The prepared samples were irradiated at room temperature with 150 MeV Ni^{+3} ions at a fluence of 8E7 at IUAC, New Delhi, India. Later, the irradiated samples were UV treated (365 nm, 150 W/cm^2) for 20 minutes to increase the selectivity of the chemical etching thus favoring the formation of cylindrically shaped pores. Etching was performed in a home made one-compartment cell with a NaOH aqueous solution at room temperature for a time up to 50 min. The supported films were then immersed in an acetic acid solution and rinsed with milli-Q water at room temperature for 5 min and were then dried with hot air. It must be noted that the pore size depends both on the conditions of the ionic and UV irradiation, and on the conditions during chemical treatment of the tracks like nature and concentration of the reactants, temperature during etching, time duration for etching. UV exposure leads to photo-oxidation in the polycarbonate and is able to increase the track etch ratio by an order of magnitude [6].

Electrodeposition within these pores of the supported template was performed at room temperature in a conventional one-compartment cell, with a copper rod working as anode and the gold layer as working electrode (cathode). Electrodeposition of copper, iron and nickel was done by using the electrolytic solutions containing the following compositions: Cu ($CuSO_4 \cdot 5H_2O$, 125 g/L; H_2SO_4, 100 g/L), Fe ($FeSO_4 \cdot 7H_2O$, 120 g/L; H_3BO_3, 45 g/L) and Ni ($NiSO_4 \cdot 6H2O$, 300 g/L; $NiCl_2 \cdot 6H_2O$, 45g/L; H_3BO_3, 45 g/L). The electrodeposition of copper nano-/microstructure was carried out for 20 minutes at 2 V (current 0.0410 to 0.0 645 A) at the temperature of 60^0 C. Similarly, microstructures of iron and nickel were fabricated at potential difference of 2 volt for 15 minutes and current variation was ranged from 0.0280 to 0.360 A at 60^0 C. The deposition potential was applied using a power supply (Electromek INDIA, SAM- Model MR 85, ± 15 V) and the monitoring of current and potential drop across the cell was carried out using a digital multimeter (PHILIPS Digital Multimeter 1225). When the wire reaches the membrane surface, a cap starts to grow on top. At this point in time, the electrodeposition process is stopped, the substrate with nano-/micro wires was

immediately removed from the electrolyte, rinsed with double-distilled water and ethanol, finally dried in dry air at room temperature and subjected to further analysis. The porous thin polycarbonate membrane was removed by dissolving it in dichloromethane for 10 minutes and washed with several times with double-distilled water.

III. RESULTS AND DISCUSSION

In the present study we have carried out morphological and electrical studies of template synthesized nano-/micro structures. For morphological characterization, the fabricated nano-/micro structures were viewed under SEM at SEMCF IIT New Delhi, Fig. 1 shows the SEM images of Copper, Iron and Nickel nano/micro wires grown on the semiconducting substrate.

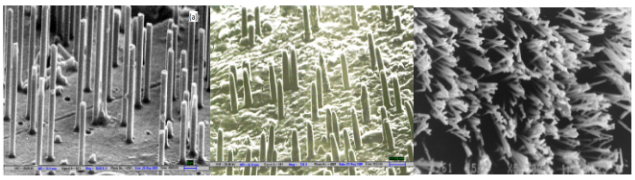

(a) (b) (c)

Figure 1: SEM image of (a) copper (b) iron and (c) nickel nano-/micro wires grown on silicon substrate.

The *in- situ* I-V characteristics of nano-/micro structures was carried out at room temperature by leaving the structures embedded in the insulating template membrane itself . A KEITHLEY 2400 source meter was used for the measurement. The Fig 2 shows the voltage vs current characteristics for the nano-/micro structures, it's the collective behavior of nanowires lying parallel to each other.

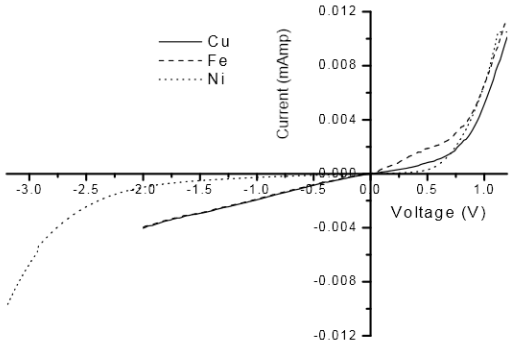

Figure 2 I-V characteristics of embedded nano-/micro copper, iron and nickel wires on Silicon substrate.

Plot shows that at the metal- semiconductor contact system behaves non-ohmic when forward biased but in reverse biased region, variation is ohmic.

Under the forward biased V at a fixed temperature

$I = I_0[\exp\{(q(v-IR_s)/nkT)-1\}]$

n is the ideality factor and R_s is the diode series resistance. For a pure thermionic emission n=1. Fit of linear region of the forward biased semilog IV curve (where $V>3k_Bt$ and R_s is negligible. Extrapolation of straight line portion of the plot to V=0 gives I_0 and the slope S=d(lnI)/dV gives n. Using I_0 barrier height may also be calculated using the equation

$\Phi_B=(kT/q)(AA^*T^2/I_0)$

Where A* is the Richardson constant and A is the electrical contact area [7]

Table 1: Table showing the slope intercept and spreading resistance values for the nanostructures grown on semiconducting substrates.

Metal	Slope(mA/Volts)	Intercept (Amps)
Cu	2.22	14.38
Fe	1.24	12.78
Ni	2.62	11.50

As the plots show the measured I-V curve is non-linear. Sze (1981) asserted that if thermionic emission is dominant, which is the major current flow mechanism for low impurity concentration, the curve should be linear. Padovani and Stratton [8] reported that even if thermionic-field emission is dominant, which occurs at a highly doped metal semiconductor interface, the I-V curve is approximately linear [9]. While Lepselter and Andrews [10] explained that if direct tunneling is dominant, the current is directly proportional to applied bias which implies that the contact is Ohmic. However, our results indicate that the contact does not follow any of the three models.

ACKNOWLEDGMENT

The financial assistance to one of the author (Jaskiran Kaur) by CSIR New Delhi and heavy ion-irradiation facility provided by the IUAC, New Delhi is gratefully acknowledged. Thanks are also due to Dr Chatar Singh, IIT New Delhi for carrying out SEM analysis.

REFERENCES

[1] X. Duan, Y. Huang, Y. Cui, J. Wang, and C. M. Lieber, 2001 Nature London 409, 66.

[2] Chakarvarti S. K. , Vetter J., 1993 Micromech. Microeng., 3,57-59.

[3] Chakarvarti S.K.,Vetter J., 1998 Rad. Meas., 29(2)149-159.

[4] K.D. Hirschman, L. Tsybeskov, S.P. Duttagupta, P.M.Fauchet, 1996 Nature 384,338.

[5] M.H. Huang, S. Mao, H. Fieck, H. Yan, Y. Wu, H. Kind, E. Weber, R. Russo, P. Yang, 2001, Science 292,1897.

[6] Chakarvarti, S.K., Singh, P., Mahna, S.K., Sud L.V., 1990 Indian J Physics A, 64A(3), 229-232.

[7] S. M. Sze, Physics of Semiconductor Devices, 2nd ed. Wiley, New York, 1981, Chap. 5.

[8] F. A. Padavani and R. 1966, Stratton Solid State Electronics, 9, 695-707.

[9] S. L. Pan, D.D. Zeng, H.L. Zhang and H.L.Li (2000) Appl. Phys. A 70, 637-640.

[10] M.P. Lepselter and J.M. Andrews (1969) The Electrochemical Society Symposium Series, New York 159-189.

Growth of nanostructured tin oxide thin films for gas sensing applications

Kamalpreet Khun Khun
Dept. of Physics, Khalsa College, Amritsar-143005, India.

***Abstract*— Tin oxide thin films comprising of nanostructures with different morphologies have been obtained on glass substrates using an ultrasonic spray pyrolysis technique. The effect of post deposition annealing on the structure and morphology of the films deposited at 400°C is studied using XRD and FESEM. The studies reveal that the annealing of the films at temperatures of 400 and 500°C results in the evolution of platelet like and bipyramidal nanostructures, exhibiting an enhanced response towards low concentrations of chlorine.**

***Keywords*—** Tin oxide, Nanostructures, Thin films, Annealing , Structural properties, Gas sensing.

I. INTRODUCTION

As gas sensing materials, the metal oxides are particularly attractive due their low cost, ease in fabrication, simplicity in their use and their ability to detect a wide range of gases. Among various metal oxides, tin oxide (SnO_2) is identified as one of the most important member of the semiconducting metal oxide group that has been widely investigated and used for the detection of large number of gases such as ammonia, hydrogen sulphide, nitrogen dioxide, carbon monoxide, ethanol, etc [1-4]. Its sensing mechanism is based on the conductance changes occurring due to the reaction between the adsorbed oxygen species on the oxide surface and the analyte, and is influenced largely by parameters such as crystallite size, orientation, shape, agglomeration, surface architecture etc of the sensing layer [5].Therefore several methods such as hydrothermal, solvothermal, thermal evaporation, templated growth and solid state reaction etc have been used for the growth of crystalline SnO_2 nanostructures with different morphologies for sensing applications [6-10].

In the present study, conditions for growth of a porous network comprising of platelet shaped nanostructures were identified and the prepared nanostructures were successfully used for sensing low concentrations of chlorine at low operating temperature of 150°C.

II. EXPERIMENTAL DETAILS

Stannous chloride and ethanol were used as starting materials. A precursor solution of 0.25 M concentration was prepared by dissolving 0.0125 moles of stannous chloride in 50 ml of ethanol. This solution was initially well stirred and heated at 40°C for 2 hours for attaining initial clarity. The prepared solution was then used for deposition of SnO_2 films onto glass substrates kept at temperatures of 400°C, using an ultrasonic spray pyrolysis technique. The deposited films were then subsequently annealed at temperatures of 400 and 500°C for 2 hours to study the changes in the microstructure and gas sensing behaviour with post deposition annealing.

The aerosol used for the deposition of films was generated ultrasonically by a simple medical nebulizer model OMRON NE-U17. The crystal phases in the films were studied by X-ray diffractometer (X'Pert Panalytical) operated at 40 kV, 30 mA over 20° to 70° with a scan rate of 0.002°/sec. The surface morphology of the films was investigated using FESEM (JEOL JSM 6700) with a beam voltage 25 kV. The thickness of the films was determined using a depth profiler (Dektek 3030 XT). The gas sensing response of the films was determined by studying the resistance variation upon exposure to chlorine gas at different operating temperatures ranging between (25-250°C).

The sensing response (R) of the film is calculated by the equation

$$R = \left(\frac{R_g - R_a}{R_a}\right) \text{X} 100\ \%$$

where R_g and R_a represent resistance in the presence of gas and air respectively.

Here, response time of the sensor is calculated as the time required for the resistance to reach 90% of the equilibrium value after the test gas is introduced and the recovery time is measured as the time necessary for the sensor to attain a resistance 10% above the original value in air .

III. RESULTS AND DISCUSSION

XRD patterns of the films deposited at substrate temperature (Ts) of 400° C are shown in figure 1. The patterns reveals the formation of polycrystalline films with peaks corresponding to reflections from (110), (101), (200), (211), (220), (310) and (301) planes of rutile structured SnO_2 phase.

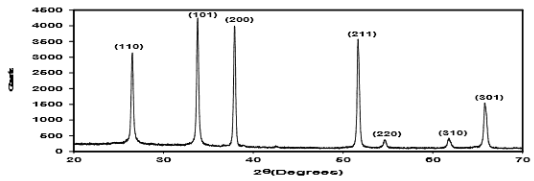

Fig. 1 XRD pattern of SnO_2 films deposited at substrate temperatures(Ts) of 400°C

Figure 2 and 3 shows the XRD patterns of the films deposited at 400°C and annealed at temperatures of 400 and 500°C respectively. The patterns show (211) as the most intense and sharp reflection for the annealed films. The intensity of the dominant reflection is found to increases with an increase in annealing temperature to 500°C and a remarkably high intensity (211) reflection is observed in case of film annealed at 500°C. The intensities of the other reflections are relatively much smaller.

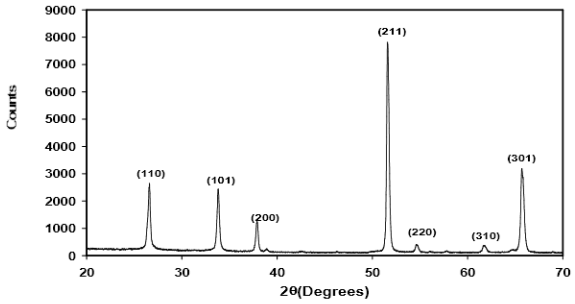

Fig 2: XRD patterns of SnO_2 films deposited at Ts = 400°C and annealed at temperature of 400°C

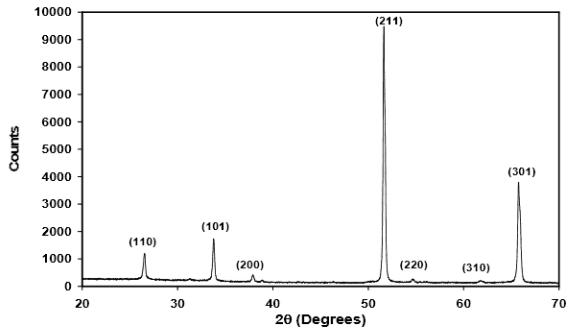

Fig 3: XRD pattern of SnO_2 films deposited at Ts = 400°C and annealed at temperatures of 500°C

The FESEM analysis of the film deposited at substrate temperature 400°C is shown in figure 4. The micrograph shows that the film is composed of cuboidal shaped crystallites.

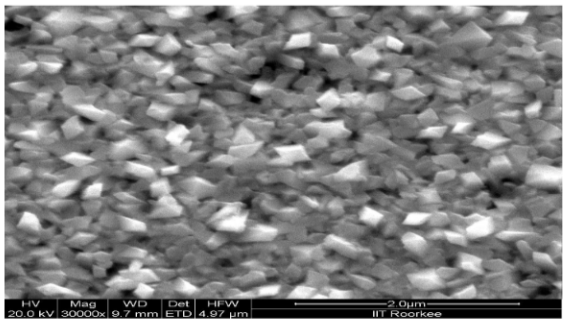

Fig 4: FESEM image of SnO_2 films deposited at substrate temperatures of 400°C

The FESEM images of the films deposited at 400°C and annealed at temperatures of 400, 500 °C are shown in figure 5 and 6 respectively. A highly porous network of platelet like crystals is evolved in case of film annealed at 400°C. At an annealing temperature of 500°C the crystals evolve into bipyramid shaped structures with uniform sizes. A close examination of these crystals reveal that the surface of the crystals is not smooth and appears to be an assembly of nanoparticles, which suggests that the obtained crystals are secondary faceted aggregates formed from primary SnO_2 nanocrystallites [11]. These variations induced in the film morphology upon annealing at different temperatures can be attributed to the occurrence of multistep stages of recrystallization, reorientation, and aggregation of SnO_2 primary crystallites on providing thermal energy to films through annealing at different temperatures.The extent of each stage at a given annealing temperature dictates the final morphology of the film at that temperature. At low annealing temperature of 400°C the thermal energy results in the partial recrystallization and reorientation of crystallites with a smaller degree of aggregation. However at higher temperatures the increased thermal energy increases the extent of orientation and aggregation due to increased multiple collisions of primary crystallites. Further during the course of aggregation the primary crystallites tend to share common faces to maximize the packing density and align their planes with similar interplanar spacing at the interface to attain coherency. The planes then spontaneously align themselves to form a low energy interface. As a result, faceted SnO_2 crystals with inherent meso-macroporosity are evolved giving a textured distribution of nanparticles with a preffered orientation. [12]

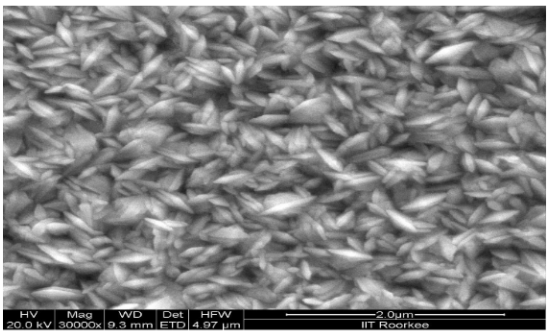

Fig 5: FESEM image of SnO_2 films deposited at Ts = 400°C and annealed at temperatures of 400°C

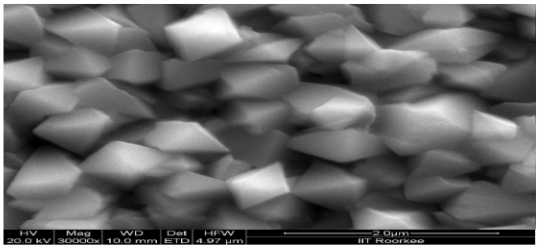

Fig 6: FESEM images of SnO_2 films deposited at Ts = 400°C and annealed at temperatures of 500°C

Gas sensing characteristics

The SnO_2 films deposited at a substrate temperature of 400°C were then tested for their gas sensing behaviour towards chlorine in the operating temperature range of 25-250°C.

Figure 7 depicts the response of film towards 10 ppm of chlorine. A high response of 173.1 % was recorded at an operating temperature of 150°C.

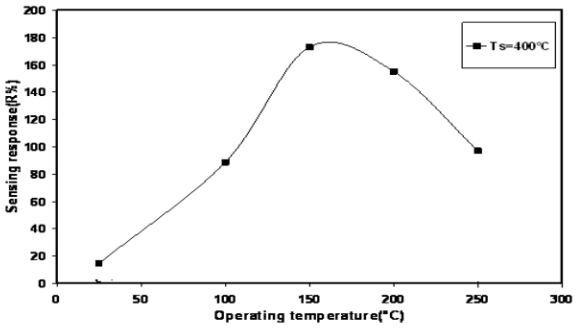

Fig 7 :Sensing response of SnO_2 films deposited at different substrate temperatures towards 10 ppm of chlorine

Figure 8 shows the gas sensing response of the films deposited at 400°C and annealed at temperatures of 400 and500 °C. It is observed that the film annealed at 400°C shows a highly improved response of 264.6% towards 10 ppm chlorine. The response was however lowered in case of films annealed at 500 °C.

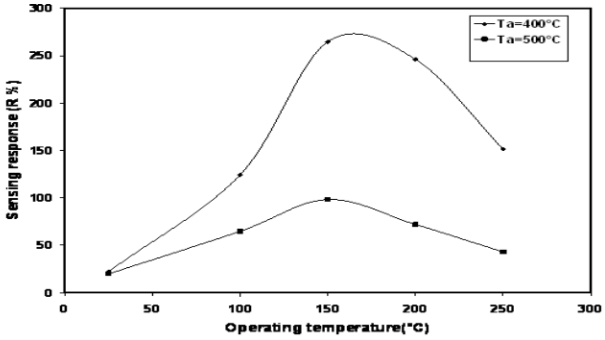

Fig 8 :Sensing response of SnO_2 films deposited at Ts=400°C and annealed at 400 and 500°C, towards 10 ppm of chlorine.

Figure 9 shows the response time curves for the film annealed at 400°C for different concentrations of chlorine (5-30 ppm).It is observed that the response was almost linear in the tested range.The maximum sensing response recorded for 30 ppm chlorine was 650.2 %.The calculated response time for sensing different concentrations of chlorine was found to be about 15 sec and the recovery time was found to lie between 20-25 sec.

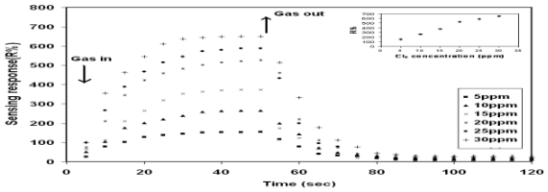

Fig 9: Response time curves for SnO_2 film annealed at 400°C for different concentrations of chlorine (5-30 ppm)

IV. CONCLUSION

The studies show the possibilities of growing nanostructured SnO_2 films by ultrasonic spray pyrolysis, with different morphologies by varying substrate and post deposition annealing temperatures. The evolution of porous platelet like agglomerates due to partial recrystallization and orientation of the SnO_2 films at annealing temperatures of 400°C were found to exhibit an enhanced response of 650.2 %towards 30 ppm chlorine, which suggests that post deposition annealing treatment of crystalline SnO_2 films prepared by ultrasonic spray pyrolysis can be used as an effective tool for modifying the structure and gas sensing behaviour of SnO_2 films towards a particular gas.

ACKNOWLEDGMENT

The author Kamalpreet Khun Khun would like to acknowledge CSIR, New Delhi for the financial assistance in the form of SRF award to carry out this research work.

REFERENCES

[1] Kamalpreet Khun Khun, Aman Mahajan, R.K bedi, Chemical Physics Letters 492 (2010) 122.

[2] 2.Li Jianping, Wang Yue, Gao Xiaoguang, Ma-Qing, Wang Li, Han Jinghong, Sensors and Actuators B 65 (2000) 111.

[3] Jaswinder kaur, V.D Vankar, M.C Bhatnagar:Sensors and Actuators B133 (2008) 650.

[4] 4. J.-H.Smatt, M.Linden, T.Wagner, C-D Kohl, M.Tiemann:Sensors and Actuators B 155(2011) 483.

[5] G.Korotcenkov, Sensors and Actuators B 107(2005)209.

[6] 6.Hui-Chi Chiu and Chen-Sheng Yeh, J. Phys. Chem. C 111(2007) 7256.

[7] Hua Wang, Qingqin Liang, Weijie Wang, Yiran An, Jinghong Li and Lin Guo, Cryst. Growth Des.11(2011) 2942.

[8] Guangcheng Xi and Jinhua Ye, Inorg.Chem. 49 (2010) 2302.

[9] Yu Lingmin, Fan Xinhui, Qi Lijun, Ma Lihe, YanWen, Applied Surface Science. 257 (2011)3140.

[10] ETH Tan,GW Ho ,ASW Wong ,S Kawi and A T SWee, Nanotechnology19 (2008) 255706.

[11] 11. R.N. Goyal , D. Kaur, A.K.Pandey, Materials Chemistry and Physics 116(2009)638-644

[12] X.Wang, Y.Ma, A.Suganan, J.Qin, M.S.Toprak, B.Zhu, M.Muhammed, Journal of Nanoparticle Research, 13(2011)5879-5885

Preparation and Characterisation of Rare Earth Doped Phosphate Glasses

Manpreet Kaur[a], Mehak Mahajan[a], Mohini Bhatia[a], Sarabjit Kaur[a], Lakhwant Singh[e]
[a]Department of Physics, DAV College, Amritsar, India
[e]Department of Physics, GNDU, Amritsar, India
manpreetaurora@gmail.com

***Abstract*— Phosphate glasses with composition $50P_2O_5$-30CaO-(20-x) Na_2O-xCeO_2 with x varying from 0-2.0 mol % were prepared using the conventional melt quench technique. The amorphous nature of prepared glasses was confirmed from the XRD spectra. The density and Molar volume of the glasses was found using the Archimedes principle. The value of the density lies in the range 3.58-3.71 g/cm^3. The density of the prepared glasses was found to increase with the concentration of CeO_2. This was explained as the molecular weight of CeO_2 is more as compared to molecular weight of Na_2O. The Raman spectra was obtained for the prepared glass samples and it was found that the no new peaks are formed with the doping of CeO_2, only there is a change in the intensity of peaks and the peaks are red shifted. The bandgap energy is found to decrease with CeO_2 doping due to formation of more NBOs.**

***Keywords*—** Band gap energy, Density, Molar Volume, Phosphate Glass, Raman Spectra

I. INTRODUCTION

In recent years extensive work has been done on rare earth doped phosphate glasses due to wide range of applications offered by them such as solid state laser hosts, glass to metal seals, optical glasses, bioactive glasses and many more [1-2]. Phosphate glasses are known to possess low melting temperature (as compared to silicate glasses), low glass transition temperature and high thermal expansion coefficient. In addition phosphate glasses can also exist as ultra, meta, pyro and ortho structural units which facilitates the tailoring of new materials for specific technological application [3]. Rare earth ions are important as they can be used to probe the local structural variations in the host glass matrix due to their 4f electronic configuration. Among rare earths cerium oxide is known as good UV absorber and it also possess the radiation damage resistance properties from X rays and gamma rays. Cerium exists as Cerous (Ce^{3+}) and Ceric (Ce^{4+}) states in oxide glasses. In the radiation resistance mechanism Ce^{4+} acts as electron traps and Ce^{3+} acts as hole traps, which avoids the formation of colour centers when the samples are irradiated [4-5]. The solubility of rare earth ions in oxide glasses changes drastically from one glass former to the other. Phosphate glasses can accommodate large amounts of RE ions as compared to silicate and borate glasses. RE ions with concentration > 1 mol% are found to form clusters in the silicate glasses. It is proposed that phosphorus- oxygen polyhedral serves as the solvation shells around the RE ions which helps them to accommodate large concentration of RE ions without phase separation [6]. It has been found that 16 times more cerium oxide can be doped in phosphate glasses as compared to the silicate glasses while maintaining the same colour and ability to absorb ultraviolet radiation. In the present research paper we have synthesised the glass with composition 50 P_2O_5-30 CaO- (20-x)Li_2O-x CeO_2 with x varying from 0 -2.0 mol %. The glasses are then characterised with UV - Visible and Raman spectroscopy for their optical and structural properties.

II. EXPERIMENTAL DETAILS

A. *Preparation of glasses*

The glasses having composition 50 P_2O_5-30 CaO- (20-x) Li_2O-x CeO_2 with x varying from 0 -2.0 mol % were prepared using the conventional melt quench technique. All the chemicals were weighed and were mixed in a ball mill to form a homogeneous mixture. This batch was then melted in an electric furnace at 1100^{0}C for 1 hour. The melt was then poured onto preheated steel plates to obtain the bubble free transparent glasses.

B. *XRD*

XRD studies of the prepared glass samples were carried out using CuKα radiation with XRD -7000 Shimadzu X Ray Diffractometer at scanning rate of 5^0 per minute in the range of 20^0 - 80^0.

C. *Density Measurements*

Density of prepared glass samples was calculated using the Archimedes Principle with Xylene as the immersion liquid. The density of the samples was calculated using the formula

$$\rho = \frac{W_a}{W_a - W_l}\,\rho_l$$

Where W_a is the weight of glass in air, W_l is the weight of glass in liquid and ρ_l is the density of immersion liquid. The molar volume of the glasses was found as

$$V_m = {}^{Molecular\ weight\ of\ glass}/_{Density\ of\ glass}$$

D. *UV Visible Absorption Spectra*

The optical absorption spectra of polished glass samples having thickness in range of 1-2 mm were recorded using double beam spectrophotometer Shimadzu 1601 in the range from 200-1100 nm. These spectra were used to

calculate the bandgap energy of glasses.

E. *Raman Spectra*

Raman spectra of polished glass samples were recorded using 488 He-Ne Laser in 400-1500 cm^{-1} range.

III. RESULT AND DISCUSSIONS

A. *XRD Analysis*

Fig. 1 shows the XRD spectra of powdered glass samples. Absence of any sharp peak in the spectra confirms the amorphous nature of prepared glasses.

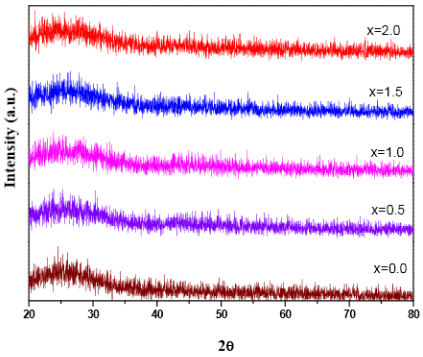

Fig. 1
XRD Spectra of 50 P_2O_5-30 CaO- (20-x) Li_2O-x CeO_2 glasses

B. *Density and Molar Volume*

Fig. 2 shows the density and molar volume as concentration of Cerium oxide. The density of glass samples is found in the range of 3.58-3.71 g/cm^3. The density of phosphate glasses is largely affected by the packing fraction of structural units present. The density of phosphate glasses was found to increase with the CeO_2 concentration as the molecular weight of CeO_2 is more than that of Na_2O. This also shows that with CeO_2 addition the cross linkages between NBOs increases which makes the glass structure more dense. Also with increase in concentration of CeO_2 the molar volume is found to increase.

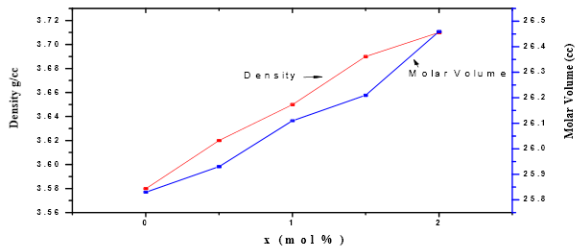

Fig.2 Density and Molar Volume variation with CeO_2 concentration

C. *Optical Properties*

Fig.3 shows the UV-Visible optical absorption spectra of prepared glasses in 300- 800 nm range. The characteristic curve for all glasses exhibit the same behavior except the onset value of absorption edge. The absorption edge was found to be red shifted with CeO_2 doping. This is attributed to the presence of more NBOs due to CeO_2.

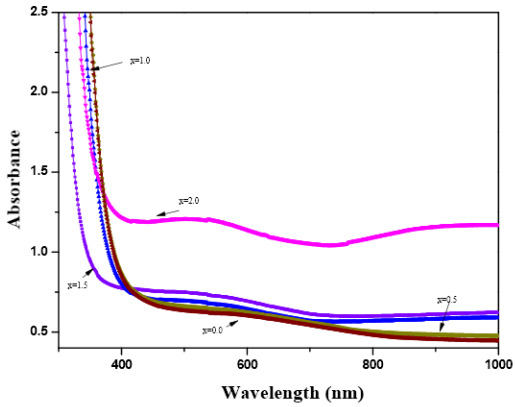

Fig. 3 Absorbance spectra of prepared glass samples

The absorption coefficient α for oxide glasses is related to $E_{optical}$ by Davis and Mott [7] power law given as

$$\alpha(\nu) = B\frac{(h\nu - E_g)^n}{h\nu}$$

Where B is a constant and n is a parameter having value 2 for glasses. Hence a plot of $(\alpha h\nu)^{1/2}$ vs hν gives a curve and if the straight line is extrapolated to x axis, it gives the value of optical bandgap.

Fig. 4 shows the indirect optical bandgap for prepared glass samples. The optical bandgap energy is found to decrease with CeO_2 concentration. This is attributed to the conversion of bridging oxygen atoms to the nonbridging oxygen atoms, which further facilitates the excitation of electrons to higher energy states and thus lowers the bandgap.

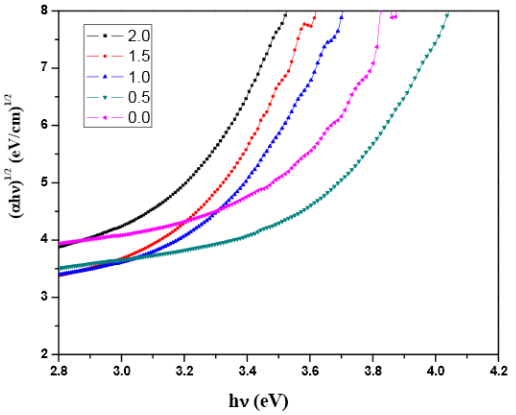

Fig.4 Optical Band gap energy for prepared glasses

The value of optical bandgap, density and molar volume is given in Table 1.

Table 1. Nominal Composition of Prepared glass series with their Density, Molar Volume and Optical bandgap

P_2O_5 (in mol %)	CaO (in mol %)	Li_2O (in mol %)	CeO_2 (in mol %)	Density (g/cc)	Molar Volume (cc)	Band gap energy (eV)
50	30	20	0	3.58	25.83	3.40
50	30	19.5	0.5	3.62	25.93	3.15
50	30	19	1.0	3.65	26.11	3.13
50	30	18.5	1.5	3.69	26.21	3.02
50	30	18	2.0	3.71	26.46	3.00

D. Raman Spectra

Fig. 5 shows the Raman spectra of prepared glass samples. The most sharp and intense band is at 1178 cm^{-1} and is attributed to the presence of symmetric PO_2 vibrations. The band at 1260 cm^{-1} is assigned to the presence of asymmetric PO_2 vibrations. The weak band at 1024 cm^{-1} is due to the symmetric $(PO_3)^{2-}$ vibrations. The band at 697 cm^{-1} is attributed to symmetric stretching vibrations of P-O-P linkages. The weak band at 920 cm^{-1} is attributed to asymmetric stretching vibrations of P-O-P linkages. As the concentration of CeO_2 is very low thus no new bands are formed. With CeO_2 doping only the intensity of various bands changes [5].

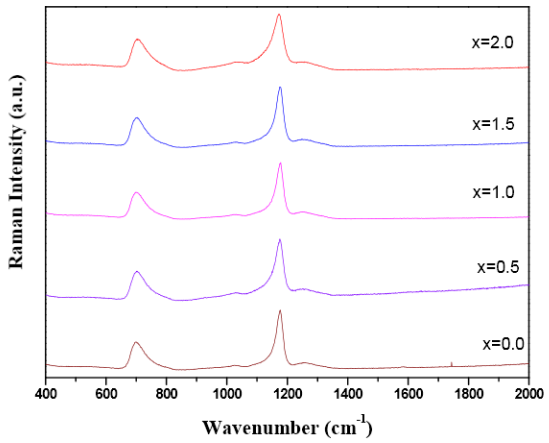

Fig. 5 Raman Spectra of prepared glass samples

IV. CONCLUSIONS

The density of prepared glass samples was found to increase with cerium dioxide which makes the glass structure denser. In Raman spectra only slight variation in intensity of bands was observed with the doping of CeO_2 upto 2 mol%. The optical bandgap was found to decrease with CeO_2 content due to formation of more NBOs.

ACKNOWLEDGMENT

The authors wish to thank Dr. Atul Khanna, Department of Physics, Guru Nanak Dev University, Amritsar for providing facilities like XRD, Raman and UV-Visible spectrophotometer. We are also thankful to Principal DAV College Amritsar for their support.

REFERENCES

[1] Dheeraj Jain, V Sudarsan, RK Vatsa , CGS Pillai, "Luminescence studies on ZnO-P_2O_5 glasses doped with Gd_2O_3:Eu nanoparticles and Eu_2O_3" J. of Luminescence, 129, 439-443 (2009).

[2] K. Venkata Rao, YC Ratnakaram, M Seshadri, JL Rao, "Optical and Luminescence studies of Pr^{3+} and Er^{3+} doped different phosphate glasses," Physica B, 405, 2297-230 (2010).

[3] R. K. Brow, "Structure of Simple Phosphate Glasses," J. Non-Cryst. Solids, 263-264, 1-28 (2000).

[4] Jincheng Du, Leopold Kokou, Jennifer L. Rygel, Yongsheng Che, Carlo G. Pantano , "Structure of Cerium Phosphate Glasses : Molecular Dynamics simulation," J. Am. Ceram. Soc., 94 [8] 2393-2401 (2011).

[5] Jennifer L, Yongsheng Che, Rygel, Carlo G. Pantano, Tomohiro Shibata, Jincheng Du, Leopold Kokou, "Local Structure of Cerium in Aluminophophate and Silicophophate Glasses,"J. Am. Ceram. Soc. 94 [8] 2442-2451 (2011).

[6] MA Marzouk, HA ElBatal, AM Abdel Ghany, FM Ezz Eldin, "Ultraviolet, visible, ESR, and Infrared spectroscopic studies of CeO_2 doped lithium phosphate glasses and effect of gamma irradiation" J. Molecular Structure 997, 94-102 (2011).

[7] Babita Tiwari, V. Sudarsan, Anupam Dixit, and Govind P. Kothiyal, "Effect of TiO_2 Addition on the Optical, Thermo-Physical and Structural Aspects of Sodium Alumino-Phosphate Glasses," J. Am. Ceram. Soc.1-7 (2011).

Comparison of composite proton conducting polymer gel electrolytes containing weak aromatic acids

Rajiv Kumar
Department of Physics, G.G.D.S.D. College, Hariana, Hoshiarpur, Punjab - 144208, India
Email: rajiv_parashar17@yahoo.co.in

Abstract- **Composite proton conducting non aqueous polymer gel electrolytes have been synthesized by dispersing nano sized fumed silica to the polymer gel electrolytes containing polymethylmethacrylate (PMMA), dimethylacetamide (DMA), benzoic acid (BA) and ortho-hydroxy benzoic acid (o-OHBA). These electrolytes have been characterized by complex impedance spectroscopy, viscosity and pH measurements. The effect of acid, polymer and fumed silica on conductivity, pH and viscosity has been studied for gel electrolytes. Maximum conductivity of 2.95 x 10^{-4} S/cm and viscosity of 1.64 x 10^{5} mPas at 25°C has been obtained. The conductivity of composite gels does not show any appreciable change with time and only a small change in conductivity is observed over the operational range of temperature, which is desirable for their use in device applications.**

Keywords— Conductivity, Dimethylacetamide, Fumed Silica, Polymethylmethacrylate, Viscosity.

I. INTRODUCTION

Fuel cells are projected as the clean energy sources of the next generation and depending upon the electrolyte used, different types of fuel cells are available in the market [1]. Proton exchange membrane fuel cells (PEMFCs) which use a solid polymer membrane as the electrolyte are favoured for stationary, portable and mobile applications as these can operate at normal temperatures [2]-[5]. The most important part of PEMFCs is the membrane which must conduct protons and should have good mechanical properties. The Nafion membrane presently used is very costly and is suitable for limited temperature range applications due to its humidity dependent conductivity. Hence there is a growing need to develop an alternate proton conducting membrane which have high value of ionic conductivity and can be used over wide temperature range. Polymers containing functional acidic groups in the hydrated state [6] and in hetrocycles such as imidazole, pyrazole or benzimidazole [7] have also been reported. Proton conducting polymer gel electrolytes containing weak acids–namely aromatic carboxylic acids and aliphatic dicarboxylic acids have recently been reported to show high value of conductivity at 25°C and being non-aqueous in nature could be used over wide range of temperature [8]-[10]. Another advantage of these materials is that the addition of different polymers has been reported to result in an increase in conductivity alongwith an increase in viscosity. The dimensional stability of these polymer gel electrolytes can be further improved by dispersing small size insulating particles in these electrolytes. The aim of the present work is to develop nano-dispersed non-aqueous polymer gel electrolytes with high value of conductivity and good dimensional stability which could find applications in PEMFCs and other devices.

In the present study nano dispersed polymer gel electrolytes obtained by dispersing nano sized fumed silica to proton conducting non-aqueous polymer gel electrolytes containing polymethylmethacrylate (PMMA) in the solutions of ortho-hydroxy benzoic acid in dimethylacetamide (DMA) has been investigated. The effect of the concentration of acid, polymer and fumed silica as well as temperature on the conductivity and viscosity of electrolytes has been studied. The effect of the molecular weight of the polymer on the conductivity and viscosity behaviour of polymer gel electrolytes has also been studied. The change in free H^+ concentration in the electrolytes has also been monitored by pH measurements.

II. EXPERIMENTAL

Polymethylmethacrylate (PMMA) (Aldrich) with average molecular weights 15,000; 120,000 and 996,000; dimethylacetamide (DMA) (Merck) (ε = 37.8, η = 1.937 cP, M.P. = -20°C, B.P. = 165°C), benzoic acid (C_6H_5COOH) (Lancaster) ortho-hydroxy benzoic acid (C_6H_4OH COOH) (Lancaster) and fumed silica (Aldrich) with surface area 380 m^2/g and grain size 7 nm were used as the starting materials. Liquid electrolytes were prepared by dissolving benzoic acid and ortho-hydroxy benzoic acid in different concentrations (expressed in molarity values) in DMA and polymer gel electrolytes were obtained by adding PMMA in different amounts (expressed as wt% of liquid electrolyte) to the liquid electrolytes alongwith continuous stirring by magnetic stirrer. Nano-dispersed gels were then prepared by dispersing nano sized fumed silica in different concentrations (expressed as wt% of polymer gel electrolytes) to the polymer gel electrolytes alongwith continuous stirring to ensure homogenization. Electrolytes containing different concentrations of ortho-hydroxy benzoic acid, PMMA and fumed silica have been studied in the present work.

The electrical conductivity of electrolytes was measured by complex impedance spectroscopy using HP4284A precision LCR meter in the 20Hz-1MHz frequency range

with a cell having platinum electrodes. The conductivity was also measured in the 20–90°C temperature range by using a temperature controlled furnace in steps of 5°C. pH of the electrolytes was measured by systronics 335 pH meter. The viscosity of different electrolytes was measured by Fungilab rotating viscometer (Visco Basic L) at different temperatures in water circulator (Julabo F12-EC) which could control the temperature with an accuracy of ± 0.1°C.

III. RESULTS AND DISSCUSSION

The conductivity of liquid electrolytes obtained by adding benzoic acid and ortho–hydroxy benzoic acid (o-OHBA) to dimethylacetamide (DMA) was measured at 25°C as a function of acid concentration and the results are given in Fig.1. The conductivity of solvent (~10^{-6} S/cm) increases by two orders of magnitude with the addition of acid and reaches a value of 1.55 x 10^{-4} S/cm for liquid electrolytes containing 1M o-OHBA. The acid upon dissociation provides free H^+ ions which take part in the conduction process and as a result conductivity increases. However the rate of increase of conductivity with acid concentration in not constant and is less at higher acid concentrations which is generally explained to be due to the formation of ion aggregates which do not take part in the conduction process. Although the solvent used (DMA) in the present study has high dielectric constant (ε = 37.8 at 25°C) yet some undissociated acid will also be present in these liquid electrolytes as the acid used is a weak acid with dissociation constant (1.40 x 10^{-3}) less than one in an aqueous solution. Due to lower dielectric constant of DMA as compared with water (ε=80) the amount of undissociated acid will be higher in liquid electrolytes containing DMA.

For comparison the conductivity variation for electrolytes containing benzoic acid is also given in Fig.1. The lower conductivity of electrolytes containing benzoic acid is due to its low dissociation constant (8 x 10^{-5}) which is less than that for o-hydroxy benzoic acid and as a result benzoic acid is not fully dissociated in the solvent.

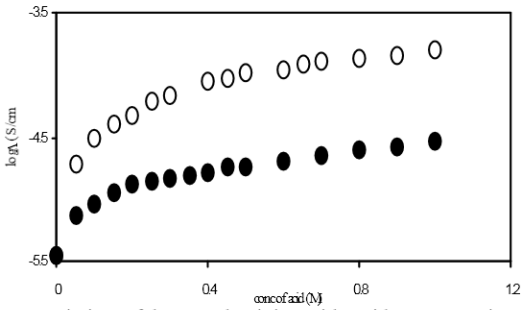

Fig.1 Variation of log conductivity with acid concentration for liquid electrolytes containing benzoic acid (•), and o-hydroxy benzoic acid (o) in DMA.

The increase in free H^+ ion concentration with the addition of o-OHBA in liquid electrolytes has been studied by pH measurements and the variation of pH with acid concentration is given in Fig.2. pH decreases with an increase in acid concentration. As pH in an aqueous solution is given by pH = -log [H^+(aq.)] so a decrease in pH corresponds to an increase in acidity or an increase in free H^+ ion concentration. A comparison of Fig.1 and Fig.2 shows that a decrease in pH is accompanied by a corresponding increase in conductivity. At high acid concentrations, the rate of decrease of pH with acid concentration also decreases. Although the electrolytes used in the present case are non-aqueous in nature yet a decrease in pH shall correspond to an increase in free H^+ ion concentration in the electrolyte. The addition of acid to DMA also results in an increase in viscosity of the electrolyte and the variation of viscosity with acid concentration is given in Fig.3. Viscosity increases linearly with the concentration of acid but due to only a small increase in viscosity, its effect on conductivity shall also be negligible.

Although liquid electrolytes possess high value of conductivity (~10^{-4} S/cm) at 25°C yet they cannot be used in various devices due to their liquid nature. The polymer gel electrolytes obtained by immobilizing liquid electrolytes with the addition of a suitable polymer matrix can partly overcome the above drawbacks of liquid electrolytes. Polymer gel electrolytes were prepared by adding PMMA with average molecular weight 15,000 to liquid electrolytes containing 0.5 and 1M o-OHBA in DMA and the variation of conductivity at 25°C as a function of PMMA concentration is given in Fig.4. The conductivity of liquid electrolytes containing 0.5 as well as 1M o-OHBA increases with the addition of PMMA, reaches a maximum value at around 3–4wt% PMMA and then shows a small decrease at higher PMMA concentrations. The addition of polymer generally results in an increase in viscosity[11-13] which shall lower ionic mobility and secondly the addition of polymer also results in a net decrease in acid concentration as no additional acid has been added alongwith PMMA and both these factors – lower mobility and lower acid concentration shall result in lower conductivity. Despite this the conductivity of liquid electrolytes increases with the addition of PMMA and this increase although small but is quite significant and σ(gel) > σ(liquid) has been observed at all PMMA concentrations [12]-[13].

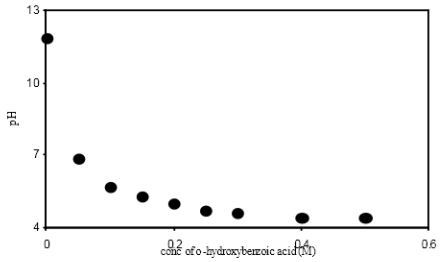

Fig.2 Dependence of pH on acid concentration for liquid electrolytes containing o-hydroxy benzoic acid in DMA.

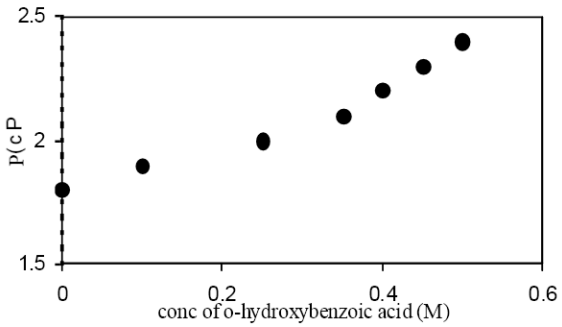

Fig.3 Change of viscosity with acid concentration for liquid electrolytes containing o-hydroxy benzoic acid in DMA.

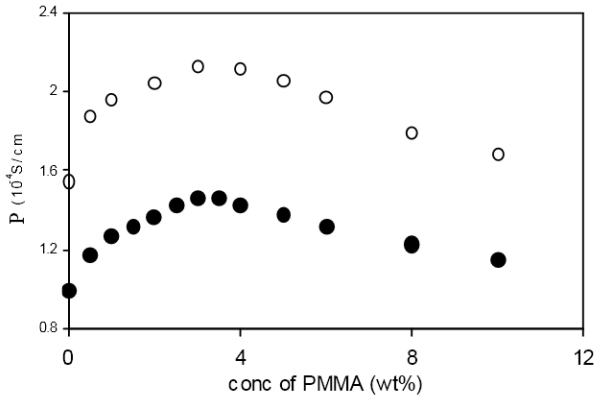

Fig.4 Variation of conductivity with PMMA concentration for polymer gel electrolytes containing 0.5M (•), 1M (o) o-hydroxy benzoic acid in DMA.

The presence of a maxima in the conductivity vs PMMA concentration plot (Fig.4) indicates the simultaneous presence of two competing processes in these gel electrolytes which are free ion concentration at low PMMA concentration and viscosity at high PMMA concentrations [14]. This was experimentally checked by pH and viscosity measurements on these polymer gel electrolytes. The variation of pH of gel electrolytes containing 0.5M o-OHBA as a function PMMA concentration is given in Fig.5. pH decreases with an increase in PMMA concentration and the decrease is more upto about 3wt% and thereafter the decrease in pH is very small. The low PMMA concentration range in which pH decreases corresponds to the region in which conductivity increases with PMMA addition as given in Fig.4. The decrease in pH corresponds to an increase in free H^+ ion concentration which contributes to an increase in conductivity. As the acid used in the present study is a weak acid so some undissociated acid is present in these gel electrolytes and the increase in free H^+ ion concentration is possibly due to the dissociation of undissociated acid with the addition of PMMA. The small change in pH at high PMMA concentrations is an expected behaviour because the amount of undissociated acid present in liquid electrolytes is fixed and with the addition of PMMA some of the undissociated acid gets dissociated resulting in a decrease in the amount of undissociated acid. This shall lead to a small change in pH at higher PMMA concentrations.

The viscosity of polymer gel electrolytes containing 0.5M o-OHBA was also measured as a function of PMMA concentration and the results are given in Fig.6. The viscosity increases linearly with PMMA concentration and the decrease in conductivity observed in Fig.4 at high PMMA concentration is due to the dominant role played by viscosity which is large at high PMMA concentrations. Although viscosity increases with increase in PMMA concentration yet its low value is due to the use of PMMA with low molecular weight (15,000). The role of viscosity in conductivity modification of polymer gel electrolytes was also investigated in more detail. However it may be pointed out that the viscosity measured experimentally by rotating viscometer is the macroscopic viscosity whereas it is the microscopic viscosity which is related to ionic mobility and hence conductivity. Literature reports on different polymer gel electrolytes report that the addition of polymer increases the viscosity of gel electrolytes which is accompanied by a small decrease in conductivity [11]. The conductivity is related to the viscosity by the relation

$$\sigma = e^2 n / 6\pi r \eta$$

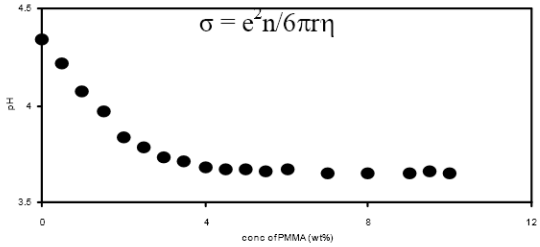

Fig.5 Dependence of pH on PMMA concentration for polymer gel electrolytes containing 0.5M o-hydroxy benzoic acid in DMA.

which suggests that an increase in viscosity shall lead to a decrease in conductivity.

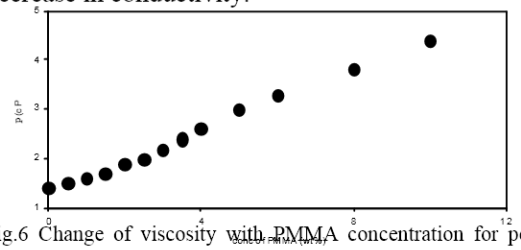

Fig.6 Change of viscosity with PMMA concentration for polymer gel electrolytes containing 0.5M o-hydroxy benzoic acid in DMA.

Further the viscosity of a particular polymer also depends upon its average molecular weight and it increases with an increase in the molecular weight of the polymer. Thus the viscosity of polymer gel electrolytes shall also depend upon the molecular weight of the polymer used. As pointed out in the above section that the viscosity of electrolytes plays a dominant role in conductivity modification at high polymer concentrations so the use of polymer with different molecular weights shall affect the conductivity by different amounts. This was studied in the present case by using PMMA with average molecular weight 15,000; 120,000 and 996,000 [12]. Polymer gel electrolytes were prepared by adding

PMMA with different molecular weights to the 0.5M solution of o-OHBA in DMA and the variation of conductivity with PMMA concentration is given in Fig.7. The conductivity of liquid electrolytes increases with the addition of PMMA having different molecular weights and the variation is similar to that observed in Fig.4. However the increase in conductivity observed with PMMA addition depends upon the molecular weight of PMMA used and is less for PMMA with higher molecular weights. However the conductivity of all the gel electrolytes containing PMMA with different molecular weights is higher than the corresponding liquid electrolyte at all concentrations of PMMA. Similar type of behaviour observed in the variation of conductivity with PMMA concentration for gel electrolytes containing PMMA with different molecular weights suggests that same type of mechanism is responsible for conductivity modification in these electrolytes. At low PMMA concentration the free H^+ ion concentration plays a dominant role whereas at high PMMA concentration, viscosity plays a dominant role in conductivity behaviour.

pH of polymer gel electrolytes containing PMMA with different molecular weights was also measured as a function of PMMA concentration and the results are given in Fig.8. In each case the pH decreases at low PMMA concentrations and shows a near saturation value at high PMMA concentrations. However the extent of decrease in pH is also related to the molecular weight of PMMA used and the decrease in pH is more for gel electrolytes containing low molecular weight (15,000) PMMA. A comparison of the results in Fig.7 and Fig.8 shows that an increase in conductivity with PMMA addition also leads to a decrease in pH which is due to an increase in free H^+ ion concentration which can take place due to the dissociation of undissociated acid present in these gel electrolytes containing weak acid. However as free ion concentration and viscosity are simultaneously affecting the conductivity behaviour so the use of high molecular weight PMMA (120,000 and 996,000) results in higher viscosity and as a result the decrease in pH is small as compared with gel electrolytes containing PMMA with low molecular weight (15,000).

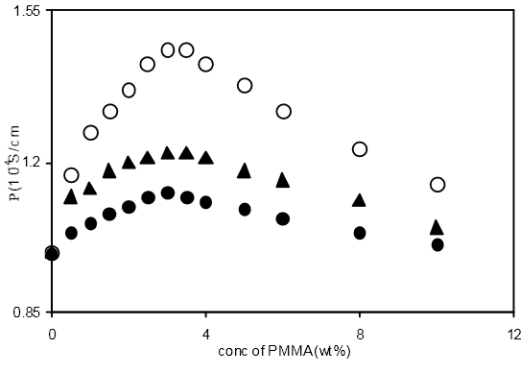

Fig.7 Dependence of conductivity on PMMA (av. mol. wt. 15,000 (o), 120,000 (▲) and 996,000 (•)) concentration for polymer gel electrolytes containing 0.5M o-hydroxy benzoic acid in DMA.

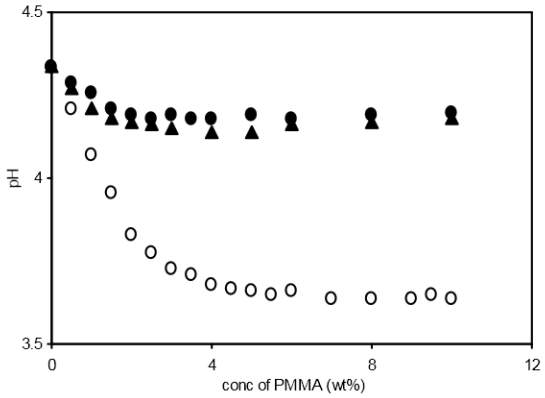

Fig.8 Variation of pH with PMMA (av. mol. wt. 15,000 (o), 120,000 (▲) and 996,000 (•)) concentration for polymer gel electrolytes containing 0.5M o-hydroxy benzoic acid in DMA.

The dependence of viscosity of polymer gel electrolytes upon the molecular weight of PMMA used was also studied by measuring the viscosity of polymer gel electrolytes containing PMMA with different molecular weights and the results are given in Fig.9. The viscosity of gel electrolytes depends upon the molecular weight of PMMA used and is higher for gels with high molecular weight PMMA. In each case, at low PMMA concentrations the viscosity is low whereas at high PMMA concentrations the viscosity is very large and plays a dominant role and results in a decrease in conductivity as observed in Fig.7. Thus the results of the variation of conductivity, pH and viscosity as given in Figs.7–9 for polymer gel electrolytes containing PMMA with different molecular weights are compatible with each other. In each case the increase in free H^+ ion concentration at low PMMA concentration is responsible for an increase in conductivity whereas the large viscosity at high PMMA concentrations plays a dominant role and results in a decrease in conductivity.

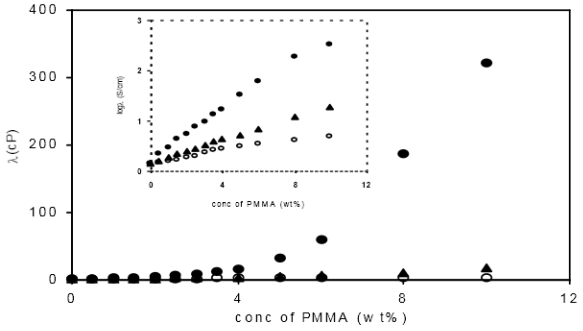

Fig.9 Variation of viscosity with PMMA (av. mol. wt. 15,000 (o), 120,000 (▲) and 996,000 (•)) concentration for polymer gel electrolytes containing 0.5M o-hydroxy benzoic acid in DMA. (inset shows the variation of log viscosity with PMMA concentration).

The effect of the dissociation constant of the acid used on the conductivity behaviour of polymer gel electrolytes was also studied by synthesizing polymer gel electrolytes containing benzoic acid. Fig.10 show the variation of conductivity with PMMA (av. mol. wt. 15,000) concentration for polymer gel electrolytes containing 1M benzoic acid in DMA. The conductivity increases with the addition of PMMA and gel electrolytes with conductivity higher than the corresponding liquid electrolytes are obtained for all concentrations of PMMA. However the increase in conductivity at low concentrations of PMMA is very large and is by 1-2 orders of magnitude as compared with that observed in Fig.4 for gel electrolytes containing o-hydroxy benzoic acid. Secondly the conductivity does not show a decrease at high PMMA concentrations as observed for o-OHBA although the rate of increase of conductivity decreases at high concentrations of PMMA. This could be explained as follows:

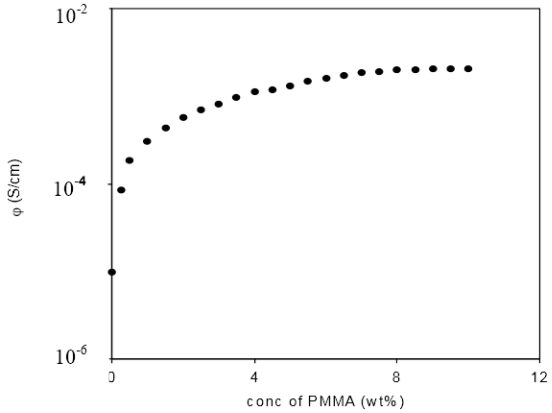

Fig.10 Variation of conductivity with PMMA (av. mol. wt. 15,000) concentration for polymer gel electrolytes containing 1M benzoic acid in DMA.

The benzoic acid used has very low value of dissociation constant (8 x 10^{-5}) which is even less than that of o-OHBA and as a result a large amount of undissociated acid shall be present in these electrolytes. As the addition of PMMA results in the dissociation of undissociated acid so the increase in free ion concentration will be large and shall play a dominant role at all PMMA concentrations upto 10wt%. The effect of viscosity at high PMMA concentrations does not play a dominant role due to the dominant role of free ion concentration.

The change in free H^+ ion concentration in polymer gel electrolytes containing benzoic acid was studied by pH measurements and Fig.11 gives the variation of pH as a function of PMMA concentration for polymer gel electrolytes containing 1M benzoic acid in DMA. pH shows a linear decrease with an increase in PMMA concentration which shows that the concentration of H^+ ion increases with PMMA addition upto 10wt% and this is reflected in the increase in conductivity with PMMA addition as given in Fig.10. Thus in electrolytes containing benzoic acid, the amount of undissociated acid is large and the addition of PMMA results in the dissociation of benzoic acid even upto 10wt% PMMA.

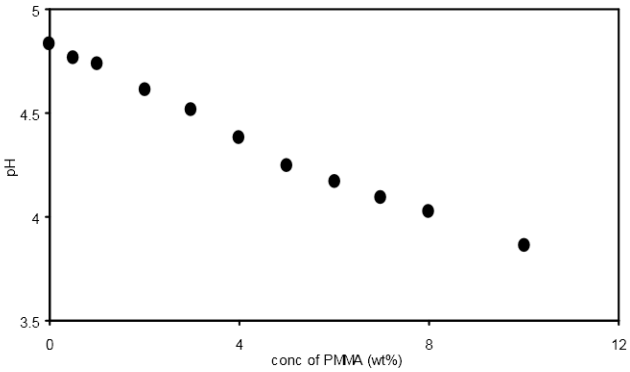

Fig.11 Change of pH with PMMA (av. mol. wt. 15,000) concentration for polymer gel electrolytes containing 1M benzoic acid in DMA.

On the basis of above studies it has been found that polymer gel electrolytes obtained by adding PMMA with molecular weight 15,000; 120,000 and 996,000 to the 0.5 and 1M solutions of o-OHBA in DMA show high conductivity as well as higher viscosity at 25°C than the corresponding liquid electrolytes. Despite this, a further improvement in the dimensional stability of these polymer gel electrolytes shall be needed for their use as electrolytes in various devices.

In 1973 Liang reported that the addition of an insulating material (Al_2O_3) to a poor ionic conductor (LiI) resulted in an increase in conductivity and these are known as composite electrolytes [15]. The increase in conductivity was later found to depend upon the particle size (the increase in conductivity was more for smaller particles) and concentration of insulating matrix [16]-[20]. Later on in the case of composite polymer electrolytes, the addition of insulating particles to the polymer electrolytes was also reported to result in an increase in the mechanical properties alongwith conductivity enhancement [21]-[26]. A similar approach has been employed in the present case to improve the mechanical strength of polymer gel electrolytes. Fumed silica with large surface area of 380m^2/g and having grain size 7 nm has been used in the present study as an insulating matrix.

Nano dispersed polymer gel electrolytes were obtained by adding fumed silica in different concentrations (expressed as wt% of polymer gel electrolytes) to the polymer gel electrolytes containing 10wt% PMMA with average molecular weight 15,000 in the 0.5 and 1M solutions of o-OHBA in DMA. The conductivity was measured at 25°C as a function of the concentration of fumed silica and the results are given in Fig.12 for electrolytes containing 0.5 and 1M o-OHBA respectively. The results show the presence of two maxima – one at

very low concentrations (<1 wt%) of fumed silica and the second at ~8wt% fumed silica. The measurements have been made upto 10wt% fumed silica only as the composite gel electrolytes become highly viscous and more silica could not be added. Two maxima in the conductivity behaviour has also been reported earlier for composite polymer electrolytes PEO – NH_4I – Al_2O_3 [27], $(PEO)_8$ – $LiClO_4$ – SiO_2 and $(PEO)_8$ - $LiN(CF_3SO_2)_2$ – SiO_2 [28], $RbHSO_4$ – SiO_2 [29], $(PEO)_9$ – $LiCF_3SO_3$ – Al_2O_3 [30] and $(PEO)_{10}$ –$LiClO_4$ – SiO_2 [24].

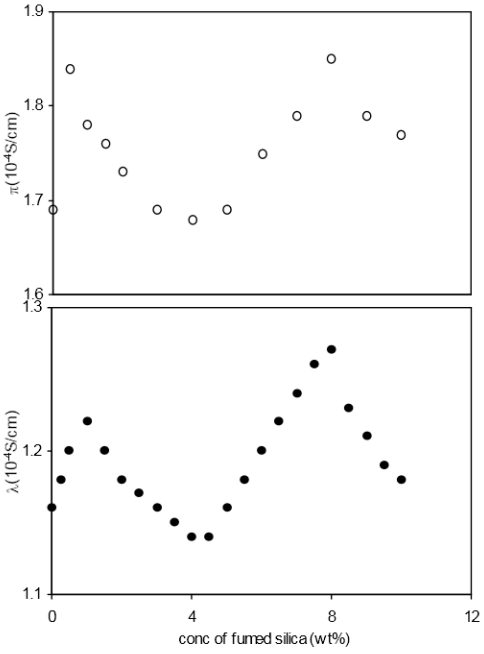

Fig.12 Conductivity variation with fumed silica concentration for nano-dispersed polymer gel electrolytes containing 10wt% PMMA in solution of 0.5M (•), 1M (o) o-hydroxy benzoic acid in DMA.

While studying the variation of conductivity of polymer gel electrolytes with PMMA concentration, the results of Fig.4 shows that conductivity is maximum for polymer gel electrolytes containing 4wt% PMMA. In order to obtain optimum value of conductivity, polymer gel electrolytes containing 4wt% PMMA were also used to prepare nano dispersed polymer gel electrolytes. The conductivity of nano dispersed polymer gel electrolytes containing 4wt% PMMA in 0.5 and 1M solutions of o-OHBA in DMA was also measured as a function of the concentration of fumed silica and the results are given in Fig.13. The variation of conductivity is similar to that for gels containing 10wt% PMMA and two maxima at approximately the same concentrations of fumed silica are observed. Thus nano dispersed polymer gel electrolytes containing different concentrations (0.5 and 1M) of ortho-hydroxybenzoic acid and containing different (4 and 10wt%) amounts of PMMA with average molecular weight 15,000 show similar conductivity behaviour as a function of fumed silica concentration. The presence of two maxima in the variation of conductivity of nano dispersed gels with fumed silica could be explained as follows:

The presence of the first maxima at very low fumed silica concentration (<1wt%) is due to an increase in the dissociation constant of acid with the addition of nano sized fumed silica. Due to the charged surface of fumed silica particles, the H of hydroxyl (-OH) group in o-hydroxy benzoic acid shall be attracted towards the oxygen of fumed silica. This shall lead to an increase in the inductive effect which shall result in an increase in the dissociation constant of the acid [31]. This shall lead to an enhanced dissociation of the acid. The enhanced dissociation of the weak o-OHBA acid present in these electrolytes shall contribute to an increase in free H^+ ion concentration and as a result an increase in conductivity is observed. However one could miss this maxima if measurements at very small concentrations of fumed silica are not taken. Irrespective of the concentration of o-OHBA and PMMA, this maxima is observed in each of the four systems studied in the present case.

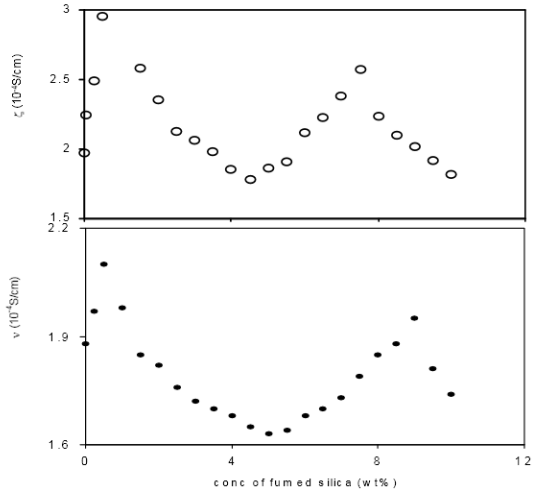

Fig.13 Conductivity variation with fumed silica concentration for nano-dispersed polymer gel electrolytes containing 4wt% PMMA in solution of 0.5M (•), 1M (o) o-hydroxy benzoic acid in DMA.

The presence of the first maxima at very low concentrations of the fumed silica was also checked by studying polymer gel electrolytes containing benzoic acid which does not contain any hydroxyl group. Fig.14 shows the variation of conductivity with the concentration of fumed silica for nano dispersed gel containing 10wt% PMMA in the 1M solution of benzoic acid in DMA. It does not show any maxima at low concentrations of fumed silica as observed for electrolytes containing o-OHBA. pH of the electrolytes also does not show any decrease with the addition of fumed silica in this case. Thus the addition of fumed silica does not enhance the dissociation of benzoic acid as observed in the case of electrolytes containing o-hydroxy benzoic acid.

The presence of second conductivity maxima at ~8wt% of fumed silica in Fig. 12 and 13 is due to the interlocking of fumed silica particles within the PMMA chains which increases viscosity alongwith promoting composite nature and as a result the second maxima is due to the formation

of high conducting interfacial layer between the particles of fumed silica and PMMA gel [32]. As the grain size of fumed silica is quite small (7nm) so maxima is observed at low concentrations of fumed silica whereas in the case of micron size Al_2O_3 the maxima is generally observed at higher concentrations (20-30wt%) of insulating materials in the composite polymer electrolytes.

The enhanced dissociation of o-OHBA with the addition of fumed silica at low concentrations was also examined by pH measurements. The variation of pH with the concentration of fumed silica for nano dispersed polymer gel electrolytes containing 4 and 10wt% PMMA in 0.5 and 1M o-OHBA solutions in DMA are given in Fig. 15. Similar behaviour has been observed in each case. pH has been found to decrease with the initial addition of fumed silica and then reaches a saturation value. The decrease in pH indicates an increase in acidity which is due to an increase in free H^+ ion concentration due to the enhanced dissociation of undissociated acid as proposed above while explaining conductivity results. In Fig. 15 the decrease in pH of polymer gel electrolytes containing 10wt% PMMA is less than those containing 4wt% PMMA which could be due to higher viscosity of polymer gel electrolytes containing 10wt% PMMA. The nearly constant value of pH above around 2wt% fumed silica suggests that the second maxima observed at ~8 wt% fumed silica is not related to a change in free H^+ ion concentration.

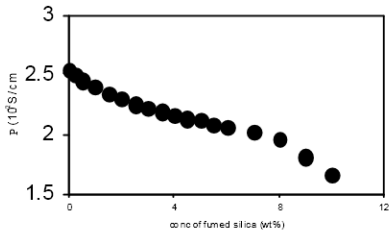

Fig.14 Variation of conductivity with fumed silica concentration for nano-dispersed polymer gel electrolytes containing 10wt% PMMA in solution of 1M benzoic acid in DMA.

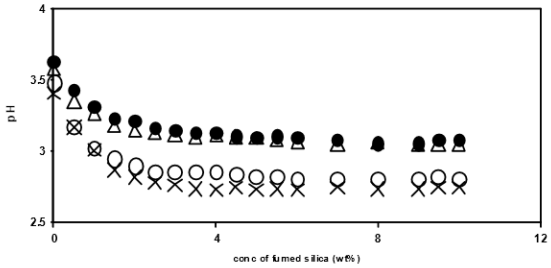

Fig.15 Change of pH with fumed silica concentration for nano-dispersed polymer gel electrolytes containing 4 (o) and 10 (•) wt% PMMA in solution of 0.5M o-hydroxy benzoic acid and for electrolytes containing 4 (x) and 10 (Δ) wt% PMMA in solution of 1M o-hydroxy benzoic acid in DMA.

The addition of fumed silica also results in a large increase in viscosity and viscosity of nano dispersed polymer gel electrolytes was also measured as a function of the concentration of fumed silica and the results are given in Fig.16 and 17 for electrolytes containing 4 and 10wt% PMMA and 0.5 and 1M o-OHBA. From the results it has been observed that the viscosity of electrolytes containing 10wt% PMMA is higher than those containing 4wt% PMMA at all concentrations of fumed silica. The viscosity of electrolytes containing 1M o-OHBA is higher than those containing 0.5M o-OHBA at all concentrations of fumed silica. The viscosity of different nano–dispersed polymer gel electrolytes at low fumed silica concentrations is lower than at high fumed silica concentrations. The change in slope observed in Fig. 17 indicates higher viscosity at high fumed silica concentrations which plays a dominant role in conductivity modification and the decrease in conductivity above 8wt% fumed silica is due to this reason.

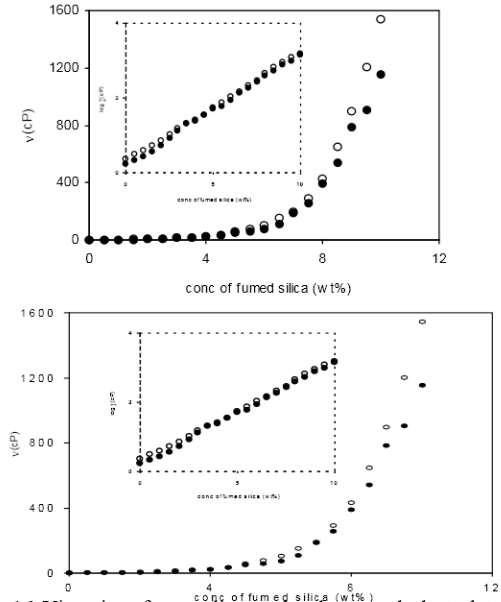

Fig.16 Viscosity of nano dispersed polymer gel electrolytes containing 4wt% PMMA in solution of 0.5M (•), 1M (o) o-hydroxy benzoic acid in DMA as a function of fumed silica concentration.

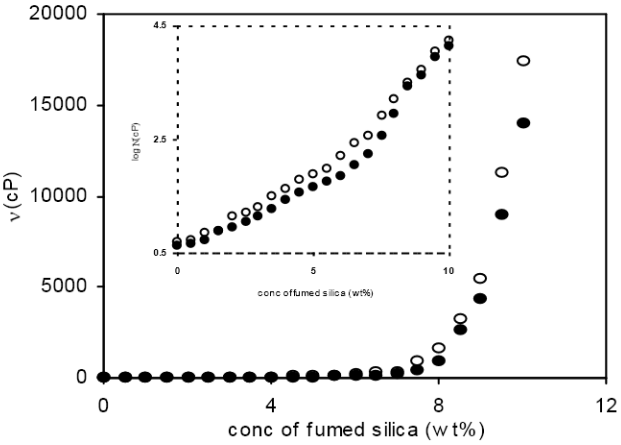

Fig.17 Viscosity of nano dispersed polymer gel electrolytes containing 10wt% PMMA in solution of 0.5M (•), 1M (o) o-hydroxy benzoic acid in DMA as a function of fumed silica concentration.

The conductivity of polymer gel electrolytes containing 10wt% PMMA in the 0.5M solution of o-OHBA in DMA and the corresponding nano dispersed polymer gel

electrolytes obtained by adding 10wt% fumed silica was measured as a function of temperature and the variation of log conductivity vs reciprocal temperature is given in Fig.18. The conductivity of nano dispersed gels is higher than the corresponding gel electrolytes at all temperatures and the change in conductivity over the operational range of temperature is very small which is desirable for their use in various devices. For a good electrolyte the conductivity should also not change with time and this was studied by measuring the conductivity of nano dispersed gel electrolytes as a function of time over a period of three weeks and the results are given in Fig.19. There is no appreciable change in the conductivity of nano dispersed gel electrolytes for this period.

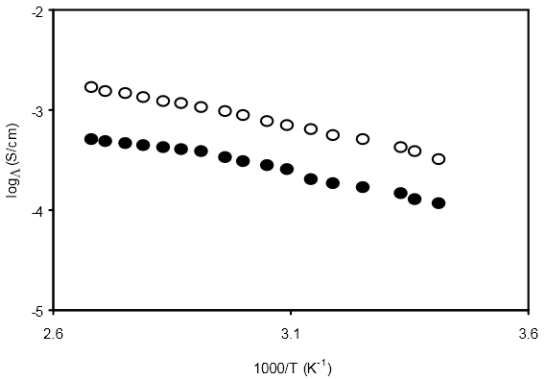

Fig.18 Conductivity as a function of temperature for gel electrolytes (•) containing 10wt% PMMA in solution of 1M o-hydroxy benzoic acid in DMA and nano dispersed gel electrolyte (o) containing 10wt% fumed silica.

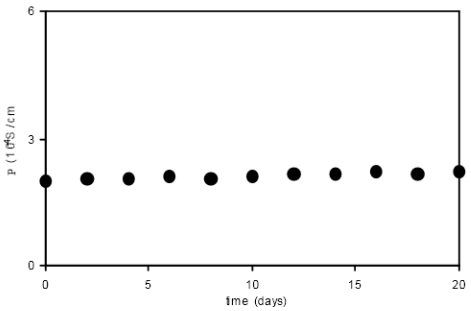

Fig.19 Variation of conductivity of nano dispersed gel electrolytes (DMA + 1M o-hydroxy benzoic acid + 10wt% PMMA + 10wt% fumed silica) as a function of time.

From above studies it has been observed that nano dispersed gels obtained by adding nano sized fumed silica to proton conducting polymer gel electrolytes containing a weak acid (o-hydroxy benzoic acid) show high conductivity (10^{-4} S/cm) at 25°C alongwith high viscosity (~10^5 cP). The conductivity remains constant with time and there is only a small change over the operational range of temperature. Thus these nano dispersed gel electrolytes are suitable for use as electrolytes in polymer electrolyte membrane fuel cells and other devices over a wide temperature range. However their compatibility with electrodes etc. have to be checked before their actual use.

IV. CONCLUSIONS

Nano dispersed polymer gel electrolytes with conductivity of 10^{-4} S/cm at 25°C alongwith good dimensional stability have been obtained. The enhanced dissociation of o-hydroxy benzoic acid with the addition of PMMA monitored by pH measurements results in an increase in conductivity and σ(gel) > σ(liquid) have been observed. The increase in conductivity and viscosity with polymer addition has been found to depend upon the molecular weight of the polymer used. The addition of nano sized fumed silica to polymer gel electrolytes also results in further conductivity enhancement alongwith an improvement in mechanical strength. The increase in conductivity at low fumed silica concentration has been explained to be due to the enhanced dissociation of o-hydroxy benzoic acid whereas at high fumed silica concentrations it is due to the formation of a high conductivity interfacial region between the particles of fumed silica and polymer gel electrolytes. The change in conductivity with temperature is very small and no change in conductivity has been observed with time which is desirable for the applications of nano dispersed gels in fuel cells and other devices.

ACKNOWLEDGEMENTS

The author is thankful to University Grants Commission, New Delhi for financial support in the form of research scheme No. 8-2(172)/2011 (MRP/NRCB).

REFERENCES

[1] L. Carrette, K. A. Friedrich, U. Stimming, "Fuel Cells – Fundamentals and Applications" *Fuel Cells*, vol. 1, pp. 5-39, 2001.

[2] J. C. Lassagues, in: P. Colomban (Ed.), Proton Conductors: solids, membranes and gel-materials and devices, Cambridge University Press, Cambridge, Ch. 20, 1992.

[3] H. P. Dhar, " On solid polymer fuel cells" *J. Electroanal. Chem,*. Vol. 357, pp. 237-250, 1993.

[4] O. Savadogo, "Emerging membranes for electrochemical systems: (I) solid polymer electrolyte membranes for fuel cell systems" *J. New Mater. Electrochem. Syst..,* Vol. 1 pp. 47-66, 1998.

[5] P. Costamagna, S. Srinivasan, "Quantum jumps in the PEMFC Science and technology from the 1960s to the year 2000: Part 1. Fundamentals Scientific aspects" *J. Power Sources*, vol. 102, pp. 242-252, 2001.

[6] K. D. Kreuer, A. Fuchs, M. Ise, M. Spaeth, "Imidazole and pyrazole-based proton conducting

polymers and liquids" *J. Maier, Electrochim. Acta,* vol. 43, pp. 1281-1288, 1998.

[7] J. S. Wainright, J. Wang, D. Weng, R. F. Savinell, M. Litt., "Acid-doped polybenzimidazoles: A new polymer electrolyte" *J. Electrochem. Soc.*, Vol. 142, pp. L121-L123, 1995.

[8] A. M. Grillone, S. Panero, B. A. Retamal, B. Scrosati, "Proton polymeric gel electrolyte membranes based on polymethylmethacrylate" *J. Electrochem. Soc,*. Vol. 146, pp. 27-31, 1999.

[9] S. Chandra, S. S. Sekhon, N. Arora, "PMMA based protonic polymer gel electrolytes" *Ionics,* vol. 6**,** pp. 112-118, 2000.

[10] W. Wieczorek, G. Zukowska, R. Borkowska, S. H. Chung, S. Greenbaum, "A basic investigation of anhydrous proton conducting gel electrolytes" *Electrochim. Acta,* vol. 46 pp. 1427-1438, 2001.

[11] A. Webber, "Conductivity and viscosity of solutions of $LiCF_3SO_3$, $Li(CF_3SO_2)_2N$, and their mixtures" *J. Electrochem. Soc.,* Vol. 138, pp. 2586-2590, 1991.

[12] R. Kumar, S. S. Sekhon, "Effect of molecular weight of PMMA on the conductivity and viscosity behavior of polymer gel electrolytes containing $NH_4CF_3SO_3$" *Ionics*, vol. 14, pp. 509-514, 2008.

[13] O. Bohnke, G. Frand, M. Rezrazi, C. Rousselot, C. Truche, "Fast ion transport in new lithium electrolytes gelled with PMMA. 1. Influence of polymer concentration" Solid State Ionics vol. 66, pp. 97-104, 1993.

[14] R. Kumar, S. S. Sekhon, "Conductivity, FTIR studies and thermal behavior of PMMA-based proton conducting polymer gel electrolytes containing triflic acid*", Ionics,* vol. 19, pp. 1627-1635, 2013.

[15] C. C. Liang, "Conduction characteristics of the lithium iodide – aluminum oxide solid electrolytes" *J. Electrochem. Soc.,* Vol. 120, pp. 1289-1292, 1973.

[16] C. W. Nan, "Conduction theory of ionic conductor containing dispersed second phase" Acta Phys. Sin., vol. 36, pp. 191-198, 1987.

[17] W. Wieczorek, Z. Elorjanczyk, J. R. Stevens, "Proton conducting polymer gels based on a polyacrylamide matrix" *Electrochim. Acta*, vol. 40, pp. 2327-2330, 1995.

[18] F. Croce, G. B. Appetecchi, L. Persi, B. Scrosati, "Nanocomposite polymer electrolytes for lithium batteries" Nature vol. 394, pp. 456-458, (1998.

[19] G. B. Appetecchi, P. Romagnoli, B. Scrosati, "Composite gel membranes: A new class of improved polymer electrolytes for lithium batteries" *Electrochem. Commu.* vol. 3, pp. 281-284, 2001.

[20] H. J. Walls, J. Zhou, J. A. Yerian, P.S. Fedkiw, S.S. Khan, M.K. Stove, G.L. Baker, "Fumed silica-based composite polymer electrolytes: Synthesis, rheology, and electrochemistry" *J. Power Sources* vol. 89, pp. 156-162, 2000.

[21] J. E. Weston, B. C. H. Steele, "Effects of inert fillers on the mechanical and electrochemical properties of lithium salt-poly(ethylene oxide) polymer electrolytes" *Solid State Ionics*, vol. 7, pp. 75-79, 1982.

[22] W. Wieczorek, K. Such, H. Wycislik, J. Plocharski, " Modifications of crystalline structure of PEO polymer electrolytes with ceramic additives" Solid State Ionics vol. 36, pp. 255-257, 1989.

[23] B. Scrosati, F. Croce, L. Persi, "Impedance spectroscopy study of PEO-based nanocomposite polymer electrolytes" *J. Electrochem. Soc.,* vol. 5 pp. 1718-1721, 2000.

[24] L. Z. Fan, C. W. Nan, M. Li, "Effect of modified SiO_2 on the properties of PEO-based polymer electrolytes" *Solid State Ionics* vol. 164, pp. 81-86, 2003.

[25] D. Kumar, S. A. Hashmi, "Ion transport and ion–filler-polymer interaction in poly(methyl methacrylate)-based, sodium ion conducting, gel polymer electrolytes dispersed with silica nanoparticles", *J. Power Sources,* vol. 195, pp. 5101–5108, 2010.

[26] P. Zhang, L C. Yang, L. L. Li, M. L. Ding, Y. P. Wu, R. Holze, "Enhanced electrochemical and mechanical properties of P(VDF-HFP)-based composite polymer electrolytes with SiO_2 nanowires", *J. Membrane Sci.,* vol. 379, pp. 80-85, 2011.

[27] A. Chandra, P. C. Srivastava, S. Chandra, Solid State Ionics: Materials and Applications, (Eds. B. V. R. Chowdari, S. Chandra, Shri Singh, P. C. Srivastava), World Scientific, Singapore, p. 397, 1992.

[28] C. Capiglia, P. Mustarelli, E. Quartarone, C. Tomasi, A. Magistris, "Effects of nanoscale SiO_2 on the thermal and transport properties of solvent-free, poly(ethylene oxide) (PEO)-based polymer electrolytes" *Solid State Ionics* vol. 118 pp. 73-79, 1999.

[29] V. G. Ponomareva, G.V. Lavrova, L.G. Simonova, "Effect of SiO_2 morphology and pores size on the proton nanocomposite electrolytes properties" *Solid State Ionics*, vol. 119, pp. 295-299, 1999.

[30] M. A. K. L. Dissanayake, P. A. R. D. Jayathilaka, B. S. P. Bokalawala, I. Albinsson, B. E. Mellander, "Effect of concentration and grain size of alumina filler on the ionic conductivity enhancement of the $(PEO)_9LiCF_3SO_3$:Al_2O_3composite polymer electrolyte" *J. Power Sources*, vol. 119-121, pp. 409-414,(2003.

[31] R. Kumar, S. S. Sekhon, "Conductivity modification of proton conducting polymer gel electrolytes containing a weak acid (ortho-hydroxy benzoic acid) with the addition of PMMA and fumed silica" *J. Appl. Electrochem.,* Vol. 39, pp. 439-445, 2009.

[32] R. Kumar, "Nano-composite polymer gel electrolytes containing ortho-nitro benzoic acid: Role of dielectric constant of solvent and fumed silica" *Ind. J. Phys.,* Unpublished.

Plastics and FRP material used in Railways

Pawan Malik
Dept. of Chemistry
SLBawa DAV College,Batala,(Punjab),India

Abstract- **The emergence of Plastic industry has become a boon for various engineering application. Plastics are durable, light weight material, easy to transport. The major advantage of plastics is recyclable nature. Recyclable nature helps to conserve landfill space and natural resources and reduce pollution. Earlier, In railways, wooden, concrete, steel sleepers are used. Due to high cost and limited life span, Plastics sleepers are used all over the world at large scale. An attempt has been made to study various engineering plastics used in railways, advantages of plastics over other construction material. Moreover, a special attention is given to Fiber reinforced plastics (FRP) i.e. plastics composites. The study concluded that how plastics composites are more reliable, more economically viable and longer life span.**

Keywords: Plastics, polymer, recycle plastics, railway sleepers, plastics composites

1.0 INTRODUCTION

A substance that can be easily formed or moulded into desired shape is Plastic. Plastic are formed by polymerization, condensation and copolymerization reaction. These reaction give high molecular weight materials which soften on heating and become rigid on cooling [1].

In the manufacture of Plastics, raw material are coal, petroleum, cellulose(prepared from wood and cotton), salt, sulphur, limestone, air water etc. are used. These are subjected to several processes of chemical decomposition and recombination giving intermediate which are them made into plastics. Plastics when mixed with tar have wide application in the construction of road. This not only enhances the strength of road but also increase the durability of road. Using this composition, constructed road get not easily spoiled even during rainy days. These may go at least for 10 years and save the money of nation. In Indian plastic industry, the production of phenol formaldehyde started in 1946.Polystyrene and polyethylene in 1957.Polyvinyl chloride in 1961 and cellulose acetate in 1963.

2.0 PLASTICS AS ENGINEERING MATERIALS

The important engineering plastics used in railways.

1. ABS(Acrylonitrile-Butadiene-Styrene)
2. Polyoxymethylene
3. Nylon-6
4. Nylon-66
5. PBT
6. PET
7. Polycarbonate
8. HDPE

Apart from these, LDPE sheet is widely used for roofing and covering of goods in the wagon [2]. Some important plastics polymers which are used in Indian railways with their application are given as:

2.1 POLYETHYLENE: Polyethylene is formed by polymerization of ethane. It is wax like thermoplastics which can become soften at 80^0-100^0C.This has excellent electrical insulation and chemically resistance. Its density is less than water. To increase its efficiency, carbon black is generally added. Its thin films are transparent. Its uses are in our daily life are house wares, bottles, trays, toys, food stuffs carrying containers.ink pen refilling tubes,wires and cables.

2.2 PTFE (Teflon):-When tetrafluoro ethylene is subjected to polymerization in the presence of acetyl peroxide, the product obtained are highly heat resistant, high thermal stability having melting point around 327^0C. Teflon is tough, flexible, excellent resistant to heat, chemical and electric current. It has very low co-efficient of friction, good weathering resistance. It is widely used in variety of seals, Gaskets, packing, valve and pump parts and lab equipments. It is also used in transformers, condensers, laminates for PCBs, coating for reducing the friction.

2.3 NYLON: - Nylon-6 is a polymer of cyclohexane, get polymerizes in the water. Nylon-66 is combination of hexamethylene diamine and adipic acid. It has properties such as toughness, rigidity, abrasion resistance, heat resistance make it for special purposes. It has variety of application in mechanical engineering parts such as gears, bearings, bushes, valves, seals. Different types of Nylon like Nylon films, Nylon filaments are being used. Nylon films have high clarity, low odour transmission. Nylon filaments are being used in brush, surgical items, sports, fishing nets. Its flexible nature used for tubing and pipe for chemicals and petrol. Its powder form used in chemical resistant coating.

2.4 POLYCARBONATE:-Polycarbonate is special plastics having melting point is 225-250^0C.It is quite rigid and tough which is stable up to 140^0C.This

plastics is transparent and high electrical insulation. Its properties such as low water absorption, high dimensional stability, used in application in electrical and electronics engineering covers for time switches, relays, batteries. This polymer has widely used in domestic purposes such as food processors bowl, power tool, hair drier, electric razor, microwave cookware.

2.5 POLYPROPYLENE(PP):-Polypropylene is widely used in fibers, films and injection mouldings. It is excellent resistance to continued faxing. It is also used in lunch boxes, car accelerators pedals. In car, it is used in battery cases, bumpers, radiator grills, chairs, flower pets. Its monofilaments are used in rope, nets and packaging.

2.6 UREA-FORMALDEHYDE(UF): Urea-formaldehyde has physical properties such as hardness, toughness make it suitable for strong knock resistant electrical fittings. It is also scratch resistant and good electrical insulation. These properties make it suitable for engineering application [3].

2.7 BAKELLITE- It is polymerization of Phenol-formaldehyde in basic medium. It is widely used in Adhesive, electrical goods, combs, fountain pen, mica table tops

2.8ACRYLOPLASTICS(PMMA):
Polymethyl(meth)acrylate (PMMA) is hard, rigid, transparent material with good weather resistance. It has good electrical; insulation and optical properties.

The chief engineering materials advantages of Plastics over the construction material.

a) Light weight
b) Low fabrication cast
c) Resistance to corrosion and solvents.
d) They have decorative effects.
e) Plastics can be used in conjunction with other metal.
f) Good electrical and thermal resistance
g) Low Thermal expansion
h) They are optically clear.
i) Plastics reduce noise and vibration in machine.
j) Low cost and durability
k) Easy fabrication of intricate parts.
l) Good surface polish with option of inbuilt coloring.

3.0 FIBER REINFIRCED PLASTICS (FRP)

A fiber reinforced resins system is a composite material consists of a network of reinforcing fibre embedded in a mixture of thermo setting resins[4].The resins used consists of a syrupy liquid which when combined with a suitable catalyst or hardner, lead to formation of cross linked hard infusible solid.

By impregnating the fibrous material with the catalyzed resin to form composite material or laminated material. When glass fiber is used, it form laminated and when carbon fiber is used, it form composite [5].

Resins used:

1. Unsaturated polyester resins-most widely used.
2. Epoxide resins (Shrinkage-1to 2%)
3. Vinyl ester resins
4. Furan resins
5. Others-Phenolics, Silicones, Polyamides, melamine

3.1 ADVANTAGES OF FRP: FRP has wide variety of application in term of technical properties, summarized as follows [6].

1. Weight—25% to 35% lighter than steel.

2. Manufacturing—easier to assemble, less cost, less complexibility, and dynamic design process.

3. Damaging Resistance: Dent superior to aluminium and steel panels

4. Tooling: Less than half cost (40% of steel stamping)

5. Corrosion resistance: Better corrosion resistance than most of the material

6. Internal damping: Less noise, less vibration, less harshness.

7. Design: More versatile-molding offer geometric shapes and shape complexcity.

Some more highlighted properties are described as:

- High tensile strength
- Ease of fabrication
- .Wide range of manufacturing techniques.
- Low capital outlay.
- Design versatility
- One off or few off moulding at reasonable cost.
- Water resistance
- Chemical resistance
- Weathering and UV resistance
- Maintenance and finish
- Good electrical and thermal properties
- Fire retardant.

4.0 PLASTICS COMPOSITES

There is trend to change railway sleeper from traditional timber to ultra-modern composites. No doubt, wooden sleeper still used in many parts of world where lighter less busy lines providing a resilient track vibration noise. Wooden sleepers are cheap, easy to carry and easy to maintain. Wood is more susceptible to wear and tear than any other modern materials. Now, the modern material used is plastics composites which have all

natural counterpart, Life span of plastics composites is more than 50 years. These plastics composites can be placed alongside older wooden sleepers. One advantage is that it is generally made from recycled material [7]. Fig. 1 shows plastics composites in railways sleepers. Recent study reveals that for one mile of wooden sleeper require 810 mature oak trees but using plastics composites uses only two millions plastics bottles, 8.9 millions plastics bags and 10,800 post consumer tyres.

Fig. 1 Plastic composite in Sleepers

So, plastics composites emerge like a new and advanced technology which is environmentally friendly. As far as economic analysis, the cost of manufacturing is very less as compared to concrete and timber market. The use of plastics composites in railway sleeper has following ability-

- Increasing life span of railway sleepers.
- Minimize vibration and noise.
- Solve the problem of waste plastics.

Plastics composites consists of waste or recycled polyolefin's (Polyethylene), Propylene polymer, Propylene-ethylene copolymer and combination of these polymers[8]

Properties:

1. High thermal coefficient expansion.
2. Environmental friendly.
3. Completely recycle material
4. Superior in performance
5. Minimum maintenance cost
6. Viable replacement of wooden sleepers.

5.0 CONCLUSION

No doubt, Plastics have been great discovery in modern world. Plastics and polymer become part of our life. Recycled plastics are alternative promising technology to save our environmental pollution. There is dire need to generate awareness among scientific community and industries to change their mind sets and develop advanced techniques to prepare such composites having high durability, low cost and higher life span. The ultimate goal of research is to convert plastics into recycled one and prepare composites, which is environmental friendly. There is need of industrial research to develop innovation for making melt-blended composites from old waste materials. Need to stress on improved methods for melt-blended fiber and plastics on commercial scale.

REFERENCE:

[1].Miller, E.Plastic products design handbook, CRC Press (1983)

[2] Erhard,G. Designing with plastics. Trans. Martin Thompson Munich: Hanser Publisher (2006)

[3] www.technologystudent.com

[4] Smallman, R.E.Bishop.R.J.Modern physical metallurgy and materials engineering; 6th ed Oxford; Butterworth-Heineman (1993)

[5] Donald, V.R.Dominick, V; Rosato and Murphy, J.Elsevier.Reinforced plastics handbook (2004)

[6] www.atkearney.es

[7] Baksi, S.Biswas, S.Composites in chemical industry. Proceeding of national convention of chemical engineering, Udaipur (2013)

[8] www.mpponline.in/waste plastics in railway sleepers.

Effect of Gamma irradiation on structural and optical properties of Muscovite Mica

Sukhnandan Kaur, Surinder Singh, Lakhwant Singh

Department of Physics, Guru Nanak Dev University, Amritsar-143005, Punjab

**Corresponding Author's Email:sukhnandanphy@gmail.com*

***Abstract*— Present work reports the structural and optical properties of pristine and gamma irradiated muscovite mica. The XRD spectra are used to estimate structural parameters such as crystallite size and micro strain of pristine and irradiated samples. Williamson Hall analysis is employed to calculate crystallite size and micro strain of pristine and irradiated sheets. UV-VIS analysis provides the value of optical indirect, direct band gap and Urbach energy. It was found that the value of optical indirect and direct band gap increases with the increase of gamma dose upto 100 kGy and then decreases with further increase in gamma dose upto 2000 kGy. Thus, the increase of optical band gap makes natural muscovite fits for efficient optoelectronic devices.**

***Keywords*—** Gamma Radiation, Natural muscovite, XRD, UV-VIS.

I. INTRODUCTION

Muscovite mica [KAl_2 ($AlSi_3O_{10}$) (F, $OH)_2$] is abundant mineral on the earth and has a layered structure of aluminium silicate sheets weekly bonded together by layers of potassium ions. These potassium ion layers produce the perfect cleavage [1]. Muscovite is used chiefly as an insulating material and for fireproofing and are presently being used as dosimeter for monitoring absorbed doses in radiation rich environments. It is well established that the exposure of any material to ionizing radiations produces changes in the microstructural properties of the material, which in turn affects the structural and optical properties [2]. Thus, it is important to understand the effect of ionizing radiation on the structural and optical properties of these materials.

A lot of information is available on the optical [3-7] properties of natural muscovite mica without irradiation. Moreover, the effect of gamma irradiation on these properties has not been investigated so far. Therefore, in the present work, the effect of gamma dose on structural and optical properties of natural muscovite mica have been investigated to utilize this material for innovative applications in radiation technology and opto-electronic devices.

II. EXPERIMENTAL TECHNIQUES

Thin sheets of Natural muscovite mica (procured from Bhilwara mines in Rajasthan) samples were irradiated with ^{60}Co source to different doses ranging from 1 kGy to 2000 kGy at IUAC, New Delhi. The structural changes were studied using XRD-7000 SHIMADZU X-ray diffractometer. The optical changes were analysed with UV-1800 Shimadzu UV-Vis spectroscopy in the wavelength range 200-600 nm.

III. RESULTS AND DISCUSSION

A. Structural Analysis

Figure 1 shows the XRD pattern for pristine and gamma irradiated natural muscovite mica. Five peaks are observed in pristine muscovite mica at 2θ = 8.99°, 17.90°, 26.94°, 36.12° and 45.59° corresponding to crystallographic planes (003), (006), (009), (0012) and (0015), respectively. No shift in peak positions is observed after gamma irradiation.

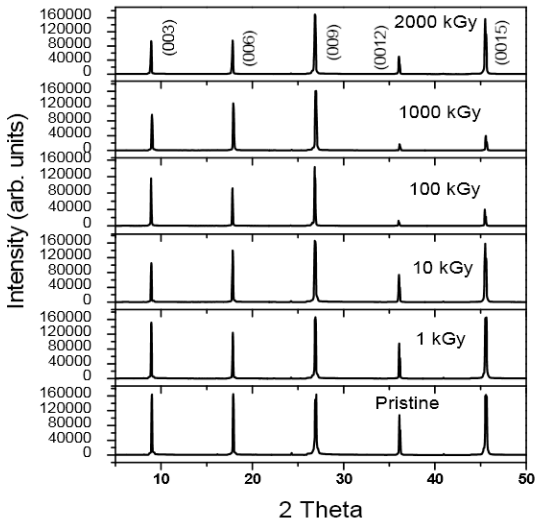

Fig. 1 X- ray diffraction pattern for pristine and gamma irradiated muscovite mica.

The average particle size and the microstrain for the pristine and gamma irradiated samples were determined using the Williamson Hall (W-H) analysis [8]. Fig. 2 shows the W-H plots for the pristine and the gamma irradiated muscovite at different absorbed doses. The values of crystallite size (D) and microstrain (ε) obtained from the intercept and slope of WH plots are listed in table

1. The crystallite size increases with the gamma dose upto 100 kGy; microstrain decreases in the dose range 1- 100 kGy. For gamma doses upto 2000 kGy, the crystallite size decreases however, unlike the microstrain which increase. This means that in the lower gamma dose range, 1 -100 kGy, the irradiation binds the crystallites in clusters, increasing their size and decreasing the microstrain. At higher gamma doses, i.e. 1000, 2000 kGy, the crystallite size decreases and the microstrain increase which indicates that the muscovite moves to a disordered structure.

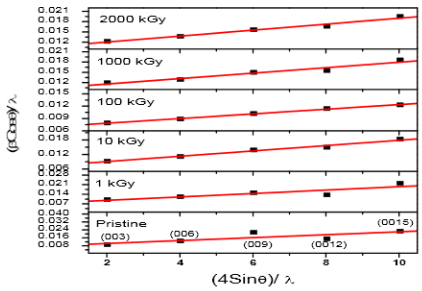

Fig. 2 W-H plots for the pristine and gamma irradiated muscovite mica.

Table 1 Variation of structural and optical parameters with gamma dose

Gamma Dose (kGy)	D nm	ε (10^{-3})	E_g (eV)		E_u (eV)
			Indirect	Direct	
Pristine	135.50	1.47	3.25	3.81	0.45
1	140.65	1.24	3.28	3.83	0.44
10	145.35	1.10	3.33	3.87	0.39
100	148.81	0.57	3.46	3.91	0.32
1000	100.10	0.79	3.30	3.85	0.43
2000	97.09	0.87	3.21	3.76	0.44

B. Optical Analysis

Fig. 3 presents the UV–visible absorption spectra of the pristine and gamma-irradiated (1-2000 kGy dose) natural muscovite mica samples. The absorption edge is shifted towards lower wavelength values by increasing the dose up to 100 kGy. However by further increasing the dose upto 2000 kGy, the absorption edge shifts towards higher wavelength values.

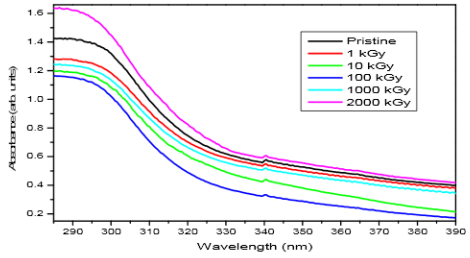

Fig. 3 UV-Vis spectra of pristine and gamma irradiated muscovite mica.

The optical band gap was determined using the following equation [9]:

$$\alpha(h\nu) = B(h\nu - E_g)^n / h\nu \quad (1)$$

where $h\nu$ is the energy of the incident photons, E_g is the value of the optical energy gap between the valance band and the conduction band, B is a constant. The value of n as 1/2 and 2 stands for direct allowed and indirect allowed transitions, respectively. The calculated values of direct and indirect optical band gap for pristine and irradiated samples are given in table 1. The values of optical indirect and direct band gap increase from 1 to 100 kGy and decrease by further increasing the gamma dose upto 2000 kGy.

The irregularities in the band gap level can be defined in terms of Urbach energy (E_u) and were estimated using relation [8]:

$$\alpha(\nu) = \alpha_o \exp(h\nu/E_u) \quad (2)$$

where α_o is a constant, E_u is an Urbach energy and ν is the frequency of radiation. The calculated values of Urbach energy for pristine and gamma irradiated muscovite at different doses are listed in table 1. The decrease of the Urbach energy at increasing γ-doses, from 1 kGy to 100 kGy, indicates the decrease in the structural disorder. By further increasing the dose upto 2000 kGy, the Urbach energy increase may be attributed to increasing of the structural disorder.

IV. CONCLUSION

Gamma irradiation upto 100 kGy leads to the increase in crystallite size and reduction in the defects, structural disorder and microstrain. Thus, irradiation of natural muscovite mica with gamma rays improves its crystallinity. The results of UV-VIS spectra show that the direct and indirect optical band gap can be monitored with the help of gamma irradiations. The increase of optical band gap with gamma irradiation makes natural muscovite fits for efficient optoelectronic devices.

ACKNOWLEDGMENT

Authors are highly thankful to Health physics and material science group at IUAC, New Delhi for providing the Gamma Irradiation, XRD and UV-Vis facilities. Financial support given by UGC, New Delhi, in the form Senior Research Fellowship is also gratefully acknowledged.

REFERENCES

[1] J. Sinkankas, Mineralogy: A First Course; East-west press Pvt. Ltd: New Delhi, 1969.
[2] B.N. Singh, J. Comput-aided Mater. Des. 6 (1999) 195-214.
[3] Popper, P. Nature. **1951**, 168, 1119-1120.
[4] Grum-Grzhimails, S.V., Anikina, L.I., Belova, E.N., Tolstikhins, K.I. Chem. Abst. **1958**, 52,13551.
[5] Dhar, R. N., Das, S.R. Nature. **1966**, 209, 185-186.

[6] Davidson, A.T., Vickers, A.F. J. Phys. C: Solid State Phys. **1972,** 5, 879-887.
[7] Le Calvez, Y., Stephen, G., Robin, S. Opt. Acta. **1968**, 15, 583-594
[8] S. Kaur, S. Singh, L. Singh and S.P. Lochab, *Nucl. Instr. Meth. B* **301,** 17-22 (2013).function networks," *IEEE Trans. Neural Networks*, vol. 4, pp. 570–578, July 1993.
[9] N. F. Mott and E.A. Davies, "Electronic processes in non crystalline materials. Claredon press, Oxford.

ISBN : 978-81-924867-2-7

Amritsar College
of Engineering & Technology

12 km Stone, Amritsar-Jalandhar G.T. Road, Amritsar, Punjab.INDIA
Phone: 0183-5010432, Fax: 0183-5069535
e-mail: contact@acetamritsar.org Website: www.acetamritsar.org

Designed By: Abhi Vatsal Arora (Student, ACET)